UNIVERSITÄT LEIPZIG

REPORT
Institute für Physik
The Physics Institutes

2013

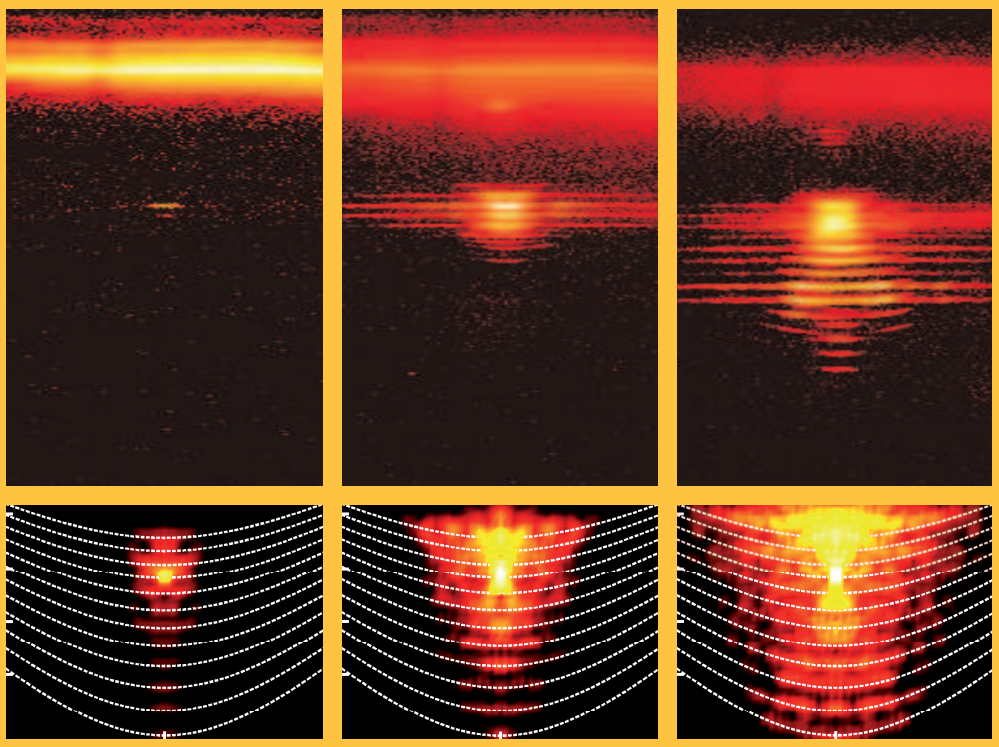

The Physics Institutes of Universität Leipzig, Report 2013
M. Grundmann (Ed.)

Technical Editor: Anja Heck

Printed in Germany by
MERKUR Druck und Kopierzentrum GmbH, Leipzig

online available at
http://nbn-resolving.de/urn:nbn:de:bsz:15-qucosa-148925

Front cover
Rising light: The front cover image shows the energy-momentum intensity pattern of the emission from a multimodal whispering-gallery-mode exciton-polariton Bose-Einstein condensate as function of excitation power (left to right: below, at, above threshold). Bosonic parametric scattering populates coherently discrete states onto the polariton ladder. Upper panels: experiment, lower panels: theoretical simulation. (Fig. 9.48)

Back covers
Recent publications.

Institut für Experimentelle Physik I
Institut für Experimentelle Physik II
Institut für Theoretische Physik

Fakultät für
Physik und Geowissenschaften

Universität Leipzig

Institute for Experimental Physics I
Institute for Experimental Physics II
Institute for Theoretical Physics

Faculty of Physics and Earth Sciences

Universität Leipzig

Report 2013

Addresses

Institute for Experimental Physics I

Linnéstraße 5
D-04103 Leipzig, Germany
Phone: +49 341 97-32551
Fax: +49 341 97-32599
WWW: http://www.uni-leipzig.de/~gasse/nysid_a/inst/exp_1.htm
Mailing address: Postfach 100 920, D-04009 Leipzig, Germany

Institute for Experimental Physics II

Linnéstraße 5
D-04103 Leipzig, Germany
Phone: +49 341 97-32650
Fax: +49 341 97-32668
WWW: http://www.uni-leipzig.de/~exph2
Mailing address: Postfach 100 920, D-04009 Leipzig, Germany

Institute for Theoretical Physics

Brüderstraße 16
D-04103 Leipzig, Germany
Phone: +49 341 97-32420
Fax: +49 341 97-32548
WWW: http://www.physik.uni-leipzig.de
Mailing address: Postfach 100 920, D-04009 Leipzig, Germany

Preface

Welcome to the 2013 Report of the Physics Institutes of the Universität Leipzig. We like to present to you an interesting overview of our research activities. We have enjoyed scientific interaction with colleagues and partners worldwide and are grateful to our guests for enriching our academic year with their contributions in the colloquium and within the work groups.

In January Prof. Jan Meijer has started as head of the nuclear solid state physics group in the Institute for Experimental Physics II. He is renown for high precision implantation of single ions and the creation and investigation of NV centers in diamond. He will expand activities with the LIPSION ion accelerator and also closely cooperate with the Leibniz Institute for Surface Modification (IOM). Prof. Dr. Alois Würger from the Université Bordeaux I in France has been awarded with the Leibniz professorship of the Universität Leipzig and has joined the faculty from April to July 2013 working on the theory of non-equilibrium colloidal transport in solution. In spring 2013 Prof. Josef Käs turned down the offer of a W3 professorship at the Westfälische Wilhelms-Universität Münster. In fall, Prof. Jürgen Haase was reelected as dean of the faculty and Prof. Marius Grundmann was elected as vice dean for research.

The 5th International Conference "Diffusion Fundamentals" was held at the Universität Leipzig for four days in August. This conference involving more than 130 scientists from all over the world was organized as a highlight of the second funding period by researchers of the Saxonian Research Unit 877 "From Local Constraints to Macroscopic Transport" (Prof. Cichos, Prof. Kroy, Prof. Kärger and Dipl.-Phys. Andrea Kramer). More than 20 renowned speakers and almost 100 scientific posters focused on interdisciplinary diffusion related research with highlights from single particle and single molecules tracking experiments in material science and biology as well as new concepts of artificial self-propelled machines.

In October the 4th "Physics of Cancer" symposium took place in Leipzig. The symposium was organized by Prof. Käs and Prof. Mierke from the Institute of Experimental Physics I, Prof. Valerie Weaver, University of California, USA and Prof. Harald Herrmann, German Cancer Research Center. Around 100 scientists from worldwide pioneering groups of many different countries such as the USA, England, France and Japan participated in the symposium and discussed recent progress in the field of cancer research and physical mechanisms underlying cancer progression.

The BuildMoNa 2013 minisymposium and FAHL Academia "Quantum Structures for Energy Applications" was covering topics which are researched in the ESF-funded Young Researcher Group "Effiziente Energienutzung: Neue Konzepte und Materialien". Together with Prof. Orrit (Leiden/Netherlands) and Prof. Barrat (Grenoble/France), Prof. Cichos continued the very successful 2012 BuildMoNa minisymposium on "Hot

Nanostructures" as a one week workshop in October at the Lorentz Center at the University of Leiden. About 60 international participants discussed the newly developing field involving nano-optics, plasmonics, heat generation and transport as well thermodynamics in temperature gradients.

At the end of November the traditional 14th International Workshop on "Recent Developments in Computational Physics" (CompPhys13) organized by Prof. Janke took place in Leipzig. Around 60 scientists from over 10 different countries exchanged ideas and discussed recent progress in several fields of computational physics.

Work in the newly established BMBF-funded VIP project transMEda ("Transparent MESFET for digital applications") has started in fall of 2013. Also the EU-funded (FP7) project piezoMAT ("High-resolution fingerprint sensing with vertical Piezoelectric nanowire MATrices") started in which ZnO nanowire arrays are developed by the semiconductor physics group within an international consortium lead by CEA, Grenoble. The International Graduate College “Statistical Physics of Complex Systems” funded by the Deutsch-Französische Hochschule (DFH-UFA) and run by the computational physics group has successfully been renewed in 2013 and commenced its third funding period in January 2014. Besides the main partner Université de Lorraine in Nancy, France, now also Coventry University, UK, and the Institute for Condensed Matter Physis of the National Academy of Sciences of Ukraine in Lviv, Ukraine, participate as associated partners. Work has successfully continued in the Centers of Excellence (Sonderforschungsbereiche) SFB 762 "Functionality of Oxide Interfaces" and SFB TRR 102 "Polymers under multiple constraints: restricted and controlled molecular order and mobility" and DFG research units.

The 2013 Katharina-Windscheid Prize of the Research Academy Leipzig for an outstanding thesis was awarded to Dr. Helena Franke for her work on the ballistic propagation of exciton-polariton condensates in ZnO-based microcavities.

The extent of our activities is only possible with the generous support from various funding agencies for which we are very grateful and which is individually acknowledged in the brief reports.

Leipzig,
June 2014

M. Grundmann
W. Janke
J. Käs
Directors

Contents

1

Structure and Staff of the Institutes

1.1 Institute for Experimental Physics I

1.1.1 Office of the Director

Prof. Dr. Josef A. Käs (director)
Prof. Dr. Frank Cichos (vice director)

1.1.2 Molecular Nano-Photonics, Molekulare Nanophotonik [MON]

Prof. Dr. Frank Cichos

Technical staff

Dipl.-Phys. Uwe Weber

PhD candidates

Subhasis Adhikari
Nicole Amecke
Marco Braun
Andreas Bregulla
André Heber
Lars Heerklotz
Selmke Markus
Nils Neubauer
David Plotzki
Martin Pumpa
Romy Schachoff
Rebecca Wagner

1.1.3 Molecular Physics, Molekülphysik [MOP]

Prof. Dr. F. Kremer

Secretary

Kerstin Lohse

Technical staff

Dipl.-Phys. Cordula Bärbel Krause
Dipl.-Ing. (FH) Jörg Reinmuth
Dipl.-Phys. Wiktor Skokow

Academic staff

Dr. Mahdy M. Elmahdy (till February 2013)
Dr. Christof Gutsche (till November 2013)
Dr. Ciprian Ghiorghita Iacob (till September 2013)

PhD candidates

Dipl.-Phys. Markus Anton
Wycliffe Kiprop Kipnusu, M. Sc.
Dipl.-Phys. Wilhelm Kossack
Emmanuel Urandu Mapesa, M. Sc.
Dipl.-Phys. Tim Stangner
Dipl.-Phys. Martin Treß
Dipl.-Phys. Olaf Ueberschär (till March 2013)
Dipl.-Phys. Carolin Wagner (till March 2013)

Students

Patrick Beer
Ludwig Popp
Lisa Schade
Benjamin Schott
Benjamin Suttner

1.1.4 Physics of Interfaces, Grenzflächenphysik [GFP]

PD. Dr. Frank Stallmach
Prof. Dr. Jörg Kärger (retired)
Prof. Dr. Dieter Freude (retired)

Technical staff

Lutz Moschkowitz
Stefan Schlayer

Academic staff

Dr. Christian Chmelik
Dr. Rustem Valiullin

PhD candidates

Dipl.-Phys. Steffen Beckert
Dipl.-Phys. Tomas Binder
Dipl.-Phys. Carsten Horch
Dipl.-Math. Daria Kondrashova
Alexander Lauerer, M.Sc.
Mgr. Mikulas Peksa
Dipl.-Phys. Anne-Kristin Pusch
Dipl.-Phys. Christian Reichenbach
Dipl.-Phys. Alexander Shakhov
Dipl.-Phys. Tobias Titze
Dipl.-Phys. Philipp Zeigermann

Students

Hiralal Gadaili
Sebastian Merker
Friederike Pielenz
Stefan-Johannes Reich
Michael Rippert
Tobias Splith

1.1.5 Soft Matter Physics, Physik der weichen Materie [PWM]

Prof. Dr. Josef A. Käs

Secretary

Claudia Brück

Technical staff

Dr. Undine Dietrich
Dipl.-Phys. Bernd Kohlstrunk
Ing. Elke Westphal

Academic staff

Dr. Claus Fütterer
Dr. Mareike Zink

PhD candidates

Silke Agte, M. Sc.
Uta Allenstein, M. Sc. (zusammen mit Prof. Mayr)
Dipl.-Phys. Anatol Fritsch
Dipl.-Phys. Tina Händler
Paul Heine, M. Sc.
Thomas Fuhs, M. Sc.
Martin Glaser, M. Sc.
Tom Golde, M. Sc.
Markus Gyger, M. Sc.
Dipl.-Phys. Chris Händel
Dipl.-Phys. Tobias Kießling
Dipl.-Math. Melanie Knorr
Hans Kubitschke, M. Sc.
Erik Morawetz, M. Sc.
Kenechukwu David Nnetu, M. Sc.
Dipl.-Phys. Steve Pawlizak
Saddam Moyazur Rahman, M. Sc. (BBZ, Forschergruppe M. Zink)
Susanne Rönicke, M. Sc.
Dipl.-Phys. Sebastian Schmidt
Dipl.-Phys. Jörg Schnauß
Dipl.-Phys. Carsten Schuldt
Dipl.-Ing. Roland Stange
Dipl.-Phys. Dan Strehle
Dipl.-Phys. Enrico Warmt
Dipl.-Phys. Franziska Wetzel
Emilia Wisotzki, M. Sc.
Dipl.-Phys. Lydia Woiterski

Students

Dave Ahrens
Hendrik Brehme
Tobias Eggebrecht
Sabrina Friebe
Nico Herbig
Michael Krahe
Tom Kunschmann
Tony Kurth
Erik Morawetz
Till Möhn
Peter Palm

Stefanie Puder
Florian Rämisch
Lydia Reuter
Stefanie Riedel
Erik Schmidt
Markus Sommerfeld
Tobias Thalheim
Astrid Weidt
Iris Wenzel
Benjamin Winkler

1.1.6 Biological Physics, Biologische Physik [BIP]

Prof. Dr. Claudia Mierke

Secretary

Kerstin Lohse

Technical staff

Dipl.-Ing. Kathrin Koch

Academic staff

PhD candidates

Stefanie Puder, M.Sc.
Dipl.-Phys. Tony Kurth
Kunschmann, M.Sc.

Students

Faranak Zamani
Stefanie Riedel
Tamara Heredia
Yadav Bashyal
Alexander Hayn
Jeremy Perez
Sebastian Haupt
Jacek Zlotowski
Mirko Kirchner

1.2 Institute for Experimental Physics II

1.2.1 Office of the Director

Prof. Dr. Marius Grundmann (director)
Prof. Dr. Pablo Esquinazi (vice director)

1.2.2 Magnetic Resonance of Complex Quantum Solids, Magnetische Resonanz Komplexer Quantenfestkörper [MQF]

Prof. Dr. Jürgen Haase

Secretary

Sophie Kirchner

Technical staff

Gert Klotzsche
Tilo Pilling

Academic staff

PD Dr. Marko Bertmer
Dr. Bettina Jee
Prof. Dr. Andreas Pöppl
Dr. Damian Rybicki

PhD candidates

Stefan Friedländer, M. Sc.
Nataliya Georgieva, M. Sc.
Farhana Gul-E-Noor, M. Sc.
Dipl.-Phys. Alexander Jäger
Michael Jurkutat, M. Sc.
Dipl.-Phys. Jonas Kohlrautz
Anusree V. Kuttatheyil, M. Sc.
Kathrin Lorenz, M. Sc.
Thomas Meier, M. Sc.
Dipl.-Phys. Thomas Meiner
Dipl.-Phys. Matthias Mendt
Steven Reichardt, M. Sc.
Dipl.-Phys. Sebastian Sambale
Emmanouil Veroutis, M. Sc.

Students

Robin Gühne
Tobias Herzig
Arafat Hossain Khan
Richard Lange
Mantas Simenas
Marufa Zahan

1.2.3 Nuclear Solid State Physics, Nukleare Festkörperphysik [NFP]

Prof. Dr. Jan Meijer

Technical staff

Dipl.-Phys. Steffen Jankuhn (since August 2013)
Carsten Pahnke
Dipl.-Ing. Joachim Starke

Academic staff

Dr. Sébastien Pezzagna (since May 2013)
Dr. Jürgen Vogt

PhD candidates

Dipl.-Phys. Tobias Andrea (till October 2013)
Nirav Barapatre, M.Sc. (till September 2013)
Ralf Wunderlich, M.Sc.

Students

Sascha Becker, B.Sc.
Dipl.-Math. Roger John (since October 2013)
Chenyang Lan, B.Sc.
Jan Lehnert, B.Sc. (since August 2013)
Tobias Lühmann, B.Sc. (since October 2013)
Michael Mensing, B.Sc.
Olga Naumov, B.Sc. (till September 2013)
Lukas Rogée (since October 2013)

1.2.4 Semiconductor Physics, Halbleiterphysik [HLP]

Prof. Dr. Marius Grundmann

Secretary

Anja Heck
Birgit Wendisch

Technical staff

Sascha Bader
Dipl.-Phys. Gabriele Benndorf
Monika Hahn
Dipl.-Ing. Holger Hochmuth
Dipl.-Phys. Jörg Lenzner
Dipl.-Phys. Axel Märcker
Gabriele Ramm
Roswitha Riedel

Academic staff

Dr. Christof Peter Dietrich
Dr. Helena Franke
Dr. Heiko Frenzel
Prof. Dr. Michael Lorenz
PD Dr. Rainer Pickenhain
Prof. Dr. Bernd Rheinländer (retired)
Dr. Rüdiger Schmidt-Grund
Dr. Chris Sturm
Dr. Holger von Wenckstern

PhD candidates

Henner Bieligk, M.Sc.
Dipl.-Phys. Tammo Böntgen
Michael Bonholzer, M.Sc.
Dipl.-Phys. Kerstin Brachwitz
Dipl.-Phys. Eike Lennart Fricke
Marcus Jenderka, M.Sc.
Robert Karsthof, M.Sc.
Sherzod Khujanov, M.Sc.
Tom Michalsky, M.Sc.
Dipl.-Phys. Fabian Klüpfel
Dipl.-Phys. Christian Kranert
Abdurashid Mavlonov, M.Sc.
Dipl.-Phys. Stefan Müller
Anna Reinhardt, M.Sc.
Steffen Richter, M.Sc.
Dipl.-Phys. Friedrich-Leonhard Schein
Peter Schlupp, M.Sc.
Dipl.-Phys. Florian Schmidt

Peter Schwinkendorf, M.Sc.
Alexander Shkurmanov, M.Sc.
Daniel Splith, M.Sc.
Dipl.-Phys. Marko Stölzel
Martin Thunert, M.Sc.
Haoming Wei, M.Sc.
Marcel Wille, M.Sc.
Zhang Zhipeng, M.Sc.

Students

Sofie Bitter
Christian Dähne
Raffael Deichsel
David Diering
Tobias Dörfler
Simon Englisch
Felix Gutt
Christian Heinrichs
Sören Herath
Oliver Herrfurth
Agnes Holtz
Max Kneiß
Oliver Kramer
Hannes Krauß
Silvia Kunz
Stefan Lange
Tobias Lühmann
Karim Nafis Imtias
Markus Purfürst
Katharina Rudisch
Michael Scheibe
Thorsten Schultz
Robert Staacke
Franz Vogt
Tobias Weiß
Anna Werner
Vitaly Zviagin

1.2.5 Solid State Optics and Acoustics, Festkörperoptik und -akustik [FKO]

Secretary

Annette Käthner

Technical staff

PTA Hans-Joachim vom Hofe
Dipl.-Ing. (FH) Ulrike Teschner

1.2.6 Superconductivity and Magnetism, Supraleitung und Magnetismus [SUM]

Prof. Dr. Pablo Esquinazi

Secretary

Mrs. Sandy Ehlers

Technical staff

Dr. Winfried Böhlmann
Dipl.-Krist. Annette Setzer

Academic staff

Dr. José Barzola-Quiquia
Dr. Yogesh Kumar
Dr. Israel Villalba-Lorite
Prof. Dr. Michael Ziese

PhD candidates

Ana Ballestar, M.Sc.
Francis Bern, M.Sc.
Santiago Muiños Landín, M.Sc.
Bogdan Sememenko, M.Sc.
Dandan Wang, M.Sc.
Chunhai Yin, M.Sc.

Students

Tom Schilling
Manuel Lindel
Johann Schmidt
Tiago Rafael Silva Cordeiro
Justus Krüger
Markus Stiller
Julia Tesch
Mahsa Zoraghi

1.3 Institute for Theoretical Physics

1.3.1 Office of the Director

Prof. Dr. Wolfhard Janke

Secretary

Susan Hussack
Gabriele Menge
Lea Voigt

1.3.2 Computational Quantum Field Theory, Computerorientierte Quantenfeldtheorie [CQT]

Prof. Dr. Wolfhard Janke

Technical staff

–

Academic staff

Dr. Stefan Schnabel
Dr. Jonathan Gross
Dr. Suman Majumder

PhD candidates

Dipl.-Phys. Mathias Aust
Dipl.-Phys. Rainer Bischof
Johannes Bock, M.Sc.
Dipl.-Phys. Niklas Fricke
Momchil Ivanov, M.Sc.
Dipl.-Phys. Martin Marenz
Dipl.-Phys. Marco Müller
Dipl.-Phys. Hannes Nagel
Dipl.-Phys. Andreas Nußbaumer
Dipl.-Phys. Jeremi Ochab (jointly with Jagiellonian University Krakow)
Philipp Schierz, M.Sc.
Dipl.-Phys. Sebastian Schöbl
Dipl.-Phys. Micha Wiedenmann
Johannes Zierenberg, M.Sc.

Students

Kieran Austin
Benjamin Schott

Christoph Vogelsberg
Henrik Christiansen
Karl Horn
Dorian Nothaaß
David Oberthür
Paul Spitzner
Andreas Wagner
Marius Bause
Hans Hepach
Jan Meischner
Tobias Weiss

1.3.3 Molecular Dynamics / Computer Simulation, Moleküldynamik / Computersimulation [MDC]

PD Dr. S. Fritzsche (Speaker)

Academic staff

PD Dr. S. Fritzsche

PhD candidates

P. Pilvar, M.Sc.
U. Arsawang, M.Sc.

Students

P. Schierz

1.3.4 Quantum Field Theory and Gravity, Quantenfeldtheorie und Gravitation [QFG]

Prof. Dr. Gerd Rudolph (Speaker)
Prof. Dr. Rainer Verch

Academic staff

PD Dr. Michael Bordag
Dr. Gandalf Lechner
Dr. José M. Muñoz-Castañeda
Dr. Matthias Schmidt

Retired

Prof. em. Bodo Geyer
Prof. em. Armin Uhlmann

PhD candidates

Andreas Andersson, M.Sc.
Zhirayr Avetisyan, M.Sc.
Dipl.-Phys. Benjamin Eltzner
Erik Fuchs, M.Sc.
Michael Gransee, M.Sc.
Dipl.-Phys. Thomas Ludwig
Dipl.-Phys. Jan Zschoche

Students

Richard Busch
Tobias Diez
Bärbel Hanle
Mathias Hänsel
Danny Krause
Adam Reichold
Johannes Zähle

1.3.5 Statistical Physics, Statistische Physik [STP]

Prof. Dr. Bernd Rosenow

Academic staff

Dr. Mats Horsdal
Dr. Daniel D. Scherer

PhD candidates

Dipl. Phys. Alexander Janot
Lukas Kimme, M.Sc.
Mirco Milletari, M.Sc.
Martin Treffkorn, M.Sc.
Dipl. Phys. Björn Zocher

Students

Christoph Lehmann
Enrico Lohman
Christian Scheidler

Johann Schmidt
Alexander Schneider
Alexander Uhlig
Heinrich-Gregor Zirnstein

1.3.6 Theory of Condensed Matter, Theorie der kondensierten Materie [TKM]

Prof. Dr. Ulrich Behn (Speaker)
Prof. Dr. Klaus Kroy

Prof. Dr. Dieter Ihle (retired)
Prof. Dr. Adolf Kühnel (retired)

PhD candidates

Dipl.-Phys. Jakob Bullerjahn
Gianmaria Falasco, M.Sc.
Dipl.-Phys. Andrea Kramer
Rüdiger Kürsten, M.Sc.
Dipl.-Phys. Marc Lämmel
Anne Meiwald, M.Ed.
Dmitrii Mishagli, M.Sc.
Dipl.-Phys. Holger Schmidtchen
Dipl.-Phys. Sebastian Sturm
Guillermo Zecua, M.Sc.

Students

Sven Auschra, B.Sc.
Mona Guthardt, B.Sc.
Michaela Kettner, B.Sc.
Richard Pfaller, B.Sc.
Nicolas Preuß, B.Sc.
Robert Schulz, M.A.
Andreas Hübner
Helena Stage, RISE intern (17.6.–6.9.2013)

1.3.7 Theory of Elementary Particles, Theorie der Elementarteilchen [TET]

Prof. Dr. Stefan Hollands (head) Prof. Dr. Klaus Siboldt (retired)

Academic staff

Dr. M. Dütsch
PD Dr. R. Kirschner

Dr. H. Perlt
Dr. J. Sanders
PD Dr. Arwed Schiller

PhD candidates

G. Collini
M. Talismitherani, M.Sc.

Students

Mr. T. Jerabek, B.Sc.

I

Institute for Experimental Physics I

2

Molecular Nano-Photonics

2.1 Introduction

The challenge of experimental physics on the nanoscale is to access local phenomena, that occur for example at interfaces, at specific molecular sites or at certain places within nano-structured materials. These local phenomena may control molecular dynamics, drive self-organization, cause charge separation or alter light propagation. Their importance extends to almost every field involved in future nanotechnology. The research of the molecular nano-photonics group thus aims at the development and application of optical techniques to access nanoscale (dynamical) processes in various fields such as chemical physics, biology or semiconductor physics. The understanding of these dynamical processes shall ultimately lead to a control over single molecules and other nano-objects by applying heat, flow, shear forces, electric fields or current.

The main experimental tool within our research is optical single molecule detection by ultra-sensitive microscopic techniques including time-resolved confocal microscopy, wide-field fluorescence or photothermal microscopy. Single molecules, semiconductor quantum dots or single metallic nanoparticles provide ideal local probes to access nanoscale physical properties inside materials while keeping the information on the heterogeneity of the system. Using these techniques recent projects focused on the

- Thermally propelled particles and micromachines
- Transmission Microscopy of Rayleigh- and Mie-Particles
- Heat conduction at the nanoscale
- Electrochemical manipulation of the emission of colloidal semiconductor nanocrystals
- Angle resolved spectroscopy of photonic crystals

During the year 2013 the Molecular Nanophotonics Group has celebrated a number of achievements. Among them are:

- Prof. Dr. Alois Würger has been a guest in the group and was awarded with Leibniz professorship at the university. Prof. Würger has worked during his stay

in Leipzig on the theory of self-propelled artificial microswimmers. The collaboration with Prof. Würger resulted in a joint project application at DFG and its french partner agency ANR, which has been accepted at the end of 2013.

- The group has actively taken part in the organization of two international conferences, the 5th International Conference "Diffusion Fundamentals" at the Universität Leipzig from the 26th to 29th of August and the second symposium on "Hot Nanostructures" from 21st - 25th October at the Lorentz Center at the University of Leiden.
- Several group members have been awarded with poster prizes at international conferences and published research in high impact factor peer-reviewed journals.

Collaborations with the group of Prof. Dr. Klaus Kroy (Universität Leipzig), Prof. Dr. Michael Mertig (TU Dresden) and Prof. Dr. Haw Yang (Princeton University) have been very fruitful. Collaborative measurements with the groups of Prof. Dr. Friedrich Kremer and Prof. Dr. Marius Grundmann have been carried out.

Frank Cichos

2.2 Stochastic Localization by Photon Nudging

A. Bregulla, F. Cichos

Temperature gradients along the surface of micro- and nanoparticles in solution cause an interfacial liquid flow, which leads to a phoretic motion of particles. Such temperature gradients can either be created externally by heat sources or by the particle itself. The latter case has been explored in this project by coating polystyrene particles partly with a thin gold layer (so called Janus particles). This thin gold layer can be heated optically via its plasmon resonance. It has been shown in previous experiments by the group, that this temperature gradient leads to a self-propelled motion of the particles with a velocity of several micrometers per second. The particle moves with the uncoated side forward but its motion is randomized by rotational diffusion. In collaboration with the group of Prof. Haw Yang at the Princeton University, we have demonstrated that a simple optical feedback mechanism can be applied to exploit the rotational diffusion to trap or steer the particles in solution without optical gradient forces. This feedback mechanism is termed photon nudging and analyzes the orientation and position of a Janus particle in real time. If the particle direction is pointing towards a target, a laser is switched on to drive the self-propelled motion towards the target. Thus the rotational diffusion is used to stochastically drive the particle at the right times. Thereby, trapping and steering have been achieved (see Figure 2.1). The localization accuracy achieved is about the particle diameter and scales with the particle radius. Thus it shall be possible to achieve even better localization accuracies for smaller particles. This is a considerable advantage as compared to optical tweezers, since they require extremely high trapping intensities for small particles. This method is extendable to multiple particles which can be steered simultaneously on individual trajectories. In summary, this switchable self-propelled motion of Janus particles delivers new ways to control particle motion by feedback mechanisms. Thus new studies of the interaction and dynamics of swarming particles will become possible.

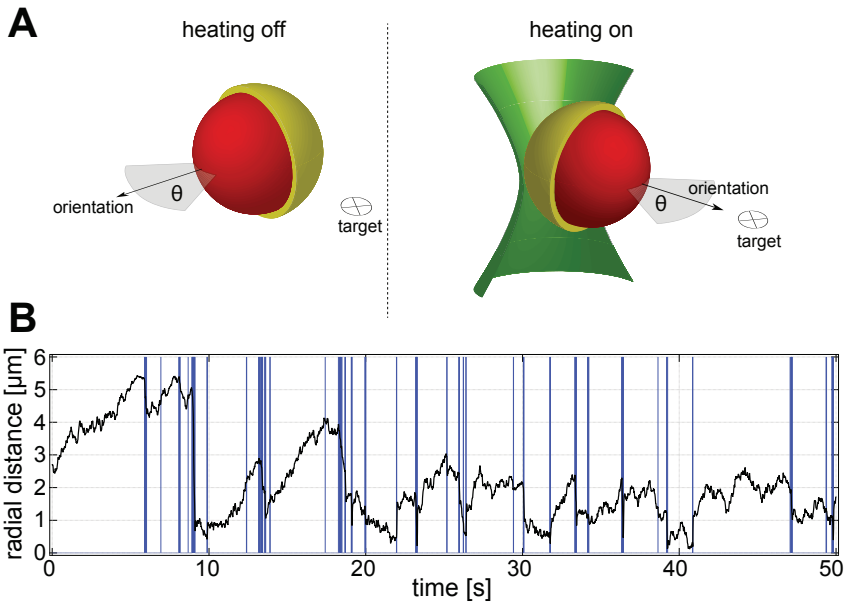

Figure 2.1: *a)* Principle of the Janus particle steering. The particle position and orientation is analyzed in real time. If the particle orientation points towards the target, the gold cap of the particle is heated to cause a directed motion. *b)* (left) Representative experimental time trace showing the stochastic heating periods (blue bars) and the distance from the target (black line) for a Janus particle with a radius of R=0.625 μm.

2.3 Thermophoretic Trapping of Single Nano-Objects

M. Braun, F. Cichos

The manipulation and trapping of nano-objects that undergo Brownian motion are of increasing interest in soft-matter sciences. Optical tweezing is the most common technique for the trapping of individual particles in solution and is based on the optical gradient force. Hence, a sufficiently high polarizability of the particle in the solution is required. While it is thus easy to trap single dielectric particles larger than 100 nm, a trapping of smaller objects such as single molecules by means of optical forces can hardly be realized. Molecular trapping can be achieved e.g. by a technique called Anti-Brownian Electrokinetic trap (ABEL trap), which exploits the feedback controlled electric field of four electrodes. However, the latter technique requires electrical contacts, which introduce difficulties when fabricating multiple traps. In this project we have develop an all-optical technique which replaces the electric fields by highly localized thermal fields. The so-called thermophoretic trap exploits thermophoretic interactions of a particle placed in a temperature gradient in solution, which locally distorts the screening of the surface charges and by that induces a particle drift. In our approach, the temperature field is generated by an optically heated gold nanostructure. Due to the small dimensions of the heat sources, even a small temperature increase introduces large temperature gradients causing a strong thermophoretic drift through which the motion of a diffusing particle can be manipulated.
To realize this trap, a circular hole in a gold film ($\sim$ 8 nm in diameter and 50 nm in height) is manufactured by microsphere lithography, where gold is thermally evaporated onto a monolayer of polystyrene microspheres, which are later removed by sonification.

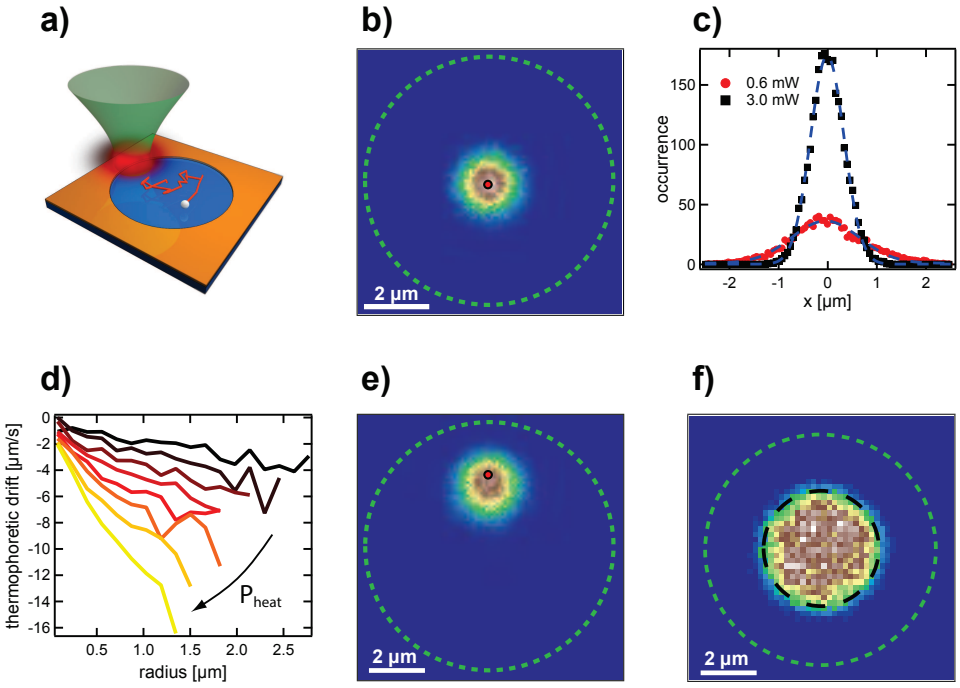

Figure 2.2: *a)* Sketch of the focussed heating beam, only a local spot of the gold structure is heated at a time. *b)* Positional distribution histogram of a 200 nm PS sphere thermally trapped within a gold structure. *c)* Positional distribution line profile for two heating beam intensities. *d)* Radial thermophoretic drift velocity for increasing heating beam power. *e)* Trapping of a 200 nm PS sphere at an arbitrary point within the trapping region. *f)* Trapping of a 200 nm PS sphere within a circular region (2D-box potential).

Colloidal nano-particles, which are carrying our 2-dimensional Brownian motion are then confined between a cover slide carrying the gold array and a blank cover slide. By means of a resonant focussed laser beam the circumference of the gold structure is heated, resulting in a strongly localized temperature field and steep temperature gradients. By tracking the colloidal particles position in real-time, a temperature field can be generated at an appropriate position to drive the particle in a particular direction by thermophoretic interaction (see Fig. 2.2a). Doing so enables a restriction of the Brownian motion of a particle to a small trapping region as shown in Fig. 2.2b. The temperature gradient induces a thermophoretic drift of the particle in radial direction, see Fig. 2.2d, which increases with increasing heating power. Hence, the strength of the confinement can be adjusted by the heating beam intensity (Fig. 2.2c). By an active feed-back, the particle can be steered within the sample region (Fig. 2.2e) or the trapping potential can be shaped in an arbitrary way, e.g. a 2D-box potential (Fig. 2.2f).
This new all-optical technique for the manipulation of nano-objects enables long-time observations of not only single but also multiple nano-objects without applying strong optical or electric fields.

2.4 Transmission Microscopy of Rayleigh/Mie-Particles

M. Selmke, I. Neugebauer, F. Cichos

Transmission microscopy [1] represents a sensitive method to detect [2] and characterize single nano-particles. A laser beam which is focused onto a particle induces a scattered field which interferes with the beam field in its propagation direction. The far-field detected transmission under this seemingly simple situation of interference exhibits a rich phenomenology. We have studied these energy-redistribution and absorption characteristics for Rayleigh- as well as for arbitrarily sized Mie-scatterers [3].

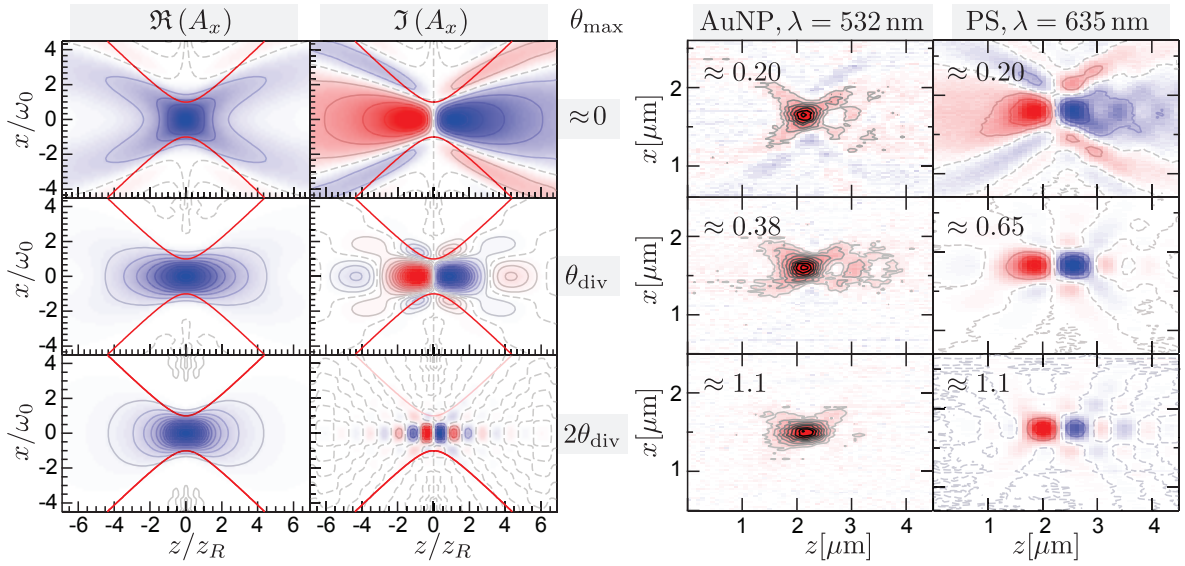

Figure 2.3: *Left plot-group)* Theoretical relative transmission signals $\Delta P_d/P_d$ (red: negative, blue: positive). $\Re(A_x)$ determines absorptive signals, $\Im(A_x)$ determines pure interference signals. *Right plot-group)* Measured transmission for a $R = 30\,\mathrm{nm}$ gold nanoparticle using a resonant $\lambda = 532\,\mathrm{nm}$ laser (right column) and a $R = 100\,\mathrm{nm}$ PS sphere using $\lambda = 635\,\mathrm{nm}$, both in PDMS. The imaging system consists of an afocal system comprised of a $\mathrm{NA}_{\mathrm{ill}} = 1.4$ and a $\mathrm{NA}_d = 1.3$ oil immersion objective for focusing and detection, respectively. The collection domain was varied using a variable iris aperture before the recording photodiode.

Starting with the generalized Lorenz-Mie theory for vectorial scattering by spherical particles, we were able to explicitly relate the particle's complex-valued polarizability α to the relative change in the transmitted power, $\Delta P_d/P_d$, for focused Gaussian beams. The signal has two contributions, one of which is related to the real part of the polarisability, and another one which is related to the imaginary part and therefore associated with absorption. These universal features sensitively depend on the particles position relative to the focus and the fraction of the light which is collected, i.e. the ratio of the collection angle to the illuminating beam's angle of divergence, $\theta_{\max}/\theta_{\mathrm{div}}$. Figure 2.3 shows a comparison of the predicted patterns $\Delta P_d(x,z) \propto \Im(\alpha)\,\Re(A_x) + \Re(\alpha)\,\Im(A_x)$ along with experimental scans of gold and polystyrene particles, representative of particles whose polarizability is primarily imaginary- or real-valued at the chosen wavelengths. The coordinates correspond to particle displacements along and perpendicular to the optical axis. An interactive tool which visualizes such scans for arbitrary Rayleigh particles can be found on the group's homepage.
Not only the patterns, but also their amplitudes depend on the collection angle. While absorption measurements require a large collection angle, the maximum relative transmission change for dielectric particles occurs at low collection angles and vanishes for

angles exceeding $2\theta_{\mathrm{div}}$. Understanding the characteristics of energy redistribution and absorption is thus useful for signal optimization as well as for quantitative particle and beam characterization.

[1] J. Hwang, W. E. Moerner: *Interferometry of a single nanoparticle using the Gouy phase of a focused laser beam*, Opt. Commun. 280(2): 487-491 (2007).
[2] S. Wennmalm, J. Widengren: *Interferometry and Fluorescence Detection for Simultaneous Analysis of Labeled and Unlabeled Nanoparticles in Solution*, J. Am. Chem. Soc., 134(48):19516-19519 (2012).
[3] M. Selmke, F. Cichos: *Energy Redistribution Signatures in Transmission Microscopy of Rayleigh- and Mie-particles*, arXiv:1404.0567 (2014).

2.5 Heat conduction on the nanoscale

A. Heber, M. Selmke, F. Cichos

The general principle behind the measurements of thermal diffusivities κ is to heat an area and measure how the temperature around that area evolves. In most schemes physical contact to the sample is required. We have realised a contact free measurement of thermal diffusivity measurements using photothermal microscopy. Photothermal

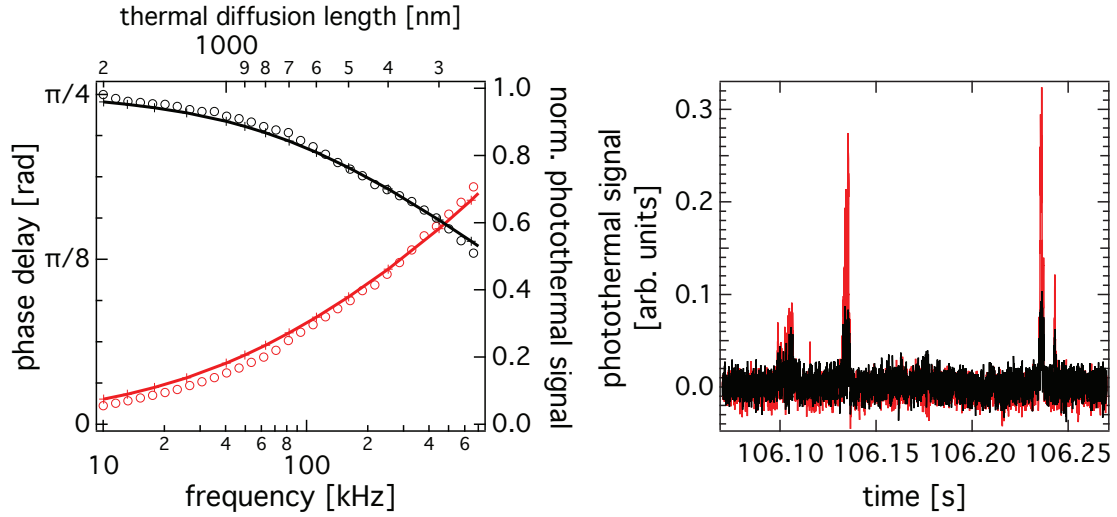

Figure 2.4: *a)* Modulation amplitude (black) and phase delay (red) are plotted against the frequency. Experimental (circles) and numerical data (solid lines) agree very well in their dependence on frequency. The comparison gives a thermal diffusivity of $(1.3 \pm 0.1) \cdot 10^{-7}\,\mathrm{ms}^{-2}$. *b)* The nano-particles are diffusing freely. Whenever a nano-particle passes the laser foci signal burst are recorded with an in phase and out-of-phase response.

microscopy is a technique that images nano-objects and molecules absorbing light and relaxing non-radiatively. Therefore the temperature of the nanoparticle is increased and a temperature around the particle is established. Due to thermal expansion the refractive index is lower in proportionality to the temperature increase. The changes of the optical properties are detected by a second laser beam. A heterodyne detection

scheme is used to make these small changes of the optical properties visible. Due to the lock-in detection scheme the heating laser is modulated which results in the emission of thermal waves. Thermal waves are critically damped oscillations that are characterised by the thermal diffusion length $R_{\mathrm{th}} = \sqrt{\kappa/\pi f}$.

If the heating laser is modulated at frequencies of more than $f = 100\,\mathrm{kHz}$ the signal of the detection laser gets delayed with respect to the heating laser. In particular it is observed in the experiments that the modulation amplitude of the detection signal decreases and phase delay increases as the modulation frequency is increased. The thermal diffusivity is determined from the comparison of numerical scattering calculations and experiments. The values determined by photothermal microscopy agree very well with laser flash measurements if the features of the laser beam are modeled in detail. It was also shown that photothermal microscopy is able to measure thermal diffusivities in liquids. Here the nanoparticles diffuse freely and pass the laser foci only from time to time. These events are recorded as signal bursts. These bursts also have a well defines phase. From a large number of events histograms are created to determine the phase of the signal bursts. Comparing experimentally determined phase and calculation also gives the thermal diffusivity.

2.6 Electrochemical Manipulation of CdSe/ZnS Quantum Dots

N. Amecke, D. Plotzki, F. Cichos

CdSe/ZnS semiconductor quantum dots (QDs) are very efficient, photostable, wavelength-tunable sources of light in the visible range. They show interrupted emission (blinking) with spectral diffusion and fluctuating lifetime. Those interruptions and shifts are generally assumed to originate from charge tunneling in and out of the QD core or simply residing and diffusing in its close vicinity. They can lead to non-radiative exciton decay channels (e.g. Auger processes or trap assisted decay) and transition energy shifts (Stark effect). However, which charge - electron or hole - is more likely to be ejected and if this is really what intermittently quenches the fluorescence, still needs to be determined.The reversible luminescence decrease of QD ensembles under illumination stresses the importance of excited carriers in the blinking process. This research project is devoted to the study of CdSe/ZnS QDs with externally injected and extracted charges. For this purpose we have constructed an electrochemical cell with a transparent thin electrode, which consists of an ITO coated glass cover slip with a 20 nm ZnO spacer deposited in the HLP group. Ensemble or single QD concentrations where spin coated on the electrode to be investigated with a confocal microscope while its potential is varied. We find high luminescence only at a preferred potential region just below the conduction band (CB) edge, see Fig. 2.5 a). At more negative potentials, electrons are injected in the CB and the fluorescence is quenched due to Auger processes. Electron extraction from the valence band (VB) is not observed. Instead decreasing mid-gap potentials quench luminescence. Electron injection into the CB proceeds equally well in the dark, as shown in 2.5 b). Mid-gap potentials only quench luminescence under excitation, see 2.5 c). This strongly supports the presence of accessible electron trap states within the band gap. When the electron is trapped, residing holes can either

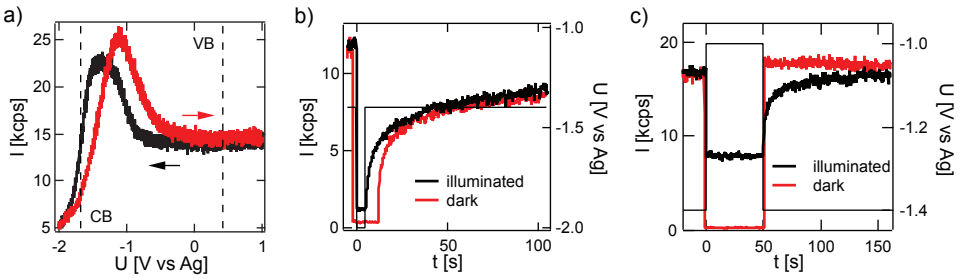

Figure 2.5: a) Intensity vs. voltage of a QD-film on a ZnO/ITO electrode detected in a triangular voltage scan at scan rate 10 mV/s. Arrows indicate scan direction. Expected QD-conduction (CB) and valence band (VB) are indicated. b) Excitation dependence of electron injection into the conduction band. c) Excitation dependence of quenching at mid-gap potentials. Excitation is blocked where the intensity falls below 1 kcps.

lead to Auger quenching themselves or induce non-radiative recombination centers at the interface or surface. Excitation induced QD quenching is also observed in blinking statistics. We thus find strong evidence for a connection of blinking with electron tunneling to trap states.

2.7 Fast Detection of Photonic Stop Bands by Back Focal Plane Imaging

R. Wagner, F. Cichos

Photonic Crystals (PCs) consist of dielectric particles with a size in the range of the wavelength of visible light. These particles are arranged in a crystal lattice. The periodic variation of the dielectric constant leads to the formation of a photonic band structure that can also contain stop bands. The stop bands inhibit the propagation of light with a certain wavelength for some directions in the PC. The dependence of the stop band position on wavelength and direction can for instance be probed by angle dependent fluorescence spectroscopy. Typically, this requires a movement of the detector for every measurement, which is time consuming. Another challenge is to ensure, that light from the same sample volume is probed for every direction.

We developed a method that detects the fluorescence intensity at a fixed wavelength for many directions in a single measurement (Fig. 2.6).[1] The fluorescence from the sample is collected by a microscope objective lens. All light that was emitted into the same direction is focused into one point in the objective's back focal plane (BFP). Every point in the BFP therefore corresponds to a certain emission direction. The distance r of this point from the optical axis is related to the emission angle ϑ_0 by the Abbe sine condition

$$\sin(\vartheta_0) = \frac{r\mathrm{NA}}{r_{\max} n_0},$$

where NA is the numerical aperture of the objective, $r_{\max}$ the maximum radius of the BFP and n_0 the effective refractive index of the PC. The BFP is imaged onto a camera

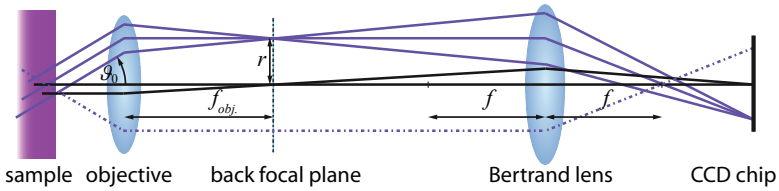

Figure 2.6: Scheme of the back focal plane imaging setup. Light emitted into one direction is focused into one spot in the BFP of the objective lens. The BFP is imaged to a camera using the Bertrand lens. Fig. taken from [1].

chip, where the intensity emitted into the different directions can be observed. Bandpass filters are applied to achieve spectral resolution.

This method was applied to PCs created by self-assembly of polystyrene beads with diameters between 260 nm and 498 nm. They form a close packed fcc lattice. The fluorescence of the polystyrene beads was excited locally by a focused laser. Using different combinations of bead diameters d and bandpass transmission wavelength λ, BFP images can be recorded for various reduced frequencies $\tilde{F} = \sqrt{2}d/\lambda$. Fig. 2.7 shows some examples of the observed patterns. The stop bands are visible as dark rings and ring sections, since less light is emitted into the corresponding directions. Obviously the radius of these rings grows with increasing frequency as expected from theory.

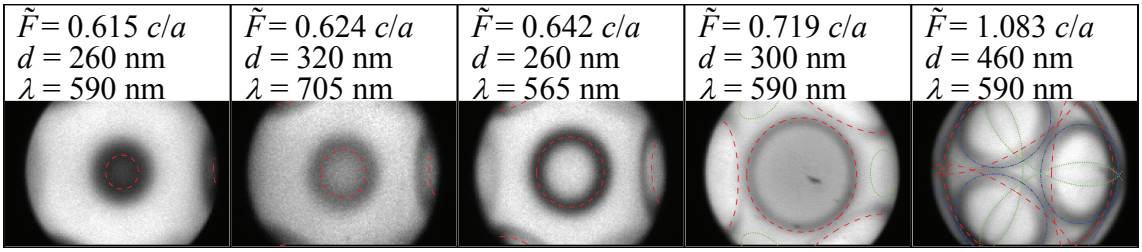

Figure 2.7: BFP images for different frequencies $\tilde{F}$ measured on PCs with bead diameter d. Various bandpass filters, transmitting at wavelength λ, are used. Stop bands appear as dark rings or ring sections. The lines indicate their theoretical positions. The different lattice plane families causing the stop bands are represented by different colors (red: {111}, green: {200}, blue: {220}).

[1] R. Wagner, and F. Cichos, *Phys. Rev. B*, 87, 165438,(2013)

2.8 Heterogeneous Single Molecule Dynamics in Polymers near T_g

S. Adhikari, F. Cichos

The dynamics in polymers close to the glass transition temperature (T_g) becomes drastically slow and deviates from homogeneous liquid behavior such as non-Arrhenius temperature dependence and non-exponential relaxation. Recently, single molecule experiments in polymers have shown that the dynamics of a single probe molecule is

both spatially and temporally heterogeneous. The understanding of heterogeneous dynamics in polymers is expected to provide detailed insight into the glass transition phenomenon. The heterogeneous dynamics in the polymers poly (methyl acrylate)

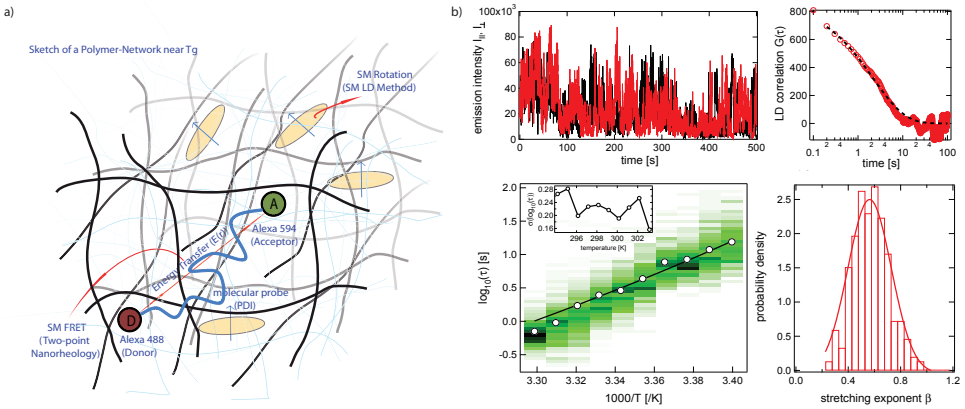

Figure 2.8: a) A sketch of polymer near T_g is shown. SM linear dichroism (LD) and SM-FRET methods are used to study heterogeneous dynamics in polymers. b) SM results from rotational studies in PMA using LD method are shown. (top left) The intensities in two polarization channels (black and red lines) fluctuate due to the rotational diffusion of the transition dipole of a single molecule. (top right) The autocorrelation of the linear dichroism calculated from intensity traces shown in the left is well fitted by a stretched exponential. (bottom left) The rotational times are log-normally distributed and mean rotational times closely follow the temperature dependence predicted by the Debye-Stokes-Einstein (DSE) relation using the polymer's bulk viscosity. (bottom right) A Gaussian distribution of stretching exponents are shown at temperature of 301 K.

(PMA) and poly (vinyl acetate) (PVAc) have been studied close to their glass transition temperatures (Tg) using single molecule (SM) techniques. The SM linear dichroism (LD) method has been applied to study diffusive rotational dynamics of single perylene-dimide (PDI) dye molecules over an extended temperature range of 10K. The autocorrelation function of the fluctuating LD of a single PDI molecule is found to be described well by a stretched exponential relaxation. Rotational times (τ) and stretching exponents (β) are broadly distributed at each temperature. The stretched exponential LD autocorrelation decay implies that the dynamics of a single PDI molecule is temporally heterogeneous. All SM results are discussed using a simple model of dynamical heterogeneity based on a Gaussian distribution of activation energies. SM results are compared to the results from dielectric experiments and viscosity data. The mean rotational times follow the Debye-Stokes-Einstein (DSE) relation using the bulk polymer viscosity but decouple from segmental motions. Further information on the heterogeneous dynamics is expected from an extension of two-point nanorheology to single molecule optical studies based on fluorescence resonance energy transfer (FRET). We have therefore synthesized a dual dye-labeled (Alexa 488 and Alexa 594) polystyrene polymer. A very high energy transfer efficiency (0.7) is observed in solution.

2.9 Funding

Light Emission of Single Emitters in 3-dimensional Photonic Crystals
Frank Cichos
CI 33/5-2

FG 877: Constrained Single Molecule Dynamics in Glassy Polymer Systems
Frank Cichos
CI 33/7-1

FG 877: Hot Brownian Motion
Frank Cichos
CI 33/7-2

FG 877: Static and dynamic properties of DNA-based polymer structures under constraints and confinement
Frank Cichos
CI 33/11-2

FG 877: From Local Constraints to Macroscopic Transport
Frank Cichos
CI 33/12 -1

BuildMoNa, ESF-NFG: Funktionale multiskalige Strukturen

BuildMoNa, ESF-NFG: Effiziente Energienutzung: Neue Konzepte und Materialien

SFB TRR102, Interaction of Single Polymer Chains in a Thermophoretic Trap

DFG-ANR, Thermoelektrische Effekte auf der Nanometerskala
Frank Cichos, Alois Würger
CI 33/14-1

2.10 Organizational Duties

Frank Cichos

- Speaker of the DFG Research Unit 877 "From Local Constrainst to Macroscopic Transport"
- Head of the Eignungsfeststellungskommission Fakultät für Physik und Geowissenschaften
- Vice head Promotionsausschuss
- Member of the Prüfungsausschuss
- Referee: Phys. Rev. B, Phys. Rev. Lett., Nature, Chem. Phys. Lett., Appl. Phys. Lett., ACS Petroleum Research Fund; Medical Research Council

2.11 External Cooperations

Academic

- TU Dresden
  Prof. Dr. Michael Mertig
- Unviversité Bordeaux
  Prof. Alois Würger
- TU Dresden
  Dr. Ralf Seidel
- TU Chemnitz
  Prof. Dr. Christian von Borczyskowski
- TU Chemnitz
  Dr. Harald Graaf
- Universität Mainz
  Prof. Dr. T. Basché
- Princeton University
  Prof. Dr. H. Yang
- MPI Kohleforschung Mühlheim
  Dr. Frank Marlow

2.12 Publications

Journals

M. Selmke, F. Cichos, *Photothermal Single Particle Rutherford Scattering Microscopy* Phys. Rev. Lett. 101, (2013) 103901.

M. Selmke, M. Braun, R. Schachoff, F. Cichos, *Photothermal Signal Distribution Analysis*, Phys. Chem. Chem. Phys. 15, (2013) 4250-4257.

M. Selmke, F. Cichos, *Photonic Rutherford Scattering: A Classical and Quantum mechanical analogy in Ray- and Wave-optics* Am. J. Phys. 81 (6), (2013) 405-413.

M. Braun, F. Cichos *Optically Controlled Thermophoretic Trapping of Single Nano-Objects*, ACS Nano 7 (12), (2013) 11200-11208.

M. Selmke, M. Braun, F. Cichos *Harnessing Thermal Fluctuations for Purposeful Activities: The Manipulation of Single Micro-swimmers by Adaptive Photon Nudging*, Chem. Sci. 4, (2013) 1420-1429.

R. Wagner, F. Cichos, *Fast Measurement of Photonic Stop Bands by Back Focal Plane Imaging*, Phys. Rev. B 87, (2013) 165438.

A. Heber, M. Selmke, F. Cichos, *Metal Nanoparticle Based All-Optical Photothermal Light Modulator*, ACS Nano 8 (2), (2014) 1893-1898.

Talks

M. Braun, F. Cichos: Thermophoretic trapping of single nano-objects, Annual Build-MoNa Conference, Leipzig, 04.-05. March 2013

M. Braun, F. Cichos: Thermophoretic trapping of single nano-objects, Second Retreat of the SFB/TRR 102, Bad Blankenburg, 06.-08. March 2013

A. Heber, F. Cichos: Photothermal control of light propagation, 78. DPG Spring Meeting, Regensburg, 10.-15. March 2013

A. Bregulla, F. Photon nudging of self propelled Janus Particles, 78. DPG Spring Meeting, Regensburg, 10.-15. March 2013

A. Bregulla, H. Yang, F. Cichos: Photon nudging of self propelled Janus Particles, OSA conference, Hawaii, 21.-25. April 2013

M. Selmke, I. Neugebauer, F. Cichos: Single particle interferometry in the generalized Lorenz-Mie framework, 78. DPG Spring Meeting, Berlin, 17.-21. March 2014

F. Cichos, A. Bregulla, H. Yang: Thermophoretic Trapping and Steering of Janus-type Particles, Ringberg Meeting on Active Particles and Microswimmers, Schloss Ringberg, 8.-11.7.2013

F. Cichos, A. Bregulla, M. Braun, H. Yang: Keynote Lecture: Trapping and Steering of Single Colloids with Plasmonic Nanostructures, International Soft Matter Conference 2013, Rom, 17.9.2013

Posters

A. Heber, M. Selmke, M. Braun, F. Cichos: Photothermal Microscopy in Liquid Crystals, 78. DPG Spring Meeting, Regensburg, 10.-15. March 2013

A. Bregulla, H. Yang, F. Cichos: Photon nudging of self propelled Janus Particles, OSA conference, Hawaii, 21.-25. April 2013

A. Bregulla, H. Yang, F. Cichos: Photon nudging of self propelled Janus Particles, Hot Nanostructures, Leiden, 21.-25. October 2013

M. Braun, F. Cichos: Gold nanostructure assisted thermophoretic trapping of single nano-objects, Diffusion Fundamentals V, Leipzig, 26.-28. August 2013

A. Heber, M. Selmke, F. Cichos: Thermal diffusivity measurements with a single nanoparticle, Diffusion Fundamentals V, Leipzig, 26.-28. August 2013

A. Heber, M. Selmke, F. Cichos: Thermal Diffusivity Measurements with a Single Nanoparticle, Hot Nanostructures, Leiden, 21.-25. October 2013

M. Braun, F. Cichos: Gold nanostructure assisted thermophoretic trapping of single nano-objects, Hot Nanostructures, Leiden, 21.-25. October 2013

A. Bregulla, H. Yang, F. Cichos: Photon nudging of self propelled Janus Particles, Hot Nanostructures, Leiden, 21.-25. October 2013

Irene Neugebauer, M. Selmke, F. Cichos: Nanoparticle Characterization by Laser Transmission Microscopy, 78. DPG Spring Meeting, Berlin, 17.-21. March 2014

2.13 Graduations

Master

- Alice Abend
  Thermophoretic Trapping
  March 2014
- Thomas Heyn
  Dynamics of Particles under a controlled Thermal Gradiets
  Januar 2013
- André Heber
  Photothermal Microscopy in Liquid Crystals. The Photothermal Transistor
  Januar 2013

2.14 Guests

- Alois Würger as Leibniz Professor at the Universität Leipzig
  Laboratoire Ondes et Matiiére d'Aquitaine, Université Bordeaux, Bordeaux, France
  Summer 2014
- Eli Barkai, Bar-Ilan University, Israel, August 2013
- Clemens Bechinger, Universität Stuttgart, August 2013
- Paul Chaikin, New York University, USA, August 2013
- Debashish Chowdhury, Indian Institute of Technology, India, August 2013
- Cees Dekker, Delft University of Technology, August 2013
- Ernst-Ludwig Florin, University of Texas at Austin, USA, August 2013
- Matthias Fuchs, Universität Konstanz, August 2013
- Steve Granick, University of Illinois at Urbana-Champaign, USA, August 2013
- Paul Heitjans, Universität Hannover, August 2013
- Werner Köhler, Universität Bayreuth, August 2013
- Ingolf Kühn, Helmholtz Centre for Environmental Research, Halle, August 2013
- Akihiro Kusumi, Kyoto University, Japan, August 2013
- Peter Reimann, Universität Bielefeld, August 2013
- Masaki Sano, The University of Tokyo, Japan, August 2013
- Erik Schäffer, Universität Tübingen, August 2013

- Gerhard Schmid, Universität Augsburg, August 2013
- Thomas Schmidt, Leiden University, The Netherlands, August 2013
- Nicholaas Stolwijk, Universität Münster, August 2013
- Matthew Turner, University of Warwick, UK, August 2013
- Ilpo Vattulainen, Tampere University of Technology, Finland, August 2013

3

Molecular Physics

3.1 Introduction

Science has a sportive component as well. One may for instance raise the question: is it possible to measure the molecular dynamics of isolated condensed polymer chains? The answer is yes. By employing nanostructured electrode arrangements - developed in collaboration with Dr. M. Reiche from the Max-Planck-Institute for Microstructure Physics in Halle - combined with Broadband Dielectric Spectroscopy (BDS), M. Tress et al. (M. Tress et al., Science 2013) manage to prove that even nanodroplets, so small that they contain on average just a single polymer chain, show a molecular dynamics which is well comparable to that of the bulk liquid. This fits with the findings from a multitude of experiments which were carried out on nanometric thin polymer layers in recent years. Additionally, combined studies of intra- and intermolecular dynamics in the course of the dynamic glass transition turned out to be very fruitful; detailed molecular understanding far beyond the existing coarse-grained descriptions was realized. The optical tweezers' activities are currently focused on dynamic force spectroscopy of single receptor ligand binding events. This has delivered detailed insights for the example a synthetic tau-peptide and phosphorylation-specific monoclonal antibodies.

Friedrich Kremer

3.2 Glassy dynamics of condensed isolated polymer coils

M. Treß, E.U. Mapesa, W. Kossack, W.K. Kipnusu, M. Reiche*, F. Kremer

*Max-Planck-Institute for Microstructures, Weinberg 2, 06120 Halle (Saale)

The glassy dynamics of condensed isolated poly(2-vinylpyridine) (P2VP) polymer chains is studied by means of Broadband Dielectric Spectroscopy (BDS).[1] For this purpose, a recently developed nano-structured electrode arrangement is refined to achieve an electrode-to-electrode distance of only 35 nm (Sec. 3.3). The polymer coils are deposited on highly conductive silicon electrodes, a subsequent annealing removed the solvent. Atomic Force Microscopy (AFM) scans of the identical samples reveal that the mean volume of the coils resembles that calculated for a single chain. ~ 30 % of the

segments directly contact the substrate (Fig. 3.1) which are hence expected to exhibit traces of interfacial interaction.

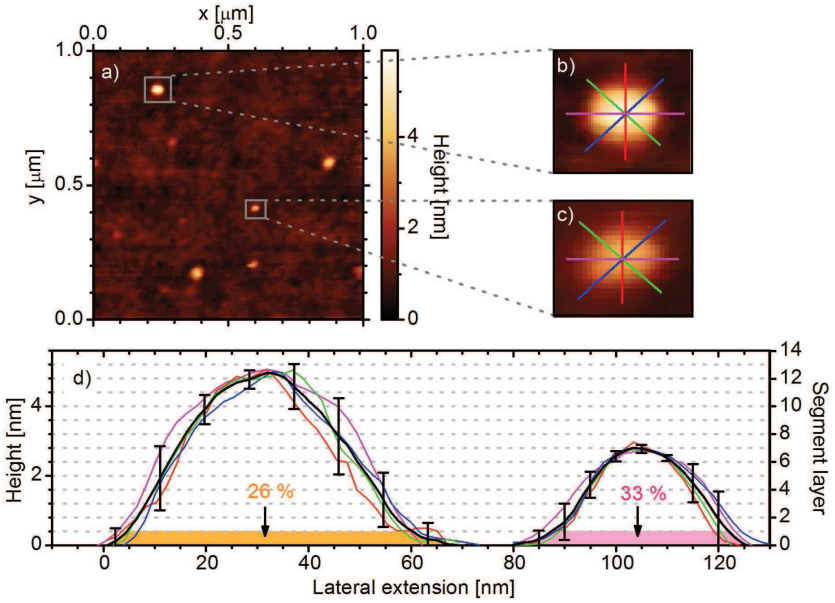

Figure 3.1: a) AFM image of isolated P2VP chains in a condensed coil conformation on silica. b) and c) show enlargements of two of these coils with colored lines indicating the traces of the height profiles taken for further analysis. d) depicts these profiles (in the same color as the respective line in b and c) along with the mean (black line) and the volume fraction of the segments which are in direct contact with the substrate (orange and pink area).

The BDS measurements show, that even isolated condensed polymer chains exhibit glassy dynamics. Further, the mean relaxation time corresponds to the bulk (Fig. 3.2). This demonstrates that glassy dynamics relies on fluctuations of 2-3 segments[2], a unit much smaller than the coil (which is in accord with results from thin layers[3–5]). An extensive analysis of the relaxation time distribution reveals a broadening at lower frequencies: 12 % of the mobile segments are slower than in bulk. The mismatch by a factor of ~ 2 with the fraction of segments directly contacting the interface is due to the fact that only half of the latter establish bonds with the substrate surface (Sec. 3.10).

[1] M. Tress, E.U. Mapesa, W. Kossack, W.K. Kipnusu, M. Reiche and F. Kremer, Science 341 1371 (2013)
[2] I. Bahar, B. Erman, F. Kremer and E. Fischer, Macromol 25 816 (1992)
[3] E.U. Mapesa, M. Tress, G. Schulz, H. Huth, C. Schick, M. Reiche and F. Kremer, Soft Matter 9 10592 (2013)
[4] W.K. Kipnusu, M.M. Elmahdy, M. Tress, M. Fuchs, E.U. Mapesa, D.-M. Smilgies, J. Zhang, C. Papadakis and F. Kremer, Macromol 46 9729 (2013)
[5] F. Kremer, E.U. Mapesa, M. Tress and M. Reiche, in Recent Advances in Broadband Dielectric Spectroscopy, Springer Netherlands 163-178 (2013)

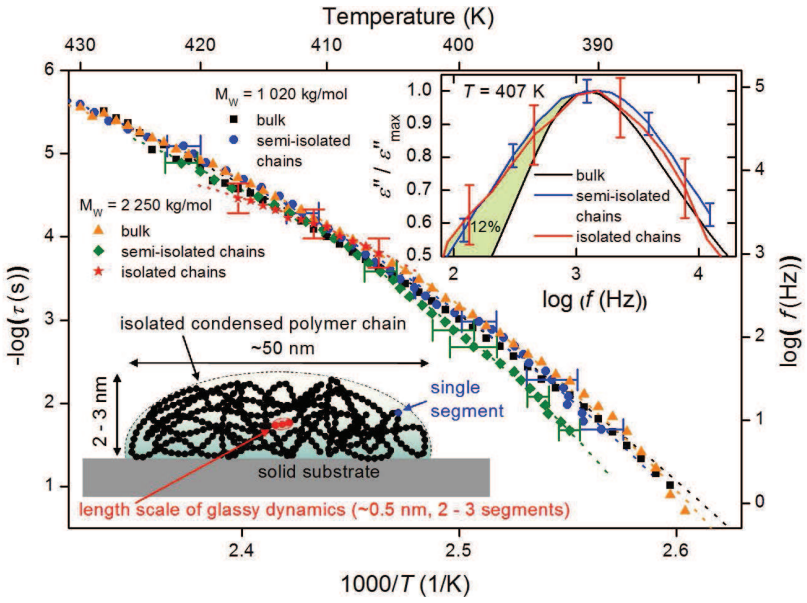

Figure 3.2: Mean relaxation time of segmental motion *vs.* inverse temperature for P2VP bulk, semi-isolated and isolated condensed polymer chains of different molecular weight as indicated. Inset: loss spectra corrected for artificial contributions (conductivity and wafer resistance) and normalized with respect to the peak maximum. Scheme: comparing dimensions of a single polymer chain and intrinsic length scale of glassy dynamics.

3.3 Nano-structured electrode arrangements

M. Treß, E.U. Mapesa, M. Reiche*, F. Kremer

*Max-Planck-Institute for Microstructures, Weinberg 2, 06120 Halle (Saale)

To investigate thin polymeric layers by means of Broadband Dielectric Spectroscopy, recently, an arrangement of highly conductive silicon electrodes covered with insulating silica nano-structures as spacers has been developed.[1] This approach enabled to examine the glassy dynamics of thin polymer layers with a free upper interface[2–5] and even isolated condensed polymer coils[6]. To analyze results obtained with this technique in detail, the consideration of all components in-between the electrodes is required which can be done in terms of equivalent circuits. Since several descriptions are possible, four different models are tested (Fig. 3.3).

Employing fit functions of these models to an exemplary data set of a thin polymer layer (where only selected parameters are free) reveals that all four circuits can similarly describe the data (Fig. 3.4). While for some quantities, like the dielectric strength of the polymer, the results are subject to large variation, others, like mean relaxation rate and broadening of the relaxation peak, do not depend on the model and can therefore be reliably deduced.

[1] A. Serghei and F. Kremer, Rev Sci Inst 79 026101 (2008)
[2] A. Serghei, H. Huth, C. Schick and F. Kremer, Macromol 41 3636 (2008)
[3] M. Erber, M. Tress, E.U. Mapesa, A. Serghei, K.-J. Eichhorn, B. Voit and F. Kremer, Macromol 43 7729 (2010)

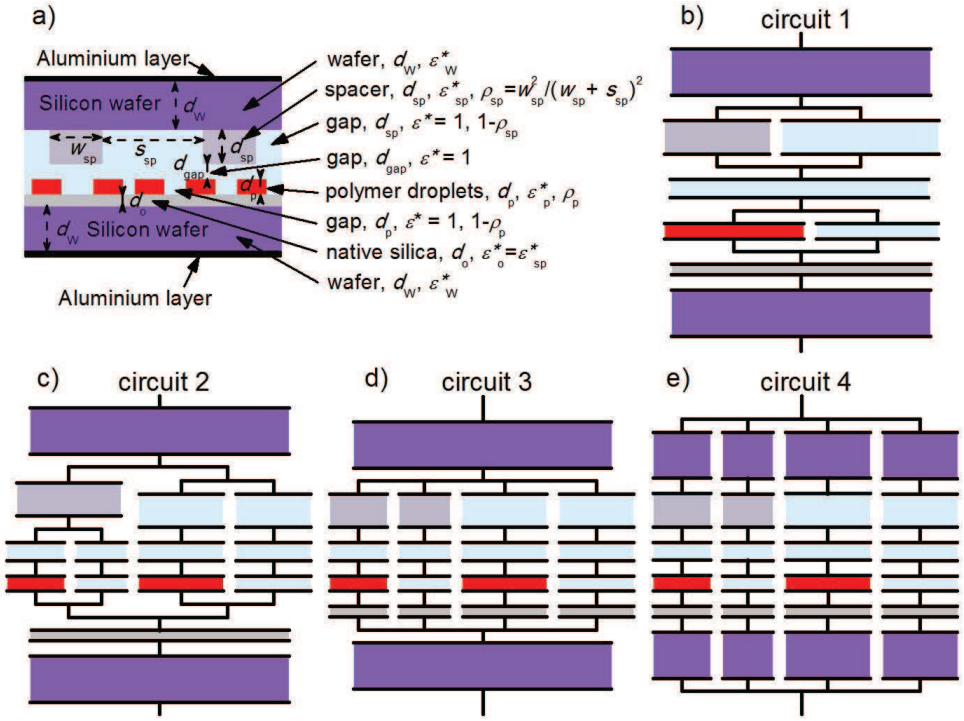

Figure 3.3: a) Schematic cross-section in the nano-structured electrode arrangement. b) - e) Equivalent circuits for respective modeling. The same color code is used in all panels.

[4] M. Tress, M. Erber, E.U. Mapesa, H. Huth, J. Müller, A. Serghei, C. Schick, K.-J. Eichhorn, B. Voit and F. Kremer, Macromol 43 9937 (2010)
[5] E.U. Mapesa, M. Erber, M. Tress, K.J. Eichhorn, A. Serghei, B. Voit and F. Kremer, Eur Phys J: Spec Top 189 173 (2010)
[6] M. Tress, E.U. Mapesa, W. Kossack, W.K. Kipnusu, M. Reiche and F. Kremer, Science 341 1371 (2013)

3.4 Molecular dynamics of poly(cis-1,4-isoprene) in 1- and 2-D confinement

E.U. Mapesa, L. Popp, M. Treß, M. Reiche*, F. Kremer,

*Max-Planck-Institute for Microstructures, Weinberg 2, 06120 Halle (Saale)

Poly(*cis*-1,4-isoprene) (*cis*-PI) belongs to the so-called Type A polymers which have a non-zero component of the dipole moment along the chain diection. It is therefore an apt candidate for studying - by Broadband Dielectric Spectroscopy - the dynamics of the molecule under conditions of geometrical confinement. This is due to the fact that two distinct relaxation processes occurring at different length scales can be probed: the segmental motion which involves structures of about one nanometer in size and the normal mode which represents the fluctuation of the end-to-end vector[1]. We have taken advantage of this and studied *cis*-PI in the 1-dimensional confinement of ultra-

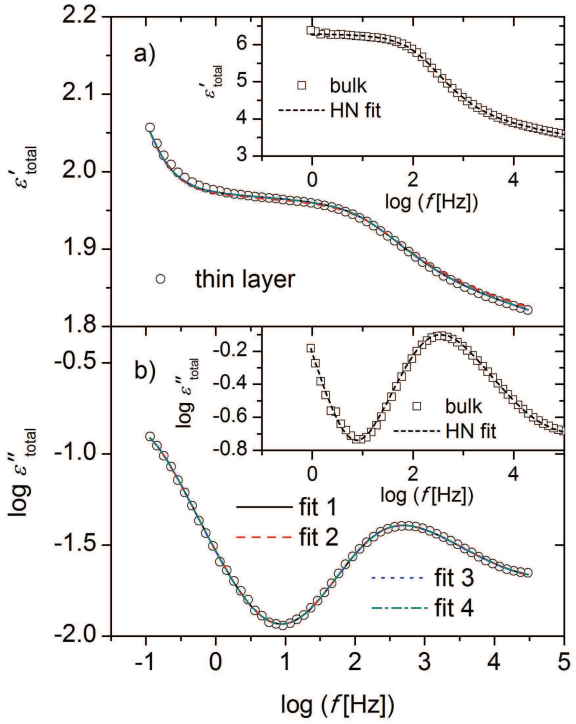

Figure 3.4: a) Permittivity and b) loss spectra of a 30-nm-thin polymer layer in the nano-structured electrode arrangement at a temperature of 400 K and fits according to the four equivalent circuits as indicated. Insets: permittivity and loss spectra of bulk (T = 400 K).

thin layers[2] as well as the 2-D confining space of uni-directional Anodic Aluminium Oxide (AAO) membranes[3].

It is observed (Fig. 3.5) that: (i) the mean spectral position of the segmental mode remains unchanged, when 1- and 2-D confined systems are compared to bulk data; (ii) the segmental mode is broadened in the AAO nanopore matrix, a phenomenon not observed for 1-D confinement; (iii) the broadening of the segmental mode is pore-size dependent (inset-Fig. 3.5); and (iv) the (remaining) normal mode (referred to as the terminal subchain mode,) becomes faster with reducing pore diameter.

[1] I. Bahar, B. Erman, F. Kremer, E.W. Fischer, Macrom. (1992) 25, 816
[2] E.U. Mapesa et al. Soft Matter (2013) 9, 10592
[3] E.U. Mapesa et al. "'Molecular dynamics of poly(cis-1,4-isoprene) in 1- and 2-dimensional confinement"' in Dynamics in Confinement (Vol. 2), edited by Friedrich Kremer, Springer 2014 (in press)

3.5 Molecular dynamics of PMPS in 1D & 2D geometrical confinements - a comparison

W.K. Kipnusu, E.U. Mapesa, F. Kremer

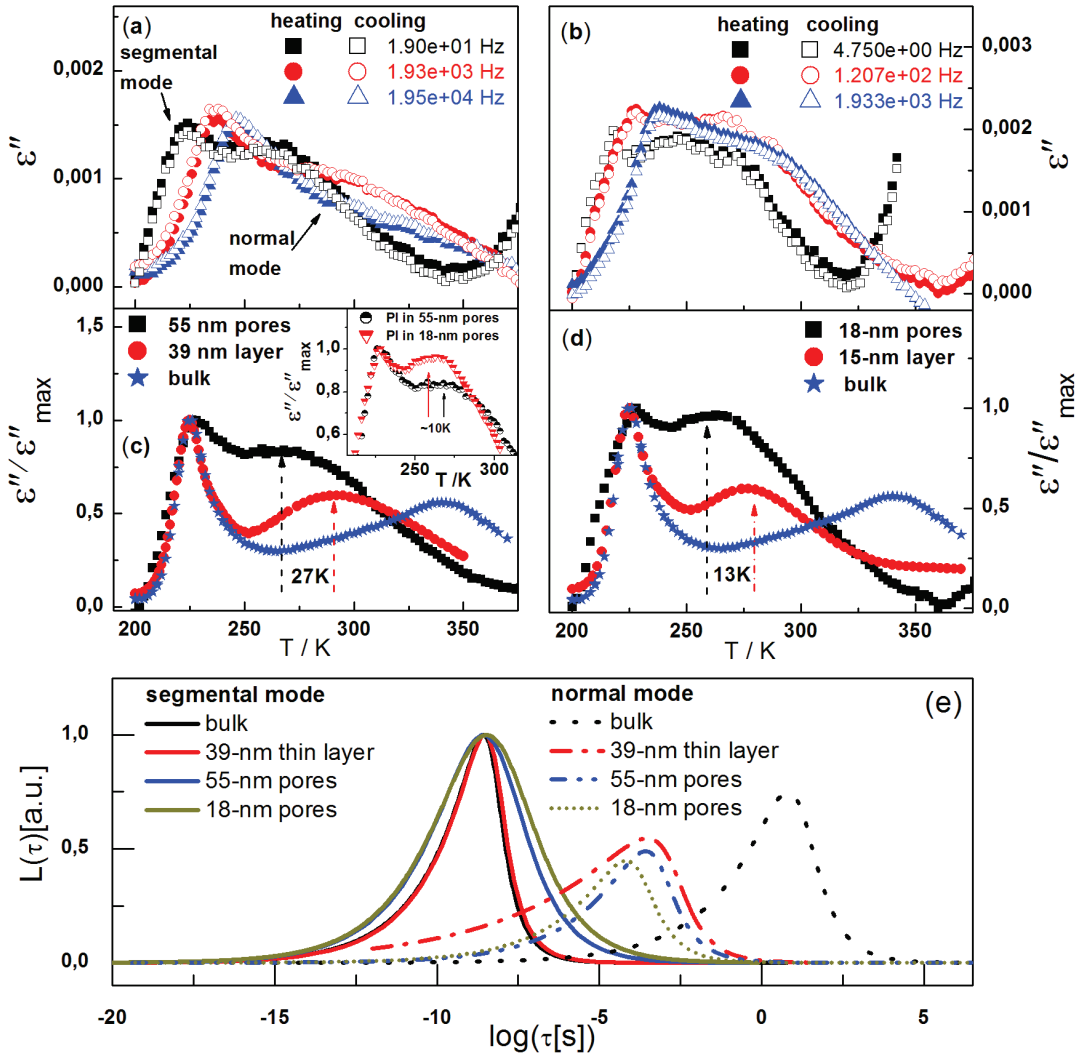

Figure 3.5: Temperature dependence of the dielectric loss, ϵ , (heating and cooling runs) for PI-53 measured in AAO templates with pores of diameter (a) 55 nm and (b) 18 nm. In (c) and (d), a comparison of normalized data is made for PI measured (at 120 Hz) in pores and in thin films of comparable size to the pore-diameter, as indicated. Bulk data is included as well for completeness. Panel (e) shows the respective distribution functions of the mean relaxation times at T = 312 K. Inset: Normalized loss data (measured at 120 Hz) plotted as function of temperature for PI in 55- and 18 – nm pores.

Broadband Dielectric Spectroscopy (BDS) is employed to study molecular dynamics of polymethylphenylsiloxane (PMPS) in 1D and 2-D geometrical constraints. The α-relaxation (segmental mode) of PMPS under the former confinement of thin films down to thickness of 4 nm remain bulk like while in the later, (PMPS infiltrated in uni-directional nanopores) α-relaxation increases with decreasing pore sizes (8 – 4 nm) when approaching the calorimetric glass transition. (Fig. 3.6a & b) This is ascribed to the reduced density of the molecules contained in nanopores. Additionally, a slower surface induced mode is observed for both 1D and 2D confined molecules which is removed after silanization of the pores (Fig. 3.6a) leading to a slight reduction in structural dynamics (Fig. 3.6b). This proves the counter balance between surface and

confinement effects as well as the impact of dimensionally of confinement.

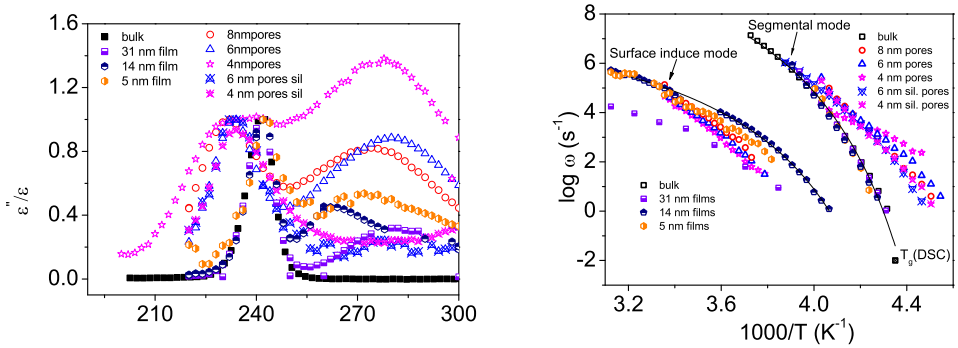

Figure 3.6: (a) Dielectric loss spectra normalized with respect to the maxima of structural relaxation peaks of PMPS: bulk (filled squares), confined in native silica nanopores (open symbols), and coated pores (crossed symbols), PMPS in thin films (half filled symbols). (b) Activation plots of 1 and 2-D confined PMPS: bulk (open squares), thin films (half-filled symbols), native nanoporous silica (open symbols) and coated pores (crossed symbols). Solid lines are VFT fits).

[1] S. H. Anastasiadis, K. Karatasos and G. Vlachos, PRL (2000) 84, 915-918
[2] W.K.Kipnusu, E.U. Mapesa and F. Kremer, under preparation

3.6 Molecular Order and Dynamics of Nanometric Thin Layers of Poly(styrene-b-1,4 isoprene) Diblock Copolymers

W.K. Kipnusu, M.M. Elmahdy, M. Treß, M. Fuchs, E.U. Mapesa, D.M. Smilgies*, J. Zhang†, C.M. Papadakis†, F. Kremer

*Cornell University, Ithaca, New York 14853
†Technische Universität München, Arcisstraße 21, 80333 München

Order and dynamics of poly(styrene-block-isoprene-1.4), P(S-*b*-I) diblock copolymers in nanometer thin layers with different isoprene volume fraction (f_{PI}) and identical molecular weight of the styrene blocks are studied by a combination of Grazing-Incidence Small-Angle X-ray Scattering (GISAXS), Atomic Force Microscopy (AFM) and Broadband Dielectric Spectroscopy (BDS). GISAXS and AFM reveal randomly oriented lamellar structures in the films and a parallel orientation at the top surface, respectively. Fig. 3.7 shows the GISAXS and BDS results for f_{PI} = 0.55. From BDS, three well separated relaxation processes are detected, (i) and (ii) the dynamic glass transitions (segmental mode) in the styrene and isoprene blocks respectively and (iii) the normal mode relaxation representing fluctuations of the isoprene chain as a whole or parts of it.[1] While the two former do not show any thickness dependence in their spectral positions, the latter becomes faster with decreasing sample thickness.[2] This reflects the difference in the length-scale on which the molecular fluctuations take place.

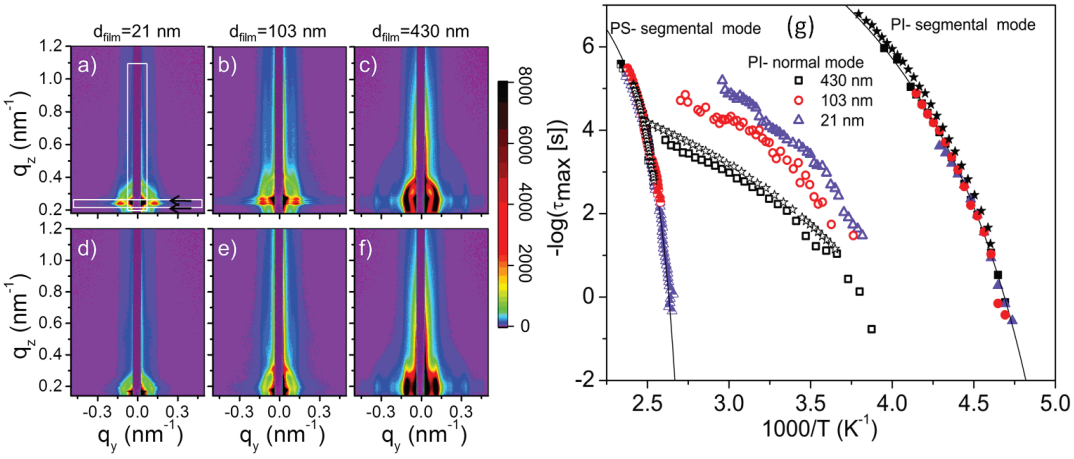

Figure 3.7: 2D GISAXS images of P(S-*b*-I) films with $f_{PI} = 0.55$. (a-c) $\alpha_i = 0.14°$ and (d-f) $\alpha_i = 0.09°$ (g) activation plot for the relaxation processes in P(S-*b*-I). The film thicknesses are indicated.

[1] E.U. Mapesa, M. Tress, G.Shulz, H. Huth, C. Schick, M. Reine and F. Kremer, Softmater, (2013) 9,10592-10598
[2] W.K. Kipnusu, M.M. Elmahdy, M. Tress, M. Fuchs, E.U. Mapesa, D.M. Silgies, J. Zhang, C.M. Papadakis and F.Kremer, Macromolecules, (2013) 46, 9729-9737

3.7 Dynamics of Poly(2-Vinyl-Pyridine) polymer brushes

N. Neubauer, M. Treß, R. Winkler*, P. Uhlmann*, M. Reiche†, F. Kremer

* Leibniz-Institut für Polymerforschung Dresden e. V.,Hohe Str. 6, 01069 Dresden
†Max-Planck-Institute for Microstructures, Weinberg 2, 06120 Halle (Saale)

A tethered polymer layer with a large grafting density is called a polymer brush. The polymer chains are stretched as the distance between grafting points is smaller than the size of the chains.[1] By means of Broadband Dielectric Spectroscopy (BDS)[2, 3] the dynamics of poly(2-vinylpyridine) (P2VP) polymer brushes are investigated. To graft the P2VP chains on a highly conductive silicon wafer, a two-step "'grafting-to"' preparation is applied. First, a thin layer (~ 2 nm) of PGMA (M_n = 17. 5kg/mol) is deposited from a 0.02 % solution in chloroform. This layer of PGMA attached to the silicon wafer serves as an anchoring layer. Next, carboxyl terminated poly(2-vinylpyridine) (P2VP-COOH, Mn = 40.6 kg/mol) is spin-coated from a 1 % THF solution. After annealing and extraction a P2VP-brush with $7-8$ nm thickness is formed, corresponding to a grafting density of about 0.1 chains/nm^2 and a distance between grafting points of approximately 3 nm (smaller than R_g ~ 5 nm). For the dielectric measurements a nanostructured electrode arrangement is used.[4, 5] Silica structures serve as spacers, leading to a distance of around $40-50$ nm between the electrodes. First experiments show different relaxation modes. From 300 K to 400 K a weak relaxation from 10^3 to 10^5 Hz is observable, which is most likely a PGMA ?-relaxation. At higher Temperatures ($400-480$ K) a stronger relaxation from 10^1 to 10^3 Hz appears, originating from the P2VP

brushes. It is not yet clear how this relaxation is related to the P2VP segmental mode.[5] Further investigations have to be done to clearly identify and describe the behavior of these relaxation modes.

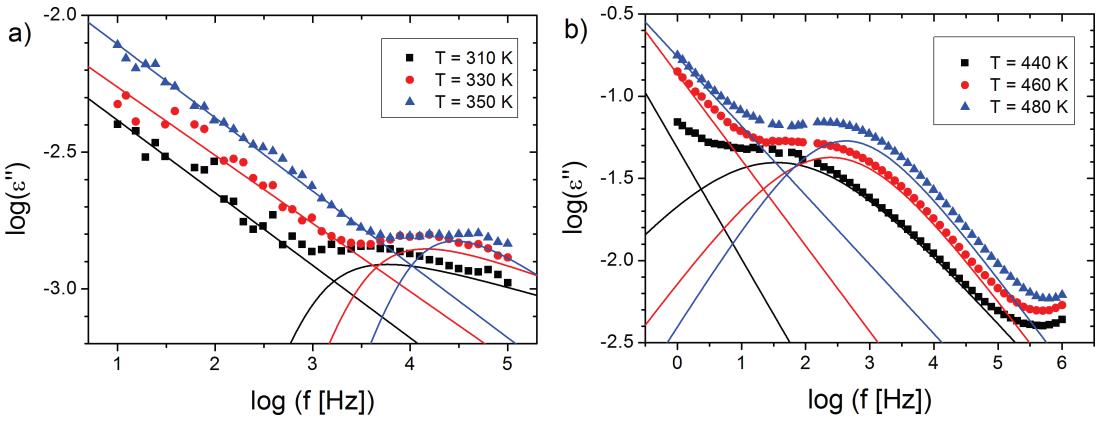

Figure 3.8: Dielectric loss (ϵ'') spectra of P2VP brushes. a) From 300 K to 370 K a weak relaxation mode, presumably a PGMA ?-relaxation, and b) from 400 K to 480 K a P2VP-relaxation mode is observed.

[1] R. Advincula, W. J. Brittain, K. Caster, J. Rühe, Polymer Brushes, Wiley-VCH, 2004
[2] E.U. Mapesa et al., Soft Matter 9, 10592-10598 (2013)
[3] Tress et al., Macromolecules 43, 9937-9944 (2010)
[4] A. Serghei and F. Kremer, Review of Scientific Instruments (2008) 79, 026101
[5] M. Tress et al., Science 341 (6152), 1371-1374 (2013)

3.8 Intra- and inter-molecular dynamics in the course of vitrification in organic glass forming materials

L. Popp, W. Kossack, M. Treß, W.K. Kipnusu, F. Kremer

The intra- and inter-molecular interactions of the organic glass forming model systems benzophenone, d-sorbitol and xylitol are studied by Fourier-Transform Infrared- (FTIR) and Broadband Dielectric Spectroscopy (BDS). By analyzing the temperature dependencies of specific IR absorption bands it is demonstrated that each molecular moiety in the glass-formers has its own signature in the course of the dynamic glass transition[1]: while some do not show any change at the calorimetric glass transition temperature others exhibit a pronounced kink. The effects cannot be attributed solely to the effect of a microscopic thermal expansion, but instead indicate gradual conformational changes[2]. The ease of application of this approach to a variety of systems in different geometries and external conditions can assist the modelling of glasses and the understanding of the coupling between the intra-and intermolecular interactions in the course of vitrification[3].

[1] W. Kossack et al., Phys Chem Chem Phys (2013), 15(47): 20641-50
[2] P. Papadopoulos et al., Soft Matter (2013) 9, 1600-1603
[3] W. K. Kipnusu et al., Soft Matter (2013) 9, 4681-4686.

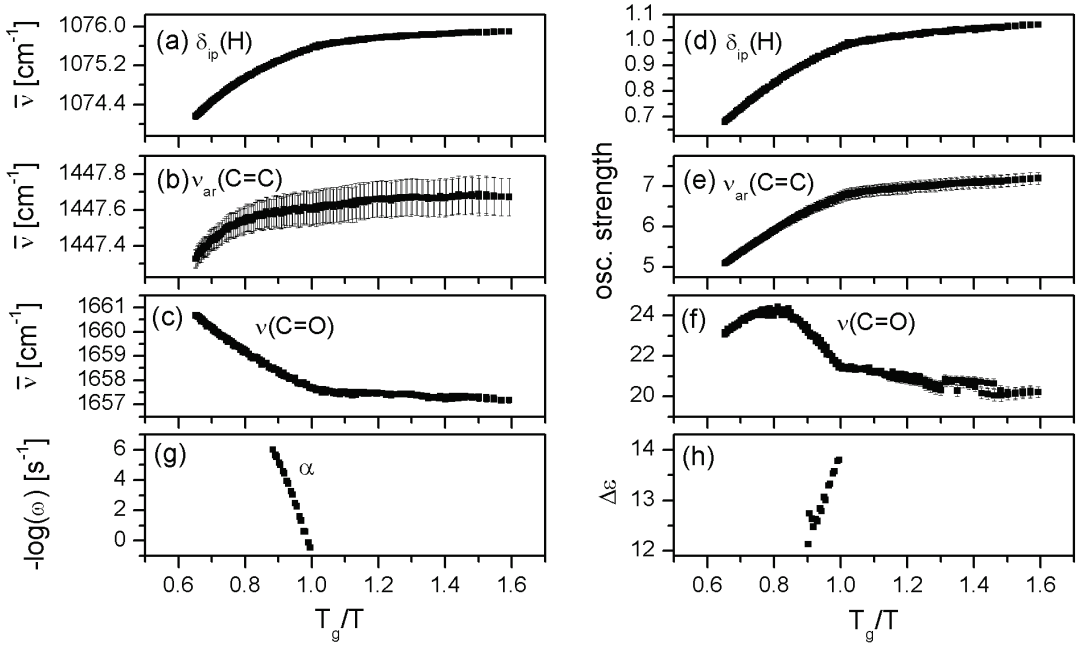

Figure 3.9: Comparison of the shift of specific IR vibrational modes and the intermolecular dynamics (from BDS) of benzophenone as a function of scaled temperature T (with T_g = 212 K). The peak positions of the (a) hydrogen in-plane bending vibration δ_{ip}(H), the (b) aromatic carbon-carbon stretching vibration ν_{ar}(C=C), the (c) carbon-oxygen stretching vibration ν(C=O) and their corresponding oscillator strengths (d-f) as well as (g) the α-relaxation rate and (h) the $\Delta\epsilon$ (from BDS) are shown.

3.9 Kinetics of mutarotation of fucose measured by Broadband Dielectric Spectroscopy (BDS) and FTIR

W. Kossack, W.K. Kipnusu, K. Kaminski*, M. Paluch*, F. Kremer,

*Institue of Physics, University of Silesia, ul. Uniwersytecka 4, 40-007 Katowice, Poland

Cyclic sugars such as fucose but also glucose and fructose appear in different isomeric states, which are dynamically converted into each other (Fig 3.10a).[1] The equilibrium concentrations of these as well as the rates of conversion depend on temperature (Fig. 3.10b). In the IR fingerprint region vibrations are assigned specifically to the α- and β-L-fucopyranose anomers.[2] Recording the height of these absorption bands when the sample is out of equilibrium, enables one to follow the equilibration of composition in time and determine the corresponding rates, k (Fig. 3.10d,e). During this process the dielectrically observable α-relaxation-time (τ_α) slows down by more than one decade (c).[3] The k's obtained from FTIR and BDS for temperatures between 313 and 333 K follow an Arrhenius like activation (b) with different activation energies, E_a. Respectively, for α- and β-fucopyranose an E_a of 102 kJ/mol and 111 kJ/mol was obtained, whereas the rates obtained from τ_α are much slower and exhibit a higher E_a of ~ 140 kJ/mol indicating a supramolecular origin of the shift of the α-relaxation.

[1] R. S. Shallenberger, Pure Appl. Chem., 50, 1409-1420, 1978

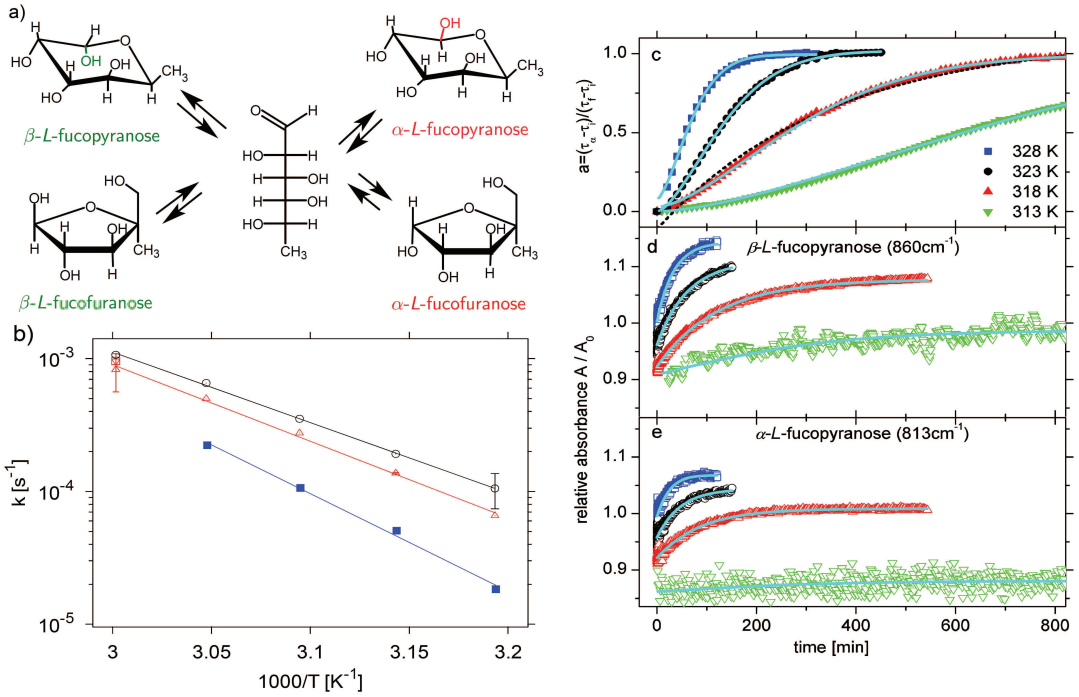

Figure 3.10: a): scheme of mutarotation, showing the transitional state (center) and the possible anomers; b) activation plot with rates determined from FTIR (hollow) for α- (black) and β-fucopyranose (red) as well as from BDS (filled), Straight lines represent fits according to an Arrhenius dependence. Errorbars are drawn if not smaller than the symbol-size. c) normalized shift of the α-relaxation upon time; d) and e) represent the growth of the integrated absorbance normalized to the value at the start of the experiment.

[2] N. Dujardin, et. al., Solid State Commun., 148, 78-82, 2008
[3] P. Wlodarczyk, et. al., J. Phys. Condens. Matter, 25, 375101, 2013

3.10 Specific surface interactions studied by FTIR

W. Kossack, W.K. Kipnusu, M. Treß, K. Kaminski*, F. Kremer

*Institue of Physics, University of Silesia, ul. Uniwersytecka 4, 40-007 Katowice, Poland

Fourier Transform Infrared Spectroscopy (FTIR) is a sensitive technique for specific intramolecular vibrations. If the intramolecular (or interatomic) potentials of a certain moiety are modified e.g. by an attractive interaction with a nearby surface, the vibrational frequencies of this group change. In nanoporous silica (pSiO) membranes the surface to volume ratio is extraordinarily high making them perfect model systems to study surface interactions (Fig. 3.11a).[1, 2]

Such interactions can be mediated by the OH terminated pore walls, and consequently strong changes of the OH stretching band (b) of ethylhexanol (ETHOH, a) are found when imbibed into pores. The removal of the surface hydroxyls (by silanization) leads to a scenario where confiment effects dominate, as the specific surface interaction is eliminated.

Interestingly, Poly-2-Vinyl-Pyridine (P2VP, inset in e) shows specific interactions of the ring with the surface hydroxyl as can be seen by the reduction in height of its stretching vibration (d) and the additional ring stretching band at ~ 1600 cm^{-1}, found when P2VP is incorporated into the pSiO (e).[3]

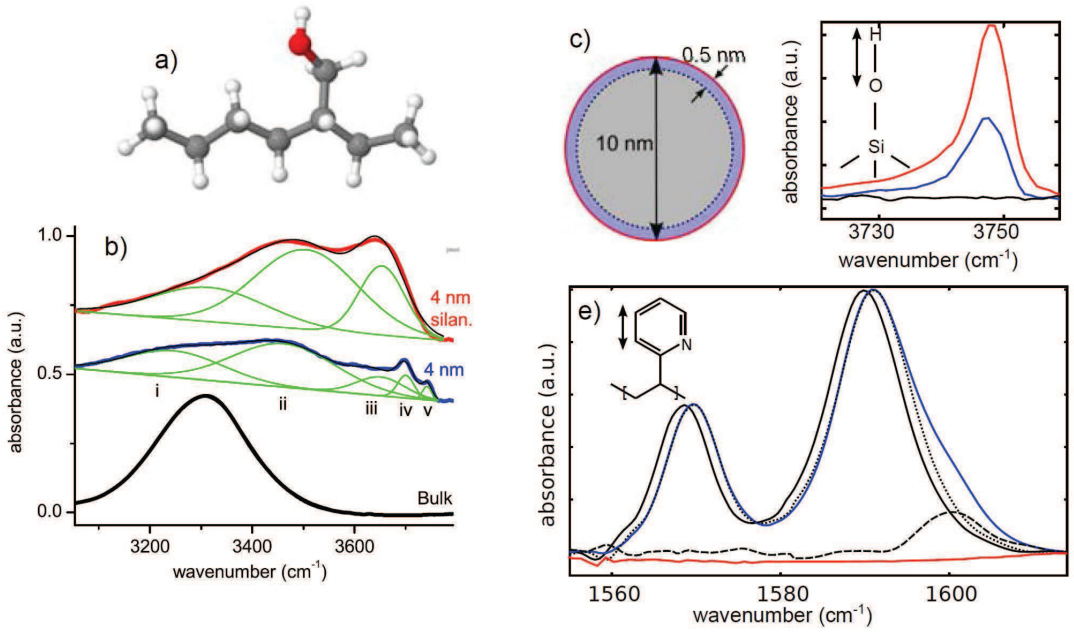

Figure 3.11: a) and inset in e) chemical structure of ETHOH and P2VP; b) IR spectra of bulk ETHOH (black) and in pSiO (blue) and silanized pSiO; Due to confinement bands ii and iii are found, whereas the the surface interaction leads to iv and v. c) scheme of a single pore, with an estimated 0.5 nm thick surface layer; d) reduction in pSiO OH stretching due to interactions with P2VP; e) additional band (dashed) originating from interactions of the pyridine ring with surface hydroxyls. The bulk spectrum (black solid) is shifted (dotted) to accommodate for density and polarity effects. In d) and e) the red and blue lines represent IR spectra of empty and P2VP filled pSiO, the geometry of the vibrations is shown in the insets.

[1] C. Iacob, et. al., Soft Matter 8, 289-293, 2011
[2] W. K. Kipnusu, W. Kossack, et. al., Z. Für Phys. Chem., 226, 797-805, 2012
[3] M. Tress, E. U. Mapesa, W. Kossack, et. al., Science, 341, 1371-1374, 2013

3.11 Intra- and intermolecular dynamics in organic glass-forming liquids

W. Kossack, K.-B. Suttner, F. Kremer

The intra and inter molecular dynamics of organic, glass forming molecular liquids is studied by Fourier Transform Infrared Spectroscopy (FTIR). By tracing the oscillator strength and spectral position of absorption bands specific for the different molecular moieties, characteristic changes of microscopic interactions can be identified. In the case of glycerol the dominant role of the hydrogen bonding network is concluded from

the strong blue shift (~ 60 cm^{-1}) of the OH stretching band (ν OH) with increasing temperature, T (Fig. 3.12c, chemical structure and displacements upon vibration depicted in Fig. 3.12b).[1] Contrary to measurements of other molecular glass formers (*e.g.* alkyl-citrates or salol) a blue shift of the CH stretching vibrations (ν CH) is observed upon heating indicating an attractive inter-molecular interaction of the alkylic H, that weakens the C-H bond itself (Fig. 3.12c).[2, 3] The spatially extended C-C-O stretchings on the other hand show a red shift with a distinct kink at the calorimetric glass transition temperature, T_g. Such pronounced changes in slope are not observed in the oscillator strength, A/A_0, which exhibit a continuous bending down when lowering temperature.

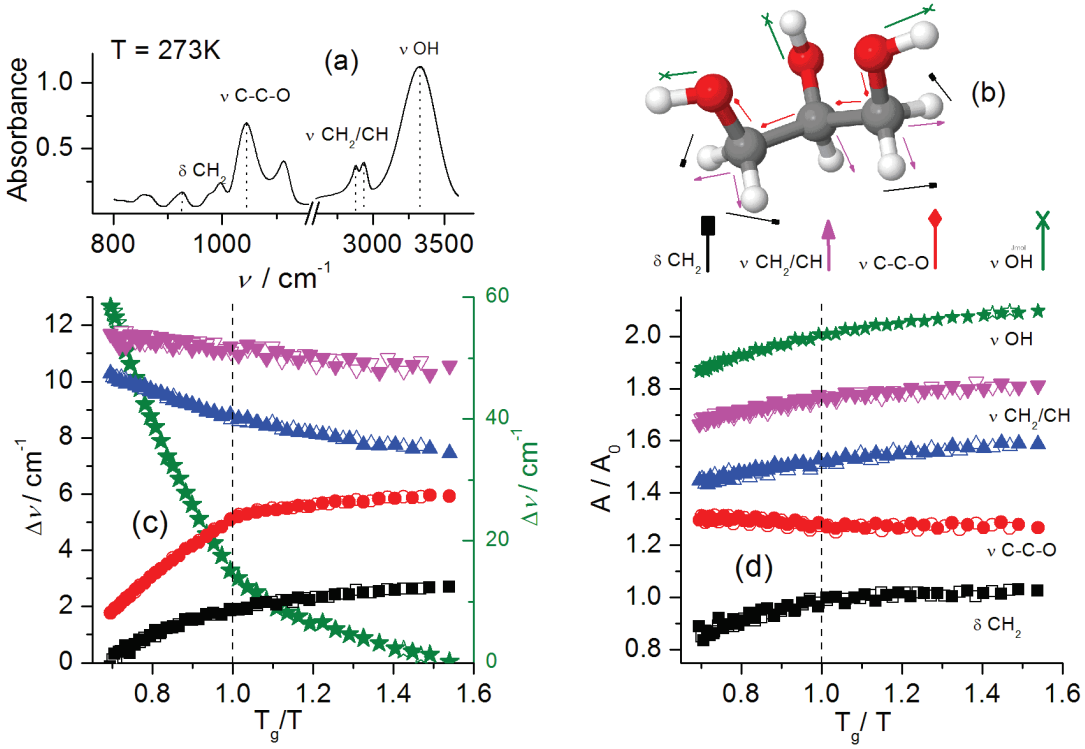

Figure 3.12: (a) IR spectrum of glycerol. (b) Molecule with vibration modes. (c),(d) Results from temperature dependent IR measurements of glycerol as functions of T_g/T. Filled symbols represent data obtained upon heating and empty symbols upon cooling. The oscillator strength is normalized to the value at T_g and shifted with an offset of 0.25 between two charts. Green stars: stretching of H-bonded OH (ν OH) (right y axis), black squares: δ CH_2, red circles: ν C-C-O, blue triangle up: ν_{sym} CH_2/CH, purple triangle down: ν_{asym} CH_2/CH.

[1] W. Kossack, et al., Phys. Chem. Chem. Phys (2013), 15, 20641
[2] P. Papadopoulos et al., Soft Matter (2013) 9, 1600
[3] W. K Kipnusu et al., Soft Matter (2013) 9, 4681

3.12 The influence of processing on orientation and mechanical properties of S-S/B-S triblock copolymers

N. Mahmood*, A.M. Anton, F. Kremer, M. Beiner*†

*1 Martin-Luther-Universität Halle-Wittenberg, Institut für Chemie, Kurt-Mothes-Straße 2, 06120 Halle (Saale)

†2 Fraunhofer Institut für Werkstoffmechanik IWM, Walter-Hülse-Straße 1, 06120 Halle (Saale)

Triblock copolymers providing a rubbery middle block made of random poly(styrene-*stat*-butadiene) (S/B) surrounded by polystyrene outer blocks are in the focus of recent research. In addition to the overall the material's properties depending on composition, softening and interfacial behavior can be fine-tuned by varying the middle block's styrene content[1, 2].

Structure resolving techniques, as SAXS, TEM or TMOA for instance, have been employed to shed light on the sample's microstructure and are combined with tensile tests to clarify the structure's influence on the material's mechanical properties.

It can be found that on mesoscale (10 - 100 nm) the triblock copolymer tends to phase separate forming lamellae not-affected through processing, while on segmental scale (< 1nm) the structure appears completely unordered. Supplementary, mechanical measurements reveal a coincidence between mesostructure and E moduli in accordance to the composite model[3]. Hence, one can assume that processing conditions are affecting on mesoscale, while the segmental scale remains inaccessible. Vice versa, mesoscale structures determine the processed copolymer's mechanical properties, while the influence of the segmental scale seems to be minor[4].

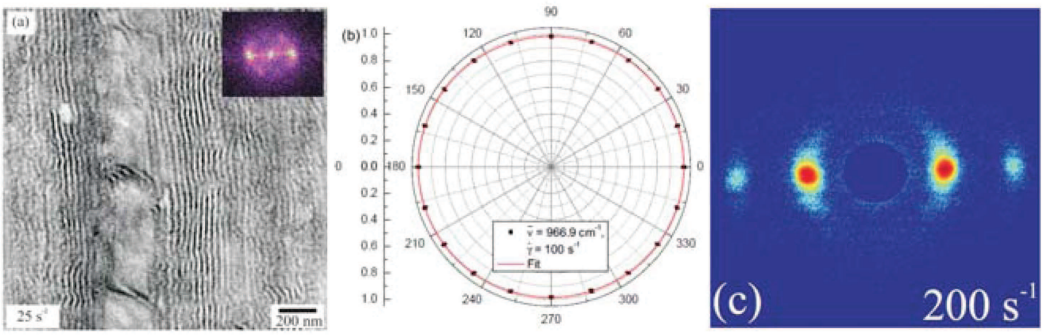

Figure 3.13: TEM (a), TMOA (b), and SAXS (c) measurement of S-S/B-S triblock copolymer. On the mesocale well-defined and well-aligned lamella structures are evident (a and c). In contrast, the circular shape of the polarization-dependent oscillator strength indicates absence of any orientation on the segmental scale (b).

[1] M. Thunga et al., J.Polym. Sci.B (2008) 46 329-343
[2] S. Hölzer et al., Europ.Polym. J.(2013) 4, 261-269
[3] P. Allan, M. J. Journal of Physics D (1991) 24 1381-1390
[4] manuscript in preparation

3.13 Study on the hierarchical structure and resulting constraints in spider silk by means of pressure- dependent FTIR-spectroscopy

A.M. Anton, W. Kossack, R. Figuli(Ene)*, P. Papadopoulos†, C. Gutsche, F. Kremer

*Karlsruher Institut für Technologie, Institut für Technische Chemie und Polymerchemie, Engesserstraße 18, 76128 Karlsruhe

†Max Planck Institut für Polymerforschung, Ackermannweg 10, 55128 Mainz

Its outstanding mechanical properties elevate spider silk to a promising material for mechanically highly demanding applications, e.g. bullet-proved vests[1–3]. Its unique structure, namely β-sheet polyalanine nanocrystals reinforcing a glycine-rich amorphous glassy matrix, that serially interconnects these crystals through pre-strained chains, is believed to be essential.

To gain insight into this structure FTIR-spectroscopy is combined with external mechanical fields. Uniaxial stress is created during stretching the sample controlled by micrometer screws monitored with a force sensor, while hydrostatic pressure is applied by means of a diamond anvil cell (DAC) determined through the pressure-dependent ruby fluorescence[4]. Since both load experiments are performed on the same material, the interplay between nanocrystals and amorphous phase can be better understood.

The non-overlapping N-C_a polyalanine stretching vibration at $\overline{\nu}$ = 965 cm^{-1} is employed as molecular force sensor located within the ?-sheet nanocrystals.[1–3] enabling to study the microscopic response to external mechanical fields while monitoring a stress-, respectively pressure-dependent shift of this vibration. In the case of applied stress a linear red shift can be found, whereas hydrostatic pressure causes a blue shift also linear on two regimes and fully reversible up to 7 GPa. The seamless connection of negative and positive pressure regimes corroborate quantitatively our structural model[5].

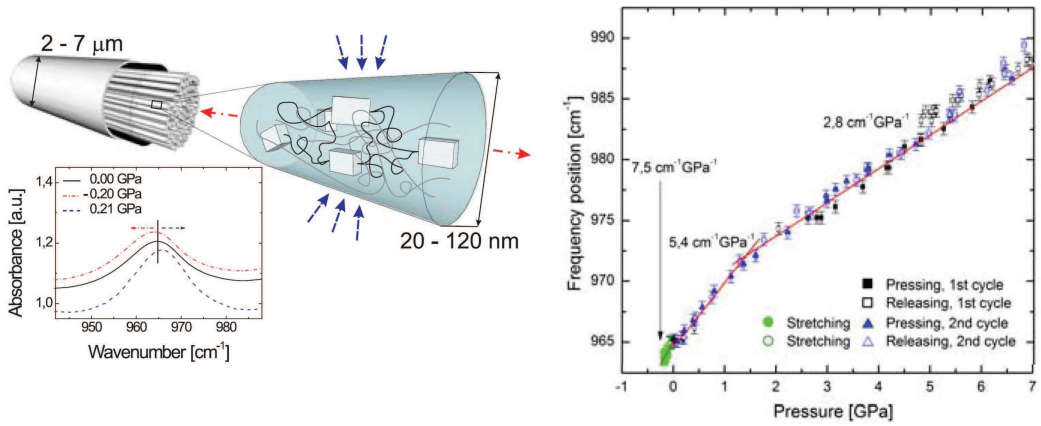

Figure 3.14: Illustration of spider silk's structure: A fiber made of fibrils is composed of nanocrystals and pre-stressed chains embedded in an amorphous matrix. The application of uniaxial stress induces a red shift of the vibration at $\overline{\nu}$ = 965 cm^{-1}, whereas hydrostatic pressure causes a blue shift.

[1] P. Papdopoulos et al., Eur. Phys. J. E (2007) 24 193-199
[2] P. Papdopoulos et al., Colloid. Polym. Sci. (2009) 287 231-236
[3] R. Ene et al., Soft Matter (2009) 5 4568-4574
[4] K. Syassen, High Press. Res. (2008) 28 75-126
[5] A. M. Anton et al. Macromol. (2013) 46 4919-4923

3.14 Determining the Specificity of Monoclonal Antibody HPT-101 to Tau-Peptides with Optical Tweezers

T. Stangner, C. Wagner, D. Singer[*], S. Angioletti-Uberti[†], C. Gutsche, J. Dzubiella, R. Hoffmann[*‡], F. Kremer

[*]Biotechnologisch-Biomedizinisches Zentrum Leipzig, Deutscher Platz 5, 04103 Leipzig
[†]Helmholtz-Zentrum Berlin für Materialien und Energie, Hahn-Meitner-Platz 1, 14109 Berlin
[‡]Technische Universität Berlin, Straße des 17. Juni 135, 10623 Berlin

Optical tweezers-assisted dynamic force spectroscopy is employed to investigate specific receptor-ligand-interactions on the level of single binding events. In particular, we analyze binding of the phosphorylation-specific monoclonal antibody (mAb) HPT-101 to synthetic tau-peptides with two potential phosphorylation sites (Thr231 and Ser235), being the most probable markers for Alzheimer's disease. Whereas the typical interpretation of enzyme-linked immunosorbent assay (ELISA) suggests that this monoclonal antibody binds exclusively to the double-phosphorylated tau-peptide, we show here by DFS that the specificity of mAb HPT-101 is only apparent. In fact, binding occurs also to each sort of the monophosphorylated peptides. Therefore, we characterize the unbinding process by analyzing the measured rupture force distributions, from which the lifetime of the bond without force τ_0, its characteristic length x_{ts} and the free energy of activation ΔG are extracted for the three mAb/peptide combinations. This information is used to build a simple theoretical model to predict features of the unbinding process for the double-phosphorylated peptide purely based on data on the monophosphorylated ones. Finally, we introduce a method to combine binding and unbinding measurements to estimate the relative affinity of the bonds. The values obtained for this quantity are in accordance with ELISA, showing how DFS can offer important insights about the dynamic binding process which are not accessible to this common and widespread assay.

[1] Stangner et al., Phys. Biol. 2013, 10, 749, 46004
[2] Stangner et al., ACS Nano 2013, 7, 12, 11388

3.15 Amino acid-sequence dependent interactions between receptors and ligands studied with Optical Tweezers

T. Stangner, D. Singer[*], D. Knappe, C. Wagner, S. Angioletti-Uberti[†], C. Gutsche, J. Dzubiella[†], R. Hoffmann[*‡], F. Kremer

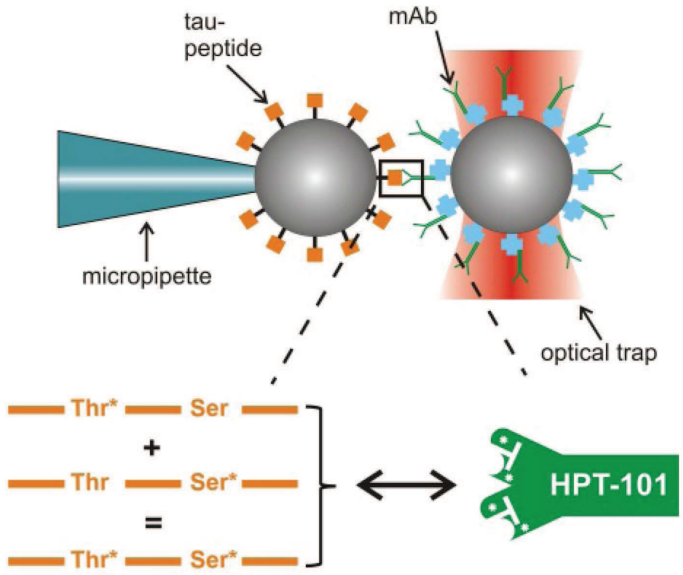

Figure 3.15: Experimental setup. One peptide-coated colloid is immobilized at the tip of a custom-made micropipette by capillary force and a second colloid, bearing the mAb HPT-101 on its surface, is trapped with the optical tweezers. (Inset) It is shown by our measurements and a simple theoretical model that the binding of mAb HPT-101 to the doubled phosphorylated peptide can be describe as the sum of the two monophosphorylated cases.

*Biotechnologisch-Biomedizinisches Zentrum Leipzig, Deutscher Platz 5, 04103 Leipzig
†Helmholtz-Zentrum Berlin für Materialien und Energie, Hahn-Meitner-Platz 1, 14109 Berlin
‡Technische Universität Berlin, Straße des 17. Juni 135, 10623 Berlin

For diagnostic procedures that rely on monoclonal antibodies (mAbs), it is imperative to know whether the antibody (e.g. mAb HPT-101) recognizes the epitope of its target peptide/protein (e.g. tau-protein) specific or whether possible cross-reactions to other forms of the protein may occur. In a previous study[1] non-specific interactions of the phosphorylation-specific mAb HPT-101 to tau-peptides with similar epitopes, differing only by a single isolated phosphorylation site, were detected. Based on this result, it is obvious that the specificity of mAb HPT-101 refers not exclusively to the phosphorylation pattern but depends also on the surrounding amino acid sequence in the tau peptide. Here, we investigate with the help of optical tweezers assisted dynamic force spectroscopy[2] the influence of single amino acids on the binding of mAb HPT-101 to the doubled phosphorylated peptide tau[pThr231/Ser235]. For this purpose, we characterize the unbinding process by analyzing the measured rupture force distributions, from which the lifetime of the bond without force τ_0, its characteristic length x_{ts}, and the free energy of activation ΔG are extracted for the all mAb/peptide combinations. Furthermore, the binding process is specified by means of the relative binding frequency. Using these parameter, it is possible to identify essential as well as secondary amino acids for the interaction between mAb HPT-101 and tau[pThr231/pSer235].

[1] Wagner et al., Soft Matter, 2011, 7, 4370-4378
[2] Stangner et al., ACS Nano 2013, 7, 12, 11388

Table 3.1: Epitop mapping of monoclonal antibody HPT-101. The antibody specific phosphorylation sites are underlined (abbreviation: p = phosphorylation) and essential amino acids are shown in red. Secondary amino acids, which contribute to the binding, are highlighted in orange. White fields are not significant for the specific interaction between antigen and antibody.

Sequence	V	A	V	V	R	pT	P	P	K	pS	P	S	S	A	K
HPT-101 (pT & pS)	V	A	V	V	R	pT	P	P	K	pS	P	S	S	A	K

3.16 Funding

FOR 877 "From local constraints to macroscopic transport" TP 7 "Electric field driven motion of single polyelectrolyte grafted colloids"
Prof. Dr. F. Kremer and Prof. Dr. K. Kroy
KR 1138/21-2 (2011-2014)

SPP 1369 "Polymer-Solid Contacts: Interfaces and Interphases"
TP "Interfacial dynamics of polymers in interaction with solid substrates"
Prof. Dr. F. Kremer
KR 1138/23-2 (2011-2014)

Graduate School "Leipzig School of Natural Sciences – Building with Molecules and Nano-object" BuildMoNa, TP 15 "Dynamics of DNA under tension and in confinement"
Prof. Dr. F. Kremer
GSC 185/1 (2008-2013)

IRTG "Diffusion in Porous Materials"
TP "Molecular Dynamics in Interntionally Tailored Nanopores"
Prof. Dr. F. Kremer
GRK 1056/02 (2009-2013)

SFB/TRR 102 "Polymers under multiple constraints: restricted and controlled molecular order and mobility"
TP B05 "Structural levels of organisation in spider-silk – a combined mechanical and IR-spectroscopic study"
TP B08 "Broadband Dielectric Spectroscopy to study the molecular dynamics in nanometer thin layers of block copolymers"
Prof. Dr. F. Kremer
(2011-2015)

3.17 Organizational Duties

Friedrich Kremer

- Principal Investigator in the "Leipzig School of Natural Sciences – Building with Molecules and Nano-Objects" in the framework of a Graduate School funded by the "Ferderal Excellence Initiative". This supports several Ph.D. projects.
- Principal Investigator and Lecturer in the International Research Training Group "Diffusion in Porous Materials" headed by Prof. Dr. R. Gläser and Prof. Dr. F. Kapteijn.
- Deputy chairman of the SFB-TRR 102 on "Polymers under multiple constraints: restricted and cotrolled molecular order and mobility" of the Universities of Halle and Leipzig.

3.18 External Cooperations

Academic

- Max-Planck-Institute for Microstructure Physics, Halle
  Dr. Manfred Reiche
- Cornell University, Ithaca, New York
  D.M. Smilgies
- Technische Universität München
  Prof. Dr. C.M. Papadakis, J. Zhang
- Leibniz-Institut für Polymerforschung Dresden
  Dr. P. Uhlmann, R. Winkler
- University of Silesia, Katowice
  Prof. Dr. M. Paluch, Dr. K. Kaminski
- Martin-Luther-Universität Halle-Wittenberg
  PD Dr. M. Beiner, N. Mahmood
- Fraunhofer Institut für Werkstoffmechanik IWM, Halle
  PD Dr. M. Beiner
- Karlsruher Institut für Technologie
  Dr. R. Figuli (Ene)
- Max Planck Institut für Polymerforschung, Mainz
  Dr. P. Papadopoulos
- Helmholtz-Zentrum Berlin für Materialien und Energie, Berlin
  Prof. Dr. J. Dzubiella, Dr. S. Angioletti-Uberti
- Biotechnologisch-Biomedizinisches Zentrum Leipzig
  Prof. Dr. R. Hoffmann, Dr. D. Singer

Industry

- Novocontrol, Hundsangen, Germany

- BOREALIS Polyolefine GmbH, Linz, Austria
- IST METZ GmbH, Nürtingen, Germany
- Süd-Chemie AG, München, Germany
- MERCK KGaA, Darmstadt, Germany

3.19 Publications

Journals

P. Papadopoulos, W. Kossack, F. Kremer: *Intra- and inter-molecular dynamics in glass-forming liquids*, Soft Matter **9**, 1600-1603 (2013)

I. Semenov, S. Raafatnia, M. Sega, V. Lobaskin, C. Holm, F. Kremer: *Electrophoretic mobility and charge inversion of a colloidal particle studied by single-colloid electrophoresis and molecular dynamics simulations*, Physical Review **87**, 022302 (2013)

K. Kaminski, W. Kipnusu, K. Adrjanowicz, E. Mapesa, C. Iacob, M. Jasiurkowska, P. Wlodarczyk, K. Grzybowska, M. Paluch, F. Kremer: *Comparative study on the molecular dynamics of a series of polypropylene glycols*, Macromolecules **46** (5), 1973-1980 (2013)

W.K. Kipnusu, W. Kossack, C. Iacob, P. Zeigermann, M. Jasiurkowska, J.R. Sangoro, R. Valiullin, F. Kremer: *The interplay between inter- and intramolecular dynamics in a series of alkylcitrates*, Soft Matter **9**, 4681-4686 (2013)

M. Anton, W. Kossack, C. Gutsche, R. Figuli (Ene), P. Papadopoulos, J. Ebad-Allah, C. Kuntscher, F. Kremer: *Pressure-Dependent FTIR-Spectroscopy on the Counterbalance between External and Internal Constraints in Spider Silk of Nephila pilipes*, Macromolecules **46**, 4919-4923 (2013)

T. Stangner, D. Singer, C. Wagner, C. Gutsche, O. Ueberschär, R. Hoffmann, F. Kremer: *FACS-sorted particles reduce the data variance in optical tweezers assisted dynamic force spectroscopy measurements*, Physical Biology **10**, 046004 (2013)

E.U. Mapesa, M. Tress, G. Schulz, H. Huth, C. Schick, M. Reiche, F. Kremer: *Segmental and chain dynamics in nanometric layers of poly (cis-1,4-isoprene) as studied by Broadband Dielectric Spectroscopy and temperature-modulated Calorimentry*, Soft Matter **9** (44), 10592-10598 (2013)

M. Tress, E.U. Mapesa, W. Kossack, W.K. Kipnusu, M. Reiche, F. Kremer: *Glassy Dynamics in Condensed Isolated Polymer Chain*, Science **341** (6152), 1371-1374 (2013)

P.J. Griffin, J.R. Sangoro, Y. Wang, A.P. Holt, V.N. Novikov, A.P. Sokolov, Z. Wojnarowska, M. Paluch, F. Kremer: *Dynamic crossover and the Debye-Stokes-Einstein relation in liquid N,N-diethyl-3-methylbenzamide (DEET)*, Soft Matter **9**, 10373-10380 (2013)

T. Stangner, C. Wagner, D. Singer, S. Angioletti-Uberti, C. Gutsche, J. Dzubiella, R. Hoffmann, F. Kremer: *Determining the Specificity of Monoclonal Antibody HPT-101 to tau-Peptides with Optical Tweezers*, ACS Nano **7**, 11388-11396 (2013)

W. Kossack, K. Adrjanowicz, M. Tarnacka, W.K. Kipnusu, M. Dulski, E.U. Mapesa, K. Kaminski, S. Pawlus, M. Paluch, F. Kremer: *Glassy dynamics and physical aging in fucose saccharides as studied by infrared- and broadband dielectric spectroscopy*, Phys. Chem. Phys. **15**, 20641-20650 (2013)

W.K. Kipnusu, M. M. Elmahdy, M. Tress, M. Fuchs, E.U. Mapesa, D.M. Smilgies, J. Zhang, C.M. Papadakis, F. Kremer: *Molecular Order and Dynamics of Nanometric Thin Layers of Poly(styrene-b-1,4-isoprene) Diblock Copolymers*, Macromolecules **46**, 9729-9737 (2013)

P.J. Griffin, A.P. Holt, Y. Wang, V.N. Novikov, J.R. Sangoro, F. Kremer: *Interplay Between Hydrophobic Aggregation and Charge Transport in the Ionic Liquid Methyltrioctylammonium Bis(trifluoromethylsulfonyl)imide*, J. Phys. Chem. B **118**, 783-790 (2013)

M. Solar, E.U. Mapesa, F. Kremer, K. Binder, W. Paul: *The dielectric-relaxation in polymer films: A comprison between experiments and atomistic simulations*, EPL **104**, 66004 (2013)

3.20 Graduations

Doctorate

- Dipl.-Phys. Carolin Wagner
  Kraftspektroskopie mittels optischer Pinzetten zur Untersuchung einzelner Rezeptor/Ligand-Komplexe
  04/2013
- Dipl.-Phys. Olaf Ueberschär
  Mikrofluidische Studien an blanken und DNA-gepfropften Mikrokugeln in verdünnten-DNA-Lösungen
  06/2013

Bachelor

- Lisa Schade
  Struktur-Eigenschaftsbeziehungen von Spinnenseide (Nephila edulis) unter uniaxialem Stress
  09/2013

3.21 Guests

- Dr. Mahdy M. Elmahdy
  Leibniz-Institut für Polymerforschung Dresden e. V., Dresden, Germany
  01 - 09/2013

4

Physics of Interfaces

4.1 Introduction

The department of Physics of Interfaces (Grenzflächenphysik, GFP) is in a transition state since April 2009. From the 14 scientists employed in the group at the end of 2013, 12 were financed as PhD students or post-docs via third party funding. The good situation with respect to third party funding allowed us to successfully contribute to teaching and research within the Institute of Experimental Physics I. Teaching obligations in several main courses of Experimental Physics were taken over by scientists of the group. In April 2013 after nine years of funding by DFG and NWO, the successful cooperation within the Dutch-German International Research Training Group *Diffusion in Porous Materials* (IRTG GK 1055/2) came to an end. Our group continues to contribute with several projects to the DFG Priority Research Programs *Porous Metal-Organic Frameworks* (SPP 1362) and *Porous Media with Defined Pore Structures - Modeling, Application and Synthesis* (SPP 1570).

Dr. R. Valiullin submitted his habilitation thesis. He was awarded the academic degree *Privatdozent* (PD) by our Faculty in June 2013. After finishing their studies within the IRTG *Diffusion in Porous Materials*, Steffen Beckert and Tomas Binder obtained their PhD degrees in 2013, left our group and continued their careers elsewhere.

PD Dr. F. Stallmach

4.2 NMR relaxometry at elevated gas pressures on metal organic frameworks for gas storage applications

C. Horch, F. Stallmach, U. Müller* L. Arnold* S. Marx*, M. Weickert*

*BASF SE, Ludwigshafen, Germany

The storage of natural gas in microporous adsorbents like metal organic frameworks (MOFs) for mobile application will become an important technology [1, 2]. We recently proposed to use low-field NMR relaxometry at elevated methane pressures to characterize the gas storage properties of such microporous materials [2, 3].

In this project [2], transverse (T_2) relaxation time distributions of methane adsorbed in powders and in cylindrical pellets of the MOF-based Basolites Z1200 and Z520 (produced by BASF SE) were measured as function of methane pressure. For the powder of Basolite Z 1200 (MOF ZIF-8) only one peak is observed, see fig. 4.1. The relaxation rates of the gas phase and the adsorbed phase methane obviously averaged due to fast exchange via the external MOF surface. For the Z 1200 pellets, three peaks are visible. Two of them appear at very short relaxation times indicating the adsorbed methane. The strong left shift of these peaks points towards an increased host-guest interaction in the Z 1200 pellets. The gas phase methane is also shifted to shorter relaxation times. This is caused by an exchange with the adsorbed phase via the transport pores and the external surface of the pellets. For more details we refer the reader to ref. [2].

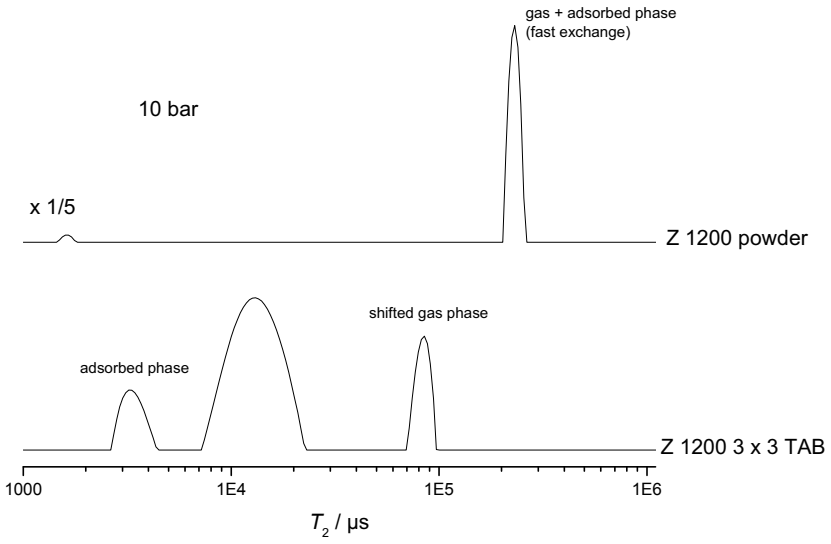

Figure 4.1: Low-field ^{1}H NMR relaxation time distribution (T_2) of methane adsorbed in powder and pellets (3 × 3 TAB) of Basolite Z 1200 at 10 bar gas pressure [2].

[1] U. Müller et al., J. Mater. Chem. **16**, 626 (2006) DOI: 10.1039/b511962f
[2] L. Arnold et al., Chemie Ingenieur Technik **85**, 1726 (2013) DOI: 10.1002/cite.201300093
[3] C. Horch et al., J. Magn. Reson. **240**, 24 (2014) DOI: 10.1016/j.jmr.2014.01.002

4.3 Solid-liquid transitions in confined spaces

D. Kondrashova, R. Valiullin

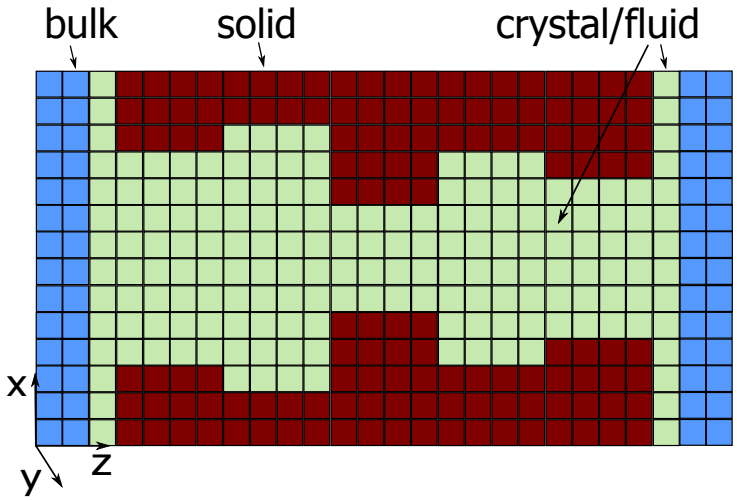

Figure 4.2: Solid-liquid lattice model for studying melting and freezing phenomena in confined spaces with arbitrary pore geometries.

Measurements of confinement-induced effects upon phase transitions are widely used as a method of structural characterization of mesoporous solids [1]. The use of the solid-liquid transitions, potentially yielding high spatial resolution, is however impeded by the lack of theoretical models providing description of solid-liquid equilibria under confinement on a microscopic level. In our work, we develop a lattice solid-fluid model (see Fig. 4.2), which is capable to model freezing and melting behaviors of fluids confined to pores with arbitrary organization of the pore spaces [2]. Using this model, we show in particular that, for fluids with sufficiently large Jackson factors, the Gibbs-Thompson equation can reasonably be used to model the confinement effects upon the the both freezing and melting transition temperatures in pores with cylindrical pore geometry. By introducing a transition dynamics-based criterion for identifying the equilibrium transition, we prove that, in the absence of homogeneous nucleation delay, it coincides with the freezing transition for cylindrical pores with open ends. We demonstrate further that melting-freezing hysteresis, which results from the metastable nature of the melting transition, can be eliminated by closing one of the pore ends. The model is further used to get deeper insight into the freezing and melting phenomena in disordered porous materials.

[1] J. Rouquerol, et al., *Pure Appl. Chem.* 66, 1739 (1994).
[2] D. Kondrashova, R. Valiullin, *Microporous Mesopororous Mat.* 178, 15 (2013).

4.4 An improved NMR probe system for diffusion studies in interface systems

S. Schlayer, F. Stallmach

NMR self-diffusion studies of molecules in interface systems represent one of the key competences of the department [1–3]. For new challenges in materials research, an improved PFG NMR diffusion probe for application of intensive pulsed field gradients was designed. The required additional magnetic flux density is generated by an actively screened gradient-field Helmholtz coil system. Its design was optimized with respect to gradient strength and homogeneity using finite element analysis (see ref. [4]).

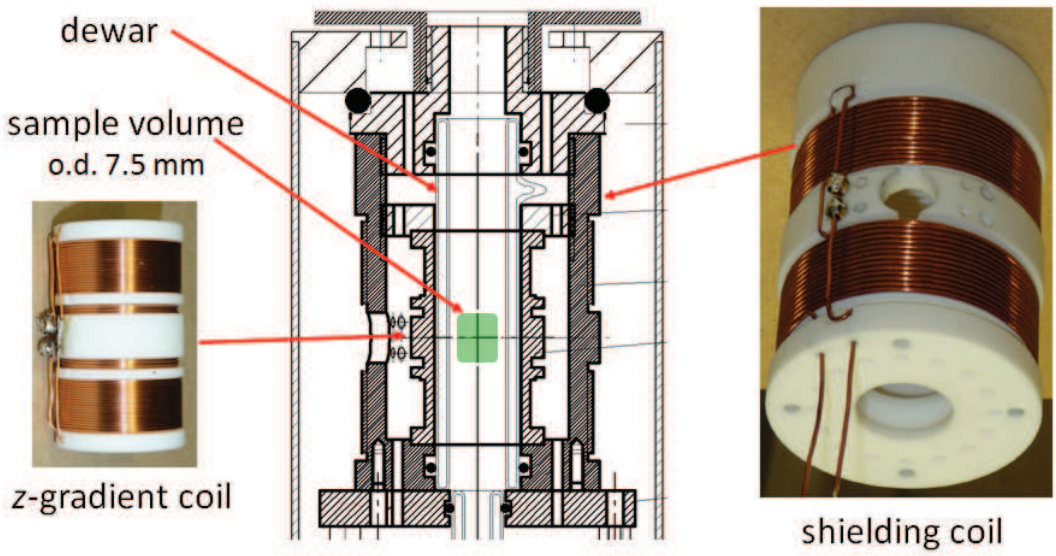

Figure 4.3: Center: Drawing of the top section of the new z-gradient probe for PFG NMR diffusion studies. The rf parts are omitted for clarity. Left and right: Photographs of the main z-gradient and the shielding coils [4].

The gradient coil was constructed using the glass ceramic MACOR as support material. Figure 4.3 shows the main components of the z-gradient NMR probe system. It allows us to vastly switch pulsed field gradients of up to 37 Tm^{-1} with the gradient current amplifier and control system described in ref. [2]. The functionality of the system for studying slow diffusion processes in interface systems was demonstrated by observing isotropic and anisotropic diffusion in aqueous solutions of a highly viscose PEO-PPO-PEO triblock-copolymer and of methane adsorbed in microporous ZIF-8 and ZSM-58. For more details we refer the reader to ref. [4] and to section 4.5.

[1] F. Stallmach, J. Kärger, Adsorption **5**, 117 (1999)
[2] F. Stallmach, P. Galvosas, Annual Rep. on NMR Spectroscopy **61**, 51 (2007)
[3] J. Kärger, D. M. Ruthven, D. Theodorou, *Diffusion in Nanoporous Materials*, Wiley-VCH, Weinheim 2012
[4] S. Schlayer et al., Chemie Ingenieur Technik **85**, 1755 (2013) DOI: 10.1002/cite.201300087

4.5 PFG NMR study of the self-diffusion anisotropy of methane and carbon dioxide in zeolite ZSM-58

T. Splith, A.K. Pusch, F. Stallmach, B.T.L. Bleken*, K.P. Lillerud*

*Center for Materials Science and Nanotechnology, Department of Chemistry, University of Oslo, Norway

^{1}H and ^{13}C PFG NMR studies were performed on methane and carbon dioxide adsorbed as unitary gases and as 1:1 mixtures in the zeolite ZSM-58. The zeolite has a two-dimensionally interconnected pore system with narrow 8-ring windows (free window diameter $d_w \sim 0.4$ nm), which may act as molecular sieve for both gases.

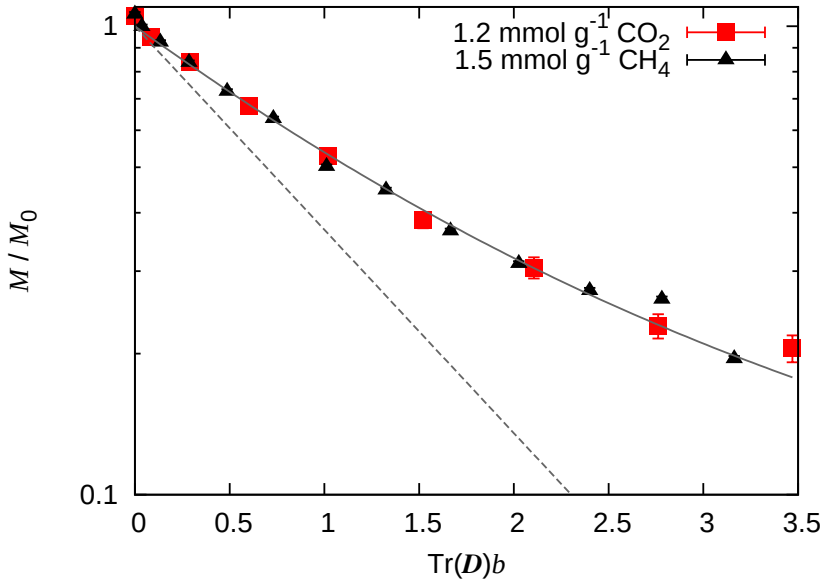

Figure 4.4: ^{1}H and ^{13}C PFG NMR spin echo attenuations of methane and carbon dioxide as a function of Tr (**D**) b [1]. The continuous line represents the attenuation curve for two dimensional diffusion [2] while the dashed line represents the attenuation curve for isotropic diffusion.

Figure 4.4 shows the PFG NMR spin echo attenuations of methane and carbon dioxide as masterplot. Tr (**D**) denotes the trace of the diffusion tensor **D** and b represents the increasing pulsed gradient intensity of the PFG NMR experiment. The spin echo attenuations of both molecules are found to coincide, indicating that the diffusion takes place in the same two-dimensional pore system. However, the diffusion coefficients of methane in zeolite ZSM-58 is about two orders of magnitude smaller than that of the smaller carbon dioxide. This demonstrates the molecular sieving effect of the pore network [1].

The diffusion coefficients for different loadings of methane and carbon dioxide and of binary mixtures of both adsorbates were compared to results obtained by MD [3] and kMC [4] simulations. For more details we refer the reader to ref. [1].

[1] B. T. L. Bleken et al., Microporous and Mesoporous Materials **182**, 25 (2013)
[2] P. T. Callaghan et al., Biophysical Journal **28**, 133 (1979)

[3] R. Krishna et al., Chemical Physics Letters **429** 219 (2006)
[4] S. E. Jee, D. S. Sholl, Journal of the American Chemical Society **131** 7896 (2009)

4.6 Desorption with increasing partial pressure: The remarkable uptake patterns of hexane isomer mixtures in zeolite MFI

T. Titze*, C. Chmelik*, J. Kärger*, J.M. van Baten† R. Krishna†

*University of Leipzig
†University of Amsterdam

Zeolites of type MFI belong to the most important zeolites for industrial applications. In this study their potential for the separation of alkane isomers is highlighted. While linear alkanes such as n-butane (nC4), and n-hexane (nC6) can adsorb at any location within the MFI zeolite pore network, configurational considerations cause the branched isomers iso-butane (iC4), and 2-methylpentane (2MP) to locate preferentially at the channel intersections. For adsorption of nC4/iC4, and nC6/2MP mixtures, Infra-Red Microscopy (IRM) measurements show that the adsorption selectivity favors the linear isomer by about one order of magnitude when the total mixture loading, Θ_t, exceeds 4 molecules per unit cell at which all the intersection sites are fully occupied. The IRM data are in quantitative agreement with Configurational-Bias Monte Carlo (CBMC) simulations (see fig. 4.5) [1]. IRM monitoring of the transient uptake of nC6/2MP mixtures within crystals of MFI exposed to step increases in the pressures show that the configurational entropy also leaves its imprint on the uptake characteristics: For loadings $\Theta_t > 4$ an overall pressure increase in equimolar nC6-2MP mixtures reduces rather than enhances the 2MP uptake, irrespective of its increasing partial pressure! Our IRM studies demonstrate the potential for separating linear and branched alkane isomers by exploiting the synergistic influence of configuration entropy and intersection blocking.

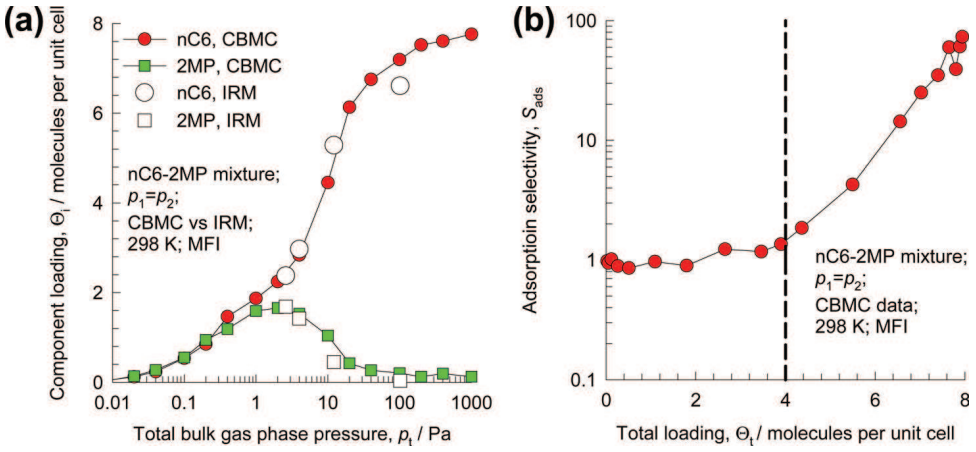

Figure 4.5: (a) IRM vs. CBMC adsorption isotherms for a nC6/2MP mixture with partial pressures $p_1 = p_2$ at 298 K. (b) Calculations of the adsorption selectivity, S_{ads}, for mixture adsorption equilibrium [1].

[1] T. Titze et al., J. Phys. Chem. C **118**, 2660 (2014) DOI: 10.1021/jp412526t

4.7 Guest-Induced Phase Transitions in zeolite MFI

T. Binder*, C. Chmelik*, J. Kärger*, H. Krautscheid*, W. Schmidt†

*University of Leipzig
†MPI für Kohlenforschung, Mülheim

There is currently a great deal of attention in the published literature on guest-induced structural changes in crystalline materials. Phenomena such as gate opening and breathing can be exploited to achieve enhanced separation performance. An industrially important example is that of separation of aromatic mixtures containing benzene and xylenes, using MFI zeolite. Starting with concentrations of about 4 molecules per unit cell, changes in the lattice structure occur. Such transitions can be shown to be associated with a re-distribution of the molecules, resulting in their shift from the pore channel intersections as their preferred locations at low loadings into the channel interiors. The exploration of benzene uptake by microimaging in MFI-type zeolites lead to surprising findings: After an initial period of normal uptake (characterized by guest profiles evolving along the channel system in x and y direction), concentration profiles evolve in the crystal's longitudinal (z) extension (see fig. 4.6) [1]. The propagation of the concentration front can thus not be referred anymore to mass transfer. It must rather be considered as an indication of long-term phase changes in the host-guest system which, accordingly, give also rise to changes in the corresponding equilibrium concentrations of the guest molecules.

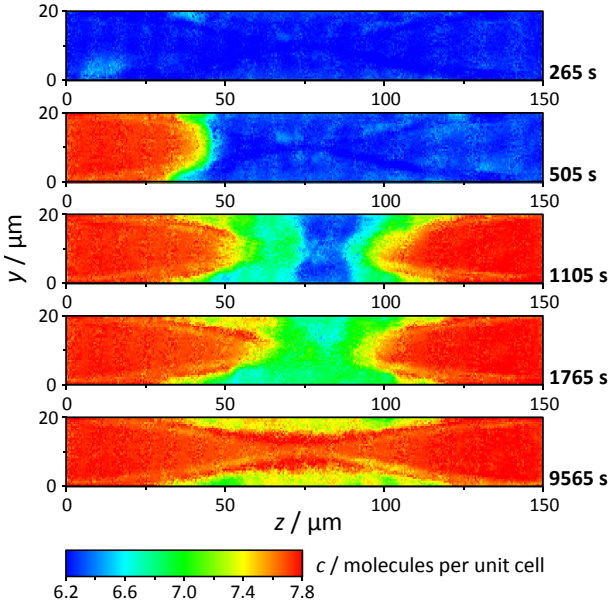

Figure 4.6: Benzene adsorption in MFI-type zeolite (pressure step 0.5 to 1 kPa): Imaging of a guest-induced phase transition. The concentration profiles evolve perpendicular to the channels [1].

[1] J. Kärger et al., Nat. Mater. **13**, 333 (2014) DOI: 10.1038/nmat3917

4.8 Funding

Fundamental Host-Guest Interactions in Porous Metal Organic Frameworks. A Combined Experimental and Theoretical Approach.
PD Dr. F. Stallmach
DFG STA 648/1-2, within SPP 1362 MOFs

Knowledge-based development of supported ZIF membranes for liquid mixture separation by pervaporation
Dr. Ch. Chmelik, Prof. Dr. J. Kärger,
DFG CH 778/1-2, within SPP 1362 MOFs

Separating mixutures of chiral anesthetic gases by modified porous glasses
Dr. Ch. Chmelik
DFG CH 778/2-1 and 778/2-2, within SPP 1570

International Research Training Group Diffusion in porous Materials
PD Dr. F. Stallmach, Prof. Dr. J. Kärger, Dr. R. Valiullin
DFG IRTG GK 1056/2

Driven diffusion in nanoscaled materials
Dr. R. Valiullin
DFG VA 463/5-2

Assessing pore structure via diffusion measurements
Dr. R. Valiullin
DFG VA 463/4-1

Correlating diffusion processes in complementary pore spaces using NMR and theoretical modelling
Prof. Dr. J. Kärger, Prof. Dr. A. Bunde, Dr. R. Valiullin
DFG KA 953/30-1

Measuring Intracrystalline Profiles of Diffusion and Reactions in Zeolites by IR Microscopy
Prof. Dr. J. Kärger, Dr. Ch. Chmelik
DFG KA 953/20-2

NMR relaxation time studies on sediment samples at elevated methane gas pressures
PD Dr. F. Stallmach
Baker Hughes Inc., Houston, USA

NMR-Untersuchungen an verstrangten Katalysatoren
PD Dr. F. Stallmach
BASF SE Ludwigshafen

4.9 Organizational Duties

Frank Stallmach

- deputy chair and member of the steering committee of the MRPM Division of the Groupement AMPERE; conference series "Magnetic Resonance in Porous Media" (MRPM)
- faculty board member, member of several commissions of the faculty board
- referee: Micropor. Mesopor. Mat., Angewandte Chemie, J. Magnetic Resonance, J. Phys. Chem., Chemical Engineering Technology, Surface Geophysics
- Project Reviewer: Research-University of Crete (Greece)

Jörg Kärger
- Membership in the Programme Committee "Diffusion Fundamentals V" (Leipzig, 2013) and "FEZA conference (Leipzig, 2014)
- Editor: Diffusion Fundamentals; Membership in Editorial Boards: Adsorption, Micropor.Mesopor.Mat.
- Referee: Nature, Phys. Rev., Phys. Rev. Lett., Angew. Chem., Europhys. Lett., J. Chem. Phys., J. Phys. Chem., Langmuir, Micropor. Mesopor. Mat., Phys. Chem. Chem. Phys., J. Magn. Res.
- Project Reviewer: Deutsche Forschungsgemeinschaft

Rustem Valiullin
- Editorial Board Online Journal "Diffusion Fundamentals", Editorial Board "Dataset Papers in Physical Chemistry"
- Referee: J. Phys. Chem., J. Am. Chem. Soc., Adsorption, Micropor. Mesopor. Mat., Phys. Rev. B, Phys. Rev. E, Phys. Rev. Lett., Langmuir, Soft Matter, Chem. Soc. Rev.

Christian Chmelik
- Editorial Board Online Journal "Diffusion Fundamentals"
- Co-Guest-Editor of the Open-Access-Journal "Materials"
- Referee: J. Phys. Chem., Micropor. Mesopor. Mat., Ind. Eng. Chem. Res., J. Am. Chem. Soc.

4.10 External Cooperations

Academic

- Delft University, Inst.Chem. Tech., Delft, The Netherlands
  Prof. Kapteijn
- Institut de Recherches sur la Catalyse, CNRS, Villeurbanne, France
  Dr. Jobic
- Max Planck Institut für Kohlenforschung, Mülheim
  Dr. Schmidt, Prof. Schüth
- Ruhr-Universität Bochum, Lehrstuhl für Anorganische Chemie 2, Organometallics and Materials Chemistry
  PD Dr. Schmid
- Universität Hannover, Dept. Phys. Chem., Hannover
  Prof. Caro, Prof. Wiebcke

- Universität Leipzig, Institut für Technische Chemie, Leipzig
  Prof. Einicke, Prof. Gläser, Prof. Enke
- Universität Leipzig, Institut für Anorganische Chemie, Leipzig
  Prof. Krautscheid
- Universität Leipzig, Institut für Medizinische Physik und Biophysik, Leipzig
  Prof. Huster
- TU Dresden, Inst. Biophysik, Dresden
  Prof. Brunner
- Universität Stuttgart, Institut für Technische Chemie, Stuttgart
  Prof. Klemm, Prof. Hunger
- University Athens, Dept Chem. Engn., Athens, Greece
  Prof. Theodorou, Prof. Papadopoulos
- University of Amterdam, Faculty of Science, The Netherlands
  Prof. Krishna
- University of Maine, Dept. Chem. Eng., USA
  Prof. Ruthven
- Victoria University of Wellington, MacDiarmid Institute for Advanced Materials and Nanotechnology, School of Chemical and Physical Sciences, New Zealand
  Dr. Galvosas
- LMU München, Dept. Chemistry and Biochemistry
  Prof. Bräuchle, Dr. C. Jung
- University of Massachusetts, Dept. of Chemical Engineering, Amherst, USA
  Prof. P.A. Monson
- Northwestern University, Dept. of Chem. Eng., Evanston, USA
  Prof. Snurr
- University of Florida, Dept. of Chem. Eng., Gainesville (FL), USA
  Prof. Vasenkov
- University College London, UK
  Prof. Coppens
- Otto-von-Guericke-Universität Magdeburg, Institut für Verfahrenstechnik, Magdeburg
  Prof. Seidel-Morgenstern

Industry

- BASF SE, Ludwigshafen, Germany
  Dr. U. Müller
- Baker Hughes INTEQ GmbH, Celle, Germany
  Dr. Th. Kruspe, Dr. H. Thern
- SINTEF, Oslo, Norway
  Prof. Stöcker
- Clariant, Berlin, Germany
  Dr. Tissler, Dr. Tufar, Dr. Lutz, Dr. Rakoczy

4.11 Publications

Journals

S. Beckert, F. Stallmach, H. Toufar, D. Freude, J. Kärger, J. Haase: *Tracing Water and Cation Diffusion in Hydrated Zeolites of Type Li-LSX by Pulsed Field Gradient NMR*, J. Phys. Chem. C **117**, 24866-24872 (2013)

C. Rajappa, C. Krause, B.J. Borah, Z. Adem, P. Galvosas, J. Kärger, S. Yashonath: *Diffusion of pentane isomers in faujasite-type zeolites: NMR and molecular dynamics study*, Microporous and Mesoporous Materials **171**, 58-64 (2013)

L. Arnold, G. Averlant, S. Marx, M. Weickert, U. Müller, J. Mertel, C. Horch, M. Peksa, F. Stallmach: *Metal Organic Frameworks for Natural Gas Storage in Vehicles*, Chemie Ingenieur Technik **85**/11, 1726-1733 (2013)

T. Binder, C. Chmelik, J. Kärger, A. Martinez-Joaristi, J. Gascon, F. Kapteijn, D. Ruthven: *A Diffusion Study of Small Hydrocarbons in DDR Zeolites by Micro-Imaging*, Microporous and Mesoporous Materials **180**, 219-228 (2013)

C. Chmelik, A. Mundstock, P.D.C. Dietzel, J. Caro: *Idiosyncrasies of Co_2(dhtp): In situ-annealing by methanol*, Microporous and Mesoporous Materials **183**, 117-123 (2013)

J. Kullmann, C. Küster, T. Titze, C. Chmelik, R. Gläser, D. Enke, L. Prager: *Potenzial des IR Micro-Imaging zur In-situ-Untersuchung chemischer Reaktionen in nanoporösen Katalysatoren*, Chemie Ingenieur Technik **85**/11, 1-7 (2013)

T. Chokbunpiam, R. Chanajaree, O.Saengsawang, S. Reimann, C. Chmelik, S. Fritzsche, J. Caro, T. Remsungnen, S. Hannongbua: *The importance of lattice flexibilityfor the migration of ethane in ZIF-8: Molecular dynamics simulations*, Microporous and Mesoporous Materials **174**, 126-134 (2013)

P. Zeigermann, J. Kärger, R. Valiullin: *Diffusion in microporous materials with embedded mesoporosities*, Microporous Mesoporous Mat. **178**, 84-89 (2013)

R. Valiullin: *Diffusion in nanoporous host systems*, in Annual reports on NMR spectroscopy, A.G. Webb, Editor., Academic Press: Burlington. **79**, 23-72 (2013)

D. Kondrashova, R. Valiullin: *Improving structural analysis of disordered mesoporous materials using nmr cryoporometry*, Microporous Mesoporous Mat., **178**, 15-19 (2013)

W.K. Kipnusu, W. Kossack, C. Iacob, P. Zeigermann, M. Jasiurkowska, J.R. Sangoro, R. Valiullin, F. Kremer: *The interplay between inter- and intra-molecular dynamics in a series of alkylcitrates*, Soft Matter **9**, 4681-4686 (2013)

J. Kärger, R. Valiullin: *Mass transfer in mesoporous materials: The benefit of microscopic diffusion measurement*, Chem. Soc. Rev., **42**, 4172 - 4197 (2013)

J. Kärger, C. Chmelik, R. Valiullin: *Die innere Größe macht's*, Physik Journal **12**, 39-45 (2013)

W.-D. Einicke, D. Enke, M. Dvoyashkin, R. Valiullin, R. Gläser: *The mechanism of pseudomorphic transformation of spherical silica gel into mcm-41 studied by pfg nmr diffusometry*, Materials **6**, 3688-3709 (2013)

M. Bonilla, T. Titze, F. Schmidt, D. Mehlhorn, C. Chmelik, R. Valiullin, S. Bhatia, S. Kaskel, R. Ryoo, J. Kärger: *Diffusion study by IR micro-imaging of molecular uptake and release on mesoporous zeolites of structure type CHA and LTA*, Materials **6**, 2662-2688 (2013)

W.-D. Einicke, H. Uhlig, D. Enke, R. Gläser, Ch. Reichenbach, S.G. Ebbinghaus: *Synthesis of hierarchical micro/mesoporous Y-zeolites by pseudomorphic Transformation*, Colloids and Surfaces A: Physicochem. Eng. Aspects **437**, 108-112 (2013)

C. Reichenbach, D. Enke, J. Möllmer, D. Klank, M. Klauck, G. Kalies: *Slow Gas Uptake and Low Pressure Hysteresis in Nanoporus Glasses: The Influence of Equilibration Time and Particle Size*, Microporous and Mesoporous Materials **181**, 68-73 (2013)

P. Bottke, D. Freude, M. Wilkening: *Ultraslow Li Exchange Processes in Diamagnetic Li_2ZrO_3 As Monitored by EXSY NMR*, Journal of Physical Chemistry C **117**, 8114-8119 (2013)

S. Schlayer, F. Stallmach, T. Splith, A.-K. Pusch, F. Pielenz, M. Peksa: *Konstruktion und Test eines Gradientensystems für NMR-Diffusionsuntersuchungen in Grenzflächensystemen*, Chemie Ingenieur Technik **85**/11, 1755-1760 (2013)

B.-T. L. Bleken, K. P. Lillerud, T. Splith, A.-K. Pusch, F. Stallmach: *PFG NMR diffusion measurements of CH_4 and CO_2 through large ZSM-58-crystals*, Microporous and Mesoporous Materials **182**, 25-31 (2013)

S. Beckert, M. Gratz, J. Kullmann, D. Enke, F. Stallmach: *Concentration dependent self-diffusion of water in aqueous solutions of lithium chloride confined to porous glasses*, Appl. Magn. Reson. **44**, 827-836 (2013)

D. Freude, S. Beckert, F. Stallmach, R. Kurzhals, D. Täschner, H. Toufar, J. Kärger, J. Haase: *Ion and water mobility in hydrated Li-LSX zeolite studied by 1H, 6Li and 7Li NMR spectroscopy and diffusometry*, Microporous and Mesoporous Materials **172**, 174-181 (2013)

P. Zeigermann, R. Valiullin: *Transport properties of gas-expanded liquids in bulk and under confinement*, J. Supercrit. Fluid **75** 43 - 47 (2013)

Books

none

Talks

F. Stallmach: *Rotationsmechanik*, 130. öffentliche Sonntagsvorlesung der physikalischen Institute, University of Leipzig, Leipzig, Germany, January 13, 2013

J. Kärger: *Physik des Fahrrades*, Experimental-Vortrag im Rahmen *Physikolympiade Leipzig der Klassenstufen 6 bis 10*, University of Leipzig, Leipzig, Germany, February 27, 2013

R. Valiullin: *Transport in hierarchical micro-mesoporous materials*, 25. Deutsche Zeolith Tagung, Hamburg, Germany, March 6 - 8, 2013

F. Hibbe, A. Lauerer, J. Kärger, C. Chmelik, J.M. van Baten, R. Krishna, V.R.R. Marthala, J. Weitkamp: *Enhancing diffusion selectivities in FER-type structures by molecular traffic control*, 25. Deutsche Zeolith-Tagung, Hamburg, Germany, March 6 - 8, 2013

J. Kärger: *Stofftransport in Nanoporen: Paradigmenwechsel durch neue Experimente*, Plenarvortrag at *Sächsischen Akademie der Wissenschaften zu Leipzig*, March 8, 2013

J. Kärger: *Potentials and benefit of microscopic techniques of diffusion measurement in nanoporous materials*, 3rd ENMIX Workshop *Zeolites, MOFs, and Porous Carbons - Advanced Preparation and Innovative Applications*, Leibniz University Hannover, Hannover, March 25 - 27, 2013

M. Peksa: *Rotational and translational mobility of adsorbed CO_2 in MOF Zn2(bdc)2dabco*, 16th IRTG Workshop *Diffusion in porous Materials*, TU Delft, Delft, Netherlands, April 2 - 4, 2013

C. Horch: *Low-Field NMR porosimetry at elevated gas pressures*, 16th IRTG Workshop *Diffusion in porous Materials*, TU Delft, Delft, Netherlands, April 2 - 4, 2013

A. Lauerer: *IR Micro-Imaging of mesoporous silicon as a model system for the investigation of hysteresis phenomena*, 16th IRTG Workshop *Diffusion in porous Materials*, TU Delft, Delft, Netherlands, April 2 - 4, 2013

M. Peksa, S. Bureekaew, R. Schmid, J. Lang, F. Stallmach: *13C NMR study of CO_2 mobility in microporous metal-organic framework Zn2(bdc)2dabco*, 28th Central European NMR meeting, Valtice, Czech Republic, April 22 - 24, 2013

J. Kärger: *Potentials and Benefit of Microscopic Techniques of Diffusion Measurement in Nanoporous Materials* ExxonMobil Research, Clinton, USA - NJ, May 17, 2013

R. Valiullin: *Sorption behavior in ink-bottle mesoporous silicon*, Fundamentals of Adsorption, Baltimore, USA, May 19-24, 2013

R. Valiullin: *Application of DMFT to linear pores with ink-bottle and side stream pore structures*, Fundamentals of Adsorption, Baltimore, USA, May 19-24, 2013

J. Kärger: *Exploring the Hierarchy of Transport Phenomena during Adsorption in Hierarchical Pore Networks by Microscopic Diffusion Measurement*, Fundamentals of Adsorption 11, Baltimore, USA - MD, May 19 - 24, 2013

T. Binder, F. Hibbe, C. Chmelik, J. Kärger, F. Kapteijn, D.M. Ruthven: *Investigation of Single-component and Mixture Adsorption in Nanoporous Materials by Means of Micro-imaging*, Fundamentals of Adsorption 11, Baltimore, USA - MD, May 20 - 24, 2013

J. Kärger: *The Beauty of Diffusion in Nanoporous Materials: Impact of Phases and Phase Transitions*, Quantachrome Instruments, Boynton Beach, USA - FL, May 15, 2013

J. Kärger: *Potentials and Benefit of Microscopic Techniques of Diffusion Measurement in Nanoporous Materials*, University of California, Santa Barbara, USA - CA, May 29, 2013

J. Kärger: *In-depth Study of Surface Resistances in Nanoporous Materials by Microscopic Diffusion Measurement*, 17th International Zeolite Conference, Moscow, Russia, July 7 - 12, 2013

F. Stallmach, Ch Chmelik: *Guest diffusivity and host flexibility - Experimental studies of structure-mobility relations in MOFs*, University Dresden, Dresden, Germany, August 21, 2013

R. Valiullin: *Transport properties of mesoporous zeolites: Towards intelligent structure design*, 1st International Symposium on Mesoporous Zeolites, Indianapolis, USA, September 8-12, 2013

J. Kärger: *Exploring Mass Transfer in DDR Single Crystals by Micro-Imaging*, 63rd Canadian Chemical Engineering Conference, Fredericton, Canada, October 21, 2013

J. Kärger: *Diffusion in Porous Materials: Insights, Miracles and Surprises*, University of Maine, Bangor, USA - ME, October 25, 2013

F. Stallmach: *NMR porosimetry and diffusometry in porous materials*, Charles University Prague, Prague, Czech Republic, November 18, 2013

Posters

A.-K. Pusch, T. Splith, S. Schlayer and F. Stallmach: *Single component and binary mixture self-diffusion studies of carbon dioxide and methane in ZIF-8 at elevated pressures* , 25. Deutsche Zeolith Tagung, Hamburg, Germany, March 05 - 08, 2013

A. Shakhov, C. Reichenbach, D. Enke and R. Valiullin: *Structural and transport properties of nanoporous glasses with tuned micro- and mesoporosity*, 25. Deutsche Zeolith Tagung, Hamburg, Germany, March 05 - 08, 2013

T. Titze, C. Chmelik, D. Enke, R. Gläser, J. Kullmann, J. Kärger, L. Prager, J. Weitkamp: *Exploring intra-particle diffusion and reaction by IR micro-imaging*, 25. Deutsche Zeolith Tagung, Hamburg, Germany, March 05 - 08, 2013

A. Lauerer, P. Zeigermann, J. Lenzner, C. Chmelik, R. Valiullin, J. Kärger: *IR Micro-Imaging of mesoporous silicon as a model system for the investigation of hysteresis phenomena*, 25. Deutsche Zeolith-Tagung, Hamburg, Germany, March 5 - 8, 2013

D. Kondrashova, R. Valiullin: *Solid-Liquid Equilibria in Disordered Mesoporous Solids*, 11th International Conference on Fundamentals of Adsorption, Baltimore, MD, USA, May 19-24, 2013

T. Binder, F. Hibbe, C. Chmelik, J. Kärger, A. Martinez-Joaristi, F. Kapteijn, D.M. Ruthven: *Intra-Crystalline diffusion in ZSM-58: An interference microscopy study*, 3rd ENMIX Workshop, Hannover, Germany, March 25 - 27, 2013

M. Peksa, S. Bureekaew, J. Lang, F. Stallmach, R. Schmid: *Mobility of CO2 in the MOF Zn2(bdc)2dabco*, EUROMAR 2013, Hersonissos, Greece, June 30 - July 5, 2013.

P. Zeigermann, D. Mehlhorn, J. Kärger, R. Valiullin: *Correlating phase ptate and transport in hierarchical mesoporous materials*, 11th International Conference on Fundamentals of Adsorption, Baltimore, MD, USA, May 19-24, 2013

C. Chmelik, F. Hibbe, A. Lauerer, J. Kärger, J.M. van Baten, R. Krishna, V.R.R. Marthala, J. Weitkamp: *Enhancing diffusion selectivities in FER-type structures by molecular traffic control*, 17th International Zeolite Conference, Moscow, Russia, July 7 - 12, 2013

T. Titze, C. Chmelik, D. Enke, R. Gläser, J. Kullmann, J. Kärger, L. Prager, J. Weitkamp: *Exploring diffusion and reaction in nanoporous catalysts by IR micro-imaging*, 17th International Zeolite Conference, Moscow, Russia, July 07 - 12, 2013

A. Lauerer, P. Zeigermann, J. Lenzner, C. Chmelik, R. Valiullin, J. Kärger: *IR microimaging of mesoporous silicon as a model system for the investigation of hysteresis phenomena*, IZC-17, Moscow, Russia, July 7 - 12, 2013.

P. Zeigermann, D. Mehlhorn, J. Kärger, R. Valiullin: *Correlating phase state and transport in hierarchical mesoporous materials*, Diffusion Fundamentals V, Leipzig, Germany, August 25 - 28, 2013

F. Feil, S. Naumov, J. Michaelis, R. Valiullin, D. Enke, Ch. Bräuchle, J. Kärger: *Single-particle and ensemble diffusivities - Test of ergodicity*, Diffusion Fundamentals V, Leipzig, Germany, August 25 - 28, 2013.

D. Kondrashova, P. Zeigermann, R. Valiullin: *Propagation of solid-liquid interfaces under disordered confinements*, Diffusion Fundamentals V, Leipzig, Germany, August 25 - 28, 2013

M. Peksa, S. Bureekaew, J. Lang, F. Stallmach, R. Schmid: *On the nature of adsorption sites for CO2 in MOF Zn2(bdc)2dabco*, Diffusion Fundamentals V, Leipzig, Germany, August 26 - 28, 2013.

A. Shakhov, J. Kärger and R. Valiullin: *Tracing Molecular Propagation in Dextran Solution by Pulsed Field Gradient NMR*, Diffusion Fundamentals V, Leipzig, Germany, August 25 - 28, 2013

T. Binder, C. Chmelik, J. Kärger, D.M. Ruthven: *Mass-transfer of binary mixtures in DDR single crystals*, Diffusion Fundamentals V, Leipzig, Germany, August 26 - 28, 2013., Leipzig, Germany, August 25 - 28, 2013

C. Chmelik, F. Hibbe, A. Lauerer, J. Kärger, J.M. van Baten, R. Krishna, V.R.R. Marthala, J. Weitkamp: *Enhancing diffusion selectivities in FER-type structures by molecular traffic control*, Diffusion Fundamentals V, Leipzig, Germany, August 26 - 28, 2013.

S. Fritzsche, P. Schierz, W. Janke, S. Hannongbua, O. Saengsawang, C. Chmelik: *Diffusion investigation for hydrogen guest molecules in an adapted force field for ZIF-11*, Diffusion Fundamentals V, Leipzig, Germany, August 26 - 28, 2013.

T. Chokbunpiam, R. Chanajaree, O. Saengsawang, S. Fritzsche, C. Chmelik, W. Janke, J. Caro, T. Remsungnen, S. Hannongbua: *Diffusion and adsorption of N2 and C2H6 in ZIF-8 MD and MC simulations*, Diffusion Fundamentals V, Leipzig, Germany, August 26 - 28, 2013.

T. Titze, C. Chmelik, D. Enke, R. Gläser, J. Kullmann, J. Kärger, L. Prager, J. Weitkamp: *Exploring diffusion and reaction in nanoporous catalysts by IR micro-imaging*, Diffusion Fundamentals V, Leipzig, Germany, August 26 - 28, 2013.

A. Lauerer, P. Zeigermann, J. Lenzner, C. Chmelik, R. Valiullin, J. Kärger: *IR Micro-Imaging of mesoporous silicon as a model system for the investigation of hysteresis phenomena*, Diffusion Fundamentals V, Leipzig, Germany, August 26 - 28, 2013.

M. Peksa, S. Bureekaew, J. Lang, F. Stallmach, R. Schmid: *On the ability of Zn-BDC-DABCO to maintain orientation of fast diffusing CO2 molecules*, International MOF symposium, Dresden, Germany, September 16 - 17, 2013

P. Schierz, S. Fritzsche, W. Janke, S. Hannongbua, O. Saengsawang, C. Chmelik: *Adsorption and diffusion of hydrogen guest molecules in the Metal-OrganicFramework ZIF-11*, International MOF symposium, Dresden, Germany, September 16 - 17, 2013

T. Chokbunpiam, R. Chanajaree, O. Saengsawang, S. Fritzsche, C. Chmelik, W. Janke, J. Caro, T. Remsungnen, S. Hannongbua: *MD simulations of self-diffusion of several small guest molecules in ZIF-8*, 24th International MOF symposium, Dresden, Germany, September 16 - 17, 2013

4.12 Graduations

Habilitation

- Rustem Valiullin
  Translational Dynamics and Phase Transitions under Spatial Confinements
  June 2013

Doctorate

- Steffen Beckert
  NMR-Untersuchungen zur kollektiven Diffusion von Wasser und gelösten Ionen: Die dynamische Hydratationszahl
  May 2013
- Tomas Binder
  Mass Transport in Nanoporous Materials: New Insights from Micro-Imaging by Interference Microscopy
  October 2013

Master

- Hiralal Gadaili
  Nuclear magnetic resonance cryoporometry using ionic liquids
  October 2013
- Tobias Splith
  Strukturdirigierte Diffusion im Zeolith ZSM-58 und in der flexiblen metall-organischen Gerüstverbindung DMOF-1
  December 2013

Bachelor

- Sebastian Merker
  Optimierung der Magnetfelder für einen Inside-Out NMR-Sensor im Jackson-Design mittels Finiter Elemente Simulationen
  February 2013
- Michael Rippert
  Untersuchungen zum Sorptionsverhalten organischer Gase in meso- und mikroporösen Stoffen mittels Infrarotspektroskopie
  October 2013

4.13 Guests

- J. Cousin
  Vrije Universiteit Brussel, Belgium
  October 08 - 10, 2013
- Dr. P. Galvosas
  Victoria University of Wellington, New Zealand
  September 09 - 11, 2013
- Prof. N. Fatkullin
  Kazan Federal University, Russia
  August 22, 2013
- Dr. H. Li
  Karlsruher Institut für Technologie (KIT), Germany
  July 07, 2013
- Prof. A. Bunde
  University Gießen, Germany
  June 25, 2013
- Dr. U. Müller and Dr. A. N. Parvulescu
  BASF SE, Germany
  February 26, 2013
- Prof. S. Vasenkov
  University of Florida, Gainesville, USA
  January 28 - 31, 2013

5

Soft Matter Physics

5.1 Introduction

Our research is dedicated to the broad field of biological physics. In particular, our work focuses on the study of mechanical properties and behavior of polymer networks as well as whole biological cells. It is our primary objective to investigate the underlying physical mechanisms responsible for the observed active and passive behavior of biological soft matter. Special attention is given to the exploration of cancer as well as neuronal growth. A wide range of sophisticated experimental techniques are applied, such as optical instruments, scanning force microscopes, traction force microscopy, rheometer and many others. The optical stretcher, a laser-based technique for contact-free measurement of cell mechanics, is one of the major working horses of our group. Several research projects within our group investigate the function of biological cells from nanometer to macroscopic length scales. The aim is to understand the underlying mechanisms and forces that are required for cell motion and function such as proliferation. Moreover, how and to what extent can cellular mechanisms change during malignant transformation and how these changes can be described from a physical perspective, is the most important research aim. To this end, the group works in close collaboration with different physics, biology and medicine groups all over the world, such as the National Cancer Institute (NCI), USA and the Institute Curie, Paris.

Josef A. Käs

5.2 Thermorheology of living cells - impact of temperature variations on cell mechanics

T.R. Kießling, R. Stange, J.A. Käs, A.W. Fritsch

The mechanical properties of living cells are widely considered to play a fundamental role for many physiologically relevant processes. Therefore, a variety of studies have investigated the response of cellular matter to external forces, aiming on a deeper understanding of the origin of the mechanical properties of single cells. Those studies, are often conducted using optical traps, particularly the so-called optical stretcher has been continuously developed and employed in our laboratory to measure the response of whole living cells to optical forces. In this study, the impact of sudden temperature variations (as caused by the absorption of laser light in optical traps) on the deformability of whole living cells has been investigated for the first time. We observe a significant systematic shift of creep compliance curves, J(t), for single living breast epithelial cells upon temperature changes. Using the optical stretcher, temperature jumps can be induced within milliseconds, while simultaneously measuring the mechanical response of whole cells to optical force. The cellular mechanical response was found to differ between sudden temperature changes compared to slow, long-term changes implying adaptation of cytoskeletal structure. Surprisingly, creep curves of living cells obtained at different temperatures strongly suggest the applicability of the time temperature superposition (TTS) principle, a scaling concept known from rheological measurements on simple polymers. Based on the empirical observation that material functions (e.g. creep compliance) show similar shapes when measured at different temperatures, creep compliance curves recorded at different temperatures can be rescaled to overlap, resulting in a single master curve. The said curve is frequently used to extend the experimentally accessible time or frequency range, whereas the scaling factors provide an insight into underlying molecular dynamics. We propose TTS, a widely used concept in polymer physics, as the leading term to rationalize the observed temperature dependence of the creep compliance J(t) of cells: for sudden temperature changes that do not exceed a critical temperature T_{crit}, we observe thermorheologically simple behavior, meaning that J(t,T) superpose by only a rescaling of the time axis. However, temperature changes on timescales of several minutes and hours or above T_{crit} demand for additional scaling of the modulus axis, indicating delayed adaptation of cellular matter to temperature changes. As being a fundamental physical quantity for viscoelastic deformation, temperature is a vital parameter which is worthwhile being further investigated in cell mechanical measurements. While temperature, undoubtedly, is used as a control parameter in many physical fields, temperature-related studies are rather underrepresented in biophysical research, particularly cell mechanical research. Thermorheological measurements such as those presented in this study could significantly contribute to a better understanding of the origin and contribution of stress relaxation processes in living cells.

[1] T. R. Kießling et al.: New Journal of Physics **15**, 045026 (2013)

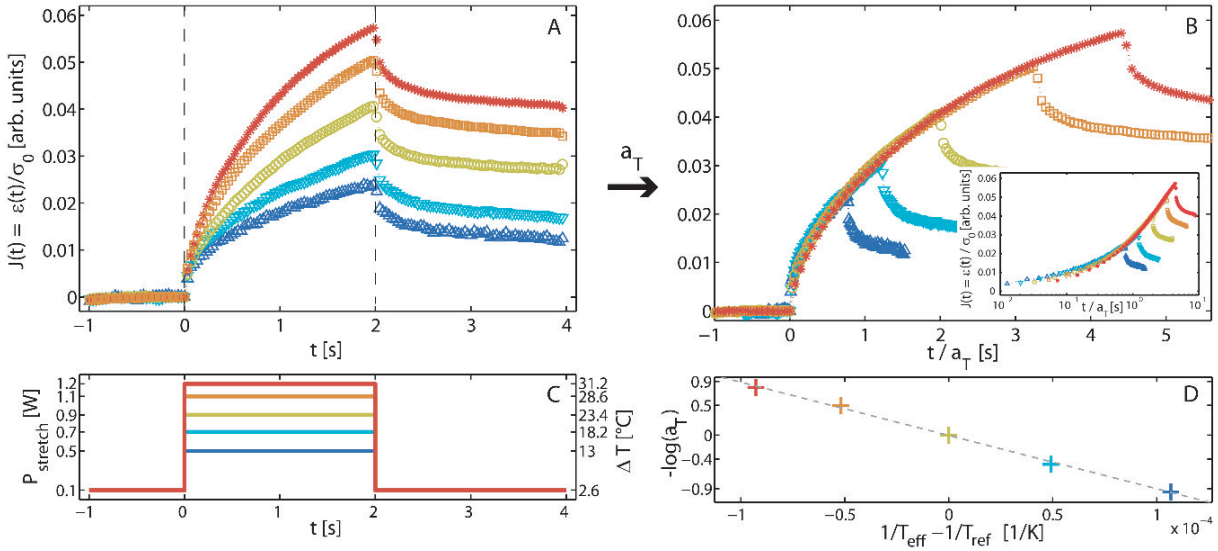

Figure 5.1: Mean creep compliance curves (J(t)) of single living breast epithelial cells measured at different temperatures (A/C). By individually rescaling of the time axis, curves obtained at different temperatures can be superposed to a master curve (B). The scaling factors, a_T, surprisingly show Arrhenius behavior (D).

5.3 Analysis of multiple physical parameters for mechanical phenotyping of living cells

T.R. Kießling, M. Herrera*, K.D. Nnetu, E.M. Balzer†, M. Girvan*, A.W. Fritsch, S.S. Martin†, J.A. Käs, W. Losert*

*Dept. of Physics, IPST, and IREAP, University of Maryland, College Park, USA
†Medical School, University of Maryland, Baltimore, USA

Since the cytoskeleton is known to regulate many cell functions, an increasing amount of effort to characterize cells by their mechanical properties has occurred. Despite the structural complexity and dynamics of the multicomponent cytoskeleton, mechanical measurements on single cells are often fit to simple models with two to three parameters, and those parameters are recorded and reported. However, different simple models are likely needed to capture the distinct mechanical cell states, and additional parameters may be needed to capture the ability of cells to actively deform. In this study, we presented a new approach is to capture a much larger set of possibly redundant parameters from cells' mechanical measurement using multiple rheological models as well as dynamic deformation and image data. Principal component analysis and network-based approaches are used to group parameters to reduce redundancies and develop robust biomechanical phenotyping. Network representation of parameters allows for visual exploration of cells' complex mechanical system, and highlights unexpected connections between parameters. To demonstrate that our biomechanical phenotyping approach can detect subtle mechanical differences, we used a Microfluidic Optical Cell Stretcher to mechanically stretch circulating human breast tumor cells bearing genetically-engineered alterations in c-src tyrosine kinase activation, which is known to influence reattachment and invasion during metastasis. Just by analyzing the mutual

relation between 47 parameters extracted individually for single creep experiments, we can identify differences between cell lines with only a minimum set of assumptions. First, we find that intensity and intensity fluctuations from phase contrast images are good discriminators among the 5 studied cell lines, which show variations in src expression and different tendencies to form microtentacles. Second, network-based grouping of parameters indicate, that creep deformation and relaxation are dominated by two different relaxation processes. Third, surprisingly, the propensity to form microtentacles has only a small impact on whole cell deformability, implying complex (counteracting) effects in the architecture of the cytoskeleton of genetically altered cells. We believe that systematic data exploration approaches, such as the network analysis presented here, will become increasingly important for the analysis of large biomechanical datasets. Visualization of the network provides an excellent tool for intuitive exploration of biophysical measures and for the development of realistic mechanical models. Including complex connections between parameters will ultimately be important for the identification of characteristic signatures of patient cells. Whether for differentiation between malignant and non-malignant cells, or for quantification of the metastatic competence of primary cell samples, one inescapably faces greater heterogeneities in cell types and behaviors in comparison to cell cultures. Therefore, the ability to classify cells by multiple parameters simultaneously can accelerate the identification of characteristic parameters and the definition of biomechanical phenotypes. Moreover, network analysis tools are extensively used in systems biology approaches. Thus, a representation of biomechanical data in this framework will help to establish the as yet missing link between biomechanics and molecular cell biology.

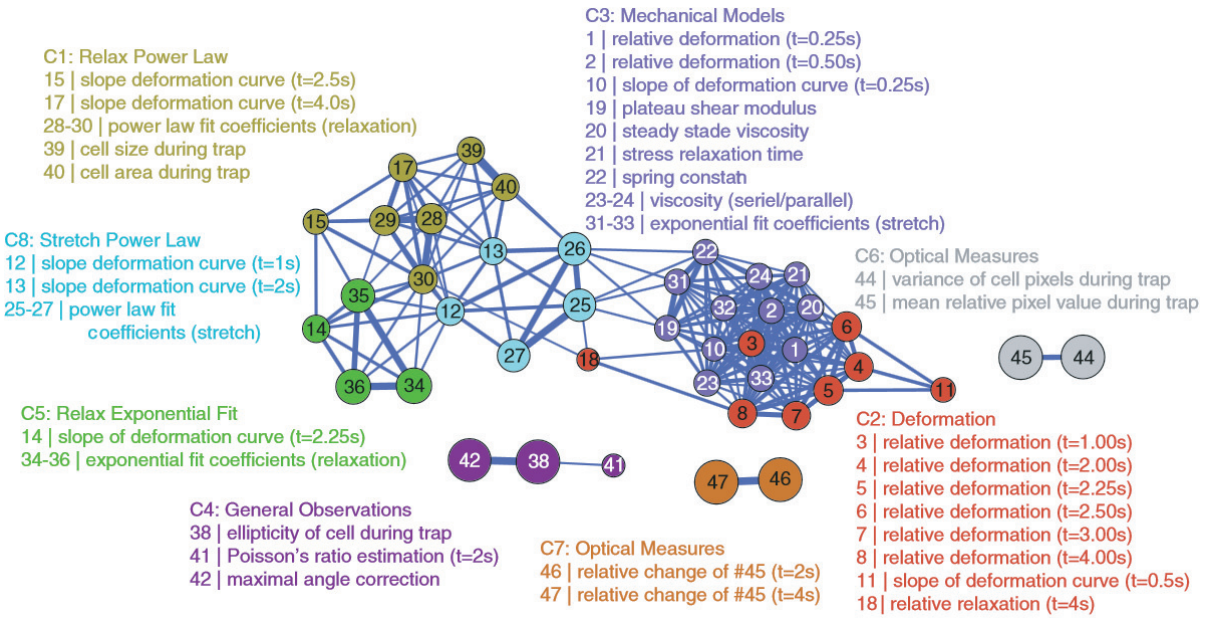

Figure 5.2: Parameter network of rheological parameters derived from single cell experiments. Each node represents one of 47 parameters, extracted for each measured cell. The mutual relations between parameters are represented by the structure of the network, allowing for widely unbiased characterization of cell samples.

[1] T. R. Kießling et al.: European Biophysics Journal **42**, 383-394 (2013)

5.4 Keratins significantly contribute to cell stiffness and impact invasive behavior

K. Seltmann*, A.W. Fritsch, J.A. Käs, T.M. Magin*

*Translationszentrum für Regenerative Medizin, Institut für Biologie

Cell motility and cell shape adaptations are crucial during wound healing, inflammation and malignant progression. These processes require the remodeling of the keratin cytoskeleton, to facilitate cell-cell and matrix adhesion. However, the role of keratins for biomechanical properties and invasion of epithelial cells are only partially understood. Here, we address this issue in murine keratinocytes lacking all keratins upon genome engineering. In contrast to prediction, keratin-free cells show about 60% higher cell deformability even for small deformations (figure 5.3). This is compared to less pronounced softening effects for actin depolymerization induced via latrunculin A. To relate these findings with functional consequences, we use invasion and three-dimensional growth assays. These reveal higher invasiveness of keratin-free cells. Re-expression of a small amount of the keratin pair K5/K14 in keratin-free cells reverses the above phenotype for the invasion but does not with respect to cell deformability. Our data shows a novel role of keratins as major player of cell stiffness influencing invasion with implications for epidermal homeostasis and pathogenesis. This study supports the view that downregulation of keratins observed during epithelial-mesenchymal transition directly contributes to the migratory and invasive behavior of tumor cells. In summary, we show for the first time, using the optical stretcher, that the keratin cytoskeleton is a major contributor to cell stiffness and decreases cell invasiveness. Based on the findings reported here and elsewhere we suggest that by providing cell stiffness and maintaining desmosome-dependent intercellular adhesion, keratins assist in the maintenance of the epithelial phenotype and protect epithelial cells against acquisition of a metastatic phenotype.

[1] K. Seltmann et al.: PNAS **110**, Issue 46, 18507-18512 (2013)

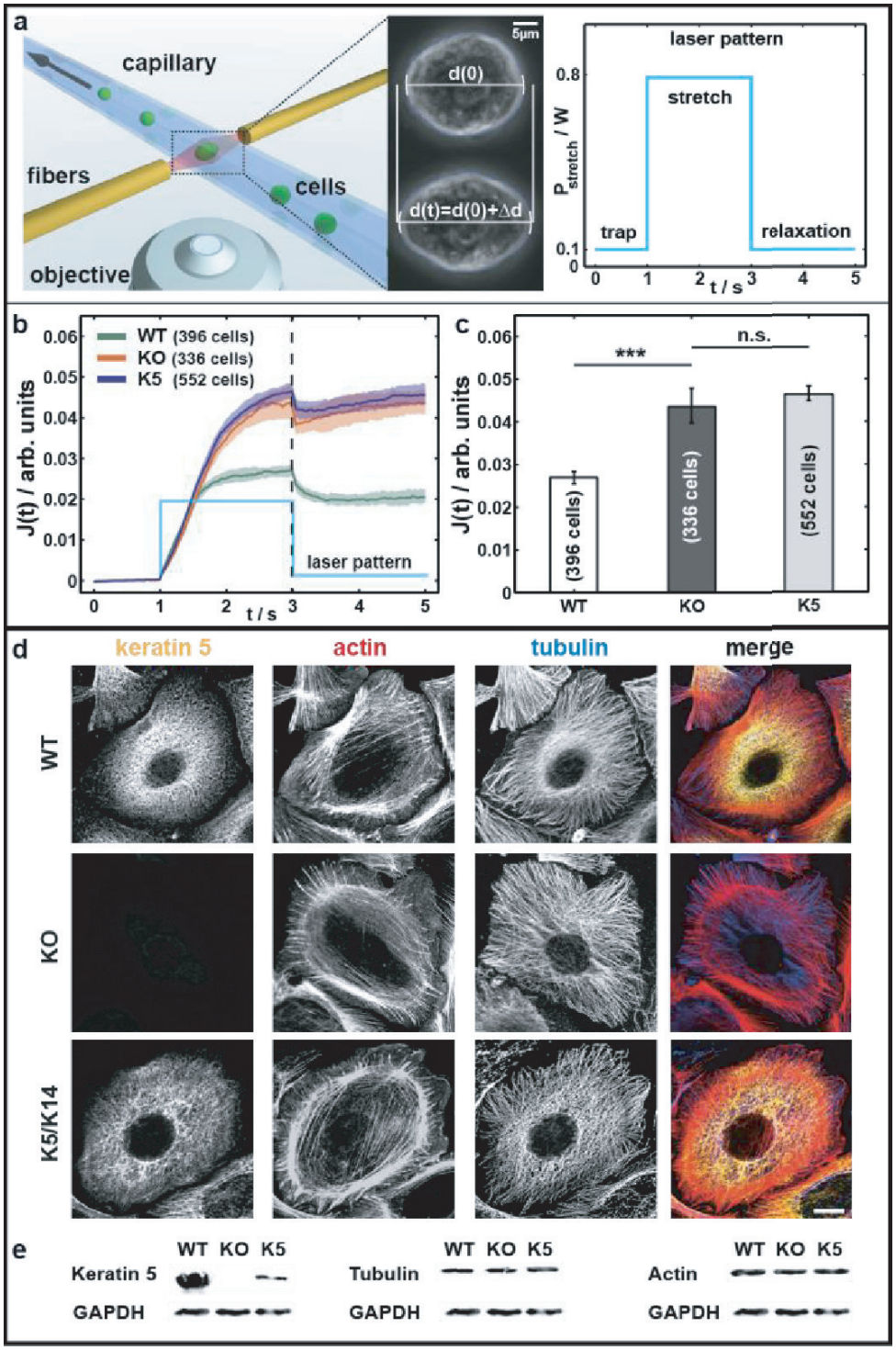

Figure 5.3: Keratins are major determinants of cell stiffness. **a:** Left: schematic of the μOS setup showing a strongly deforming KO cell treated with latA. Right: laser-pattern used for all μOS measurements. **b, c:** Data sets from optical stretcher measurements of keratin-free and K5/K14 re-expressing cells compared to WT cells. Characterized by J(t=3s) (b) and creep deformation curves J(t) (c). **d:** Immunofluorescence analysis using keratin and tubulin antibodies and phalloidin staining (actin). **e:** Keratin 5 , tubulin and actin expression detected by Western blotting of total protein lysates. Bar, 10 μm.

5.5 Evaluation of single cell biomechanics as potential marker for oral squamous cell carcinomas: a pilot study

J. Runge[*], T.E. Reichert[†], A.W. Fritsch, J.A. Käs, J. Bertolini[‡], T.W. Remmerbach[* §]

[*]Universitätsklinikum Leipzig, Zahnklinik, Sekt. f. Klinische u. Experimentelle Orale Medizin
[†]Klinik und Poliklinik für Mund-, Kiefer- und Gesichtschirurgie, Universität Regensburg
[‡]Universitätsklinikum Leipzig, Institut für Pathologie
[§]Griffith Institute of Health and Medical Research, Griffith University, Australia

Early detection of oral cancer is a major health issue. The objective of this pilot study was to analyze the deformability of healthy and cancer cells using a microfluidic optical stretcher. Different cancer cell lines, primary oral cancer cells and their healthy counterparts were cultivated and characterized respectively. A measurable deformation of the cells along the optical axis was detected, caused by surface stress, which is optically induced by the laser power. All cells revealed a visco-elastic extension behavior and showed a characteristic deformation response under laser light exposure. The CAL-27/-33 cells exhibited the highest relative deformation. All other cells achieved similar values, but on a lower level. The cytoskeleton reacts sensitively of changing environmental conditions, which may be influenced by growth behavior of the cancer specimens. Nevertheless, the statistical analysis showed significant differences between healthy and cancer cells. Generally malignant and benign cells showed significantly different mechanical behavior. Cancer related changes influence the composition of the cytoskeleton and thus affect the deformability, but this effect may be superimposed by cell cultivation conditions, or cell doubling time. These influences had to be substituted by brush biopsies to minimize confounders in pursuing investigations.

5.6 Different Modes of Growth Cone Collapse

P. Rauch, P. Heine, B. Goettgens[*], J.A. Käs

[*]Fakultät für Biowissenschaften, Pharmazie und Psychologie, Institut für Biologie

The directed motility of growth cones at the tip of neuronal processes is a key function in neuronal path - finding and relies on a complex system of interacting cytoskeletal components. A growth cone at the tip of every neurite detects, integrates and follows multiple guidance cues which regulate outgrowth and initiate directional changes through cytoskeletal rearrangements. Even though tremendous effort has been put into researching this interesting process, not all aspects of the involved cytoskeletal dynamics have been identified. Especially the function of microtubules has been largely underestimated, as most force - generating mechanisms are attributed to actin-myosin based structures and processes.

We were able to implement a combination of custom written MATLAB algorithms to semi - automatically detect and track growth cone contours in laser scanning microscope image series of NG108-15 growth cones transiently transfected with mCherry-

LifeAct and pCS2+/EMTB-3XGFP for filamentous actin and microtubules. While the main focus of research lies on the cytoskeletal dynamics underlying growth cone advancement, we investigated collapse and retraction mechanisms. Using fluorescence time lapse microscopy we could classify two discrete modes of growth cone collapse leading either to neurite retraction or to a controlled halt of neurite extension (figure 5.4). In the latter case, lateral movement and folding of actin bundles (filopodia) confine microtubule extension and constrict microtubule - based expansion processes without the necessity of a constantly engaged actin turnover machinery. We call this previously unreported additional type fold collapse and propose that it marks an intermediate type of growth regulation which closes the gap between full retraction and small scale fluctuations.

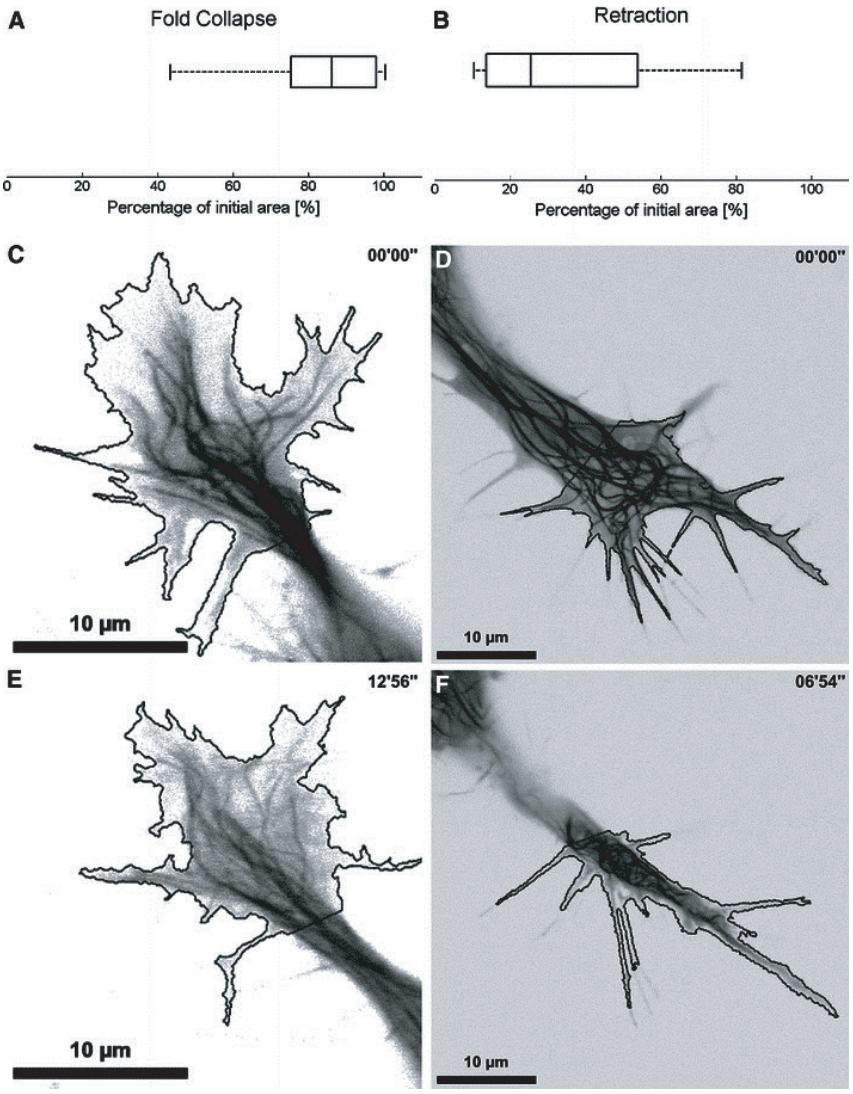

Figure 5.4: Reduction of growth cone area for the two discrete cases of retraction, shown in histograms and before and after images for these events.

[1] P. Rauch et al.: European Biophysics Journal **42**, Issue 8, 591-605 (2013)

5.7 Fluorescent beads disintegrate actin networks

T. Golde, C. Schuldt, J. Schnauß, D. Strehle, M. Glaser, J.A. Käs

The viscoelastic properties of F-actin networks, a model system for semiflexible polymer networks, can be explored with passive microrheology. For this technique the thermal fluctuations of tracer particles are used to calculate the complex shear modulus. This allows to obtain both the bulk properties and their microscopic origins. A common microrheological method is video particle tracking of fluorescent tracer particles with the help of an epifluorescent microscope.

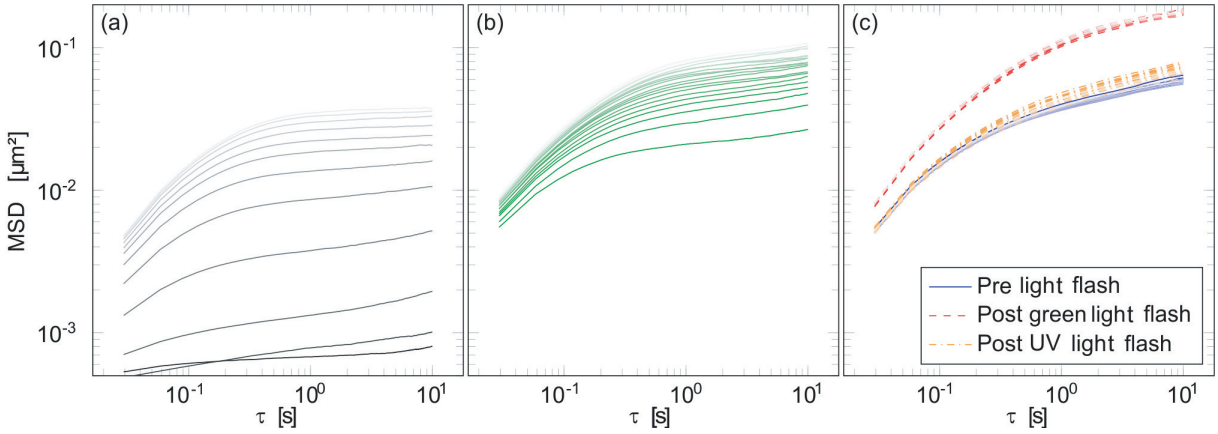

Figure 5.5: Time dependent mean-squared displacement (MSD) of 1 μm NYO beads in 1 mg/ml actin networks. Additionally, the cross-linked sample contained 1.34 μM heavy meromyosin. The MSD was calculated for consecutive time courses every 100 s and is plotted against the lag time τ with a truncation after 10 s. Consecutive time courses are represented by a fade in color. **(a)** The cross-linked network was observed for 1200 s, and **(b)** the entangled network was observed for 1800 s with fluorescent light. **(c)** The entangled network was observed for 1900 s with bright field microscopy before and after a 60 s high intensity flash of green and UV lights, respectively [1].

Using this method, we found that illumination of fluorescent beads with their appropriate excitation wavelength leads to a striking "light-induced softening" of actin gels. Illumination with other wavelengths and the usage of bright field microscopy do not influence thermal bead fluctuations. The addition of oxygen scavengers cannot significantly reduce the light-induced softening. We conclude that fluorescent beads impair results and recommend bright field imaging for studying the microrheology of actin networks [1].

[1] T. Golde et al.: Physical Review E **88**, 044601 (2013)

5.8 Emergent complexity of the cytoskeleton: from single filaments to tissue

F. Huber*, J. Schnauß, S. Rönicke, P. Rauch, K. Müller, C. Fütterer, J.A. Käs

*FOM Institute AMOLF, Amsterdam, The Netherlands

In January 2013 we published the article "Emergent complexity of the cytoskeleton: from single filaments to tissue" in Advances in Physics. We have been invited to contribute to this journal, which is ranked number one in the discipline of condensed matter physics (impact factor 34.29). The article is among the top fifthy of most downloaded papers 2013. Physics of different scales (levels of complexity) in biological systems are reviewed providing a broad collection of fundamental achievements in the field. Biophysical investigations and theoretical approaches were presented aiming to introduce the physics of the cytoskeleton. To explain this intra-cellular biopolymer scaffold appropriately, effects ranging from single biopolymer filaments to cells and multicellular organisms are summarized. In that course a wide range of phenomena is presented and the intertwined nature of different levels of complexity is emphasized. Numerous emergent properties are explained by the means of self-organization or self-assembly.

These physical levels as well as according backgrounds correspond to the research in our group. Thus, this review was a perfect opportunity to present our current work and to highlight connections and applications to other fields.

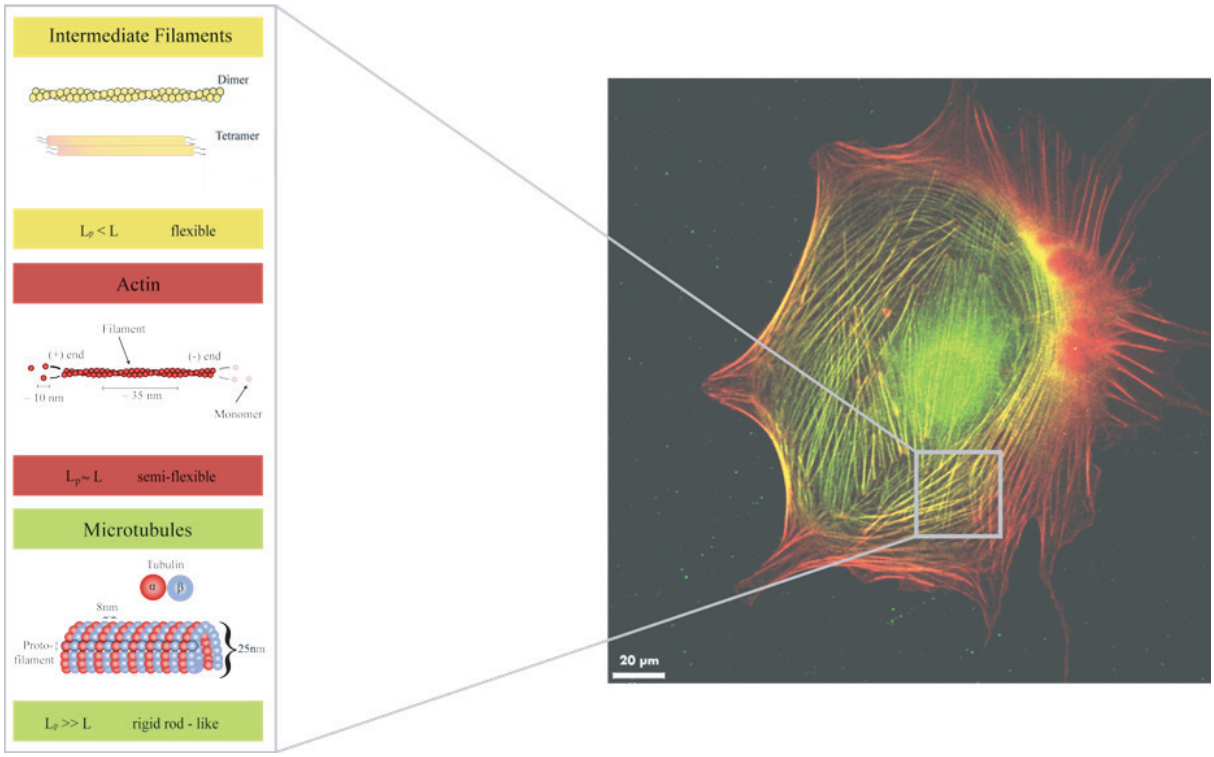

Figure 5.6: The cellular cytoskeleton consists of three main components. Due to the cytoskeleton cells can remain organized and various higher ordered structures can emerge.

[1] F. Huber et al.: Advances in Physics **62**, Issue 1, 1-112 (2013)

5.9 Functionalization of FePd Ferromagnetic Shape Memory Alloys for Biomedical Applications - An Experimental and Theoretical Survey

U. Allenstein, Y. Ma*, A. Arabi-Hashemi*, F. Szillat*, S.G. Mayr*, M. Zink

*Leibniz-Institut für Oberflächenmodifizierung, Translationszentrum für Regenerative Medizin

Magnetic shape memory alloys are capable to perform strains of up to 5 % by applying a moderate external magnetic field. This shape memory effect occurs due to variant reorientation and is only observable for a high mobility of twinning dislocations and a high magneto-crystalline anisotropy and is very promising for biomedical applications like actuators, stents and valves. Up to now, only few materials known to fulfill these requirements. Fe_7Pd_3 is the only one of them also potent to show a sufficient biocompatibility, which we investigated in *in vitro* experiments with NIH 3T3 fibroblasts, MCF 10A epithelial cells and HOB osteoblasts on vapor-deposited single crystalline Fe_7Pd_3 thin films [1]. We were able to demonstrate good proliferation and adhesion of all investigated cell types. No harmful morphological changes or cytotoxic effects could be observed. On this basis, we investigated how cellular behavior can be mediated by common protein coatings, such as fibronectin, laminin and poly-L-lysine and found significant differences in the morphology and proliferation behavior of the cells as illustrated in figure 5.7.

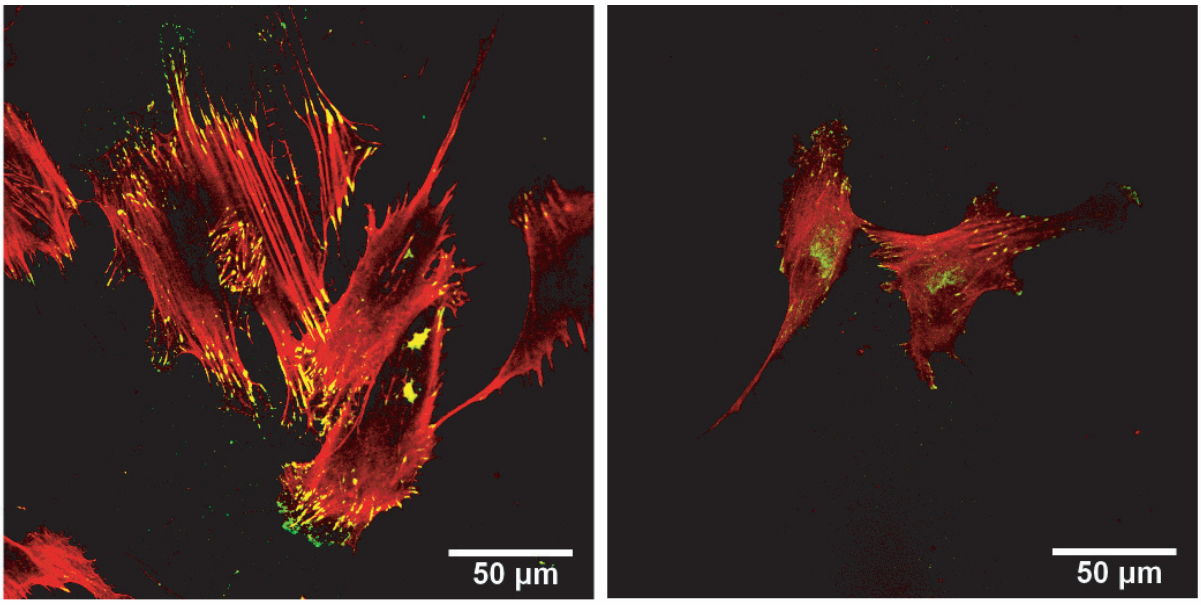

Figure 5.7: Human osteoblasts on Fe_7Pd_3 coated with different specific binding agents. Cells in the left image (fibronectin coating) show a much more spread morphology and focal adhesion density than those in the right image (laminin coating).

A more detailed investigation was carried out on coatings with the RGD amino acid sequence, which is a component of fibronectin and of fundamental importance to integrin interaction and thus cellular adhesion. Through delamination tests and cell culture assays we proved decent adhesion of RGD to the substrate, and cells to

the RGD, respectively. Theoretical ab initio calculations via density functional theory confirm the experimental results and explain the strong connection between RGD and Fe_7Pd_3 in a fundamental physical way: it is mainly mediated by coordinate bonds between iron atoms of the films and nitrogen/oxygen atoms of the RGD [2]. Thus surface functionalization with biological coatings is possible and desirable.

[1] U. Allenstein et al.: Acta Biomaterialia **9**, Issue 3, 5845-5853 (2013)
[2] M. Zink et al.: Advanced Functional Materials **23**, Issue 11, 1383-1391 (2013)

5.10 Funding

Leipziger Schule der Naturwissenschaften - Bauen mit Molekülen und Nano-Objekten (BuildMoNa)
Prof. Dr. E. Hey-Hawkins, Prof. Dr. M. Grundmann und Prof. Dr. J. A. Käs
GSC 185/1

InterNeuro
Prof. Dr. J. A. Käs, Mitglied im DFG-Graduiertenkolleg "InterNeuro", Projekte 5 und 7
GRK 1097

Optische Messung zellulärer Materialeigenschaften für pharmakologische Hochdurchsatz-Technologie ("Agescreen")
Prof. Dr. J. A. Käs
BMBF-Projekt, 13N109 35

Von lokalen Einschränkungen bis zum makroskopischen Transport - From local constraints to macroscopic transport
Prof. Dr. J. Käs, Dr. Stephan Diez et al.
DFG Forschergruppe FOR 877, Teilprojekt 6, KA 1116/ 7-1

Light propagation through the retina: Vertebrate retinal optics
Prof. Dr. J. A. Käs, Prof. Dr. A. Reichenbach et al.
DFG, RE 849/15-1

Untersuchung funktioneller Änderungen von Tumorzellen als Ursache unsymmetrischer Verteilungsfunktionen des Zelldeformationsverhaltens
Prof. Dr. J. A. Käs, Dr. M. Zink
DFG, KA 1116/9-1

Rezidivprognose zur Entwicklung von effektiven Brusttumortherapeutika
Prof. Dr. J. A. Käs, Prof. Dr. A. Beck-Sickinger, Prof. Dr. E. Hey-Hawkins
SAB, 33707045

Nanostrukturierte Substrate zur organotypischen Langzeitkultivierung adulter Gewebe: Neuartige Verfahren für in vitro Wirkstoffscreening am Beispiel von Augenerkrankungen
Dr. M. Zink, Prof. Dr. J. A. Käs, Prof. Dr. A. Robitzki (BBZ)
SAB,100121467

Invasion und initiale Schritte bei der Metastasierung solider Tumore (Karzinome)
Prof. Dr. J. A. Käs
ESF-Nachwuchsforschergruppe, SAB, 100147954

Werkzeuge und Technologien für die rationale Wirkstoffentwicklung
Prof. Dr. J. A. Käs
ESF-Nachwuchsforschergruppe, SAB, 100148830

Peptid-vermitteltes Tumortargeting: Diagnostik und Therapie
Prof. Dr. J. A. Käs, Prof. Dr. A. Beck-Sickinger, Prof. Dr. E. Hey-Hawkins, Prof. Dr. A. Robitzki
SMWK 70

Erforschung und Entwicklung eines Sortier-Chips zur Analyse seltener Zellen
Prof. Dr. J. A. Käs, Cellastix GmbH (S. Rönicke, R. Stange, B. Hofmann)
SMWK, 4-7531.60/32/2

Dynamisch-mechanische Manipulation and Charakterisierung von Zellen mit Hilfe magnetischer Dehnung
Dr. M. Zink
DFG, Zi-1330/2-1

5.11 Organizational Duties

Prof. J. A. Käs

- Senator der Universität Leipzig
- Direktor des Instituts für Experimentelle Physik I
- Member of the Organizing Committee: 4th Annual Symposium - Physics of Cancer, Leipzig, September 2013
  involved organizers: Prof. Dr. C. Mierke, Prof. Dr. H. Herrmann, Prof. V. M. Weaver
- PWM Winterschool Spindlermühle CZ, February 2013
- Journal review: Nature, Science, Cell, Physical Review Letters, Biophysical Journal, Biophysica and Proceedings of the National Academy of Science, Langmuir, Angewandte Chemie, Nature Physics, Journal of Biophotonics, Cytoskeleton, Optics Express, New Journal of Physics
- Grant review: National Science Foundation, Div. of Materials Research; National Science Foundation, Div. of Cellular Organization; National Science Foundation, Div. of Computational Biology; National Science Foundation, Div. of Physics, Special Programs; Deutsche Forschungsgemeinschaft, Alexander von Humboldt Foundation, Deutsche Studienstiftung, Centre National de Recherche

5.12 External Cooperations

Academic

- ESPCI, Paris, France
  Prof. Dr. J. Prost

- Princeton University, USA
  Prof. Dr. R. Austin
- Albert Einstein Institute of Medicine, U.S.A.
  Prof. Dr. J. Condeelis
- Deutsche Gesellschaft für Zellbiologie (DGZ)
  Prof. Dr. H. Herrmann
- Max-Delbrück-Zentrum für molekulare Medizin
  Dr. M. Falcke
- Deutsches Krebsforschungszentrum
  Prof. Dr. R. Eills
- Charité Berlin, MR Elastographie
  Prof. Dr. I. Sack
- Westfälische Wilhelms-Universität Münster
  Dr. J. Schnekenburger
- Ludwig-Maximilians-Universität München, Fakultät für Chemie und Pharmazie
  Prof. Dr. A. Vollmar
- Universität Bonn, Institut für Genetik
  Prof. Dr. K. Rottner
- Universität Leipzig, Klinik u. Poliklinik für Frauenheilkunde
  Prof. Dr. M. Höckel
- Universität Leipzig, Institut für Pathologie
  Prof. Dr. L.-C. Horn
- Universität Leipzig, Institut für Anorganische Chemie
  Prof. Dr. E. Hey-Hawkins
- Universität Leipzig, Institut für Biochemie
  Prof. Dr. A. Beck-Sickinger
- Universität Leipzig, Klinik u. Poliklinik f. Mund-, Kiefer- u. Plast. Gesichtschirurgie
  Dr. T. Remmerbach
- Universität Leipzig, Klinik u. Poliklinik f. Dermatologie, Venerologie u. Allergologie
  Prof. Dr. J. Simon
- Universität Leipzig,Translationszentrum für Regenerative Medizin
  Prof. Dr. T. Magin
- Universität Leipzig, Klinik u. Poliklinik f. Dermatologie, Venerologie u. Allergologie
  Prof. Dr. M. Kunz
- Universität Leipzig, Institut für Biochemie
  Prof. Dr. T. Pompe
- Universität Leipzig, Institut für Medizinische Physik und Biophysik
  Prof. Dr. D. Huster
- Universität Leipzig, Institut für Experimentelle Physik I
  Prof. Dr. C. Mierke

Industry

- Beiersdorf AG, Hamburg
  Dr. C. Schulze
- JPK Instruments, Berlin
  Dr. T. Müller
- Niendorf & Hamper, Hamburg
  Prof. A. Niendorf
- ibidi GmbH, Martinsried
  Dr. V. Kahl
- Inventages, London, GB
  Prof. Dr. T. Bayerl
- Cellastix GmbH, Leipzig
  S. Rönicke

5.13 Publications

Journals

M. Zink, F. Szillat, U. Allenstein, S. G. Mayr: *Interaction of Ferromagnetic Shape Memory Alloys and RGD Peptides for Mechanical Coupling to Cells: from Ab Initio Calculations to Cell Studies*, Advanced Functional Materials **23**, Issue 11, 1383-1391 (2013)

P. Rauch, P. Heine, B. Goettgens, J. A. Käs: *Forces from the rear: deformed microtubules in neuronal growth cones influence retrograde flow and advancement*, New Journal of Physics, **15**, 015007 (2013)

P. Rauch, P. Heine, B. Goettgens, J. A. Käs: *Different modes of growth cone collapse in NG 108-15 cells*, European Biophysics Journal **42**, Issue 8, 591-605

M. Krahe, I. Wenzel, K.-N. Lin, J. Fischer, J. Goldmann, M. Kästner, C. Fütterer: *Fluctuations and differential contraction during regeneration of Hydra vulgaris tissue toroids*, New Journal of Physics **15**, 035004 (2013)

U. Allenstein, Y. Ma, A. Arabi-Hashemi, M. Zink, S. G. Mayr: *Fe-Pd based ferromagnetic shape memory actuators for medical applications: Biocompatibility, effect of surface roughness and protein coatings*, Acta Biomaterialia **9**, Issue 3, 5845-5853 (2013)

L. Woiterski, T. Claudepierre, R. Luxenhofer, R. Jordan, J. A. Käs: *Stages of neuronal network formation*, New Journal of Physics **15**, 025029 (2013)

F. Huber, J. Schnauß, S. Rönicke, P. Rauch, K. Müller, C. Fütterer, J. A. Käs: *Emergent complexity of the cytoskeleton: from single filaments to tissue*, Advances in Physics **62**, Issue 1 (2013)

T. R. Kießling, M. Herrera, K. D. Nnetu, E. M. Balzer, M. Girvan, A. W. Fritsch, S. S. Martin, J. A. Käs, W. Losert: *Analysis of multiple physical parameters for mechanical phenotyping of living cells*, European Biophysics Journal **42**, Issue 5, 383-394 (2013)

T. R. Kießling, R. Stange, J. A. Käs, A. W. Fritsch: *Thermorheology of living cells - impact of temperature variations on cell mechanics*, New Journal of Physics **15**, Issue 4 (2013)

K. D. Nnetu, M. Knorr, S. Pawlizak, T. Fuhs, J. A. Käs: *Slow and anomalous dynamics of an MCF-10A epithelial cell monolayer*, Soft Matter **9**, 9335-9341 (2013)

J. Runge, T. E. Reichert, A. Fritsch, J. A. Käs, J. Bertolini, T. W. Remmerbach: *Evaluation of single cell biomechanics as potential marker for oral squamous cell carcinomas: a pilot study*, Oral Diseases, first published online (2013)

K. Seltmann, A. W. Fritsch, J. A. Käs, T. M. Magin: *Keratins significantly contribute to cell stiffness and impact invasive behavior*, PNAS **110**, Issue 46 (2013)

T. Fuhs, M. Gögler, C. A. Brunner, C. W. Wolgemuth, J. A. Käs: *Causes of retrograde flow in fish keratocytes*, Cytoskeleton, accepted and published online before printing (2013)

T. Golde, C. Schuldt, J. Schnauß, D. Strehle, M. Glaser, J. A. Käs: *Fluorescent Beads Disintegrate Actin Networks*, Physical Review E **88**, Issue 4, 044601 (2013)

M. Gyger, T. Kießling, R. Stange, A. Fritsch, A. G. Beck-Sickinger, M. Zink, J. A. Käs: *Active contractions in single suspended epithelial cells*, European Biophysics Journal, accepted (2013)

Books

M. Zink *Thin Films and Coatings in Biology*, Chapter 2 (11 - 67), Soroush Nazarpour (Ed.), Springer, Berlin Heidelberg (2013)

Talks

J. A. Käs *The Physical Bounds of In Vivo Cell Motility*, DPG Spring Meeting Regensburg, March 2013

M. Zink, V. Dallacasagrande, A. Jakob, M. Müller, A. Reichenbach, J. A. Käs, S. G. Mayr *Tailoring substrates for long-term organotypic culture of adult neuronal tissue*, DPG Spring Meeting, Regensburg, March 2013

S. Pawlizak, A. Fritsch, J. A. Käs *On the Relevance of Cellular Adhesion for Compartmentalization*, DPG Spring Meeting, Regensburg, March 2013

E. Warmt, T. Kießling, R. Stange, A. Fritsch, J. A. Käs *Impact of Temperature on Cell Nuclei Integrity*, DPG Spring Meeting, Regensburg, March 2013

U. Allenstein, Y. Ma, A. Arabi-Hashemi, S. G. Mayr, M. Zink *Biocompatibility of Fe-Pd ferromagnetic shape memory alloys - influence of surface roughness and protein coatings*, DPG Spring Meeting, Regensburg, March 2013

J. A. Käs *The Physical Bounds of In Vivo Cell Motility*, Joint International Meeting of the German Society for Cell Biology (DGZ) and the German Society for Developmental Biology (GfE), Heidelberg, March, 2013 (invited talk)

S. Pawlizak, A. Fritsch, J. A. Käs *Is Compartmentalization Driven by Adhesion? - Probing Cellular Adhesion Forces Using a Modified BioAFM*, 5th AFM BioMed Conference, Shanghai (China) May 2013

J. A. Käs *The Physical Bounds of In Vivo Cell Motility*, International Focus Workshop on "Connecting Theory and Experiments in Active Matter", Dresden, June 2013 (invited talk)

J. A. Käs *The Physical Bounds of In Vivo Cell Motility*, 4th Annual Symposium - Physics of Cancer, Leipzig, September 2013

J. A. Käs *The Physical Bounds of In Vivo Cell Motility*, VI Meeting of Epithelial-Mesenchymal Transition International Association (TEMTIA), "Systems and Mathematical Modelling of EMT", Alicante (Spain), November 2013 (invited talk)

M. Zink, V. Dallacasagrande, A. Reichenbach, J. A. Käs, S. G. Mayr *Investigating Super-Hydrophilic Nanotube Arrays for Long-Term Organotypic Culture of Adult Retina and Brain Tissue*, Materials Research Society Fall Meeting, Boston (USA), December 2013

M. Zink, F. Szillat, U. Allenstein, S. G. Mayr *Interaction of Ferromagnetic Shape Memory Alloys and RGD Peptides for Promotion of Cell Adhesion: From Ab-Initio-Calculations to Cell Studies*, Materials Research Society Fall Meeting, Boston (USA), December 2013

Posters

J. Schnauß, F. Huber, D. Strehle, J. A. Käs *Actin bundle assembly in higher ordered structures - a new liquid crystal phase?*, Annual Conference of the Graduate School BuildMoNa, Leipzig, March 2013

S. Pawlizak, A. Fritsch, J. A. Käs *On the Relevance of Cellular Adhesion for Compartmentalization*, Annual Conference of the Graduate School BuildMoNa, Leipzig, March 2013

R. Stange, T. Kießling, A. Fritsch, S. Rönicke, J. A. Käs *Automated Optical Stretching*, DPG Spring Meeting, Regensburg, March 2013

R. Stange, D. K. Nnetu, J. A. Käs *Cell stiffening and softening evoked by optical stress application*, European Biophysics Congress, Lisbon (Portugal), July 2013 and Diffusion Fundamentals, Leipzig, August 2013

E. Warmt, T. Kießling, A. Fritsch, R. Stange, J. A. Käs *Temperature Induced Sudden Loss of Cell Nuclei Integrity*, 4th Annual Symposium - Physics of Cancer, Leipzig, September 2013

S. Grosser, A. Fritsch, T. Kießling, R. Stange, F. Meinhövel, J. A. Käs *Refractometry of single, suspended cells in a dual-beam optical trap*, 4th Annual Symposium - Physics of Cancer, Leipzig, September 2013

S. Pawlizak, T. Thalheim, A. Fritsch, J. A. Käs *Challenges in Probing Cellular Adhesion Forces Using Atomic Force Microscopy*, 4th Annual Symposium - Physics of Cancer, Leipzig, September 2013

T. Golde, C. Schuldt, J. Schnauß, D. Strehle, M. Glaser, J. A. Käs *Fluorescent Beads Disintegrate Actin Networks*, 4th Annual Symposium - Physics of Cancer, Leipzig, September 2013

C. Schuldt, T. Golde, J. Schnauß, M. Glaser, J. A. Käs *Entropic contraction of actin networks*, 4th Annual Symposium - Physics of Cancer, Leipzig, September 2013

J. Schnauß, T. Golde, C. Schuldt, D. Strehle, J. A. Käs *Entropic contraction of actin bundles*, 4th Annual Symposium - Physics of Cancer, Leipzig, September 2013

F. Wetzel, A. Fritsch, S. Schmidt, S. Pawlizak, T. Kießling, R. Stange, L.-C. Horn, K. Bendrat, M. Oktay, A. Niendorf, M. Höckel, J. Condeelis, M. Zink, J. A. Käs *Biomechanical Screening of Primary Mammary Carcinoma*, 12th Leipzig Research Festival for Life Sciences, December 2013

T. Golde, C. Schuldt, J. Schnauß, D. Strehle, M. Glaser, J. A. Käs *Influence of fluorescent beads on actin networks*, 12th Leipzig Research Festival for Life Sciences, December 2013

M. Zink, U. Allenstein, A. Weidt, Y. Ma, F. Szillat, S. G. Mayr *Tuning Biocompatibility of Single Crystalline $Fe_{70}Pd_{30}$ Ferromagnetic Shape Memory Films for Cell Sensing*, Materials Research Society Fall Meeting, Boston (USA), December 2013

5.14 Graduations

Doctorate

- Silke Agte
  Light Guidance in Müller Cells of the Vertebrate Retina
  18.03.2013
- Kenchukwu David Nnetu
  A hierarchical study on cell mechanics and dynamics
  15.07.2013
- Philipp Rauch
  Neuronal Growth Cone Dynamics - The Back and Forth of it -
  16.09.2013
- Markus Gyger
  Active and Passive Biomechanical Measurements for Characterization and Stimulation of Biological Cells
  16.09.2013
- Thomas Fuhs
  Intracellular Polymer Network as Source of Cell Motility
  16.09.2013
- Lydia Woiterski
  Meeting at the Membrane - Confined Water at Cationic Lipids & Neuronal Growth on Fluid Lipid Bilayers
  16.12.2013

Diploma

- Hendrik Brehme
  Reliability of Chemical Guidance Methods in Neuronal Growth Cone Motility
  September 2013
- Nico Herbig
  Systematic study of the development of a basic rheological model for measurements obtained by an optical stretcher
  September 2013
- Tony Kurth
  An Evaluation Of Techniques To Chemically Guide Neurons
  September 2013

Master

- Michael Krahe
  Fluctuations and Symmetry Breaking in the Early Regeneration of Hydra vulgaris Tissues
  January 2013
- Benjamin Winkler
  From Actin Flow to Cellular Forces
  July 2013
- Stefanie Puder
  Impact of Chemotherapeutic Drugs on Biological Materials
  September 2013
- Tom Kunschmann
  Influence of Water Isotopes on Mechanical Properties of Cells
  October 2013

Bachelor

- Tobias Thalheim
  Measuring Cell-Cell Adhesion Forces of the MCF-10A Cell Line with Atomic Force Microscopy
  January 2013

5.15 Guests

- Valentina Dallacasagrande M. Sc.
  EU-research assistant at the Paul-Flechsig-Institut for brain research and the Dept. Softmatter Physics, Universität Leipzig, March 2010 - 2013

6

Biological Physics

6.1 Introduction
Cellular Biophysics in the Field of Cancer Research

Most cancer-related deaths during the malginant cancer progression are caused by the ability of cancer cells to metastasize. The process of metastasis follows a linear propagation of several steps. It starts with the spreading of cancer cells from the primary tumor, which then migrate into the local tumor microenvironment. The cancer cells can transmigrate into blood or lymph vessels (intravasation), get transported through the vessel flow, adhere to the endothelial cell lining, grow and form a secondary tumor directly inside the vessel or the cancer cells possibly transmigrate through the endothelial vessel lining (extravasation) into the extracellular matrix of connective tissue. After this step, the cancer cells migrate further into the targeted tissue (possibly another organ), grow and form a secondary tumor (i.e. the tumor metastasizes). Despite of all current findings based on biochemistry and even the novel approaches based on genomics and proteomics cancer research did not fundamentally change cancer death rates, but still improved clinical diagnosis substantially in the field of cancer research regarding the classification and detailed staging of tumors, numerous marker proteins and mapping of specific human cancer-types. Thus, a main criticism to these methods is that the expression levels of numerous genes and molecules, which are differently regulated during cancer progression, depend on the cancer disease stage. In particular, it is still not fully understood how they regulate cancer progression. A reason may be that these genomic and proteomic based methods do not account for the localization of the molecules in special compartments such as lipid rafts, their activation or assembly state, their life-time, turn-over-, modification- and recycling rate. Thus, we and others propose that the biomechanical properties are crucial for the efficiency and speed of cancer cell invasion and subsequently, for metastases formation. In more detail, classical physical approaches will be adopted to complex soft matter such as cancer cells and novel biophysical methods will be developed in order to adopt them to cancer research. These novel physical approaches have so far changed or will still alter the direction of recent cancer research. Moreover, even the role of the endothelium during the transmigration and invasion of cells is not clear, it has been seen as passive barrier, but this could not explain all novel findings as our finding that this endothelial layer of vessels can enhance the invasiveness of cancer cells. Thus, we will investigate how cancer cells alter

the structural, biochemical and mechanical properties of the endothelium to regulate their own invasiveness through extracellular matrices and hence, through the tissue microenvironment. Moreover, we will investigate how the mechanical properties of cancer cells regulate the functional properties such as cancer cell invasion and transendothelial migration. Finally, our research will shed light on the mechanical properties of cancer cells and the interacting endothelium and will point out the importance of the mechanical properties as a critical determinant for the efficiency of cancer cell invasion and the overall progression of cancer. In conclusion, we suggest that the regulation of the endothelial cell's biomechanical properties by cancer cells and the mechanical properties of cancer cells are a critical determinants of cancer cell invasiveness and may affect the future development of new cancer treatments.

Claudia Mierke

6.2 Phagocytized beads reduce the $\alpha 5\beta 1$ integrin facilitated invasiveness of cancer cells by regulating cellular stiffness

C.T. Mierke

Cell invasion through the extracellular matrix (ECM) of connective tissue is an important biomechanical process, which plays a prominent role in tumor progression. The malignancy of tumors depends mainly on the capacity of cancer cells to migrate and metastasize. A prerequisite for metastasis is the invasion of cancer cells through connective tissue to targeted organs. Cellular stiffness and cytoskeletal remodeling dynamics have been proposed to affect the invasiveness of cancer cells. Here, this study investigated whether highly invasive cancer cells are capable of invading into dense 3D-ECMs with an average poresize of 1.3 or 3.0 μm when phagocytized beads (2.7 and 4.5 μm diameter) increased their cellular stiffness and reduced their cytoskeletal remodeling dynamics compared to weakly invasive cancer cells. The phagocytized beads decreased the invasiveness of the $\alpha 5\beta 1$ (high) cancer cells into 3D-ECMs, whereas the invasiveness of the $\alpha 5\beta 1$(low) cancer cells was not affected. The effect of phagocytized beads on the highly invasive $\alpha 5\beta 1$(high) cells was abolished by specific knock-down of the $\alpha 5$ integrin subunit or addition of an anti-$\alpha 5$ integrin blocking antibody. Furthermore, the reduction of contractile forces using MLCK and ROCK inhibitors abolished the effect of phagocytized beads on the invasiveness of $\alpha 5\beta 1$(high) cells. In addition, the cellular stiffness of $\alpha 5\beta 1$(high) cells was increased after bead phagocytosis, whereas the bead phagocytosis did not alter the stiffness of $\alpha 5\beta 1$(low) cells. Taken together, the $\alpha 5\beta 1$ integrin dependent invasiveness was reduced after bead phagocytosis by altered biomechanical properties, suggesting that the $\alpha 5\beta 1$(high) cells need an appropriate intermediate cellular stiffness to overcome the steric hindrance of 3D-ECMs, whereas the $\alpha 5\beta 1$(low) cells were not affected by phagocytized beads.

6.3 Physical break-down of the classical view on cancer cell invasion and metastasis

C.T. Mierke

Eight classical hallmarks of cancer have been proposed and are well-defined by using biochemical or molecular genetic methods, but are not yet precisely defined by cellular biophysical processes. To define the malignant transformation of neoplasms and finally reveal the functional pathway, which enables cancer cells to promote cancer progression, these classical hallmarks of cancer require the inclusion of specific biomechanical properties of cancer cells and their microenvironment such as the extracellular matrix and embedded cells such as fibroblasts, macrophages or endothelial cells. Nonetheless a main novel ninth hallmark of cancer is still elusive in classical tumor biological reviews, which is the aspect of physics in cancer disease by the natural selection of an aggressive (highly invasive) subtype of cancer cells. The physical aspects can be analyzed by using state-of-the-art biophysical methods. Thus, this review will present current cancer research in a different light and will focus on novel physical methods to investigate the aggressiveness of cancer cells from a biophysicist's point of view. This may lead to novel insights into cancer disease and will overcome classical views on cancer. In addition, this review will discuss how physics of cancer can help to reveal whether cancer cells will invade connective tissue and metastasize. In particular, this review will point out how physics can improve, break-down or support classical approaches to examine tumor growth even across primary tumor boundaries, the invasion of single or collective cancer cells, transendothelial migration of cancer cells and metastasis in targeted organs. Finally, this review will show how physical measurements can be integrated into classical tumor biological analysis approaches. The insights into physical interactions between cancer cells, the primary tumor and the microenvironment may help to solve some "old" questions in cancer disease progression and may finally lead to novel approaches for development and improvement of cancer diagnostics and therapies.

6.4 The role of focal adhesion kinase in the regulation of cellular mechanical properties

C.T. Mierke

The regulation of mechanical properties is necessary for cell invasion into connective tissue or intra- and extravasation through the endothelium of blood or lymph vessels. Cell invasion is important for the regulation of many healthy processes such as immune response reactions and wound healing. In addition, cell invasion plays a role in disease-related processes such as tumor metastasis and autoimmune responses. Until now the role of focal adhesion kinase (FAK) in regulating mechanical properties of cells and its impact on cell invasion efficiency is still not well known. Thus, this review focuses on mechanical properties regulated by FAK in comparison to the mechano-regulating protein vinculin. Moreover, it points out the connection between cancer cell invasion and metastasis and FAK by showing that FAK regulates cellular mechanical properties

required for cellular motility. Furthermore, it sheds light on the indirect interaction of FAK with vinculin by binding to paxillin, which then impairs the binding of paxillin to vinculin. In addition, this review emphasizes whether FAK fulfills regulatory functions similar to vinculin. In particular, it discusses the differences and the similarities between FAK and vinculin in regulating the biomechanical properties of cells. Finally, this paper highlights that both focal adhesion proteins, vinculin and FAK, synergize their functions to regulate the mechanical properties of cells such as stiffness and contractile forces. Subsequently, these mechanical properties determine cellular invasiveness into tissues and provide a source sink for future drug developments to inhibit excessive cell invasion and hence, metastases formation.

6.5 Tetracycline-encapsulated P(3HB) microsphere-coated 45S5 Bioglass-based scaffolds for bone tissue engineering

D. Meng[*], L. Francis[†], I.D. Thompson[‡], C.T. Mierke H. Huebner, [§], A. Amtmann[§], I. Roy[†], A.R. Boccaccini[*]

[*]Department of Materials, Imperial College London
[†]Department of Molecular and Applied Biology, University of Westminster, London
[‡]Biomaterials Unit, Dental Institute, Kings College London
[§]Institute of Bioprocess Engineering, University of Erlangen, Nürnberg

Bioglass-based scaffolds for bone tissue engineering have been developed, which can also serve as carriers for drug delivery. For this, P(3HB) microspheres (PMSs) loaded with tetracycline were fabricated and immobilised on the scaffold surfaces by a modified slurry dipping technique. The sustained drug delivery ability in simulated body fluid was confirmed by using UV-Vis absorption spectroscopy measurements. The MTT assay using mouse fibroblast cells provided evidence that the tetracycline loaded microspheres produced in this study show limited cytotoxicity. The scaffolds developed in this work provide mechanical support, adequate 3D surface roughness, bioactivity and controlled drug delivery function, and are thus interesting candidates for bone tissue engineering applications.

6.6 LMX1B is essential for the maintenance of differentiated podocytes in adult kidneys

T. Burghardt[*], J. Kastner[*], H. Suleiman[*], E. Rivera-Milla[†], N. Stepanova[*], C. Lottaz, [‡], M. Kubitza[*] C.A. Böger, [§], S. Schmidt, [¶], M. Gorski, [‖], U. deVries[*], H. Schmidt[*], I. Hertting[*], J. Kopp, [**], A. Rascle[*], M. Moser[¶], I.M. Heid, [††], R. Warth[‡‡], R. Spang[‡], C.T. Mierke C. Englert[†], R. Witzgall[*]

[*]Institute for Molecular and Cellular Anatomy, University of Regensburg, Regensburg, Germany
[†]Leibniz Institute for Age Research, Fritz Lipmann Institute, Jena, Germany

‡Institute for Functional Genomics, University of Regensburg, Regensburg, Germany
§Department of Internal Medicine II, University Hospital Regensburg, University of Regensburg, Regensburg, Germany
¶Max-Planck-Institute of Biochemistry, Department of Molecular Medicine, Martinsried, Germany
‖Department of Epidemiology and Preventive Medicine, University Hospital Regensburg, University of Regensburg, Regensburg, Germany
**Kidney Disease Section, National Institute of Diabetes and Digestive and Kidney Diseases, National Institutes of Health, Bethesda, Maryland
††Department of Epidemiology and Preventive Medicine, University Hospital Regensburg, University of Regensburg, Regensburg, Germany; Institute of Epidemiology, Helmholtz Zentrum München, Neuherberg, Germany
‡‡Institute for Medical Cell Biology, University of Regensburg, Regensburg, Germany

Mutations of the LMX1B gene cause nail-patella syndrome, a rare autosomal-dominant disorder affecting the development of the limbs, eyes, brain, and kidneys. The characterization of conventional Lmx1b knockout mice has shown that LMX1B regulates the development of podocyte foot processes and slit diaphragms, but studies using podocyte-specific Lmx1b knockout mice have yielded conflicting results regarding the importance of LMX1B for maintaining podocyte structures. In order to address this question, we generated inducible podocyte-specific Lmx1b knockout mice. One week of Lmx1b inactivation in adult mice resulted in proteinuria with only minimal foot process effacement. Notably, expression levels of slit diaphragm and basement membrane proteins remained stable at this time point, and basement membrane charge properties also did not change, suggesting that alternative mechanisms mediate the development of proteinuria in these mice. Cell biological and biophysical experiments with primary podocytes isolated after 1 week of Lmx1b inactivation indicated dysregulation of actin cytoskeleton organization, and time-resolved DNA microarray analysis identified the genes encoding actin cytoskeleton-associated proteins, including Abra and Arl4c, as putative LMX1B targets. Chromatin immunoprecipitation experiments in conditionally immortalized human podocytes and gel shift assays showed that LMX1B recognizes AT-rich binding sites (FLAT elements) in the promoter regions of ABRA and ARL4C, and knockdown experiments in zebrafish support a model in which LMX1B and ABRA act in a common pathway during pronephros development. Our report establishes the importance of LMX1B in fully differentiated podocytes and argues that LMX1B is essential for the maintenance of an appropriately structured actin cytoskeleton in podocytes

6.7 Funding

International Meeting of the German Society for Cell Biology 4th Annual Symposium Physics of Cancer in Leipzig Physics of Cancer 2013 in Leipzig
Prof. C. T. Mierke
DFG, MI1211/11-1

Functional Role of Endothelial Cells during transendothelial Migration and Invasion of Cancer Cells

Prof. C. T. Mierke
German Cancer Foundation (Deutsche Krebshilfe)

Invasion und initiale Schritte bei der Metastasierung solider Tumore (Karzinome) "Eine biochemische und biophysikalische Untersuchung der Tumorzellen bei dem epithelialen-mesenchymalen Übergangsprozess und der Tumor-Mikroumgebung zur Ermittlung neuer therapeutischer Ziele"
Prof. C. T. Mierke
ESF-SAB Research Group

6.8 Organizational Duties

C. T. Mierke

- Referee: Cancer Research, Journal of Cell Science, Advanced Biomaterials, Acta Biomaterials, British Journal of Cancer, Journal of Pharmacy and Pharmacology, Molecular Vision, International Journal of Nanomedicine, Plos One, Eur. J. Biophysics
- Organization of the 4th International Physics of Cancer Conference in Leipzig (sponsored by DFG and DGZ, 120 participants, 2013)
- Special Issue Guest Editor for Physical Biology

6.9 External Cooperations

Academic

- Imperial College London, Department of Materials, London,UK
  Prof. Dr.-Ing. habil. Aldo R. Boccaccini
- Netherlands Cancer Institute Amsterdam, Netherlands
  Dr. Arnoud Sonnenberg
- University of Regensburg, Institute for Molecular and Cellular Anatomy, Regensburg, Germany
  Prof. Dr. Ralph Witzgall
- Philipps-University Marburg, Department of Neurosurgery, Germany
  Prof. Dr. J. W. Bartsch
- Department of Paediatric Kidney, Hannover medical School, Germany
  Prof. Dr. Hermann Haller , Dr. rer. nat. Wolfgang Ziegler
- University of Bonn, Institute of Genetics Actin Dynamics and Motility Unit, Germany
  Prof. Dr. Klemens Rottner
- University of Leipzig, Translational Center for Regenerative Medicine, Germany
  Prof. Dr. Thomas Magin
- University of Leipzig, Center for Biotechnology and Biomedicine (BBZ), Germany
  Prof. Dr. A. Robitzki

6.10 Publications

Journals

C. T. Mierke: *The integrin alphav beta3 increases cellular stiffness and cytoskeletal remodeling dynamics to facilitate cancer cell invasion*, New Journal of Physics 15 **23**, 015003 (2013)

C. T. Mierke: *Phagocytized beads reduce the α5β1 integrin facilitated invasiveness of cancer cells by regulating cellular stiffness*, Cell Biochem. Biophys **66**, 599-622 (2013)

D. Meng, L. Francis, I. D. Thompson, C. T. Mierke, H. Huebner, A. Amtmann, I. Roy, A. R. Boccaccini: *Tetracycline-encapsulated P(3HB) microsphere-coated 45S5 Bioglass-based scaffolds for bone tissue engineering*, J Mater Sci Mater Med**24**, 2809-2817 (2013)

T. Burghardt, J. Kastner, H. Suleiman, E. Rivera-Milla, N.Stepanova, C.Lottaz, M. Kubitza, C. A. Böger, S. Schmidt, M. Gorski, U. de Vries, H. Schmidt, I. Hertting, J. Kopp, A. Rascle, M. Moser, I. M. Heid, R. Warth, R. Spang, J. Wegener, C. T. Mierke, C. Englert, R. Witzgall: *LMX1B is Essential for the Maintenance of Differentiated Podocytes in Adult Kidneys*, J Am Soc Nephrol **24**, 1830-1848 (2013)

C. T. Mierke: *Physical break-down of the classical view on cancer cell invasion and metastasis*, Eur J Cell Biol **92**, 89-104 (2013)

C. T. Mierke: *The role of focal adhesion kinase in the regulation of cellular mechanical properties*, Physical Biology 10 **6**, 065005 (2013)

C. T. Mierke: *Meeting Report: International Meeting of the German Society for Cell Biology*, Physics of Cancer 2013, Cell News **03**, 24-28 (2013)

Books

C. T. Mierke: *Cancer Metastasis and Biomechanics of the Endothelium*, Mechanobiology of the Endothelium, 2013

6.11 Guests

- Prof. Dr. Harald Herrmann
  German Cancer Research Center, Heidelberg, Germany
  17.04.2013
- Prof. Dr. rer. nat. Jörg W. Bartsch
  Philipps-Universität Marburg, Labor der Klinik für Neurochirurgie, Germany
  11.06.2013

II

Institute for Experimental Physics II

7

Magnetic Resonance of Complex Quantum Solids

7.1 Introduction

The electronic properties of quantum-solids in which the electrons exhibit strong correlations with each other or with the lattice are particularly rich and will be of special importance in future functional materials. In addition, such solids are challenging for experiment, aswell as theory, as the more than twenty five-year history of high-temperature superconductivity shows: we still do not understand the electronic structure of these systems. One particular aspect of strongly correlated electronic materials is their tendency towards nano-scale electronic phase separation. Even in perfect lattices, electronic nano-structures can form. The investigation of such materials requires the use of methods that can give detailed information. Here, magnetic resonance, on nuclei and electrons, is of particular interest as they not only have atomic scale resolution, but also yield bulk information in contrast to surface techniques. We explore the properties of these materials with tailored new techniques at the frontiers of magnetic resonance. For example, we are the leading laboratory when it comes to NMR at highest pressures and magnetic fields.

Jürgen Haase

7.2 ^{75}As NMR study of overdoped $CeFeAsO_{0.8}F_{0.2}$

D. Rybicki*, T. Meißner, G.V.M. Williams†, S.V. Chong‡, M. Lux, J. Haase

*AGH University of Science and Technology, Faculty of Physics and Applied Computer Science, Department of Solid State Physics, Kraków, Poland

†SCPS, Victoria University of Wellington, Wellington, New Zealand

‡Callaghan Innovation Research Limited, Lower Hutt, New Zealand

We report on the results from a ^{75}As nuclear magnetic resonance (NMR) study of the overdoped iron pnictide superconductor $CeFeAsO_{0.8}F_{0.2}$. We find two As sites with different shifts at temperatures as high as 100 K, which is above the superconducting transition temperature of 39 K, and hence they cannot be attributed to the effect of

vortices in the superconducting state as previously suggested (Ghoshray et al 2009 Phys. Rev. B 79 144512). The much larger spin-lattice relaxation rate compared with that found in other pnictides without magnetic rare earth ions, and the temperature dependence of the ^{75}As NMR shifts for the two central lines, are consistent with the hyperfine coupling from magnetic Ce to As. The low temperature spectra indicate that there are As ions with two different quadrupole splittings. Our findings appear to be consistent with an electronic phase segregation into regions with two different F dopings or the presence of a correlated spatial charge and spin density variations.

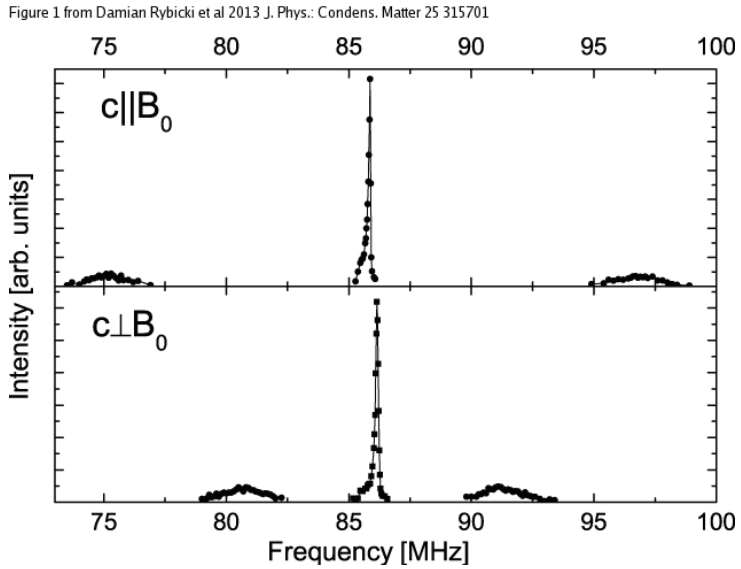

Figure 7.1: ^{75}As spectra of $CeFeAsO_{0.8}F_{0.2}$ at 11.75 T and at 297 K for two orientations of the external field with respect of the c axis, i. e. $c \parallel B_0$ and $c \perp B_0$. (©IOP Publishing Ltd – see [1] for more information).

[1] Journal of Physics: Condensed Matter 25 (2013) 315701, iopscience.iop.org/0953-8984/25/31/315701/

7.3 Charge Inhomogeneity in Electron-Doped $Pr_{1.85}Ce_{0.15}CuO_4$ Determined with ^{63}Cu NMR

M. Jurkutat, J. Haase, A. Erb*

*Walther-Meissner-Institute for Low Temperature Research, Garching, Germany

Nuclear Magnetic Resonance (NMR) of Cu and O has been applied successfully to probe locally the charge distribution in the CuO_2 plane of the hole-doped cuprates. However, for the electron-doped systems, only insufficient Cu NMR data are available. Here, with a set of new ^{63}Cu NMR experiments including double-resonance experiments, we examine the quadrupole interaction for a single crystal of $Pr_{1.85}Ce_{0.15}CuO_4$. From the data, we deduce that the doped electrons mainly enter the Cu $3d_{x^2-y^2}$ orbital resulting in an almost vanishing electric field gradient. In addition, we observe a substantial

variation across the CuO_2 plane that, however, remains largely axially symmetric. We estimate 13 % doped carriers at 15 % nominal doping with a charge density variation of at least 4 % for this optimally doped sample.

7.4 Magnetic resonance imaging at frequencies below 1 kHz

I. Hilschenz*, R. Körber*, H.-J. Scheer*, T. Fedele†, H.-H. Albrecht*, A.M. Cassará‡, S. Hartwig*, L. Trahms*, J. Haase, M. Burghoff*

*Physikalisch-Technische Bundesanstalt (PTB), Berlin, Germany
†Department of Neurology, Charité Campus Benjamin Franklin, Berlin, Germany
‡Museo Storico della Fisica e Centro Studi e Ricerche E. Fermi, Rome, Italy

Within the magnetic resonance imaging (MRI) community the trend is going to higher and higher magnetic fields, ranging from 1.5 T to 7 T, corresponding to Larmor frequencies of 63.8-298 MHz. Since for high-field MRI the magnetization increases with the applied magnetic field, the signal-to-noise-ratio increases as well, thus enabling higher image resolutions. On the other hand, MRI is possible also at ultra-low magnetic fields, as was shown by different groups. The goal of our development was to reach a Larmor frequency range of the low-field MRI system corresponding to the frequency range of human brain activities ranging from near zero-frequency (near-DC) to over 1 kHz. Here, first 2D MRI images of phantoms taken at Larmor frequencies of 100 Hz and 731 Hz will be shown and discussed. These frequencies are examples of brain activity triggered by electrostimulation of the median nerve. The method will allow the magnetic fields of the brain currents to influence the magnetic resonance image, and thus lead to a direct functional imaging modality of neuronal currents.

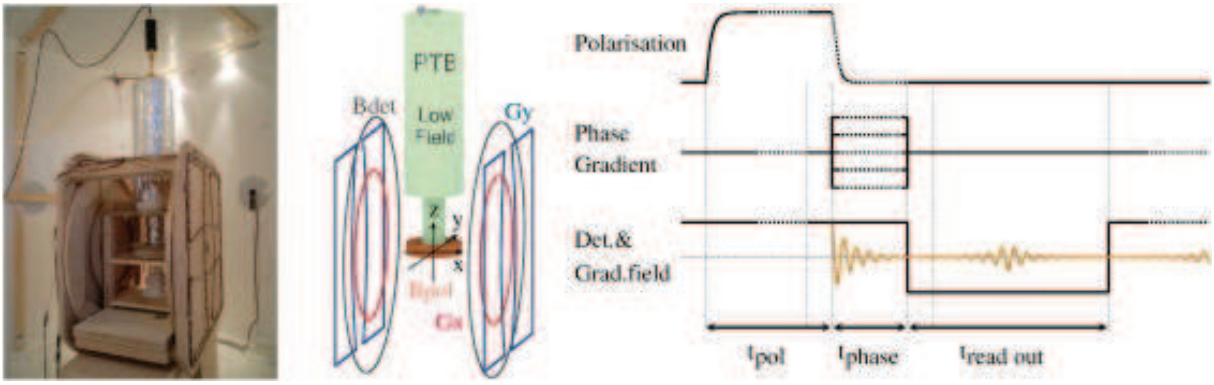

Figure 7.2: (Left) Picture of the imaging setup inside the magnetically shielded room. (Middle) schematic imaging setup showing MRI coils $B_{det} \parallel$ x, $B_{pol} \parallel$ z. (Right) 2D Fourier imaging sequence with gradient echo. (©Elsevier B. V. – see [1] for more information).

[1] Magnetic Resonance Imaging 31 (2013) 171-177, dx.doi.org/10.1016/j.mri.2012.06.014

7.5 Ion and water mobility in hydrated Li-LSX zeolite studied by ^{1}H, ^{6}Li and ^{7}Li NMR spectroscopy and diffusometry

D. Freude, S. Beckert, F. Stallmach, R. Kurzhals*, D. Täschner*, H. Toufar†, J. Kärger, J. Haase

*Clariant Produkte GmbH, Werk Bitterfeld, Bitterfeld-Wolfen, Germany
†Süd-Chemie INC - a Clariant Group Company, Louisville, USA

Crystallites of zeolite LSX with a diameter of about 10 Î¼m were synthesized. Crystals of this size are shown to allow the simultaneous investigation of intracrystalline mass transfer phenomena of water molecules and lithium ions in hydrated zeolite Li-LSX by NMR diffusometry. By MAS NMR spectroscopy with the ^{1}H and ^{6}Li nuclei, the water molecules and lithium ions are found to yield two signals, a major and a minor one, which may be attributed to locations in the sodalite cages and the supercages, respectively. By ^{1}H and ^{6}Li exchange spectroscopy the mean residence times in the sodalite cages at 373 K are found to be about 150 ms for the water molecules and about 40 ms for the lithium cations. PFG NMR self-diffusion measurements at 373 K yield a diffusivity of about 2 x 10^{-11} m^2 s^{-1} for the lithium ions, which is about one order of magnitude below the water diffusivity.

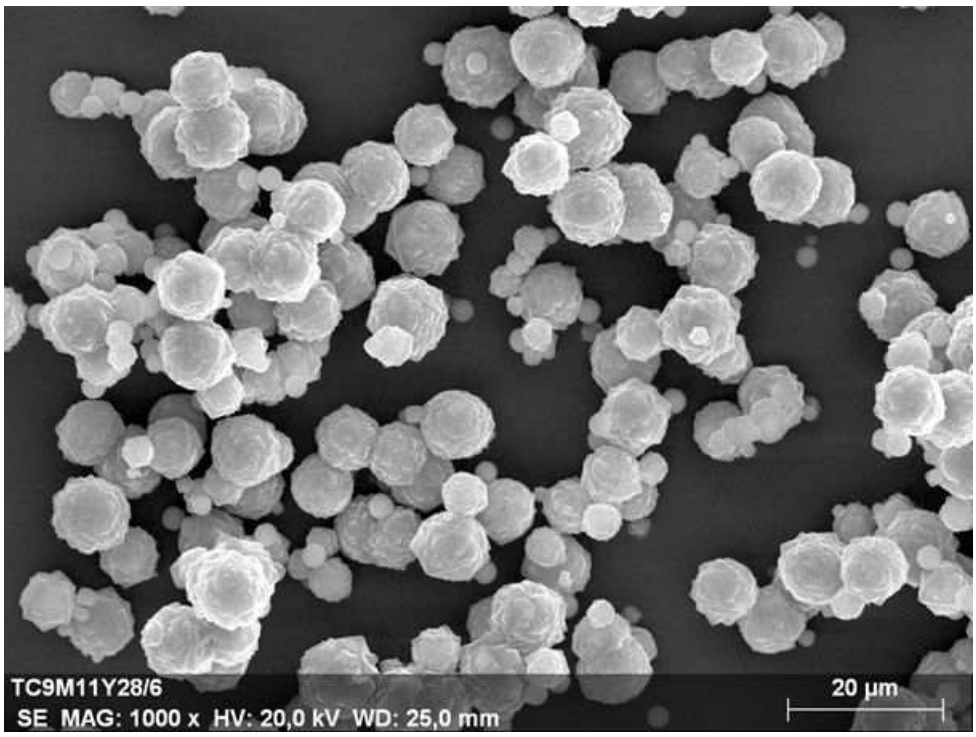

Figure 7.3: Electron microscopic picture of the LSX crystallites. (©Elsevier B. V. – see [1] for more information).

[1] Microporous and Mesoporous Materials 172 (2013) 174-181, dx.doi.org/10.1016/j.micromeso.2013.01.011

7.6 Tracing Water and Cation Diffusion in Hydrated Zeolites of Type Li-LSX by Pulsed Field Gradient NMR

S. Beckert, F. Stallmach, H. Toufar*, D. Freude, J. Kärger, J. Haase

*Süd-Chemie INC - a Clariant Group Company, Louisville, USA

The pulsed field gradient (PFG) technique of NMR is exploited for recording the time-dependent mean diffusion path lengths of both the water molecules (via ^{1}H NMR) and the cations (via ^{7}Li NMR) in hydrated zeolite Li-LSX. The observed propagation patterns reveal, for both the water molecules and the cations, two types of transport resistances, acting in addition to the diffusion resistance of the genuine pore network. They are attributed to the interfaces at the boundary between the purely crystalline regions (crystallites) within the Li-LSX particles (intergrowths) under study and to the external surface of either the particles themselves or crystallite aggregates within these particles. The cation diffusivity is retarded by about 1 order of magnitude in comparison with the water diffusivity. This notably exceeds the retardation of cation diffusion in comparison with water in free solution, reflecting the particular influence of the zeolite lattice on the guest mobility.

7.7 Investigation of the spin-lattice relaxation of ^{13}CO and $^{13}CO_2$ adsorbed in the metal-organic frameworks $Cu_3(btc)_2$ and $Cu_{3-x}Zn_x(btc)_2$

F. Gul-E-Noor, D. Michel, H. Krautscheid, J. Haase, M. Bertmer

The ^{13}C nuclear spin-lattice relaxation time of ^{13}CO and $^{13}CO_2$ molecules adsorbed in the metal-organic frameworks (MOFs) $Cu_{2.97}Zn_{0.03}(btc)_2$ and $Cu_3(btc)_2$ is investigated over a wide range of temperatures at resonance frequencies of 75.468 and 188.62 MHz. In all cases a mono-exponential relaxation is observed, and the ^{13}C spin-lattice relaxation times (T_1) reveal minima within the temperature range of the measurements and both frequencies. This allows us to carry out a more detailed analysis of the ^{13}C spin relaxation data and to consider the influence due to the spectral functions of the thermal motion. In a model-free discussion of the temperature dependence of the ratios T_1 (T)/$T_{1,min}$ we observe a motional mechanism that can be described by a single correlation time. In relation to the discussion of the relaxation mechanisms this can be understood in terms of dominating translational motion with mean jump distance being larger than the minimum distances between neighboring adsorption sites in the MOFs. A more detailed discussion of the jump-like motion observed here might be carried out on the basis of self-diffusion coefficients. From the present spin relaxation measurements activation energies for the local motion of the adsorbed molecules in the MOFs can be estimated to be 3.3 kJ/mol and 2.2 kJ/mol, for CO and CO_2 molecules, respectively. Finally, our findings are compared with our recent results derived from the ^{13}C line shape analysis.

7.8 Time dependent water uptake in $Cu_3(btc)_2$ MOF: Identification of different water adsorption states by ^1H MAS NMR

F. Gul-E-Noor, D. Michel, H. Krautscheid, J. Haase, M. Bertmer

The hydration process in a deuterated $Cu_3(btc)_2$ (d-$Cu_3(btc)_2$) metal-organic framework (MOF) was followed by ^1H solid state NMR. Various hydrated states of d-$Cu_3(btc)_2$ are studied at definite time intervals after exposition of the MOF to atmospheric water. ^1H MAS NMR spectra indicate different positions of the water molecules inside the $Cu_3(btc)_2$ framework, and a distribution of chemical shifts. The change of the different water signals with time is followed by an intensity analysis. Fast exchange dynamics is observed when the amount of water is above two molecules per copper atom.

7.9 Adsorption of Small Molecules on $Cu_3(btc)_2$ and $Cu_{3-x}Zn_x(btc)_2$ Metal-Organic Frameworks (MOF) As Studied by Solid-State NMR

F. Gul-E-Noor, M. Mendt, D. Michel, A. Pöppl, H. Krautscheid, J. Haase, M. Bertmer

Static and MAS ^{13}C NMR techniques are used to investigate the interaction of CO and CO_2 molecules with the host structure of the MOFs $Cu_3(btc)_2$ and $Cu_{2.97}Zn_{0.03}(btc)_2$. A defined amount of ^{13}C-enriched molecules per copper atom was adsorbed. The ^{13}C chemical shift anisotropy and isotropic chemical shift were studied over a temperature range from 10 to 353 K. Already above 30 K an isotropic line for CO is found superimposed to the solidlike spectra belonging to the majority of adsorbed CO molecules. For adsorbed CO_2 an isotropic line can be detected above 70 K. This observation reflects differences in the local motion of both molecules. At high temperatures it is found that CO is desorbed more easily from the MOF framework in comparison to CO_2. This is in agreement with conclusions derived from desorption measurements on $Cu_3(btc)_2$. From the temperature dependence of the chemical shift for adsorbed CO_2 molecules (measured by means of ^{13}C MAS NMR between 213 and 353 K) and from the deconvolution of the overlapping ^{13}C NMR lines for adsorbed CO molecules (between 180 and 323 K), the activation energy for the local motion of the adsorbed molecules was determined as 3.3 and 6.1 kJ/mol, respectively. Additionally, the motion is accompanied by a partial desorption of the adsorbed species.

[1] Journal of Physical Chemistry C 117 (2013) 7703-7712, pubs.acs.org/doi/abs/10.1021/jp400869f

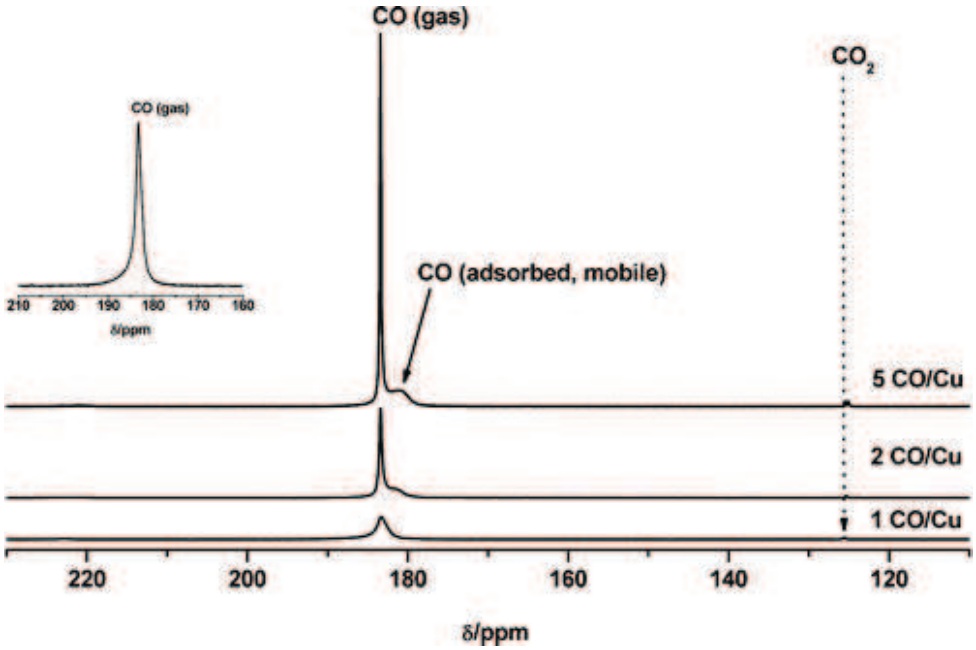

Figure 7.4: ^{13}C MAS NMR spectra of 1, 2, and 5 CO/Cu recorded at 298 K. For a better visual inspection, the spectrum for 1 CO/Cu is also shown enlarged in the inset. (©American Chemical Society – see [1] for more information).

7.10 Synthesis, Crystal Structure, and Solid-State NMR Investigations of Heteronuclear Zn/Co Coordination Networks - A Comparative Study

A.V. Kuttatheyil, D. Lässig, J. Lincke, M. Kobalz, M. Baias*, K. König†, J. Hofmann†, H. Krautscheid, C.J. Pickard‡, J. Haase, M. Bertmer

*Universitè de Lyon, Centre de RMN á très hauts champs, CNRS/ENS Lyon/UCBL, Villeurbanne, France
†Institut fÃ¼r Nichtklassische Chemie e. V., Leipzig, Germany
‡Department of Physics & Astronomy, University College London, London, United Kingdom

Synthesis and solid-state NMR characterization of two isomorphous series of zinc and cobalt coordination networks with 1,2,4-triazolyl benzoate ligands are reported. Both series consist of 3D diamondoid networks with four-fold interpenetration. Solid-state NMR identifies the metal coordination of the ligands, and assignment of all ^{1}H and ^{13}C shifts was enabled by the combination of ^{13}C editing, FSLG-HETCOR spectra, and 2D ^{1}H-^{1}H back-to-back (BABA) spectra with results from NMR-CASTEP calculations. The incorporation of Co^{2+} replacing Zn^{2+} ions in the MOF over the full range of concentrations has significant influences on the NMR spectra. A uniform distribution of metal ions is documented based on the analysis of ^{1}H T_1 relaxation time measurements.

7.11 A Solid-Solution Approach to Mixed-Metal Metal-Organic Frameworks - Detailed Characterization of Local Structures, Defects and Breathing Behaviour of AI/V Frameworks

O. Kozachuk*, M. Meilikhov*, K. Yusenko*, A. Schneemann*, B. Jee, A.V. Kuttatheyil, M. Bertmer, C. Sternemann†, A. Pöppl, R.A. Fischer*

*Chair of Inorganic Chemistry II, Organometallics and Materials Chemistry, Ruhr-University Bochum, Bochum, Germany
†Fakultät Physik/DELTA, Technische Universität Dortmund, Dortmund, Germany

The doping of $[Al(OH)L]_n$ [L = 1,4-benzenedicarboxylate (bdc) or 1,4-naphthalenedicarboxylate (ndc)] with vanadium ions yields crystalline porous mixed-metal solid-solution metal-organic frameworks (MOFs) of general formula $[(AlOH)_{1-x}(VO)_xL]_n$ (x can be varied in the whole range from 0 to 1). Several characterization methods, including powder X-ray diffraction (PXRD), electron paramagnetic resonance (EPR), solid-state NMR and FTIR spectroscopy, strongly support the effective incorporation of vanadium cations. The Al/V-doped MOFs are isostructural to the parent monometallic MOFs and show a characteristic uniform dependence of the cell parameters on the metal ratios. Detailed spectroscopic investigation provided evidence that the introduced species are fairly well ordered. Interestingly, for low amounts of doped vanadium for both activated and as-synthesized Al/V phases, the EPR results revealed the presence of vanadyl units as local defects in pseudo-octahedral or square-pyramidal environments, which are different from those in the parent MIL-47(V). This observation matches the nonlinear response of the adsorption properties on variation of the composition. Remarkably, the presence of such mixed Al/V chains strongly affects the breathing behaviour of the materials. Both CO_2 sorption and in situ PXRD studies validated a gradual change from highly flexible (with easily induced phase transitions) to totally rigid structures upon increasing vanadium content.

7.12 Binary and Ternary Metal-Organic Hybrid Polymers in Aqueous Lead(II)-Dicarboxylic Acid-(Phen) Systems. The Influence of O- and S-Ligand Heteroatoms on the Assembly of Distinct Lattice Architecture, Dimensionality, and Spectroscopic Properties

C. Gabriel*, C.P. Raptopoulou†, A. Terzis†, V. Psycharis†, F. Gul-E-Noor, M. Bertmer, C. Mateescu‡, A. Salifoglou*

*Department of Chemical Engineering, Laboratory of Inorganic Chemistry, Aristotle University of Thessaloniki, Thessaloniki, Greece

[†]Institute of Advanced Materials, Physicochemical Processes, Nanotechnology and Microsystems, Department of Materials Science, NCSR Demokritos, Aghia Paraskevi, Attiki, Greece
[‡]Banats University of Agricultural Sciences and Veterinary Medicine from Timisoara, Timisoara, Romania

Poised to understand the influence of O- and S-heteroatoms on the chemical reactivity of dicarboxylic acids toward Pb(II), leading to crystalline metal-organic hybrid materials with distinct lattice architecture, dimensionality, and spectroscopic properties, the synthesis and physicochemical properties of binary/ternary Pb(II)-(O,S)-dicarboxylic acid-(phenanthroline) systems was investigated in aqueous media. pH-specific hydrothermal reactions of Pb(II) with O- and S-dicarboxylic acid ligands and phenanthroline (phen) afforded the variable dimensionality metal-organic Pb(II) polymers $[Pb_3(oda)_3]_n$ (1), $[Pb(phen)(oda)]_n$ (2), $[Pb(tda)]_n$ (3), and $[Pb(phen)(tda)]_n$ (4). The choice of O- vs S-ligands in the aqueous systems of Pb(II) and phenanthroline is linked to the emergence of distinct lattice composition-dimensionality (2D-3D) changes at the binary and ternary level, bestowing spectroscopic fingerprint identity to Pb(II) coordination and luminescence activity.

7.13 H_2, D_2 and HD adsorption upon the metal-organic framework $[Cu_{2.97}Zn_{0.03}(btc)_2]_n$ studied by pulsed ENDOR and HYSCORE spectroscopy

B. Jee, M. Hartmann[*], A. Pöppl

[*]Erlangen Catalysis Resource Center, Universität Erlangen-Nürnberg, Erlangen, Germany

The adsorption of hydrogen has become interesting in terms of gas separation as well as safe and reversible storage of hydrogen as an energy carrier. In this regard, metal-organic framework compounds are potential candidates. The metal-organic framework $[Cu_{2.97}Zn_{0.03}(btc)_2]_n$ as a partially Zn-substituted analogue of the well known compound HKUST-1 is well suited for studying adsorption geometries at cupric ions by electron paramagnetic resonance (EPR) methods due to the formation of few mixed Cu/Zn paddle wheel units with isolated $S = 1/2$ electron spins. The adsorption of hydrogen (H_2) as well as the deuterium (D_2) and HD molecules were investigated by continuous wave EPR and pulsed ENDOR and HYSCORE spectroscopy. The principal values of the proton and deuterium hyperfine coupling tensors A^H and A^D were determined by spectral simulations as well as of the deuterium nuclear quadrupole tensor Q^D for adsorbed HD and D_2. The results show a side-on coordination of HD and D_2 with identical Cu-H and Cu-D distances r_{CuX} = 2.8 Åwith the tensors $A^{H,D}$ and Q^D aligned parallel to the C_4 symmetry axis of the paddle wheel unit. A thermodynamic non-equilibrium state with $J = 1$, $m_J = \pm 1$ is indicated by the experimental data with $A^{H,D}$ and Q^D averaged by rotation around C_4.

7.14 A Combined Pulsed Electron Paramagnetic Resonance Spectroscopic and DFT Analysis of the $^{13}CO_2$ and ^{13}CO Adsorption on the Metal-Organic Framework $Cu_{2.97}Zn_{0.03}(btc)_2$

B. Jee, P.St. Petkov*, G.N. Vayssilov*, T. Heine† M. Hartmann‡, A. Pöppl

*Faculty of Chemistry and Pharmacy, University of Sofia, Sofia, Bulgaria
†School of Engineering and Science, Jacobs University Bremen, Bremen, Germany
‡Erlangen Catalysis Resource Center, Universität Erlangen-Nürnberg, Erlangen, Germany

$Cu_3(btc)_2$ (btc = 1,3,5-benzenetricarboxylate), also called HKUST-1, is one of the well-known representatives of the metal-organic framework (MOF) compounds. It exhibits a large surface area and a high pore volume. Due to the coordinatively unsaturated metal centers as preferential adsorption sites, $Cu_3(btc)_2$ is particularly interesting for the separation of CO_2 and CO in gaseous mixtures. We studied the interactions of ^{13}C-enriched carbon dioxide ($^{13}CO_2$) and carbon monoxide (^{13}CO) with the Cu^{2+} centers in the zinc-substituted homologue $Cu_{2.97}Zn_{0.03}(btc)_2$ using continuous wave (cw) and pulsed electron paramagnetic resonance (EPR) spectroscopy (Davies or Mims electron nuclear double resonance (ENDOR) and hyperfine sublevel correlation (HYSCORE)). Upon adsorption of $^{13}CO_2$ and ^{13}CO, the coordination geometry of the Cu^{2+} centers changed from square planar to square pyramidal. The cupric ion g-tensor and the $^{63/65}Cu$ hyperfine coupling tensor A^{Cu} show the changes in the ligand field of Cu^{2+}. Moreover, the interaction with the ^{13}C nuclei of the gas molecules is reflected in the isotropic coupling constant $A_{iso}{}^{C}$ and the dipolar coupling parameter T^C which are derived from the ^{13}C hyperfine coupling tensor A^C obtained by the pulsed EPR experiments. From the experimentally obtained parameters, we derived a geometrical model for the adsorption of $^{13}CO_2$ and ^{13}CO at the Cu^{2+} ions that is consistent with our DFT calculations. The ^{13}CO molecule is found to coordinate linearly at the Cu^{2+} center via the ^{13}C atom and perpendicular to the CuO_4 plane with a Cu-C distance of r_{CuC} = 2.57(10) Å(DFT, 2.42 Å). The $^{13}CO_2$ molecule is coordinated slightly tilted via the O atom with a Cu-C distance of r_{CuC} = 3.34(10) Å(DFT, 3.27 Å). The Cu-O distance for adsorbed $^{13}CO_2$ is not directly accessible to EPR measurements but could be estimated from geometrical considerations in the range of r_{CuO} = 2.53-2.73 Å(DFT, 2.39 Å). The results provide detailed insight into the geometry of adsorbed CO_2 and CO in porous materials and show the potential of EPR spectroscopy for analyzing adsorption complexes.

[1] Journal of Physical Chemistry C 117 (2013) 8231-8240, pubs.acs.org/doi/abs/10.1021/jp4003033

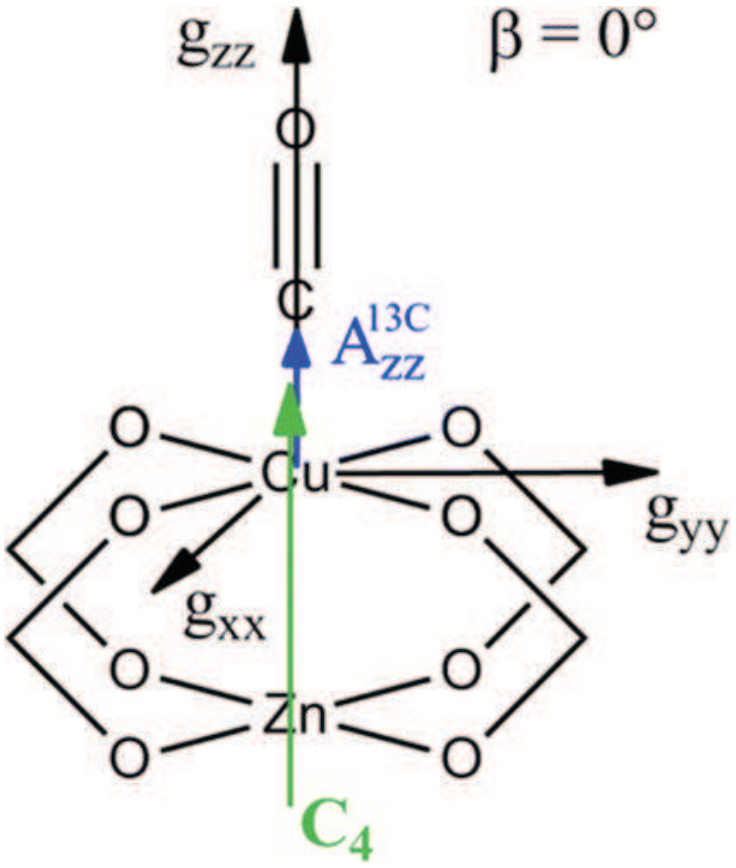

Figure 7.5: Schematic representation of the coordination geometry of ^{13}CO adsorbed at Cu^{2+} ions in $[Cu_{2.97}Zn_{0.03}(btc)_2]_n$ derived from pulsed ENDOR and HYSCORE experiments. The z-axes of the g- and A^C-tensor are coaxial ($\beta = 0°$). The Cu-^{13}C distance is $r_{CuC} = 2.57$ Å. (©American Chemical Society – see [1] for more information).

7.15 Superhyperfine Interactions of the Nitrogen Donors in 4H SiC Studied by Pulsed ENDOR and TRIPLE ENDOR Spectroscopy

D.V. Savchenko[*] [†], E.N. Kalabukhova[†], E.N. Mokhov[‡], A. Pöppl

[*]Institute of Physics, AS CR, Prague, Czech Republic
[†]V.E. Lashkaryov Institute of Seminconductor Physics, NASU, Kiev, Ukraine
[‡]A.F. Ioffe Physical Technical Institute, RAS, St. Petersburg, Russia

The nitrogen donors residing at quasi-cubic lattice site (N_k) in 4H SiC were investigated by field sweep electron spin echo (FS ESE), pulsed electron nuclear double resonance (ENDOR) and pulsed General TRIPLE ENDOR spectroscopy. The ^{29}Si and ^{13}C superhyperfine lines observed in the FS ESE and ENDOR spectra of N_k in n-type 6H SiC were assigned by pulsed General TRIPLE resonance spectroscopy to the specific carbon (C) and silicon (Si) atoms located in the nearest environment of N_k in 4H SiC. The superhyperfine interaction constants and their relative signs for N_k with ^{29}Si and ^{13}C nuclei located in the nearest-neighbor shells are found from the General TRIPLE

ENDOR spectra to be positive for C atoms and negative for Si atoms.

7.16 Combined proton NMR wideline and NMR relaxometry to study SOM-water interactions of cation-treated soils

G.E. Schaumann[*], D. Diehl[*], M. Bertmer, A. Jäger[*], P. Conte[†], G. Alonzo[†], J. Bachmann[‡]

[*]University of Koblenz-Landau, Institute for Environmental Sciences, Department of Environmental and Soil Chemistry, Landau, Germany
[†]Dipartimento dei Sistemi Agro-Ambientali, Università degli Studi di Palermo, Palermo, Italy
[‡]Leibniz University Hannover, Institute of Soil Science, Hannover, Germany

Focusing on the idea that multivalent cations affect SOM matrix and surface, we treated peat and soil samples by solutions of NaCl, CaCl2 or AlCl3. Water binding was characterized with low field 1H-NMR-relaxometry (20 MHz) and 1H wideline NMR spectroscopy (400 MHz) and compared to contact angles. From 1H wideline, we distinguished mobile water and water involved in water molecule bridges (WaMB). Large part of cation bridges (CaB) between SOM functional groups are associated with WaMB. Unexpectedly, 1H NMRrelaxometry relaxation rates suggest that cross-linking in the Al-containing peat is not stronger than that by Ca. The relation between percentage of mobile water and WaMB water in the context of wettability and 1H NMR relaxation times confirms that wettability controls the water film surrounding soil particles. Wettability is controlled by WaMB-CaB associations fixing hydrophilic functional groups in the SOM interior. This can lead to severe water repellency. Wettability decreases with increasing involvement of functional groups in CaB-WaMB associations. The results demonstrate the relevance of CaB and WaMB for the dynamics of biogeochemical and hydrological processes under field conditions, as only a few percent of organic matter can affect the physical, chemical, and biological functioning of the entire 3-phase ecosystem.

7.17 Restructuring of a Peat in Interaction with Multivalent Cations: Effect of Cation Type and Aging Time

Y.K. Mouvenchery[*], A. Jäger[*], A.J.A. Aquino[†], D. Tunega[†], D. Diehl[*], M. Bertmer, G.E. Schaumann[*]

[*]University of Koblenz-Landau, Institute for Environmental Sciences, Department of Environmental and Soil Chemistry, Landau, Germany
[†]University of Natural Resources and Life Sciences, Vienna Institute of Soil Research, Vienna, Austria

It is assumed to be common knowledge that multivalent cations cross-link soil organic matter (SOM) molecules via cation bridges (CaB). The concept has not been explicitly

demonstrated in solid SOM by targeted experiments, yet. Therefore, the requirements for and characteristics of CaB remain unidentified. In this study, a combined experimental and molecular modeling approach was adopted to investigate the interaction of cations on a peat OM from physicochemical perspective. Before treatment with salt solutions of Al^{3+}, Ca^{2+} or Na^{+}, respectively, the original exchangeable cations were removed using cation exchange resin. Cation treatment was conducted at two different values of pH prior to adjusting pH to 4.1. Cation sorption is slower (»2 h) than deprotonation of functional groups (<2 h) and was described by a Langmuir model. The maximum uptake increased with pH of cation addition and decreased with increasing cation valency. Sorption coefficients were similar for all cations and at both pH. This contradicts the general expectations for electrostatic interactions, suggesting that not only the interaction chemistry but also spatial distribution of functional groups in OM determines binding of cations in this peat. The reaction of contact angle, matrix rigidity due to water molecule bridges (WaMB) and molecular mobility of water (NMR analysis) suggested that cross-linking via CaB has low relevance in this peat. This unexpected finding is probably due to the low cation exchange capacity, resulting in low abundance of charged functionalities. Molecular modeling demonstrates that large average distances between functionalities (3 nm in this peat) cannot be bridged by CaB-WaMB associations. However, aging strongly increased matrix rigidity, suggesting successive increase of WaMB size to connect functionalities and thus increasing degree of cross-linking by CaB-WaMB associations. Results thus demonstrated that the physicochemical structure of OM is decisive for CaB and aging-induced structural reorganisation can enhance cross-link formation.

7.18 Ultraslow Li Exchange Processes in Diamagnetic Li_2ZrO_3 As Monitored by EXSY NMR

P. Bottke*, D. Freude, M. Wilkening*

*Institute for Chemistry and Technology of Materials, Graz University of Technology, Graz, Austria

Two-dimensional (2D) ^{6}Li exchange magic angle spinning (MAS) nuclear magnetic resonance (NMR) spectroscopy was used to probe extremely slow lithium hopping processes in a polycrystalline powder sample of lithium zirconate, Li_2ZrO_3. In agreement with the crystal structure of Li_2ZrO_3, the ^{6}Li MAS NMR spectra recorded are composed of two signals (- 0.10 and 0.26 ppm) with equal intensity. They reflect the two magnetically (and electrically) inequivalent Li sites in Li_2ZrO_3. The mixing-time dependent 2D MAS NMR spectra, which were acquired at a bearing gas temperature of ca. 310 K, clearly reveal off-diagonal intensities indicating Li exchange processes with exchange rates as low as 60 jumps/hour. To our knowledge, this is by far one of the slowest Li solid-state diffusion processes ever probed by ^{6}Li 2D exchange MAS NMR spectroscopy.

7.19 Funding

Aufkärung des Ladungstransports in funktionalisierten porösen Organosilikaten und Kompositmembranen mit MAS-NMR-Spektroskopie und Diffusometrie
Prof. Dr. Jürgen Haase, Prof. Dr. Michael Wark
DFG, HA 1893/9-1

MOFs as carrier for nitric oxide delivery in biological systems - microscopic fundamentals of adsoprtion and controlled release studied by infrared and electron and nuclear spin resonance spectroscopy
PD Dr. Marko Bertmer, Prof. Dr. Andreas Pöppl, Prof. Dr. Martin Hartmann, Prof. Dr. Michael Fröba
DFG, BE 2434/4-2, PO 426/8-2

A coordinated approach to access, experimental developement and scientific exploitation of all European large infrastructures for high magnetic fields
Dr. Geert L. J. A. Rikken, Prof. Dr. J. C. Maan, Prof. Dr. Joachim Wosnitza, Prof. Dr. Jürgen Haase, Prof. Robin Nicholas, Ago Samoson, Prof. Lucio Frydman
EU, 228043

Charakterisierung der [2+2]-Photodimerisierung von photoaktiven Substanzen auf der Basis von Zimtsäure eingebaut in Polymeren oder in supramolekularen Strukturen mit Festkörper-NMR-Spektroskopie
PD Dr. Marko Bertmer
DFG, BE 2434/2-3

Paramagnetic adsorption sites in microporous crystalline solids studied by electron paramagnetic resonance spectroscopy from single crystals to oriented thin films
Prof. Dr. Andreas Pöppl
DFG, PO 426/11-1

7.20 Organizational Duties

Professor Dr. Jürgen Haase

- Dean of the Faculty
- Vice Director of the Magnetic Resonance Center Leipzig
- Board Member of the Heisenberg Gesellschaft e. V.
- Full Member of the Saxonian Academy of Sciences in Leipzig
- Member of the German Physical Society
- Member of the American Physical Society
- Member of the "ICAM Board of Goveners" of the Institute for Complex Adaptive Matter
- Referee: Physical Review, Science, IOP, German-Israeli Foundation for Scientific Research and Developement

Prof. Dr. Andreas Pöppl

- Referee: Journal ofMagnetic Resonance, Journal ofAmericanChemical Society, Physical Chemistry Chemical Physics, Chemical Physics Letters

- Project Reviewer: German-Israeli Foundation for Scientific Research and Development

PD Dr. Marko Bertmer
- Referee: AngewandteChemie,Chemistry ofMaterials, Journal of PhysicalChemistry, Solid State Nuclear Magnetic Resonance

Prof. Dr. Dieter Michel
- Full Member of the Saxonian Academy of Sciences in Leipzig
- Member of the German Physical Society
- Member of the Society of German Chemists
- German Coordinator of the German-Russian Centre "Applied and Computational Physics (ACOPhys)" at the St. Petersburg State University
- Member at the International Advisory Committee of the International Meeting of Ferroelectricity
- Member at the International Advisory Committee of the European Meeting of Ferroelectricity
- Member at the International Advisory Committee of the Conference "NMR of Condensed Matter St. Petersburg"
- Member of the German-Israeli Foundation for Scientific Research and Developement
- Referee: Physical Review, Journal of Physics: Condensed Matter, Langmuir, Journal of Magnetic Resonance, Phys. Stat. Sol., Materials Chemistry and Physics, German-Israeli Foundation for Scientific Research and Developement

Prof. Dr. Rolf Böttcher
- Referee: Physical Review, Journal of Physics: Condensed Matter, Langmuir, Journal of Magnetic Resonance

7.21 External Cooperations

Academic

- Technical University Munich, Physics Department, Crystal Lab, Garching, Germany
  Prof. Dr. Andreas Erb
- Cavendish Laboratory, Cambridge, UK
  S. K. Goh, P. Alireza
- Washington University, St. Louis, MO, USA
  J. Schilling, M. Conradi
- Victoria University, Physics Department, Wellington, New Zealand
  Dr. Grant V. M. Williams
- Helmholtz-Zentrum Dresden-Rossendorf, Dresden, Germany
  Prof. Dr. J. Wosnitza
- University of Minnesota, School of Physics and Astronomy, USA
  Prof. Dr. M. Greven

- University of Illinois at Urbana-Champaign, Department of Physics, USA
  Prof. Dr. C. P. Slichter
- Laboratoire National des Champs Magnétiques Pulsès, Toulouse, France
  Prof. Dr. G. Rikken
- University of New South Wales, School of Physics, Sydney, Australia
  Prof. Dr. O. Sushkov
- Washington University, Department of Chemistry, St. Louis, MO, USA
  Sophia E. Hayes
- Universität Koblenz-Landau, Abteilung Chemie, Landau, Germany,
  Prof. Dr. Gabriele Schaumann
- Martin-Luther-Universität Halle-Wittenberg, Halle, Germany
  Dr. H. T. Langhammer
- Kazan State University, Tartastan, Russian Federation
  Prof. Dr. E. N. Kalabukhova
- Universität Erlangen-Nürnberg, Erlangen Catalysis Resource Center - ECRC, Erlangen, Germany
  Prof. Dr. Martin Hartmann
- Université du Maine, Laboratoire de Physique de l'Etat Condenseé, Le Mans, France
  Prof. Dr. A. Kassiba
- University of Vilnius, Faculty of Physics, Vilnius, Lithuania
  Prof. Dr. J. Banys
- Argonne National Laboratory, Illinois, USA
  Prof. Dr. P. Littlewood
- Georgetown University Department of Chemistry, Washington, DC, USA
  Prof. Dr. YuYe Tong
- Max Planck Institute of Solid State Research, Stuttgart, Germany
  Prof. Dr. B. Keimer
- University of Illinois at Chicago, USA
  Prof. Dr. D. K. Morr
- IFW-Dresden, Dresden, Germany
  M. Richter, H. Eschrig
- Ruhr-University Bochum, Bochum, Germany
  R. A. Fischer

Industry

- NMR-Service GmbH, Erfurt, Germany
  M. Braun
- Bruker BioSpin GmbH, Rheinstetten, Germany
  F. Engelke

7.22 Publications

Journals

D. Rybicki, T. Meißner, G.V.M. Williams, S.V. Chong, M. Lux, J. Haase
^{75}As NMR study of overdoped $CeFeAsO_{0.8}F_{0.2}$
J. Phys.: Condens. Matter **25** (2013) 315701

I. Hilschenz, R. Körber, M.-J. Scheer, T. Fedele, H.-H. Albrecht, A.M. Cassará, S. Hartwig, L. Trahms, J. Haase, M. Burghoff
Magnetic resonance imaging at frequencies below 1 kHz
Magn. Reson. Imaging **31** (2013) 171-177

D. Freude, S. Beckert, F. Stallmach, R. Kurzhals, D. Täschner, H. Toufar, J. Kärger, J. Haase
Ion and water mobility in hydrated Li-LSX zeolite studied by ^{1}H, ^{6}Li and ^{7}Li NMR spectroscopy and diffusometry
Microporous and Mesoporous Materials **172** (2013) 174-181

S. Beckert, F. Stallmach, H. Toufar, D. Freude, J. Kärger, J. Haase
Tracing Water and Cation Diffusion in Hydrated Zeolites of Type Li-LSX by Pulsed Field Gradient NMR
J. Phys. Chem. C **117** (2013) 24866-24872

F. Gul-E-Noor, D. Michel, H. Krautscheid, J. Haase, M. Bertmer
Investigation of the spin-lattice relaxation of ^{13}CO and $^{13}CO_2$ adsorbed in the metal-organic frameworks $Cu_3(btc)_2$ and $Cu_{3-x}Zn_x(btc)_2$
J. Chem. Phys **139** (2013) 034202

F. Gul-E-Noor, D. Michel, H. Krautscheid, J. Haase, M. Bertmer
Time dependent water uptake in $Cu_3(btc)_2$ MOF: Identification of different water adsorption states by ^{1}H MAS NMR
Microporous and Mesoporous Materials **180** (2013) 8-13

F. Gul-E-Noor, M. Mendt, D. Michel, A. Pöppl, H. Krautscheid, J. Haase, M. Bertmer
Adsorption of Small Molecules on $Cu_3(btc)_2$ and $Cu_{3-x}Zn_x(btc)_2$ Metal-Organic Frameworks (MOF) As Studied by Solid-State NMR
J. Phys. Chem. C **117** (2013) 7703-7712

A.V. Kuttatheyil, D. Lässig, J. Lincke, M. Kobalz, M. Baias, K. König, J. Hofmann, H. Krautscheid, C.J. Pickard, J. Haase, M. Bertmer
Synthesis, Crystal Structure, and Solid-State NMR Investigations of Heteronuclear Zn/Co Coordination Networks - A Comparative Study
Inorg. Chem. **52** (2013) 4431-4442

O. Kozachuk, M. Meilikhov, K. Yusenko, A. Schneemann, B. Jee, A.V. Kuttatheyil, M. Bertmer, C. Sternemann, A. Pöppl, R.A. Fischer
A Solid-Solution Approach to Mixed-Metal Metal-Organic Frameworks - Detailed Characterization of Local Structures, Defects and Breathing Behaviour of Al/V Frameworks
Eur. J. Inorg. Chem. (2013) 4546-4557

C. Gabriel, C.P. Raptopoulou, A. Terzis, V. Psycharis, F. Gul-E-Noor, M. Bertmer, C. Mateescu, A. Salifoglou
Binary and Ternary Metal-Organic Hybrid Polymers in Aqueous Lead(III)-Dicarboxylic Acid-(Phen) Systems. The Influence of O- and S-Ligand Heteroatoms on the Assembly of Distinct Lattice Architecture, Dimensionality, and Spectroscopic Properties
Cryst. Growth Des. **13** (2013) 2573-2589

B. Jee, M. Hartmann, A. Pöppl
H_2, D_2 and HD adsorption upon the metal-organic framwork $[Cu_{2.97}Zn_{0.03}(btc)_2]_n$ studied by pulsed ENDOR and HYSCORE spectroscopy
Molecular Physics **111** (2013) 2950-2966

B. Jee, P.St. Petkov, G.N. Vayssilov, T. Heine, M. Hartmann, A. Pöppl
A Combined Pulsed Electron Paramagnetic Resonance Spectroscopic and DFT Analysis of the $^{13}CO_2$ and ^{13}CO Adsorption on the Metal-Organic Framework $Cu_{2.97}Zn_{0.03}(btc)_2$
J. Phys. Chem. C **117** (2013) 8231-8240

D.V. Savchenko, E.N. Kalabukhova, E.N. Mokhov, A. Pöppl
Superhyperfine Interactions of the Nitrogen Donors in 4H SiC Studied by Pulsed ENDOR and TRIPLE ENDOR Spectroscopy
Materials Science Forum **740-742** (2013) 439-449

G.E. Schaumann, D. Diehl, M. Bertmer, A. Jäger, P. Conte, G. Alonzo, J. Bachmann
Combined proton NMR wideline and NMR relaxometry to study SOM-water interactions of cation-treated soils
J. Hydrol. Hydromech. **61** (1) (2013) 50-63

Y.K. Mouvenchery, A. Jäger, A.J.A. Aquino, D. Tunega, D. Diehl, M. Bertmer, G.E. Schaumann
Restructuring of a Peat in Interaction with Multi-valent Cations: Effects of Cation Type and Aging Time
PLOS One **8** (6) (2013) e65359

R.M. Rakhmatullin, L.K. Aminov, I.N. Kurkin, R. Böttcher, A. Pöppl, S. Sen
Nature of size-dependent lattice distortions in doped CeO_2
J. Appl. Phys. **114** (2013) 203507

M. Lorenz, C. Schmidt, G. Benndorf, T. Böntgen, H. Hochmuth, R. Böttcher, A. Pöppl, D. Spemann, M. Grundmann
Degenerate interface layers in epitaxial scandium-doped ZnO thin films
J. Phys. D: Appl. Phys. **46** (2013) 065311

V.V. Laguta, M. Nikl, A. Pöppl, J. Rosa, D. Savchenko, S. Zazubovich
ESR and TSL study of hole capture in $PbWO_4$:Mo,La and $PbWO_4$:Mo,Y scintillator crystals
J. Phys. D: Appl. Phys. **46** (2013) 075302

P. Bottke, D. Freude, M. Wilkening
Ultraslow Li Exchange Processes in Diamagnetic Li_2ZrO_3 As Monitored by EXSY NMR
J. Phys. Chem. C **117** (2013) 8114-8119

Talks

J. Haase *Extreme NMR of Correlated Electron Superconductors*, 25. - 29.11.2013, Gordon Godfrey Workshop on Spins and Strong Electron Correlations, Sydney, Australia

J. Haase *NMR measurements on electron- and hole-doped high-T_c superconductors*, 27.06.2013, Festkörperkolloquium, Walther Meissner Institute, Garching, Germany

J. Haase, T. Meißner *Nuclear magnetic resonance at pressures of up to 10.1 GPa detects an electronic topological transition in aluminum metal*, 18. - 22.03.2013, APS Meeting 2013, Baltimore, USA

M. Bertmer: *NMR and EPR studies of small molecules adsorption in in MOFs*, 16. - 17.09.2013, International MOF Symposium 2013, Dresden, Germany

S. Friedländer: *Sensitivity Enhancement in CW-EPR - Structure Analysis with EPR-silent Dielectric Resonators and Planar Microresonators on MOF Structures at Non-Ambient Conditions*, 13.09.2013, Annual SPP 1601 Meeting, Frauenchiemsee, Germany

S. Friedländer: *Increasing Sensitivity in EPR - Approaches for Spectroscopy of Single Crystals and Thin Films*, 08.04.2013, Young Researchers Workshop SPP 1601, Berlin, Germany

A. Pöppl: *Cw and Pulsed EPR Spectroscopy of Paramagnetic Adsorption Complexes in the Metal-Organic Framework Compound $Cu_3(btc)_2$*, 10. - 12.04.2013, Workshop "Spins as Functional Probes in Solar Energy Research", Berlin, Germany

Posters

S. Friedländer: *Increasing Sensitivity in EPR - Approaches for Spectroscopy of Single Crystals and Thin Films*, 12. - 18.01.2013, 6th Advanced EPR Winter School of EFEPR, Weizmann Institute of Science, Israel

A. Jäger: *Incorporation of organic chemicals into the organic matter of a Sapril Histosol observed by Differential Scanning Calorimetry*, 07. - 12.09.2013, Jahrestagung der Deutschen Bodenkundlichen Gesellschaft, Rostock

J. Kohlrautz, S. Reichardt, J. Haase, E. Green, T. Herrmannsdörfer, J. Wosnitza: *NMR at 60 T Relaxation measurements in pulsed magnetic fields*, 04.07.2013, EUROMAR 2013, Hersonissos, Crete, Greece

A.V. Kuttatheyil, D. Lässig, J. Lincke, H. Krautscheid, J. Haase, M. Bertmer: *CO_2 and CO adsorption dynamics in a metal-organic framework without open metal sites*, 16. - 17.09.2013, International MOF Symposium 2013, Dresden

K. Lorenz, T. Mildner, A. Pampel, H.E. Möller: *Transient effects in arterial CBV quantification*, 20. - 26.04.2013, ISMRM 2013 21st Annual Meeting & Exhibition, Salt Lake City, USA

7.23 Graduations

Doctorate

- Bettina Jee
  Cw and Pulsed EPR spectroscopy of Cu^{II} and V^{IV} in metal-organic framework compounds: metal ion coordination and adsorbate interactions
  14.10.2013
- Farhana Gul-E-Noor
  $[Cu_3(btc)_2]$ and $[Cu_{3-x}Zn_x(btc)_2]$: Electronic Effects and Small Molecules Adsorption Studied by Solid-State NMR
  17.06.2013

Diploma

- Richard Lange
  Analyse von Aerosolen mittels Spinresonanz
  26.09.2013

Master

- Stefan Friedländer
  Increasing Sensitivity in EPR Approaches for Spectroscopy of Single Crystals and Thin Films
  21.05.2013
- Tobias Herzig
  Temperaturabhängige Hochdruck-NMR - Untersuchung von Aluminium im Gigapascal-Bereich bei kryogenen Temperaturen in Hochdruck-Stempelzellen
  18.11.2013

7.24 Guests

- Denis Yurievich Nefedov
  St. Petersburg State University, St. Petersburg, Russian Federation
  September - November 2013
- Prof. Dr. Elena Charnaya
  St. Petersburg State University, St. Petersburg, Russian Federation
  September - October 2013
- Prof. Dr. Lieh-Jeng Chang
  National Cheng Kung University, Tainan, Taiwan
  January 2013
- Dr. Erica Brendler
  TU Bergakademie Freiberg, Fakultät für Chemie und Physik, Freiberg, Germany
  February 2013

- Prof. Dr. Boris Fine
  Universität Heidelberg, Institut für Theoretische Physik, Heidelberg, Germany
  June 2013
- Dr. Olaf Hellmuth
  Leibniz Institute for Tropospheric Research (TROPOS), Leipzig, Germany, January 2013
- Prof. P. K. Madhu
  Tata Institute of Fundamental Research, Department of Chemical Sciences, Mumbai, India
  July 2013
- Prof. Dr. James Schilling
  Washington University, Department of Physics, St. Louis, USA
  June 2013
- Prof. Dr. Alexander Shengelaya
  Tbilisi State University, Department of Physics, Tbilisi, Georgia
  November 2013

8

Nuclear Solid State Physics

8.1 Introduction

The division of Nuclear Solid State Physics changed its scope of research activities closer to questions of material modification and investigation. One topic in this new direction is the production of artificial single defects in solids, like colour centres in diamond. Defect centres, like the NV centre, became in the last decade an attract attention due to their extraordinary quantum mechanical properties even at room temperature. This makes them applicable as highly sensitive magnetic sensors or for the fabrication of a quantum computer. We perform the production of these centres by using single ion implantation for a large number of research groups all over the world. Highlights of these cooperations in the year 2013 are the nuclear magnetic resonance (NMR) spectroscopy of a 5 nm sample volume [1] and the first entanglement of two NV centres [2]. Both papers were generated in cooperation with the group of Jörg Wrachtrup in Stuttgart. Main tool to prepare these samples is a nanoimplanter for low energy ion implantation using a pierced AFM-tip (Fig. 8.1). The system is able to achieve a lateral resolution below 15 nm and is installed and renewed at the new joint lab founded by the Leibniz-Institut für Oberflächenmodifizierung e.V. Leipzig (IOM) and the NFP department. Beside these unique implantation tools, we set up a new optical lab with a

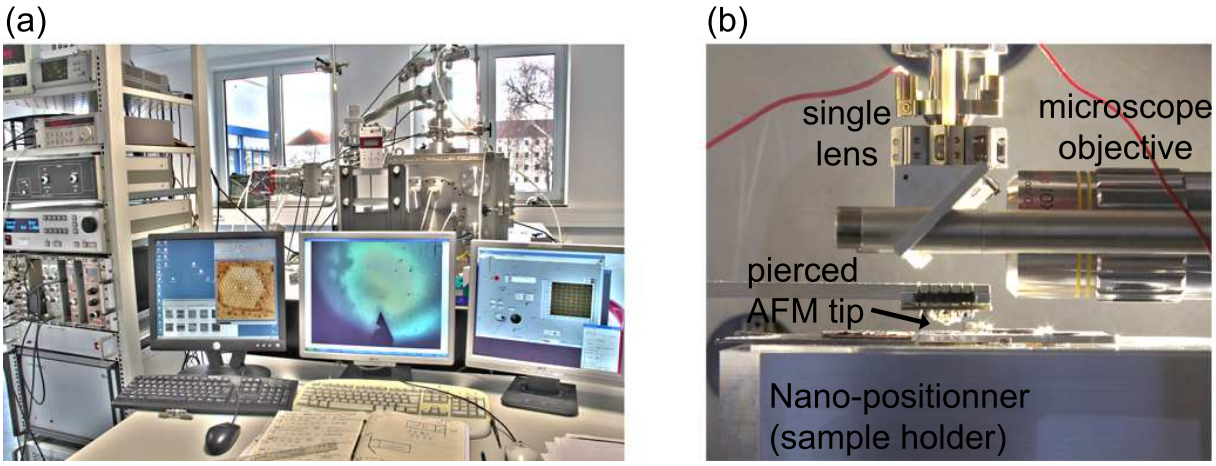

Figure 8.1: Nanoimplanter for low energy ion implantation using a pierced AFM-tip: **(a)** exterior view, **(b)** interior view.

confocal microscope and single defect spectroscopy as well as an electron microscope. We also modify the accelerator of the high energy ion microprobe LIPSION in order to accelerate heavy ions. This tool is now able to focus, e.g., nitrogen ions down to a size of a few micrometers. Additionally, we start to set up a new 150 kV implanter for nearly all types of ion species. However, the set up or rebuilding of these new equipment cost a large amount of effort. I am very happy, that we nevertheless achieved some new results like the electrical switching of NV centres using PIN junctions as well as in the study of biological questions with nano particles.

We gratefully acknowledge the financial support of our research by the DFG (FOR 1493), the VW Foundation, the BMBF, the EU, and cooperations with academic and industrial partners.

Jan Meijer

[1] T. Staudacher et al.: Science **339**, 561 (2013), doi:10.1126/science.1231675
[2] F. Dolde et al.: Nat. Phys. **9**, 139 (2013), doi:10.1038/nphys2545

8.2 Active charge state control of NV colour centres using planar pin-junctions in diamond

J. Lehnert, M. Mensing, R. Karsthof[*], C. Ronning[†], A. Lohrmann[‡], M. Grundmann[*], S. Pezzagna, J. Meijer

[*]Division of Semiconductor Physics
[†]Institute for Solid State Physics, Friedrich-Schiller-Universität Jena
[‡]RUBION, Ruhr-Universität Bochum

The manufacturing of the *quantum-computer* is one of the main challenges in the 21th century. Therefore, the so called *nitrogen-vacancy (NV) centre* is very important, because they can be used as qubits. Qubits are the centrepiece of the quantum computer and are utilised by the controlled charge state manipulation from NV^- over NV^0 to NV^+ and the individual addressing of the centres. In this work, we present the charge state control from NV^- to NV^0 by applying a voltage at a p-i-n diode structure. These diodes were fabricated in CVD-diamond by ion implantation with support of UV-lithographic methods. For the p-type region and the n-type we used B and P implantation, respectively (Fig. 8.2). The i-layer thickness in the diodes varied between 6 µm and 13 µm. The diodes were characterised by measuring of the *I-V*-characteristics. These measurements were performed at room temperature after several annealing steps at 1200 °C and 1600 °C each for 4 h. The pure diode *I-V*-characteristic was obtained only after the sample was annealed at the temperature of 1600 °C. By applying a voltage on the diode, it was possible to change the charge state of several NV-centres in an ensemble (Fig. 8.3). This change is caused by shifting of the Fermi level within the i-gap of the diode. Computer simulations of the *I-V* characteristics were performed to confirm the shifting of the Fermi level in the diode.

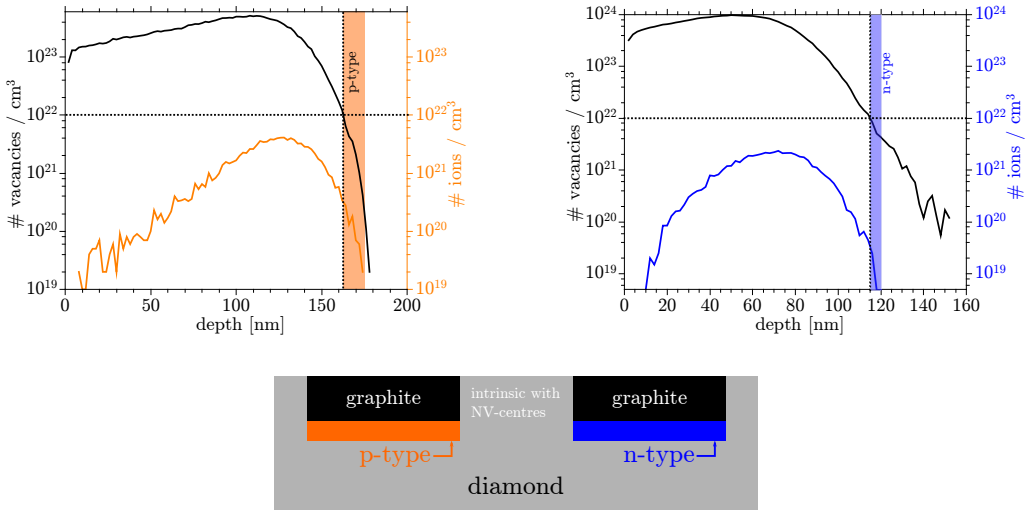

Figure 8.2: SRIM simulations for B with 70 keV (*orange*) and P with 95 keV (*blue*) as well as a schematic picture of the produced pin-diodes.

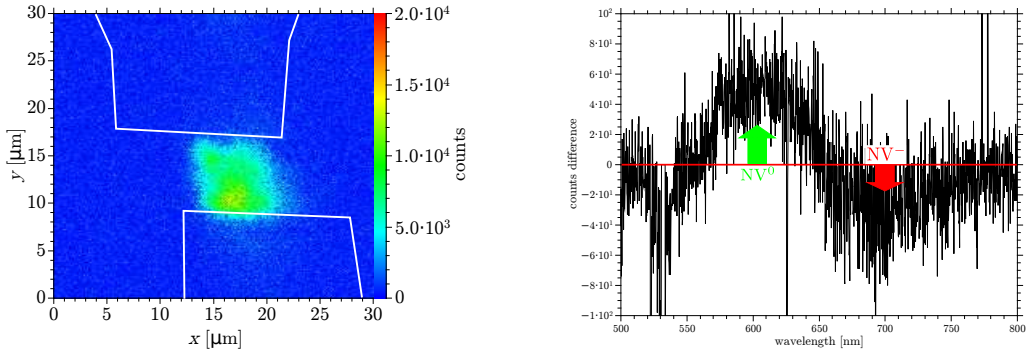

Figure 8.3: Electroluminescence picture of the NV-centres in the intrinsic layer of the pin-diode (left) and the difference of the spectra for the voltages +30 V and −30 V (right).

8.3 Passive charge-state control of Nitrogen-Vacancy centres in diamond using phosphorus and boron doping

K. Groot-Berning[*†], N. Raatz[*], I. Dobrinets[*], M. Lesik[*‡§¶], P. Spinicelli[*], A. Tallaire[‖**], J. Achard[‖**], V. Jacques[‡§¶], J.-F. Roch[‡§¶], A.M. Zaitsev[††], J. Meijer, S. Pezzagna

[*]RUBION, Ruhr-Universität Bochum
[†]QUANTUM, Universität Mainz
[‡]Laboratoire Aimé Cotton, CNRS, France
[§]Université Paris-Sud, France
[¶]Ecole Normale Supérieure de Cachan, France
[‖]Université Paris 13, Sorbonne Paris Cité, France
[**]Laboratoire des Sciences des Procédés et des Matériaux (CNRS UPR 3407), Villetaneuse, France
[††]College of Staten Island and the Graduate Center of The City University of New York, USA

The control and stabilization of the charge state of nitrogen-vacancy (NV) centres in diamond is an important issue for the achievement of reliable processing of spin-based

quantum information [1]. NV centres can be found in different charge states (NV^-, NV^0, NV^+) in the same diamond sample, depending mainly on their close environment. However, only the negative form of the defect possesses the unique optical and spin properties suitable to use single NV centres as room-temperature qu-bits. Therefore, we have been searching for different ways of controlling or stabilizing the NV charge state [2, 3]. The active control between NV^0 and NV^- using a p-i-n diode structure can be found in section 8.2. In this project, we investigate the effect of donors or acceptors (Fig. 8.4(a)) on the charge state of NV centres. In this purpose, P (donor) and B (acceptor)

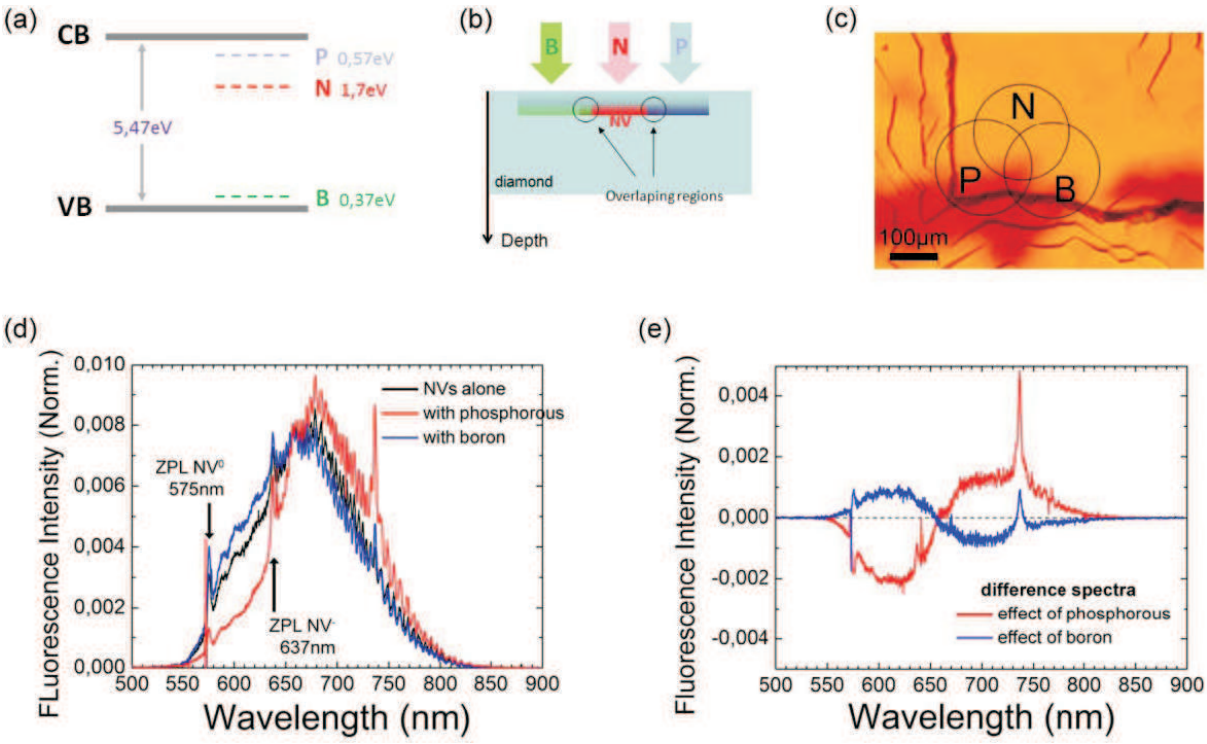

Figure 8.4: (a) Simplified energy levels of substitutional P, N, and B in the bandgap of diamond. **(b)** Ion implantation scheme used to produce an overlap between the NV ensemble and B or P doped regions. **(c)** Optical view of the selected places for implantation on the as-grown CVD layer. **(d)** Effect of co-doping with B and P (1×10^{13} cm^{-2}) on the charge state of an ensemble of NV centres. The spectra are taken in the undoped NV ensemble (*black*), in the P doped region (*red*), and in the B doped region (*blue*) in the case of an O-termination of the (100) surface of diamond. **(e)** Difference spectra comparing respectively the P doped region (*red*) and the B doped region (*blue*) with the undoped ensemble of NV centres.

doping of diamond has been achieved by ion implantation, which enables a targeted doping directly close to the NV centres (Fig. 8.4(b),(c)). More particularly, ensembles of NV centres have been produced at a depth of 60 nm in ultrapure diamond by implantation of nitrogen ions. Overlapping with the NV ensembles, donor and acceptor doped regions of different doping levels are prepared by ion implantation of P and B followed by annealing in vacuum at 1500 ℃. The charge state of the NV centres is then investigated using a home-made scanning confocal fluorescence microscope equipped with a spectrometer. NV^0 and NV^- possess distinct and well-known fluorescence with zero-phonon lines at 575 nm and 637 nm, respectively. It can be seen in Fig. 8.4(d),(e) that the charge state of the NV centres is controlled by the presence of P or B atoms in

their neighbourhood. The spectral measurements on the ensemble of NV centres reveal a higher amount of NV^0 in the case of B and a higher amount of NV^- in the case of P, as compared with undoped regions. This behavior is strengthened when the doping level is increased. This is an important result, however, the presence of P or B may reduce the coherence time of the electron spins and further experiments are in preparation. As well, the P and B doping will also be studied on single NV centres.

Interestingly, the charge state control of not only NV centres but of other defects in diamond is possible by these means. As an example, we could observe some "native" Si-vacancy defects in our sample, the charge state of which was also tuned (SiV^- with a zero-phonon line at 738 nm).

[1] F. Dolde et al.: Nat. Phys. **9**, 139 (2013), doi:10.1038/nphys2545
[2] M.V. Hauf et al.: Phys. Rev. B **83**, 081304(R) (2011), doi:10.1103/PhysRevB.83.081304
[3] B. Grotz et al.: Nat. Commun. **3**, 729 (2012), doi:10.1038/ncomms1729

8.4 Writing and Imaging Nanostructures of Single Defects in Diamond

N. Raatz*, J. Meijer, S. Pezzagna

*RUBION, Ruhr-Universität Bochum

In the last years quantum information processing developed very fast and progressive. One promising way to realise a solid state quantum computer is doping solids with single atoms. Among the variety of doping possibilities one prominent candidate is the Nitrogen Vacancy (NV) centre in diamond.

This long-known defect (present in most of natural diamonds) can easily be created by N implantation followed by thermal annealing. It possesses strong optical absorption and fluorescence which enables the optical imaging of single NV centres.

The NV centre exists in three different charge states: neutral (NV^0), negatively (NV^-) and positively charged (NV^+). The electron spin associated to the negative NV^- can be polarised and read out optically. Moreover, the coherence time of the electron spin can reach ms at room temperature in ultrapure diamond samples. Therefore, the NV centre can be used as a qubit. The entanglement of NV-qubits has already been demonstrated at room temperature [1, 2].

In order to create scalable structures based on coupled NV centres one needs to place single NV centres within distances of a few tens of nanometres. To realise the addressing of single NVs within this resolution, we developed a unique technique to implant single ions with an accuracy of below 10 nm in all three dimensions.

The nano implanter is a combination of an atomic force microscope (AFM) with a pierced hollow tip (Fig. 8.5(b)) and a low energy ion source (keV range). The drilling of the AFM tip is made with a focussed ion beam (see Fig. 8.5(a)). The collimation through this hole results in a very small ion beam about a few nm in diameter. An ion gun with a gas source provides a broad range of ion types and an integrated electron multiplier allows the detection of single ions. The created NV-pattern could be imaged with a stimulated emission depletion (STED) microscope (see Fig. 8.5(c)).

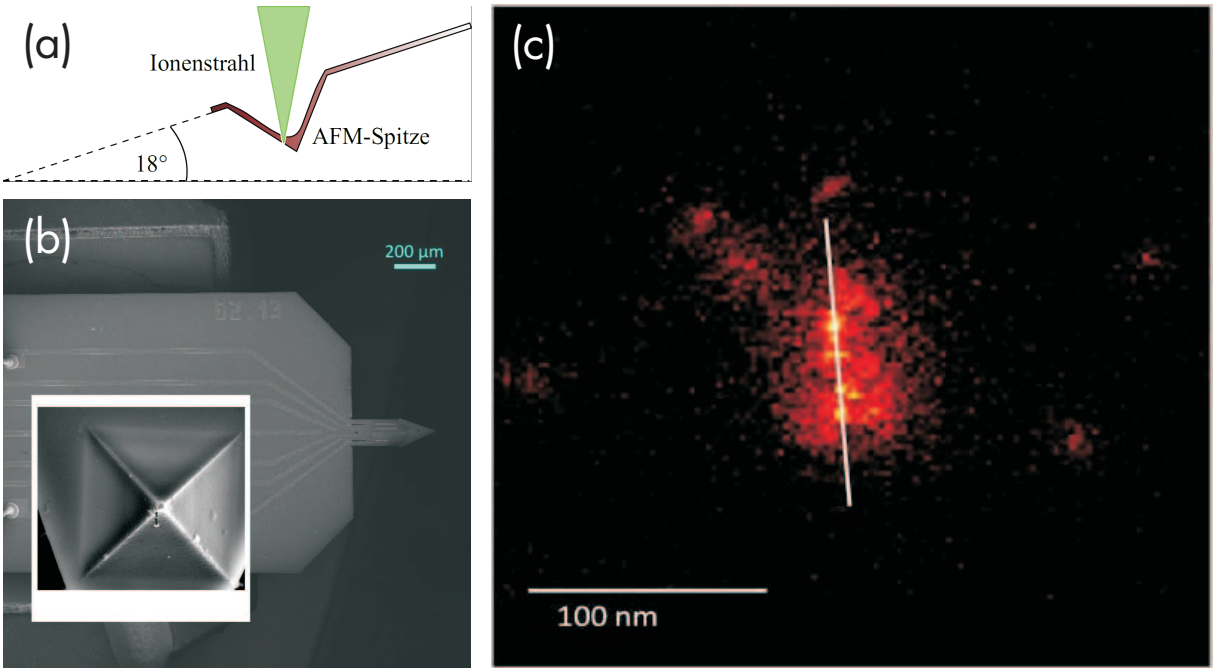

Figure 8.5: (a) Sketch of hole drilling in an AFM tip with a focussed ion beam, **(b)** SEM image of a pierced AFM tip used to collimate and address the ion beam, **(c)** stimulated emission depletion (STED) microscope image of 6 implanted single NV centres in a row.

This year we moved the nano implanter in a joint lab at the Leibniz-Institut für Oberflächenmodifizierung e.V. Leipzig (IOM).

[1] F. Dolde et al.: Nat. Phys. **9**, 139 (2013), doi:10.1038/nphys2545
[2] T. Gaebel et al.: Nat. Phys. **2**, 408 (2006), doi:10.1038/nphys318

8.5 Targeted creation and control of shallow NV centres

S. Pezzagna, J. Meijer

The nitrogen-vacancy (NV) defect centre in diamond has attracted a lot of attention in the last decade. Due to unique optical and spin properties, single NV centres are nowadays used as magnetometers or single-photon sources and are promising qubits for quantum information processing at room temperature [1–3]. However, quantum devices, based on the interaction between the spins associated to single NV centres, do require the ability to create scalable arrays of such centres with high resolution.

Low kinetic energy single-ion beam implantation enables to address atoms within a few nanometres in all three dimensions [4]. This technique seems to be the only way to produce an array of, e.g., NV centres with suitable precision as needed to fabricate a quantum array.

However, whereas the entanglement between two NV is shown, concepts of the readout and addressing of a large number of NV centres within in distance of a few nanometre is still missing. A possible solution is may be the charge state control of the NV centre [3]. But the engineering of this type of device is difficult.

[1] F. Dolde et al.: Nat. Phys. **9**, 139 (2013), doi:10.1038/nphys2545
[2] P. Neumann et al.: Science **329**, 542 (2010), doi:10.1126/science.1189075
[3] M.V. Hauf et al.: Phys. Rev. B **83**, 081304(R) (2011), doi:10.1103/PhysRevB.83.081304
[4] S. Pezzagna et al.: Small **6**, 2117 (2010), doi:10.1002/smll.201000902

8.6 Diffusion of NVs in diamond

D. Wildanger*, S. Pezzagna, J.-F. Roch†, J. Meijer

*Department of NanoBiophotonics, Max Planck Institute for Biophysical Chemistry Göttingen
†Centre National de la Recherche Scientifique (CNRS), École normale supérieure (ENS), Laboratoire Aimé Cotton (LAC), Cachan, France

Ion implantation is only the first step towards the creation of quantum devices based on NV centres in diamond. Producing artificial NV defect centres using nitrogen implantation also requires repairing the crystal implantation defects, creating the N–V bonds and stabilizing the NV charge state. This is commonly done by annealing the samples in a vacuum furnace at a temperature between (800 – 1000) ℃. Unfortunately, the creation yield of NV centres (conversion from N to N–V) is small for low ion energies; a few percent or less. Possible solutions to increase it are: a post irradiation and annealing process, a subsequent overgrowth to bury the shallow NV centres, or a surface treatment to find a suitable termination of the surface.

In this study, we investigated the diffusion and temperature stability of the NV defect centre using the combination of two methods. The idea is to check whether NV centres diffuse during a high temperature treatment (here, 1100 ℃ during 30 min). The first method consists simply in imaging a chosen pattern of NV centres before and after annealing and to evaluate whether the distance between the NV centres has changed. This is done using scanning confocal fluorescence microscopy with gives the possibility to image single defects. The separation power is somehow limited to ~ 250 nm, however the centre of mass of the so called "confocal spots" can be accurately measured (with a precision in the order of 5 nm) thanks to the brightness of the single NV centres. Within this limit, no movement of the NV centres could be observed. Therefore, a second method has been employed, based on the detection of Zeeman splitting on the electron spin of the NV centres using optically detected magnetic resonance (ODMR). The NV centres can have four different orientations in the diamond crystal lattice. By applying a magnetic field to the diamond sample, it is possible to determine in which of these four possible orientations a single NV centre is. Therefore, in the case a NV would diffuse, it is expected to see a change in orientation of the N–V bond, which would be the basic step of a diffusion process. For five selected NV centres, we did not observe any change in the electron paramagnetic resonance (EPR) signal (Fig. 8.6). We found no indication of a NV movement even at this temperature of 1100 ℃ for 30 min. This is a very important result for the engineering of quantum computer using NV centres in the future: a modification of, e.g, a stack of NV centres (by adding an additional NV center) is possible without destroying or even changing the stack.

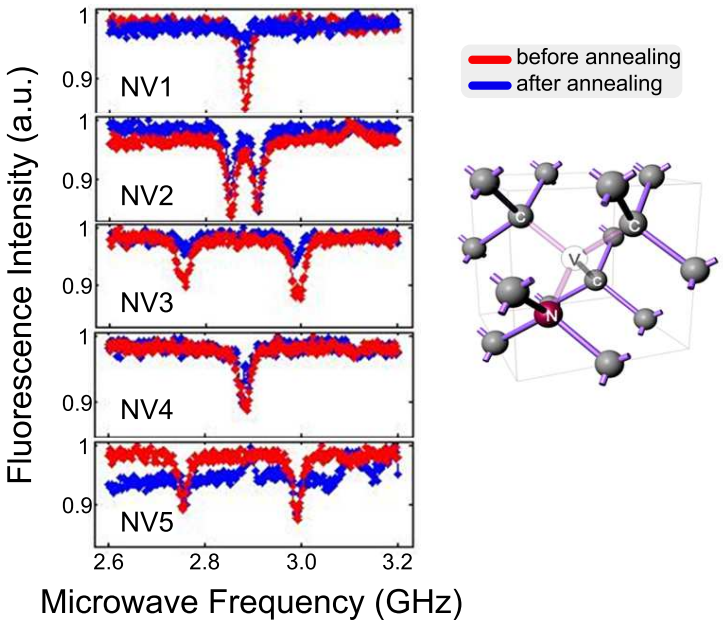

Figure 8.6: ODMR measurement of NV centres before and after a temperature treatment at 1100 °C. The measurements are performed at the optical system of MPI Göttingen (Prof. Hell).

8.7 Improving the lateral resolution in ion beam analysis by deconvolution of the point spread function of a nuclear microprobe

M. Mensing, J. Lehnert, J.L. Barzola-Quiquia*, J. Meijer, D. Spemann

*Division of Superconductivity and Magnetism

The precise knowledge of the point spread function (PSF) of a nuclear microprobe should allow to improve the lateral resolution of maps created in ion beam analysis (IBA) using mathematical deconvolution. Therefore, a resolution standard for high current ion beam applications like, e.g., particle induced X-ray emission (PIXE) or Rutherford backscattering spectrometry (RBS) was developed, fabricated and characterized. The standard consists of two concentric structures made of thick Ti film on a glassy C substrate in order to ensure elemental and topographical contrast in the IBA method used for imaging with a sufficiently high yield to avoid unreasonably long measurement times. In addition, the deconvolution software `PSFinder` was developed and optimized for the resolution standard. Both were used to determine the PSF of the ion nanoprobe LIPSION at the Universität Leipzig. The dimensions of the PSF were cross-checked with measurements of Cu- and Ni-meshes, where good agreement was obtained. Furthermore, `PSFinder` was used to increase the resolution of several element maps leading to a decrease of the edge full width at half maximum by up to 45 % after a deconvolution for structures of known dimensions. Moreover, different element maps with a low signal-to-noise ratio were deconvolved using a deconvolution algorithm based on the Wiener filter in order to investigate the limits of this approach. Here, the result was a clear improvement of the contrast and the resolution of the structures in the

map. A quantification of the improvement, however, was difficult in these cases due to the low signal-to-noise ratio in the original images. Enabling the improvement of the resolution of elemental maps, the developed resolution standard and the associated deconvolution software `PSFinder` are now integrated in the measurement protocol of the ion beam laboratory LIPSION.

8.8 Study of LbL self-assembled particles and capsules

O. Naumov[*†], C. Lan[*†], St. Jankuhn, U. Reibetanz[*]

[*]Institute for Medical Physics and Biophysics
[†]Division of Nuclear Solid State Physics

Layer-by-Layer (LbL) coated microcarriers represent a novel group of drug delivery systems which is gaining greater recognition in medical applications. The modular design of the polymer multilayer provides a multifunctional transport system: The step-by-step assembly of oppositely charged biocompatible and biodegradable polyelectrolytes on a dissolvable core allows the fabrication of polyelectrolyte multilayer capsules and simultaneous integration of active substances. Due to surface modifications the particle- or capsule-based delivery systems permit a local, target-oriented transport and time-controlled release of active agents, e.g. cancer therapeutics or anti-inflammatory substances, into certain cells or tissues. The possibility to adjust the amount of transported active agents allows to minimize side-effects of therapeutics [1].

The understanding of uptake and processing of the carriers in cells and organs play a major role concerning the development of new drug delivery systems. Hence, in the first part of this project the design of a microcarrier system for visualization of cytoplasmic processing is focused using nanoparticles as reporters followed by investigating uptake, delayed release of the reporters, and their intracellular distribution within the cell in order to provide information about the effective transport of active agents. Thus, spherical cores ($CaCO_3$) were coated with protamine/dextrane sulfate (PRM/DXS) basis multilayer and Fe_3O_4-magnetite nanoparticles (MNPs). MNPs were successfully integrated into the multilayers in different layer depths and layer numbers to demonstrate the variety of transportation of active agents. After co-incubation with Vero cells for 48 h, 72 h, 96 h, and 120 h microcarriers were detected by means of confocal laser scanning microscopy (CLSM) (Fig. 8.7(a),(b)). The direct localization of the carriers within the cytoplasm is supported by staining of cell compartments or core of the microcarrier. Here, the use of a highly effective staining for lysosomes enables the detection of microcarriers in endolysosomes [2]. In comparison, the decomposition of the multilayers in cytoplasm were visualized via particle induced X-ray emission (PIXE) spectrometry to show the advantage of multi-layered transport of active agents over single application (see Fig. 8.7(c)) [3].

In the second part of this project, hollow microcapsules were produced by one time of core dissolution with 0.1 M ethylenediaminetetraacetic acid disodium salt dihydrate (Na_2EDTA) followed by three times of water washing [4]. Controlled by CLSM (Fig. 8.8(a)-(c)), no observable Ca from the core was detected by PIXE (Fig. 8.8(d)) but traces of S and Cl from the polyelectrolyte layers — now: synthetic polymers poly(sodium 4-styrensulfonate)/poly(allylamine hydrochloride) (PSS/PAH) — could

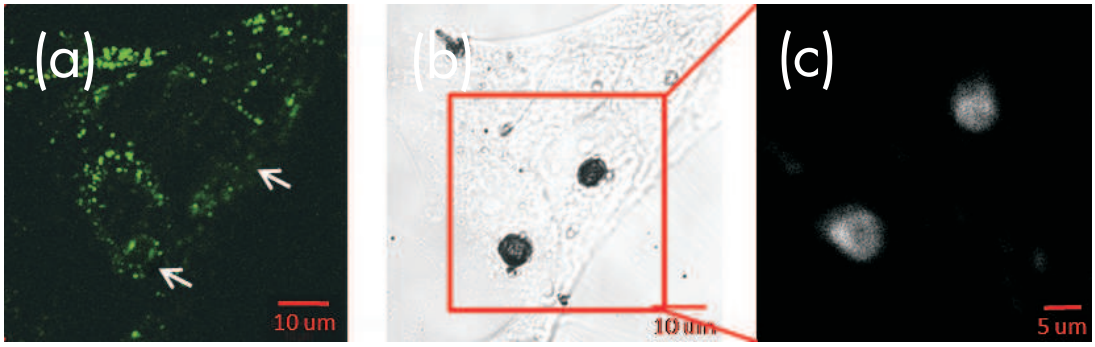

Figure 8.7: LbL-coated $CaCO_3$ microcarriers with MNPs integrated in layers 6, 10, and 14 after co-incubation with Vero cells for 120 h: **(a)** CLSM fluorescence image of a cell stained with Lysotracker-FITC (*green*) and with microcarriers in the cytoplasma (*white arrows*); **(b)** CLSM image of the transmission channel; **(c)** PIXE map of the Fe distribution on the microcarriers.

be found (Fig. 8.8(e),(f)) which means the thorough elimination of the colloidal cores while preserving the multilayers.

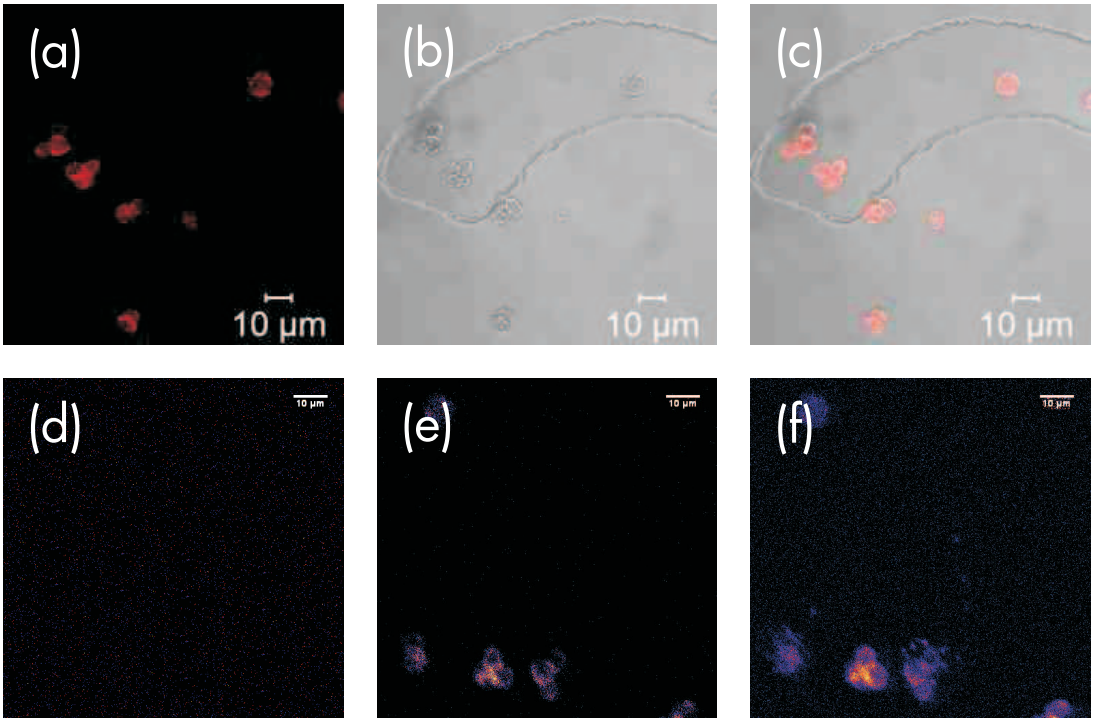

Figure 8.8: LbL-layered microcapsules: **(a)** CLSM fluorescence image of RITC-labelled microcapsules; **(b)** CLSM image of the transmission channel; **(c)** overlay of **(a)** with **(b)**; **(d)**, **(e)**, and **(f)** PIXE maps of Ca, S, and Cl distributions, respectively.

[1] L.J. De Cock et al.: Angew. Chem. Int. Edit. **49**, 6954 (2010), doi:10.1002/anie.200906266
[2] S. Rathmann et al.: Cytometry Part A **79A**, 979 (2011), doi:10.1002/cyto.a.21145
[3] U. Reibetanz et al.: Nucl. Instrum. Meth. Phys. Res. B **269**, 2281 (2011), doi:10.1016/j.nimb.2011.02.064
[4] B.G. De Geest et al.: Soft Matter **5**, 282 (2009), doi:10.1039/B808262F

8.9 Aging of diesel exhaust catalysts in use with biofuels (DieselKat Aging)

R. Eschrich*, D. Worch*, J. Böhm*, R. Gläser*, St. Jankuhn, J. Schröder†, F. Hartmann†, F. Müller-Langer†

*Institute of Chemical Technology, Universität Leipzig
†Deutsches Biomasseforschungszentrum gGmbH (DBFZ), Leipzig

In this work, field-aged catalysts for diesel exhaust aftertreatment were characterized and compared to their fresh counterparts. The analyzed samples include diesel oxidation catalysts (DOC), as well as catalysts for the selective catalytic reduction of NO_x by ammonia (NH_3-SCR). Therefore, sophisticated analytical methods like X-ray Fluorescence (XRF), Particle-induced X-ray Emission (PIXE), Transmission Electron Microscopy (TEM) and Temperature-programmed Desorption of Ammonia (TPDA) were used to investigate the material properties. A synthetic exhaust gas apparatus was developed and built in order to reveal the catalytic properties of the samples under a broad range of conditions. A slip regulation for NH_3-SCR-catalysts was implemented to determine the NO_x-conversion under realistic conditions. With the obtained data, a target-oriented poisoning routine of fresh catalysts for exhaust aftertreatment can be developed to mimic a real aged catalyst both in terms of material and catalytic properties. This is beneficial to predict the behavior of a catalyst in a wide scope of aging parameters, which interfere with variable fuel compositions and emission regimentations. For that reason, a market analysis was carried out and combined with biofuel analysis to estimate the future restrictions and challenges for diesel exhaust aftertreatment catalysts.

The intrusion depth of catalyst poisons was especially investigated by PIXE experiments. It was found that several poisons are present in different depths in the washcoat. As shown in Fig. 8.9 for a field-aged DOC the intrusion depth of S and P differ. Whereas S is only present on the washcoat probably as a component of ash deposits, P was found as well distributed within the washcoat.

With the use of an engine test bed, two sets of rapidly aged SCR- and DOC-catalysts were prepared using regular and doped biofuels. A linear correlation between amount of poisons found on the catalyst surface and the duration of aging was observed. This linear correlation was also observed for the activity of the poisoned SCR-catalysts. For DOC-catalysts the activity drops progressively with the time-on-stream.

The resulting knowledge about catalyst poisons, their amount and local distribution over the catalyst length and depth, as well as their deactivation potential was applied in poisoning experiments on the laboratory scale, which include poisoning in the liquid phase (with an evaporating poison), gas phase (with gases and particles) and supercritical phase. For the obtained samples a clear correlation between activity and material properties was found. For DOC-catalysts the effect of some poisons could be clearly linked to deactivation phenomena on different oxidation reactions (oxidation of CO, C_3H_6, or NO). These results provide a basis for a rapid aging protocol on the laboratory scale.

The authors want to thank the Research Association for Combustion Engines e.V. (FVV) and Fachagentur Nachwachsende Rohstoffe e.V. (FNR) for funding. The projects

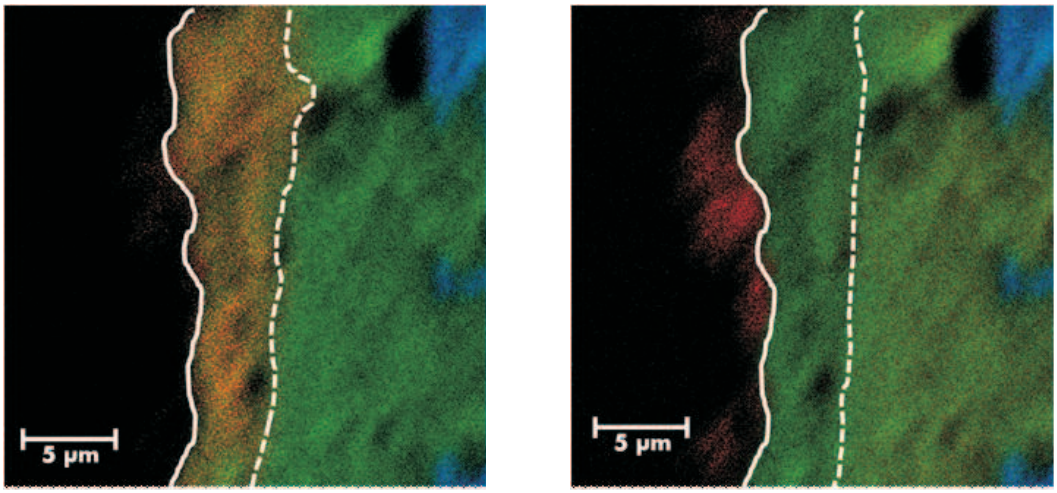

Figure 8.9: RGB image of the element mapping by PIXE from the entry part of a field-aged DOC. Al is given in *green* and Si in *blue color*. *Red* corresponds to either P (left) or S (right). The *solid line* represents the phase boundary between the catalyst surface and the gas phase, and the *dashed line* represents the boundary between the two layers of washcoat.

behind this report are 22005610 (Universität Leipzig) and 22009610 (DBFZ).

8.10 Funding

Integration of Molecular Components in Functional Macroscopic Systems: Coupling color centers into macroscopic quantum systems with an atomic nano-assembler
Prof. Dr. J. Meijer
VolkswagenStiftung

DIAmond Devices Enabled Metrology and Sensing (DIADEMS)
Prof. Dr. J. Meijer
EU FP7-ICT-2013.9.7 611143

Quantum Information with NV Centres (QINVC)
Prof. Dr. J. Meijer
CHIST-ERA VBP 01BQ1105

Diamond Materials for Quantum Application: Ultraprecise deterministic doping of diamond
Prof. Dr. J. Meijer
DFG FOR1493

8.11 Organizational Duties

J. Meijer

- Organisation: Workshop "Ionenstrahlen in Forschung und Anwendung", Leipzig, 12.–14.06.2013
- Referee: Several journals

M. Mensing
- Member of the Faculty Student Representatives

S. Pezzagna
- Referee: Diam. Relat. Mater.

J. Vogt
- Member of the Faculty Board

8.12 External Cooperations

Academic

- City University of New York, College of Staten Island, Department of Engineering Science and Physics, USA
  Assoc. Prof. Dr. A.M. Zaitsev
- Centre National de la Recherche Scientifique (CNRS), École normale supérieure (ENS), Laboratoire Aimé Cotton (LAC), Cachan, France
  Prof. Dr. J.-F. Roch
- Centre National de la Recherche Scientifique (CNRS), Laboratoire des Sciences des Procédés et des Matériaux (LSPM), Fabrication Processes of Advanced Materials (PEMA), Paris, France
  Prof. Dr. J. Achard
- Commissariat à l'énergie atomique et aux énergies alternatives (CEA), Institut Rayonnement Matière de Saclay (IRAMIS), Service de Physique de l'Etat Condensé (SPEC), Quantronique, Saclay, France
  Prof. Dr. D. Esteve
- ETH Zürich, Physikdepartement, Laboratorium für Festkörperphysik, Spin Physics and Imaging, Switzerland
  Prof. Dr. C. Degen
- Fraunhofer-Institut für Angewandte Festkörperphysik Freiburg, Mikro- und Nanosensoren
  Dr. C.E. Nebel
- Hebrew University of Jerusalem, Israel
- Humboldt-Universität zu Berlin, Mathematisch-Naturwissenschaftliche Fakultät I, Institut für Physik, AG Nanooptik
  Prof. Dr. O. Benson
- Hungarian Academy of Sciences, Wigner Research Centre for Physics, Institute for Solid State Physics and Optics, Budapest, Hungaria
- Interuniversitair Micro-Electronica Centrum (imec) Leuven, Belgium
- Julius-Maximilians-Universität Würzburg, Fakultät für Chemie und Pharmazie, Institut für Organische Chemie
  Prof. Dr. A. Krüger

- Leibniz-Institut für Oberflächenmodifizierung e.V. Leipzig
  Prof. Dr. Dr. h.c. B. Rauschenbach, Prof. Dr. B. Abel
- Leibniz-Universität Hannover, Institut für Anorganische Chemie, AK Analytik
  Prof. Dr. C. Vogt
- Ludwig-Maximilians-Universität München, Fakultät für Physik, Experimentelle Quantenphysik
  Prof. Dr. H. Weinfurter
- Max-Planck-Institut für biophysikalische Chemie Göttingen, Karl-Friedrich-Bonhoeffer-Institut, Abt. NanoBiophotonik
  Prof. Dr. Dr. h.c. St.W. Hell
- Technische Universität München, Walter Schottky Institut, E25: Spins and Defects in Semiconductors
  Prof. Dr. M.S. Brandt
- Universität Basel, Department of Physics, Quantum-Sensing Lab, Switzerland
  Prof. Dr. P. Maletinsky
- Universität Konstanz, Mathematisch-Naturwissenschaftliche Sektion, Fachbereich Physik, Lehrstuhl für Ultrakurzzeitphysik und Photonik
  Prof. Dr. A. Leitenstorfer
- Universität Leipzig, Medizinische Fakultät, Institut für Medizinische Physik und Biophysik
  Prof. Dr. E. Donath, Dr. I. Estrela-Lopis, Dr. U. Reibetanz, Dipl.-Biochem. M. Dorn
- Universität Leipzig, Fakultät für Chemie und Mineralogie, Institut für Technische Chemie
  Prof. Dr. R. Gläser, D. Worch, M.Sc.
- Universität Mainz, Fachbereich Physik, Mathematik und Informatik, Institut für Physik, Arbeitsgruppe Quanten-, Atom- & Neutronenphysik (QUANTUM)
  Prof. Dr. F. Schmidt-Kaler, Priv.-Doz. Dr. K. Singer
- Universität Stuttgart, Fakultät Mathematik und Physik, 3. Physikalisches Institut
  Prof. Dr. J. Wrachtrup
- Universität Ulm, Fakultät für Naturwissenschaften, Institut für Quantenoptik
  Prof. Dr. F. Jelezko
- Universität Ulm, Fakultät für Naturwissenschaften, Institut für Theoretische Physik, Controlled Quantum Dynamics Group
  Prof. Dr. M.B. Plenio
- University of Warwick, Department of Physics, Condensed Matter Physics, Magnetic Resonance Cluster, Coventry, UK
  Prof. Dr. M. Newton
- Westfälische Wilhelms-Universität Münster, Physikalisches Institut
  Prof. Dr. R. Bratschitsch

Industry

- ARTTIC Paris, France

- attocube systems AG München
- Element Six Ltd. Shannon, Co. Clare, Ireland
- THALES Research & Technology Palaiseau, France

8.13 Publications

Journals

S. Borhani-Haghighi, M. Kieschnick, Y. Motemani, A. Savan, D. Rogalla, H.-W. Becker, J. Meijer, A. Ludwig: *High-Throughput Compositional and Structural Evaluation of a* $Li_a(Ni_xMn_yCo_z)O_r$ *Thin Film Battery Materials Library*, ACS Comb. Sci. **15**, 401 (2013), doi:10.1021/co4000166

T. Butz: *Comment on "Oxidation of Hafnium and Diffusion of Hafnium Atoms in Hexagonal Close-Packed* Hf*; Microscopic Investigations by Perturbed Angular Correlations" by C.C. Dey, Z. Naturforsch.* ***67a****, 633 (2012)*, Z. Naturforsch. **68a**, 315 (2013), doi:10.5560/ZNA.2013-0012

T. Butz, S.K. Das, C.C. Dey, S. Dey, S. Ghoshal: *Recoil Induced Room Temperature Stable Frenkel Pairs in α-Hafnium Upon Thermal Neutron Capture*, Z. Naturforsch. **68a**, 610 (2013), doi:10.5560/ZNA.2013-0039

T. Butz, R. Vianden: *The temperature dependence of the nuclear quadrupole interaction of* ^{44}Ti*(EC)*^{44}Sc *in rutile*, Hyp. Interact. **221**, 99 (2013), doi:10.1007/s10751-012-0675-7

D. Diering, D. Spemann, J. Lenzner, St. Müller, T. Böntgen, H. von Wenckstern: *Greyscale Proton Beam Writing in p-type Gallium Arsenide*, Nucl. Instrum. Meth. Phys. Res. B **306**, 275 (2013), doi:10.1016/j.nimb.2012.11.049

F. Dolde, I. Jakobi, B. Naydenov, N. Zhao, S. Pezzagna, C. Trautmann, J. Meijer, P. Neumann, F. Jelezko, J. Wrachtrup: *Room-temperature entanglement between single defect spins in diamond*, Nat. Phys. **9**, 139 (2013), doi:10.1038/nphys2545

P. Esquinazi, W. Hergert, D. Spemann, A. Setzer, A. Ernst: *Defect-Induced Magnetism in Solids*, IEEE Trans. Magn. **46**, 4668 (2013), doi:10.1109/TMAG.2013.2255867

A.M. Jakob, M. Hennes, M. Müller, D. Spemann, S.G. Mayr: *Coupling of Micromagnetic and Structural Properties Across the Martensite and Curie Temperatures in Miniaturized* Ni-Mn-Ga *Ferromagnetic Shape Memory Alloys*, Adv. Funct. Mater. **23**, 4694 (2013), doi:10.1002/adfm.201300165

N. Klingner, J. Vogt, D. Spemann: *Optimizing the Rutherford Backscattering Spectrometry setup in a nuclear microprobe*, Nucl. Instrum. Meth. Phys. Res. B **306**, 44 (2013), doi:10.1016/j.nimb.2012.12.062

M. Lesik, P. Spinicelli, S. Pezzagna, P. Happel, V. Jacques, O. Salord, B. Rasser, A. Delobbe, P. Sudraud, A. Tallaire, J. Meijer, J.-F. Roch: *Maskless and targeted creation of arrays of colour centres in diamond using focused ion beam technology*, phys. stat. sol. A **210**, 2055 (2013), doi:10.1002/pssa.201300102

M. Lorenz, C. Schmidt, G. Benndorf, T. Böntgen, H. Hochmuth, R. Böttcher, A. Pöppl, D. Spemann, M. Grundmann: *Degenerate interface layers in epitaxial Scandium-doped* ZnO *thin films*, J. Phys. D: Appl. Phys. **46**, 065311 (2013), doi:10.1088/0022-3727/46/6/065311

C. Osterkamp, J. Scharpf, S. Pezzagna, J. Meijer, T. Diemant, R.J. Behm, B. Naydenov, F. Jelezko: *Increasing the creation yield of shallow single defects in diamond by surface plasma treatment*, Appl. Phys. Lett. **103**, 193118 (2013), doi:10.1063/1.4829875

T. Staudacher, F. Shi, S. Pezzagna, J. Meijer, J. Du, C.A. Meriles, F. Reinhard, J. Wrachtrup: *Nuclear Magnetic Resonance Spectroscopy on a (5-Nanometer)*^{3} *Sample Volume*, Science **339**, 561 (2013), doi:10.1126/science.1231675

M. Wortmann, A. Ludwig, J. Meijer, D. Reuter, A.D. Wieck: *High-resolution mass spectrometer for liquid metal ion sources*, Rev. Sci. Instrum. **84**, 093305 (2013), doi:10.1063/1.4822275

R. Wunderlich, N. Klingner, J. Vogt, D. Spemann: *Quantitative elemental microscopy on lateral highly inhomogeneous meteorite samples using ion beam analysis*, Nucl. Instrum. Meth. Phys. Res. B **306**, 85 (2013), doi:10.1016/j.nimb.2012.11.048

J. Zippel, M. Lorenz, A. Setzer, M. Rothermel, D. Spemann, P. Esquinazi, M. Grundmann, G. Wagner, R. Denecke, A.A. Timopheev: *Defect-induced magnetism in homoepitaxial manganese-stabilized zirconia thin films*, J. Phys. D: Appl. Phys. **46**, 275002 (2013), doi:10.1088/0022-3727/46/27/275002

Talks

D. Lehmann
Erster Störfall in der Geschichte der Kernkraft (Leipziger Uranmaschinen-Versuche)
Carl von Ossietzky-Universität, Oldenburg, 06.03.2013

J. Meijer
A scheme for addressing of individual NV centers by an active charge state control?
Advice Meeting, Cachan, France, 19.02.2013

M. Lesik, S. Pezzagna, P. Spinicelli, V. Jacques, A. Tallaire, J. Achard, A. Gicquel, J. Meijer, J.-F. Roch
Improved properties of buried NV centres in diamond with nanometre positioning
Diamond Workshop SBDD XVIII, Hasselt, Belgium, 27.02.–01.03.2013

J. Meijer
Single ion implantation in diamond with high lateral resolution: The key technology for the fabrication of quantum devices?
FWI Institutskolloquium, Helmholz-Zentrum Dresden–Rossendorf, 21.03.2013

J. Meijer
Defect engineering in diamond
2. Research Coordination Meeting of the "Utilization of Ion Accelerators for Studying and Modelling of Radiation Induced Defects in Semiconductors and Insulators" IAEA CRP No. F11016, Vienna, Austria, 13.–17.05.2013

J. Meijer
Erzeugung von NV Zentren in Diamant mit hoher lateraler Auflösung
Technische Universität Ilmenau, 16.05.2013

J. Meijer
Einzelionenimplantation als Schlüsselexperiment für Quantencomputer
IFK Institutsseminar, Friedrich-Schiller-Universität Jena, 17.05.2013

J. Meijer
Schema zur Herstellung eines Quantencomputers auf Basis von NV Zentren in Diamant
Antrittsvorlesung, Fakultätskolloquium, Universität Leipzig, 28.05.2013

J. Meijer
N *shallow implantation with* 0.5 keV *to* 5 keV
DIADEMS Kick off Meeting, Paris, France, 12./13.07.2013

J. Meijer
Wiring up NV color-centers
Symposium VWStiftung, Hannover, 23./24.10.2013

J. Meijer
New developments in ion implantation: From high power diodes to quantum devices
Seminar, Nanoscale Science Department, Max-Planck-Institut für Festkörperphysik Stuttgart, 07.11.2013

J. Meijer
Defect engineering in diamond
IAEA Technical Meeting, Vienna, Austria, 10.–15.11.2013

J. Meijer
Pathway to a scalable solid state quantum computer using NVs?
Seminar, Graduate School of Engineering Science, Osaka University, Japan, 12.11.2013

O. Naumov, St. Jankuhn, U. Reibetanz
Untersuchung der intrazellulären Dekomposition LbL-beschichteter Mikropartikel mittels PIXE
Workshop Ionenstrahlen in Forschung und Anwendung, Leipzig, 12.–14.06.2013

S. Pezzagna, J. Meijer
A scheme for addressing of individual NV centers by an active charge state control?
Workshop on Diamond – Spintronics, Photonics, Bio-applications, Hong Kong, 27.–29.04.2013

S. Pezzagna
High-resolution ion implantation for optical centres in diamond
Workshop Ionenstrahlen in Forschung und Anwendung, Leipzig, 12.–14.06.2013

S. Pezzagna, J. Meijer
Targeted defect generation and diffusion of vacancies in diamond
17. International Conference on Radiation Effects in Insulators (REI), Helsinki, Finland, 30.06.–05.07.2013

M. Lesik, P. Spinicelli, N. Raatz, S. Pezzagna, V. Jacques, A. Tallaire, J. Achard, A. Gicquel, J. Meijer, J.-F. Roch
Preserved pattern of very shallow implanted nitrogen-vacancy centres in diamond deeply buried by overgrowth
International Conference on Diamond and Carbon Materials, Riva del Garda, Italy, 02.–05.09.2013

S. Pezzagna, J. Meijer
Targeted creation and control of shallow NV centers
Workshop on Quantum Information using NV Centers in Diamond, Hefei, China, 13.–17.10.2013

F. Schmidt, H. von Wenckstern, S. Müller, D. Spemann, M. Grundmann
Irradiation studies on differently orientated ZnO *thin films*
DPG-Frühjahrstagung, Regensburg, 10.–15.03.2013

D. Spemann
Trace element content and magnetic properties of commercial HOPG samples studied by ion beam microscopy and SQUID magnetometry
Workshop Ionenstrahlen in Forschung und Anwendung, Leipzig, 12.–14.06.2013

8.14 Graduations

Doctorate

- T. Andrea
  3D-Visualization of Cells by Limited-angle Ion Micro-tomography and Proton Beam Sculpting
  October 2013
- N.D. Barapatre
  Application of Ion Beam Methods in Biomedical Research - Quantitative Microscopy with Trace Element Sensitivity
  September 2013

Master

- O. Naumov
  Untersuchung der intrazellulären Dekomposition LbL-beschichteter Mikropartikel mittels PIXE
  August 2013

Bachelor

- Ch. Lan
  Investigation of the Core Dissolution Process of Layer-by-Layer Coated Calcium Carbonate Microparticles by Means of PIXE and CLSM
  December 2013

- M. Mensing
  The Determination of the Point Spread Function of a Nuclear Microprobe
  September 2013

8.15 Guests

- Assoc. Prof. Dr. J.C. McCallum
  University of Melbourne, School of Physics, Centre for Quantum Computation and Communication Technology, Australia
  17.–19.07.2013
- Prof. Dr.-Ing. I. Rangelow
  Technische Universität Ilmenau, Fakultät für Elektrotechnik und Informationstechnik, Institut für Mikro- und Nanoelektronik, FG Mikro- und nanoelektronische Systeme
  21.06.2013
- Prof. Dr. C. Ronning
  Friedrich-Schiller-Universität Jena, Institute for Solid State Physics
  17.12.2013
- Prof. Dr. J. Wrachtrup
  Universität Stuttgart, Fakultät Mathematik und Physik, 3. Physikalisches Institut
  07./08.10.2013

9

Semiconductor Physics

9.1 Introduction

2013 turned out to be a fruitful year with many new and exciting findings. We established an innovative pulsed-laser deposition method with a single, segmented target and succeeded in the facile fabrication of thin films with continuous composition spread in the systems (Mg,Zn)O and $(In,Ga)_2O_3$. The (Mg,Zn)O films have been used to fabricate ultraviolet photodetectors with defined center wavelength and narrow spectral bandwidth. We have expanded our work on the deposition of sesquioxide thin films of the type $(In,Ga,Al)_2O_3$ towards the fabrication of diodes. Remarkable is the ideal behavior of Ga_2O_3 Schottky diodes at elevated temperatures (550 K). Several approaches to bipolar oxide diodes yielded devices with high rectification including $ZnCo_2O_4$/ZnO, CuI/ZnO and the all-amorphous system of p-type zinc cobalt oxide on n-type zinc tin oxide (ZCO/ZTO). For NiO/ZnO in addition efficient photovoltaic energy conversion in the UV was found, making this heterostructure a suitable approach to transparent photovoltaics on windows. Our patent application for transparent rectifying contacts was granted in the EU (EP 2 446 484 B1) and the United States (US 8,445,904 B2).

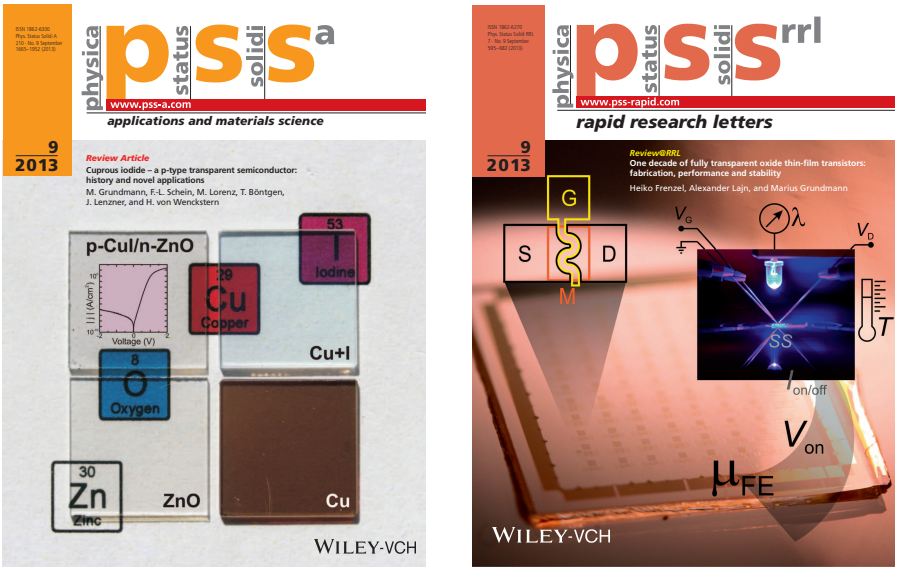

Figure 9.1: Journal covers of 2013 publications of the semiconductor physics group

We are very grateful to our funding agencies in particular Deutsche Forschungsgemeinschaft (DFG) and European Social Fund (ESF). We are grateful for the continued funding of Sonderforschungsbereich SFB 762 "Functionality of Oxide Interfaces" (2012–2015) and our project on nanowire heterostructures in the Forschergruppe FOR 1616 "Nanowire Optoelectronics" (2012–2014). Also we thank Sächsische Aufbaubank to support our new work on Ga_2O_3 thin films and oxide solar cells. The generous support of Universität Leipzig allowed us to install in 2013 a new high resolution X-ray diffraction setup and a multi-target sputter chamber for oxides. In 2014 we can continue our work on ZCO and CuI bipolar electronics with two new DFG grants. The work of our students and researchers together with our academic and industrial partners near and far was fruitful and enjoyable and thus it is with pleasure that the semiconductor physics group presents their progress report.

Marius Grundmann

9.2 One decade of fully transparent oxide thin film transistors: fabrication, performance and stability

H. Frenzel, A. Lajn*, M. Grundmann,

*now at Advanced Mask Technology Center GmbH & Co. KG, Rähnitzer Allee 9, D-01109 Dresden

We review the history of *fully* transparent oxide thin film transistors (TTFT). TTFT have gained much attention during the past decade, inspiring scientists to develop invisible electronics that could be integrated as transparent displays in windshields, windows, mobile devices or everyday objects. For the approach using metal-insulator-semiconductor field-effect transistors (MISFET), highly insulating dielectrics with preferably high dielectric constants are used. Alternatively, metal-semiconductor field-effect transistors (MESFET) can be used applying a transparent rectifying contact (TRC) as gate diode [1].

The first TTFTs, published in 2003, were based on polycrystalline oxides. Hoffman *et al.* used an ion-beam-sputtered (IBS) ZnO channel and a commercially available $Al_2O_3/TiO_2/Al_2O_3$ (ATO) stack on an indium tin oxide (ITO) layer as common back-gate diode on glass for a transistor with an on/off-ratio of 10^7 and a channel mobility of 0.45 cm^2/Vs [2]. Since then, the ATO/ITO coated glass have been the most popular basis for the fabrication of TTFT. Nomura *et al.* published the record mobility of 80 cm^2/Vs using single-crystalline indium-gallium-zinc-oxide (IGZO) on yttria-stabilized zirconia (YSZ) substrate with HfO_2 dielectric [3]. In contrast to that, Fortunato *et al.* set up an approach using room-temperature grown amorphous oxides as channel layer for TFTs, having nearly the same performance [4].
A tentatively complete list of published results on the performance of TTFT since 2003 is compiled in [5]. Despite of all efforts to achieve low source-drain- and gate-voltages using gate dielectrics with higher dielectric constants like Al_2O_3, HfO_2 and a stack of ATO, only 16% of all TTFT exhibit a V_{SD} <= 5 V and only 10% a ΔV_G <= 5 V, which is recommended in mobile applications or meeting the requirements for integration with

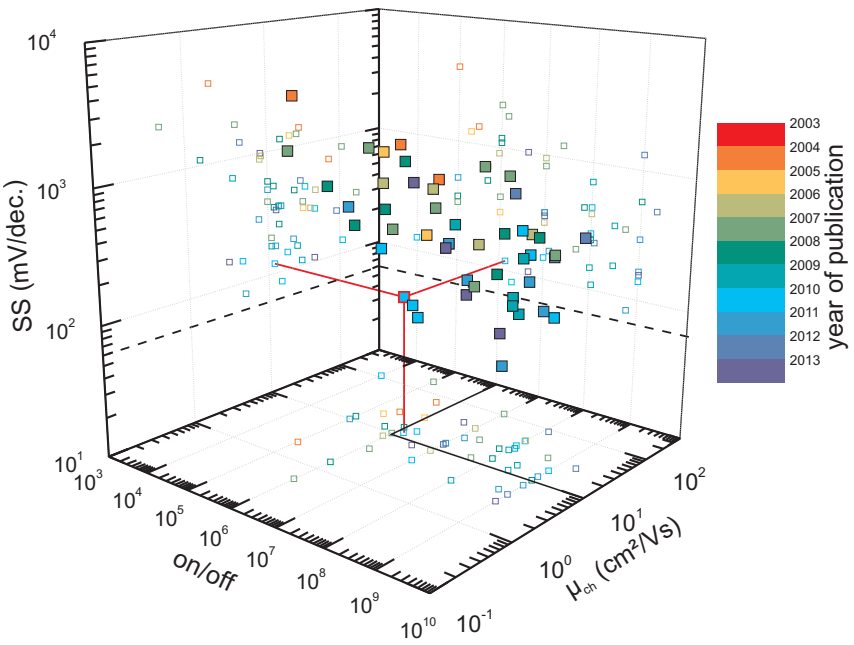

Figure 9.2: Subthreshold slope *SS*, on/off-ratio and channel mobility μ_{ch} of TTFT (data from [5]). Color code represents the year of publication. The dashed line indicates the thermodynamic limit of *SS* at room temperature. The dash-dotted line indicates the minimum desired on/off ratio and μ_{ch}. The red-marked point is a TMESFET according to this work; other points are MISFET.

silicon technology. One of the few exceptions is our approach of a TMESFET using TRC based on AgO_x or PtO_y [1].

Figure 9.2 visualizes the most important figures of merit as indicated in the caption. The lowest *SS* values coincide with devices using novel gate-diode structures. In recent past, many MISFET using conventional gate dielectrics suffer from high *SS* and low μ_{FE}. High mobilities can be achieved using more sophisticated growth methods for the insulator such as atomic layer deposition (ALD), high-temperature pulsed-laser deposition (PLD). However, these methods are not practicable for large-scale fabrication of transparent electronics, where sputtering techniques are used. In fact, in 70% of the TTFT magnetron sputtering (MS) was used for the fabrication of the channel layer. This percentage has increased during the past decade. The usage of transparent amorphous oxide semiconductors (TAOS) as channel material has become a strong trend in the past ten years.

We compare the published properties about bias stress stability, stability towards illumination, at elevated temperatures and longterm stability of TMISFET with our TMESFET technology. To study bias stress stress stability, our TMESFET were biased in either positive (PBS) or negative (NBS) direction for 20000 seconds. For PBS, μ_{FE}, *SS*, I_{on}/I_{off} and V_{SS} stay constant for Pt- and Ag-based TRC. For NBS, both devices respond differently: whereas Pt-TMESFET remain constant, the Ag-based TMESFET exhibits significant degradation in the first 1000 seconds. Compared to TMISFET, our Pt-based TMESFET is among the best devices regarding a V_{SS}-shift.

Operation stability towards the illumination with visible light is crucial for transparent devices. For our TMESFET, there is an increasing influence of the illumination with shorter wavelength. The induced photocurrent increases the off-current and subsequently the subthreshold slope of the transistor. Simultaneously, a photo voltage is generated leading to a shift of the switching voltage. Without additional biasing, the parameters of our TMESFET are competitive to TMISFET [5]. V_{SS} is fairly constant but all TMISFET show a higher significant increase of I_{off} compared to our TMESFET. With an additional negetave gate bias (NBIS), the voltage shift of the transfer curve tends to

be larger due to light enhanced charge trapping in the gate insulator.
The influence of elevated temperatures on the performance of TTFT has been investigated. Our Pt-TMESFET are more stable than Ag-TMESFET, whose degradation already starts shortly after room temperature, implying a reduction of the on/off-ratio by a factor of 10, a 20% decreasing mobility and a 30% higher subthreshold slope due to an increase of the off-current. For both devices V_{SS} exhibits a positive shift, which is attributed to traps in the channel or channel/gate interface. Usually for MISFET, a larger *negative* voltage shift occurs with increasing temperature, which is explained by temperature activated trap states in the insulator.
Longterm stability has been studied storing our TMESFET for 151 days in dry air. They exhibit a 30 to 40% reduction of μ_{FE} due to the indiffusion of compensating defects with time. The Pt-based TMESFET are more stable than the Ag-based device. Its on/off-ratio decreases by a factor of 3 during the first month, but then stays constant for the remaining 4 months. On the other hand, I_{on}/I_{off} for Ag drops over 3 decades due to an increase of the off-current. Despite of the apparently decreasing net doping concentration, the switching voltage for both devices remains constant. In contrast, there are significant voltage shifts for the TMISFET [5]. We assume, that the stability can be further improved by encapsulation and passivation of the devices.

[1] H. Frenzel, *et al.* Adv. Mat. **22**(47), 5332–5349 (2010).
[2] R. L. Hoffman, *et al.* Appl. Phys. Lett. **82**(5), 733–735 (2003).
[3] K. Nomura, *et al.* Science **300**, 1269–1272 (2003).
[4] E. Fortunato, *et al.* Journal of Non-Crystalline Solids **338-340**, 806 – 809 (2004).
[5] H. Frenzel, *et al.* phys. stat. sol. (RRL) **7**, 605 – 615 2013.

9.3 Electrical properties of transparent rectifying Schottky contacts

H. von Wenckstern, A. Lajn, P. Barquinha*, E. Fortunato*, R. Martins*, M. Grundmann

*CENIMAT/I3N, Departamento de Ciência dos Materiais, Faculdade de Ciências e Tecnologia, FCT, Universidade Nova de Lisboa and CEMOP-UNINOVA, 2829-516 Caparica, Portugal

We compare electrical properties of fully transparent rectifying contacts (TRC) on crystalline and amorphous transparent semiconducting oxides (TSO). The TRCs have transparency exceeding 70% in the visible spectral range and exhibit high rectification on ZnO bulk single crystals, heteroepitaxial ZnO thin films grown by pulsed-laser deposition on a-plane sapphire as well as on room temperature RF-sputtered amorphous GaInZnO layers on glass substrate [1]. The transport mechanism for temperatures above 100 K is thermionic emission independent of the crystallinity of the TSO. As typical for real Schottky barrier diodes (SBD) the barrier potential has lateral fluctuation that can be described Gaussian distribution with standard deviation σ around a mean barrier height $\Phi_{B,m}$ [23]. These characteristic parameters of real SBDs were determined from temperature-dependent current-voltage characteristics [1]. In Fig. 9.3 (a) a clear

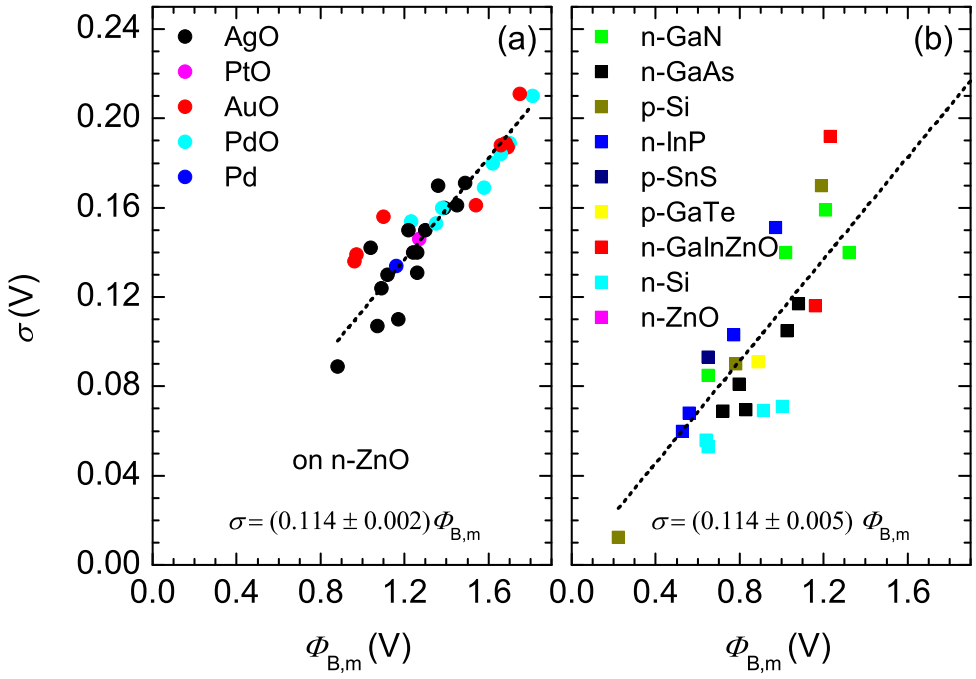

Figure 9.3: Correlation between mean barrier height and barrier distribution width for Schottky contacts fabricated (a) on n-ZnO (data from this work and [2–5]) and (b) on various semiconductors using various contact metals (data from this work and [6–23]). The dotted lines are linear fits through (0/0).

correlation between the standard deviation σ and the mean barrier height $\Phi_{B,m}$ is observed. A linear fit of the data reveals that $\sigma = (0.114 \pm 0.002)\Phi_{B,m}$. In Fig. 9.3 (b) we plot data of numerous reported SBDs on elemental, III-V and several II-VI semiconductors in conjunction with the data of our SBDs on crystalline and amorphous TSOs and find the same relation between standard deviation and mean barrier height. This suggests a fundamental origin of the Schottky barrier height fluctuations which we tentatively address to the polycrystalline nature of the Schottly barrier contacts compiled in Fig. 9.3.

This work has been supported by Deutsche Forschungsgemeinschaft in the framework of SFB 762 "Functionality of Oxide Interfaces" and the Graduate School "Leipzig School of Natural Sciences - Building with Molecules and Nano-objects" (BuildMoNa).

[1] A. Lajn, H. von Wenckstern, M. Grundmann, G. Wagner, P. Barquinha, E. Fortunato, R. Martins J. Appl. Phys. **113**, 044511 (2013).
[2] Holger von Wenckstern, Gisela Biehne, R. Abdel Rahman, Holger Hochmuth, Michael Lorenz, and Marius Grundmann, Appl. Phys. Lett., **88**, 092102 (2006).
[3] A. Lajn, H. von Wenckstern, Z. Zhang, C. Czekalla, G. Biehne, J. Lenzner, H. Hochmuth, M. Lorenz, M. Grundmann, S. Künzel, C. Vogt, and R. Denecke, J. Vac. Sci. Technol. B, **27**,1769 (2009).
[4] Alexander Lajn, *Reactively sputtered Schottky contacts on epitaxial zinc oxide*, Master thesis, Universität Leipzig, 2008.

[5] Hogyoung Kim, Haeri Kim, and Dong-Wook Kim, J. Appl. Phys., **108**, 074514 (2010).
[6] F.E. Cimillia, M. Saglama, H. Efeoglub, and A. Türüt, Physica B, **404**, 1558 (2009).
[7] M. Siva Pratap Reddy, A. Ashok Kumar, and V. Rajagopal Reddy, Thin Solid Films, **519**, 3844 (2011).
[8] Ö. Güllü, M. Biber, S. Duman, and A. Türüt, Appl. Surf Sci., **253**, 7246 (2007).
[9] M.K Hudait, P Venkateswarlu, and S.B Krupanidhi, Solid-state Electron., **45**, 133 (2001).
[10] M. Biber, Physica B, **325**, 138 (2003).
[11] Jiang Yu-Long, Ru Guo-Ping, Lu Fang, Qu Xin-Ping, Li Bing-Zong, Li Wei, and Li Ai-Zhen, Chinese Phys. Lett., **19**,553 (2002).
[12] Ilbilge Dökme, Microelectron. Reliab., **51**, 360 (2011).
[13] M. Soylu and B. Abay, Microelectron. Eng., **86**,88 (2009).
[14] A. Ashok Kumar, V. Janardhanam, V. Rajagopal Reddy, and P. Narasimha Reddy, Superlattices Microstruct., **45**, 22 (2009).
[15] B. Abay, G. Cankaya, H. S. Güder, H. Efeoglu, and Y. K. Yogurtcu, Semicond. Sci. Tech., **18**, 75 (2003).
[16] P.G. McCafferty, A. Sellai, P. Dawson, and H. Elabd, Solid-state Electron., **39**, 583 (1996).
[17] S. Acar, S. Karadeniz, N. Tugluoglu, A. B. Selcuk, and M. Kasap, Appl. Surf Sci., **233**, 373 (2004).
[18] S. Karadeniz, M. Sahin, N. Tugluoglu, and H. Safak, Semicond. Sci. Tech., **19**, 1098 (2004).
[19] A. Gumus, A. Türüt, and N. Yalcin, J. Appl. Phys., **91**, 245 (2002).
[20] M. Mamor, J. Phys: Condens Mat., **21**, 335802 (2009).
[21] Hyunsoo Kim, Seongjun Kim, Kyoung-Kook Kim, Sung-Nam Lee, and Kwang-Soon Ahn, Jpn. J. Appl. Phys., **50**, 105702 (2011).
[22] Shiyang Zhu, R.L. Van Meirhaeghe, C. Detavernier, F. Cardon, Guo-Ping Ru, Xin-Ping Qu, and Bing-Zong Li, Solid-state Electron., **44**, 663 (2000).
[23] J. H. Werner and H. H. Güttler, J. Appl. Phys., **69**, 1522 (1991).

9.4 Eclipse pulsed laser deposition grown Schottky contacts on ZnO thin films

S. Müller, H. von Wenckstern, F. Schmidt, D. Splith, R. Heinhold*, M.W. Allen*, M. Grundmann

*The MacDiarmid Institute for Advanced Materials and Nanotechnology, University of Canterbury, Christchurch 8043, New Zealand

In the past decade oxide semiconductors were investigated with a renewed interest. One prime candidate of large band gap oxide semiconductors is zinc oxide (ZnO). Here, we present high quality IrO_x Schottky contacts (SCs) prepared by eclipse pulsed laser deposition (E-PLD) on ZnO thin films. The ZnO thin films are also grown by PLD on *a* - plane sapphire substrates and consist of two different layers. First, a highly aluminum doped layer with a thickness of about 50 nm is deposited. This layer is used as ohmic

back contact [1]. Afterward a nominally undoped ZnO thin film with a thickness of about 1 µm is grown. Both layers were deposited at a growth temperature of 650 °C and an oxygen partial pressure of 0.016 mbar. Circular SCs with a diameter of 320 µm were defined using photolithography. The E-PLD grown SCs were ablated from a metallic Ir target at room temperature and a oxygen partial pressure of 0.13 mbar (0.1 Torr). A more precise description of the conditions used is give elsewhere [2]. The thickness of IrO_x layer is approximately 50 nm. As capping layer we used a (sputtered Au nochmal nachschauen) layer with a thickness of about 50 nm.

Figure 9.4(a) depicts a room temperature current-voltage (*I-V*) characteristic of one of

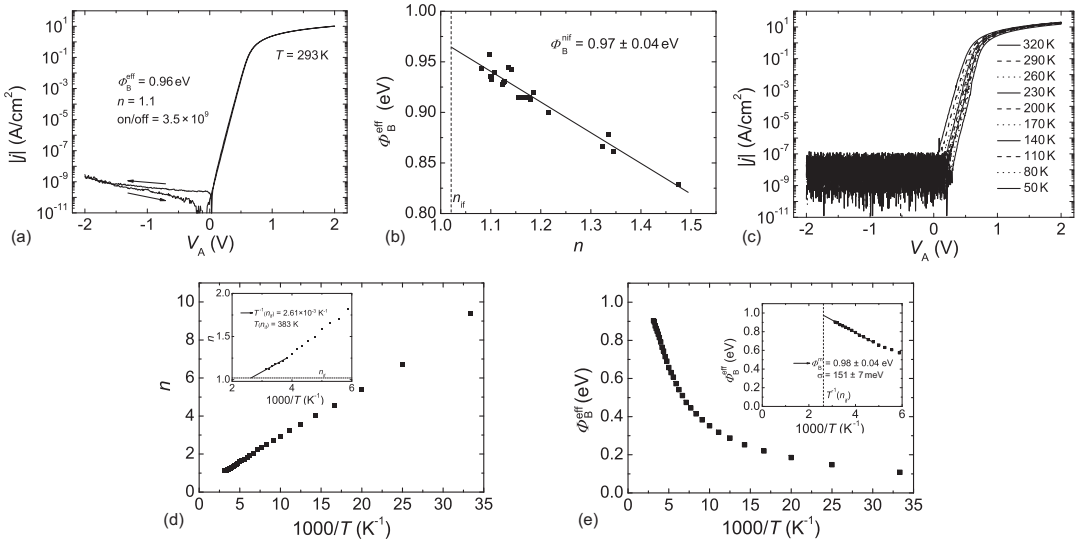

Figure 9.4: (a) a) Room temperature *I-V* characteristic of one of the best IrO_x/ZnO SCs fabricated by reactive eclipse pulsed laser deposition. The black arrow indicates the measurement direction. (b) Effective barrier height in dependence on the ideality factor of all IrO_x/ZnO SCs on this sample. (c) Temperature-dependent *I-V* characteristics between 50 K and 320 K of a IrO_x/ZnO SC fabricated by reactive eclipse pulsed laser deposition. (d) Ideality factor height and (e) effective barrier height vs inverse temperature of the SC shown in (c).

the best IrO_x SC investigated. In forward direction up to 0.5 V is a single exponential slope visible. A fit of the forward region using thermionic emission theory yields for this diode an effective barrier height of 0.96 eV and an ideality factor of 1.1. Both values are comparable with SCs grown with E-PLD on ZnO single crystals [2] and better than SCs fabricated by other techniques on ZnO thin films [1, 3, 4]. The large effective barrier height also results in a large on/off ratio of 3.5×10^9. We observe a small hysteresis of the *I-V* characteristics for reverse voltages. The reverse current is in general smaller if the sweep direction is from negative to positive voltages. The direction of the respective measurement is indicated by the black arrows in Fig. 9.4(a). Differences between both measurements are highest for voltages close to 0 V. The splitting of the zero crossing for the two sweep directions is due to a charging and discharging current of an additional parallel capacitance which is caused e.g. by surface states. For forward voltages the diode current is independent of the sweep direction.

The effective barrier height in dependence on the ideality factor of all working 22 SCs on the investigated sample is depicted in Fig. 9.4(b). We see a linear dependence between both parameters as expected for SCs with barrier height inhomogeneities. The ideality

factor of all of the investigated IrO_x/ZnO SCs is below 1.5. More than 80% of the investigated SCs have an ideality factor below 1.2 substantiating the good homogeneity of this type of SCs. Fitting the linear dependence the homogeneous barrier height is determined to be 0.97eV.
A temperature dependent *I-V* measurement from 50 K to 320 K of one IrO_x/ZnO SC is depicted in Fig. 9.4(c). In backward direction we see at all measured temperatures a current coinciding with the noise floor of the setup used. However, compared to the room-temperature measurement in the wafer prober system is the noise level in the cryostat system by 2 orders of magnitude increased. In forward direction the current again increases with increasing temperature as expected from TE. For temperatures below 260 K a kink in the IV characteristic is noticeable for small forward bias. This kink is caused by barrier inhomogeneities. The ideality factor und effective barrier height in dependence on the inverse temperature determined from the measurement depicted in Fig. 9.4(c) is shown in Fig. 9.4(d) and (e). The ideality factor strongly decreases with increasing temperature and approaches unity for high temperatures. The inset Fig. 9.4(d) shows the ideality factor for temperature above 170 K. At high temperatures we see a decrease of the slope of $n(T^{-1})$. Therefore, we determined the temperature where the image force lowered ideality factor is reached within this region to be 383 K. The determination in the high temperature region also has the advantage that the current transport is well described by TE and other possible transport mechanism like tunneling or trap-assisted tunneling can be ignored. The barrier height also shows a strong dependence on the temperature. At low temperatures we see a small increase of the effective barrier with increasing temperature. With increasing temperature the slope increases until the slope is linearly dependent on the inverse temperature for temperature above 200 K. We used this region for the determination of the mean barrier height, which is for this SC 0.98 eV. Note, that the mean barrier height for this contact is in very good agreement with the homogeneous barrier height of this sample.

This work has been supported by Deutsche Forschungsgemeinschaft in the framework of SFB 762 "Functionality of Oxide Interfaces".

[1] H. von Wenckstern, G. Biehne, R. Abdel Rahman, H. Hochmuth, M. Lorenz, and M. Grundmann, Appl. Phys. Lett. **88**, 092102 (2006), doi:10.1063/1.1638898
[2] M. W. Allen, R. J. Mendelsberg, R. J. Reeves, and S. M. Durbin, Appl. Phys. Lett. **94**, 103508 (2009), doi:10.1063/1.3089871
[3] A. Lajn, H. v. Wenckstern, Z. Zhang, C. Czekalla, G. Biehne, J. Lenzner, H. Hochmuth, M. Lorenz, M. Grundmann, S. Wickert, C. Vogt and R. Denecke, J. Vac. Sci. Technol. B **27**, 1769 (2009), doi:10.1116/1.3086718
[4] S. Müller, H. Von Wenckstern, O. Breitenstein, J. Lenzner, and M. Grundmann, IEEE Transactions on Electron Devices **59**, 536 (2012), doi:10.1109/TED.2011.2177984.

9.5 Barrier height of Cu Schottky contacts on β-Ga_2O_3 thin films

D. Splith, S. Müller, H. von Wenckstern, M. Grundmann

Oxide semiconductors like β-gallium oxide (β-Ga_2O_3) are promising materials for a new generation of transparent electronic devices. Due to its large band gap of 4.9 eV, β-Ga_2O_3 is especially of interest for application in high power electronics and solar-blind photonic devices. For the realization of such devices the fabrication of rectifying Schottky contacts (SCs) is important. SCs are the key elements of unipolar electronic devices like Schottky diodes and metal-semiconductor field-effect transistors. Further, such contacts enable electrical characterization by capacitance-voltage measurements or deep-level transient spectroscopy.

Recently, Au and Ni SCs on β-Ga_2O_3 single crystals and homoepitaxial thin films were reported [1, 2]. Since the growth of β-Ga_2O_3 single crystals is a lengthy and expensive procedure and presently limited to 2" wafers, heteroepitaxial growth of β-Ga_2O_3 thin films and the fabrication of devices thereon is of increasing interest.

We investigated SCs on heteroepitaxial β-Ga_2O_3 thin films grown by pulsed laser deposition of a ceramic Ga_2O_3 target with 1 wt.% Si. The SCs were fabricated by dc sputtering or thermal evaporation. Beside the Cu SCs discussed here, deposition of other metals like Ag, Fe or W also resulted in rectifying contacts. The current-voltage (I-V) characteristics of Cu SCs on β-Ga_2O_3 grown on c-plane sapphire substrate exhibit a rectification with rectification ratios (at $V = \pm 2$ V) of almost 10^7. Since both, the Schottky and the ohmic contact are on top of the β-Ga_2O_3 thin film, a high series resistance of about 10 $k\Omega$ limits the current in forward direction. In order to reduce this series resistance we employed a different sample structure were the β-Ga_2O_3 thin film was grown on an highly Ga-doped ZnO layer on an a-plane sapphire substrate [5]. The Ga-doped ZnO layer acts as a back contact layer (bcl). Cu SCs on such samples have a series resistance of only 100 Ω, increasing the rectification ratio to almost 10^9[6]. Assuming thermionic emission as dominant transport mechanism, effective barrier heights up to 1.05 eV and ideality factors n down to 1.2 were determined at room temperature. The deviation of the ideality factor from unity indicates that the barrier of the contact is laterally inhomogeneous. Temperature dependent I-V measurements between 50 and 320 K substantiate this picture. By fitting, we determined the linear dependence of the effective barrier height and $n^{-1}-1$ on the inverse temperature shown in Fig. 9.5 (a) which is in accordance to the model of thermionic emission over a laterally inhomogeneous barrier [3]. From a linear fit, the mean barrier height is determined to be 1.32 eV with a standard deviation of 0.13 eV. Further, from the I-V characteristic at a temperature of 550 K, which is shown in Fig. 9.5 (b) an ideality factor of 1.03 was determined. The small deviation of the ideality factor from unity is in principle due to the image force lowering of the barrier. Hence, the influence of the barrier height inhomogeneities has vanished at this temperature and the contact is close to ideality. The effective barrier height at this temperature is 1.36 eV, which coincides with the mean barrier height determined before. By fitting the reverse characteristic at this temperature taking image force lowering of the barrier into account [4] (see inset of Fig. 9.5 (b)), a flat-band barrier height of 1.55 eV and the image force lowering of 0.17 eV was determined. Therefore, the mean barrier height determined from the measurement at low temperatures, the homogeneous barrier height and the barrier height of 1.38 eV of the image force lowered flat-band barrier are in good agreement.

This work has been supported by the European Regional Development Fund "Leistungselektronik auf Basis von Galliumoxid" (100132251).

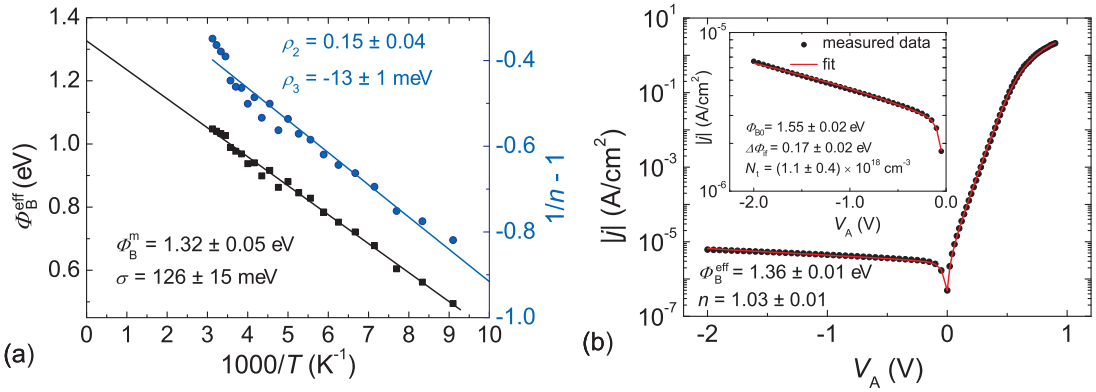

Figure 9.5: (a) Effective barrier height and $n^{-1} - 1$ in dependence on the inverse temperature and linear fit. (b) *I-V* characteristic at 550 K and fit with the model of thermionic emission. The inset shows the fit of the reverse characteristics with an enhanced model, taking into account the image force lowering.

[1] K. Irmscher *et al.*, J. Appl. Phys., 110, 6: 063720 (2011)
[2] M. Mohamed *et al.*, Appl. Phys. Lett., 101, 13: 132106 (2012)
[3] J. H. Werner and H. H. Güttler, J. Appl. Phys., 69, 3: 1522 (1991)
[4] M. W. Allen *et al.*, IEEE Trans. Electron Dev., 56, 9: 2160-2164 (2009)
[5] H. von Wenckstern *et al.*, Appl. Phys. Lett., 88, 9: 092102 (2006)
[6] D. Splith, *et al.*, phys. stat. sol. (a) 211, 40 (2014)

9.6 MIS-diodes based on Si-doped β-Ga_2O_3

A. Reinhardt, H. von Wenckstern, M. Grundmann

We report on the fabrication of MIS-diodes based on Si-doped β-Ga_2O_3. The β-Ga_2O_3 thin films were grown from a Ga_2O_3-target with 1 wt% SiO_2 at a growth temperature of T_G = 650°C in an oxygen ambient of 10^{-3} mbar using pulsed-laser deposition (PLD). Prior to the growth of the 350 nm thick Ga_2O_3 thin film a degenerately doped ZnO:Ga (ZGO) layer serving as ohmic back contact and subsequently a nominally undoped ZnO layer of about 500 nm have been deposited on an *a*-plane sapphire substrate at a growth temperature and oxygen partial pressure of about 650°C and 0.016 mbar, respectively [3]. The inset in Fig.1(a) depicts the schematic device structure. For the realization of MIS-diodes we used room-temperature PLD-grown aluminum oxide (Al_2O_3) as dielectric and direct-current (DC) sputtered gold (Au) as metal-contacts. The electrical properties of the MIS-diodes were varied via the thickness of the dielectric and the oxygen partial pressure ($p(O_2)$) during deposition of the dielectric. Current-voltage measurements (*IV*) reveal minimal leakage current densities of down to 3×10^{-10} Acm^{-2} for a dielectric thickness of $d_i \approx 120$ nm and $p(O_2) = 0.002$ mbar. In order to determine the dielectric constant of the insulator, we performed quasi-static capacitance-voltage measurements. For the PLD-grown Al_2O_3 we find a dielectric constant in the range of 7-9, which is in good agreement with reported values of 8-10 [1, 2]. Furthermore, the possible origin of conduction through the insulator is investigated by means of temperature-dependent *IV*-measurements. Fig. 9.6(a) depicts *IV*-characteristics of a

MIS-diode with 40 nm Al_2O_3 in a temperature range between 25°C and 150°C. As expected, the leakage current density increases with increasing temperature. From the analysis of the forward current density at 4 V vs. the inverse temperature (see Fig. 9.6(b)) Schottky emission (SE) and Frenkel-Poole emission (FP) are deduced as dominant conduction mechanisms yielding a barrier height $\phi_B = 0.95$ eV from the fit at higher temperatures.

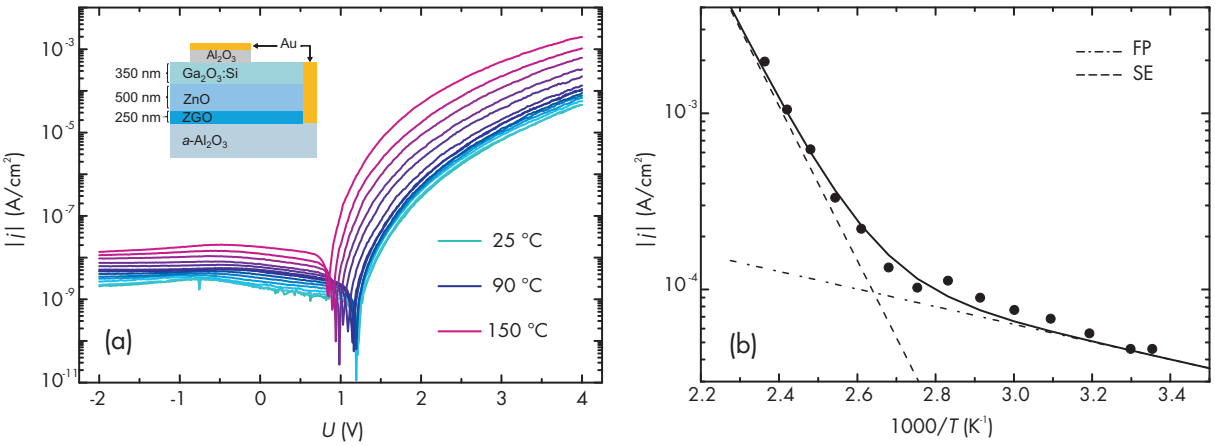

Figure 9.6: (a) Temperature-dependent *I-V*-characteristics of a MIS-diode based on Si-doped β-Ga_2O_3. The inset shows the schematic device structure. (b) Current density j vs. 1000/T. The solid line is a fit to determine the barrier height ϕ_B.

This work has been supported by the European Regional Development Fund "Leistungselektronik auf Basis von Galliumoxid" (SAB 100132251).

[1] D. Splith *et al.*, Phys. Status Solidi A **211**, No. 1, 40-47 (2014)
[2] J. Robertson, Eur. Phys. J. Appl. Phys. **28** , 265-291 (2004)
[3] P. Katiyar *et al.*, Acta Materialia **53**, 2617-2622 (2005)

9.7 Highly rectifying contacts on amorphous zinc oxide tin films

P. Schlupp, F.-L. Schein, H. von Wenckstern, M. Grundmann

For a cost-efficient fabrication of semiconducting thin films the usage of amorphous oxides is advantageous. They can be deposited at room-temperature (RT) and with that plastic or even paper can be used as substrate. Having electron mobilities in the order 10 cm^2/Vs or even higher [1, 2] they are a promising alternative to amorphous silicon. Zinc tin oxide (ZTO) consisting of highly abundant zinc and tin is such a promising material that is already used as channel layer in field effect transistors [3]. Here, we present highly rectifying contacts on amorphous ZTO thin films. At first Schottky diodes and after that a heterojunction-diode consisting of *n*-type ZTO and *p*-type zinc cobalt oxide (ZCO) will be discussed.
All ZTO thin films were fabricated by pulsed laser deposition at room temperature.

Ohmic contacts were realized by dc-sputtered gold layers. To create Schottky contacts the metal was sputtered reactively in 50%/50% argon/oxygen atmosphere. However, the first contacts showed only weak rectification. Temperature dependent *jV*-measurements indicate that tunneling is the dominant transport mechanism. In order to avoid that we introduced an ultra-thin insulating ZTO layer between the thin film and the metal. Figure 9.10a shows the (arithmetic-) mean current-density-voltage characteristics of *k* Schottky diodes realized on ZTO thin films with free electron denisities ranging from 5×10^{13} cm^{-3} to 10^{19} cm^{-3}. Our best Schottky diodes exhibit current rectifications as high as $I(1.6\,\mathrm{V})/I(1.6\,\mathrm{V}) = 10^7$.
In order to create a bipolar diode a *p*-type semiconductor is required. We chose ZCO because it is *p*-type even in the amorphous state [4]. Similar to the first Schottky diodes the rectification of our first *pn*-diode was poor. Again, the introduction of an insulating ZTO layer, resulting in a *pin*-heterodiode, improves the rectification considerable. Fig 9.10b depicts the mean *jV*-characteristics of the heterojunction diodes with free electron densities from 10^{16} cm^{-3} to 10^{19} cm^{-3} in the *n*-ZTO layer. The ZCO films are always deposited by PLD in 3 Pa oxygen atmosphere. Our best heterojunction-*pin*-diodes exhibit current on/off ratios as high as 5×10^6 at $\pm$ 1.6V.
This value outperforms the best fully amorphous *pn*-diodes, fabricated up to now, by far [5, 6]. In conclusion we demonstrate highly rectifying Schottky and heterojunction diodes deposited at RT which are required for RT-fabricated transistor applications.

This work has been supported by the European Social Fund (SAB 100124929) and and the Graduate School "Leipzig School of Natural Sciences - Building with Molecules and Nano-objects (BuildMoNa).

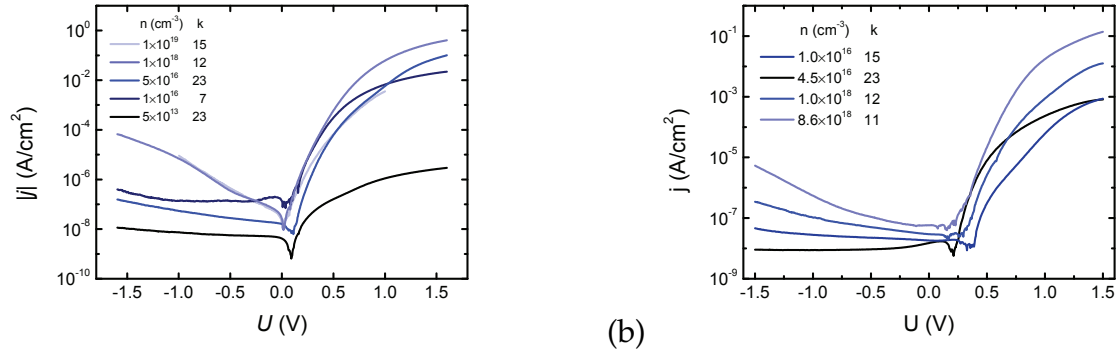

Figure 9.7: Mean *jV*-characteristics averaged over *k* single devices for (a) Schottkybarrier diodes and (b) heterojunction diodes on ZTO thin films with different free electron densities.

[1] M. K. Yajaraj, K. J. Saji, K. Nomura, T. Kamiya, H. Hosono: J. Vac. Sci. Technol. B **26**, 495 (2008)
[2] K. Nomura, A. Takagi, T. Kamiya, H. Ohta, M. Hirano, H. Hosono: Jpn. J. Appl. Phys. **45**, 4303 (2006)
[3] H. Q. Chiang, J. F. Wager, R. L. Hoffman, J. Jeong, D. A. Keszler: Appl. Phys. Lett. **86**, 013503 (2005)
[4] F.-L. Schein, H. v. Wenckstern, H. Frenzel, M. Grundmann: IEEE Electron Device Letters **33**(5), 676 (2010)

[5] S. Kim, J. A. Cianfrone, P. Sadik, K.-W. Kim, M. Ivill, D. P. Norton: J. Appl. Phys. **107**(10), 103538 (2010)
[6] S. Narushima, H. Mizoguchi, K. Shimizu, K. Ueda, H. Ohta, M. Hirano, T. Kamiya, H. Hosono: Adv. Mater. **15**(17), 1409 (2003)

9.8 Highly rectifying *p*-$ZnCo_2O_4$/*n*-ZnO heterojunction diodes

F.-L. Schein, M. Winter, T. Böntgen, H. von Wenckstern, M. Grundmann

We used pulsed-laser deposition to fabricate long-term stable, highly rectifying bipolar heterojunctions consisting of *n*-ZnO and *p*-$ZnCo_2O_4$ [1]. Hall and Seebeck effect as well as scanning capacitance spectroscopy were used to evaluate hole conduction of $ZnCo_2O_4$ (ZCO). Among (semi)transparent *p*-type oxides the Zn spinels ZnM_2O_4 (M = Co, Rh, Ir) are exceptional due to the preservation of their hole conductivity in the amorphous state [2]. Both types of heterostructure, ZnO/ZCO and ZCO/ZnO, showed diode characteristics. We used *a*-sapphire as substrate and dc-sputtered Au for ohmic contacts. For the first diode type consisting of ZnO on top of ZCO with both layers grown at 460 °C, a current rectification ratio of $I_f/I_r = 4300$ at ±2 V and an ideality factor of $\eta = 2.6$ was achieved. For the other diode type we used an optimized growth temperature for ZnO (650 °C) followed by room temperature grown ZCO. Current-voltage characteristics revealed $\eta = 2.04$ and I_f/I_r up to 2×10^{10}. Best values reported in the literature on fully or partly amorphous (semi)transparent oxide diodes are $\eta = 2.3$ [2] and $I_f/I_r = 3\times10^3$ at ±1 V [3]. Additionally, the ZCO/ZnO diodes turned out to be long-term stable since the current-voltage characteristics changed only little after more than one year (393 days). This is shown in Fig. 9.10. The average ideality factor of 34 diodes on the same substrate even improved from 2.07 to 1.98 while series resistance increased from 520 Ω to 1848 Ω resulting in slight decrease of the mean rectification ratio from 7.0 to 6.4 orders of magnitude. This demonstrates the stability of the *pn*-heterointerface, changes are only due to parasitic effects. For future applications the substitution of crystalline ZnO may lead to fully amorphous, highly rectifying all-oxide diodes.

This work has been supported by Deutsche Forschungsgemeinschaft in the framework of SFB 762 "Functionality of Oxide Interfaces" and the Graduate School "Leipzig School of Natural Sciences - Building with Molecules and Nano-objects (BuildMoNa).

[1] F.-L. Schein *et al.*, Appl. Phys. Lett. **104**, 022104 (2014), doi:10.1063/1.4861648
[2] S. Narushima *et al.*, Adv. Mater. **15**, 1409 (2003), doi:10.1002/adma.200304947
[3] E. Azaceta *et al.*, Electrochim. Acta **71**, 39 (2012), doi:10.1016/j.electacta.2012.03.093

9.9 Semi-transparent ZnO/NiO UV solar cells

R. Karsthof, P. Räcke, Z. Zhang, H. von Wenckstern, M. Grundmann

Photovoltaic cells with high transmittance in the visible spectral range (350 – 650 nm) are a promising possiblilty to generate electric power on areas inaccessible to

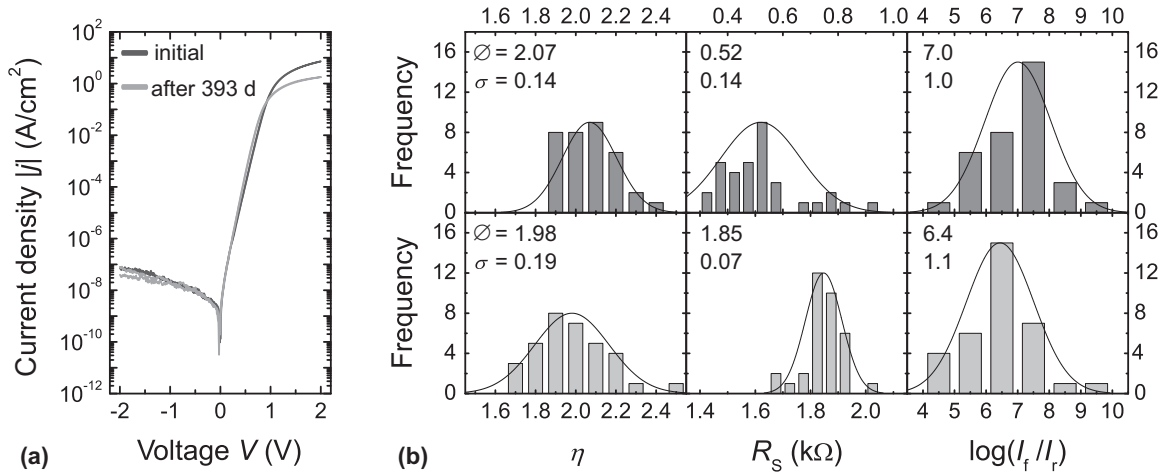

Figure 9.8: (a) Current density vs. voltage characteristic of a typical *p*-ZCO/*n*-ZnO diode initially after fabrication (*dark-gray*) and more than one year later (*light-gray*). **(b)** Histograms of fit parameters ideality factor η and series resistance R_S as well as logaritm of rectification ratio. Mean value $\varnothing$ and standard deviation σ are labeled.

conventional technologies, e.g. windows or glazed roofs. According to calculations by R. Lunt a solar cell that only operates in the UV and IR could reach a total conversion efficiency of 21% [1]. Even if only photons from the UV were converted, more than 1% efficiency would be feasible.

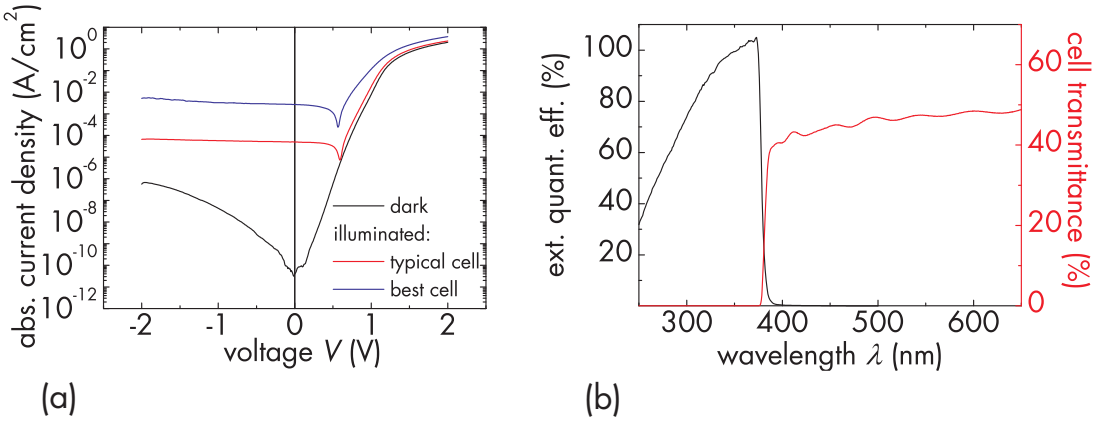

Figure 9.9: (a) *jV* characteristics of ZnO/NiO contacts under dark conditions (black) and under illumination for a typical (red) and a record (purple) cell. (b) transmittance and external quantum efficiency

In this work we focused on the fabrication of UV-active solar cells based on *n*-ZnO/*p*-NiO heterojunctions. The ZnO layers were grown by pulsed laser deposition (PLD) on top of *a*-plane sapphire substrates. A highly Al-doped ZnO layer serves as transparent back contact. Nominally undoped ZnO was grown on top with a thickness of 1μm. Afterwards, circular-shaped NiO contacts were grown by reactive DC-magnetron sputtering of metallic Ni in an Ar/O_2 atmosphere with a metal shadow mask fixed on top of the substrate. The NiO pillars were then covered with thin Au contact layers. The full stack has an average transmittance slightly below 50% in the visible spectral range, as shown in Fig. 9.9(b). The contacts were electrically characterized by means of current-

voltage measurements (see Fig. 9.9(a)). Under dark conditions high rectification ratios of up to 9 orders of magnitude at ±2 V were detected. Upon illumination with a solar simulator (AM1.5G solar spectrum, optical power density 100 mW/cm^2) the devices show a photovoltaic effect with open-circuit voltages of above 500 mV. The measured short-circuit current densities for most cells were only around 0.05 mA/cm^2. In some cases, however, j_{sc} values of more than 1 mA/cm^2 were achieved. In such a record device the quantum efficiency in the UV range is around 100% (Fig. 9.9(b)). Fill factors were close to 0.5, resulting in power conversion efficiencies of 1.5% in record cells and around 0.02% in the general case. In order to investigate the mechanism behind the frequent case of poor cell performance, an analysis of the voltage dependence of the charge carrier collection probability was carried out. This technique has been described in the literature in detail [2, 3] and can be used to investigate collection loss mechanisms in the layer with the lowest doping concentration, which in the present case is the ZnO absorber. From this analysis it can be concluded that the collection of photo-generated charge carriers within the ZnO layer is very efficient. We thus attribute the observed low j_{sc} values to recombination processes in the NiO.

This work has been supported by the European Regional Development Fund "Transparente photovoltaische Zellen" (SAB 1001112104).

[1] R. Lunt, Appl. Phys. Lett. 101, 043902 (2012)
[2] K.W. Mitchell, A.L. Fahrenbruch, R.H. Bube, J. Appl. Phys. 48, 4365 (1977)
[3] S. Hegedus, D. Desai, C. Thompson, Prog. Photovolt.: Res. Appl. 15, 587 (2007)

9.10 Flicker noise in ZnO thin films

F.J. Klüpfel, H. von Wenckstern, M. Grundmann

ZnO based devices have been proposed for sensor applications, e.g. photodetectors[1] and pH sensors[2]. The noise produced by such devices is a crucial parameter, as it limits the achievable sensitivity. While reports for the noise in ZnO based photodetectors[3] or varistors[4] exist, no results for ZnO based thin-film transistors have been published yet.

We measured the low frequency current noise in mesa structures etched from PLD grown ZnO films on a-sapphire substrates with thicknesses between 15 nm and 70 nm. We observed a dominating 1/f contribution, often called flicker noise, in agreement with the results published for other ZnO devices. A typical series of noise power density spectra for varied bias voltage is shown in Fig. 9.10. For zero bias the constant thermal noise is dominating, while for increasing bias the 1/f contribution becomes the only relevant noise source. Measuring mesa with different width W and length L revealed that the 1/f noise scales with $1/(WL)$. This is a proof that the noise originates in the channel material, as otherwise only a scaling according to the current, and thus W/L, would be expected.

Based on these results we examined the noise of ZnO based metal-semiconductor-metal field-effect transistors (MESFETs). The gate voltage V_{GS} was set to 0 V and the noise of the drain current measured. Again 1/f noise was dominating. Using the relation derived by van Vliet[5] for generation-recombination noise, one can relate the noise

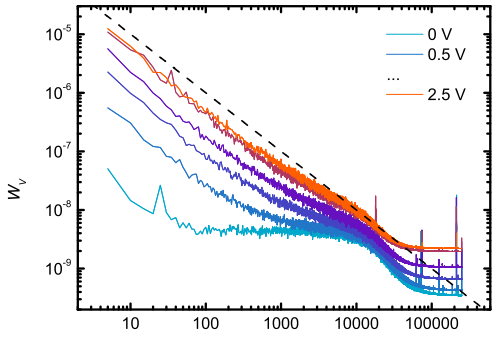

Figure 9.10: Noise power density spectra for a ZnO mesa with thickness 25 nm, length 50 μm, and width 30 μm.

amplitude measured for MESFETs with that for mesa without gate. This is illustrated in Fig. 9.11.

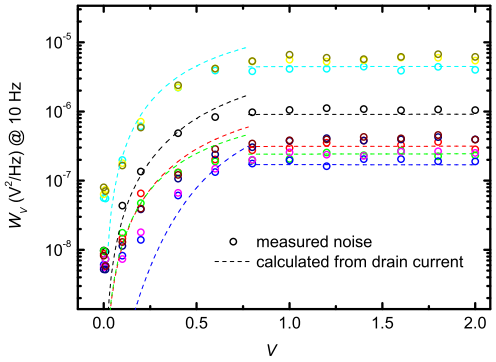

Figure 9.11: Noise power density at 10 Hz for ZnO based MESFETs with different geometries (V_{GS} = 0 V).

It was found, that the noise magnitude is within the same order of magnitude, and thus most probably of the same origin. Consequently, the limiting factor when using such MESFETs as sensors is the channel material. Surface traps, which are as commonly charged with causing 1/f noise, can be ruled out here, as the depletion layer of the MESFET seperates the channel current from the semiconductor surface. With further experiments on ZnO structures using different preparation methods we hope to link the flicker noise to material parameters like crystal quality, clarifying its origin.

[1] Zhang *et al.*, Applied Physics Letters, 99, 083502 (2011)
[2] Batista *et al.*, Applied Physics Letters, 87, 143508 (2005)
[3] Li *et al.*, Japanese Journal of Applied Physics, 52, 084101 (2013)
[4] Prudenziati *et al.*, Journal of Applied Physics, 58, 345 (1985)
[5] van Vliet *et al.*, Electron Devices, 22, 616 (1975)

9.11 Variation of reduced effective mass of Al-doped (Mg,Zn)O thin films grown by pulsed laser deposition

A. Mavlonov, S. Richter, H. von Wenckstern, R. Schmidt-Grund, M. Grundmann

ZnO is a promising II-VI compound semiconductor for transparent conductive electrode applications because of its high transparency in the visible (VIS) and near infrared (NIR) ability of wet chemical etching and high n-type dopability [1, 2]. Furthermore, there is interest in conducting electrodes exhibiting optical transparency into the ultraviolet range to produce solar cells harvesting solar energy also in that part of the solar spectrum [3]. For these purposes, the band gap of ZnO can be increased by alloying with MgO [4]. One of the main issue for electrode applications is the fabrication of highly conducting (Mg,Zn)O films. In this work, we report on optical and electrical properties of Al-doped (Mg,Zn)O thin films grown on 2 inch size glass substrate by pulsed-laser deposition (PLD) using a continuous composition spread (CCS) approach [5]. For that segmented targets consisting of binary ZnO, 8 wt-% MgO:ZnO and 5 wt-% Al_2O_3:ZnO, respectively, were used. The spatial variation of chemical composition in the thin film was investigated by energy-dispersive X-ray (EDX) spectroscopy. The thin film properties were characterized in dependence on the Mg content x and Al doping concentration. In order to perform optical and electrical measurements, the film was cut into pieces, $5 \times 5\text{mm}^2$ in size using diamond saw.

We investigated the fundamental absorption edge and corresponding optical band gap in the near-ultraviolet part of the spectrum using UV-VIS-NIR spectrometer (Lambda 19, PERKIN ELMER) and the plasma frequency in the near- and mid-infrared part of the spectrum by infrared spectroscopic ellipsometry (IRSE).

Figure 9.12(a) shows the variation of the optical band gap of the films as a function of Mg content x and free carrier density (which corresponds to the Al doping). Using the following equation which accounts for an increasing optical band gap due to the Burstein-Moss shift by an amount that depends on the curvature of both the conduction and valence bands,

$$\Delta E_g = \frac{h^2}{8m_r^*}\left(\frac{3}{\pi}\right)^{2/3} n^{2/3}.$$

we determined values reduced effective mass m_r^* for a given Mg-content from the slope of the optical band gap versus the free carrier density (Figure 9.12(b)) to be 0.56m_e, 0.60m_e, 0.78m_e for x=0.01, 0.03 and 0.05, respectively. However, for the carrier densities of the samples investigated here, many body effects cannot be excluded. The plasma frequency of the sample allows in principle separation of the reduced mass into electron and hole effective masses; first results of infrared spectroscopic ellipsometry measurements are depicted in Fig. 9.12(c) but do not allow separation of the reduced mass due to the aforementioned many body effects.

This work has been supported by the Islamic Development Bank (IDB), Merit Scholarship Programme for High Technology (A.Mavlonov, Grant No. 91/UZB/P32).

[1] H. von Wenckstern, M. Grundmann, The (Mg,Zn)O Alloy. Handbook of Zinc Oxide and Related Materials, Vol. 1 Materials. Taylor and Francis/CRC Press (2012).

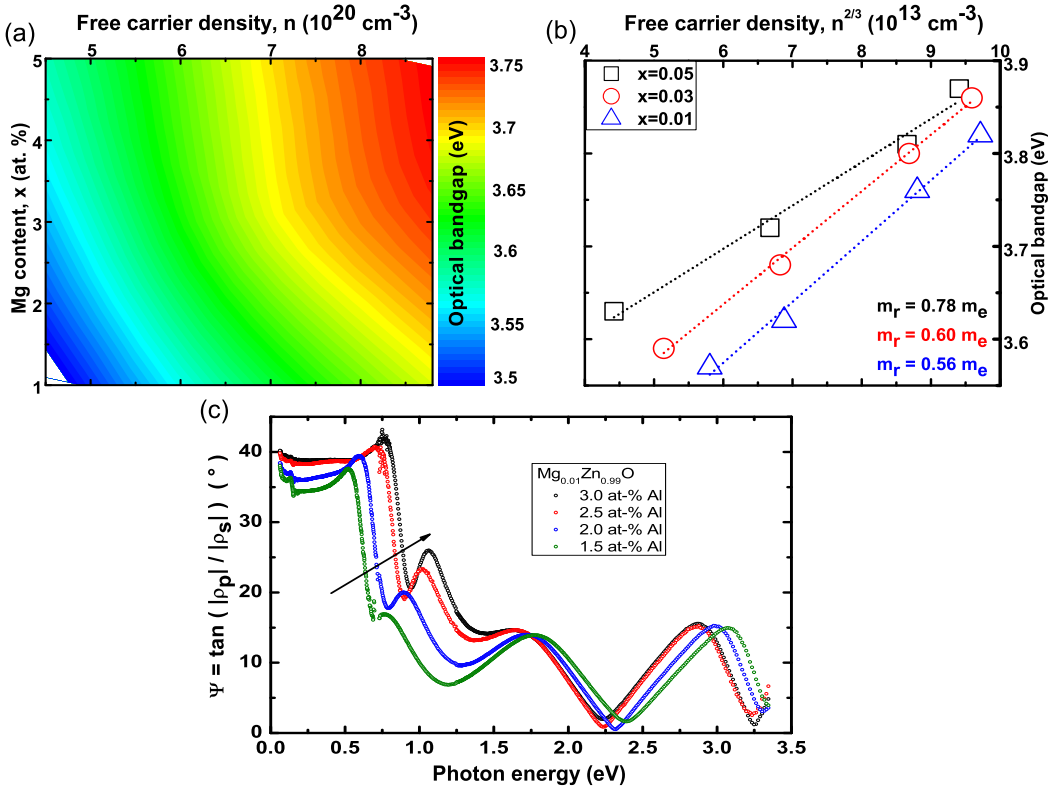

Figure 9.12: (a) The optical bandgap as function of Mg content and free carrier density, (b) the calculated reduced electron mass, and (c) ellipsometric parameter Ψ measured at an angle of incidence of 65 ° for the sample divisions with 1 at-% Mg showing the increasing plasma frequency with increasing Al concentration (arrow).

[2] R.G. Gordon, MRS Bulletin **25**, (2000) 52 - 57.
[3] T. Minemoto, Y. Hamakawa, Thin Solid Films **372**, (2000) 173 - 176.
[4] H. von Wenckstern, K. Jug, Progress in Solid State Chemistry **37**, (2009) 153 - 172.
[5] H. von Wenckstern, M. Grundmann, CrystEngComm **15**, (2013) 10020-10027.

9.12 A continuous composition spread approach towards wavelength-selective monolithic multichannel ultraviolet photodiodes based on (Mg,Zn)O thin films

Z. Zhang, H. von Wenckstern, J. Lenzner, H. Hochmuth, M. Lorenz, M. Grundmann

In recent years, ultraviolet (UV) photodiodes (PDs) based on wide bandgap semiconductors find applications for remote sensing, surveillance purpose and chemical/biological sensors [1]. In comparison with conventional photomultiplier tubes with metal photocathode, which are bulky, fragile and require a large bias, UV-PDs employing wide bandgap semiconductors have significant advantages [1]. For wavelength-selective detection based on Si, SiC or GaP, an expensive external dichroic filter is required, due to their sensitivity to visible and infrared radiation. This is not necessary

for wide bandgap material like ternary semiconductor (Mg,Zn)O [2, 3] with integrated optical filter layer being only sensitive in a defined narrow spectral range.

In this report, we demonstrate monolithic multichannel UV-PDs with wavelength- and bandwidth-selectivity in the visible-blind spectral range. The PDs are fabricated on (Mg,Zn)O thin films grown by pulsed-laser deposition (PLD) with continuous composition spread (CCS) [5] using a single segmented target. Both the active as well as the filter layer were grown by this CCS approach on opposite sides of a 2 inch a-plane sapphire wafer. Due to the CCS the Mg-content and with that the fundamental bandgap of both layers change linearly along the composition gradient. The photo response stems from a metal-semiconductor-metal (MSM) structure on the active layer and the varying spectral bandwidths are enabled by the optical filter layer.

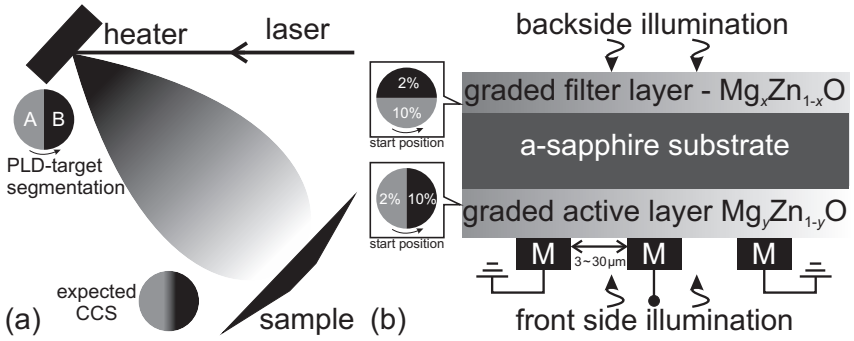

Figure 9.13: (a) Schematic representation of PLD-setup with a two-fold segmented target of constituent A and B, respectively, enabling compositionally graded profile on the sample; (b) schematic layout of the device with graded-filter/a-sapphire/graded-active structure under front as well as backside illumination, the Mg-contents of the segmented target are 2 at.% and 10 at.%, respectively.

Circular ZnO targets containing 2 at.% and 10 at.% MgO, respectively, are prepared by ball milling, cold pressing and sintering [6]. The targets are then cut into two semicircular pieces and assembled in a two-fold segmented target as illustrated in FIG. 9.23 (a,b). The rotation of the substrate and PLD-target is synchronized. First, the optical filter layer is grown on one side of a 2 inch double-sided polished a-plane sapphire wafer. After turning the substrate, the active layer is subsequently deposited on the opposite side of the substrate, but with a starting position for which the boundary is perpendicular to the edge of the 2 inch wafer. Such design leads to a spatial decoupling of both layers allowing a minimization of the bandwidth and shift of cutoff energies of the PD arrays [6, 7].

The dependence of the fundamental bandgap of (Mg,Zn)O is linear within the composition range investigated here. Hence, a variation of bandgap can be determined from a cathodoluminescence (CL) measurements in FIG. 9.24 (d,e) as related to a change of Mg-content. The Mg-composition of both layers is measured by energy dispersive X-ray spectroscopy (EDX) and mapped in FIG. 9.24 (d,e), respectively. As obvious from the CL-maps, the $E_{CL,max.}$ determined from the spectra of the near band-edge emission [3], shifts continuously with increasing Mg-content to higher energies, along the composition gradient as indicated by white dashed arrows across the wafer. As expected [7], the resultant directions of the composition gradient of both layers with an angle of about 72° to each other, are consistent with the starting positions of the two-fold

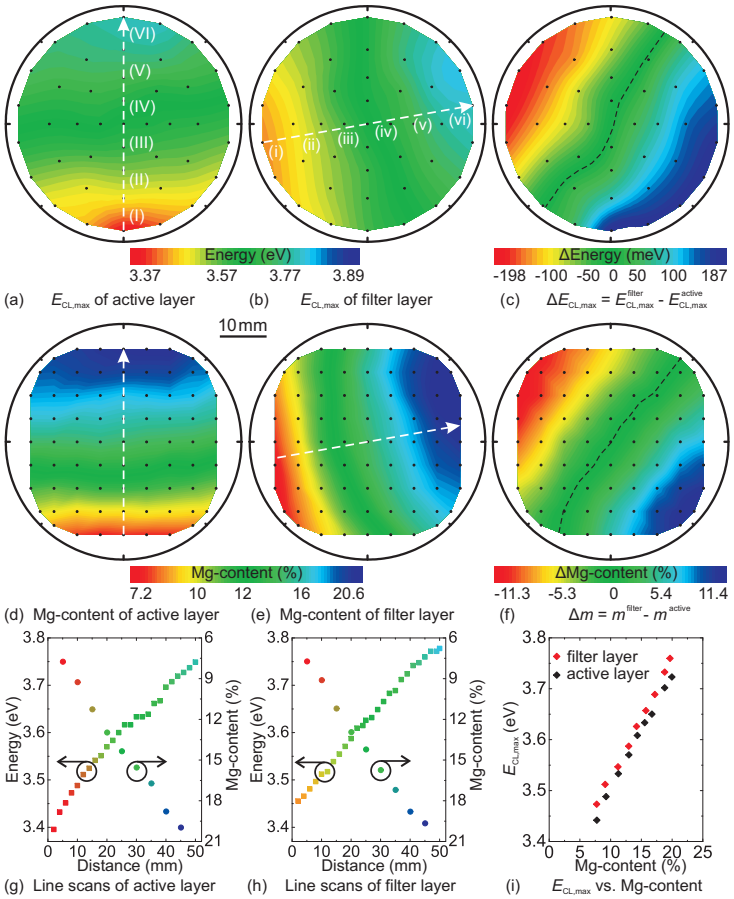

Figure 9.14: Contour plots (black points depict measuring positions) of the maximum emission energy $E_{\mathrm{CL,max.}}$ of room temperature CL- and Mg-content observed by EDX-measurements of the (a,d) active and filter layer (b,e), respectively; contour plots of (c) $\Delta E_{\mathrm{CL,max.}}$ and (f) Δm between filter and active layer, the black dashed line shows the dividing line of $\Delta E_{\mathrm{CL,max.}} = \Delta m = 0$; line scans of $E_{\mathrm{CL,max.}}$ and m of (g) active (h) filter layer along the Mg-composition gradient as indicated marked by white dashed arrows in figures (a,b), respectively; (i) dependence of $E_{\mathrm{CL,max.}}$ on Mg-content at measuring spot from figures (g,h).

PLD-target of its own (cf. FIG. 9.23 (b)). FIG. 9.24 (g,h) show the line scans of $E_{\mathrm{CL,max.}}$ and Mg-content of both layers along the gradient. $E_{\mathrm{CL,max.}}$ of the active (filter) layer across the wafer has a difference of about 350 (320) meV and increases linearly on the lateral position ($\Delta E^{\mathrm{active\,(filter)}}_{\mathrm{CL,max.}}/\Delta d = 7.4\,(6.7)$ meV/mm). Mg-content $\Delta m^{\mathrm{active\,(filter)}}/\Delta d = 0.306\,\%\,(0.298\,\%)$/mm has the same trend as CL-measurements. On the same Mg-content, a slight higher $E_{\mathrm{CL,max.}}$ of the filter layer is observed (cf. FIG. 9.24 (i)) due to the surface reheating during the deposition of active layer.

The structural properties of the CCS thin films are characterized by X-ray diffraction (XRD) measurements. Both layers are single-phase, crystalline, c-axis oriented and have wurtzite structure. A shift of (0002) reflection to higher angles with higher Mg incorporation along the composition gradient on lateral position is observed due to a different distribution of the growth temperature on the PLD-heater.

The cutoff energy E_{cutoff} of a PD is defined by $\sqrt{1/2}\,E_{\mathrm{max.}}$. All cutoff energies (cf. FIG. 9.15 (a,b)) of the PDs are achieved in the UVA spectral range (3.10−3.94 eV) illustrated as gray shadows in FIG. 9.15 (a,b). For the front side illumination (dashed lines),

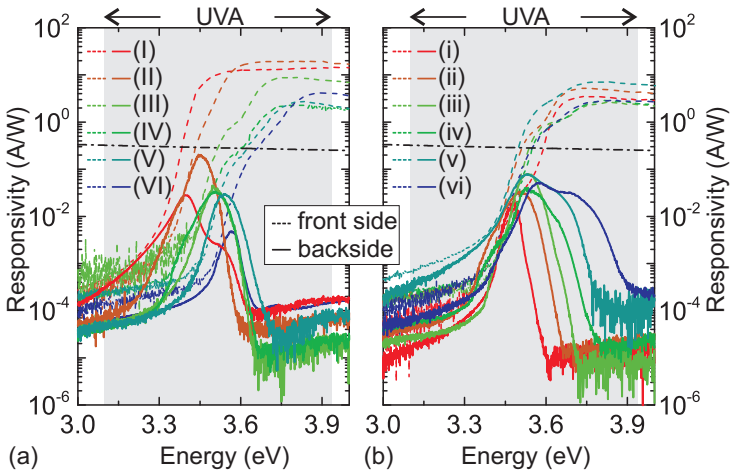

Figure 9.15: spectral responsivity (A/W) of multichannel MSM-PDs versus photon energy at $V_{\text{ext}} = 4.0\,\text{V}$ under front- (dashed lines) and backside (solid lines) illuminations for positions selected along the gradient as depicted in FIG. 9.24 (a,b) of (a) active and (b) filter layer, respectively, the dashed-dotted lines show the maximum external quantum efficiency of 100 %

the photo response extends to deep UV range keeping a constant responsivity due to an inactive filter layer [3]. As expected from the CL- and EDX-measurements, along the Mg-composition gradient of the active layer from position (I) to (VI), a blue-shift of the absorption onset of the photo response is observed. In directions perpendicular to the gradient only a slight variation of $E_{\text{cutoff}}^{\text{front}}$ from positions (i) to (vi) is observed.

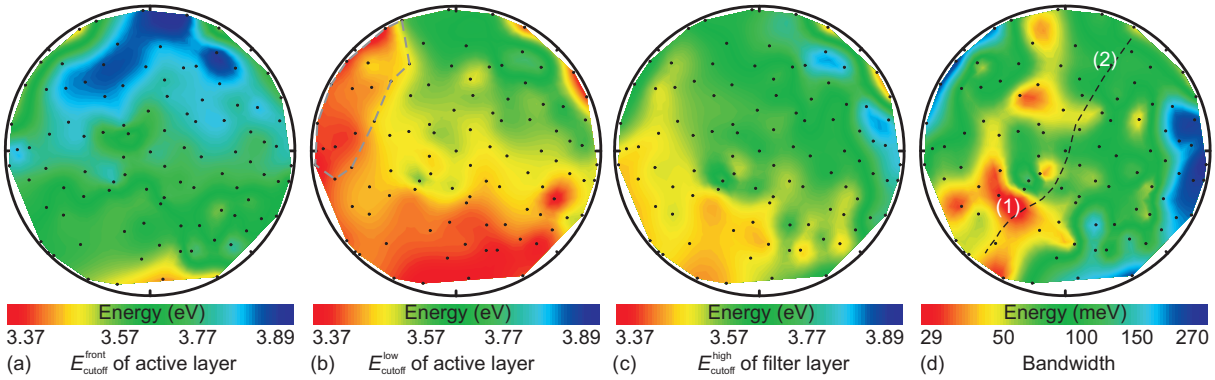

Figure 9.16: False color maps showing the 2 inch wafer of (a) $E_{\text{cutoff}}^{\text{front}}$ of photo response under front side, (b,c) $E_{\text{cutoff}}^{\text{low,high}}$ and (d) bandwidth under backside illumination, respectively; the black points depict positions of selected 98 MSM-PDs corresponding the wafer.

The spatial dependence of $E_{\text{cutoff}}^{\text{front}}$ of 98 fabricated MSM-PDs on the lateral positions indicated as black points, are shown as a false color representation in FIG. 9.16 (a). As can be seen, a wavelength-selective PD with defined bandwidth can be only realized by backside illumination (solid lines). The low cutoff energy $E_{\text{cutoff}}^{\text{low}}$ of PDs referred to the absorption edge of the active layer has also a blue-shift from position (I) to (VI) in FIG. 9.16 (a). Compared to $E_{\text{cutoff}}^{\text{front}}$ and/or $E_{\text{cutoff}}^{\text{low}}$, a blue-shift of $E_{\text{cutoff}}^{\text{high}}$ along the Mg-gradient of the filter layer (cf. FIG. 9.15 (b), FIG. 9.16 (c)) from (i) to (vi) is also observed, while there is only a slight variation on lateral positions from (I) to (VI).

The spectral bandwidth of photon energy $E_{\text{bandwidth}}$ is defined by the difference of

both cutoff energies shown as a false color map in FIG. 9.16 (d). As can be seen, the largest bandwidth of 270 meV (ca. 25 nm) is observed at the measuring position of maximal $\Delta E_{\mathrm{CL,max.}}$ and Δm (cf. FIG. 9.24 (c,f)). The lowest bandwidth should be measured at the positions near the boundary of $\Delta E_{\mathrm{CL,max.}} = \Delta m = 0$. But apparently, the narrowest bandwidth of 29 meV is observed at the position (1) not (2), although the $\Delta E_{\mathrm{CL,max.}}$ for both positions has a same value of 26 meV. It is caused by the limited FWHM of photo response due to alloy broadening [8], for which the Mg-contents of both layers at position (2) are higher than that of (1) (cf. FIG. 9.24 (d-f)). Thus, the bandwidth can be adjusted not only by appropriate choice of the target constituents [3], but also can be realized ($\Delta E_{\mathrm{bandwidth}} = 241$ meV) by using of two angled CCS thin films with a same target constituent.

We have realized wavelength/bandwidth-selective, monolithic, and multichannel photodiode arrays by using a design of decoupling of two separated continuous composition spreads. The onset of the absorption edge is tuned over 430 meV within the UVA range under front side illumination and the spectral bandwidth can be controlled from 270 meV down to 29 meV.

This work has been supported by Deutsche Forschungsgemeinschaft in the framework of SFB 762 "Functionality of Oxide Interfaces".

[1] M. Razeghi and A. Rogalski, J. Appl. Phys. **79**, 7433 (1996)
[2] Z.P. Zhang, H. von Wenckstern, M. Schmidt, and M. Grundmann, Appl. Phys. Lett. **99**, 083502 (2011)
[3] Z.P. Zhang, H. von Wenckstern, and M. Grundmann, Appl. Phys. Lett. **103**, 171111 (2013)
[4] H. von Wenckstern, R. Schmidt-Grund, C. Bundesmann, A. Müller, C. P. Dietrich, M. Stözel, M. Lange, and M. Grundmann, "The (Mg,Zn)O alloy", in *Handbook of Zinc Oxide and Related Materials*, edited by Z. C. Feng, (Taylor and Francis/CRC Press, Boca Raton, Florida, USA, 2012), Chapter 10, p. 257
[5] J.J. Hanak, J. Mater. Sci. **5**, 964 (1970)
[6] H. von Wenckstern, Z.P. Zhang, and M. Grundmann, CrystEngComm **15**, 10020 (2013)
[7] H. von Wenckstern, Z.P. Zhang, J. Lenzner, F. Schmidt, and M. Grundmann, MRS Proceedings **1633**, DOI: http://dx.doi.org/10.1557/opl.2014.19 (2014)
[8] M. Grundmann and C.P. Dietrich, J. Appl. Phys. **106**, 123521 (2009)

9.13 Low Rate Deep Level Transient Spectroscopy – A powerful tool for defect characterization in wide bandgap semiconductors

F. Schmidt, H. von Wenckstern, O. Breitenstein*, R. Pickenhain, M. Grundmann

*Max Planck Institute of Microstructure Physics, Weinberg 2, 06120 Halle, Germany

Deep Level Transient Spectroscopy (DLTS) is widely used to detect electronic defects in semiconductors [1]. In the last decades many special DLTS techniques have

been developed, from which ODLTS (DLTS working under permanent monochromatic light illumination [3, 4]) is used to determine optical capture cross sections (absorption spectra). For doing this, the optical emission rate must be at least in the order of the lowest experimentally accessible rate window of the DLTS system, which is for commercial DLTS systems about 1 s^{-1}. The photon flux of conventional light source is often not sufficient to produce optical emission rates above that critical value. For such cases the extension of available rate windows into the mHz-range is required. It also may allow to separate energetically close-lying levels, whose peaks are overlapping in the usual rate window range. Moreover, for wide bandgap materials it extends the detection range of defect levels to higher activation energies, as illustrated in Fig. 9.17 (a). Such low rate windows are outside of the parameter range of standard DLTS systems.

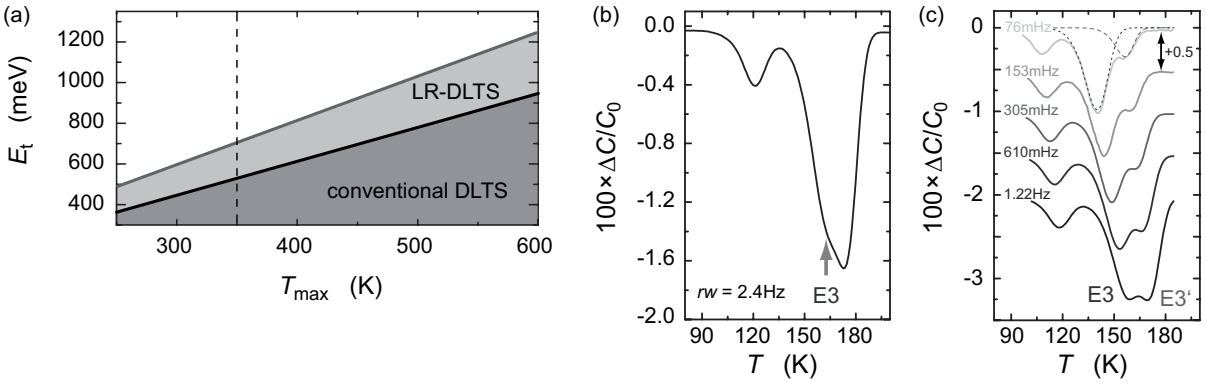

Figure 9.17: (a) Accessible thermal activation energy E_t versus maximal applied temperature T_{max} for a rate window of 10 Hz (conventional DLTS) and 10 mHz (LR-DLTS), respectively. (b) DLTS signal using a rate-window of 2.4 Hz and (c) rate-windows between 76 mHz and 1.22 Hz. The lines in (c) have been shifted for clarity in vertical direction in equidistant steps of 0.5.

For detecting low emission rates the tuning state of the DLTS capacitance (C) meter is fixed during each isothermal transient measurement. During a temperature (T) scan the basic capacitance of the sample changes by typically 10%, and also the conductive loss changes considerably. If the tuning of the C-meter stays constant during the whole T-scan, its dynamic range must cover this large capacitance and conductance changes. This usually means that the C-meter is not in its most sensitive range, which is only assured if both the capacitance and the conductance are perfectly tuned in the bridge circuit. In this contribution a novel C-meter concept is introduced, combining high detection sensitivity with a permanent tuning of the basic capacitance. For performing LR-DLTS, a special DLTS spectrometer was used, which was developed at Max Planck Institute Halle. It combines maximum possible detection sensitivity with a continuously tuning of the basic capacitance and conductance inbetween the transient measurements in two independent feedback loops. The C-meter is based on the resonance-tuned bridge design described in Ref. [5]. This design was extended for automatic C- and G-compensation by using a varicap and an LED-driven photoresistor.

The setup opens up the possibility for further refined measuring techniques such as double DLTS, ODLTS with permanent and pulsed photon excitation, capacitance-voltage measurements, photo-capacitance measurements, and photo-current measurements [9]. Finally it is possible to store the whole outcome of a measurement with

each single transient for further external evaluation e.g. a deconvolution with aid of Laplace-DLTS [6].

Within the sizeable number of electrically active defects in zinc oxide (ZnO) the E3 defect is certainly one of the most prominent. This is due to the fact, that E3 seems to be omnipresent in ZnO; it is incorporated in ZnO independent of the growth method in bulk crystals, thin films and microwires from carbothermal evaporation. The thermal activation energy E_a and the apparent capture cross-section σ determined via DLTS are reported in the range from 275 to 300 meV and from 1×10^{16} cm^2 to about 8×10^{16} cm^2, respectively. However, the microscopic origin of E3 is still under debate.

By using high-resolution Laplace-DLTS [6], Auret *et al.* [7] revealed that a defect labeled E3' exists in ZnO thin films on ZnO:Al buffer causing a DLTS signal in the vicinity of that of E3. In a conventional DLTS scan recorded by using the smallest rate-windows being in the range of 1 Hz, E3' usually occurs only as a shoulder on the high temperature side of the E3 peak; for higher rate-windows the signals of E3 and E3' merge making the determination of the individual trap parameters difficult if not impossible.

With LR-DLTS is is possible to apply rate-windows in the order of 1 mHz, for which the DLTS peaks of E3 and E3' are shifted to lower temperatures, at which the emission rate of E3 and E3', respectively, and with that the DLTS signals are easily distinguishable [9]. In Fig. 9.17 (b) a conventional thermal DLTS measurement is shown for a comparatively small rate-window of 2.4 Hz. A shoulder on the low temperature side of the E3' signal is visible and is due to the E3 defect. The data, however, does not allow to determine trap parameters of E3' or E3. Now, LR-DLTS extends the accessible range of emission rates by at least three orders of magnitude. With that, the signals of E3 and E3' are measurable at temperatures for which they are clearly separated. On the basis of the LR-DLTS data an Arrhenius plot can be constructed using lineshape fits as shown by the dashed lines in Fig. 9.17 (c) for a rate window of 76 mHz.

Optical emission rates of deep levels can be investigated by means of ODLTS. In this example we observe only an interaction between the defect and free electrons in the conduction band. This is because in our *n*-type ZnO thin film hole emission can be neglected. Defects were charged using a filling pulse having the same shape and length as applied before in the conventional DLTS experiment, i.e. a reverse bias of 3 V, a filling pulse height of 4 V and a filling pulse length of 1 ms. The measurement was conducted at 300 K, where the emission rate of E3 is too high to contribute to the ODLTS signal. The concentration of E4, on the other hand, is too low and hardly visible in the thermal DLTS scan. Therefore, thermal emission processes can be neglected and the emission rate is given by the optical emission. Figure 9.18 (a) shows the ODLTS spectrum as a contour plot. Under illumination with photon energies of 1550 meV and 2900 meV the defects T4 [8] and TH1 [8] can be recharged, respectively, and therefore contribute to the ODLTS signal. The energetic position of the T4 step shows that the level is situated in the midgap region, where thermal emission processes can be excluded. Hence, the capacitance transient stems from the optical electron emission and subsequent optical hole emission of the midgap level. The TH1 defect, on the other hand, is located in the vicinity of the valence band edge. Its signal occurs due to the photo-ionisation by photons with an energy above 3.1 eV and a subsequent thermal emission of the generated hole into the valence band.

The optical capture cross-section σ_n^o is determined by the optical emission rate e_n^o and

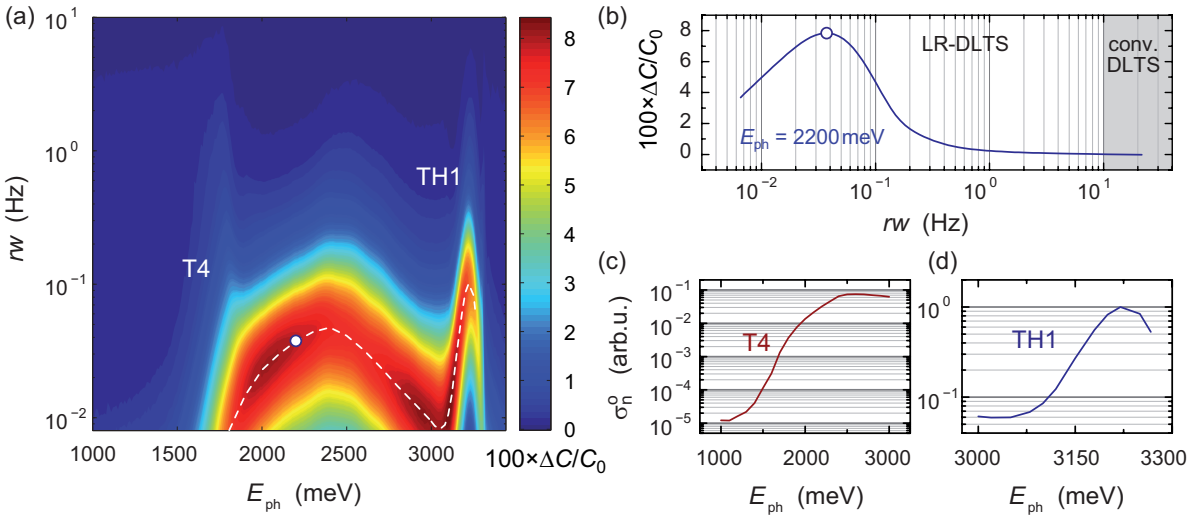

Figure 9.18: (a) Contour plot of the optical DLTS measurement. The dashed line represents the position of the maximum ODLTS signal in dependence of $h\nu$. (b) Normalized ODLTS signal for a photon energy of 2200 meV. The circle represents the maximum (cf. Fig. 9.18 (a)). (c) Optical capture cross-section of T4 and (d) TH1. Both signals were normalized on the maximum of TH1.

the photon flux ϕ, which is determined by the light source used and therefore usually fixed. To obtain σ_n^o in a wide energy range, it is necessary to assign the maximum ODLTS signal for each photon energy as shown exemplary for $E_{ph} = 2200$ meV in Fig. 9.18 (b). With LR-DLTS it is now possible to measure rate-windows in the mHz range and for a given photon energy $h\nu$ a by 3 orders of magnitude smaller optical emission rate and with that optical capture cross-section $\sigma_{n,p}^o$. This allows to determine $\sigma_{n,p}^o$ over a wide photon energy range. Figure 9.18 (c) and (d) show σ_n^o for T4 and TH1, respectively. The optical capture cross-section can be associated with absorption measurements and is therefore a fingerprint of a certain defect. Via the normalized peak height of the ODLTS signal $\varnothing/C_0$ and the net-doping density obtained from CV-measurements we determined the concentrations of T4 and TH1 to be 1×10^{16} cm^{-3} in each case. It is worth to recall that T4 and TH1 are the dominating compensating deep defects in ZnO and are not accessible with thermal DLTS.

[1] D. V. Lang, J. Appl. Phys. **45**, 3023 (1974).
[2] D. V. Lang, Physica B **401-402**, 7 (2007).
[3] A. Chantre, G. Vincent, D. Bois, Phys. Rev. B **23**, 5335 (1981).
[4] S. Brehme, R. Pickenhain, Phys. Status Solidi A **88**, K63 (1985).
[5] O. Breitenstein, Phys. Status Solidi A **71**, 159 (1982).
[6] L. Dobaczewski, A. R. Peaker, K. B. Nielsen, J. Appl. Phys. **96**, 4689 (2004).
[7] F. D. Auret, W. Meyer, P. J. van Rensburg, M. Hayes, J. Nel, H. von Wenckstern, H. Schmidt, G. Biehne, H. Hochmuth, M. Lorenz, M. Grundmann, Physica B **401-402**, 378 (2007).
[8] M. Schmidt, H. von Wenckstern, R. Pickenhain, M. Grundmann, Solid-State Electron. **75**, 48 (2012).
[9] F. Schmidt, H. von Wenckstern, O. Breitenstein, R. Pickenhain, M. Grundmann, Solid State Electron. **92**, 40 (2014).

9.14 Deep defects in ZnO microwires

F. Schmidt, S. Müller, H. von Wenckstern, C.P. Dietrich, R. Heinhold*, H.-S. Kim*, M.W. Allen*, M. Grundmann

*The MacDiarmid Institute for Advanced Materials and Nanotechnology, University of Canterbury, Christchurch 8043, New Zealand

Self organized grown zinc oxide microstructures have gained much attention due to their promising properties for applications in microscale and nanoscale technologies [1, 2]. ZnO micro- and nanostructures of high crystalline quality are key structures for modern photonic devices such as microresonators, ultraviolet detectors and electrically driven nanolasers [2]. However, the presence of defects greatly impacts material properties, such as carrier lifetime, mobility, and UV emission efficiency. Understanding the incorporation of defects is therefore an essential step towards the development and optimization of future applications. In this study we report on a detailed investigation of the defect nature of a ZnO microwire grown by carbo-thermal evaporation, a ZnO thin film grown by pulsed-laser deposition on an *a*-plane sapphire, and a hydrothermally grown Zn-face ZnO single crystal (Tokyo Denpa Co. Ltd.). The samples were investigated by means of current-voltage (*IV*) measurements, capacitance-voltage (*CV*) measurements, and deep-level transient spectroscopy (DLTS).

Room temperature *IV* measurements were applied using an Agilent 4156C precision semiconductor parameter analyzer and are shown in Fig. 9.19 (a) for all three ZnO structures.

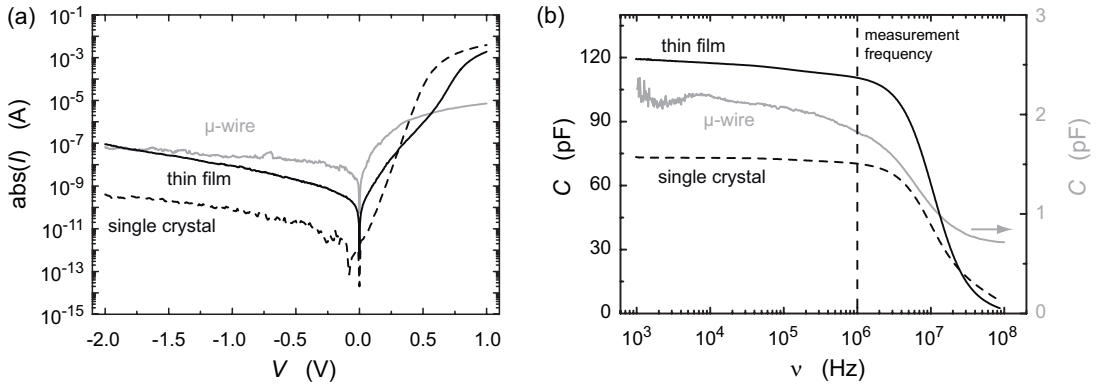

Figure 9.19: (a) Room temperature current-voltage characteristic of the microwire, thin film and single crystal, respectively. (b) Frequency-dependence of the capacitance of all samples investigated. Pictures adapted from Ref. [3].

The series resistance R_s, the shunt resistance R_p, and the rectification ratio RR defined by $I(+1\,\mathrm{V})/I(-1\,\mathrm{V})$ were determined and are summarized in Tab. 9.1.

Frequency-dependent capacitance measurements reveal the influence of the series resistance on the cut-off frequency ν_{co} and on the frequency dependence of the capacitance. Since ν_{co} is inversely proportional to R_s and this value is quite high for the microwire (80 kΩ, cmp. Tab. 9.1), it was necessary to check that ν_{co} was above the 1 MHz measuring frequency of our DLTS system. This was confirmed for all diodes used in this study, as shown in Fig. 9.19 (b). All samples are therefore suitable for investigations by DLTS.

Table 9.1: Series resistance R_s, shunt resistance R_p and rectification ratio RR obtained from room-temperature IV - characteristics of ZnO Schottky diodes.

Sample	R_s (Ω)	R_p (Ω)	RR
microwire	80k	40M	3×10^2
thin film	61	6M	2×10^5
single crystal	115	9G	6×10^7

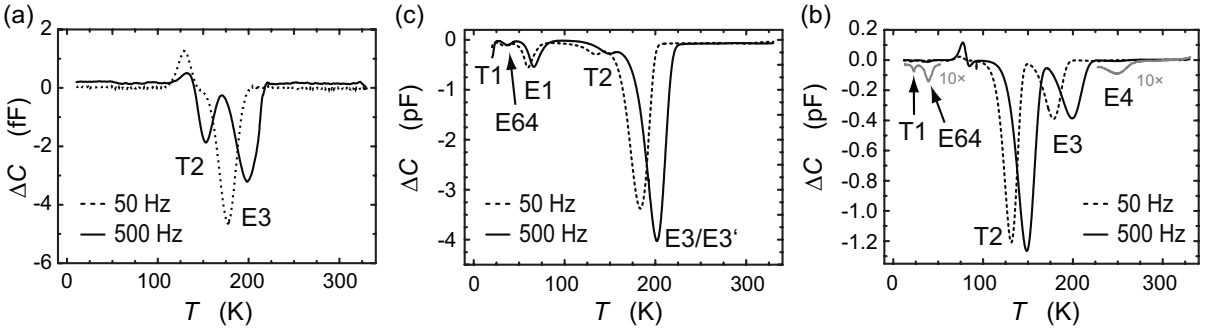

Figure 9.20: DLTS scans of (a) the microwire, (b) the thin film and (c) the single crystal sample using a rate window of 500 Hz and 50 Hz, respectively.

DLTS was applied in a temperature range from 10 K to 330 K. A description of the DLTS system can be found in Ref. [4]. The samples were biased at $V = -2$ V and excited using a filling pulse of $V = 2.5$ V applied for $t_p = 1$ ms. Rate windows in the range of 2.5 Hz to 2000 Hz were used. The DLTS scans of the microwire, the thin film and the single crystal sample are shown in Fig. 9.20 (a) to (c) for rate windows of 50 Hz and 500 Hz, respectively.

For the ZnO microwire, we found DLTS peaks that correspond to the carrier emission of the defects T2 and E3. The E3 defect, which is commonly observed in ZnO, was also present in the thin film and single crystal samples (cmp. Fig. 9.20 (b) and (c)). The defect activation energy of approximately 300 meV was also determined by temperature dependent Hall-effect measurements on an undoped ZnO microwire [5]. It was shown that the activation energy and apparent capture cross section σ_n of T2 depends on its concentration. The trap parameters of T2 in the microwire sample would therefore allow an estimation of the defect concentration $N_{t,T2}$. By extrapolation of the σ_n versus $N_{t,T2}$ relation (inset in Fig. 2 in Ref. [6]) we determined the concentration to be below 10^{14} cm^{-3}. In general the appearance of E3 and T2 in the microwire sample is a strong indication for their connection to intrinsic defects.

The concentration of T2 is enhanced in ZnO under annealing in vacuum and an oxygen ambient as shown in melt grown single crystal ZnO and PLD grown ZnO, respectively. While this is confirmed in the low-Li bulk sample prepared at nominally 1400°C ($N_{t,T2} = 3 \times 10^{15}$ cm^{-3}) as well as in the PLD thin film grown at 650°C ($N_{t,T2} = 4 \times 10^{14}$ cm^{-3}), surprisingly the concentration of T2 in the microwire is lowest (since E_t is highest) even at intermediate growth temperatures of 950°C. We therefore suggest that the position of the Fermi level E_F significantly affects the concentration of T2. Based on a model introduced by Schmidt *et al.*, the T2 defect is assumed to be a donor-acceptor complex. Although our experimental methods are not sensitive to the chemical nature of either the donor or the acceptor, we would propose the zinc vacancy

V_{Zn} as a possible candidate for an acceptor. First-principles studies reveal that V_{Zn} has a lower formation energy for a higher Fermi level [7]. Due to the naturally high concentration of donors in ZnO it is reasonable that the T2 concentration is determined by the concentration of that acceptor and with that the position of the Fermi level. This is supported by the net-doping density $N_d - N_a$, which is a measure for E_F in our samples. $N_d - N_a$ was obtained from CV measurements for the PLD thin film and the low-Li bulk sample to be $1 \times 10^{17}\,cm^{-3}$ and $4 \times 10^{16}\,cm^{-3}$, respectively. Due to the large uncertainty of the effective contact area we can only estimate the net doping density for the microwire to be about $10^{16}\,cm^{-3}$. This value is consistent with the apparent free carrier concentration $n_H = 2 \times 10^{16}\,cm^{-3}$ determined from Hall effect measurements of similar wires. Therefore, we conclude that the acceptor is most likely formed in the PLD thin film followed by the bulk sample and the microwire, which is consistent with the model proposed for T2. Freeze-out due to the comparatively large degree of compensation in the microwire sample and the as-grown ZnO-bulk sample supports the assumption that V_{Zn} is preferably formed in the PLD thin film having a high Fermi level, while the generation of the defect is less distinct in the compensated microwire or only occurs after thermal treatment as it is the case for the two bulk samples.

[1] M. S. Gudiksen, L. J. Lauhon, J. Wang, D. C. Smith, C. M. Lieber, Nature **415**, 617 (2002).
[2] M. H. Huang, S. Mao, H. Feick, H. Yan, Y. Wu, H. Kind, E. Weber, R. Russo, P. Yang, Science **292**, 1897 (2001).
[3] F. Schmidt, S. Müller, H. von Wenckstern, C. P. Dietrich, R. Heinhold, M. W. Allen, M. Grundmann, Appl. Phys. Lett. **103**(6), 062102 (2013).
[4] F. Schmidt, H. von Wenckstern, D. Spemann, M. Grundmann, Appl. Phys. Lett. **101**, 012103 (2012).
[5] C. P. Dietrich, M. Brandt, M. Lange, J. Kupper, T. Böntgen, H. von Wenckstern, and M. Grundmann, J. Appl. Phys. **109**, 013712 (2011).
[6] M. Schmidt, M. Ellguth, R. Karsthof, H. von Wenckstern, R. Pickenhain, M. Grundmann, G. Brauer, F. C. C. Ling, Phys. Status Solidi B **249**, No. 3, 588 (2012).
[7] F. Oba, M. Choi, A. Togo, I. Tanaka, Sci. Technol. Adv. Mater. **12**, 034302 (2011).

9.15 Defect studies on Ar-implanted ZnO thin films

F. Schmidt, S. Müller, R. Pickenhain, H. von Wenckstern, S. Geburt*, C. Ronning*, M. Grundmann

*Friedrich-Schiller-Universität Jena, Institut für Festkörperphysik, Max-Wien-Platz 1, 07743 Jena, Germany

Zinc oxide (ZnO) and related compounds are interesting for optoelectronic devices working in the near UV. Ion implantation is commonly used in the device fabrication process for e.g. LEDs in GaN [1], however, it is not yet routinely applied in ZnO. A profound understanding of ion induced damage in such wide band gap semiconductors is necessary to optimize suitable implantation and annealing conditions for certain applications.

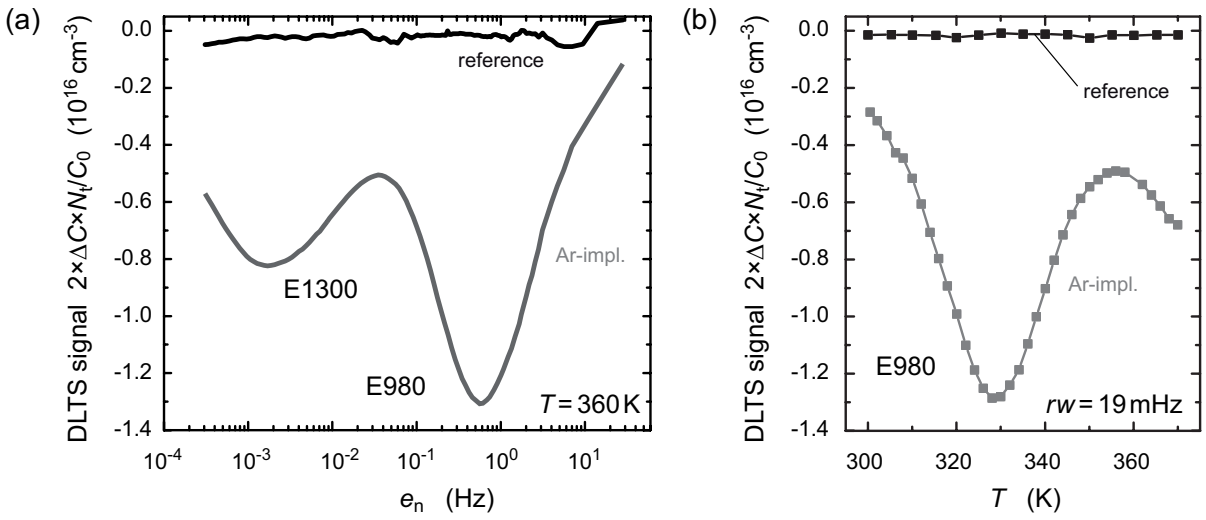

Figure 9.21: DLTS signal versus (a) emission rate e_n and (b) temperature T for thin film samples annealed at different temperatures. Figures adapted from Ref. [8].

In this study we present a combination of low-rate deep level transient spectroscopy (LR-DLTS) [2, 3] and optical deep level transient spectroscopy (ODLTS) to study native deep-level defects introduced into ZnO thin films by Ar ion implantation. The ZnO thin film with a thickness of approx. 1 μm was grown by pulsed laser deposition (PLD) [4] on an *a*-plane sapphire wafer. The wafer was divided into smaller pieces from which one piece was kept as as-grown reference and one was implanted with ^{40}Ar ions.

Figure 9.21 (a) and (b) show the DLTS signals multiplied with the net-doping N_t density obtained from *CV*-measurements versus the thermal emission rate e_n^{th} and the temperature, respectively. In this representation the signal height is directly proportional to the concentration of the emitting defect level.

In Fig. 9.21 (a) DLTS signals of the reference sample (black line) and the argon-implanted sample (grey line) are depicted for a fixed measurement temperature of 360 K, respectively. Apparently, the argon-implantation introduces two deep levels resulting in peaks at $e_n^{th} = 1.7$ mHz and $e_n^{th} = 0.56$ Hz, respectively. Figure 9.21 (b) shows the DLTS signals in a temperature range between 300 K and 370 K for a fixed rate window of 19 mHz. In the thermal DLTS scan only the shallower defect is visible in the temperature range accessible with our setup. Both defects are absent in the reference sample. The defects have activation energies E_a of 980 meV and 1300 meV, respectively, and apparent capture cross sections σ_n of 2.4×10^{-13} cm^2 and 1.4×10^{-11} cm^2, respectively.

Optical DLTS (ODLTS) [3, 5] was carried out using an IR-laser diode having a wavelength of 1064 nm ($E_{ph} = 1.17$ eV). The ODLTS scan of E980 is shown by the orange line in Fig. 9.22 (a) for a rate window of 19 mHz. The black line represents the DLTS signal under dark conditions using the same rate window. At low temperatures ($T <$ 310 K) the DLTS signal is dominated by the optical emission of carriers, since $e_n^{opt} \gg e_n^{th}$. At high temperatures ($T >$ 360 K) the thermal emission process is predominant and leads to a drop of the ODLTS signal. The difference of the ODLTS signal between 310 K and 360 K should correspond to the sum of the concentration of E980 and E730. However, this is not the case, since the drop of the ODLTS signal is larger than the DLTS maximum of E980 including the signal of E730 under dark conditions. Hence,

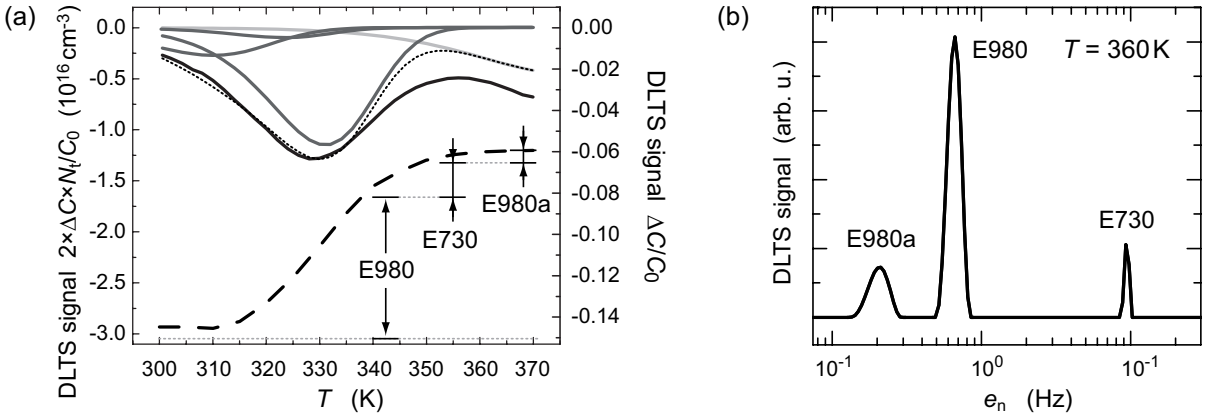

Figure 9.22: (a) Thermal DLTS (black line) and ODLTS scan (dashed line). (b) Isothermal LDLTS spectrum at $T = 360\,\mathrm{K}$. The dotted line in (a) represents the calculated DLTS signal taking into account the signal heights and the emission rates obtained from the LDLTS measurement. Figures adapted from Ref. [8].

we conclude that more than those two deep levels contributes to the overall signal and therefore applied high resolution Laplace DLTS (LDLTS) [6] as described in the following. A LDLTS spectrum for $T = 360\,\mathrm{K}$ is shown in Fig. 9.22 (b). The deconvolution of isothermal capacitance transients reveals contributions of 3 deep levels labelled E980, E730 and E980a.

Since only changes in the charge state of defects are measured, space charge spectroscopic methods, in particularly DLTS, are chemically blind. However, we assign the oxygen vacancy V_O as a possible candidate for E730, E980 or E1300. It was shown from first-principle studies that the oxygen vacancy is a deep donor in ZnO with the transition $V_O^{2+} \rightarrow V_O^0$ at approximately 1.0 eV below the conduction band edge [7]. Due to its high formation energy of $\approx +3.5\,\mathrm{eV}$ it is neither likely that V_O is incorporated during growth nor that the defect is responsible for unintentional *n*-type conductivity of ZnO. By the implantation of high energetic ions, on the other hand, such energies can be easily transferred to the lattice and therefore lead to the formation of defects e.g. vacancies [8].

[1] S. J. Pearton, C. R. Abernathy, and F. Ren, Gallium Nitride Processing for Electronics, Sensors and Spintronics (Springer, 2006).
[2] D.V. Lang, J. Appl. Phys. **45**(7), 3023 (1974).
[3] F. Schmidt, H. von Wenckstern, O. Breitenstein, R. Pickenhain, M. Grundmann, Solid-State Electron. **92**, 40 (2014).
[4] M. Lorenz, in: K. Elmer, A. Klein, B. Rech (Eds.), Transparent Conductive Zinc Oxide: Basics and Applications, Springer, 2008, pp. 77-122.
[5] A. Chantre, G. Vincent, D. Bois, Phys. Rev. B **23**, 5335 (1981).
[6] L. Dobaczewski, A. R. Peaker, and K. B. Nielsen, J. Appl. Phys. **96**, 4689 (2004).
[7] A. Janotti and C. G. Van de Walle, Appl. Phys. Lett. **87**, 122102 (2005).
[8] F. Schmidt, S. Müller, R. Pickenhain, H. von Wenckstern, S. Geburt, C. Ronning, M. Grundmann, Phys. Status Solidi B, published online, DOI 10.1002/pssb.201451011 (2014).

9.16 Epitaxial growth of $LaAlO_3$ and $LaNiO_3$ thin films and multilayers by PLD

H.M. Wei, M. Lorenz, M. Grundmann

$LaNiO_3$ (LNO) is an interesting material exhibiting Pauli paramagnetic metallic behavior at any temperature [1]. Over the past few years, research interest in this compound was the development of highly conductive elctrodes for ferroelectric thin-film devices [2]. Recently, LNO superlattices (SLs) have been drawing enormous attention since the prediction of a possible high-temperature superconductivity [3]. Furthermore, theory predicts the appearance of topological phases in $LaNiO_3/LaAlO_3$ SLs (where $LaAlO_3$ is a wide band-gap insulator) [4, 5]. However, up to date, little experimental work has been done.

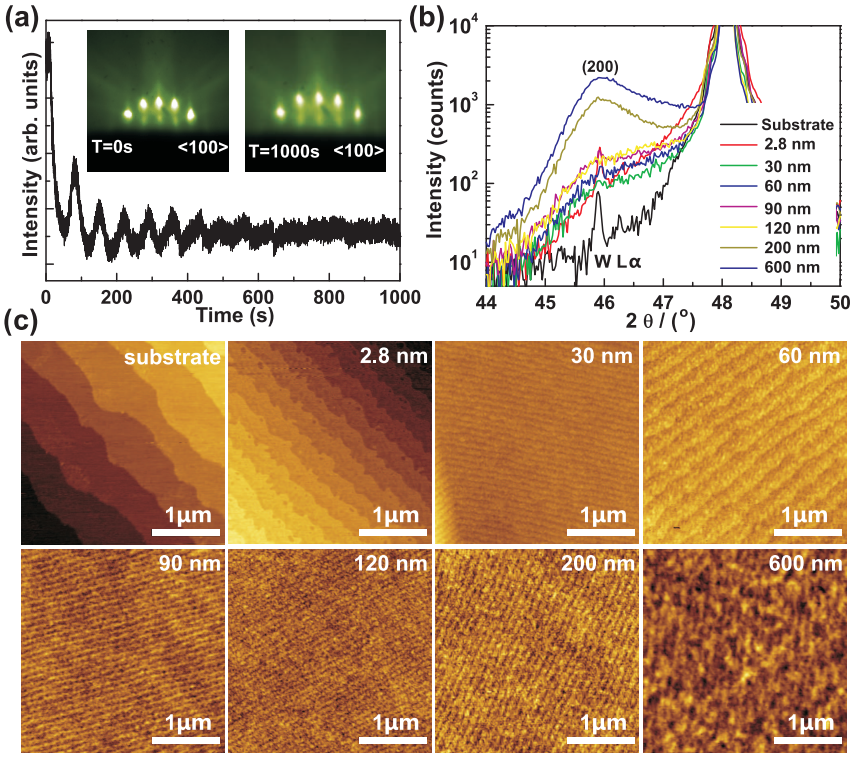

Figure 9.23: (a) RHEED oscillations of 2.8 nm LAO film grown on LAO substrate (inset are RHEED patterns before and after deposition). (b) XRD $2\theta - \omega$ scans of annealed LAO substrate and thin films with different thickness. (c) AFM images of LAO substrate and thin films. Thickness values were estimated from the numbers of laser pulses using an ellipsometry measurement (30000 pulses ≈ 600 nm).

We have grown LAO and LNO thin films and $10 \times$ [LNO(d nm)/LAO(d nm)] multilayers (MLs) by PLD on various substrates. Before deposition, the substrates are annealed in a tube furnace in order to obtain single-terminated and atomically flat steps. Reflection high-energy diffraction (RHEED) was utilized to monitor the two-dimensional growth process and control the thickness of thin films. As shown in Fig. 9.23 (a), RHEED intensity oscillations are clearly observed during growth of the first LAO layer. In addition, Fig.1 (a) shows RHEED patterns before and after deposition of 14 layers. The sharp pattern with clear Kikuchi lines confirms an atomically

flat surface. All LAO films with different thickness have consistent out-of-plane lattice constant and smooth surface with root mean square (rms) roughness below 0.17 nm as shown in Fig. 9.23 (b,c).

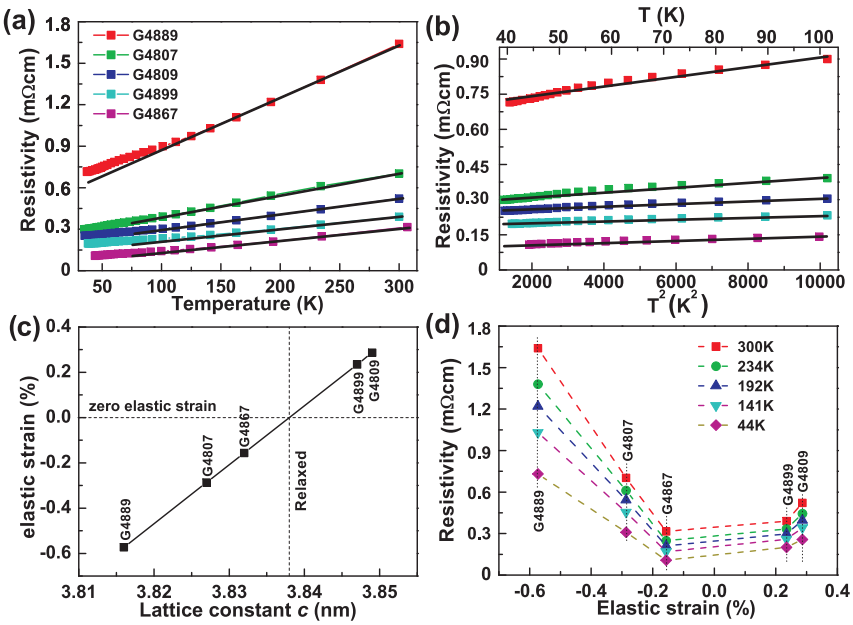

Figure 9.24: (a) Temperature-dependent resistivity of LNO films. (b) ρ vs. T^2 curve below 100 K. (c) Residual elastic strain in perpendicular direction of samples corresponding to (a). (d) Plot of resistivity of LNO films as a function of elastic out-of-plane strain.

Table 9.2: Characteristics of the LNO films: strain, electron-phonon coupling constant λ, carriers mean free path l and Kadowaki-Woods ratio γ_{KW}. Out-of-plane strain was adjusted by the PLD growth parameters.

Sample no.	strain	λ	l (Å)	γ_{KW}
G4889	-0.57	0.915	4.05	11.02
G4807	-0.29	0.383	9.37	5.441
G4867	-0.16	0.205	20.9	2.217
G4899	0.23	0.194	16.85	2.159
G4809	0.29	0.269	12.67	3.049

The lattice constant and strain of LNO films could be controlled by adjusting the growth conditions. All LNO films show metallic conductive behavior with a positive resistivity temperature coefficient as shown in Fig. 9.24 (a). At higher temperatures (T above 100 K), $\rho(T)$ follows a linear relation: $\rho = \rho_0 + A\,T$. Such a behavior of ρ is related to the typical electron-phonon ($el-ph$) scattering. The $el-ph$ coupling λ can be estimated from the slope of the resistivity using [6]: $\lambda = (\hbar\omega_p^2/8\pi^2 k_B)[\rho(T) - \rho(0)]/T = 0.246\,(\hbar\omega_p^2)\,A$, where $\hbar\omega_p$ is the plasmon energy, ω_p is the plasmon frequency, k_B is the Boltzmann constant, and A is the slope of the $\rho(T)$. The values of λ for our samples are between about 0.2 and 0.9 (see Tab. 1) . Compared with λ value of about 0.14 for heat treated $LaNiO_3$ film [7], the larger λ obtained here indicates a stronger coupling between electrons and phonons in our films. The free path l can be obtained

by using the relation [6]: $l = 4.95 \times 10^{-4} v_F / \rho(\hbar\omega_p^2)$, where v_F is the Fermi velocity (about $1.05 \times 10^{-7}\, cm \cdot s^{-1}$ for LNO). At lower temperature (T below 100 K), as shown in Fig. 9.24 (b), ρ fits to the following equation: $\rho = \rho_0 + B\,T^2$. In general, the T^2 term originates from electron-electron ($el - el$) scattering. The Kadowaki-Woods ratio γ_{KW} is given by [8]: $\gamma_{KW} = B/\gamma^2$, where γ is the electronic specific heat coefficient and this value for LNO is about 13.8 $mJ \cdot mol^{-1} \cdot K^{-2}$ [9]. We obtained larger γ_{KW} values, which indicates a stronger $el - el$ Coulomb interaction that is related to the 3 d electrons [10]. In order to clarify the origin of the resistivity differences, out-of-plane lattice constants and elastic strains were measured using the following equation: $e^{\perp} = ((c - c_{bulk})/c_{bulk}) \times 100\%$ (Fig. 9.24 (c)). The resistivity of LNO films is plotted as a function of the strain as shown in Fig. 9.24 (d). According to our results, we observe a correlation between elastic strain and the resistivity, i.e. as strain increases, both tensile and compressive, we observe a clear increase of resistivity.

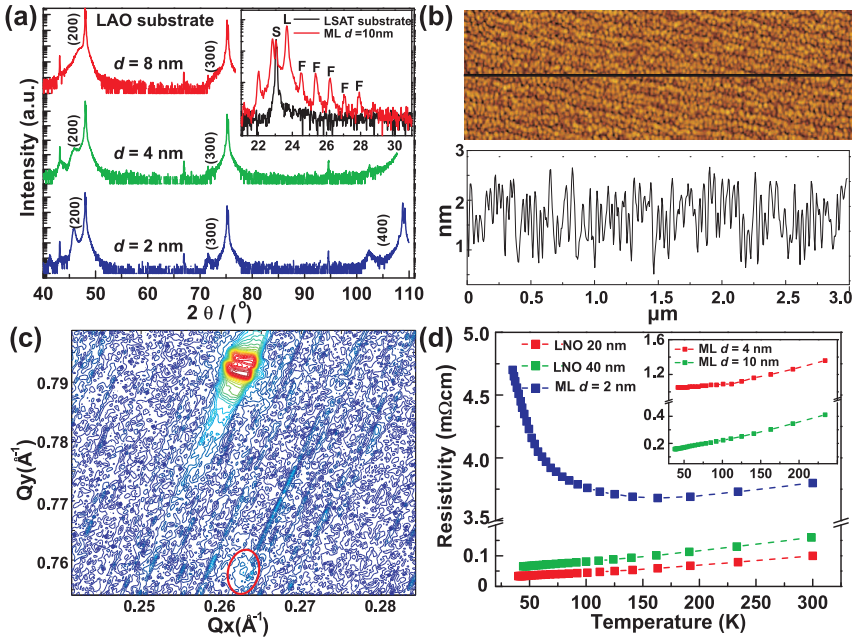

Figure 9.25: (a) XRD $2\theta - \omega$ of LNO/LAO MLs on LAO substrate with different single layer thickness (inset shows the layer fringes of ML deposited on LSAT substrate). (b) AFM image with line scan and corresponding height profile of ML with $d = 2$ nm. (c) Reciprocal space map around the asymmetric LAO (-103) peak of ML with $d = 2$ nm. The red ellipse marks the ML peak. (d) Temperature-dependent resistivity of single LNO thin films and ML with $d = 2$ nm (inset are MLs with $d = 4$ nm and 10 nm).

Fig. 9.25 (a) displays the XRD $2\theta - \omega$ scans of LNO/LAO MLs with different monolayer thickness which could be controlled by the number of laser pulses. As shown in the inset, layer fringes are observed clearly. From the layer fringes, a single layer thickness of $d = (10 \pm 1)$ nm is obtained. As shown in the AFM image in Fig. 9.25 (b), ML with $d = 2$ nm has a smooth surface with rms roughness of about 0.47 nm. Fig. 9.25 (c) shows a reciprocal space map for the ML in the vicinity of the perovskite (-103) peak. Q_x of the ML is almost equal to that of substrate indicating a good in-plane lattice match, i.e. pseudomorphic growth. Single LNO films remain metallic when the thickness is reduced as shown in Fig. 9.25 (d). LNO film with thickness of 20 nm shows a low resistivity about 100 $\mu\Omega$·cm at 300 K. Interestingly, a 10 × [LNO/LAO] ML with $d = 2$ nm

shows a resistivity minimum at about 150 K which is related to the weak localization effect [11].

In summary, LAO and LNO thin films and 10 × [LNO/LAO] MLs have been grown by PLD. Structural, morphological and electrical properties were studied in detail. Further work will focus on the optimization of PLD conditions to further improve layer-by-layer growth and the in-depth investigation of band structure by photoconductivity and IR-ellipsometry.

[1] J. Son et al.: Appl. Phys. Lett. **97**, 202109 (1996), doi:10.1063/1.3511738
[2] Y. W. Li et al.: Appl. Phys. Lett. **92**, 042901 (2008), doi:10.1063/1.2837534
[3] M. Gibert et al.: Nat. Mater. **11**, 195 (2012), doi:10.1038/nmat3224
[4] K. Y. Yang et al.: Phys. Rev. B **84**, 201104(R) (2011), doi:10.1103/PhysRevB.84.201104
[5] A. Ruegg et al.: Phys. Rev. B **85**, 245131 (2012), doi:10.1103/PhysRevB.85.245131
[6] M. Gurvitch et al.: Phys. Rev. Lett. **59**, 1337 (1987), doi:10.1103/PhysRevLett.59.1337
[7] G. P. Mambrini et al.: Phys. Rev. Lett. **102**, 043708 (2007), doi:10.1063/1.2769349
[8] S. Y. Li et al.: Phys. Rev. Lett. **93**, 056401 (2004), doi:10.1103/PhysRevLett.93.056401
[9] K. Screedhar et al.: Phys. Rev. B **46**, 6382 (1992), doi:10.1103/PhysRevB.46.6382
[10] L. Qiao et al.: Europhys. Lett. **93**, 57002 (2011), doi:10.1209/0295-5075/93/57002
[11] R. Scherwitzl et al.: Appl. Phys. Lett. **95**, 222114 (2009), doi:10.1063/1.3269591

9.17 2D layer by layer growth of TiN for use as bottom electrode in zinc ferrite based magnetic tunnel junctions

M. Bonholzer, M. Lorenz, M. Grundmann

Spinel oxides such as magnetite (Fe_3O_4) and zinc ferrite ($ZnFe_2O_4$) show promising properties for spintronic applications, i.e. semiconducting behavior and a high spin polarization [1–4]. We use zinc ferrite as ferromagnetic electrodes in order to realize room temperature operation of oxide based magnetic tunnel junctions (MTJs). A highly conductive interlayer is required for a successful device implementation of these spinel oxides in MTJs [1]. To reduce the series resistance of our devices we add a highly conductive titanium nitride (TiN) layer between the magnesium oxide (MgO) substrate and the $ZnFe_2O_4$ layer. A critical issue in MTJs is the interface quality. In order to support the tunneling process, the interfaces must be as flat as possible.
We succeeded to grow atomically smooth hetero-epitaxial TiN and $ZnFe_2O_4$ thin films on (001) MgO single crystals by pulsed laser deposition (PLD). In order to generate perfect conditions for two-dimensional growth of TiN on MgO, the substrates have to be annealed at 950°C for 2h in vacuum using a CO_2 laser heater. The annealed substrates show smooth and uniformly stepped surfaces. The terrace height is half a unit cell of MgO; a value of 0.21nm was measured by atomic force microscopy (AFM).
On these substrates we grew TiN thin films by pulsed laser deposition (PLD). In situ RHEED oscillations indicate two-dimensional (2D) growth mode up to a film thickness of about 50 nm. This is confirmed by AFM measurements. The TiN films show smooth, stepped surfaces with a uniform terrace height of about 0.21 nm. X-ray diffraction

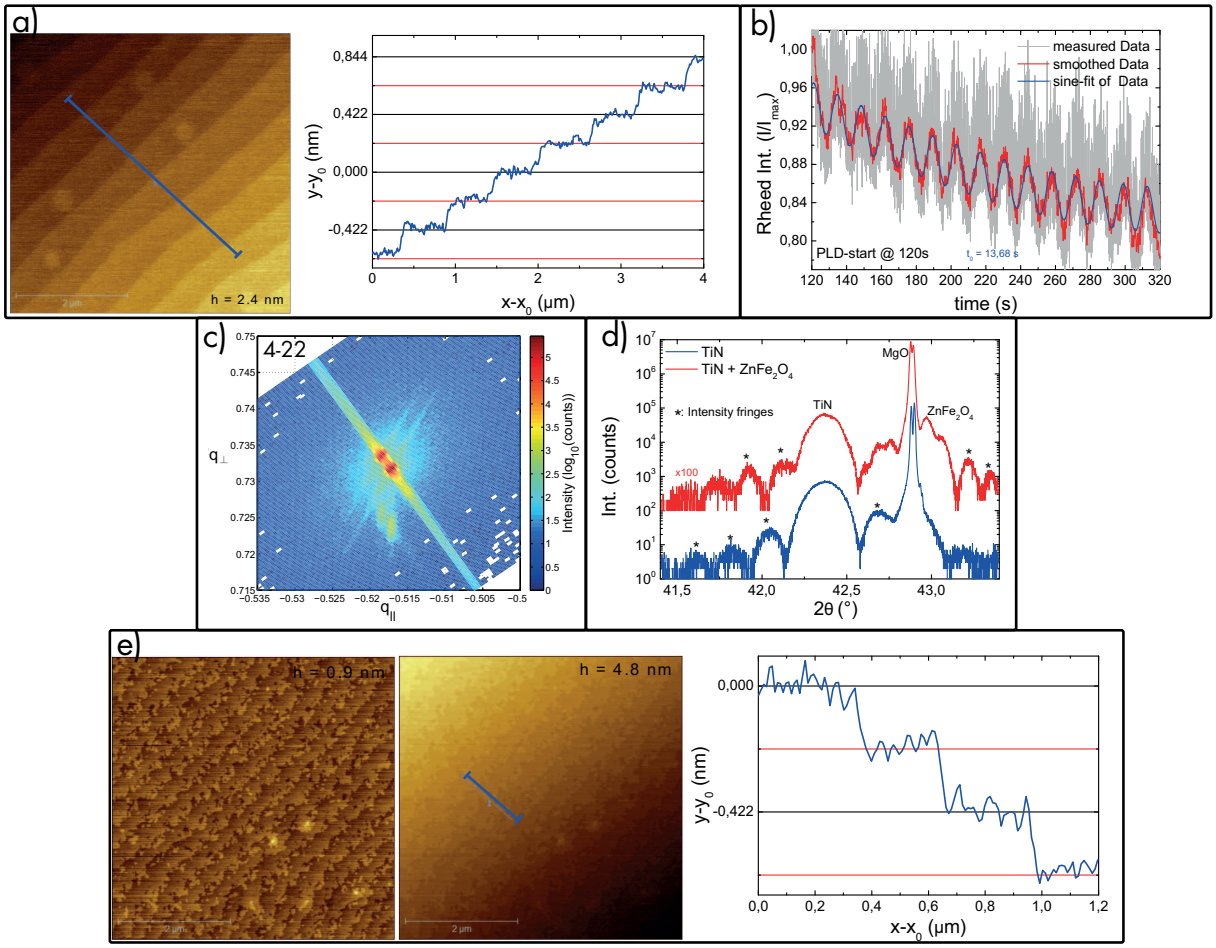

Figure 9.26: a) AFM-image (5x5 µm^2) of the surface of a 43 nm thick TiN thin film grown by PLD. One can clearly observe the steps with a height of 1/2 the lattice constant. b) RHEED intensity of the (0,1) spot as function of growth time for the first 400 pulses. The intensity oscillations indicate a 2D growth mode. c) X-ray reciprocal space map around the (4-22) peak of MgO. The vertical alignment of the centered substrate and the weaker film peaks below indicates the pseudomorphic growth. The broadening of the TiN-peak only parallel to $q_\perp$ due to finite film thickness shows the high film quality. d) High resolution X-ray diffraction 2Θ-ω scan shows strained TiN and $ZnFe_2O_4$. The presence of intensity fringes for both, TiN and $ZnFe_2O_4$ indicates a good crystal and surface quality. e) AFM-image (5x5 μm^2) of the surface of a 70 nm thick $ZnFe_2O_4$ thin film grown by PLD on top of TiN/MgO(100). The steps with a height of 1/4 the lattice constant are clearly visible.

reciprocal space maps of asymmetric reflections show strained, pseudomorphic growth of TiN on MgO. The in-plane lattice constant of TiN is with 4.22 Å the same as MgO, the out-of plane lattice constant is 4.25 Å (bulk TiN: a = 4.24 Å). A peak broadening only in $q_\perp$ due to the finite film thickness indicates a high film quality. The occurrence of intensity fringes in the high resolution X-ray pattern indicates a smooth film surface and interface, as well.

On top of the TiN layer the $ZnFe_2O_4$ layer (magnetic bottom electrode) is also grown by PLD. X-ray diffraction measurements show a clear zinc ferrite peak and also intensity fringes linked to this layer. The spacing of this fringes gives a layer thickness of 70 nm. AFM images show a stepped surfaces with a step height of 1/4 of the unit cell. This

result is also found on magnetite (Fe_3O_4) films, which have a similar crystal structure to zinc ferrite (spinel). The step height is explained by a B-layer termination [5, 6].
This high quality films of TiN and $ZnFe_2O_4$ with their smooth, stepped surfaces will be used as bottom electrode for $ZnFe_2O_4$ based MTJs.

This work has been supported by Deutsche Forschungsgemeinschaft in the framework of SFB 762 "Functionality of Oxide Interfaces".

[1] M. Opel *et al.*, Phys. Status Solidi A **208**, 232 (2011)
[2] C.E. Rodríguez Torres *et al.*, Phys. Rev. B **84**, 064404 (2011)
[3] K. Brachwitz *et al.*, Appl. Phys. Letters **102**, 172104 (2013)
[4] M. Lorenz *et al.*, Phys. Status Solidi RRL **5**, 438 (2011)
[5] B. Stanka *et al.*, Surface Science **448**, 49 (2000)
[6] G. Parkinson *et al.*, Surface Science **605**, 15 (2011)

9.18 Heteroepitaxial thin films of layered perovskite Li_2IrO_3 grown by pulsed laser deposition

M. Jenderka, H. Frenzel, R. Schmidt-Grund, M. Grundmann, M. Lorenz

The layered perovskite oxides A_2IrO_3 (A = Na, Li) have been studied in recent years in terms of a physical realization of spin-liquid [1] and topological insulator [2] phases, desired within certain quantum computation proposals. Subsequent experiments showed that, while Na_2IrO_3 is clearly within an antiferomagnetically ordered phase, Li_2IrO_3 is close to the desired spin liquid phase [3]. There is yet no direct experimental evidence of a topological insulator phase in both materials. However, theoretical studies predict that a topological insulator phase can still be achieved by application of strain [2, 4]. Hence, the fabrication of epitaxial thin films is a first step in exposing a possible topological insulator phase and generally paves the way for future device applications.
Recently, we successfully grew heteroepitaxial Na_2IrO_3 thin films. We observed three-dimensional Mott variable range hopping conductivity (Mott-VRH) and signatures of a weak antilocalization effect that can be associated with topological surface states [5]. Experimental data on Li_2IrO_3 were so far restricted to polycrystalline samples. Here, we report on the pulsed laser deposition (PLD) of heteroepitaxial Li_2IrO_3 films on ZrO_2:Y(001) (YSZ) single crystalline substrates. A typical x-ray diffraction (XRD) 2Θ-ω pattern of a Li_2IrO_3 film is displayed in Fig. 9.27(a). As in Na_2IrO_3 [5], the pattern is indexed on the basis of a monoclinic $C2/c$ unit cell. [3] The pattern shows pronounced symmetric peaks related to a preferential (001) out-of-plane crystalline orientation. Investigation of the in-plane epitaxial relationship is done by high-resolution XRD ϕ scans of the asymmetric Li_2IrO_3 (131) and YSZ (111) reflections, shown in Fig. 9.27(b). We observe that the epilayer aligns in-plane within 12 "strong" plus 12 "weak" rotational domains. The precise origin of this large number of rotational domains is at present unknown.
Resistivity ρ between 35 and 300 K is dominated by a three-dimensional Mott-VRH mechanism (see Fig. 9.27(c)). Infrared optical transmission from 0 to 1.85 eV, measured by Fourier transform infrared spectroscopy, reveals a small optical gap $E_{go} \approx 300$ meV.

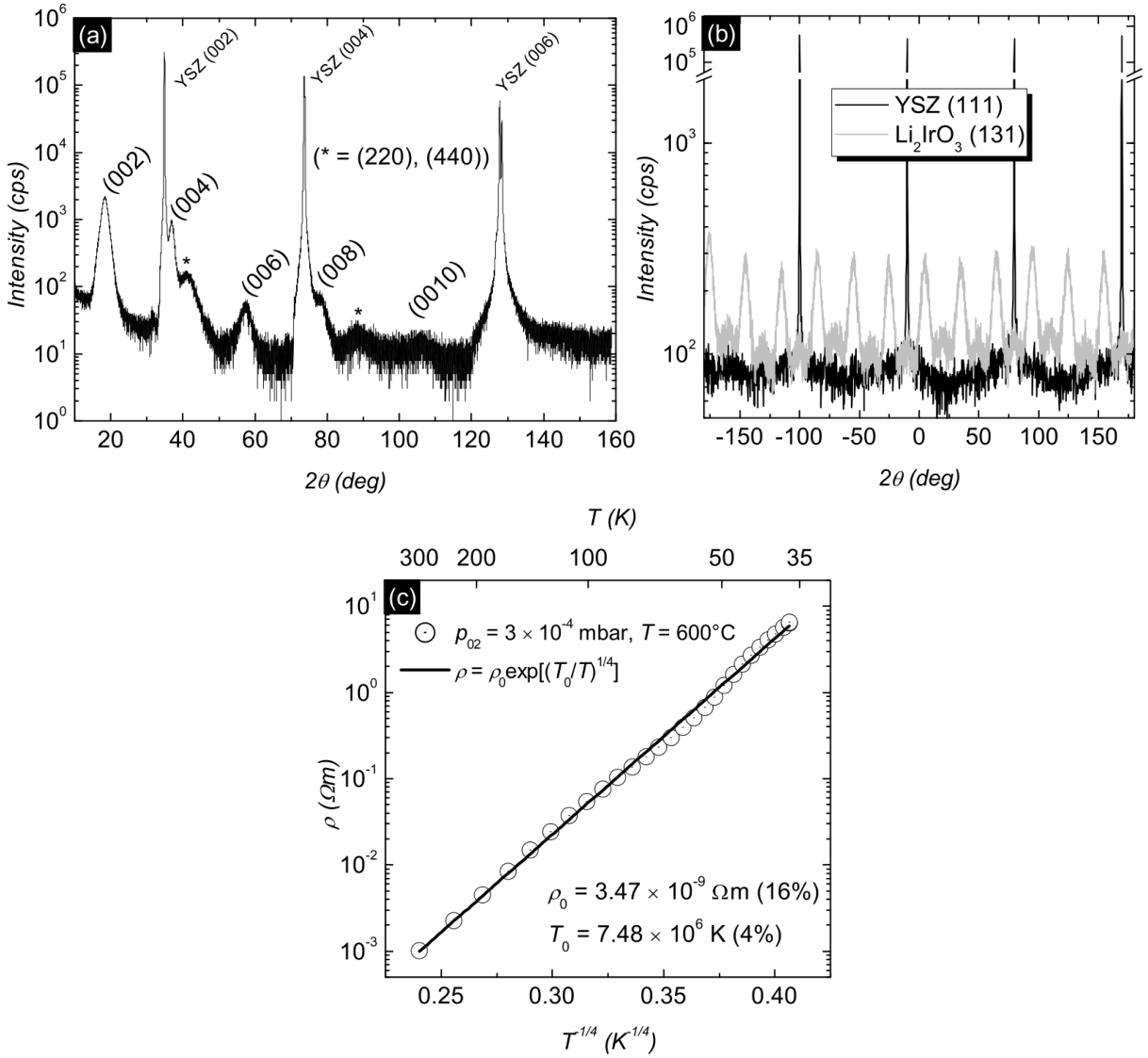

Figure 9.27: PLD-grown Li_2IrO_3(001) thin film on YSZ(001). (a) XRD 2Θ-ω scan. (b) High-resolution XRD ϕ scans of asymmetric Li_2IrO_3 (131) and YSZ (111) reflections. (c) Temperature-dependent resistivity plotted in log ρ versus $T^{-1/4}$. Straight line fit indicates dominant Mott-VRH mechanism.

By means of spectroscopic ellipsometry, we measured the dielectric function in the spectral range between 0.03 and 3.50 eV. The calculated absorption coefficient confirms the value for E_{go}.

This work has been supported by Deutsche Forschungsgemeinschaft within the project "Oxidische topologische Isolator-Dünnfilme – Darstellung und elektronische Eigenschaften" (Lo 790/5-1).

[1] J. Chaloupka *et al.*, Physical Review Letters **105**, 027204 (2010).
[2] H.-S. Kim *et al.*, Physical Review B **87**, 165117 (2013).
[3] Y. Singh *et al.*, Physical Review Letters **108**, 127203 (2012).
[4] C. Kim *et al.*, Physical Review Letters **108**, 106401 (2012).
[5] M. Jenderka *et al.*, Physical Review B **88**, 045111 (2013).

9.19 Multiferroic Composite and Multilayer Thin Films, based on $BaTiO_3$ and $BiFeO_3$

P. Schwinkendorf, M. Lorenz, V.V. Lazenka*, K. Brachwitz, T. Böntgen, M. Grundmann

*Institute for Nanoscale Physics and Chemistry, KU Leuven, Belgium

Multiferroics are a promising new class of materials for potential use in future electronic devices. Their unique property is the coexistence and coupling of two or more ferroic order parameters. The most desirable properties are ferromagnetism and ferroelectricity which may create the possibility of switching a materials electric polarization via a magnetic field or its magnetization via an electric field.
Up to now there is only one single phase room temperature multiferroic material known, namely $BiFeO_3$. Besides investigating complex oxides such as double perovskites for their multiferroic behavior it is our aim to improve the electrical and magnetic properties of $BiFeO_3$ thin films by combination with $BaTiO_3$ as either composite films or multilayer films.
For this purpose we used samples grown by pulsed laser deposition on 5×5 mm^2 and 10×10 mm^2 $SrTiO_3$ (100), MgO (100), and $MgAl_2O_3$ (001). For composite films we ablated mixed targets with content ratios of 33 % $BaTiO_3$ / 67 % $BiFeO_3$ and 67 % $BaTiO_3$ / 33 % $BiFeO_3$ [1]. The multilayers consist of 30 alternating $BaTiO_3$ and $BiFeO_3$ layers of 1000 laser pulses each. X-ray diffraction was performed verifying c-oriented growth of both the composites and the multilayers. Samples grown at higher oxygen partial pressure (0.25 mbar) tend to exhibit lower out-of-plane lattice constants probably indicating non-lattice-matched film growth in comparison to low pressure samples (0.01 mbar). In AFM measurements we find a generally much smoother surface for multilayers (rms ca. 1 nm) than for composites (rms ca. 8 nm).

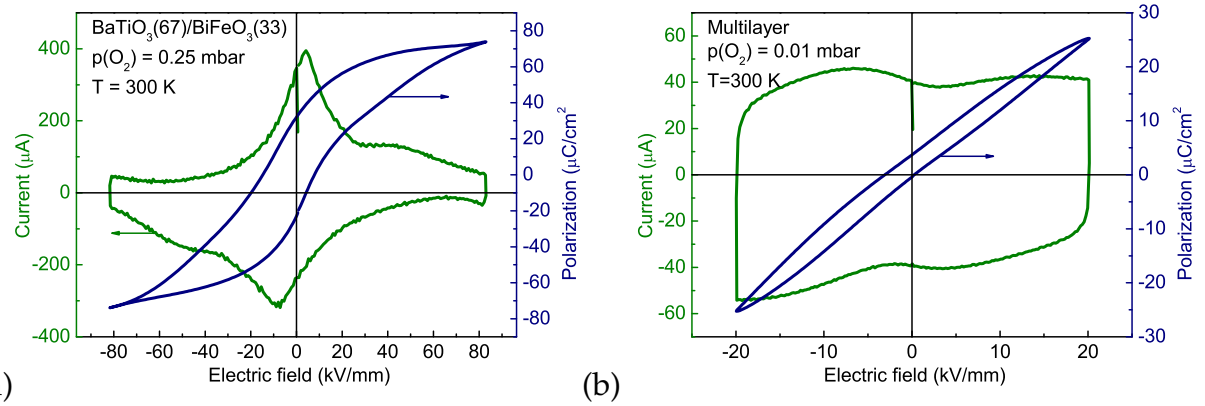

Figure 9.28: Ferroelectric hysteresis of (a) $BaTiO_3$ 67 % / $BiFeO_3$ 33 % – composite and (b) 15 × $BaTiO_3$ / $BiFeO_3$ multilayer thin film taken at 300 K. The composite shows very high electric field stability and high saturation polarization.

All samples (surprisingly even pure $BaTiO_3$ – probably due to oxygen vacancies) exhibit weak magnetism as well as ferroelectricity and can thus be considered multiferroic. However, pure $BiFeO_3$ thin films often suffer from high dc leakage covering its ferroelectric switching. A rising $BaTiO_3$ content in composite films increases their

resistivity while preserving a high ferroelectric polarization of over 60 μC/cm^2 (Figure 1 (a)). Multilayers also feature lower leakage currents, but at the expense of a significantly reduced ferroelectric polarization (Figure 1 (b)).
The advantage of multilayer films becomes obvious regarding the magnetization as they surpass pure $BiFeO_3$ by nearly 100 % at room temperature reaching values of over 10^{-3} T/μ_0 at 300 K and 3×10^{-3} T/μ_0. We attribute this effect to a coupling of the different particular magnetic moments of both the $BaTiO_3$ and the $BiFeO_3$ at the layer interfaces in contrast to the composite films.
The magnetoelectric coefficient $\alpha_{ME}=\partial E/\partial H$ was determined as a function of applied DC magnetic field as well as temperature using a longitudinal AC method in Leuven. Figures 2 (a) and (b) show α_{ME} of the 0.01 mbar multilayer (8.76 V/cmOe) being significantly larger than that of the 0.01 mbar $BaTiO_3$ 67 % / $BiFeO_3$ 33 % composite (1.61 V/cmOe). Another composite sample grown at 0.25 mbar oxygen partial pressure reached an even higher α_{ME} of 20.75 V/cmOe [1].
Besides the intrinsic ME coupling in $BiFeO_3$, an additional ME effect in multilayer multiferroic films is created at the interfaces. There is an elastic coupling at the interface: an applied magnetic field produces an elastic strain in the magnetostrictive phase ($BiFeO_3$) which is stress coupled to that of the piezoelectric ($BaTiO_3$), resulting in an induced voltage.

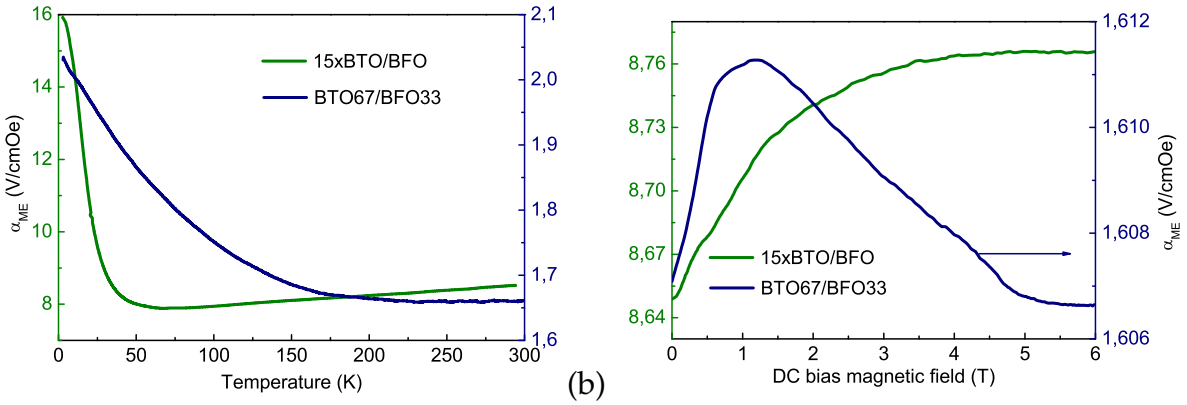

Figure 9.29: ME coefficient α_{ME} as a function of temperature (at 0 T) and DC magnetic field (at 300 K) for 15 × $BaTiO_3$ / $BiFeO_3$ multilayer and $BaTiO_3$ 67 % / $BiFeO_3$ 33 % composite thin films both grown at 0.01 mbar.

[1] Michael Lorenz, Vera Lazenka, Peter Schwinkendorf, Francis Bern, Michael Ziese, Hiwa Modarresi, Alexander Volodin, Margriet J. Van Bael, Kristiaan Temst, André Vantomme, Marius Grundmann; J. Phys. D: Appl. Phys, **47**, 135303 (2014)

9.19.1 Cuprous Iodide - a p-type transparent semiconductor: history and novel applications

M. Grundmann

Cuprous iodide was described by Bädeker as the first transparent conductive material in 1907 [1]. We have reviewed the literature on CuI bulk, thin films and nanostructures

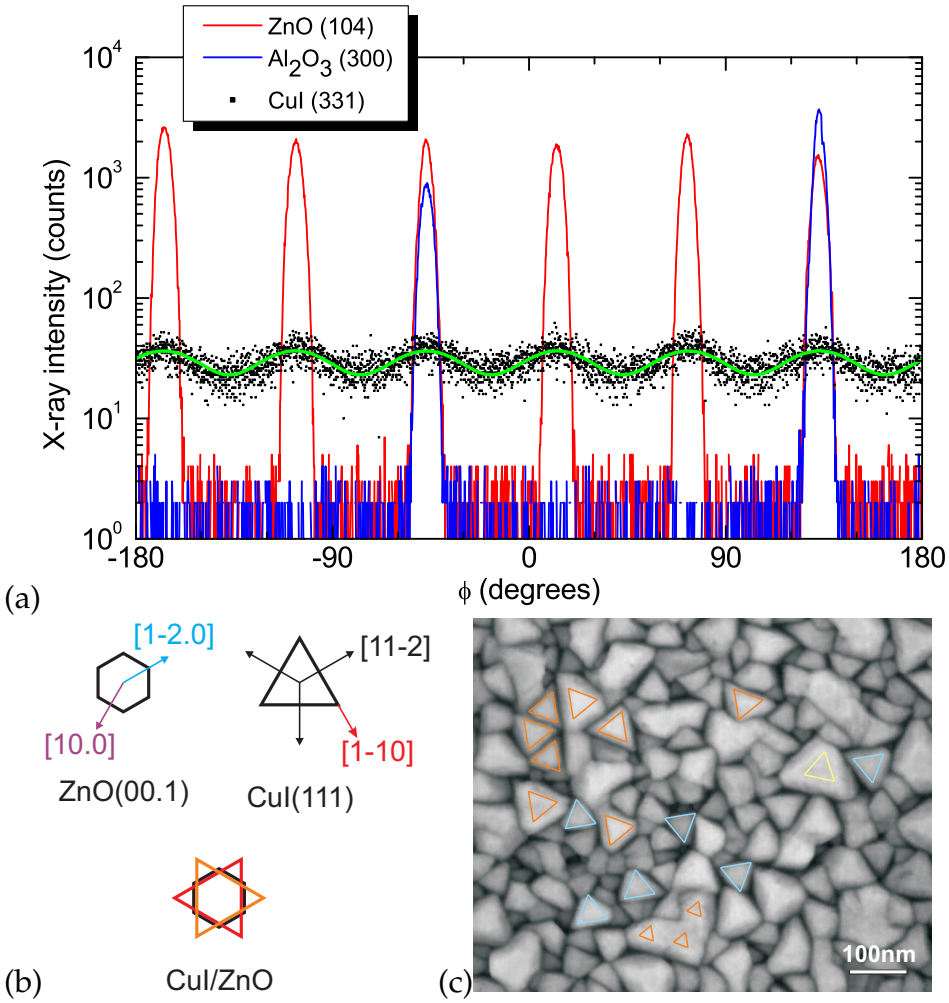

Figure 9.30: (a) X-ray diffraction azimuthal ϕ-scan of 100 nm evaporated CuI on $\approx 1\,\mu$m heteroepitaxial ZnO thin film on a-Al_2O_3 heterostructure around substrate normal for Al_2O_3 (300) and ZnO (104) (red and blue lines) and CuI (331) (black dots) reflections. The angular intensity of Cu(331) is fitted with a sinusoidal curve (green line). (b) Graphical representation of the in-plane epitaxial relationship and rotation domain formation. (c) SEM image of an evaporated CuI epilayer on ZnO(00.1). The preferred domain orientation is indicated with orange triangles corresponding to (b). Grain orientation rotated by 30° is indicated with blue triangles; another domain rotated by about 9° is indicated with a yellow triangle. Three small orange triangles indicate area of coalescence of similarly oriented epitaxial domains.

[2]. In this publication we also have presented first evidence for epitaxial growth of CuI(111) on ZnO(00.1) (on Al_2O_3) (Fig. 9.30). This combination of p-CuI and the ZnO n-type oxide results in diodes with high rectification (6×10^6 at ±2 V) and ideality factor around 2 as reported in [3].

[1] K. Bädeker, *Über die elektrische Leitfähigkeit und die thermoelektrische Kraft einiger Schwermetallverbindungen*, Analen der Physik **327**, 749–766 (1907).
[2] M. Grundmann, F.-L. Schein, M. Lorenz, T. Böntgen, J. Lenzner, H. von Wenckstern, phys. stat. sol. (a) **210**(9), 1671–1703 (2013).
[3] F.-L. Schein, H. von Wenckstern, M. Grundmann, Appl. Phys. Lett. **102**(9), 092109 (2013).

9.19.2 Umweganregung of ZnO Bulk and Thin Films

M. Grundmann, M. Lorenz, J. Bläsing*, A. Krost*

*Otto-von-Guericke Universität Magdeburg

We have investigated Umweganregung reflections (Renninger scans, X-ray multiple reflections) for (*HK.L*) = (00.1), (00.3) and (00.5) (Fig. 9.31a) for a number of wurtzite structure ZnO samples, namely various bulk crystals (substrates), two ZnO thin films and a ZnO:Mg thin film, grown by pulsed laser deposition on a-plane sapphire [1]. Using a low divergence setup, we achieve a high angular resolution of 0.1° or better (a factor of ten better than previous published work).
We have derived an analytical formula for peak positions as a function of wavelength λ and the lattice parameters a and c. The three investigated ZnO substrates exhibit all expected (kinematically allowed) reflections for Cu K_{α_1}, K_{α_2} and K_β (Fig. 9.31b).

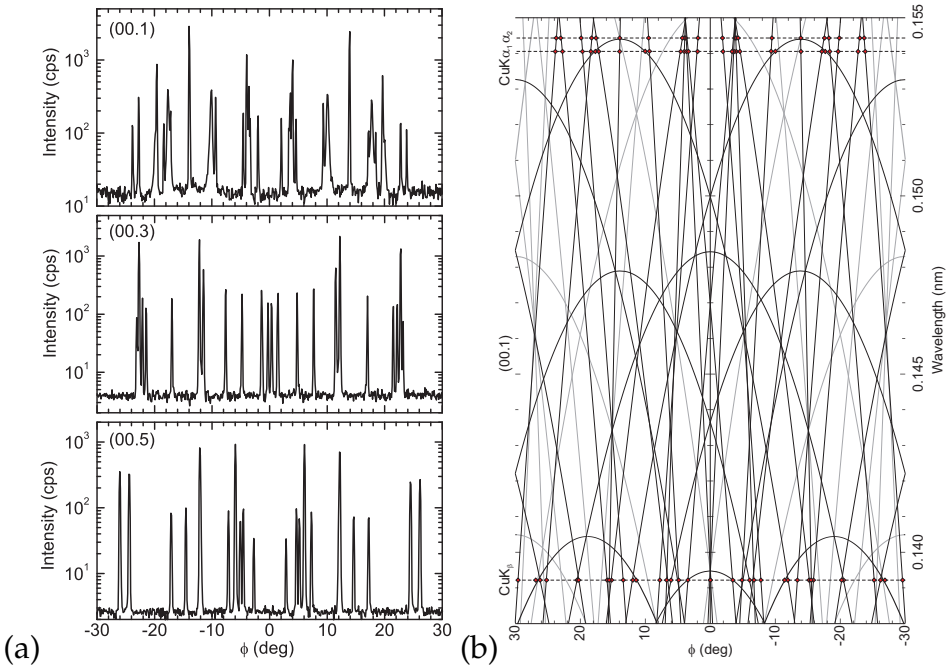

Figure 9.31: (a) Umweganregung scans for ZnO bulk (substrate from CrysTec) and excitation with Cu K_{α_1}. (b) Azimuthal angular position of all possible Umweganregungen for ZnO for (*HK.L*) = (00.1) primary reflection as a function of X-ray wavelength λ. The kinematically forbidden Umweganregungen are shown in grey. The wavelengths for the Cu K_{α_1}, K_{α_2} and K_β lines are shown as horizontal dashed lines. Experimental data from a ZnO substrate (Tokyo Denpa) are shown as symbols.

A lineshape analysis of the multiple reflection peaks shows that the width of certain reflections (e.g. (*hk.l*) = ($4\bar{4}$.1) in Fig. 9.32a and (*hk.l*) = (12.4) in Fig. 9.32b) is determined by the spectral linewidth of the exciting copper lines. The thin films exhibit only slight broadening of the peaks but disappearance of several reflections. The *a* lattice constant can be determined directly and with high precision from the azimuthal peak positions.

[1] M. Grundmann, M. Scheibe, M. Lorenz, J. Bläsing, A. Krost, phys. stat. sol. (b) (2014), doi:10.1002/pssb.201350297

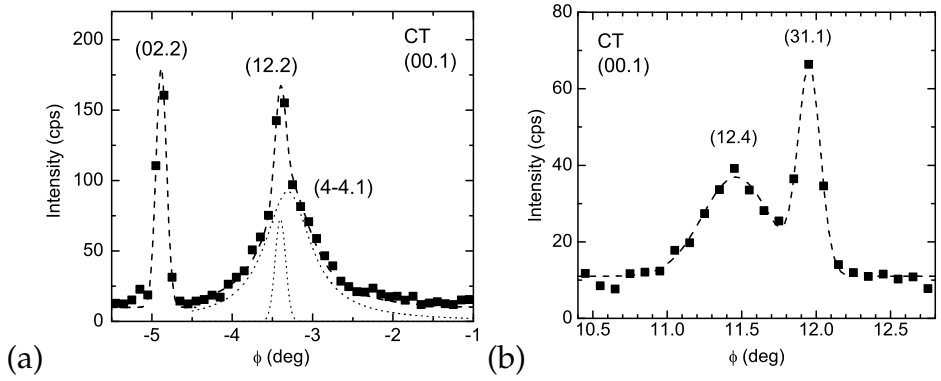

Figure 9.32: (a) Umweganregung peaks for ZnO substrate (CrysTec), (*HK.L*)=(00.1) in the vicinity of (*hk.l*) = (12.2) for excitation with Cu K_β. Experimental data (symbols) and lineshape fit with a Gaussian for (02.2), a Gaussian for (12.2) and a Lorentzian for (4$\bar{4}$.1) (dashed and dotted lines). (b) Umweganregung peaks for ZnO substrate (CrysTec), (*HK.L*)=(00.1) in the vicinity of (*hk.l*) = (12.4) for excitation with Cu K_β. Experimental data (symbols) and lineshape fit with two Gaussians (dashed line).

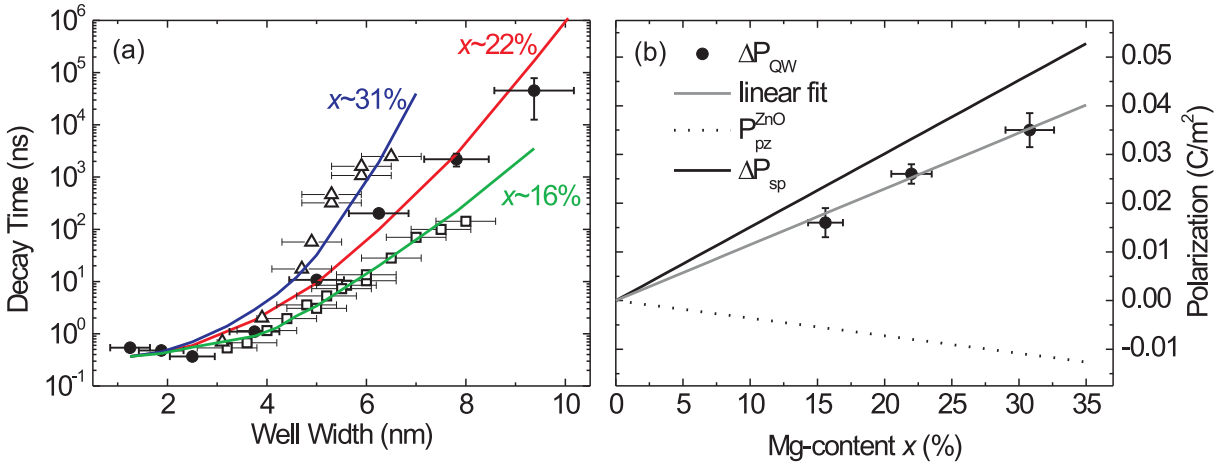

Figure 9.33: (a) Dependence of the single-exciton decay time on the QW width for ZnO/(Mg, Zn)O-QWs with three different Mg-contents x in the barriers. Dots represent planar samples with $x = 22\%$. Triangles ($x = 31\%$) and squares ($x = 16\%$) represent wedge-shaped samples. The solid lines represent the simulated data for the indicated Mg-content in the barrier layers. (b) Linear fit (grey line) of the experimentally determined total polarization difference ΔP_{QW} (dots) between QW and barrier layers. The piezoelectric polarization (dotted line) has been calculated for the ZnO-QW. For the relaxed barrier layers P_{pz} equals zero. The black line represents the determined difference of the spontaneous polarization between ZnO and (Mg, Zn)O in dependence on the Mg-content.

9.20 Spontaneous and piezoelectric polarization in ZnO/$Mg_xZn_{1-x}O$ quantum wells

M. Stölzel, A. Müller, G. Benndorf, H. Hochmuth, M. Lorenz, M. Grundmann

Due to the higher bandgap of (Mg, Zn)O compared to ZnO, it is commonly used as a barrier material for ZnO based quantum wells (QWs). Wurtzite ZnO as well as wurtzite

(Mg, Zn)O are polar materials exhibiting a spontaneous polarization (sp) along the *c*-axis. For pseudomorphic growth of the structure at least one of the materials is strained leading to an additional piezoelectric polarization (pz). The resulting electric field across the QW $E = \Delta P_{\mathrm{QW}}/\varepsilon$ is determined by the differences of the components of the polarization of the layers $\Delta P_{\mathrm{QW}} = \Delta P_{\mathrm{sp}} + \Delta P_{\mathrm{pz}}$. Up to now, only calculations exist for the spontaneous polarization of wurtzite (Mg, Zn)O differing widely, e.g. listed in Ref. [1].

We performed low temperature (T = 2 K) time-resolved photoluminescence (PL) measurements on polar ZnO/(Mg, Zn)O QWs grown by pulsed laser deposition in an oxygen ambient on *a*-plane sapphire (T = 650 °C, p = 0.004 mbar). For QW widths larger than the Bohr radius of the exciton (~ 2 nm), the internal electric field separates electrons and holes inside the QW, which decreases the transition energy (triangular potential for electrons and holes) and largely increases the decay time, known as the quantum-confined Stark effect. The single-exciton transition energy is very hard to determine with a sufficiently high signal-to-noise ratio by continuous-wave PL as well as by time-resolved experiments because screening effects must be considered even at moderate excitation densities (~ 1 W/cm^2). In contrast to that, the decay time of the unscreened single-exciton inside the QW can be well determined from the measured energetic dependence of the decay time by means of an extended relaxation model [2]. In Fig. 9.33 (a) the dependence of the single-exciton decay time on the well width is shown for samples incorporating three different Mg-contents in the barriers. It has been simulated by a self-consistent solution of the Schrödinger and Poisson equation. The details of the calculations as well as the parameters are described in Ref. [2].

The simulation yields the polarization across the QW for the three Mg-contents (shown in Fig. 9.33 (b)). A linear approximation gives ΔP_{QW} in dependence on the Mg-content. It should be noted that the barrier layers are unstrained. The piezoelectric polarization equals zero for the barrier layers. Therefore ΔP_{QW} only consists of the difference of the spontaneous polarizations of the two materials as well as the piezoelectric polarization of the pseudomorphic grown ZnO-QW. With the determined elastic stiffness constants (C_{ij}) [3] and components of the piezoelectric tensor (e_{ij}) [4] for the binary material ZnO, the piezoelectric polarization can be calculated by $P_{\mathrm{pz}} = 2(a_{\mathrm{s}} - a_{\mathrm{e}})/a_{\mathrm{e}} \cdot (e_{31} - e_{33}C_{13}/C_{33})$ [5], where a_s and a_e represents the lattice constants of the unstrained bottom layer and the pseudomorphic grown film in equilibrium. Using the dependence of the lattice constant on Mg-content determined by X-ray diffraction $a(x)[\text{Å}] = 3.244 + 0.058 \cdot x$ [6] we calculate $P_{\mathrm{pz}}^{\mathrm{ZnO}}$ as indicated by the dotted line in Fig. 9.33 (b). Subtracting $P_{\mathrm{pz}}^{\mathrm{ZnO}}$ from ΔP_{QW} finally gives the difference in spontaneous polarization of the materials. With $P_{\mathrm{sp}}^{\mathrm{ZnO}} = 0.057\,\mathrm{C/m^2}$ [4] the spontaneous polarization of wurtzite (Mg, Zn)O results in $P_{\mathrm{sp}}^{\mathrm{MgZnO}} = (0.057 + (0.151 \pm 0.016) \cdot x)\,\mathrm{C/m^2}$ in dependence on the Mg-content. The determined dependence is by a factor of five larger compared to the theoretical predictions [1].

This work has been supported by Deutsche Forschungsgemeinschaft in the framwork of SFB 762 "Functionality of Oxide Interfaces".

[1] S.-H. Jang *et al.*: J. Appl. Phys. **112**, 073503 (2012), doi:10.1063/1.4757023
[2] M. Stölzel *et al.*: Phys. Rev. B **88**, 045315 (2013), doi:10.1103/PhysRevB.88.045315
[3] G. Carlozzi *et al.*: J. Phys. Condens. Matter **7**, 9147 (1995), doi:10.1088/0953-8984/7/48/006
[4] F. Bernardini *et al.*: Phys. Rev. B **56**, R10024 (1997), doi:10.1103/PhysRevB.56.R10024

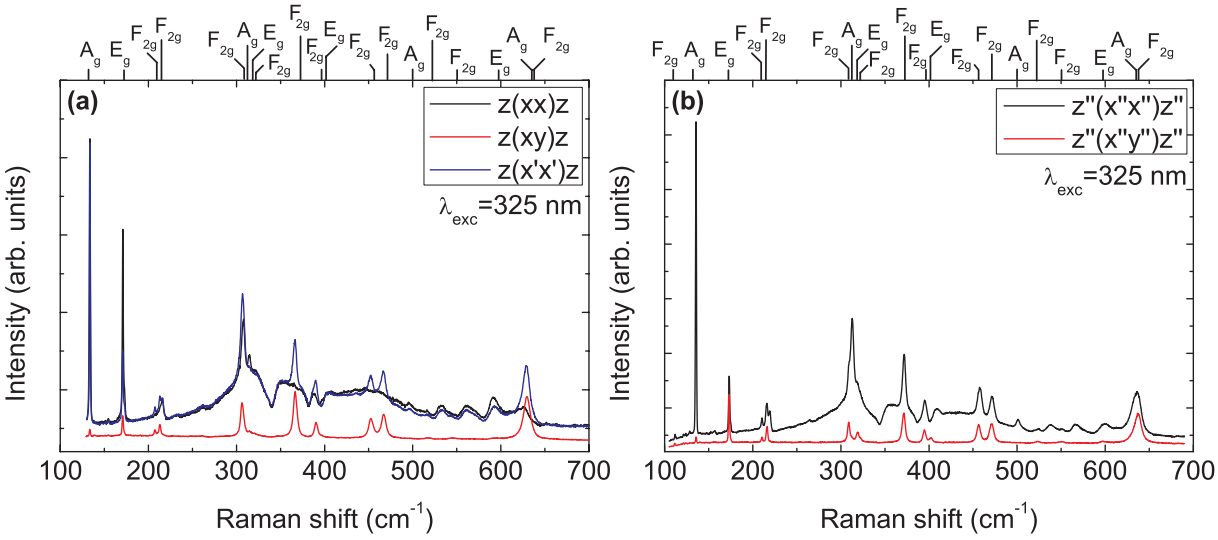

Figure 9.34: Raman spectra of In_2O_3 thin films at $T = 10\,K$ excited at $\lambda_{exc} = 325\,nm$. (a) (100)-oriented film grown on (100)-oriented YSZ and (b) mainly (111)-oriented film grown on (0001)-oriented Al_2O_3.

[5] A. Reale *et al.*: J. Appl. Phys. **93**, 400 (2003), doi:10.1063/1.1527989
[6] A. Rahm: diploma thesis, Universität Leipzig (2003)

9.21 Phonon modes and dielectric function of $(In_xGa_{1-x})_2O_3$ thin films

C. Kranert, R. Schmidt-Grund, C. Dähne, T. Böntgen, H. Krauß, J. Lenzner, M. Lorenz, H. von Wenckstern, M. Grundmann

We investigated the phonon modes (Sects. 9.21.1 and 9.21.2) and optical properties (Sec. 9.21.3), i.e. the refractive index dispersion and the energy of the optical absorption edge, of $(In_xGa_{1-x})_2O_3$ in dependence on the composition by means of Raman spectroscopy and spectroscopic ellipsometry. The samples studied are thin films grown by pulsed laser deposition. For the composition dependent investigations, films with a continuous composition spread (CCS) on *c*-sapphire substrates with an In concentration ranging from 0 to roughly 90 at. % (composition determined by EDX) were used. The CCS sample allowed us to adjust the composition of the material for each measurement simply by selecting the position of the excitation spot on the sample. A further benefit of this technique is that virtually any composition can be found in the samples eliminating gaps of information in our data. Additionally, we investigated pure (001)- and (111)-oriented In_2O_3 films on yttria stabilized zirconia (YSZ) and on *c*-sapphire substrates, respectively.

9.21.1 Raman scattering in bixbyite-type In_2O_3 thin films

Raman spectra of most bixbyite-type In_2O_3 samples excited off-resonantly, as it was done exclusively in all reports on this topic before, show only a small fraction (five to

six) of the 22 phonon modes [1, 2] predicted by group theory:

$$\Gamma = 4A_g + 4E_g + 14F_{2g}. \tag{9.1}$$

Only Garcia-Domene *et al.* [3] observed 16 distinct peaks in their Raman spectra of bulk-like In_2O_3 powder. However, they could not experimentally verify the symmetry of the phonon modes due to the indefinite orientation of the crystallites. Consequently, the knowledge on the Raman active phonons of this material was incomplete. We investigated the Raman spectrum of In_2O_3 for resonant excitation near its optical band gap, which is around 3.6 eV [4] and approximately 800 meV larger than the fundamental band gap. For this, we use the $\lambda_{exc} = 325$ nm emisson of a HeCd laser, so that the exciting photons have an energy of 3.81 eV which is reasonably close to the optical gap. This increases the overall intensity of the scattered light as well as selectively enhances the scattering cross section for several modes not observed for non-resonant excitation [5], making them easily detectable even in thin film samples.

The excitation conditions are shifted even closer towards resonance by cooling the sample down to $T = 10$ K. Measurements at this low temperature also benefit from a decreased line broadening facilitating the spectral separation of the individual phonon modes. As a result, we were able to observe all Raman active phonon modes of In_2O_3, many of which have not been observed before, and assign the symmetry for 19 of them based on the Raman selection rules. Particularly, based on the polarization dependence of the Raman lines of (001)- and (111)-oriented films (see Fig. 9.34), we could assign the observed phonon modes to the 4 modes each with A_g and E_g symmetry and to 11 of the 14 modes with F_{2g} symmetry, as labelled in Fig. 9.34. We also observe peaks in the spectral range where modes with F_{2g} symmetry are predicted theoretically by Garcia-Domene *et al.* [3], but could not verify their predicted symmetry due to the very weak intensity.

9.21.2 Phonon modes in $(In_xGa_{1-x})_2O_3$

We investigated the phonon modes of $(In_xGa_{1-x})_2O_3$ in dependence on the composition by means of Raman spectroscopy. For indium concentrations below 20 at. %, only phonon modes related to the β-Ga_2O_3 structure are observed (see Fig. 9.35(a)). The dependence of some of these modes on the indium concentration x is shown in Fig. 9.35(c-e). All of them show a linear behaviour indicating a full incorporation of indium into the β-Ga_2O_3 lattice. The accuracy of the obtained slopes is very high due to the constant growth conditions for all compositions and the large amount of data points which could be obtained. As a result, we can determine the composition of an $(In_xGa_{1-x})_2O_3$ film from the phonon mode energies with a precision better than 1 at. %.

The Raman spectra for higher In concentrations show additional peaks. Most prominently, a peak at 260 cm^{-1} evolves with an increasing amount of indium in the film (see Fig. 9.35(b)). This can be assigned to neither a phonon mode from the β-Ga_2O_3 nor from the bixbyite-type In_2O_3 structure. Thus, this indicates an additional intermediate phase in our samples for indium concentrations above 20 at. %. Such an additional phase was also observed by X-ray diffraction, matching the values of a rhombohedral high pressure phase for $x = 50$ at. % named $InGaO_3$II [6].

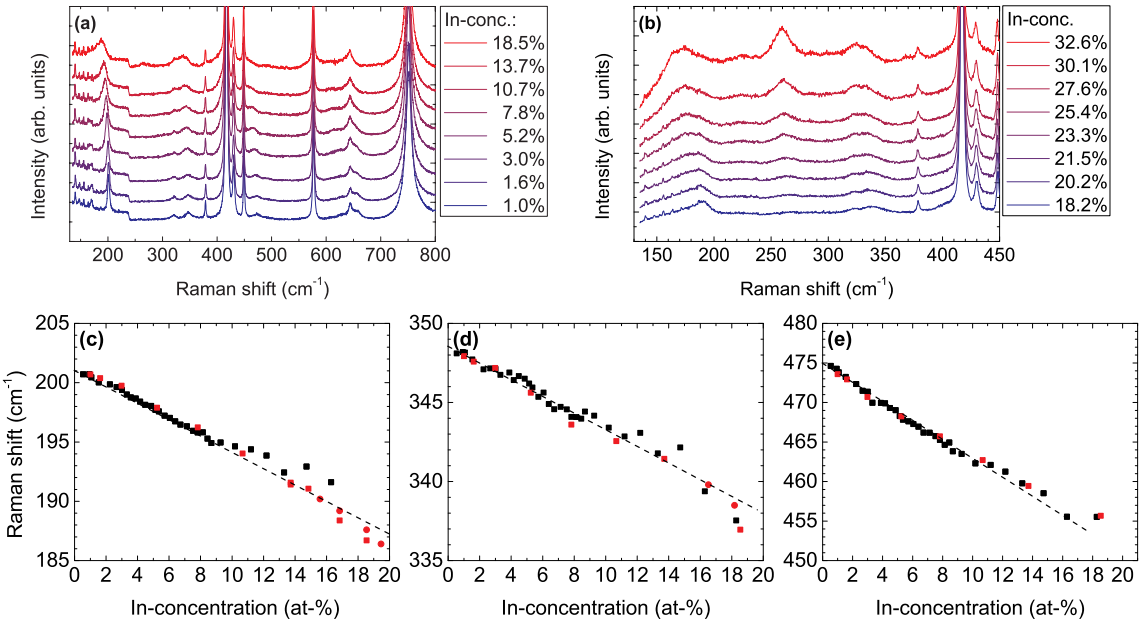

Figure 9.35: (a,b) Raman spectra of $(In_xGa_{1-x})_2O_3$ CCS samples corresponding to the given values for x. Peaks from the sapphire substrate are labelled with an asterisk. (a) Indium is fully incorporated into the β-Ga_2O_3 lattice for $x < 20$ at.% resulting in a redshift of the Raman modes. (b) For $x > 20$ at.%, additional peaks in the Raman spectra occur, most remarkably the highlighted one at 260 cm^{-1}. (c-e) Dependence of the phonon energy on the incorporated concentration of indium for three different phonon modes observable in (a). Differently coloured data points originate from different samples showing the high reproducibility of our method.

9.21.3 Dielectric function and band gap energies of $(In_xGa_{1-x})_2O_3$

We have determined the refractive index dispersion and the energy of the optical absorption edge as a function of the In concentration $x < 12$ % by means of spectroscopic ellipsometry. In the transparency spectral range, i.e. for photon energies below ≈ 3.7 eV, we applied a standard Cauchy model for the determination of the layer thickness and the refractive index dispersion $n(\lambda)$. It is found that $n(\lambda, x)$ depends linearly on x (in at.%) and follows

$$n(\lambda, x) = 1.902 + (100 + 1.2x) \times 10^{-4}\mu m^2 \times \lambda^{-2} + (410 + 10x) \times 10^{-4}\mu m^4 \times \lambda^{-4}, \lambda$$

being the light wavelength in μm. We have obtained the dielectric function in the entire spectral range (0.5 – 9 eV) by numerical inversion of the experimental ellipsometry data. From this dielectric function, we calculated the complex refractive index spectra (Fig. 9.36) and the absorption coefficient α. By a linear approximation of the onset of $(\alpha(E))^2$ (E being the photon energy) we have determined the energy of the optical absorption edge (Fig. 9.37). An almost linear redshift with In concentration is found. For In incorporation higher than 20 at. %, the optical absorption edge smears out considerably such that no reasonable band gap energy could be determined, possibly caused by the strong lattice distortion and thus a strong perturbation of the band structure.

This work has been supported by the European Social Fund (ESF).

[1] J. Gan *et al.*, Sci. Rep. **3**, 1021 (2013) doi:10.1038/srep01021.

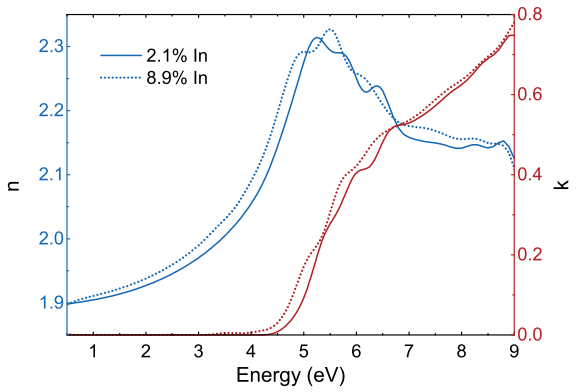

Figure 9.36: Spectra of the real (n) and imaginary part (k) of the complex refractive index of $(In_xGa_{1-x})_2O_3$ calculated from the dielectric function spectra exemplarily for two different In concentrations as labelled in the graph.

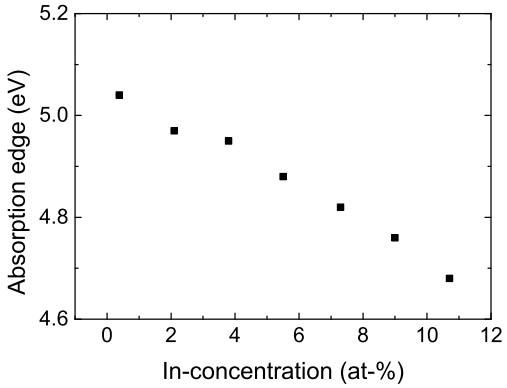

Figure 9.37: Energy of the optical absorption edge determined from the square of the absorption coefficient as a function of the In concentration.

[2] O. M. Berengue *et al.*, J. Phys. D: Appl. Phys. **43**, 045401 (2010) doi:10.1088/0022-3727/43/4/045401.
[3] B. Garcia-Domene *et al.*, J. Appl. Phys. **112**, 123511 (2012), doi:10.1063/1.4769747.
[4] P. D. C. King, Phys. Rev. B **79**, 205211 (2009) doi:10.1103/PhysRevB.79.205211.
[5] C. Kranert *et al.*: phys. stat. solid RRL, phys. stat. sol. rrl 8, 554 (2014), doi:10.1002/pssr.201409004.
[6] R. Shannon and C. Prewitt, J. Inorg. Nucl. Chem. **30**, 1389 – 1398 (1968) doi:10.1016/0022-1902(68).80277-5

9.22 Defect-induced conduction mechanism and magnetism in spinel-type ferrites

K. Brachwitz, M. Welke, T. Böntgen, A. Setzer*, M. Lorenz, R. Denecke† P. Esquinazi*, M. Grundmann

*Supraleitung und Magnetismus, Institut für Experimentelle Physik II, Universität Leipzig
†Wilhelm-Ostwald-Institut für Physikalische und Theoretische Physik, Universität Leipzig

Ferrites constitute a class of materials that has been recognized to have significant potential in applications ranging from millimeter wave integrated circuitry to magnetic recording [1]. $ZnFe_2O_4$, $CoFe_2O_4$ and $NiFe_2O_4$ are promising candidates for the application in magnetic tunnel junctions (MTJs) and spin filter materials [2–4]. The tunability of the electrical conductivity (as reported for zinc ferrite [2]) makes ferrite thin films capable for both, the application as conducting electrode and as insulating barrier in MTJs. In this respect, we have investigated $ZnFe_2O_4$, $CoFe_2O_4$ and $NiFe_2O_4$ thin films grown by pulsed-laser deposition on $SrTiO_3$(001) substrates [5]. The thin films crystallize in spinel structure. This study includes the investigation of structural, magnetic and electrical properties of thin films grown at various growth conditions. Hence, we have varied the growth temperature (T_G) in a range from (265°C < T_G < 700°C) and the

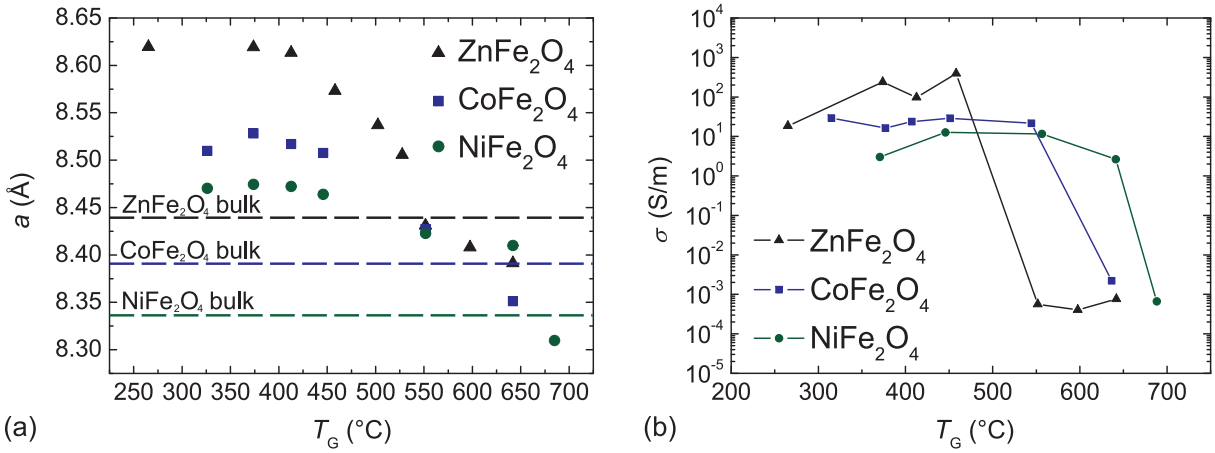

Figure 9.38: (a) Out-of-plane lattice constant a vs growth temperature T_G. High temperature grown films fit the bulk value best. (b) Electrical conductivity σ vs growth temperature T_G. High temperature grown films show the expected insulating behavior.

oxygen partial pressure ranging from 6×10^{-5} mbar to 0.1 mbar. The preferential (001) out-of-plane orientation of the films and the lattice constant were obtained by X-ray diffraction. These XRD measurements reveal an increasing out-of-plane lattice constant with decreasing substrate temperature for all investigated thin films, see Fig. 9.38(a). Furthermore, decreasing intensity of the XRD reflections with decreasing substrate temperatures during growth indicates a poorer crystalline order of the low-temperature thin films [5]. The chemical composition of the $ZnFe_2O_4$ thin films has been investigated by means of energy-dispersive X-ray spectroscopy (EDX). The determined Fe/Zn ratios are in a range from 1.6-2.6, as depicted in Fig. 9.39. Only high-temperature The origin of magnetism has been studied using X-ray circular dichroism (XMCD). By correlating the results of EDX and XPS with XMCD measurements, a partial inversion of the spinel structure could be verified. The partial inversion of the cations and hence the magnetic properties of these thin films are also affected by varying the growth parameters. The high-temperature thin films show an increasing saturation magnetization M_S with decreasing $p(O_2)$ as reported in [6]. SQUID measurements reveal also an increased magnetization of thin films with high cation inversion, cmp. Fig. 9.40 (b). The maximum at about 708 eV in Fig. 9.40 (a) corresponds to trivalent iron ions on tetrahedral sites and therefore indicates cation inversion of the low-temperature grown zinc ferrite thin films [7]. Furthermore, the electrical conductivity increases with decreasing growth temperature for all investigated ferrite materials. Temperature-dependent conductivity measurements show a thermal activation of the conduction with two different activation energies [5]. This behavior corresponds to a thermally activated hopping mechanism of electrons between divalent and trivalent iron ions. The temperature dependent behavior can also be attributed to conduction between three-dimensional clusters, which are embedded in an amorphous matrix [8]. This model is in good agreement with the results of the XRD measurements. The dominating defects in the ferrite thin films can be concluded from correlating the results of above mentioned methods of investigation. On the one hand, there are defects on atomic scale, like cation disorder and presence of divalent iron ions in zinc ferrite, which affect the magnetic and electric properties. On the other hand, the occurrence of three-dimensional clusters in

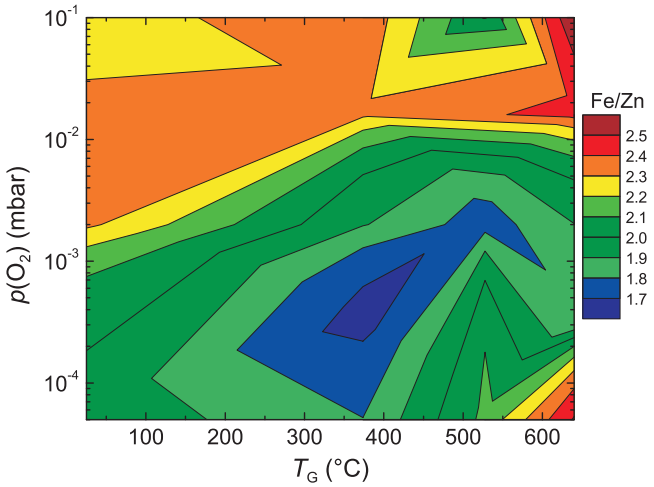

Figure 9.39: Iron-zinc ratios determined by EDX. Green areas are within the experimental accuracy of the EDX measurements.

an amorphous matrix may explain the dependence of the structural properties and the temperature dependence of the electrical conductivity of the low-temperature thin films.

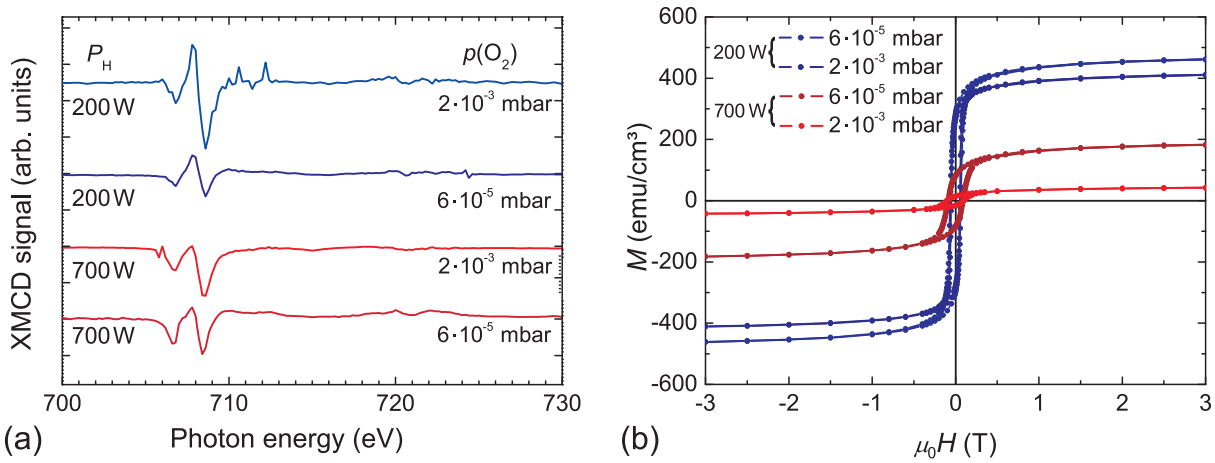

Figure 9.40: (a)

This work has been supported by Deutsche Forschungsgemeinschaft in the framework of SFB 762 "Functionality of Oxide Interfaces".

[1] Y. Suzuki, Annu. Rev. Mater. Res. **31**, 265 (2001)
[2] M. Lorenz *et al.*, Phys. Status Solidi RRL **5**, 438 (2011)
[3] A.V. Ramos *et al.*, Appl. Phys. Lett. 91, 122107 (2007)
[4] U. Lüders *et al.*, Adv. Mater. **18**, 1733 (2006)
[5] K. Brachwitz *et al.*, Appl. Phys. Lett. 102 172104 (2013)
[6] C. E. Rodríguez Torres *et al.*, Phys. Rev. B **84**, 064404 (2011)
[7] R. A. D. Pattrick *et al.*, Eur. J. Mineral. **14**, 1095 (2002)
[8] P. Sheng *et al.*, Phys. Rev. Lett. **31**, 44 (1973)

9.23 (Magneto-) optical properties of spinel oxides

V. Zviagin, R. Schmidt-Grund, P. Richter *, T. Böntgen, M. Lorenz, D.R.T. Zahn *, G. Salvan *, M. Grundmann.

*Technische Universtät Chemnitz, Semiconductor Physics, Reichenheiner Str. 70, Germany.

We have investigated the optical and magneto-optical properties of the spinel type oxides $ZnFe_2O_4$ (ZFO)[1], $CoFe_2O_4$ (CFO) and $ZnCo_2O_4$ (ZCO). Inverse spinel oxides (e.g. CFO) have been in focus of research interests due to their magnetic and magneto-optical properties [2]. Normal spinel oxides (e.g. ZFO, ZCO) have only recently gained more interest due to their potential for application in data storage and spintronic devices [3].

By means of pulsed laser deposition we have grown thin films of ZFO, CFO and ZCO on MgO substrates. These samples were investigated using variable angle spectroscopic ellipsometry in a wide spectral range (0.5 – 9.0) eV and a model for the dielectric function was deduced. Because the investigated compounds share a common crystal structure, many of the optical transitions observed are expected to be similar. Thus similar models for the compounds can be proposed. The main transitions observed can be characterized as either inter-valence [x]-site transitions or inter-sublattice [x]-site transitions. The critical point transition corresponds to a transition from $O_{2p} \rightarrow Zn_{4s}$ for ZFO and ZCO and from $O_{2p} \rightarrow Co_{3d}$ for CFO. For high photon energies an additional transition (likely due to Zn) is expected for ZFO and ZCO (Fig. 9.41). Transitions in the low energy range correspond to metal *d* to *d* on-site transitions and are observed mainly for low temperature grown samples. These transitions have been observed in similar materials and are believed to become possible through the disorder in the crystal. The magneto-optical response of the dielectric tensor was obtained using magneto-optical Kerr effect (MOKE) spectroscopy in the visible spectral range (1.5 – 5.5) eV with an applied field of 1.7 T for ZFO and CFO spinels. The magneto-optical measurements showed a response at the energies of mentioned transitions, namely the critical point transition at 3.0 eV for ZFO and at 1.7 eV for CFO as well as the $O_2p \rightarrow Fe_3d$ transition at 3.7 eV for ZFO and at 3.5 eV for CFO (Fig. 9.42). Its strong dependence on the crystal quality of the films indicates that the magneto-optical response is related to disordered 2*d* and 3*d* metal lattice site occupation and thus to the occurrence of mixtures of regular and inverse spinel structure. The magneto-optical response seen at 2.5 eV for ZFO is most likely due to thickness interferences.

This work has been supported by Deutsche Forschungsgemeinschaft in the framework of SFB 762 "Functionality of Oxide Interfaces".

[1] T. Böntgen *et al.*: J. Appl. Phys. **113**, 073503 (2013) doi:10.1063/1.4790881
[2] D.L. Camphausen *et al.*: Phys. Rev. Lett. **29**, 657 (1979) doi:10.1103/PhysRevLett.29.657
[3] M. Opel *et al.*: Physica Status Solidi (a) **208**, 232 (2011) doi:10.1002/pssa.201026403

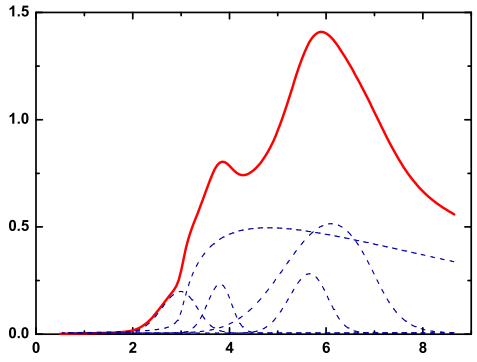

Figure 9.41: Imaginary part of the dielectric function (ε_2) of ZFO calculated from the model with the individual transition contributions (blue dashed lines) specified.

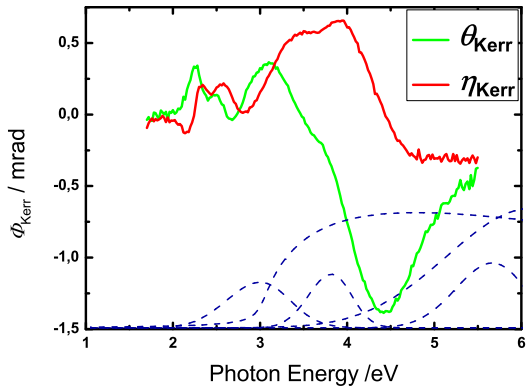

Figure 9.42: Complex MOKE spectra of the ZFO film shown in Fig. 9.41. The model contributions to ε_2 are also included for comparison.

9.24 Dielectric function tensor of a $YMnO_3$ single crystal

R. Schmidt-Grund, S. Richter, S.G. Ebbinghaus*, M. Lorenz, C. Bundesmann†, M. Grundmann

*Institut für Chemie, Martin-Luther-Universität Halle-Wittenberg, Kurt-Mothes-Straße 2, D-06120 Halle/Saale, Germany.
†Leibniz-Institut für Oberflächenmodifizierung (IOM), Permoserstr. 15, D-04318 Leipzig, Germany.

Hexagonal manganite's $RMnO_3$ (R being rare earths) are interesting due to their potential use in information processing and spintronic devices because of their strong magneto-electric interaction, caused by the interplay between Mn and O ions in a distorted close-packed configuration. Especially $YMnO_3$ is considered as a prototype multiferroic material.

We have determined crystallographic data and investigated optical properties in the wide spectral range (0.5 – 9.15) eV of a (110)-oriented hexagonal $YMnO_3$ bulk single crystal (Fig. 9.43) grown by the optical floating zone technique. Structure refinement reveals very high crystal quality. We have determined the tensor of the dielectric function (DF) by Kramers-Kronig consistent modelling of the Mueller matrix elements measured by ellipsometry. For the spectral range below 5.4 eV, our data are much more precise compared to previous reports [1], for higher energies no reports were given previously. The features observed in the DF due to electronic charge transfer transitions basically agree well with theoretical predictions [2]. However, several differences (Fig. 9.44) make refinement of electronic structure theory necessary to gain a better understanding of this prototype multiferroic material. We have found strong indications for direct band-band transitions which have not been reported so far. At energies below these transitions, pronounced discrete interband charge transfer transitions from the hybridized oxygen-Mn states to Mn–3*d* states are found at different energies for each of the linear independent principal diagonal elements of the DF tensor $\varepsilon_\perp$ and $\varepsilon_\parallel$. The index

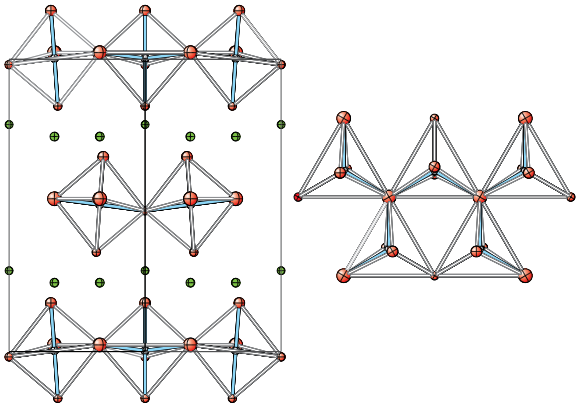

Figure 9.43: Crystal structure of $YMnO_3$ viewed along [110] (left) and [001] (right). Equivalent isotropic displacement parameters represent a 90 % probability (indicated by the size of the spheres). Y atoms are coloured green, Mn gray and oxygen red. Mn−O bonds are coloured light blue and the MnO_5-trigonal bipyramids are marked by white lines.

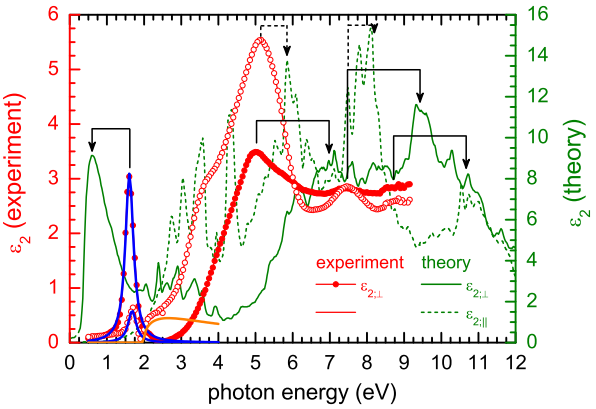

Figure 9.44: Comparison of experimentally determined $\varepsilon_{2;\perp,\parallel}$ spectra (red symbols, $\perp$: filled, $\parallel$: open) with theoretically calculated ones (Ref. [2], green lines, $\perp$: solid, $\parallel$: dashed). The arrows indicate the energy shift between peaks observed in the experiment and the theory. Please note the different scale of the ε_2-axes for experiment (left) and theory (right). The blue lines show Lorentzian lineshape approximations of the sharp peaks at 1.612 eV ($\varepsilon_{2;\perp}$) and 1.686 eV ($\varepsilon_{2;\parallel}$). The orange line represents the M0 critical point-like onset of the band-band absorption at 1.97 eV.

$\perp$ and $\parallel$ denotes the component perpendicular and parallel to the optical axis. Both transitions appear to be molecule-like with the same purely homogeneous linewidth and pseudo-transparent points, where the imaginary part of each DF tensor element approaches zero, occur at their high energy side.

This work has been supported by Deutsche Forschungsgemeinschaft in the framework of SFB 762 "Functionality of Oxide Interfaces".

[1] A. M. Kalashnikova and R. V. Pisarev, JETP Lett. **78**, 143 (2003) doi:10.1134/1.1618880
[2] M. Qian *et al.*, Phys. Rev. B **63**, 155101 (2000) doi:10.1103/PhysRevB.63.155101

9.25 Extension of the rigorous coupled wave approach for slanted structures

L. Fricke, R. Schmidt-Grund, M. Grundmann

The rigorous coupled wave approach (RCWA) is a method to simulate the interaction of light with planar dielectric structures, that exhibit periodic structuring in the layer planes and are piecewise homogeneous along the layer normal. We extended this method to be able to simulate the interaction not only with homogeneous but slanted structures as for example in sculptured thin films.

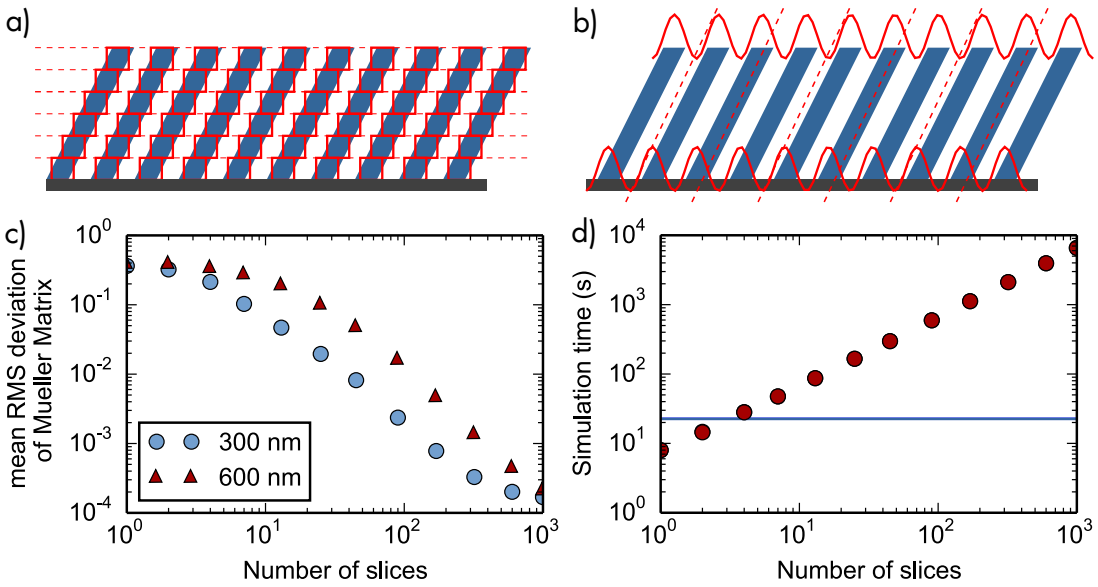

Figure 9.45: (a), (b) Illustration of the "slicing" and direct method, respectively. (c) Convergence of the "slicing" method to the direct method. A minimum of 100 slices is necessary for acceptable agreement. Gratings of 30 nm wide bars of SiO_2 with a period of 300 nm and an inclination of 45° on silicon have been simulated for two different heights (blue and red symbols). (d) Time needed to simulate the spectra as a function of number of slices. The time needed using the direct method is marked by the horizontal line. For both methods the simulation time does not depend on the height of the grating.

In the RCWA the electromagnetic field is expressed as a truncated Fourier series in the plane of the layers. The Fourier components are coupled via a dielectric matrix according to the material pattern in the layer. For this representation eigenmodes, which are plane waves in the normal direction, are calculated. At the interface between the layers the fields are joined such that they fulfil the continuity conditions. [1]

In this approach slanted structures have to be divided in small homogeneous slices (slicing method, cf. Fig. 9.45 (a)) and treated each separately, which leads to high computational effort. The slices are only shifted against each other and share the same periodic in-plane structure. The shift is expressed as a unitary transformation of the dielectric coupling matrix in the Fourier series representation. If instead the field is directly transformed in the same way into a Fourier series and inserted into the Maxwell equations, a matrix eigenvalue problem similar to the original eigenmode calculation is obtained (direct method, cf. Fig. 9.45 (b)). Here the size of the eigenvalue problem is doubled compared to the slicing method. Whereas in the original approach only the magnetic field components of the electromagnetic wave are considered in the calculation, the direct method uses both magnetic and electric field components.

We compared the simulated Mueller matrix spectra of the specular reflection. For one-dimensional structures (like gratings) the slicing method yields the same results as the direct method for a large number of slices. The convergence of the slicing method to the direct method of a sample structure for different sample heights is shown in Fig. 9.45 (c). The simulation time of the slicing method exceeds that of the direct method for acceptable number of slices as can be seen in Fig. 9.45 (d).

This new method is a powerful tool to simulate the optical response of functional

optical coatings for ellipsometry analysis in the future.

This work has been supported by Leibniz-Gemeinschaft in the framework SAW-2011-IOM-2 "Ortsaufgelöste nanomechanische Eigenschaften funktionaler Oberflächen – Experiment und Simulation".

[1] V. Liu and S. Fan: Comput. Phys. Commun. **183**, 2233 (2012), doi:10.1016/j.cpc.2012.04.026

9.26 Phonon-assisted exciton lasing in ZnO microwires

T. Michalsky, C.P. Dietrich, C. Sturm, R. Schmidt-Grund, M. Grundmann

We investigated the lasing properties of hexagonal ZnO microwires. The spectral distribution of the lasing modes reveals that the lasing is driven by a strong exciton-phonon interaction. These findings are supported by former results measuring a strong exciton-phonon interaction in ZnO [1, 2] and showing indications for an increase of the coupling strength with reduced structure size [2]. We observe lasing at the spectral position of the first (1LO) and second longitudinal optical phonon replica (2LO) of the free A exciton (FXA) at $T = 10\,\mathrm{K}$ and room temperature (2LO only).

The microwires investigated here have diameters of about $D = 7\,\mu\mathrm{m}$. They were fabricated by carbothermal vapor phase transport. The growth took place in a heatable tube furnace at temperatures larger 1000 ℃ [3].

Figure 9.46(a,b) shows spectrally resolved k-space photoluminescence (PL) emission patterns from two different, but structural very similar microwires out of the same growing charge recorded at $T = 10\,\mathrm{K}$ under the same conditions. In Fig. 9.46(a) it is clearly visible that the spectral centre of the PL emission is located in the spectral range of the 1LO. Narrow dispersionless lasing lines extended over the full observable $k_{||}$-range prove that the lasing mechanism cannot be explained only by lasing out of photonic modes (here whispering gallery modes - WGMs - where a dispersion would be expected), but is rather fed by scattering processes without momentum conservation. In contrast to that, the lasing emission from the second microwire is centred at $k_{||} = 0$ and follows the mode dispersion (Fig. 9.46(b)). It appears at energies above the energy of 1LO and could be either of photonic or even also polaritonic origin. The actual gain mechanism for the lasing is unclear so far.

Furthermore we observed phonon-assisted lasing in the spectral range of the 2LO line at $T = 10\,\mathrm{K}$ as well as at room temperature (Fig. 9.46(c,d)). Comparable to the lasing out of the 1L0 line, the brightest emission spots were detected where WGMs cross the 2LO spectral range. The real space emission pattern of the wire taken at room temperature reveals that the lasing emission couples out only at the wire edges (not shown) which is typical for WGMs [4]. The corresponding two-dimensional k-space emission pattern shows knots which belong to the WGM mode numbers crossing the 2LO line.

This work has been supported by Deutsche Forschungsgemeinschaft within the project "Extrem verzerrte Nano- und Mikrodrähte" (GR 1011/23-1).

[1] D.C. Reynolds *et al.*, J. Appl. Phys. **89**, 6189 (2001) doi:10.1063/1.1356432

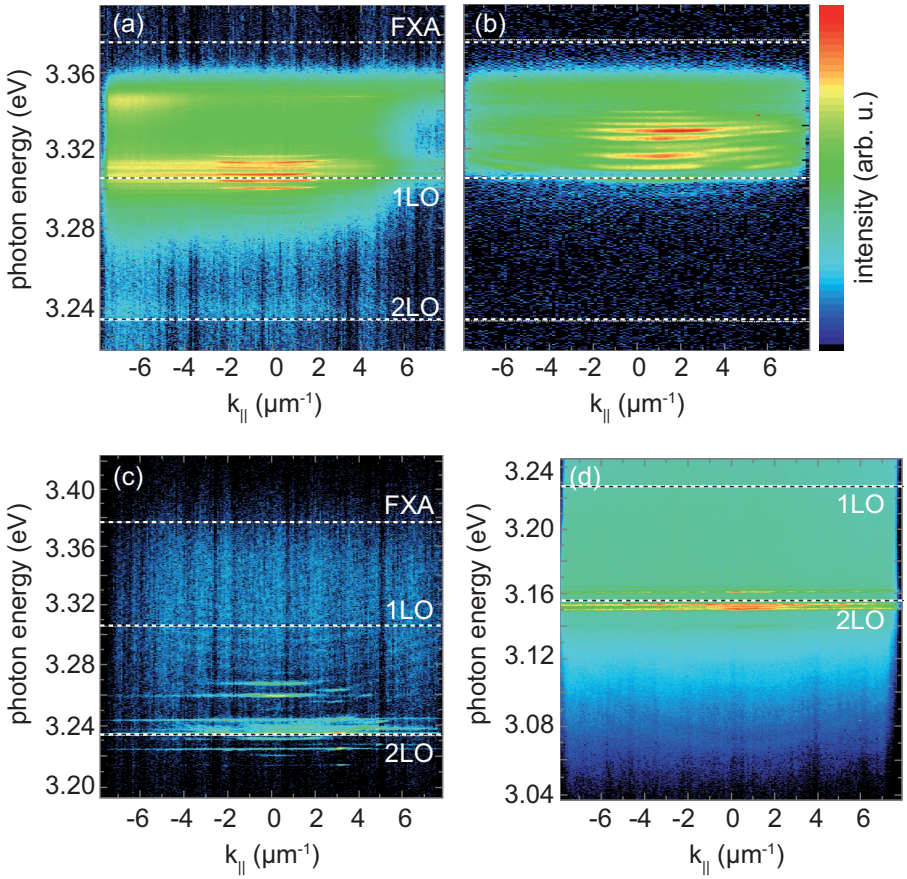

Figure 9.46: Spectrally resolved k-space PL emission patterns. $k_{||}$ refers to the absolute value of the wave vector along the wire axis. The white dashed-dotted lines indicate the positions of the first (1LO) and second longitudinal optical phonon replica (2LO) of the free A-exciton (FXA). (a-c) have been recorded at $T = 10$ K and belong to three different, but very similar microwires. (d) shows data for the same wire as in (c) but recorded at room temperature. In both cases (c,d) lasing emission can be detected where WGMs cross the spectral range of the 2LO line.

[2] H.C. Hsu *et al.*, J. Crystal Growth **261**, 520 (2004) doi:10.1016/j.jcrysgro.2003.09.040
[3] M. Grundmann *et al.*, Proc. Mat. Res. Soc. **957**, 107 (2007)
[4] J. Wiersig, Phys. Rev. A **67**, 023807 (2003) doi:10.1103/PhysRevA.67.023807

9.27 Exciton-Polaritons in ZnO-based microcavities: g-factor, coherent quantum states and mode probing

C. Sturm, H. Franke, T. Michalsky, M. Thunert, A. Janot*, S. Richter, C.P. Dietrich†, R. Johne‡, M.D. Martín§, P. Eastham¶, L. Viña§, B. Rosenow*, R. Schmidt-Grund, M. Grundmann

*Institut für Theoretische Physik, Universität Leipzig.
†now with: University of St Andrews, School of Physics and Astronomy, North Haugh, KY16 9SS, St Andrews, Fife, Scotland, United Kingdom.

‡Max Planck Institute for the Physics of Complex Systems, Nöthnitzer Straße 38, 01187 Dresden, Germany.
§Universidad Autonóma de Madrid, Departamento de Física de Materiales, C/ Francisco Tomás y Valiente, n° 7, 28049 Madrid, Spain.
¶Trinity College Dublin, College Green, Dublin 2, Ireland.

Exciton-polaritons are quasi-particles formed by the strong light-matter coupling between excitons and photons in a microcavity. The composite nature of these particles causes that they inherit the properties of both constituents: the photonic one allows their propagation in the micrometer range and the excitonic one leads to strong nonlinear interaction of the polaritons among each other and with their environment [1]. This makes them interesting for devices and some basic elements like transistors and diodes have been already realized [2]. One interesting feature of the exciton-polaritons arises from their bosonic nature and their low effective mass. Exciton-polaritons can build a macroscopic quantum state, a dynamic Bose-Einsten condensate (BEC), which exhibit lasing like emission or superfluidity.

In the first part of this report, Sec.9.27.1, we address the interaction of the exciton-polaritons with magnetic fields. These fields can be applied externally or can be caused by intrinsic effects such as the TE-TM-splitting[1]. The impact of magnetic fields on the polariton properties becomes more and more of interest, since, on the one hand, it was recently shown that the condensation threshold can be reduced by applying an external magnetic field [3], allowing for the realization of electrically injected polariton lasers [4]. On the other hand, the presence of effective internal magnetic fields causes new physical effects like the optical Spin Hall effect or the formation of spin polarized vortices. For the description of the polariton properties in magnetic fields the pseudo-spin formalism in terms of the density matrix representation is used. Here we discuss different contributions to the magnetic field acting on the exciton-polariton pseudo-spin and emphasizes their g-factor tensor properties.

The second part, Sec. 9.27.2, focusses on properties of exciton-polariton Bose-Einstein condensates in a disorder potential landscape and its relaxation behaviour in a multimode environment. For these investigations ZnO cavities were used. In the first case, we take advantage of the intrinsic defects of a planar microcavity grown by pulsed laser deposition. The $\lambda/2$ cavity was embedded between two Bragg reflectors made of 10.5 layer pairs of YSZ and Al_2O_3. A detailed description of this microcavity can be found in reference [5]. In the second case, the investigation of the relaxation behaviour, we used a ZnO microwire grown by carbothermal vapour phase transport. The whispering gallery modes (WGM) present in this wire provide a multi-mode photonic system with its ground mode energetically well separated from the exciton-resonance, typically some electron volts [6]. The multi-mode property is also inherited by the exciton-polaritons leading to new effects compared to those of (single-mode) Fabry-Pérot type which typically arise in planar cavities.

In the last part, Sec. 9.27.3, we present the realization of an angular resolved μ-reflectivity setup. This setup allows to probe the dispersion of non-occupied photon or exciton-polariton modes with high spatial resolution in the micrometer range, mandatory for a deeper understanding of the physics of exciton-polaritons in microcavities

[1]The TE-TM-splitting denotes the energetic splitting between the two orthogonal linear polarizations TE (transversal electric field) and TM (transversal magnetic field)

based on nano- and microwires.

9.27.1 Exciton-polariton pseudo-spin g-factor

The pseudo-spin of an exciton-polariton ensemble is the superposition of spin and polarization of their constituting excitons and photons, respectively. It is associated with a three-dimensional pseudovector which is defined by the Pauli spin density matrices applied to the state density matrix. Since the pseudo-spin is related to the polarization of the emitted photons, it is directly accessible by means of optical methods [7].

Similar to the spin of an electron or photon, the pseudo-spin can be manipulated by magnetic fields. These fields can be applied externally or induced intrinsically as effective fields. The latter arise in the pseudo-spin Hilbert space as a consequence of any energetic splitting of different excitonic or photonic spin respective polarization states. It is convenient to express those effective fields in terms of their Larmor vector $\vec{\Omega}$. Since exciton-polaritons are composite particles, the origin of these effective magnetic fields can be photonic ($\vec{\Omega}_{\mathrm{C},i}$), e.g. caused by optical birefringence of the resonator structure, or excitonic ($\vec{\Omega}_{\mathrm{X},i}$), e.g. caused by dichroism of the cavity materials. The resulting entire effective field $\vec{\Omega}_{\mathrm{tot}}$ is then given by $\vec{\Omega}_{\mathrm{tot}} = |X|^2 \sum_i \vec{\Omega}_{\mathrm{X},i} + |C|^2 \sum_i \vec{\Omega}_{\mathrm{C},i}$. $|X|^2$ and $|C|^2$ are the relative excitonic and photonic fractions of the exciton-polaritons, respectively, which depend strongly on their wave vector $\vec{k}$ and the energetic detuning between the cavity photon mode and the exciton.

When external fields ($\vec{B}$) are applied, the resulting magnetic field acting in the pseudo-spin space is a superposition of the apparent effective fields and that external one. For this, $\vec{B}$ in real space has to be transferred into $\vec{\Omega}_{\mathrm{ext}}$ by using a polariton $\hat{g}$-factor tensor and a space transformation matrix ($\hat{T}$), i.e. $\vec{\Omega}_{\mathrm{ext}} = \mu_{\mathrm{B}} \hat{T} \hat{g} \vec{B}/\hbar$. μ_{B} and $\hbar$ represent the Bohr magneton and the reduced Planck constant, respectively. $\hat{T}$ is expressed by a rotation matrix and transforms the magnetic field given in real space coordinates, where the z-coordinate is defined by the propagation direction, into the pseudo-spin Hilbert space. In literature, this $\hat{g}$-factor tensor is often assumed to be isotropic or investigations are principally restricted to Faraday configuration where the external field is applied in propagation direction. However, polarization resolved photoluminescence measurements on ZnO-based microcavities indicate a more sophisticated relation for general magnetic field orientations [9]. The origin of the tensorial shape of $\hat{g}$ is caused by: 1. the effective $\hat{g}$-factor of the photons $\hat{g}^{\mathrm{C}}$, which takes into account Faraday rotation and the Voigt effect (magnetic field induced optical birefringences). 2. the $\hat{g}$-factor of the excitons which itself is composed of electron (g^e) and hole (g^h) contributions. Similar to the effective field, the entire polariton $\hat{g}$-factor is composed of the photonic and excitonic $\hat{g}$-factors by

$$\hat{g}_{\mathrm{pol}} = |C|^2 \begin{pmatrix} g^{\mathrm{C}}_{Voigt} & 0 & 0 \\ 0 & g^{\mathrm{C}}_{Voigt} & 0 \\ 0 & 0 & g^{\mathrm{C}}_{Faraday} \end{pmatrix} + |X|^2 \begin{pmatrix} \pm(g^e_\perp + g^h_\perp) & 0 & 0 \\ 0 & \pm(g^e_\perp + g^h_\perp) & 0 \\ 0 & 0 & g^e_\parallel + g^h_\parallel \end{pmatrix}. \tag{9.2}$$

The indices $\perp$ and $\parallel$ denote the components perpendicular and parallel to the magnetic field. It has to be considered that $\hat{g}_{\mathrm{pol}}$ strongly depends on $\vec{k}$. This is caused by the $\vec{k}$

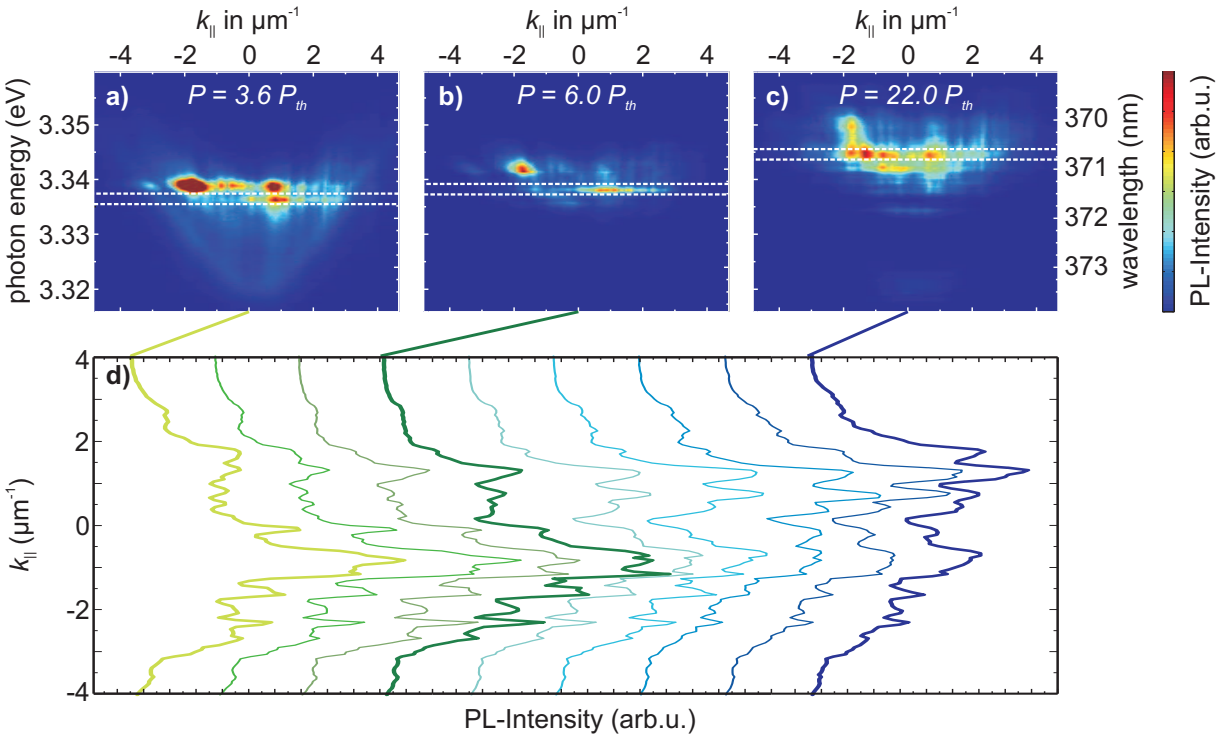

Figure 9.47: (a)-(c) Excitation power series of the far-field PL emission in a linear false color scale for $T = 10\,\mathrm{K}$ and a detuning of $\Delta = -30\,\mathrm{meV}$ ($P_{\mathrm{th}} = 46.5\,\mathrm{W/cm^{-2}}$). (d) Excitation power dependent evolution of intensity-momentum profiles of a single condensate state (integrated over a small energy range of 2 meV, indicated by the white rectangle in the far-field emission pattern (a)-(c)).

dependency of $|X|^2$ and $|C|^2$ but also the effective fields itself can change with $\vec{k}$ as it is e.g. the case for the TE-TM-splitting related field [8]. Thus, finally $\vec{\Omega}_{\mathrm{tot}}$ and therewith the polarization eigenstates of a certain polariton state depend on $\vec{B}$ and $\vec{k}$.

9.27.2 Bose-Einstein condensates in ZnO microcavities

Influence of disorder on the exciton-polariton condensate

In contrast to a BEC of atoms, the BEC formed by exciton-polaritons is not in a thermal equilibrium and dynamic effects have to be considered. So, e.g., the effect of disorder destroys the superfluid properties of a BEC, scaling with the ratio of the condensate energy, which is proportional to its density, to the disorder potential height. Usually it is considered that, if the condensate energy is large compared to the disorder potential, the superfluidity stabilizes. But as shown recently theoretically, even a weak disorder perturbs the condensate's phase stability [10]. An experimental signature for the presence of disorder is a non-homogeneous momentum distribution of the polariton condensate. For a disorder-free BEC, a smooth momentum distribution is expected. In literature, a lack of stabilization of a single-mode condensate for increasing density was observed experimentally [11]. However, theoretically the role of the disorder effects were studied only for a fixed polariton density or rather excitation power density [12]. The processes of condensate stabilization or desynchronization depending on the

strength of the disorder potential is still under discussion.

In order to gain insights into the role of disorder we exploit the intrinsic disorder effects in our microcavity. By changing the excitation density, the potential energy of the polaritons due to their repulsive interaction was varied and therewith the ratio to the disorder potential height. For all excitation densities, our experimental observations show pronounced intensity fluctuations within the far-field (momentum space) emission pattern of a single-mode condensate state (cf. Fig. 9.47). Even at high potential energies a non-homogeneous distribution of the condensate emission was observable which indicates the pronounced non-equilibrium nature of the BEC. The phase coherence of this condensate was proven by using a Michelson interferometer in mirror-retroreflector configuration which yield a clear interference pattern of the emission and therefore an evidence for the long-range coherence of polaritons with different in-plane momenta $k_{||}$.

For understanding the nature of the observed intensity fluctuations and their dependence on the strength of the disorder potential relative to the condensate energy we solved the extended Gross-Pitaevskii equation. A polariton density dependent depletion term accounts for their non-equilibrium nature [10]. Especially, this term considers microscopical polariton currents due to the disorder potential and gain-loss mechanism. A comparison of the numerical simulations with the experiment shows that the phase fluctuation length in our microcavity is similar to the condensate size and independent of the excitation power. Thus, the stabilization of the condensate is suppressed even at high excitation power. In contrast to that, for a condensate in thermal equilibrium without any phase fluctuations a stabilization would be expected. These findings underline the strong non-equilibrium dynamic character of the investigated condensate. We can also conclude that the condensate is exposed to significant structural disorder potentials which are in the same order as the potential energy of the condensate.

Parametric relaxation in whispering-gallery mode exciton-polariton condensates

Last year we reported on the formation of a BEC of multimode WGM exciton-polaritons in hexagonal ZnO microwires at low temperature [13]. At threshold, laser emission starts in modes close to the emission energy of defect-bound excitons. We propose this process to be fed by resonant excitation of polaritons by the emission from the highly populated defect-bound excitons. With further increasing excitation power, the condensates relax within the multimode whispering-gallery mode polariton ladder leading to its effective evaporative cooling. The intensity, energy and momentum evolution of this process indicates a parametric polariton-polariton scattering process. The excitation power dependent intensity evolution of the BEC emission in the energy momentum space is shown in Fig. 9.48(a).

We were now able to theoretically describe our experimental findings and thus confirm the model of parametric mixing of condensate states. We applied numerical simulations based on a model for polariton-polariton scattering [14, 15] that we have modified to resemble the multimode WGM system. Basically, the model takes into account 1.) polariton creation and annihilation at each energy-momentum state of all polariton branches, 2.) their in- and out-scattering from and into all of them, 3.) polariton-driving field interaction considering a small thermal population of the states for initiating the scattering process and 4.) a strong pump field for the resonant feeding

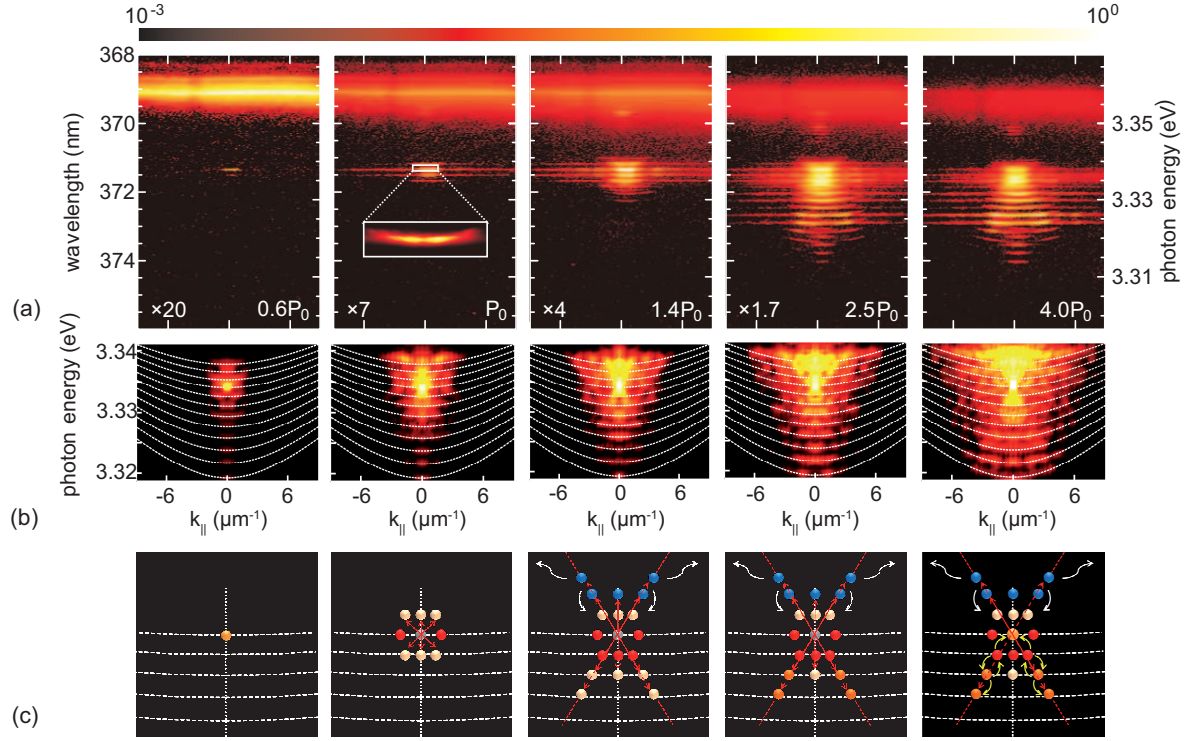

Figure 9.48: (a) Excitation-dependent PL images (T = 10 K) of a ZnO microwire (P_0 = 15 kW/cm^2). Spectra are normalized to each other (colour-coded intensity scale is in logarithmic scale). Relative excitation powers as well as intensity multiplication factors are given at the bottom. (b) Theoretically simulated polariton distribution as a function of the excitation power. (c) Schematic of the excitation power dependent scattering processes as observed in (a) and (b) (note that one out of many scattering paths is shown only for clarity). WGM polariton modes are shown as white dashed lines. The vertical white dashed line refers to k = 0. Occupied polariton states are shown as circles. The colour code from light orange to red indicates increasing occupation density. The blue circles indicate target states of the scattering processes which are not visible in the PL images due to their fast decay and relaxation. Red arrows refer to linear polariton-polariton scattering while the yellow arrows indicate the parametric mixing processes.

by the defect bound exciton. The calculated excitation power dependent polariton distribution in the energy momentum space, which is proportional to the emission intensity from the BEC decay, is shown in Fig. 9.48(b). The simulation reproduces very nicely the experimental observations. An obvious difference between experiment and the model simulation is that in the latter also states at energies higher than the initial state are heavily occupied. This is due to the finite number of polariton states considered in the simulation for calculation power reasons causing the lack of efficient drain for the high-energy polaritons.

9.27.3 Extension of the micro photoluminescence setup for angular resolved reflectivity measurements

Reflectivity and photoluminescence (PL) measurements are two complementary methods. The first one probes the dispersion and the other one the occupation of states

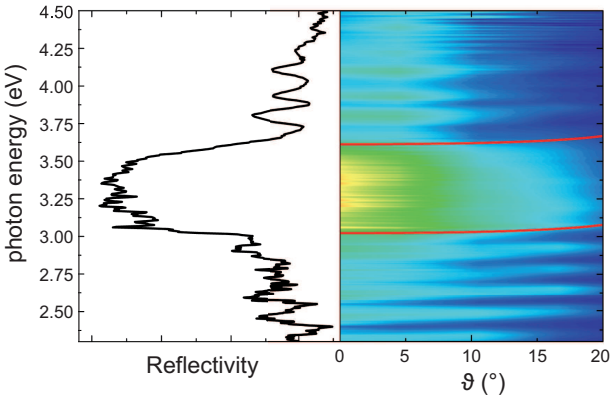

Figure 9.49: Angular resolved reflectivity image of a Bragg mirror coated ZnO nanowire clearly showing the Bragg stop band (marked with red lines) and mode dispersion.

being present in a sample. For the investigation of inhomogeneous samples, structured samples or nano-structures it is necessary to probe only a small area of few micrometers in diameter.

For the realization of a μ-reflectivity setup we extended an existing μ-photoluminescence imaging setup by a Xenon lamp as white light source which was coupled into a fibre. By imaging the end of the fibre on the sample by using an objective and a lens with a focal length of f_o and f_l, respectively, the probed area on the sample is given by $d = d_f f_o / f_l$. f_f represents the diameter of the fibre. Like for the PL measurements, the focal plane of the objective is imaged on a CCD camera which allows to perform angular resolved measurements and therewith to deduce the dispersion of the modes. In the case of a Fabry-Pérot microcavity the dispersion, i.e. the dependence of the photon energy (E) on $k_{||}$, can be determined from the angle of incidence (θ) by $k_{||} = E/(\hbar c) \sin\theta$, with $\hbar$ and c being the reduced Planck constant and the vacuum velocity of light, respectively. The high numerical aperture microscope objective (NA = 0.4) allows us to observe an angular range of about $\Delta\theta = \pm 23°$. A challenge in performing of angular resolved reflectivity measurements is to extract the reflectivity precisely from the raw data which require the measurement of a reference with a well known reflectivity. From both measurements, of the investigated and the reference sample, the signal background has to be removed which arises mainly from internal reflections of the elements of the setup (mainly from the microscope objective).

In Fig. 9.49 the angular resolved reflectivity spectra of a 2D confined microcavity consisting of a zinc oxide nanowire which was coated with a Bragg reflector [16] is shown. The photonic modes as well as the Bragg stop band are clearly observable, demonstrating the operability of the setup.

This work has been supported by Deutsche Forschungsgemeinschaft within the project "Bose-Einstein-Kondensation und Supraflüssigkeit von Exziton-Polaritonen bei Raumtemperatur" (GR 1011/20-2).

[1] F. Tassone, Y. Yamamoto: Phys. Rev. B **59**, 10830 (1999), doi:10.1103/PhysRevB.59.10830; M. Wouters *et al.*: Phys. Rev. B **77**, 115340 (2008), doi:10.1103/PhysRevB.77.115340

[2] D. Ballarini *et al.*: Nat. Commun. **4**, 1778 (2013), doi:10.1038/ncomms2734;

H.S. Nguyen *et al.*: Phys. Rev. Lett. **110**, 236601 (2013), doi:10.1103/PhysRevLett.110.236601
[3] V. P. Kochereshko *et al.*: arXiv:1309.6983 (2013), arXiv:1309.6983
[4] C. Schneider *et al.*: Nature **497**, 348 (2013), doi:10.1038/nature12036
[5] H. Franke *et al.*: New. J. Phys. **14**, 013037 (2012), doi:10.1088/1367-2630/14/1/013037
[6] C.P. Dietrich *et al.*: New. J. Phys. **13**, 103021 (2011), doi:10.1088/1367-2630/13/10/103021
[7] R.I. Dzhioev *et al.*: Phys. Rev. B, **56**, 13405 (1997)
[8] S. Sturm *et al.*: Phys. Rev. B **83**, 205301 (2011)
[9] R. Schmidt-Grund *et al.*: in *The Physics Institutes of Universität Leipzig, Report 2012*, M. Grundmann (Ed.), pp. 199, Leipzig, 2013.
[10] A. Janot *et al.*: Phys. Rev. Lett. **111**, 230403 (2013), doi:10.1103/PhysRevLett.111.230403
[11] F. Manni *et al.*: Phys. Rev. Lett. **106**, 176401 (2011), doi:10.1103/PhysRevB.83.241307
[12] D. Krizhanovskii *et al.*: Phys. Rev. B **80**, 045317 (2009), doi:10.1103/PhysRevB.80.045317; A. Trichet *et al.*: Phys. Rev. B **83**, 041302 (2011), doi:10.1103/PhysRevB.83.041302
[13] R. Schmidt-Grund et al.: in The Physics Institutes of Universität Leipzig, Report 2011, M. Grundmann (Ed.) pp. 204, Leipzig, 2012
[14] C. Ciuti, P. Schwendimann, B. Deveaud, and A. Quattropani, Phys. Rev. B **62**, R4825 (2000), doi:10.1103/PhysRevB.62.R4825
[15] C. Ciuti, P. Schwendimann, and A. Quattropani, Semiconductor science and technology **18**, S279 (2003)
[16] R. Schmidt-Grund *et al.*: phys. stat. sol. b **247**, 1351 (2010), doi:10.1002/pssb.200945530

9.28 Funding

Leipzig School of Natural Sciences - Building with Molecules and Nano-objects (BuildMoNa)
Prof. Dr. M. Grundmann
DFG GS 185/1

Polarisationswechselwirkung in Laser-MBE Wurtzit-Perowskit-Heterostrukturen
Prof. Dr. M. Lorenz
SFB 762/2-2012, TP A2 within SFB 762 *Funktionalität Oxidischer Grenzflächen*

Optische Untersuchungen zu magneto-elektro-optischen Wechselwirkungen in ihrer Dynamik in oxidischen Heterostrukturen
Dr. Rüdiger Schmidt-Grund
SFB 762/2-2012, TP B03 within SFB 762 *Funktionalität Oxidischer Grenzflächen*

Lateraler Transport in oxidischen Feldeffekt-Strukturen
Dr. H. von Wenckstern, Prof. Dr. M. Grundmann
SFB 762/2-2012, TP B04 within SFB 762 *Funktionalität Oxidischer Grenzflächen*

Spinabhängiges Tunneln in oxidischen Heterostrukturen
Prof. Dr. M. Grundmann, Prof. Dr. I. Mertig (Martin-Luther-Universität Halle-Witten-

berg)
SFB 762/2-2012, TP B06 within SFB 762 *Funktionalität Oxidischer Grenzflächen*

Bose-Einstein-Kondensation und Supraflüssigkeit von Exziton-Polaritonen bei Raumtemperatur
Prof. Dr. M. Grundmann, Dr. R. Schmidt-Grund
DFG GR 1011/20-2

Extrem verzerrte Nano- und Mikrodrähte
Prof. Dr. M. Grundmann
DFG GR 1011/23-1

Quantum Gases and Liquids in Semiconductor Rods conformally coated with Bragg Mirrors
Dr. R. Schmidt-Grund, Prof. Dr. M. Grundmann
DFG SCHM 2710/2-1, TP P1 within FOR 1616 *Dynamics and Interactions of Semiconductor Nanowires for Optoelectronics*

Oxidische topologische Isolator-Dünnfilme – Darstellung und elektronische Eigenschaften
Prof. Dr. M. Lorenz
DFG LO 790/5-1

Whispering Gallery Moden: Einfluss der Resonatorform auf Lasing-Eigenschaften
Prof. Dr. M. Grundmann
DFG GR 1011/26-1

Ortsaufgelöste nanomechanische Eigenschaften funktionaler Oberflächen – Experiment und Simulation
Prof. Dr. M. Grundmann, Prof. Dr. Dr. B. Rauschenbach (Leibniz-Institut für Oberflächenmodifizierung e. V.), Prof. Dr. S. Mayr (Leibniz-Institut für Oberflächenmodifizierung)
SAW-2011-IOM-2

Graduiertenschule: Wolken, Aerosole und Strahlung am Beispiel des Mineralstaubes
Prof. Dr. M. Grundmann, Prof. Dr. A. Macke (Leibniz-Institut für Troposphärenforschung e. V.)
SAW-2012-IfT-4

3D in situ Ellipsometrie
Dr. R. Schmidt-Grund, Dr. C. Bundesmann (Leibniz-Institut für Oberflächenmodifizierung e. V.)
Forschungs- und Entwicklungsvertrag im Rahmen der Förderung aus dem Europäischen Sozialfonds

Transparente photovoltaische Zellen
Prof. Dr. M. Grundmann
Europäischer Fonds für regionale Entwicklung (EFRE) Energie und Klimaschutz – RL EuK 2007

Leistungselektronik auf Basis von Galliumoxid
Prof. Dr. M. Grundmann
Europäischer Fonds für regionale Entwicklung (EFRE) Energie und Klimaschutz – RL EuK 2007

Effiziente Energienutzung: Neue Konzepte und Materialien
Prof. Dr. M. Grundmann
ESF-Nachwuchsforschergruppe des Freistaates Sachsen im Rahmen des Europäischen Sozialfonds

Elektron-Phonon-Wechselwirkung in Mikro- und Nanonadeln
Dipl.-Phys. Christian Kranert
Landesinnovationspromotionsstipendium des Freistaates Sachsen im Rahmen des Europäischen Sozialfonds

Magnetotunnel-Widerstände mit oxidischen Kontakten
Michael Bonholzer, M.Sc.
Landesinnovationspromotionsstipendium des Freistaates Sachsen im Rahmen des Europäischen Sozialfonds

Transparente MESFET für digitale Anwendungen
Prof. Dr. M. Grundmann, Dr. H. Frenzel
BMBF 03V0509

High-resolution fingerprint sensing with piezoelectric nanowire matrices: PiezoMat
Prof. Dr. M. Grundmann
European Union, Seventh Framework Programme 611019

Untersuchung und Verbesserung des Durchbruchverhaltens flexibler Dünnschichtsolarzellen
Prof. Dr. M. Grundmann, Solarion AG
IHK Förderung mit Projekten der regionalen Wirtschaft

Postdoctoral scholarship: Investigation of vertically stacked functional oxides
Dr. O. Sviridova
European Union: Stipendienprogramm Erasmus Mundus WEBB

9.29 Organizational Duties

M. Grundmann

- Prodekan Forschung der Fakultät für Physik und Geowissenschaften
- Direktor des Instituts für Experimentelle Physik II
- Stellvertretender Sprecher der Graduiertenschule "Leipzig School of Natural Sciences - Building with Molecules and Nano-objects" (BuildMoNa), http://www. buildmona.de
- Stellvertretender Sprecher des Sonderforschungsbereiches "Funktionalität Oxidischer Grenzflächen" (SFB762), http://www.physik.uni-halle.de/sfb762
- Sprecher der Fächerübergreifenden Arbeitsgemeinschaft Halbleiterforschung Leipzig (FAHL), http://www.uni-leipzig.de/~fahl

- Mitglied des wissenschaftlichen Beirats des Leibniz-Instituts für Oberflächenmodifizierung e. V., Leipzig (IOM)
- Member of the Advisory Committee of the 11th International Thin-Film Transistor Conference, Rennes, France
- Organizer MRS Fall Meeting, Boston, Symposium "Oxide Semiconductors"
- Project Reviewer: Deutsche Forschungsgemeinschaft (DFG), Alexander von Humboldt-Stiftung (AvH), Schweizerischer Nationalfonds zur Förderung der wissenschaftlichen Forschung (FNSNF), Fonds zur Förderung der Wissenschaften (FWF), EU, Österreichische Forschungsförderungsgesellschaft mbH (FFG), Agence Nationale de la Recherche (France)
- Referee: Appl. Phys. Lett., Electr. Lett., J. Appl. Phys., Nature, Physica E, Phys. Rev. B., Phys. Rev. Lett., Phys. Stat. Sol., Adv. Materials, u.a.

M. Lorenz

- Editorial board member J. Phys. D: Appl. Phys. (IOP)
- Project Reviewer: Deutsche Forschungsgemeinschaft (DFG)
- Referee: Advanced Functional Materials, Applied Physics Letters, Applied Surface Science , Crystal Growth and Design, European Physics Journal, IEEE Transactions on Nuclear Science, Journal of Physical Chemistry, Journal of Physics D: Applied Physics, Japanese Journal of Applied Physics, Materials Science and Engineering, Nanotechnology, Physica Status Solidi (a) and RRL, Thin Solid Films

H. von Wenckstern

- Project Reviewer: U.S. Department of Energy – Office of Science, National Research Fondation RSA
- Referee: Appl. Phys. Lett., J. Appl. Phys., Thin Solid Films, Solid State Electron., Phys. Stat. Sol., Superlatt. Microstruct., J. Electron. Mater., Turk. J. Phys., J. Mater. Sci., Mater. Electron., J. Vac. Sci. Technol., Mater. Sci. Eng. B, J. Nanosci. Nanotechnol., Microelectron. Eng., J. Phys. D, J. Cryst. Growth, Surf. Sci.

R. Schmidt-Grund

- Vice Chair of the German Association on Ellipsometry (Arbeitskreis Ellipsometrie – Paul Drude e.V.)
- Project Reviewer: Deutsche Forschungsgemeinschaft (DFG), US Department of Energy – Office of Science
- Referee: Thin Solid Films, Current Applied Physics, Phys. Stat. Sol. C, Nature Communications, Appl. Phys. Lett., Optics Express, Journal of Electromagnetic Waves and Applications, Opt. Materials, ACS Applied Materials & Interfaces

H. Frenzel

- Referee: IEEE Electronic Device Letters, Thin Solid Films, Applied Physics Letters, ETRI Journal, Journal of Applied Physics, Japanese Journal of Applied Physics, Advanced Materials, physics status solidi (a)

9.30 External Cooperations

Academic

- Leibniz-Institut für Oberflächenmodifizierung e. V., Leipzig, Germany
  Prof. Dr. B. Rauschenbach, Prof. Dr. S. Mayr, Dr. J. Gerlach, Dr. C. Bundesmann
- Universität Leipzig, Fakultät für Chemie und Mineralogie, Germany
  Prof. Dr. H. Krautscheid, Prof. Dr. R. Denecke
- Universität Halle-Wittenberg, Germany
  Prof. Dr. I. Mertig, Prof. Dr. W. Widdra, Prof. Dr. S.G. Ebbinghaus, Prof. Dr. W. Hergert
- Max-Planck-Institut für Mikrostrukturphysik, Halle/Saale, Germany
  Dr. O. Breitenstein, Dr. A. Ernst, Dr. P. Werner, Prof. Dr. D. Hesse
- Forschungszentrum Dresden-Rossendorf, Germany
  Prof. Dr. M. Helm, Dr. K. Potzger
- Technische Universität Berlin, Germany
  Prof. Dr. D. Bimberg, Prof. Dr. A. Hoffmann
- University of Aveiro, Portugal
  Prof. N. A. Sobolev
- Universität Gießen, Germany
  Prof. Dr. B. Meyer
- Universität Magdeburg, Germany
  Prof. Dr. A. Krost, Dr. J. Bläsing, Prof. Dr. J. Christen
- Universität Jena, Germany
  Prof. Dr. C. Ronning
- University of Pretoria, South Africa
  Prof. F. D. Auret
- University of Canterbury, Christchurch, New Zealand
  Prof. Dr. M. Allen
- Centre de Recherche sur l' Hétéro-Epitaxie et ses Applications (CNRS-CRHEA), Valbonne, France
  Dr. J. Zúñiga-Pérez
- Western Michigan University, USA
  Prof. Dr. S. M. Durbin
- Katholieke Universiteit Leuven, Belgium
  Dr. V. Lazenka, Prof. Dr. K. Temst

Industry

- Solarion AG, Leipzig Germany
  Dr. A. Braun, Dr. A. Rahm
- Freiberger Compound Materials GmbH, Freiberg, Germany
  Dr. G. Leibiger

9.31 Publications

Journals

T. Böntgen, K. Brachwitz, R. Schmidt-Grund, M. Lorenz, M. Grundmann: *Vacuum ultraviolet dielectric function of $ZnFe_2O_4$ thin films*, J. Appl. Phys. **113**(7), 073503 (4 pages)(2013)

K. Brachwitz, T. Böntgen, M. Lorenz, M. Grundmann: *On the transition point of thermally activated conduction of spinel-type MFe_2O_4 ferrite thin films (M=Zn,Co,Ni)*, Appl. Phys. Lett. **102**(17), 172104 (4 pages) (2013)

F. Daume, S. Puttnins, C. Scheit, H. Zachmann, A. Rahm, A. Braun, M. Grundmann: *Damp heat treatment of Cu(In,Ga)Se_2 solar cells with different sodium content*, Materials **6**, 5478-5489 (2013)

H. Frenzel, A. Lajn, M. Grundmann: *One decade of fully transparent oxide thin film transistors: fabrication, performance and stability*, phys. stat. sol. RRL **7**(9), 605-615 (2013)

M. Grundmann, F.-L. Schein, M. Lorenz, T. Böntgen, J. Lenzner, H. von Wenckstern: *Cuprous Iodide – a p-type transparent semiconductor: history and novel applications*, phys. stat. sol. (a)**210**, 1671-1703 (2013)

M. Jenderka, J. Barzola-Quiquia, Z. Zhang, H. Frenzel, M. Grundmann, M. Lorenz: *Mott variable range hopping and weak antilocalization effect in heteroepitaxial Na_2IrO_3 thin films*, Phys. Rev. B **88**(4), 045111 (6 pages) (2013)

F.J. Klüpfel, F.-L. Schein, M. Lorenz, H. Frenzel, H. von Wenckstern, M. Grundmann: *Comparison of ZnO-based JFET, MESFET, and MISFET*, IEEE Transact. Electr. Dev. **60**(6), 1828-1833 (2013)

C. Kranert, R. Schmidt-Grund, M. Grundmann: *Surface- and point-defect-related Raman scattering in wurtzite semiconductors excited above the band gap*, New J. Phys. **15**, 113048 (22 pages) (2013)

A. Lajn, H. von Wenckstern, M. Grundmann, G. Wagner, P. Barquinha, E. Fortunato, R. Martins: *Comparative study of transparent rectifying contacts on semiconducting oxide single crystals and amorphous thin films*, J. Appl. Phys. **113**(4), 044511 (13 pages) (2013)

M. Lange, C.P. Dietrich, M. Lorenz, M. Grundmann: *Excitonic and Optical Confinement in Microwire Heterostructures with Non-Polar (Zn,Cd)O/(Mg,Zn)O Multiple Quantum Wells*, J. Phys. Chem. C**117**(17), 9020-9024 (2013)

V.V. Lazenka, M. Lorenz, H. Modarresi, K. Brachwitz, P. Schwinkendorf, T. Böntgen, J. Vanacken, M. Ziese, M. Grundmann, V.V. Moshchalkov: *Effect of rare-earth ion doping on multiferroic properties of $BiFeO_3$ thin films grown epitaxially on $SrTiO_3$(100)*, J. Phys. D.: Appl. Phys. **46**(17), 175006 (9 pages) (2013)

M. Lorenz, C. Schmidt, G. Benndorf, T. Böntgen, H. Hochmuth, R. Böttcher, A. Pöppl, D. Spemann, M. Grundmann: *Degenerate interface layers in epitaxial scandium-doped ZnO thin films*, J. Phys. D: Appl. Phys. **46**(6), 065311 (10 pages) (2013)

M. Lorenz, M. Grundmann, S. Wickert, R. Denecke: *Oxidation state of tungsten oxide thin films used as gate dielectric for zinc oxide based transistors*, Proc. Mat. Res. Soc. **1494**, 1649 (4 pages) (2013)

M. Lorenz, M. Ziese, G. Wagner, P. Esquinazi, M. Grundmann: *Exchange bias and magnetoelectric coupling effects in $ZnFe_2O_4$-$BaTiO_3$ composite thin films*, Ext. Abstracts of the Nature Conference "Frontiers in Electronic Materials", Aachen, Germany (Nanosession: Multiferroic Thin Films and Heterostructures), J. Heber, D. Schlomm, Y. Tokura, R. Waser, M. Wuttig, eds., p. 334 (1 page) (2013)

M. Lorenz, M. Lange, C. Kranert, C.P. Dietrich, M. Grundmann: *Optical properties of and optical devices from ZnO-based nanostructures*, Zinc Oxide Nanostructures: Advances and Applications, (60 pages) (2013), M. Willander, ed. (Pan Stanford Publishing, Singapore, 2013), ISBN 9789814411332

A. Müller, M. Grundmann: *Tunneling dynamics of excitons in random semiconductor alloys*, Phys. Rev. B **87**(3), 035134 (5 pages) (2013)

S. Puttnins, S. Levcenco, K. Schwarzburg, G. Benndorf, F. Daume, A. Rahm, A. Braun, M. Grundmann, T. Unold: *Effect of Sodium on Material and Device Quality in Low Temperature Deposited Cu(In,Ga)Se_2*, Sol. Energy Mat. Sol. Cells **119**, 281-286 (2013)

F.-L. Schein, H. von Wenckstern, M. Grundmann: *Transparent p-CuI/n-ZnO heterojunction diodes*, Appl. Phys. Lett. **102**(9), 092109 (4 pages) (2013)

F. Schmidt, S. Müller, H. von Wenckstern, C.P. Dietrich, R. Heinhold, M.W. Allen, M. Grundmann: *Comparative Study of Deep Defects in ZnO Microwires, Thin Films and Bulk Single Crystals*, Appl. Phys. Lett. **103**(6), 062102 (4 pages) (2013)

R. Schmidt-Grund, T. Lühmann, T. Böntgen, H. Franke, D. Opper, M. Lorenz, M. Grundmann: *Temperature dependent dielectric function in the NIR-VUV spectral range of alumina and yttria stabilized zirconia thin films*, J. Appl. Phys. **114**, 223509 (8 pages)(2013)

P. Schwinkendorf, M. Lorenz, H. Hochmuth, Z. Zhang, M. Grundmann: *Interface charging effects in ferroelectric ZnO-$BaTiO_3$ field-effect transistor heterostructures*, phys. stat. sol. (a), published online (7 pages) (2013)

M. Stölzel, A. Müller, G. Benndorf, M. Brandt, M. Lorenz, M. Grundmann: *Determination of unscreened exciton states in polar ZnO/(Mg,Zn)O quantum wells with strong quantum-confined Stark effect*, Phys. Rev. B **88**(4), 045315 (6 pages) (2013)

A.A. Timopheev, A.M. Azevedo, N.A. Sobolev, K. Brachwitz, M. Lorenz, M. Ziese, P. Esquinazi, M. Grundmann: *Magnetic anisotropy of epitaxial zinc ferrite thin films grown by pulsed laser deposition*, Thin Solid Films **527**, 273-277 (2013)

H. von Wenckstern, Z. Zhang, F. Schmidt, J. Lenzner, H. Hochmuth, M. Grundmann: *Continuous composition spread using pulsed-laser deposition with a single, segmented target*, CrystEngComm **15**, 10020-10027 (2013)

Z. Zhang, H. von Wenckstern, M. Grundmann: *Energy-selective multichannel ultraviolet photodiodes based on (Mg,Zn)O*, Appl. Phys. Lett. **103**, 171111(4 pages) (2013)

J. Zippel, M. Lorenz, M. Lange, M. Stölzel, G. Benndorf, M. Grundmann: *Growth control of nonpolar and polar ZnO/$Mg_xZn_($1 – x)O quantum wells by pulsed-laser deposition*, J. Cryst. Growth **364**, 81-87 (2013)

J. Zippel, M. Lorenz, A. Setzer, M. Rothermel, D. Spemann, P. Esquinazi, M. Grundmann, G. Wagner, R. Denecke, A.A. Timopheev: *Defect-induced magnetism in homoepitaxial manganese stabilized zirconia thin films*, J. Phys. D: Appl. Phys. **46**(27), 275002 (10 pages) (2013)

J. Zippel, M. Lorenz, G. Wagner, J. Lenzner, M. Grundmann: *Martensitic phase transition and subsequent surface corrugation in manganese stabilized zirconia thin films*, Phil. Mag. **93**(18), 2329-2339 (2013)

Patents

M. Grundmann, H. Frenzel, A. Lajn, H. von Wenckstern: *TRANSPARENT RECTIFYING METAL/METAL OXIDE/SEMICONDUCTOR CONTACT STRUCTURE AND METHOD FOR THE PRODUCTION THEREOF AND USE*, CA 2765981 C (Canadian Intellectual Property Office, 2013)

M. Grundmann, H. Frenzel, A. Lajn, H. von Wenckstern: *Transparente gleichrichtende Metall-Metalloxid-Halbleiterkontaktstruktur und Verfahren zu ihrer Herstellung und Verwendung*, EP 2 446 484 B1 (European Patent Office, Munich, 2013)

M. Grundmann, H. Frenzel, A. Lajn, H. von Wenckstern: *TRANSPARENT RECTIFYING METAL/METAL OXIDE/SEMICONDUCTOR CONTACT STRUCTURE AND METHOD FOR THE PRODUCTION THEREOF AND USE*, US 8,445,904 B2 (United States Patent, 2013)

Talks

F. Daume, A. Rahm, M. Grundmann: *Admittance Spectroscopy Cu(In,Ga)Se_2 Solar Cells with respect to Na content*, 77th Spring Meeting of the German Physical Society 2013, Regensburg, Germany, March 2013

F. Daume, A. Rahm, A. Braun, M. Grundmann: *Sodium in the Degradation Process of Cu(In,Ga)Se_2 Solar Cells*, 28th EU-PVSEC, Paris, France, October 2013

C.P. Dietrich, T. Michalsky, C. Sturm, H. Franke, M. Lange, R. Schmidt-Grund, M. Grundmann: *BEC relaxation in a multimodal whispering-gallery exciton-polariton system*, 77th Spring Meeting of the German Physical Society 2013, Regensburg, Germany, March 2013

H. Frenzel, M. Lorenz, F. Klüpfel, F. L. Schein, A. Lajn, H. von Wenckstern, M. Grundmann: *Oxide-based devices for transparent electronics*, BuildMoNa Module 2013-A3/Herbstschule/ FAHL-Academia, Leipzig, Germany, October 2013

M. Grundmann: *Metalloxid-Dioden für die Dünnfilm-Elektronik*, Physikalisches Kolloquium der FNW, Otto-von-Guericke Universität Magdeburg, Magdeburg, Germany, January 2013, invited

M. Grundmann: *Das Praktikum Halbleiterphysik an der Universität Leipzig*, DPG-Schule der AG Physikalische Praktika, Bad Honnef, Germany, February 2013, invited

M. Grundmann: *Spectral and spatial overlap of oxide quantum wells and whispering gallery modes*, 77th Spring Meeting of the German Physical Society 2013, Regensburg, Germany, March 2013, invited

M. Grundmann: *Neuartige auf ZnO basierende photonische und elektronische Halbleiterstrukturen*, Physikalisches Kolloquium, Universität Paderborn, June 2013, invited

T. Jakubczyk, T. Smoleński, W. Pacuski, C. Kruse, H. Franke, M. Florian, F. Jahnke, A. Golnik, R. Schmidt-Grund, M. Grundmann, D. Hommel, P. Kossacki: *Effects of Light-Matter Weak Coupling in ZnTe-based Micropillar and Planar Cavities with CdTe Quantum Dots*, The 16th International Conference on II-VI Compound and Related Materials (II-VI 2013), Nagahama, Japan, September 2013

M. Jenderka, J. Barzola-Quiquia, Z. Zhang, H. Frenzel, M. Grundmann, M. Lorenz: *Weak Antilocalization in Na_2IrO_3 Thin Films*, Seminar, I. Physikalisches Institut, Georg-August-Universität Göttingen, Germany, April 2013

M. Jenderka, J. Barzola-Quiquia, Z. Zhang, H. Frenzel, M. Grundmann, M. Lorenz: *Mott Variable Range Hopping and Weak Antilocalization Effect in Heteroepitaxial Na_2IrO_3 Thin Films*, Seminar, Helmholtz-Zentrum Berlin für Materialien und Energie GmbH, Berlin, Germany, August 2013

F.J. Klüpfel, F.-L. Schein, M. Lorenz, H. Frenzel, H. von Wenckstern, M. Grundmann: *Comparison of ZnO-based JFET, MESFET and MISFET*, 55th Electronic Materials Conference, University of Notre Dame, USA, June 2013

C. Kranert, R. Schmidt-Grund, M. Grundmann: *The role of the surface in resonance Raman scattering in ZnO and other wurtzites*, 77th Spring Meeting of the German Physical Society 2013, Regensburg, Germany, March 2013

C. Kranert, T. Böntgen, J. Lenzner, R. Schmidt-Grund, H. von Wenckstern, M. Grundmann: *Optical properties of $(In_xGa_{1-x})_2O_3$ films grown by pulsed laser deposition*, MRS Fall Meeting, Boston, USA, December 2013

M. Lorenz, M. Jenderka: *Novel oxide semiconducting and multiferroic heterostructures by pulsed laser deposition: Weak antilocalization effect in Na2IrO3 thin films*, Seminar, I. Physikalisches Institut, Georg-August-Universität Göttingen, April 2013, invited

M. Lorenz: *From high-T_c superconductors to topological insulators – two decades pulsed laser deposition of functional oxides in Leipzig*, ICMAT2013 – The 7th International Conference on Materials for Advanced Technologies, Singapore, Republic of Singapore, July 2013, invited

M. Lorenz, J. Zippel, G. Benndorf, M. Grundmann: *Persistent layer-by layer growth for pulsed-laser epitaxy of ZnO films and nonpolar and polar QWs*, 14th Kinetikseminar – Workshop of the AK "Wachstumskinetik und Nanostrukturen" of DGKK, Berlin, Germany, November 2013

M. Lorenz: *Crystallization of fresnoite scintillator thin films by laser direct writing and in-situ CO_2 laser heating*, Indian Institute of Technology IIT Madras, Chennai, India, December 2013, invited

M. Lorenz: *Pulsed Laser Deposition of functional oxides for electronic applications*, International Conference in Asia (ICA) of the International Union of Materials Research Societies (IUMRS) IUMRS-ICA2013, Bangalore, India, December 2013, invited

T. Michalsky, H. Franke, C. Sturm, R. Schmidt-Grund, M. Grundmann: *Optically and structurally trapped exciton-polariton systems*, 77th Spring Meeting of the German Physical Society 2013, Regensburg, Germany, March 2013

S. Müller, H. von Wenckstern, F. Schmidt, D. Splith, M. Grundmann: *Structural and electrical properties of Si-doped beta-Ga_2O_3 thin films*, 77th Spring Meeting of the German Physical Society 2013, Regensburg, Germany, March 2013

S. Müller, H. von Wenckstern, F. Schmidt, D. Splith, M. Grundmann: *Structural and Electrical Properties of Si-doped beta-Ga_2O_3 Thin Films and Schottky Contacts Thereon*, 55th Electronic Material Conference 2013, University of Notre Dame, South Bend, USA, June 2013

R. Pickenhain, F. Schmidt, S. Geburt, C. Ronning, H. von Wenckstern, M. Grundmann: *Iron-induced gap states in ZnO thin films*, 77th Spring Meeting of the German Physical Society 2013, Regensburg, Germany, March 2013

S. Richter, C. Sturm, H. Franke, R. Schmidt-Grund, M. Grundmann: *Exciton-polariton pseudospin polarization in a planar microcavity*, 77th Spring Meeting of the German Physical Society 2013, Regensburg, Germany, March 2013

F.-L. Schein, H. von Wenckstern, M. Grundmann: *Transparent p-CuI/n-ZnO heterojunction diodes*, 55th Electronic Materials Conference, South Bend (IN), USA, June 2013

F.-L. Schein, P. Schlupp, H. von Wenckstern, M. Grundmann: *Highly rectifying pn-diodes based on amorphous $ZnCo_2O_4$ and ZnSnO*, 55th Electronic Materials Conference, South Bend (IN), USA, June 2013

P. Schlupp, F.-L. Schein, H.von Wenckstern, M. Grundmann: *Electrical und optical properties of room temperature deposited zinc tin oxide thin films and utilisation in all oxide amorphous heterodiodes*, 77th Spring Meeting of the German Physical Society 2013, Regensburg, Germany, March 2013

P. Schlupp, F.-L. Schein, H. von Wenckstern, M. Grundmann: *Electrical properties of highly rectifying contacts on amorphous zinc-tin-oxide thin films*, MRS Fall Meeting, Boston, USA, December 2013

F. Schmidt, S. Müller, R. Pickenhain, H. von Wenckstern, S. Geburt, C. Ronning, M. Grundmann: *Defect studies on Ar-implanted ZnO thin films*, MRS Fall Meeting, Boston, USA, December 2013

F. Schmidt, H. von Wenckstern, S. Müller, D. Spemann, M. Grundmann: *Irradiation studies on differently orientated ZnO thin films*, 77th Spring Meeting of the German Physical Society 2013, Regensburg, Germany, March 2013

D. Splith, S. Müller, H. von Wenckstern, M. Grundmann: *Schottky contacts on β-Ga_2O_3 thin films grown by pulsed laser deposition*, 77th Spring Meeting of the German Physical Society 2013, Regensburg, Germany, March 2013

M. Thunert, H. Franke, C. Sturm, R. Schmidt-Grund, A. Janot, B. Rosenow, M. Grundmann: *Influence of disorder on the propagation of polariton BEC*, 77th Spring Meeting of the German Physical Society 2013, Regensburg, Germany, March 2013

H. von Wenckstern: *Transparent semiconducting oxides – from materials to devices*, lecture at Johannes Kepler Universität, Linz, Austria, November 2013, invited

H. von Wenckstern: *Wide band-gap semiconductors: From materials to devices*, lecture, Bergakademie Freiberg, Institut für Elektronik und Sensormaterialien, Freiberg, Germany, October 2013, invited

H. von Wenckstern: *Transparent semiconducting oxides – from materials to devices*, 42nd "Jazowiec" International School and Conference on the Physics of Semiconductors, Wisla, Poland, June 2013

H. von Wenckstern: *Ga_2O_3 – Ein neues Material für Leistungselektronik*, TCO workshop of European Society of Thin Films, Dresden, Germany, June 2013

Posters

M. Bonholzer, K. Brachwitz, M. Lorenz, A. Setzer, M. Ziese, P. Esquinazi, M. Grundmann: *Zinc ferrite, an oxide for spintronics?*, 77th Spring Meeting of the German Physical Society 2013, Regensburg, Germany, March 2013

M. Bonholzer, K. Brachwitz, M. Lorenz, A. Setzer, M. Ziese, P. Esquinazi, M. Grundmann: *Zinc ferrite, an oxide for spintronics?*, ISOE 2013 Cargèse, France, September 2013

T. Böntgen, K. Brachwitz, R. Schmidt-Grund, M. Lorenz, M. Grundmann: *$ZnFe_2O_4$ dielectric function*, 77th Spring Meeting of the German Physical Society 2013, Regensburg, Germany, March 2013

T. Böntgen, J. Lorbeer, M. Teichmann, F. Frost, R. Schmidt-Grund, M. Grundmann: *Investigation of surface plasmons on structured surfaces*, 77th Spring Meeting of the German Physical Society 2013, Regensburg, Germany, March 2013

T. Böntgen, V. Zviagin, K. Brachwitz, F. Schein, M. Lorenz, R. Schmidt-Grund, M. Grundmann: *Ellipsometric study of $ZnFe_2O_4$ and $ZnCo_2O_4$ spinel oxides*, 6th International Conference on Spectroscopic Ellipsometry (ICSE-VI), Kyoto, Japan, May 2013

K. Brachwitz, T. Böntgen, A. Setzer, M. Lorenz, P. Esquinazi, M. Grundmann: *Defect-induced conduction mechanism and magnetism in spinel-type ferrites*, 6th European School on Multiferroics, Lutherstadt Wittenberg, Germany, July 2013

K. Brachwitz, T. Böntgen, M. Lorenz, M. Grundmann: *Defect-induced conduction mechanism in MFe_2O_4 thin films (M = Zn, Co, Ni)*, 77th Spring Meeting of the German Physical Society 2013, Regensburg, Germany, March 2013

F. Daume, A. Rahm, S. Puttnins, A. Braun, M. Grundmann: *Sodium in the Degradation Process of Cu(In,Ga)Se_2 Solar Cells*, MRS Spring Meeting, San Francisco, USA, April 2013

H. Franke, R. Schmidt-Grund, T. Jakubczyk, C. Sturm, T. Michalsky, W. Pacuski, C. Kruse, D. Hommel, P. Kossacki, T. Smoleński, M. Grundmann: *Lateral confinement of micro-pillar cavities by conformal distributed Bragg reflector coating*, 5th International Conference on One Dimensional Nanomaterials (ICON), Annecy, France, September 2013

L. Fricke, T. Böntgen, J. Lorbeer, J. Lenzner, R. Schmidt-Grund, M. Grundmann: *Surface modification of ZnO bulk single crystals in vacuum*, 77th Spring Meeting of the German Physical Society 2013, Regensburg, Germany, March 2013

J. Hartmann, L. Caccamo, S. Merzsch, X. Wang, M. Thunert, H. Franke, R. Schmidt-Grund, Hergo-Heinrich Wehmann, M. Grundmann, A. Waag: *DBR for 3D-GaN-LEDs*, 77th Spring Meeting of the German Physical Society 2013, Regensburg, Germany, March 2013

T. Jakubczyk, H. Franke, T. Smoleński, W. Pacuski, A. Golnik, C. Kruse, D. Hommel, R. Schmidt-Grund, M. Grundmann, P. Kossacki: *Enhancement and inhibition of spontaneous emission of CdTe quantum dots*, 42nd International School & Conference on the Physics of Semiconductors, Jaszowiec, Poland, June 2013

M. Jenderka, J. Barzola-Quiquia, Z. Zhang, H. Frenzel, M. Grundmann, M. Lorenz: *Mott Variable Range Hopping and Weak Antilocalization Effect in Heteroepitaxial Na_2IrO_3 Thin Films*, Symposium on Quantum Hall Effects and Related Topics, MPI for Solid State Research Stuttgart, Germany, June 2013

M. Jenderka, J. Barzola-Quiquia, Z. Zhang, H. Frenzel, M. Grundmann, M. Lorenz: *Mott Variable Range Hopping and Weak Antilocalization Effect in Heteroepitaxial Na_2IrO_3 Thin Films*, SPP1666 Kickoff Meeting, Frankfurt, Germany, October 2013

F.J. Klüpfel, F.-L. Schein, M. Lorenz, H. Frenzel, H. von Wenckstern, M. Grundmann: *Comparison of ZnO-based JFET, MESFET and MISFET*, 77th Spring Meeting of the German Physical Society 2013, Regensburg, Germany, March 2013

T. Lühmann, T. Böntgen, H. Franke, R. Schmidt-Grund, M. Grundmann: *Temperature dependent dielectric function of yttria stabilized zirconia and alumina*, 77th Spring Meeting of the German Physical Society 2013, Regensburg, Germany, March 2013

T. Michalsky, M. Thunert, H. Franke, C. Sturm, R. Schmidt-Grund, M. Grundmann: *Discrete relaxation of uncondensed exciton-polaritons in an inhomogeneous potential*, 14th Conference on Physics of Light-Matter Coupling in Nanostructures, Hersonissos, Crete, Greece, May 2013

T. Michalsky, S. Richter, M. Thunert, C. Sturm, H. Franke, C.P. Dietrich, M. Grundmann, R. Schmidt-Grund: *Overview of fabrication and optical characterization techniques for ZnO-based microcavities in Leipzig*, International School of Nanophotonics and Photovoltaics 2013, Maratea, Italy, August-September 2013

T. Michalsky, S. Richter, M. Thunert, C. Sturm, H. Franke, C.P. Dietrich, M. Grundmann, R. Schmidt-Grund: *Overview of current research on exciton-polaritons in ZnO-based microcavities in Leipzig*, International School of Nanophotonics and Photovoltaics 2013, Maratea, Italy, August-September 2013

T. Michalsky, H. Franke, M. Thunert, C.P. Dietrich, C. Sturm, R. Schmidt-Grund, P. Eastham, M. Grundmann: *Relaxation processes in ZnO*, 13th International Conference on Optics of Excitons in Confined Systems - OECS 13, Rome, Italy, September 2013

R. Pickenhain, F. Schmidt, O. Breitenstein, H. von Wenckstern, M. Grundmann: *Low Rate Deep Level Transient Spectroscopy: A new method for detecting deep levels in wide gap semiconductors*, 77th Spring Meeting of the German Physical Society 2013, Regensburg, Germany, March 2013

M. Purfürst, D. Splith, S. Müller, Z. Zhang, H. von Wenckstern, M. Grundmann: *Metal-semiconductor-metal photodetectors based on $(Ga_{1-x}In_x)_2O_3$ thin films*, 55th Electronic Material Conference 2013, University of Notre Dame, South Bend, USA, June 2013

M. Purfürst, D. Splith, C. Kranert, S. Müller, Z. Zhang, H. von Wenckstern, M. Grundmann: *Solar blind UV-photodetectors based on PLD-grown $(Ga_{1-x}\ In_x)_2O_3$ thin films: Characterization of the material, Schottky contacts and photoresponse*, MRS Fall Meeting, Boston, USA, December 2013

A. Reinhardt, M. Lorenz, H. von Wenckstern, M. Grundmann: *Optimization of (Mg,Zn)O-based thin-film transistors with high-k WO_3 dielectric gates*, 77th Spring Meeting of the German Physical Society 2013, Regensburg, Germany, March 2013

S. Richter, C. Sturm, H. Franke, R. Schmidt-Grund, M. Grundmann: *Exciton-polariton pseudospin in a planar ZnO-based microcavity under external magnetic fields*, 77th Spring Meeting of the German Physical Society 2013, Regensburg, Germany, March 2013

S. Richter, C. Sturm, M. Thunert, H. Franke, R. Schmidt-Grund, M. Grundmann: *Exciton-polariton pseudospin under external magnetic fields*, 14th Conference on Physics of Light-Matter Coupling in Nanostructures (PLMCN), Hernissos, Greece, May 2013

S. Richter, C. Sturm, M. Thunert, H. Franke, R. Schmidt-Grund, M. Grundmann: *Anisotropy of the g-factor of Exciton-Polaritons in a Planar Microcavity*, 13th International Conference on Optics of Excitons in Confined Systems - OECS 13, Rome, Italy, September 2013

F.-L. Schein, H. von Wenckstern, M. Grundmann: *Transparent p-CuI/n-ZnO heterojunction diodes*, 77th Spring Meeting of the German Physical Society 2013, Regensburg, Germany, March 2013

F.-L. Schein, P. Schlupp, T. Böntgen, J. Lenzner, M. Lorenz, H. von Wenckstern, M. Grundmann: *Transparent p-CuI/n-ZnO heterojunction diodes*, MRS Fall Meeting, Boston, USA, December 2013

F. Schmidt, P. Schlupp, S. Müller, C.P. Dietrich, H. von Wenckstern, M. Grundmann, R. Heinhold, H.-S. Kim, M.W. Allen: *A DLTS study of ZnO microwire, thin film and bulk material*, MRS Fall Meeting, Boston, USA, December 2013

R. Schmidt-Grund, C. P. Dietrich, T. Michalsky, H. Franke, C. Sturm, A. Meißner, M. Grundmann: *Relaxation effects in a ZnO microwire*, International Workshop "Out-of-equilibrium dynamics of 1D condensates", Palaiseau, France, May 2013.

R. Schmidt-Grund, T. Böntgen, L. Fricke, J. Lorbeer, C. Grüner, J. Bauer, C. Sturm, M. Teichmann, J. Lenzner, F. Frost, B. Rauschenbach, M. Grundmann: *Ellipsometry investigation of natural and functional nano-structured surfaces*, 6th International Conference on Spectroscopic Ellipsometry (ICSE-VI), Kyoto, Japan, May 2013

R. Schmidt-Grund, C.P. Dietrich, T. Michalsky, H. Franke, C. Sturm, M. Lange, R. Johne, P. Eastham, M. Grundmann: *ZnO whispering gallery mode resonators - weak and strong exciton-photon coupling*, 5th International Conference on One Dimensional Nanomaterials (ICON), Annecy, France, September, 2013

D. Splith, C. Kranert, S. Müller, H. von Wenckstern, M. Grundmann: *Schottky contacts on β-Ga_2O_3 thin films grown by pulsed laser deposition*, MRS Fall Meeting, Boston, USA, December 2013

M. Thunert, H. Krauß, H. Franke, C. Sturm, R. Schmidt-Grund, M. Grundmann: *Strong light-matter coupling between photons and several excitonic states in ZnO-based microcavities*, 77th Spring Meeting of the German Physical Society 2013, Regensburg, Germany, March 2013

M. Thunert, A. Janot, H. Franke, C. Sturm, T. Michalsky, S. Richter, R. Schmidt-Grund, B. Rosenow, M. Grundmann: *Influence of disorder on the propagation of polariton BEC*, 14th Conference on Physics of Light-Matter Coupling in Nanostructures (PLMCN), Hernissos, Greece, May 2013

K. Xhaxhiu, C. Kvarnström, P. Damlin, R. Schmidt-Grund, K. Bente: *Photochromatic sensors of multinary mixed valence inorganic micro needles*, 21st Annual Conference of the German Crystallographic Society, Freiberg, March 2013

V. Zviagin, T. Böntgen, R. Schmidt-Grund, M. Lorenz, M. Grundmann: *Optical and structural properties of $ZnCo_2O_4$ under different growth conditions*, 77th Spring Meeting of the German Physical Society 2013, Regensburg, Germany, March 2013

9.32 Graduations

Doctorate

- Michael Lorenz
  ZnO-basierte Metall-Isolator-Halbleiter Feldeffekttransistoren mit Wolframoxid als Gatedielektrikum
  February 2013

Diploma

- Simon Englisch
  Elektrische und optische Charakterisierung flexibler Cu(In,Ga)Se_2 Solarzellen im Rahmen des Prozesstransfers von Pilotlinie zur Massenproduktion
  June 2013

Master

- Eike Lennart Fricke
  In-situ Ellipsometrie an Zinkoxideinkristalloberflächen
  February 2013
- Christian Heinrichs
  Aufbau eines Ellipsometers zur Messung der vollständigen Müller-Matrix
  February 2013
- Oliver Kramer
  Untersuchung von elektronischen Defektzuständen in ternären MgZnO-Dünnfilmen mittels optischer Kapazitätsspektroskopie
  January 2013
- Marcus Purfürst
  Herstellung und Charakterisierung von Ultraviolett-Photodetektoren auf Indium-Galliumoxid-Basis
  July 2013
- Peter Schlupp
  Züchtung und elektrische Charakterisierung amorpher Zink-Zinn-Oxid Dünnfilme
  February 2013
- Daniel Splith
  Schottky-Kontakte auf β-Galliumoxid-Dünnfilmen: Herstellung und elektrische Charakterisierung
  March 2013

Bachelor

- Sofie Bitter
  Influence of Thermal Annealing on the Electrical and Optical Properties of Amorphous Zinc-Tin-Oxide
  February 2013
- Christian Dähne
  Ramanstreuung an Indium-Gallium-Oxid
  October 2013
- Thomas Els
  Struktur und elektrische Eigenschaften von homoepitaktischen Al-dotierten ZnO-Dünnfilmen
  May 2013
- Max Kneiß
  Charakterisierung von undotierten und Ni-, Cr- und W-dotierten Titandioxid-Dünnfilmen gezüchtet mit PLD
  April 2013

- Robert Staacke
  Kompensation von Zinkoxid-Dünnfilmen durch den Einbau von Kupfer
  July 2013
- Franz Vogt
  Ionenstrahldissoziation von Selen
  October 2013
- Tobias Weiß
  Struktur und elektronische Eigenschaften von homoepitaktischen Ga-dotierten ZnO Dünnfilmen
  November 2013

9.33 Guests

- Dr. Olga Sviridova
  Odessa National Polytechnic University, Ukraine
  September 2013 – July 2014

10

Superconductivity and Magnetism

10.1 Introduction

The main interests of the group at the division are phenomena related to superconductivity and magnetism in solids. In the last few years the research activities in superconductivity have been mainly concentrated in searching for its existence in graphite, especially at graphite interfaces between Bernal-like crystalline regions. This research issue started in our division in Leipzig in the year 2000 and became supporting experimental evidence quite recently, indicating the existence of superconductivity at temperatures above 100 K. Future work will be concentrated in the localization of the superconducting phases and the increase of the superconducting yield.

Our division was the first to show that atomic lattice defects can produce magnetic order in graphite without the need of magnetic ions. This phenomenon is known nowadays as Defect-Induced Magnetism and it is found in a broad spectrum of different materials. Within a collaborative research project we further work on the emergence of this phenomenon in nominally non-magnetic oxides, via vacancies and/or non-magnetic-ions doping. Magnetic order has been obtained already in oxide thin films as well as in nanowires. Further research topic is the study of the electrical and magnetic properties of oxide multilayers of thickness starting from a few unit cells. Main research issues are related to the magnetic coupling at the interfaces of oxide layers, i.e. exchange bias phenomena, with different magnetic properties as well as the possibility to develop a two-dimensional electron gas at the interfaces.

Pablo Esquinazi

10.2 Josephson-coupled superconducting regions embedded at the interfaces of highly oriented pyrolytic graphite

A. Ballestar, J. Barzola-Quiquia, T. Scheike, P. Esquinazi

Transport properties of a few hundreds of nanometers thick (in the graphene plane direction) lamellae of highly oriented pyrolytic graphite (HOPG) were investigated.

Current-voltage characteristics as well as the temperature dependence of the voltage at different fixed input currents provide evidence for Josephson-coupled superconducting regions embedded in the internal two-dimensional interfaces of HOPG. The resistance shows a sharp drop as a function of temperature, reaching zero resistance at low enough temperatures, see figure 10.1. The current-voltage characteristics are nonlinear and reminiscent of a Josephson junction. The temperature dependence of the critical current follows the Ambegaokar-Halperin model. Critical temperatures were in the region between 15 K and 150 K.

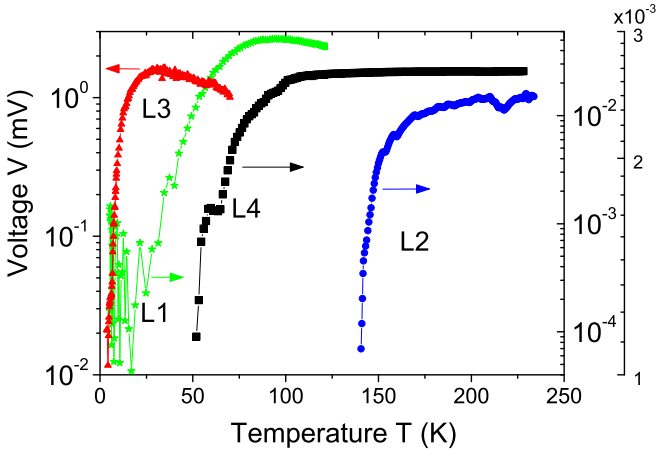

Figure 10.1: Temperature dependence of the voltage in a logarithmic scale for four samples. A clear drop in the measured voltage is observed at 15 K < T <150 K upon sample. For sample L4, the region near the onset of voltage decrease is shown (second right y-axis).

10.3 Exchange bias in manganite/$SrRuO_3$ superlattices

M. Ziese, F. Bern, I. Vrejoiu*

*Max Planck Institute of Microstructure Physics, 06120 Halle, Germany

The magnetization processes in $Pr_{0.7}Ca_{0.3}MnO_3/SrRuO_3$ and $La_{0.7}Sr_{0.3}MnO_3/SrRuO_3$ superlattices were studied. In both superlattices the ferromagnetic layers were antiferromagnetically coupled across the interfaces. Whereas superlattice $La_{0.7}Sr_{0.3}MnO_3/SrRuO_3$ showed a three-step magnetization reversal mechanism for all temperatures, superlattice $Pr_{0.7}Ca_{0.3}MnO_3/SrRuO_3$ had a compensation point with a two-step below and a three-step reversal mechanism above the compensation temperature. Exchange-bias and coercive fields, the vertical magnetization shift as well as the minor loop opening were measured as a function of the cooling field. Main findings were a change of the exchange-bias field from negative to positive values for increasing cooling fields in the two-step reversal regime and from negative values to zero for increasing cooling fields in the three-step reversal regime, see figure 10.2. Exchange-bias training occurs mostly within the first magnetization cycle. The data are consistent with the formation of interfacial domain walls.

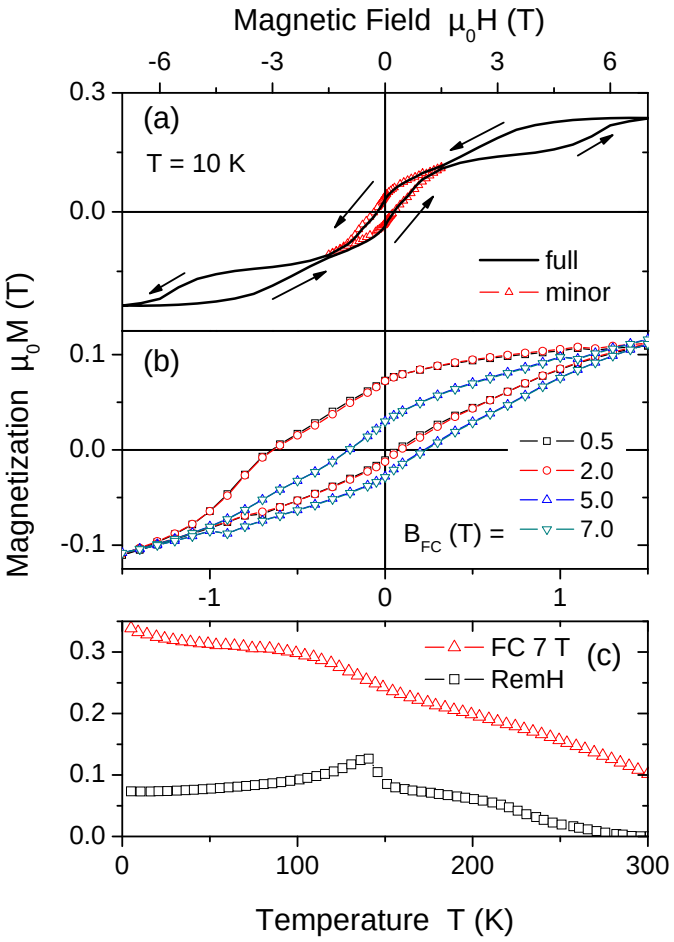

Figure 10.2: Magnetization data of sample LSMO/SRO. (a) Full hysteresis loop and minor loop with field amplitude of 1.5 T at 10 K. The minor loop was measured after ZFC and subsequent application of +7 T. (b) Minor loops measured after FC in B_{FC} at 10 K. (c) FC magnetization in 7 T and remanent magnetization (RemH) as a function of temperature. The remanence was measured after FC in +7 T and removing the field at 5 K.

10.4 Transport properties of single TiO_2 nanotubes

M. Stiller, J. Barzola-Quiquia, I. Lorite, P. Esquinazi, R. Kirchgeorg*, S.P. Albu*, P. Schmuki*†

*Chair for Surface Science and Corrosion, Department Material Science and Engineering, University of Erlangen, D-91058 Erlangen, Germany

†Department of Chemistry, King Abdulaziz University, Jeddah, Saudi Arabia

The electric transport properties of single TiO_2 nanotubes separated from an anodic titania nanotube array, see figure 10.3, were studied. The temperature dependence of the resistance measured with the conventional four point method of all investigated samples showed Mott variable range hopping behavior. The results obtained with two contacts indicate the existence of a potential barrier between the Cr/Au contacts and the sample surfaces, which influence is clearly observable at temperatures < 150 K. Impedance spectroscopy in the frequency range of 40 Hz to 1 MHz carried out at room temperature indicates that the electronic transport of these polycrystalline tubes was dominated by the grain cores.

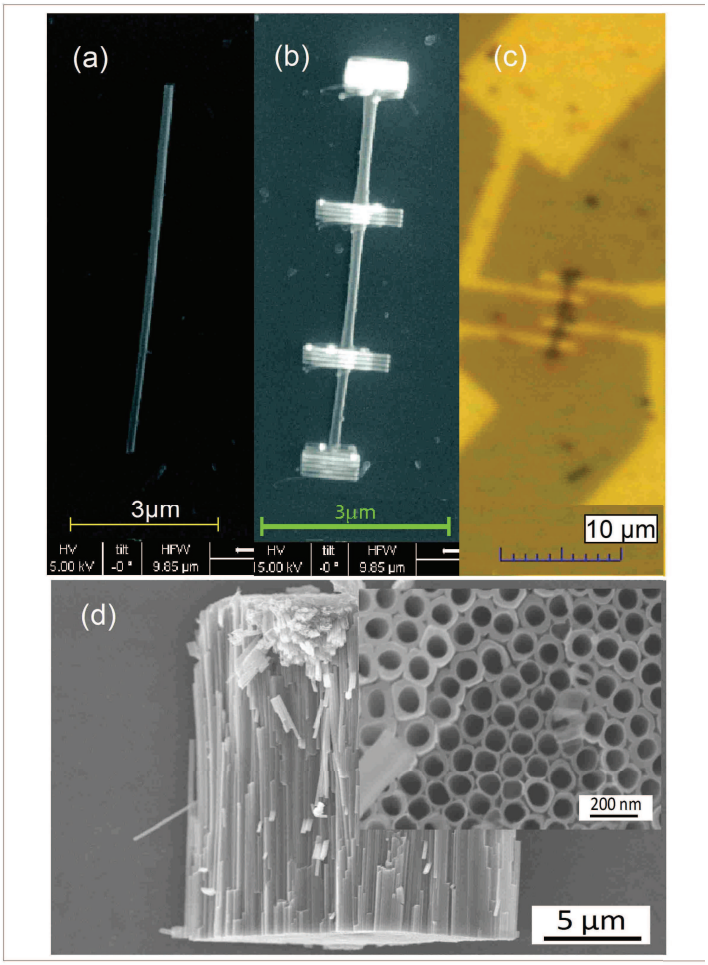

Figure 10.3: (a) A TiO_2 nanotube before fixing it on the substrate. (b) The nanotube fixed with WC_x . (c) After producing the electrical contacts. (d) Scanning electron microscope side and top views (inset) of a bundle of TiO_2 nanotubes.

10.5 Structural, magnetic and electrical properties of $SrRuO_3$ films and $SrRuO_3/SrTiO_3$ superlattices

F. Bern, M. Ziese, A. Setzer, E. Pippel*, D. Hesse,* I. Vrejoiu*

*Max Planck Institute of Microstructure Physics, 06120 Halle, Germany

$SrRuO_3$ films and $SrRuO_3/SrTiO_3$ superlattices grown on $SrTiO_3$ (001) were studied by structural, magnetic, magnetoresistance and Hall effect measurements. The superlattices showed heteroepitaxial growth with coherent interfaces and a Ru/Ti diffusion region of 1-1.5 unit cells. The resistivity had metallic character above a critical thickness of 3-4 unit cells, becoming insulating below. There was no hint of conduction processes along the interfaces. Both magnetization and magnetoresistance measurements showed an increase of the magnetic anisotropy, consistent with magnetostriction effects. The magnetostriction coefficient was estimated to $\lambda_{100} \sim 1.4 \times 10^{-4}$. Three unit cell thick $SrRuO_3$ layers in $SrRuO_3/SrTiO_3$ superlattices were found to have tetragonal crystal symmetry, as deduced from the sign change of the anomalous Hall constant,

see figure 10.4.

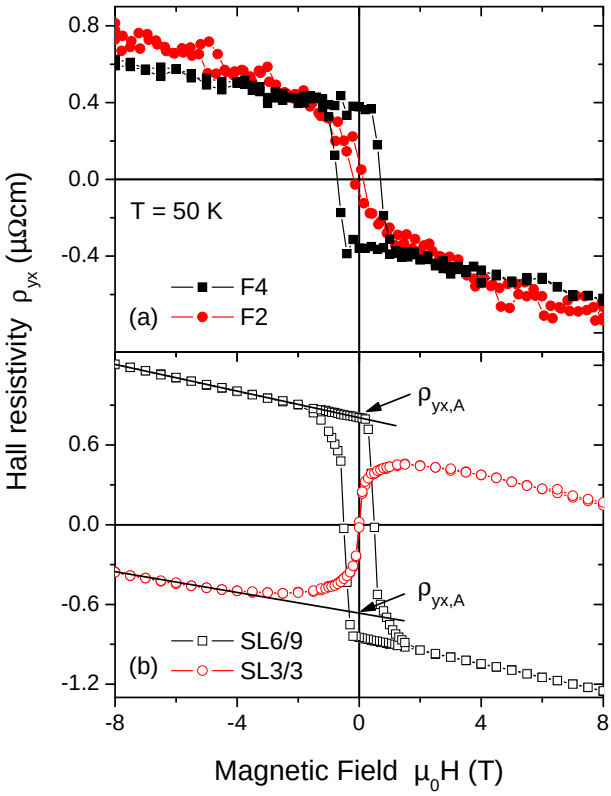

Figure 10.4: Hall effect of (a) 2 and 4 unit cell thick $SrRuO_3$ films as well as (b) superlattices SL6 u.c./9 u.c. and SL3u.c. /3 u.c. as a function of magnetic field at 50 K. The solid lines in (b) are asymptotes to the high field Hall effect. $\rho_{yx,A}$ denotes the anomalous Hall contribution as determined by the extrapolation of the high field slope to zero.

10.6 Granular superconductivity at room temperature in bulk highly oriented pyrolytic graphite samples

T. Scheike, P. Esquinazi, A. Setzer, W. Böhlmann

The magnetic response of two bulk highly oriented pyrolytic graphite (HOPG) samples with different internal microstructure was studied. For the sample with well defined interfaces, parallel to the graphene layers, the temperature and magnetic field hysteresis are similar to those found recently in water-treated graphite powders, see figure 10.5. The observed behavior suggests the existence of granular superconductivity above room temperature in agreement with previous reports in other graphite samples. The granular superconductivity behavior is observed only for fields normal to the embedded interfaces, whereas no relevant hysteresis in temperature or field is observed for fields applied parallel to them. Increasing the temperature above 400 K changes irreversibly the hysteretic response of the sample.

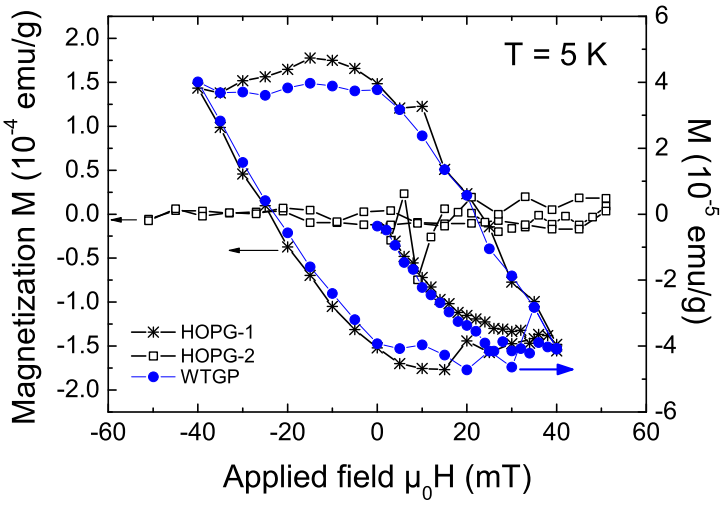

Figure 10.5: Magnetic field loops of the magnetization for fields applied normal to the graphene layers of the two HOPG samples (left *y*-axis) and of the water treated graphite powder. Linear diamagnetic backgrounds were subtracted from the measured signals

10.7 Existence of a magnetically ordered hole gas at the $La_{0.7}Sr_{0.3}MnO_3/SrRuO_3$ interface

M. Ziese, F. Bern, A. Setzer, E. Pippel*, D. Hesse,* I. Vrejoiu*

*Max Planck Institute of Microstructure Physics, 06120 Halle, Germany

The study of spatially confined complex oxides is of wide interest, since correlated electrons at interfaces might form new states of matter. Here $La_{0.7}Sr_{0.3}MnO_3/SrRuO_3$ superlattices with coherently grown interfaces and layer thicknesses down to 1 unit cell were fabricated by pulsed laser deposition. The superlattices were studied by x-ray, HRTEM, magnetization and magnetotransport measurements. For such small thicknesses $La_{0.7}Sr_{0.3}MnO_3$ *films* are antiferromagnetic and insulating. Despite the small layer thickness, the $La_{0.7}Sr_{0.3}MnO_3$ *layers* in the superlattices were ferromagnetic with Curie temperatures close to room temperature. Whereas the resistivity of the superlattices showed metallic behaviour and was dominated by the conducting $SrRuO_3$ layers, the off-diagonal resistivity showed an anomalous Hall effect with ferromagnetic loop shape even far above the Curie temperature of the $SrRuO_3$ layers as well as a positive high field slope. This indicates the presence of a highly conducting, ferromagnetically ordered hole gas at the interfaces that might be formed by a charge-transfer process. This result opens up an alternative route for the fabrication of quasi-two-dimensional systems.

10.8 Funding

Study of intrinsic and extrinsic phenomena in the electrical transport properties of multigraphene
Prof. Dr. Pablo Esquinazi
DFG ES 86/16-1

Defect-induced Magnetism in Oxides
Prof. Dr. Pablo Esquinazi
DFG SFB 762/2, B1

Magnetic and electric properties of oxide superlattices with ultrathin single layers
Prof. Dr. Pablo Esquinazi and Prof. Dr. Michael Ziese
DFG SFB 762/2, B5

Untersuchung des Einflusses von Leerstellen und Wasserstoff auf die elektrischen, magnetischen und optischen Eigenschaften von ZnO und $Mg_xZn_{1-x}O$ Nanostrukturen
Prof. Dr. Pablo Esquinazi
DAAD-PROALAR

Development of nanostructured ZnO Biosensors for the detection of very low concentration of analytes in Biomedical Applications
Prof. Dr. Pablo Esquinazi
BMBF-NANOTEC (ARG 11/033)

Superconducting Properties of Graphite Interfaces
Prof. Dr. Pablo Esquinazi
DAAD-PROBRAL

10.9 Organizational Duties

P. Esquinazi

- Dean of Studies (until October 2013)
- Project Reviewer: Deutsche Forschungsgemeinschaft (DFG), National Science Foundation (USA), German-Israeli Foundation (GIF), Israel Science Foundation, Department of Energy (Washington), DAAD
- Referee: Phys. Rev. Lett, Phys. Rev. B., Appl. Phys. Lett., Chem. Phys. Lett., Nature Physics, Nature Materials, Physica C, Phys. Lett. A, phys. stat. sol., J. Low Temp. Phys., Carbon, J. Chem. Phys., Eur. J. Phys. B, J. Magn. Magn. Mater.

M. Ziese

- Head of the Undergraduate Physics Laboratory
- Dean of Studies (from October 2013)
- Referee: Phys. Rev. Lett., Phys. Rev. B., Adv. Mater., Appl. Phys. A, Current Nanoscience, Eur. Phys. J. B, IEEE Trans. Magn., J. Phys.: Condens. Matter, J. Phys. D: Appl. Phys., J. Alloys Comp., J. Appl. Phys., J. Am. Ceram. Soc., J. Magn. Magn. Mater., J. Mater. Research, J. Mater. Science, Materials Science and Engineering B, Nanotechnology, phys. stat. sol., Thin Solid Films

W. Böhlmann

- Referee: J. Physical Chemistry, J. of American Chemical Society, Microporous and Mesoporous Materials

10.10 External Cooperations

Academic

- State University of Campinas, Campinas, Brazil
  Prof. Dr. Yakov Kopelevich
- Max-Planck Institute of Microstructure Physics, Halle, Germany
  Dr. Ionela Vrejoiu
- Max-Planck Institute of Microstructure Physics, Halle, Germany
  Prof. Dietrich Hesse
- Max-Planck Institute of Microstructure Physics, Halle, Germany
  Dr. Marin Alexe
- Max-Planck Institute of Microstructure Physics, Halle, Germany
  Dr. Arthur Ernst
- Martin-Luther Universität Halle-Wittenberg, Halle, Germany
  Prof. Ingrid Mertig
- Martin-Luther Universität Halle-Wittenberg, Halle, Germany
  Prof. Wolfram Hergert
- Martin-Luther Universität Halle-Wittenberg, Halle, Germany
  Dr. Angelika Chassé
- Martin-Luther Universität Halle-Wittenberg, Halle, Germany
  Dr. Manfred Dubiel
- Stanford Synchrotron Radiation Laboratory, USA
  Dr. Hendrik Ohldag
- Max-Planck-Institut für Metallforschung, Stuttgart, Germany
  Dr. Eberhard Goering
- Laboratorio de Física de Sistemas Pequeños y Nanotecnologíia, Consejo Superior de Investigaciones Científicas, Madrid, Spain
  Prof. N. García (Madrid)
- Forschungszentrum Dresden-Rossendorf e.V., Institut für Ionenstrahlphysik und Materialforschung, Germany
  Dr. W. Anwand
- Forschungszentrum Dresden-Rossendorf e.V., Institut für Ionenstrahlphysik und Materialforschung, Germany
  Dr. G. Brauer
- Tucuman University, Argentina
  Prof. S. P. de Heluani
- University of La Plata, Argentina
  Dr. C. E. Rodriguez Torres
- Universidad Autónoma de Madrid, Spain
  Prof. Dr. Miguel Angel Ramos
- University of Ioannina, Greece, Ioannina, Greece
  Prof. I. Panagiotopoulos

10.11 Publications

Journals

F. Bern, M. Ziese, K. Dörr, A. Herklotz, and I. Vrejoiu:
Hall effect of tetragonal and orthorhombic $SrRuO_3$ films
Phys. Status Solidi RRL **7**, 204 (2013)

M. Ziese and I. Vrejoiu:
Invited review: Properties of manganite/ruthenate superlattices with ultrathin layers
Phys. Status Solidi RRL **7** 243 (2013)

A. A. Timopheev, A. M. Azevedo, N. A. Sobolev, K. Brachwitz, M. Lorenz, M. Ziese, P. Esquinazi, and M. Grundmann:
Magnetic anisotropy of epitaxial zinc ferrite thin films grown by pulsed laser deposition
Thin Solid Films **527**, 273 (2013)

M. Ziese, F. Bern, A. Setzer, E. Pippel, D. Hesse, and I. Vrejoiu:
Existence of a magnetically ordered hole gas at the $La_{0.7}Sr_{0.3}MnO_3/SrRuO_3$ interface
Eur. Phys. J. B **86**, 42 (2013)

M. Ziese, F. Bern, and I. Vrejoiu:
Exchange bias in manganite/$SrRuO_3$ superlattices
J. Appl. Phys. **113**, 063911 (2013)

A. Ballestar, J. Barzola-Quiquia, T. Scheike, and P Esquinazi:
Josephson-coupled superconducting regions embedded at the interfaces of highly oriented pyrolytic graphite
New Journal of Physics **15**, 023024 (2013)

T. Scheike, P. Esquinazi, A. Setzer, and W. Böhlmann:
Granular superconductivity at room temperature in bulk highly oriented pyrolytic graphite samples
Carbon **59**, 140 (2013)

V. V. Lazenka, M. Lorenz, H. Modarresi, K. Brachwitz, P. Schwinkendorf, T. Böntgen, J. Vanacken, M. Ziese, M. Grundmann, and V. V. Moshchalkov:
Effect of rare-earth ion doping on the multiferroic properties of $BiFeO_3$ thin films grown epitaxially on $SrTiO_3$ (100)
J. Phys. D: Appl. Phys. **46**, 175006 (2013)

M. Gabás, A. Landa-Cánovas, J. L. Costa-Krämer, F. Agulló-Rueda, A. R. González-Elipe, P. Díaz-Carrasco, J. Hernández-Moro, I. Lorite, P. Herrero, P. Castillero, A. Barranco, and J. R. Ramos-Barrado:
Differences in n-type doping efficiency between Al- and Ga-ZnO films
J. Appl. Phys. **113**, 163709 (2013)

J. Zippel, M. Lorenz, A. Setzer, M. Rothermel, D. Spemann, P. Esquinazi, M. Grundmann, G. Wagner, R. Denecke, and A. A. Timopheev:
Defect-induced magnetism in homoepitaxial manganese-stabilized zirconia thin films
J. Phys. D: Appl. Phys. **46**, 275002 (2013)

M. Jenderka, J. Barzola-Quiquia, Z. Zhang, H. Frenzel, M. Grundmann, and M. Lorenz:
Mott variable-range hopping and weak antilocalization effect in heteroepitaxial Na_2IrO_3 thin films
Phys. Rev. B **88**, 045111 (2013)

P. Esquinazi, W. Hergert, D. Spemann, A. Setzer, and A. Ernst:
Defect-Induced Magnetism in Solids
IEEE Trans. Magnetics, **49**, 4668 (2013)

J. L. Cholula-Díaz, J. Barzola-Quiquia, H. Krautscheid, U. Teschner, P. Esquinazi:
Synthesis and magnetotransport properties of nanocrystalline graphite prepared by aerosol assisted chemical vapor deposition
Carbon **67**, 10 (2014)

P. Esquinazi:
Invited review: Graphite and its hidden superconductivity
Papers in Physics, **5**, 050007 (2013)

M. Stiller, J. Barzola-Quiquia, I. Lorite, P. Esquinazi, R. Kirchgeorg, S. P. Albu, and P. Schmuki:
Transport properties of single TiO_2 nanotubes
Appl. Phys. Lett. **103**, 173108 (2013)

F. Bern, M. Ziese, A. Setzer, E. Pippel, D. Hesse and I. Vrejoiu:
Structural, magnetic and electrical properties of $SrRuO_3$ films and $SrRuO_3/SrTiO_3$ superlattices
J. Phys.: Condens. Matter **25**, 496003 (2013)

F. Bern and M. Ziese:
Magnetotransport and Hall effect studies of $SrRuO_3/SrTiO_3$ superlattices
EPJ Web of Conferences **40**, 15013 (2013)

10.12 Graduations

Master

- B.Sc. Julia Tesch
  Thermopower measurements of micrometer-sized samples
  28.02.2013
- B.Sc. Tobias Lehmann
  Herstellung von dünnen Filmen des topologischen Isolators Bi_2Se_3 und deren Magnetotransportmessungen
  28.03.2013

Bachelor

- cand. B.Sc. Johann Schmidt
  Influence of a Deionized Water Treatment on the Electronic Transport Properties of a

Multigraphene Sample
28.02.2013

- cand. B.Sc. Manuel Lindel
Transport Properties of Multi-Wall Carbon Nanotube Bundles
24.07.2013
- cand. B.Sc. Tom Schilling
Structural and magnetic properties of $SrRuO_3$ thin films deposited on (111) $SrTiO_3$
30.09.2013

10.13 Guests

- Prof. Dr. Mónica Tirado
Laboratorio de Física del Sólido, University of Tucumán / Argentine
15.05. - 02.06.2013
- Dr. Carlos Iván Zandalazini
Laboratorio de Física del Sólido, University of Tucumán / Argentine
02.05. - 30.06.2013
- PhD Silvina Claudia Real
Laboratorio de Física del Sólido, University of Tucumán / Argentine
15.05. - 10.06.2013
- Binda Chen
Technische Universität München
23. - 27.06.2013
- Dr. David Comedi
Laboratorio de Física del Sólido, University of Tucumán / Argentine
02. - 14.06.2013
- PhD Ricardo Matías Trujillo
Laboratorio de Física del Sólido, University of Tucumán / Argentine
Time
- B.Sc. Burak Cibuk
Faculty of Engineering, Physic Engineering, University Ankara / Turkey
01.07. - 30.09.2013
- Prof. Dr. Yakov Kopelevich
Instituto de Física "Gleb Wataghin", Universidade Estadual de Campinas, São Paulo / Brazil
16.07. - 01.08.2013
- PhD Parmod Kumar
Department of Physics, Indian Institute of Technology, New Delhi / India
15.07. - 31.12.2013
- Dr. Noelia Bajales Luna
Grupo Cienca de Materials, Instituto Enrique Gaviola, (IFEG), Cordoba, Argentine
23./24.10.2013

III

Institute for Theoretical Physics

11

Computational Quantum Field Theory

11.1 Introduction

The Computational Physics Group performs basic research into classical and quantum statistical physics with special emphasis on phase transitions and critical phenomena. In the centre of interest are the physics of spin glasses, diluted magnets and other materials with quenched, random disorder, soft condensed matter physics with focus on fluctuating paths and interfaces, biologically motivated problems such as protein folding, aggregation and adsorption as well as related properties of homopolymers, and the intriguing physics of low-dimensional quantum spin systems. Our investigations of a geometrical approach to the statistical physics of topological defects with applications to superconductors and superfluids and research into fluctuating geometries with applications to quantum gravity, e.g., dynamical triangulations, build on the previous European Research Training Network (RTN) "ENRAGE": *Random Geometry and Random Matrices: From Quantum Gravity to Econophysics*, a collaboration of 13 teams throughout Europe. Moreover, initiated by a bi-national Institute Partnership with the Jagiellonian University in Krakow, Polen, supported by the Alexander von Humboldt (AvH) Foundation the statistical mechanics of complex networks is studied. In April 2012 a new AvH Institute Partnership project with the Institute for Condensed Matter Physics of the National Academy of Sciences in Lviv, Ukraine, on *Polymers in Porous Environments and on Disordered Substrates* commenced its work.

The methodology is a combination of analytical and numerical techniques. The numerical tools are currently Monte Carlo and Molecular Dynamics computer simulations as well as exact enumeration techniques. The computational approach to theoretical physics is expected to gain more and more importance with the future advances of computer technology, and is likely to become the third cornerstone of physics besides experiment and analytical theory as sketched in Fig. 11.1. Already now it can help to bridge the gap between experiments and the often necessarily approximate calculations in analytic approaches. To achieve the desired high efficiency of the numerical studies we develop new algorithms, and to guarantee the flexibility required by basic research all computer codes are implemented by ourselves. The technical tools are Fortran, C, and C++ programs running under Unix or Linux operating systems and computer algebra using Maple or Mathematica. The software is developed and tested at the Insti-

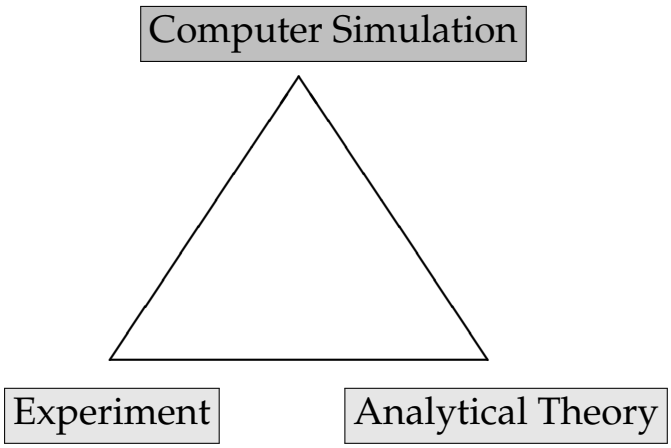

Figure 11.1: Sketch of the "triangular" relationship between experiment, analytical theory and computer simulation.

tute on a cluster of PCs and workstations, where also most of the numerical analyses are performed. Currently we are also exploring the possibilities of the rapidly developing graphics card computing, that is computer simulations on graphics processing units (GPUs) with many cores. Large-scale simulations requiring vast amounts of computer time are carried out at the Institute on quite powerful compute servers, at the parallel computers of the University computing centre, and, upon successful grant application at the national supercomputing centres in Jülich, Stuttgart and München on parallel supercomputers. This hierarchy of various platforms gives good training opportunities for the students and offers promising job perspectives in many different fields for their future career.

Within the University, our research activities are closely integrated into the Graduate School "BuildMoNa": Leipzig School of Natural Sciences – *Building with Molecules and Nano-objects*, two ESF Junior Research Groups, the International Max Planck Research School (IMPRS) *Mathematics in the Sciences*, and the International Graduate School *Statistical Physics of Complex Systems* with Université de Lorraine in Nancy, France, supported by the Deutsch-Französische Hochschule (DFH-UFA). In the second funding period 2011–2013, Coventry University in England has been integrated as an associated partner, and in the recently approved third funding period 2014–2016, also the National Academy of Sciences of Ukraine in Lviv has joined as another associated partner institution, offering our PhD students now several interesting options for secondments. The three Graduate Schools are all "Classes" of the Research Academy Leipzig (RALeipzig), providing the organizational frame for hosting visiting students and senior scientists, offering language courses, organizing childcare and for many other practical matters. At the post-graduate level our research projects are embedded into the "Sächsische DFG-Forschergruppe" FOR877 *From Local Constraints to Macroscopic Transport* jointly with the universities in Chemnitz and Dresden, and the Sonderforschungsbereich/Transregio SFB/TRR 102 *Polymers under Multiple Constraints: Restricted and Controlled Molecular Order and Mobility* together with Halle University. Our group also actively contributes to two of the top level research areas (previously "Profilbildende Forschungsbereiche (PbF)", currently being reorganized

into so-called "Profillinien") and the Centre for Theoretical Sciences (NTZ) of the University. Beside "BuildMoNa" the latter structures are particularly instrumental for our cooperations with research groups in experimental physics and biochemistry on the one hand and with mathematics and computer science on the other.

On an international scale, our research projects which are in part initiated by the European RTN "ENRAGE" and the previous AvH Institute Partnership with the Jagiellonian University in Krakow, Poland, are currently carried out in a wide net of collaborations mainly funded by the German Academic Exchange Service (DAAD) and the Alexander von Humboldt Foundation through the Institute Partnership with the National Academy of Sciences in Lviv, Ukraine, as well as their Fellowship Programmes. Further close contacts and collaborations are established with research groups in Armenia, Austria, China, France, Great Britain, Israel, Italy, Japan, Poland, Russia, Spain, Sweden, Taiwan, Turkey, Ukraine, and the United States. These contacts are refreshed and furthered through topical Workshops, Advanced Training Modules and Tutorials, and our International Workshop series *CompPhys: New Developments in Computational Physics*, taking annually place at the end of November just before the first advent weekend.

Wolfhard Janke

11.2 Morphing the energy landscape of spin glasses

S. Schnabel, W. Janke

Among the numerous systems that became accessible for investigation with the introduction of Monte Carlo simulations, spin glasses have proven to be among the most challenging. This becomes apparent when the Edwards-Anderson model [1] is studied. While being closely related to the very thoroughly examined and well-understood Ising model the introduction of disorder,

$$\mathcal{H} = \sum_{\langle ij \rangle} J_{ij} S_i S_j \,,$$

in the form of random couplings J_{ij} leads to an energy landscape that is characterized by an excessive number of local minima separated by energy barriers. This severely hampers Monte Carlo simulations since a random walker has to change frequently between high and low energies in order to sample a representative part of the state space. In consequence both the search for the ground state and the investigation of thermodynamic properties can only be performed for relatively modest system sizes. While for the former new methods keep being introduced, at least in the last two decades progress in the latter has exclusively been achieved due to an increase of computational resources.

We propose a novel technique related to the basin hopping algorithm [2]. In addition to the energy of a given configuration we evaluate the energy of the system after a short energy minimization and attribute this energy to the original configuration as well. Combining these two values it is possible to obtain a variable that retains the minima of the Hamiltonian but alters the shape of the surrounding valleys, thus facilitating the simulation and reducing autocorrelation time.

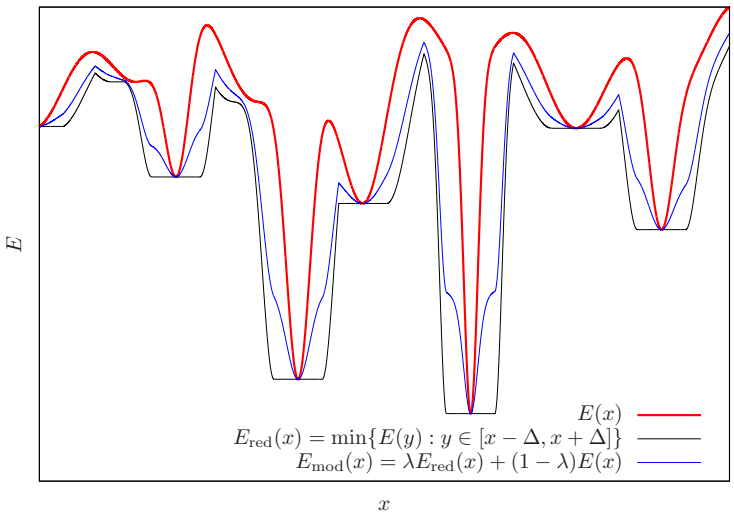

Figure 11.2: This sketch shows how a new variable (blue) with favorable characteristics can be composed from the energy (red) and a minimized energy (black).

We obtain ground-state energies that correspond well with data from the literature. Furthermore, we are able to reach lower energies in balanced simulations than possible before.

[1] S.F. Edwards, P.W. Anderson: J. Phys. F **5**, 965 (1975)
[2] D.J. Wales: J. Phys. Chem. A **101**, 5111 (1997)

11.3 Polymer adsorption onto a stripe-patterned substrate

M. Möddel*, M. Bachmann†, W. Janke

*Present address: Basycon Unternehmensberatung, Welserstraße 1, 81373 München, Germany
†Center for Simulational Physics, The University of Georgia, Athens, Georgia 30602, USA

Naturally occurring substrates almost exclusively exist with heterogeneities not just on the macroscopic, but also on the micro- or nanoscopic level. Consequently, after we developed an in-depth understanding of the statistical equilibrium behaviour of a generic self-attracting polymer model close to an attractive homogeneous substrate in recent years [1–5], the question arose how this behaviour gets modified if hetereogenities are introduced on the substrate.

The goal was to see the influence on the level of the whole pseudo-phase diagram, where "pseudo" refers to the finiteness of the simulated chain length. Since already the phase diagram of the polymer near the homogeneous substrate is very rich in transitions (cf. Fig. 11.3(a)), to extract any meaningful results the chosen surface heterogeneity needs to be easily controllable and preferably simple.

Our choice was to add to the previously investigated [1–5] bulk energy term and 9-3 Lennard-Jones (LJ) attraction between each monomer and the substrate an attractive

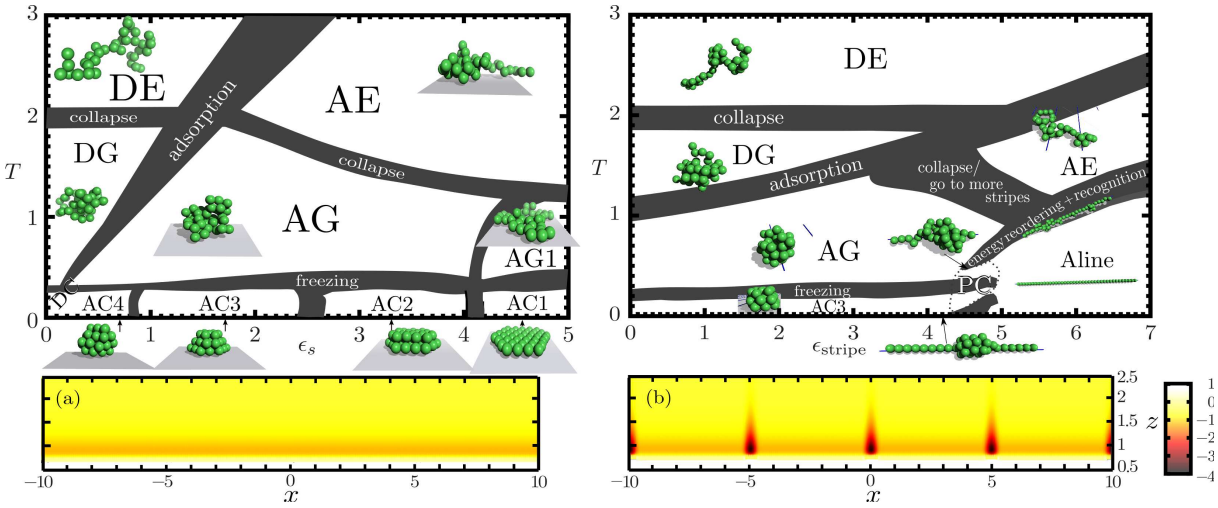

Figure 11.3: (a) Pseudo-phase diagram for polymer adsorption to a homogeneous substrate ($\epsilon_{\text{stripe}} = 0$) in the temperature ($T$) – surface attraction ($\epsilon_s$) plane and a "heat map" of the substrate potential for $\epsilon_s = 1$. (b) Analogous pseudo-phase diagram for the stripe patterned case in the T–ϵ_{stripe} plane for $\epsilon_s = 1$. Phases with "A/D" are adsorbed/desorbed, while "E", "G", and "C" denote phases with increasing order: expanded, globular, and compact. "PC" stands short for a region with phase coexistence.

cosine-square potential of distance $D = 5$ such that the energy of the system in total is

$$E_{\text{bulk}} = 4 \sum_{i=1}^{N-2} \sum_{j=i+2}^{N} \left(r_{ij}^{-12} - r_{ij}^{-6} \right) + \frac{1}{4} \sum_{i=1}^{N-2} (1 - \cos \vartheta_i) \ , \tag{11.1}$$

that is strongly dominated by a 12-6 Lennard-Jones (LJ) attraction between non-neighboring monomers, and

$$E_{\text{sur, stripe}}(x,z) = \begin{cases} \left(\frac{2}{15} z^{-9} - z^{-3}\right) \left[\epsilon_s + \epsilon_{\text{stripe}} \cos^2 \left(\pi \left(\text{mod}\left(x + \frac{D}{2}, D\right) - \frac{D}{2} \right) \right) \right], & \text{if } \left| \text{mod}\left(x + \frac{D}{2}, D\right) - \frac{D}{2} \right| \leq \frac{1}{2} \\ \left(\frac{2}{15} z^{-9} - z^{-3}\right) \epsilon_s, & \text{else.} \end{cases} \tag{11.2}$$

The impact of those stripes was described in detail with an emphasis on the onset of the "recognition" transition below which the polymer perfectly adapts the shape of the stripe. Figure 11.3(b) shows that despite some striking differences, many conclusions drawn for the adsorption of a single polymer on a homogeneous substrate remain valid in the more general hetereogeneous case [6].

[1] M. Möddel et al.: J. Phys. Chem. B **113**, 3314 (2009)
[2] M. Möddel et al.: Phys. Chem. Chem. Phys. **12**, 11548 (2010)
[3] M. Möddel et al.: Macromolecules **44**, 9013 (2011)
[4] M. Möddel et al.: Comput. Phys. Commun. **182**, 1961 (2011)
[5] M. Möddel et al.: in Proceedings of the *NIC Symposium 2012*, eds. K. Binder, G. Münster, M. Kremer, John von Neumann Institute for Computing, Jülich, NIC Series, Vol. **45**, p. 277 (2012)
[6] M. Möddel et al.: Phys. Rev. Lett. **112**, 148303 (2014)

11.4 Structural phases of stiff and flexible polymers

D.T. Seaton*, S. Schnabel, D.P. Landau*, M. Bachmann*

*Center for Simulational Physics, The University of Georgia, Athens, USA

In order to get a systematic understanding of the structural behaviour of polymers with a varying degree of stiffness we performed extensive simulations for a bead-spring model. The Hamiltonian contains three types of interactions:

- Excluded volume and hydrophobicity are modeled by a Lennard-Jones potential

$$U_{\mathrm{LJ}}(r_{ij}) = r_{ij}^{-12} - 2r_{ij}^{-6}$$

  with a minimum at $r_{ij} = 1$, acting upon all non-neighbouring monomer pairs.

- Bonds are introduced by a FENE-potential

$$U_{\mathrm{FENE}}(r_{ii+1}) = -R^2 \ln\left[1 - (r_{ii+1}/R)^2\right],$$

  with the maximum bond length $R = 1.2$. An adjusted Lennard-Jones potential is added in order to match the equilibrium distance to that of the non-bonded pairs.

- The polymer obtains stiffness via a bending energy

$$U_{\mathrm{bend}}(\Theta_l) = \kappa\,(1 - \cos\Theta_l)$$

  based on the angle between adjacent bonds Θ_l.

Employing advanced generalized-ensemble Monte Carlo techniques we were able to sample the state space for all relevant κ-values in a single simulation [1]. Transition lines were afterwards identified using thermal fluctuations of energy (Fig. 11.4) and radius of gyration.

We did not only focus on the general phases between the limits stiff and flexible but investigated the influence of finite-size effects on structure formation. This is a significant problem as it has become apparent that the structural properties of classes of short semiflexible biomolecules can significantly deviate from the standard wormlike-chain behaviour. The changed structural behaviour, therefore, needs to be considered in the understanding of biomolecular processes on short length scales and also in the nanofabrication of molecular devices.

[1] D.T. Seaton et al.: Phys. Rev. Lett. **110**, 028103 (2013)

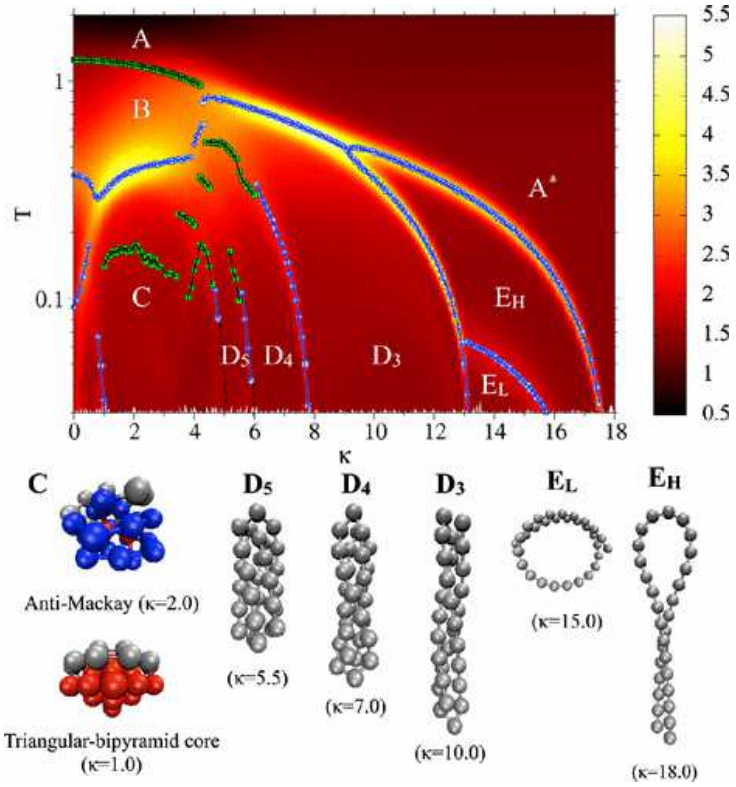

Figure 11.4: Surface plot of the specific heat for classes of polymers with $N = 30$ monomers as a function of temperature T and stiffness κ. Brighter colors correspond to higher thermal activity, signaling structural transitions. For a large number of κ values, locations of peaks and shoulders are emphasized by circles and squares, respectively, for easier identification of transition points. Conformational phases are labeled as follows: A, random coil; A^*, random rodlike; B, liquid globular; C, solid globular; D_m, rodlike bundles with m segments; and E, toroidal.

11.5 Ground-state properties of a polymer chain inside an attractive sphere potential

H. Arkın*, W. Janke

*Department of Physics Engineering, Faculty of Engineering, Ankara University, Tandogan, 06100 Ankara, Turkey

Understanding the basic mechanisms for structure formation of biomolecules at different interfaces is one of the major challenges of modern interdisciplinary research and possible applications in nanotechnology. Knowledge of the origin of structure formation is an important prerequisite for tailoring polymer adhesion to metals and semiconductors [1] and the design of biomedical implants [2] and biosensors [3]. The adsorption behaviour can also influence cellular motion, drug delivery, and other biological processes. The advances in designing and manipulating biomolecules at solid substrates on the nanoscale open new challenges for potential nanotechnological applications of hybrid organic-inorganic interfaces.

Recently, some progress has been achieved in the understanding of general properties of the conformational behaviour of homopolymers and heteropolymers near

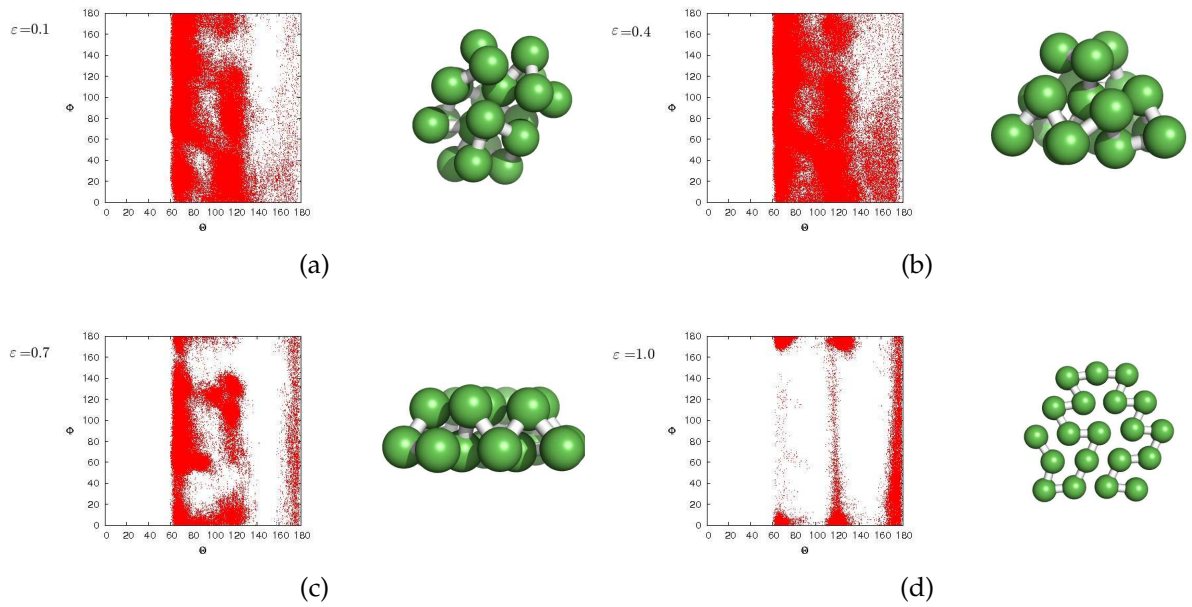

Figure 11.5: Bond and torsion angle distributions for (a) $\epsilon = 0.1$, (b) $\epsilon = 0.4$, (c) $\epsilon = 0.7$, (d) $\epsilon = 1.0$ and the associated global minimum energy conformations. The distribution of the torsion angles has reflection symmetry and therefore only the positive interval is shown.

substrates. In most cases, the substrates are considered to be planar [4]. In this work, we considered a simple off-lattice coarse-grained polymer model inside of an attractive sphere, for which we have recently constructed the finite-temperature phase diagram [5]. Here, we focused on the ground-state properties caused by different attraction strengths ϵ of the sphere within the frame of generalized-ensemble simulations [6]. In a comparative analysis based among others on various (invariant) shape parameters related to the eigenvalues of the gyration tensor, a classification of the structures formed in the accompanying adsorption process has been achieved.

The distributions of all successive pairs of virtual bond angles $\Theta_i = \pi - \vartheta_i$ and torsion angles Φ_i in the low-temperature regime ($T < 0.2$) for different values of the surface attraction strength ϵ are shown in Fig. 11.5. It is one of the most remarkable results of our study that for different parameter values of the polymer-attractive sphere system, we get conformations that fit perfectly to the inner wall of the sphere. A careful comparison with results for flat substrates has recently been presented in Ref. [7].

[1] M. Bachmann et al.: Angew. Chem. Int. Ed. **49**, 9530 (2010)
[2] E. Nakata et al.: J. Am. Chem. Soc. **126**, 490 (2004)
[3] R.F. Service: Science **270**, 230 (1995)
[4] M. Möddel et al.: J. Phys. Chem. B **113**, 3314 (2009); Phys. Chem. Chem. Phys. **12**, 11548 (2010); Comput. Phys. Commun. **182**, 1961 (2011); Macromolecules **44**, 9013 (2011); in *NIC Symposium 2012*, Proceedings, eds. K. Binder, G. Münster, M. Kremer, John von Neumann Institute for Computing, Jülich, NIC Series, Vol. **45**, 277 (2012); Phys. Rev. Lett. **112**, 148303 (2014)
[5] H. Arkın, W. Janke: Phys. Rev. E **85**, 051802 (2012)
[6] H. Arkın, W. Janke: J. Phys. Chem. B **116**, 10379 (2012)

[7] H. Arkın, W. Janke: Eur. Phys. J. – Special Topics **216**, 181 (2013)

11.6 Polymer shapes in an attractive spherical cage

H. Arkın*, W. Janke

*Department of Physics Engineering, Faculty of Engineering, Ankara University, Tandogan, 06100 Ankara, Turkey

The conformational properties of polymers and proteins confined in cages with different geometries are a subject of great interest in polymer science [1–4], playing an important role both from a physical and chemical perspective. In recent work, we considered a simple off-lattice coarse-grained polymer model inside an attractive sphere, for which we have constructed the finite-temperature phase diagram [5] and investigated the ground-state properties [6]. A careful comparison with results for flat substrates has recently been presented in Ref. [7].

In this work we found highly structured conformations that are of approximately spherical shape or form two-dimensional planar, compact to extended, random coil structures. The observed conformations range from desorbed to partially or even completely adsorbed. In the present study [8], we show that the gyration tensor and related asphericity and shape anisotropy parameters are powerful combinations to characterize the conformational pseudo-phases in detail and to identify the associated typical polymer shapes. In a comparative analysis, a classification of the structures formed in the accompanying adsorption process has been achieved. It is one of the most remarkable results of our study that for different values of the attraction-strength parameter ϵ of the polymer-attractive sphere system, we get conformations that fit perfectly to the inner wall of the sphere with two-dimensional shape.

The eigenvalues of the gyration tensor measure the extensions in the principle axis system and enable us to define several additional, partly universal shape parameters of which information about the system can be extracted that complements the physical picture obtained so far. Some of our results [8] are exemplified in Fig. 11.6, where the distributions of the eigenvalues of the gyration tensor are shown for low-temperature conformations at (a) $\epsilon = 0.1$, (b) $\epsilon = 0.4$, (c) $\epsilon = 0.7$, (d) $\epsilon = 1.0$. For $\epsilon = 0.1$ and 0.4 the eigenvalues are nearly equal to each other. There are no significant differences because these values correspond to almost spherically symmetric shapes or three-layered shapes which are also close to spherical shape. On the other hand, as we know from the T-ϵ phase diagram [5, 7] that for low temperatures the transition point is at $\epsilon \approx 0.6$, the plot for $\epsilon = 0.7$ shows a tendency of increasing values λ_1, λ_2 and decreasing λ_3. For $\epsilon = 1.0$ it can be seen that this tendency becomes more pronounced and λ_3 approaches zero whereas the other two eigenvalues are increasing to higher values. This confirms in a quantitative way that the layering transition at the inner surface of the attractive sphere is a topological transition from 3D to 2D polymer conformations.

[1] F. Takagi et al.: Proc. Natl. Acad. Sci. USA **100**, 11367 (2003)
[2] N. Rathore et al.: Biophys. J. **90**, 1767 (2006)
[3] D. Lu et al.: Biophys. J. **90**, 3224 (2006)

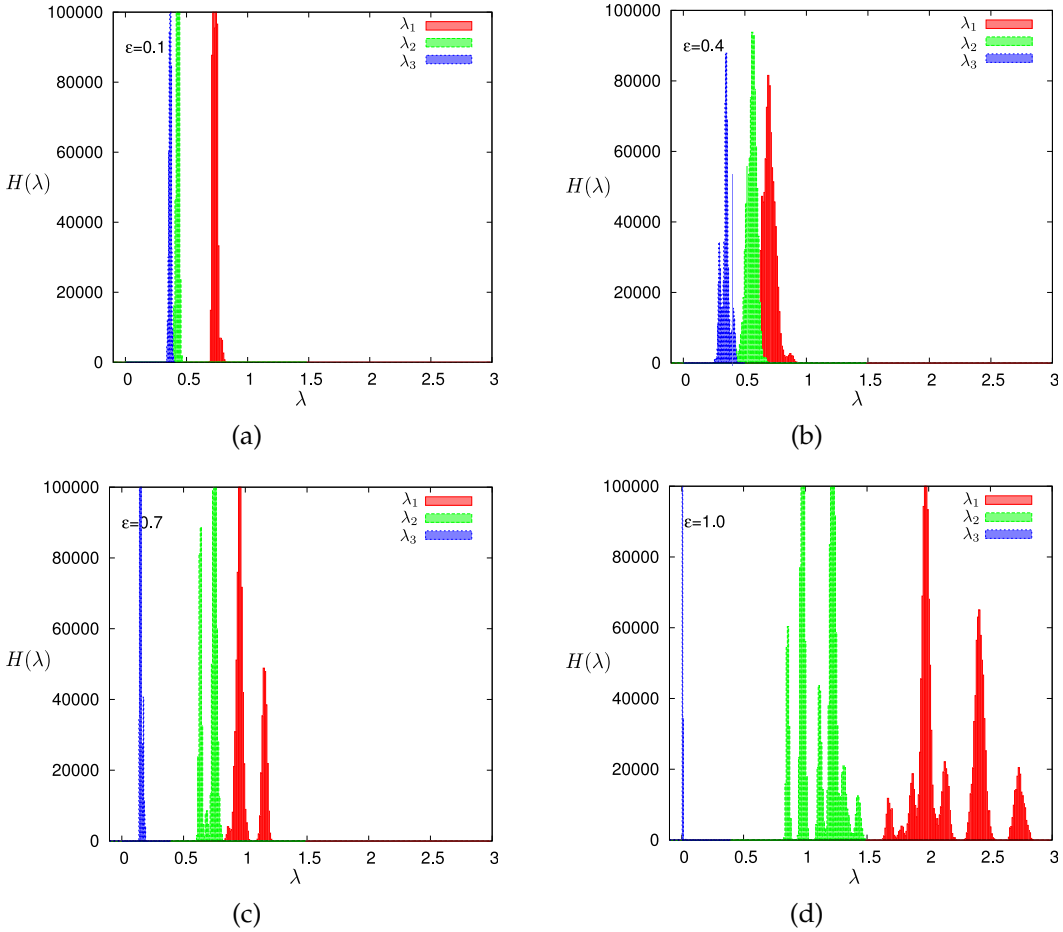

Figure 11.6: The eigenvalue distributions of the gyration tensor of low-temperature conformations for surface attraction strength (a) $\epsilon = 0.1$, (b) $\epsilon = 0.4$, (c) $\epsilon = 0.7$, (d) $\epsilon = 1.0$.

[4] M. Marenz et al.: Condens. Matter Phys. **15**, 43008 (2012)
[5] H. Arkın, W. Janke: Phys. Rev. E **85**, 051802 (2012)
[6] H. Arkın, W. Janke: J. Phys. Chem. B **116**, 10379 (2012)
[7] H. Arkın, W. Janke: Eur. Phys. J. – Special Topics **216**, 181 (2013)
[8] H. Arkın, W. Janke: J. Chem. Phys. **138**, 054904 (2013)

11.7 Effects of bending stiffness on a coarse grained polymer model

M. Marenz, W. Janke

To investigate the generic behaviour of polymers and proteins in computer simulations it is common to use generic models. On the one hand, these models neglect chemical details, which means that one cannot observe any specific behaviour. Instead the general behaviour for the type of polymer is exposed. Additionally these coarse-grained models are often the only ones which are treatable with analytical or numerical methods. One of the most used coarse-grained models is the so called bead-stick polymer. For this

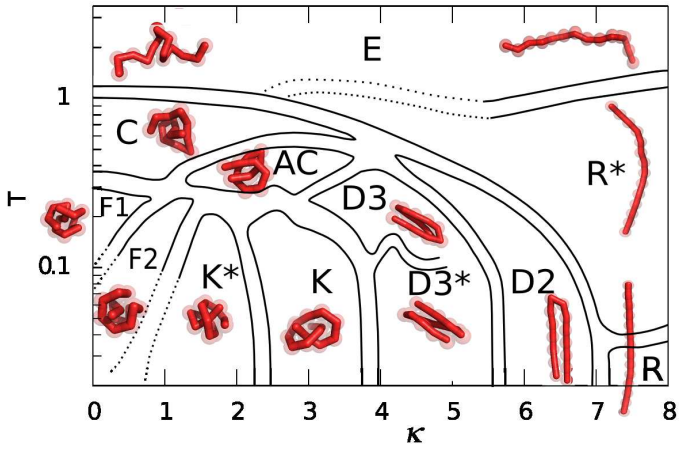

Figure 11.7: Different conformational phases of a homopolymer consisting of 14 monomers. Black lines indicate pseudo-phase transitions. The different pseudo phases are labeled as follows: E - elongated, R/R* - rod-like, C - collapsed, AC - aligned collapses, F1/F2 - frozen, K/K* knot-like, DN - bended $N-1$ times.

work, we added a bending stiffness to the Hamiltonian of this model, so that we can investigate many different kinds of polymers without reintroducing chemical details. The Hamiltonian of the simulated polymers looks as follows:

$$H = 4 \sum_{i=1}^{N-2} \sum_{j=i+2}^{N} \left(\frac{1}{r_{ij}^{12}} - \frac{1}{r_{ij}^{6}} \right) + \kappa \sum_{\theta_i} (1 - \cos \theta_i) \,,$$

where r_{ij} denote the distances between non-adjacent monomers and θ_i is the angle of two adjacent bonds.

Now we can adjust the bending stiffness by varying κ, so that the simulated polymer can be anything between flexible, semi-flexible or stiff. To investigate the different conformational phases we need results over a broad temperature range. We therefore used a parallel version of the multicanonical algorithm, which is explained in [1]. This algorithm can produce results over a large temperature range and also overcome problems arising from numerous phase transitions. These phase transitions make it problematic to simulate such models with standard Monte Carlo algorithms. We measured different observables such as the energy $\langle E \rangle$, the squared radius of gyration $\left\langle R_g^2 \right\rangle$ or the invariants of the gyration tensor and identified the different (pseudo) phase transitions from peaks in the thermal derivatives.

Despite of the simplicity of the model, the phase diagram is remarkable rich [2], see Fig. 11.7. Many of theses phases are comparable to conformations which have been observed for real polymers and proteins. Similar but in details different results have recently been observed for a different coarse-grained polymer model [3] (cf. Fig. 11.4). For the future we plan to investigate the effect of the polymer length on the different pseudo-phase transitions. Additionally, a finite-size scaling analysis at few selected

pseudo-phase transition points could yield a deeper insight into the type and scaling properties of the transitions.

[1] J. Zierenberg et al.: Comput. Phys. Commun. **184**, 1155 (2013)
[2] M. Marenz, W. Janke: Leizpig preprint, to appear in Physics Procedia (2014), in print
[3] D.T. Seaton et al.: Phys. Rev. Lett. **110**, 028103 (2013)

11.8 The role of stiffness on structural phases in polymer aggregation

J. Zierenberg, W. Janke

We have investigated the effect of stiffness on polymer aggregation and were able to show that stiffness plays a crucial role in whether a system forms an amorphous aggregate or a bundle structure [1]. Figure 11.8 shows the temperature-stiffness phase diagram of polymer aggregation for 8 polymers with 13 monomers each. We have performed the same analysis also for 2 and 4 polymers of the same length and were always able to identify a regime of flexible polymers forming uncorrelated aggregates, an intermediate regime and a regime of rather stiff polymers directly forming bundle like structures. With the help of a microcanonical analysis we investigated the intermediate stiffness regime. Here, lowering the temperature for a few polymers the aggregation first forms correlated structures followed by a first-order like transition into the "frozen" states. On the other hand, for an increasing number of polymers, lowering the temperature first drives the system into an uncorrelated aggregate, shortly followed by a second-order like transition into the correlated aggregate.

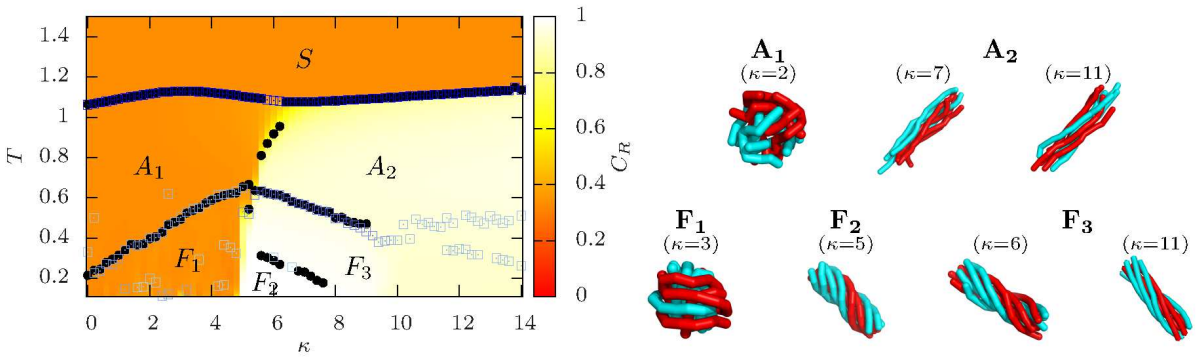

Figure 11.8: Full temperature-stiffness phase diagram of 8 polymers with 13 monomers each. The surface plot shows a correlation order parameter (1 = correlated; 1/3 = uncorrelated) and the black and blue dots represent peaks in the heat capacity and the thermal derivative of the phase separation parameter, respectively [1].

For increasing numbers of polymers, we can see that the "frozen"(low-temperature) states in Fig. 11.8 show a twisted bundle structure if the stiffness is large enough. This sort of structure has been reported before in the context of material design for specific interactions usually related to proteins. Since our study did not include any specific interactions, but instead a homopolymer with short-range attraction/repulsion with additional bending stiffness, we conclude that specific interactions are not necessary but may stabilize or destabilize those occurring structures.

In order to generate the data, we employed parallel multicanonical simulations [2] with up to 128 cores on the supercomputer JUROPA at Jülich Supercomputing Centre (JSC).

[1] J. Zierenberg, W. Janke: e-print arXiv:1401.3227, submitted
[2] J. Zierenberg et al.: Comput. Phys. Commun. **184**, 1155 (2013)

11.9 Effect of coupling constants on polymer aggregation (ISAWs)

J. Zierenberg, B. Schott, W. Janke

Interacting self-avoiding walks (ISAWs) are a first-order approximation to flexible θ-polymers and a suitable way to study generic effects of aggregation in relatively large systems. The model has been applied to a variety of problems including protein folding and surface adsorption and benefits from a discretized energy with nearest-neighbour interaction only. The Hamiltonian is given by

$$\mathcal{H} = -\left(\epsilon_i N_i + \epsilon_o N_o\right) , \tag{11.3}$$

where N_i, N_o are the number of contacts of the polymers with themselves and with each other, respectively. Here, we consider a three-dimensional cubic lattice with edge length L. The discretization allows a fast calculation of the system energy and, moreover, allows to enumerate small systems exactly.

Usually, one assumes $\epsilon_i = \epsilon_o$ which leads to competition of the polymer collapse and polymer aggregation [1]. This, we were able to recapture in principle with parallel multicanonical simulations [2] of ISAWs, showing in addition that in equilibrium the polymers homogeneously aggregate into one macroscopic aggregate [3] similar to gas condensation. Moreover, the simplified model allows to systematically study the effect of the coupling constants on the occurring transitions. To this end, we introduce the ratio $\epsilon = \epsilon_o/\epsilon_i$, expressing the inter-polymer coupling in terms of the intra-polymer coupling. The result of an exact enumeration of two polymers ($N = 9, L = 35$) is shown in Fig. 11.9. Next to the heat capacity, it also shows the maxima and minima of the temperature derivative of the energy (E), the phase separation parameter (P), and the number of intra-(N_i) and inter-(N_o) polymer contacts.

This simple but exact example shows that the collapse and the aggregation only compete in the vicinity of $\epsilon \approx 1$. For small ϵ the two polymers first collapse before aggregating, while for large ϵ the polymers aggregate already at higher temperatures followed by further rearrangement transitions. The exact enumerations are extended

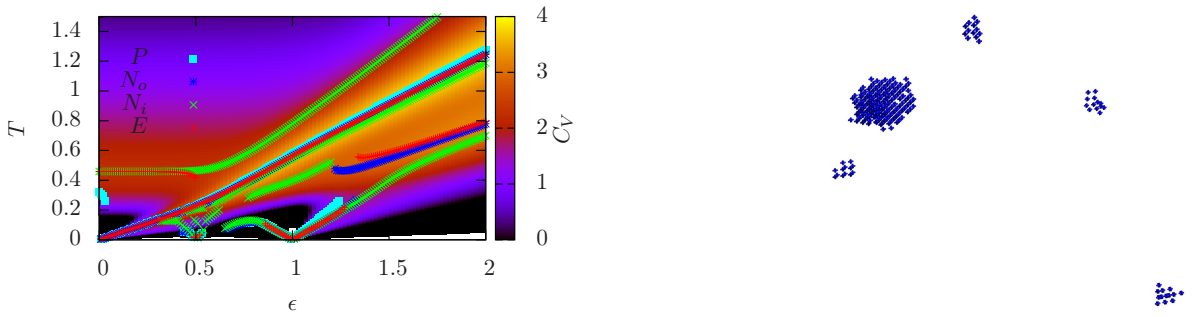

(a) (b)

Figure 11.9: (a) Pseudo-phase diagram of two polymers ($N = 9$) with variable coupling constant $\epsilon = \epsilon_o/\epsilon_i$. (b) 20 polymers ($N = 13$) in the aggregated phase.

by Monte Carlo simulations in order to better characterize the occurring phases also for larger systems, with an increasing number of longer chains.

[1] C. Junghans et al.: Europhys. Lett. **87**, 40002 (2009)
[2] J. Zierenberg et al.: Comput. Phys. Commun. **184**, 1155 (2013)
[3] J. Zierenberg, W. Janke: Leipzig preprint (2013)

11.10 Random heteropolymer models

V. Blavatska*, W. Janke

*Institute for Condensed Matter Physics, National Academy of Sciences of Ukraine, Lviv, Ukraine

The conformational properties of long heteropolymer chains are a subject of great interest in both chemical and biological physics. Typical examples are proteins, consisting of sequences of amino acid residues connected by peptide bonds. The conformations of individual macromolecules are controlled by the type of monomer-monomer interactions. In general, the constituents (monomers) of macromolecules in an aqueous environment can be characterized as hydrophilic or hydrophobic, depending on their chemical structure. Hydrophilic residues tend to form hydrogen bonds with surrounding water molecules, whereas the hydrophobic monomers effectively attract each other and tend to form a dense hydrophobic core.

We studied the conformational transitions in heteropolymers within a lattice model containing N_A monomers of type A and $N_B = N - N_A$ monomers of type B. Such a model can describe in particular the sequences of hydrophobic and hydrophilic residues in proteins [1] and polyampholytes with oppositely charged groups [2]. Restricting ourselves only to short-range interactions between any pair of monomers residing on neighboring lattice sites that are not connected by a covalent bond, we considered 5

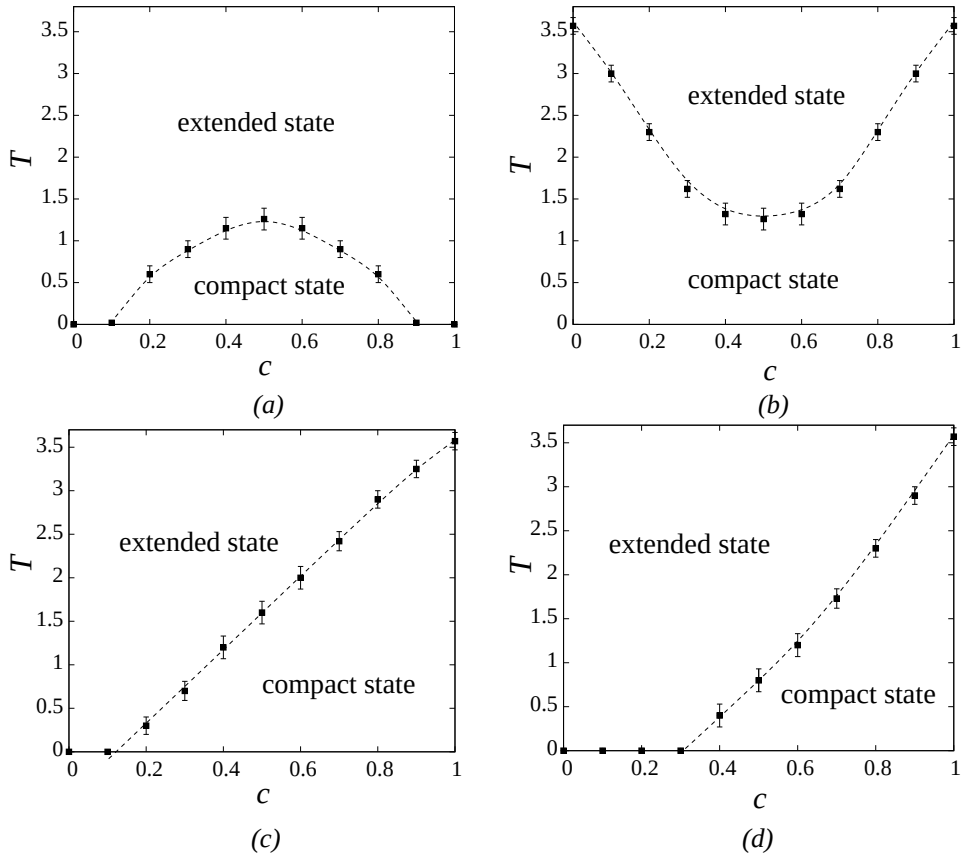

Figure 11.10: Phase diagrams of heterogeneous polymer chains in T-c space. (a) model 1, (b) model 2, (c) model 4, (d) model 5.

different parametrizations of this model. In particular, model 1 ($\varepsilon_{AA} = \varepsilon_{BB} = 1, \varepsilon_{AB} = -1$) where like monomers repel and opposite ones attract each other, refers to strongly screened Coulomb interactions [2]. The model 3 ($\varepsilon_{AA} = 1, \varepsilon_{BB} = \varepsilon_{AB} = 0$) is a particular case of model 1 and corresponds to a polymer chain containing charged (A) and neutral (B) monomers. Model 4 ($\varepsilon_{AA} = -1, \varepsilon_{BB} = \varepsilon_{AB} = 0$) refers to the (minimal) HP model [5] with hydrophobic (A) and hydrophilic (B) monomers. Models 2 ($\varepsilon_{AA} = \varepsilon_{BB} = -1, \varepsilon_{AB} = 1$) and 5 ($\varepsilon_{AA} = -1, \varepsilon_{BB} = 1, \varepsilon_{AB} = 0$) can be considered as generalizations of the two above mentioned cases.

Applying the pruned-enriched Rosenbluth chain-growth algorithm (PERM) [3] we analyzed numerically the transitions from an extended into a compact state as function of the inhomogeneity ratio $c = N_A/N$ for all five heteropolymer chain models [4]. Figure 11.10 shows that in model 3, unlike the other models, the polymer chain expands its size with lowering the temperature due to the repulsion between monomers, and the polymer chain remains in an extended state at any temperature. In model 2, the θ-transition is always present at any value of inhomogeneity ratio c, whereas models 1, 4 and 5 remain in an extended state when the concentration of attracting monomers is too small to cause a transition into the compact state. Note also that at small concentration of attractive monomers, the chains can attain the compact state only when they are long enough and have enough attractive nearest-neighbour contacts to overcome the conformational entropy. Models 2, 4 and 5 describe homogeneous polymer chains with

nearest-neighbour attractions in the limiting case $c = 1$ (for model 2 also $c = 0$) with known value of the transition temperature $T_\theta = 3.717(3)$ [3].

[1] K.A. Dill: Biochemistry **24**, 1501 (1985); K.F. Lau, K.A. Dill: Macromolecules **22**, 3986 (1989)
[2] Y. Kantor, M. Kardar: Europhys. Lett. **28**, 169 (1994)
[3] P. Grassberger: Phys. Rev. E **56**, 3682 (1997)
[4] V. Blavatska, W. Janke: J. Chem. Phys. **140**, 034904 (2014)

11.11 Hysteresis and scaling of DNA under oscillatory force

S. Kumar*, R. Kumar, W. Janke

*Department of Physics, Banaras Hindu University, Varanasi 221 005, India

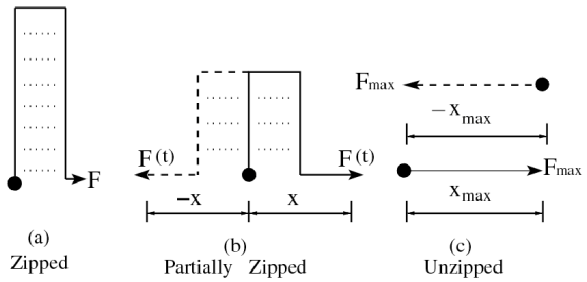

Figure 11.11: Schematic representations of DNA: (a) zipped, (b) partially zipped, and (c) unzipped. One end is kept fixed (indicated by the solid circle), while the other end may move in positive (shown by the solid line) or negative direction (shown by the dashed line), depending on the applied force direction.

Much attention has been paid in recent years to the understanding of biological processes, e.g., transcription and replication of nucleic acids, packing of DNA in a capsid, synthesis and degradation of proteins etc., which are driven by different types of molecular motors *in vivo* [1]. Experiments on biomolecules using single molecule force spectroscopy (SMFS) techniques have enhanced our understanding about these processes [2]. Unlike *in vivo*, where these motors are driven by oscillatory forces resulting from the periodic consumption of ATP to ADP, a constant force or loading rate used in SMFS experiments provides a limited picture of these processes *in vitro*. This has been highlighted in recent studies, where it was suggested that by varying the frequency and amplitude of the applied force, new aspects of a force-driven transition can be introduced [3–5], which otherwise would not be possible in the case of a steady force.

In this project, we have shown within a simplified model the existence of a dynamical transition in a system of driven DNA under the influence of an oscillatory force of amplitude F and frequency ω [6], for a sketch see Fig. 11.11. For a chain of finite length, we observe that the area of hysteresis loops shown in Fig. 11.12 scales with the same exponents as proposed in the recent study [3]. However, in the true thermodynamic

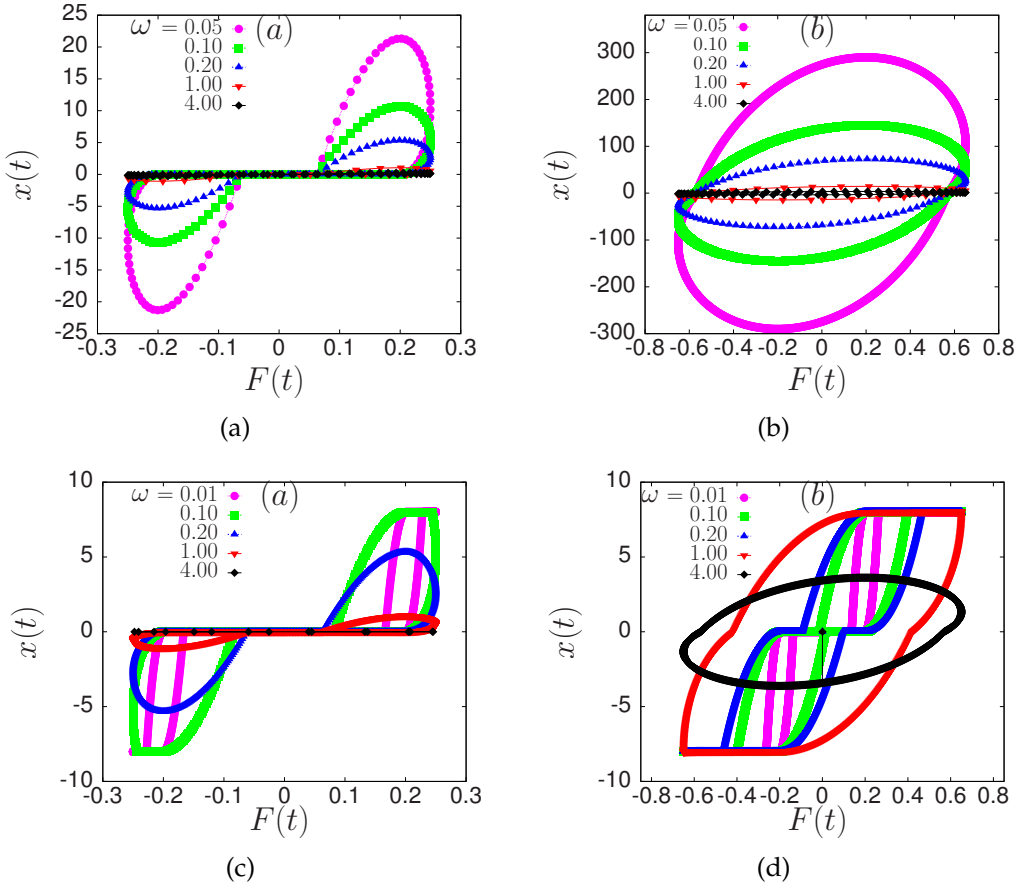

Figure 11.12: Hysteresis of the end points separation under a periodic force for different frequencies ω and (a) small amplitude ($F = 0.25$) respectively (b) large amplitude ($F = 0.65$) in the infinite chain-length limit $L = \infty$. The lower part (c), (d) of the figure shows the corresponding plots for a chain of finite length $L = 4$ where $|x(t)| \leq 8$.

limit, we find that the high-frequency scaling regime extends to lower frequencies for larger chain length L, and the system has only one scaling regime where the area of the hysteresis loop scales with $\omega^{-1}F^2$. This indicates that a true dynamical transition may not exist in the thermodynamic limit. We also show that the scaling for large but finite L at temperature $T = 0$ and $\neq 0$ remains invariant.

[1] B. Alberts et al.: *Molecular Biology of the Cell* (Garland Publishing, New York, 1994)
[2] S. Kumar, M.S. Li: Phys. Rep. **486**, 1 (2010)
[3] S. Kumar, G. Mishra: Phys. Rev. Lett. **110**, 258102 (2013)
[4] G. Mishra et al.: Phys. Rev. E **87**, 022718 (2013)
[5] R.K. Mishra et al.: J. Chem. Phys. **138**, 244905 (2013)
[6] S. Kumar et al.: Varanasi/Leipzig preprint (2014), to be published

11.12 Exact enumeration of polymers in fractal disorder

N. Fricke, W. Janke

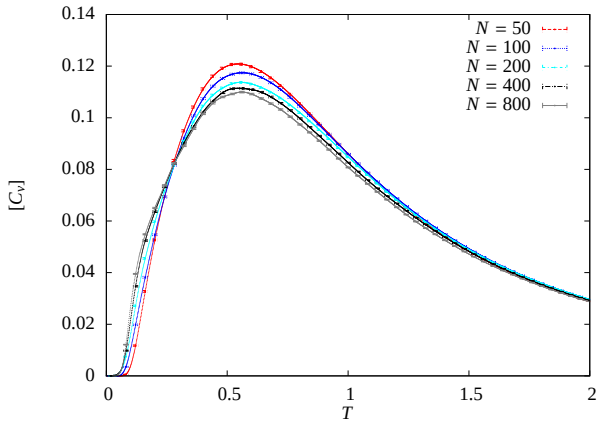

Figure 11.13: Quenched averages of the specific heat for self-attracting self-avoiding walks of varying length on critical percolation clusters.

The asymptotic scaling behaviour of flexible polymers in a good solvent is properly captured by self-avoiding walks (SAWs) on a regular lattice [1]. By including a nearest-neighbour attraction, ϵ, one can account for van der Waals forces that will cause a transition to a collapsed state at a certain temperature Θ. These so-called self-attracting self-avoiding walks (SASAWs) or Θ-polymers are characterized by three different sets of exponents: above, at, and below Θ.

To describe polymers in disordered environments such as porous rocks, one often considers quenched averages of (SA)SAWs on critical percolation clusters; see [2]. One interesting aspect there is the fractal nature of the clusters, which have non-integer Hausdorff dimensions. This model is difficult to treat analytically, and previous numerical approaches have proved rather cumbersome.

We developed a new enumeration method to exactly determine the configurational averages on a random sample of critical clusters [3–5]. Our approach makes use of the fractal geometry of the clusters and is thus considerably more efficient than any previous numerical method. The principal idea is to partition the critical cluster into a hierarchy of weakly connected regions, where the walks can be enumerated independently. The method can easily handle 10^4 steps for normal SAWs and about 6×10^3 for SASAWs on three-dimensional clusters at a fixed temperature. For shorter chains (about 800 steps), it can also be used to generate the complete density of states, Ω_E, from which the configurational averages at any temperature can be calculated. For instance, the specific heat, C_V, as a function of temperature, T which is typically studied when investigating thermal phase transitions, is obtained as:

$$C_V = \frac{1}{Nk_BT^2}\left(\frac{\sum_E \Omega_E E^2 e^{-\frac{E}{k_BT}}}{Z} - \left(\frac{\sum_E \Omega_E E e^{-\frac{E}{k_BT}}}{Z}\right)^2\right),$$

where E is a walk's total energy, N the number of monomers and Z the partition function.

For single clusters, we found that C_V typically shows sharp peaks, whereas the quenched average only has a cusp at around $T = 0.55\epsilon/k_B$ (Fig. 11.13). We are currently investigating whether this corresponds to a collapse transition.

[1] P.-G. de Gennes: *Scaling Concepts in Polymer Physics* (Cornell University Press, Ithaca, 1976)
[2] B. Barat, B.K. Chakrabarti: Phys. Rep. **258**, 377 (1995)
[3] N. Fricke, W. Janke: Europhys. Lett. **99**, 56005 (2012)
[4] N. Fricke, W. Janke: in *Computer Simulation Studies in Condensed-Matter Physics XXV*, eds. D.P. Landau, H.-B. Schüttler, S.P. Lewis, M. Bachmann, Physics Procedia **34**, 39 (2012)
[5] N. Fricke, W. Janke: Eur. Phys. J. Special Topics **216**, 175 (2013)

11.13 Kinetic growth random walks in fractal disorder

N. Fricke, J. Bock, W. Janke

The self-avoiding random walk (SAW) has been a popular model for polymers since the 1950s [1]. Of particular interest is the asymptotic scaling behaviour of its mean squared end-to-end distance with the number of steps, described by a power law with a universal exponent, $\langle R^2 \rangle \sim N^{2\nu}$. The average can be defined in two different ways: For the standard SAW, each trajectory contributes equally, corresponding to equilibrium statistics. The so-called kinetic growth walk (KGW) models a growing polymer; each trajectory contributes to the average according to the probability that it would occur in a self-avoiding growth process. On regular lattices, SAWs and KGWs appear to have different scaling exponents; see [2, 3].

To model polymers in random environments, one often constrains the walks to a critical percolation cluster, the paradigm for a highly disordered medium [4]. Our previous investigations had suggested that here, too, the exponents are different [3]. However, these results were preliminary, the number of steps and the amount of statistics having been rather small. By now we were able to significantly improve our measurements, owing to the use of more efficient algorithms: To simulate the KGWs, we used a modification of the pruned-enriched Rosenbluth method (PERM), which avoids trapping of the walks in dead ends [5]. The standard SAWs were exactly enumerated using a new technique that exploits the fractal nature of the clusters [6]. We were thus able to study SAWs and KGWs of up to 800 steps on a sample of 10^4 randomly generated clusters in two and three dimensions. The closer look revealed that while the behaviours differ initially, they clearly appear to converge when the number of steps is sufficiently increased; see Fig. 11.14. Our estimates for the exponent ν for SAWs and KGWs on critical clusters are given in Table 11.1, alongside the previously obtained full-lattice values.

Based on these findings, we conclude that the asymptotic scaling behaviour of SAWs and KGWs on critical percolation clusters is probably identical, contrary to the situation on the full lattice.

Table 11.1: Values the scaling exponent ν.

medium	ν_{2D} (SAW)	ν_{2D} (KGW)	ν_{3D} (SAW)	ν_{3D} (KGW)
full lattice	3/4	0.682(2) [3]	0.587597(7) [7]	0.520(1) [3]
perc. cluster	0.780(5) [5]	0.782(3) [5]	0.66(3) [5]	0.649(4) [5]

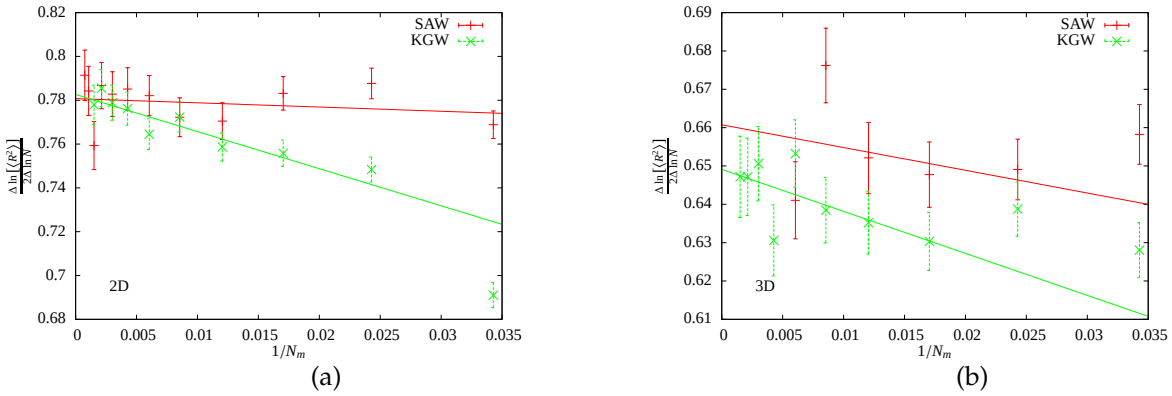

Figure 11.14: Extrapolations of $\frac{1}{2}\frac{\Delta \ln[\langle R^2 \rangle]}{\Delta \ln N}$ vs. $1/N$ to estimate the exponent ν on (a) 2D and (b) 3D percolation clusters. Only values where $1/N < 0.02$ were used for the fits. N_m denotes the mean of successive values of N.

[1] P. Flory: *Principles of Polymer Chemistry* (Cornell University Press, Ithaca, 1953)
[2] K. Kremer, J.W. Lyklema: Phys. Rev. Lett. **55**, 2091 (1985)
[3] J. Bock: Master Thesis, Universität Leipzig (2013)
[4] B. Barat, B.K. Chakrabarti: Phys. Rep. **258**, 377 (1995)
[5] N. Fricke et al.: diffusion-fundamentals.org **20**, 111 (2013)
[6] N. Fricke, W. Janke: Europhys. Lett. **99**, 56005 (2012)
[7] N. Clisby: Phys. Rev. Lett. **104**, 055702 (2010)

11.14 Dynamics of the binary frustrated unit: The effect of multiple inherent time scales

D. Labavić*, H. Nagel, W. Janke, H. Meyer-Ortmanns*

*School of Engineering and Science, Jacobs University Bremen, Germany

The motif of a self-activating species A that also activates another species B, which in turn represses its activator A, is often found in biological systems, particularly in those featuring inherent oscillatory behaviour. In such biological systems a source of delay in the interaction is essential for the observed dynamics. Thus different time scales are present in the interaction of the species. In this research, we investigated how such different inherent time scales lead to distinct dynamics in a stochastic description of such a system.

We considered a realization as a genetic circuit where two kinds of a proteins act as species A and B. The mechanism of activation and repression is modeled after genetic promoter sequences encoded before their respective regulated genes: The binding of a specific protein to an activating or inhibiting promoter region respectively increases or decreases the expression rate of the protein associated to that gene, cf. Fig. 11.15.

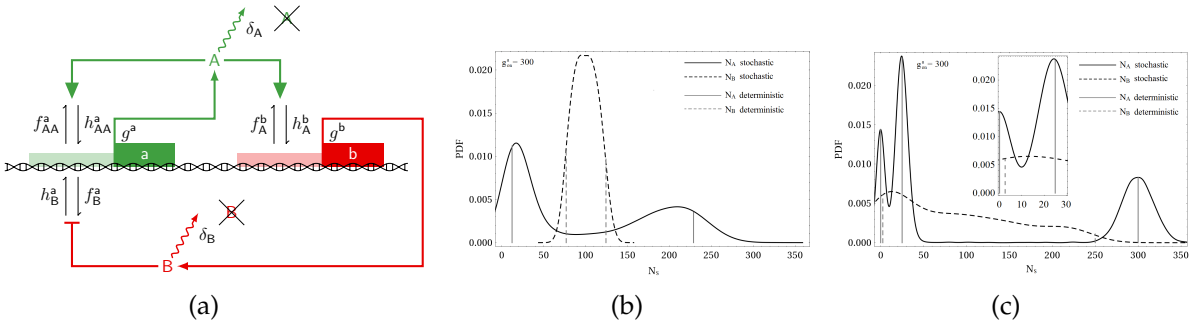

Figure 11.15: (a) Implementation of the basic motif as a genetic circuit. (b), (c) Probability density functions for populations N_A, N_B of species A, B respectively for a fast (b) and slow (c) time scale of gene activation. For slow genes (c) the bifurcation picture changes and attractors split up.

In previous work [1] we found that one source of delay can be introduced by making the species B-protein expression and decay slower than that of the A-protein and could observe oscillations. Depending on the amount of delay, these oscillations are the consequence of a limit cycle and large excursions from a fixed point in a Hopf–type bifurcation.

Here we identified and investigated the effect of a second source of delay in the activation/repression mechanism itself [2]. The corresponding time scale is defined by the binding rates of the proteins to the genes promoter regions. Employing Monte Carlo simulations as well as coarse-graining methods in the time domain we were able to identify distinct dynamic behaviours when the time scale of activation is much faster than that of species A, as fast as A and as slow as B. The bifurcational patterns change with the inherent time scales, too.

[1] A. Garai et al.: J. Stat. Mech.: Theor. Exp., P01009 (2012)
[2] D. Labavić et al.: Phys. Rev. E **87**, 062706 (2013)

11.15 Condensation shapes in a stochastic mass transport model

E. Ehrenpreis, H. Nagel, W. Janke

Generic examples for stochastic mass transport processes are traffic flow, force propagation in granular media, aggregation and fragmentation of clusters, and many others [1]. The transport is classically modeled by probabilities for hopping events from one site to another. Since such processes are usually out-of-equilibrium, it is in general difficult to predict possible stationary states. Still, under certain circumstances it is possible to identify a transition between a liquid-like phase and a phase with a condensate (e.g., a "traffic jam") that are associated with different stationary states. In the condensate a finite fraction M' of constituent particles condenses onto a finite extension W in space, sometimes even onto a single site. This is an example of spontaneous

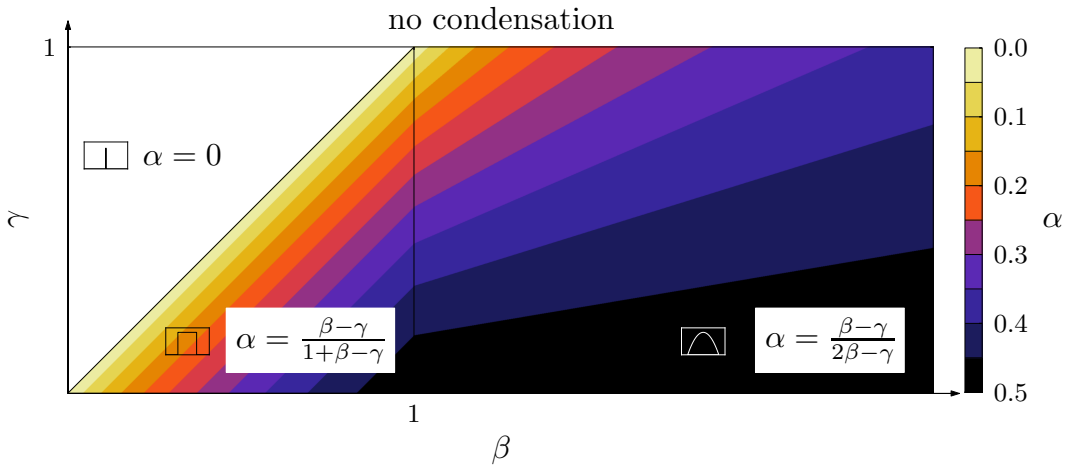

Figure 11.16: Theoretically predicted phase diagram for $K(x) \sim e^{-x^\beta}$ and $p(m) \sim e^{-m^\gamma}$, exhibiting condensed phases with point-like, rectangular and parabolic shapes (from left to right). The predicted value of the exponent α in the scaling law for the condensate extension W with the number M' of condensed particles, $W \simeq M'^\alpha$, is indicated by the color code.

symmetry breaking which, in contrast to equilibrium systems, can happen here even in a one-dimensional system.

In previous analytical work [2–4] we concentrated on a class of models with steady states that factorize over the links of arbitrary connected graphs, so-called pair-factorized steady states (PFSS). This property enables at least partially an analytic treatment of the transport properties. In one dimension we could predict the critical mass density at the condensation transition and in particular the condensate shape which turned out to be non-universal. Rather, by the competition of local (K) and ultralocal (p) interactions governing the hopping rates, it can be tuned from "extended" to "point-like" [5]. The resulting phase diagram for the choice $K(x) \propto \exp(-x^\beta)$ and $p(m) \propto \exp(-m^\gamma)$ and the analytically predicted exponent α in the scaling law for the condensate extension, $W \sim M'^\alpha$, are shown in Fig. 11.16.

The analytical treatment is based on several approximations. To assess their accuracy, we have performed extensive computer simulations of the hopping events and determined the phase diagram numerically [6]. As a result we find very nice agreement with the theoretical prediction. This is demonstrated in Fig. 11.17 where the measured condensate shapes are displayed in the β-γ plane. By performing power-law fits of the condensate widths W against the number of constituent particles M', we obtain in most parts of the β-γ plane very good agreement with the predicted values of the exponent α at a 1% accuracy level.

[1] M.R. Evans et al.: Phys. Rev. Lett. **97**, 010602 (2006)
[2] B. Wacław et al.: J. Phys. A: Math. Theor. **42**, 315003 (2009)
[3] B. Wacław et al.: Phys. Rev. Lett. **103**, 080602 (2009)
[4] B. Wacław et al.: J. Stat. Mech. P10021 (2009)
[5] B. Wacław et al.: J. Phys.: Conf. Ser. **246**, 012011 (2010)
[6] E. Ehrenpreis et al.: J. Phys. A: Math. Theor. **47**, 125001 (2014)

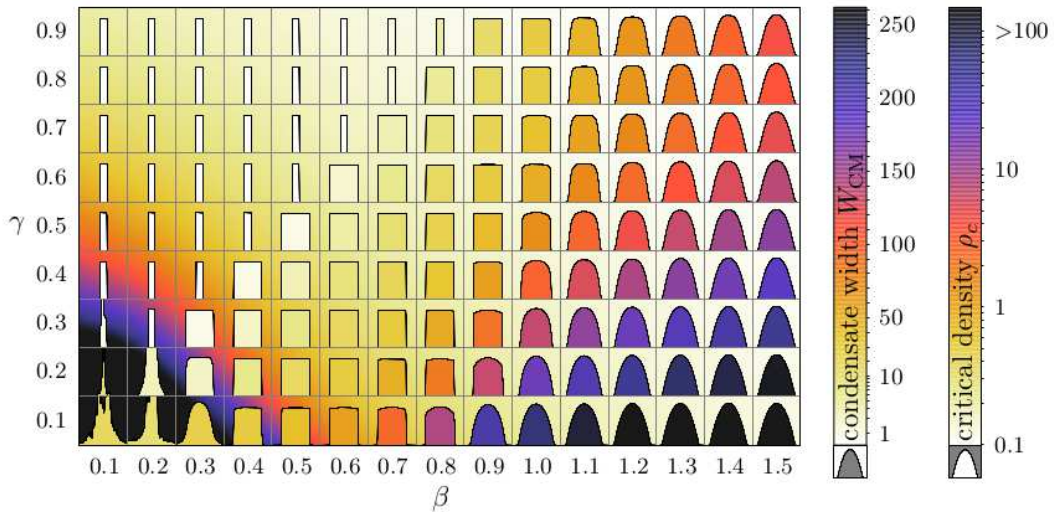

Figure 11.17: Numerically determined characteristic condensate shapes for systems of various β and γ at a condensate volume of about 10^5 masses. The shapes are formed by rescaling the width and height of all measured condensate sample shapes and only then averaging them. The fill colour inside the condensate shapes encodes the respective measured condensate width while the background colour around the shapes gives the critical density of the system. The shapes in the single-site condensate regime are plotted narrowed to give better distinction to extended shapes.

11.16 Transmuted finite-size scaling at first-order phase transitions

M. Müller, W. Janke, D.A. Johnston*

*Department of Mathematics and the Maxwell Institute for Mathematical Sciences, Heriot-Watt University, Edinburgh, UK

First-order phase transitions are ubiquitous in nature. In the limit of infinite system size they are characterized by jumps in the energy and/or order parameter and δ-function like divergences in response functions such as the specific heat. Similarly to critical phenomena, in finite systems these singularities are rounded and shifted. It is well established [1] that the finite-size corrections at a first-order phase transition scale with the inverse system volume, i.e., $1/L^3$ for an $L \times L \times L$ lattice in 3D, with the amplitudes of the correction terms being proportional to $\ln q$, where q denotes the degeneracy of the low-temperature phase. In many standard models such as the q-state Potts model, this factor is not particularly important since q is just a constant which does not change with system size.

However, if the degeneracy q of the low-temperature phase depends exponentially on the system size, say $q \propto e^L$, the usual $1/L^3$ would be modified to $1/L^2$. In [2] we noted that one model with precisely this feature is a 3D plaquette (4-spin) interaction Ising model on a cubic lattice where $q = 2^{3L}$ on an L^3 lattice [3]. This is a member of a family of so-called gonihedric Ising models [4] whose Hamiltonians contain, in general, nearest, next-to-nearest, and plaquette interactions. These were originally formulated as a lattice discretization of string-theory actions in high-energy physics which depend

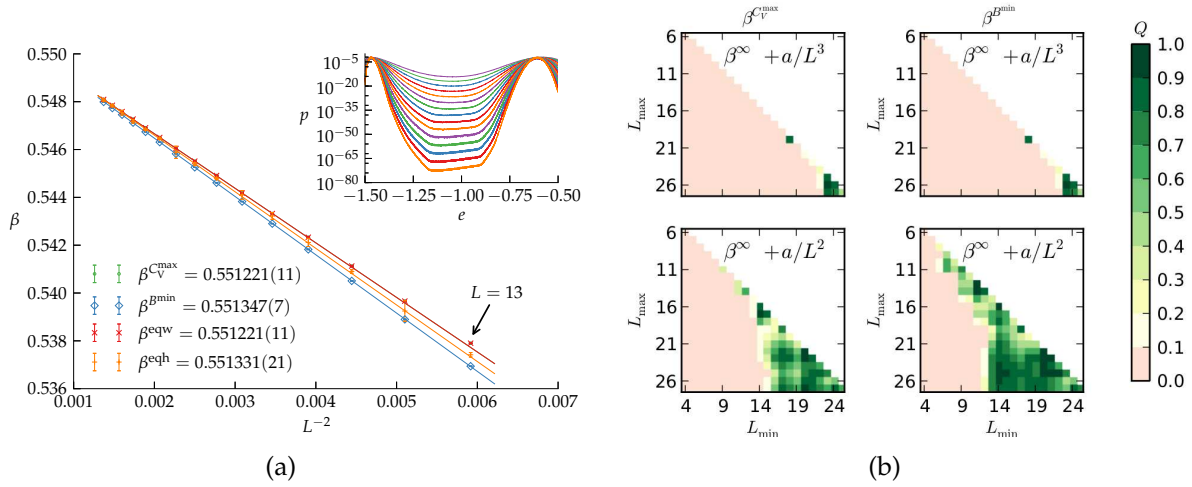

(a) (b)

Figure 11.18: (a) Best fits using the leading $1/L^2$ scaling behaviour for the gonihedric model. (b) Plot of the goodness-of-fit parameter Q for fits on the extremal locations of the specific heat, $\beta^{C_V^{\max}}$, and Binder's energy cumulant, $\beta^{B^{\min}}$, of the original model for different fitting ranges $L_{\min} - L_{\max}$. Large values of Q (green color) indicate acceptable fits. Upper row: Standard $1/L^3$ finite-size scaling ansatz. Lower row: Transmuted $1/L^2$ finite-size scaling.

solely on the extrinsic curvature of the string worldsheet [5].

We used multicanonical simulations of this model to generate high-precision data which indeed provides strong confirmation of the non-standard finite-size scaling law [2, 6], see Fig. 11.18. The dual to the gonihedric model, which is an anisotropically coupled Ashkin-Teller model [7], has a similar degeneracy and also displays the non-standard scaling [2, 6].

Our observation for the gonihedric model and its dual applies generically to any models which have a low-temperature phase degeneracy that depends exponentially on the system size. Examples range from ANNNI models to topological "orbital" models in the context of quantum computing. Numerous other systems, such as the Ising antiferromagnet on a 3D FCC lattice, have an exponentially degenerate number of ground states but a small number of true low-temperature phases. Nonetheless, they do possess an exponentially degenerate number of low-energy excitations so, depending on the nature of the growth of energy barriers with system size, an *effective* modified scaling could still be seen at a first-order transition for the lattice sizes accessible in typical simulations.

[1] C. Borgs et al.: J. Stat. Phys. **62**, 529 (1991); W. Janke: Phys. Rev. B **47**, 14757 (1993)
[2] M. Mueller et al.: Phys. Rev. Lett. **112**, 200601 (2014)
[3] R. Pietig, F. Wegner: Nucl. Phys. B **466**, 513 (1996); *ibid.* **525**, 549 (1998)
[4] G.K. Savvidy, F.J. Wegner: Nucl. Phys. B **413**, 605 (1994); D.A. Johnston, R.K.P.C. Malmini: Phys. Lett. B **378**, 87 (1996)
[5] R.V. Ambartzumian et al.: Phys. Lett. B **275**, 99 (1992); G.K. Savvidy, K.G. Savvidy: Int. J. Mod. Phys. A **8**, 3393 (1993); Mod. Phys. Lett. A **8**, 2963 (1993)
[6] M. Mueller et al.: Leipzig preprint (2014), to be published
[7] D.A. Johnston, R.P.K.C.M. Ranasinghe: J. Phys. A: Math. Theor. **44**, 295004 (2011)

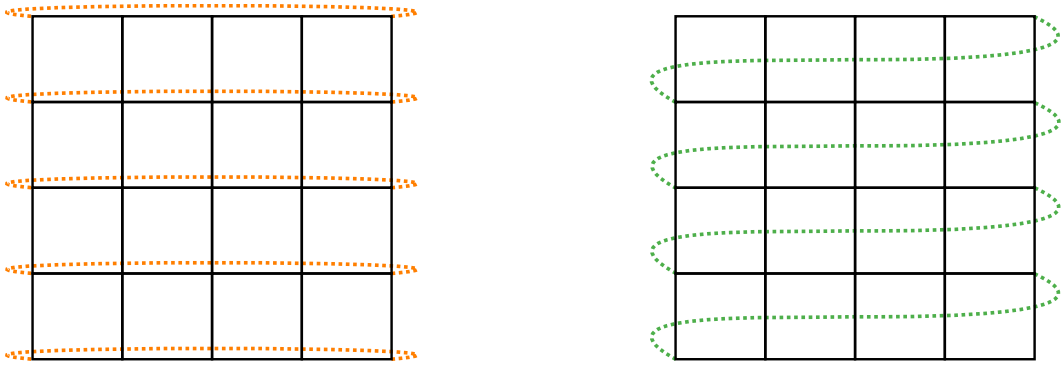

(a) PBC (b) SBC

Figure 11.19: Sketch of (a) periodic (PBC) and (b) screw-periodic boundary conditions (SBC) along the x-axis of a two-dimensional lattice. In the SBC picture the link between the lower right and the upper left corner is not shown. Equivalent boundary conditions are applied to the y-direction. Here a screw parameter of $S = 1$ is used.

11.17 First-order directional ordering transition in the three-dimensional compass model

M.H. Gerlach*, W. Janke

*Institut für Theoretische Physik, Universität zu Köln, Germany

Both the classical and the quantum version of the compass model have recently attracted much interest in the literature. The reason is its connection to interesting quantum phenomena ranging from orbital order in transition metal compounds to topologically protected qbits [1–3]. In three dimensions the classical model is defined by the Hamiltonian

$$\mathcal{H} = J \sum_{i=1}^{N} \left(\sigma_i^x \sigma_{i+e_x}^x + \sigma_i^y \sigma_{i+e_y}^y + \sigma_i^z \sigma_{i+e_z}^z \right) , \tag{11.4}$$

where $\sigma = (\sigma^x, \sigma^y, \sigma^z)$ are three-dimensional unit spin vectors, e_x, e_y, and e_z are unit vectors in x, y, and z direction, and J is a coupling constant. Although simple looking at first sight, surprisingly little is known about this model in three dimensions. Most studies so far focused on the two-dimensional analogue which still turned out to be rather hard to study numerically. It was shown to possess rich physics ranging from highly degenerate ground states to quantum phase transitions to an exciting thermal phase transition [4, 5].

In recent analyses of high-temperature series expansions of the three-dimensional quantum model (where the classical spins are replaced by Pauli matrices) it was claimed that this model does not exhibit a phase transition at any finite temperature [6]. This motivated us to consider first the three-dimensional classical model and to investigate whether this model exhibits a phase transition [7]. To this end we employed state-of-the-art Monte Carlo computer simulations using Metropolis, cluster, and parallel tempering (PT) techniques. From our previous studies in two dimensions [5] we knew

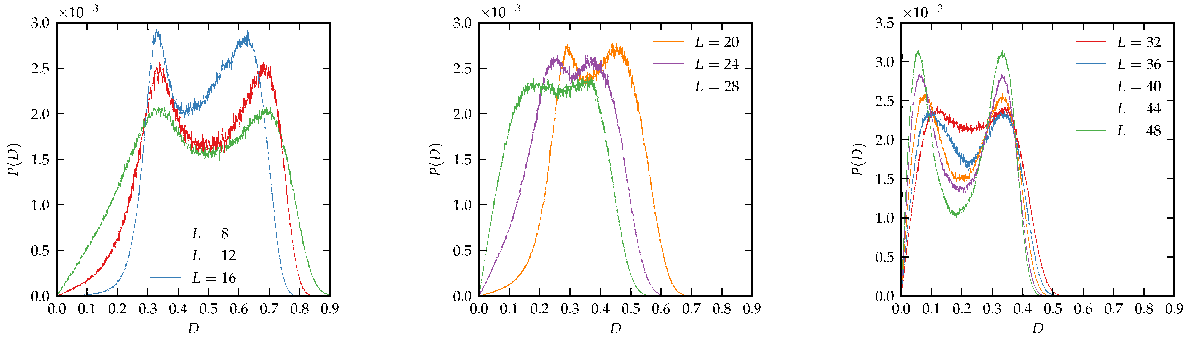

Figure 11.20: Histograms of the directional order parameter D in the three-dimensional compass model with screw-periodic boundary conditions for various lattice sizes L.

that employing so-called screw-periodic boundary conditions [8] sketched in Fig. 11.19 considerably improves the finite-size scaling behaviour of this model. As a result we obtained convincing numerical evidence for a phase transition of first-order at the temperature $T_0 = 0.098328 \pm 0.000003$. This value is in good agreement with a brief remark in Ref. [9]. The nature of the phase transition can be read off from the histograms of the directional order parameter D of the model in Fig. 11.20 which exhibit for large lattice sizes L a characteristic double-peak structure. Note the nonmonotonic behaviour as function of lattice size: Initially, the double peak becomes *less* pronounced until $L \approx 28-32$, and only from then on it becomes more pronounced with further increasing L. By analyzing the ratio of peak maximum to peak minimum, we arrive at a definitely nonzero, albeit small value for associated interface tension, $\sigma_{\mathrm{od}} \approx 3 \times 10^{-4}$.

[1] K.I. Kugel, D.I. Khomskii: Sov. Phys. Usp. **25**, 231 (1982)
[2] B. Douçot et al.: Phys. Rev. B **71**, 024505 (2005)
[3] A. Kitaev: Ann. Phys. **321**, 2 (2006)
[4] S. Wenzel, W. Janke: Phys. Rev. B **78**, 064402 (2008); see also "Publisher's Note" in Phys. Rev. B **78**, 099902(E) (2008) [Fig. 1 selected for Phys. Rev. B "Kaleidoscope" August 2008]
[5] S. Wenzel et al.: Phys. Rev. E **81**, 066702 (2010) [arXiv:1002.3508]
[6] J. Oitmaa, C.J. Hamer: Phys. Rev. B **83**, 094437 (2011)
[7] M.H. Gerlach, W. Janke: *First-order directional ordering transition in the three-dimensional compass model*, e-print arXiv:1406.1750 (cond-mat.stat-mech), submitted
[8] E. Bittner et al.: Nucl. Phys. B **820**, 694 (2009)
[9] S. Wenzel, A.M. Läuchli: Phys. Rev. Lett. **106**, 197201 (2011)

11.18 Status of our framework for programming Monte Carlo simulation (βMC)

M. Marenz, J. Zierenberg, W. Janke

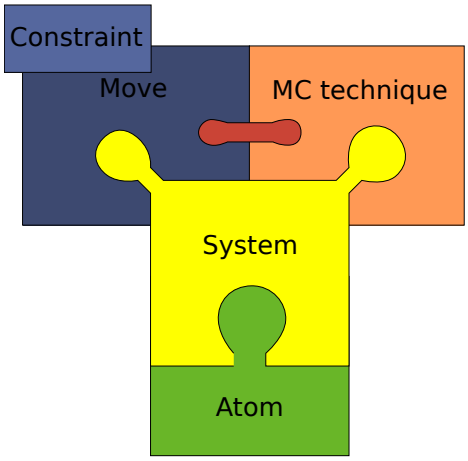

Figure 11.21: The 5 basic building blocks.

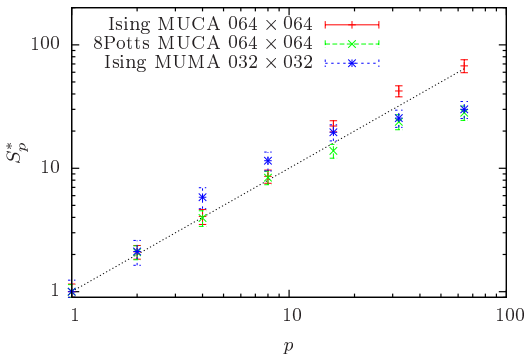

Figure 11.22: Scaling properties of the parallel multicanonical algorithm as a function of the number of processors p.

Monte Carlo (MC) computer simulations are a very powerful tool for investigating and understanding the thermodynamical behaviour of a wide variety of physical systems. These systems range from such simple ones like the Ising spin model to complex ones like the adsorption properties of proteins on surfaces [1]. In contrast to Molecular Dynamics (MD) simulations, the other important class of algorithm to simulate microscopical systems, MC simulations are not suitable to investigate dynamical properties. On the other hand, the ability of modern MC methods to explore effectively the phase space of physical systems, especially those with a phase transition, makes them a very powerful and indispensable tool.

Another difference to MD simulations is the lack of a widely used program package for generic MC simulations. One reason for this lack is the versatility of modern MC algorithms – there are various different algorithm and many different possibilities to adjust a MC simulation to a specific problem.

This was the starting point for the development of our framework for advanced MC algorithms. The aim of the framework is to enable the programmer to implement specific simulations in an easy and efficient way, without the need to implement all the tricky details for every new problem. The framework is implemented in the C++ programming language and is designed such that it separates basics parts of a MC algorithm in separate building blocks. These building blocks can be used by the programmer to implement a specific simulation.

There are 5 basic building blocks as illustrated in Fig. 11.21: The first one is the "system", which defines the Hamiltonian and the structure of the physical system. This means that the "system" building block encapsulates the energy calculation and the structure of the considered physical problem. For off-lattice system this block contains a smaller subpart, the "atom" block, which encodes the geometry of the system (e.g., boundary conditions). As systems we have implemented so far different kinds of coarse-grained homopolymers, the Lennard-Jones gas, the TIP4P water model, lattice polymers and the Potts model in different dimensions. On top of the "system" are the last two other building blocks, the "move" and the "MC technique". A "move" defines a single update proposal, propagating the system from the current state to the next one. Additionally a "constraint" can be added to every "move" in order to simulate efficiently systems with geometrical confinements. The "MC technique" implements the

Monte Carlo algorithm itself. At the moment we have implemented various algorithms such as Metropolis MC, parallel tempering, multicanonical MC, multimagnetic MC and the Wang-Landau MC algorithm. One of the most advanced MC algorithms we have implemented is a parallel version of the multicanonical algorithm [2], see Fig. 11.22.

The boundaries between these blocks are well defined, so that one can easily exchange one of them. For example one can use two different algorithm to simulate a specific system without implementing a completely new program. The framework is already in practical use for different studies, for example the investigation of the influence of bending stiffness on a coarse-grained homopolymer, the influence of a spherical confinement to pseudo-phase transitions of homopolymers, the study of polymer aggregation of several polymers for a large set of parameters (temperature, bending stiffness). Thus the framework is very useful and has let already to the publication of several papers [2–5].

[1] M. Bachmann et al.: Angew. Chem. Int. Ed. **49**, 9530 (2010) [Ang. Chem. **122**, 9721 (2010), in German]
[2] J. Zierenberg et al.: Comput. Phys. Commun. **184**, 1155 (2013)
[3] M. Marenz et al.: Condens. Matter Phys. **15**, 43008 (2012)
[4] J. Zierenberg et al.: J. Phys.: Conf. Ser. **510**, 012017 (2014)
[5] J. Zierenberg, W. Janke: e-print arXiv:1401.3227, submitted

11.19 Application of the parallel multicanonical method to a broad range of problems

J. Zierenberg, M. Wiedenmann, M. Marenz, W. Janke

We applied our recently refined parallel multicanonical method [1] to a broad range of problems and investigated the scaling properties including the Ising spin model, the q-state Potts model and bead-spring polymers [2], as well as the lattice gas model [3]. In all cases, we find a close to linear scaling with slope one for up to 128 cores used. This means, that doubling the number of involved processors would reduce the wall-clock time necessary by a factor of two. Moreover, it is a straightforward and simple implementation especially if wrapped around an existing multicanonical simulation.

A detailed analysis of optimized parameters per degree of parallelization for the q-state Potts model in the range $q = \{2, 8\}$ suggests that there exists a limit depending on emerging barriers and associated increasing integrated autocorrelation times [1, 2].

For any real-life application, we continue to consider a fixed number of sweeps per multicanonical iteration that is distributed onto the number of cores. This is the only possibility to assess larger or more complicated systems and shows the expected scaling also for first-order transitions like gas condensation in two and three dimensions, see Fig. 11.23 [3]. With this method, we were able to show that in three dimensions lattice gas condensation shows an unexpected deviation from the analytic predictions which may be explained by finite-size effects but needs additional investigations.

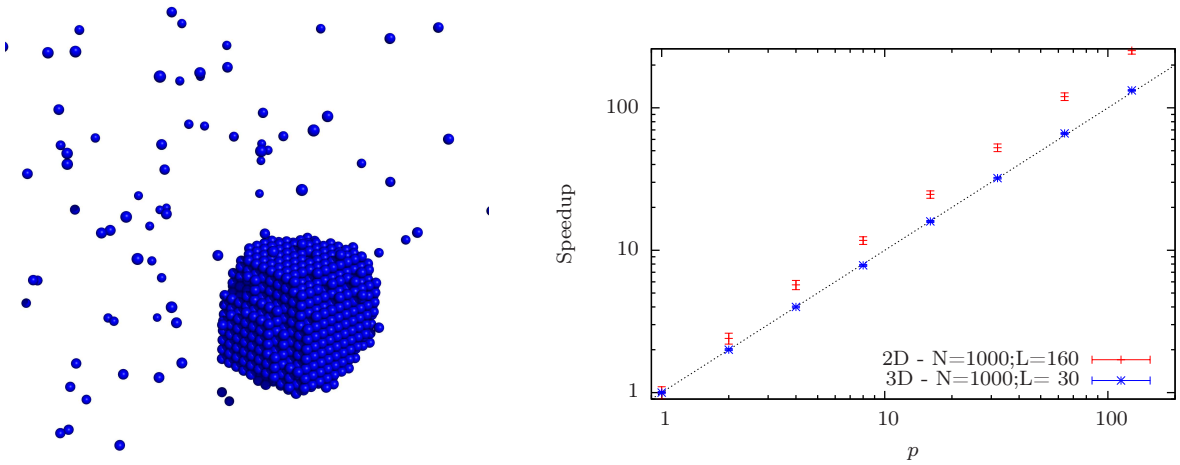

(a) (b)

Figure 11.23: (a) Lattice gas in the droplet phase as an example for (b) the speedup in a day-to-day application.

Altogether, this demonstrates the broad range of application of this parallel version of multicanonical simulations to problems in hard and soft condensed matter in any parameter that occurs linear in the Hamiltonian (temperature, field, etc.).

[1] J. Zierenberg et al.: Comput. Phys. Commun. **184**, 1155 (2013)
[2] J. Zierenberg et al.: e-print `arXiv:1312.2213`, to appear in Physics Procedia, in print
[3] J. Zierenberg et al.: J. Phys.: Conf. Ser. **510**, 012017 (2014)

11.20 Simulated tempering and magnetizing simulations of the three-state Potts model

T. Nagai*, Y. Okamoto*, W. Janke

*Department of Physics, Graduate School of Science, Nagoya University, Nagoya, Japan

The three-state Potts model in an external magnetic field has several interesting applications in condensed matter physics and serves as an effective model for quantum chromodynamics [1]. When one of the three states per spin is disfavoured in an external (negative) magnetic field (see Fig. 11.24), the other two states exhibit Z_2 symmetry and one expects a crossover from Potts to Ising critical behaviour.

To study such a crossover in a two-dimensional parameter space, generalized-ensemble Monte Carlo simulations are a useful tool [2]. Inspired by recent multi-dimensional generalizations of generalized-ensemble algorithms [3], the "Simulated Tempering and Magnetizing" (STM) method has been proposed by two of us and first tested for the classical Ising model in an external magnetic field [4]. In the conventional simulated tempering (ST) scheme [5] the temperature is considered as an additional dynamical variable besides the spin degrees of freedom. The STM method is a generalization to a two-dimensional parameter space where both the temperature *and* the magnetic field

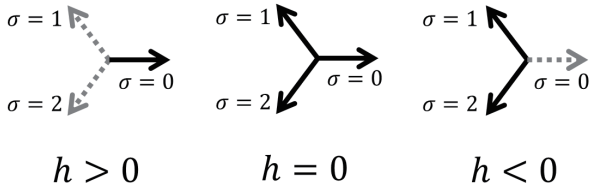

Figure 11.24: Schematic sketch illustrating the behaviour of the spins of the three-state Potts model in an external magnetic field h.

are treated as additional dynamical variables. Recently we have extended this new simulation method to the two-dimensional three-state Potts model and by this means generated accurate numerical data in the temperature-field plane [6].

Our STM simulations were performed for lattice sizes $L = 5, 10, 20, 40, 80$, and 160 with the total number of sweeps varying between about 160×10^6 and 500×10^6, where a sweep consisted of N single-spin updates with the heat-bath algorithm followed by an update of either the temperature T or the field h. By this means one can easily sample a wide range of the two-dimensional parameter space and it is straightforward to compute a two-dimensional map of any thermodynamic quantity that can be expressed in terms of the energy and magnetization. As an example, Fig. 11.25 shows (a) the specific heat and (b) the susceptibility for $L = 80$. We see a line of phase transitions starting at the Potts critical point at $h = 0$, $T_c^{\text{Potts}} = 1/\ln(1+\sqrt{3}) = 0.9950$ which approaches for strong negative magnetic fields the Ising model limit with a critical point at $h \to -\infty$, $T_c^{\text{Ising}} = 1/\ln(1+\sqrt{2}) = 1.1346$. By means of finite-size scaling analyses we confirmed that along this transition line the critical exponents indeed fall into the Ising universality class [6], as expected. For positive magnetic fields, the phase transition disappears altogether.

[1] F.Y. Wu: Rev. Mod. Phys. **54**, 235 (1982)
[2] W. Janke: Physica A **254**, 164 (1998); U.H.E. Hansmann, Y. Okamoto: in *Annual Reviews of Computational Physics VI*, ed. D. Stauffer (World Scientific, Singapore, 1999), p. 129; W. Janke (ed.): *Rugged Free Energy Landscapes: Common Computational Approaches to Spin Glasses, Structural Glasses and Biological Macromolecules*, Lect. Notes Phys. **736** (Springer, Berlin, 2008)
[3] A. Mitsutake, Y. Okamoto: Phys. Rev. E **79**, 047701 (2009); J. Chem. Phys. **130**, 214105 (2009)
[4] T. Nagai, Y. Okamoto: Phys. Rev. E **86**, 056705 (2012); Physics Procedia **34**, 100 (2012)
[5] A.P. Lyubartsev et al.: J. Chem. Phys. **96**, 1776 (1992); E. Marinari, G. Parisi: Europhys. Lett. **19**, 451 (1992)
[6] T. Nagai et al.: J. Stat. Mech.: Theor. Exp., P02039 (2013); Condens. Matter Phys. **16**, 23605 (2013)

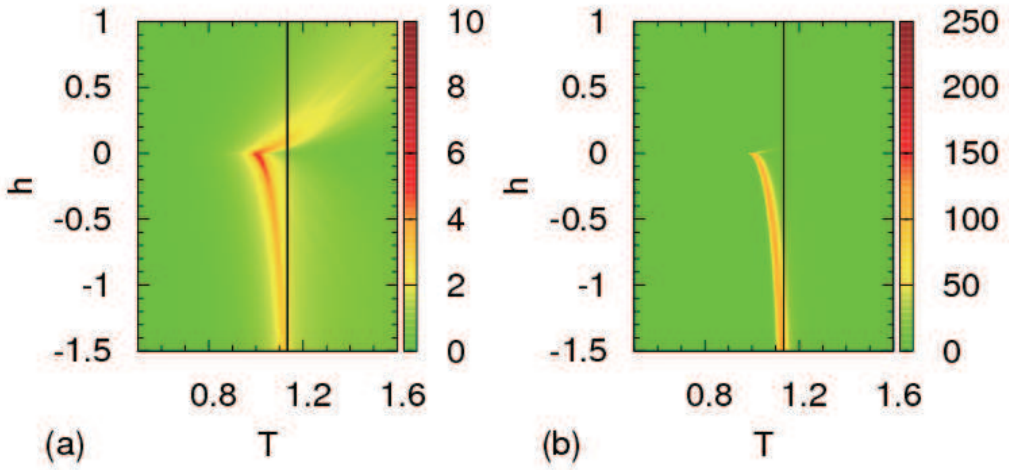

Figure 11.25: (a) Specific heat C/L^2 and (b) magnetic susceptibility χ/L^2 as functions of T and h for $L = 80$. The solid vertical line at $T = 1.1346$ shows the critical temperature of the Ising model (in 2-state Potts model normalization).

11.21 Finding the bridge between Molecular Dynamics and Monte Carlo simulations

P. Schierz, J. Zierenberg, W. Janke

Molecular Dynamics (MD) and Monte Carlo (MC) simulations are two powerful and widely used tools for the investigation of polymer properties. While MD follows the time evolution of the system by integrating Newton's equations of motion, MC simulations are based on statistical mechanics.

The starting question was to which extent we can expect the same results for both simulation techniques when we study polymer aggregation. Simulations for a many polymer system showed deviations between the results from multicanonical (MUCA) MC simulations [1] analysed in the NVE ensemble and MD (see Fig. 11.26(a)), where N is the number of polymers, V the volume, and E the total energy.

In order to find the reason for the observed deviations, similar simulations have been performed for a simpler Lennard-Jones gas. It turned out that the assumption that MD samples the NVE ensemble is not entirely correct. The NVE ensemble would allow all momenta for one configuration which are consistent with the given total energy. In MD, however, we have, for a system without boundary conditions, conservation laws for the total momentum P and total angular momentum J which leads to a restriction of the available phase space and therefore to the NVEPJ ensemble [2].

The knowledge of this ensemble allows the attempt to reweight from the MD data in the NVEPJ ensemble to the NVE ensemble. For a single homopolymer, boundary conditions are not necessary since it will remain at the starting point in an MD simulation.

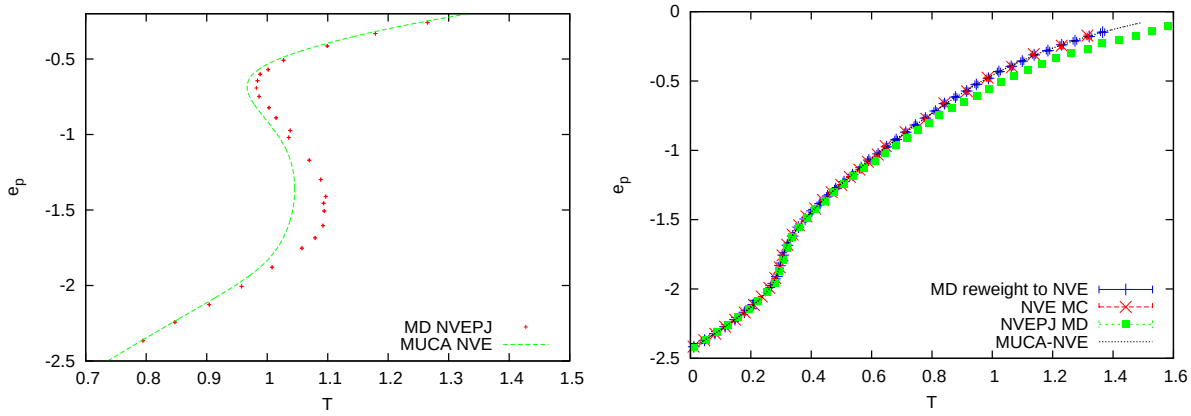

(a) (b)

Figure 11.26: (a) Comparison of the energy as function of temperature for 8 polymers with 13 monomers each, simulated with MUCA MC and MD. (b) The energy for a single polymer with 13 monomers simulated by MUCA MC, NVE MC, simple MD, and reweighted MD.

In this case the reweighting technique worked for the whole coil-globule transition, see Fig. 11.26(b). For the Lennard-Jones gas, the boundary conditions are only negligible for the condensed phase with a zero total momentum. As soon as the condensate brakes apart the periodic boundary conditions will break the angular momentum conservation and the NVEPJ ensemble is no longer valid.

[1] B.A. Berg, T. Neuhaus: Phys. Lett. B **267**, 249 (1991); Phys. Rev. Lett. **68**, 9 (1992)
[2] F. Calvo et al.: J. Chem. Phys. **112**, 22 (2000)

11.22 Funding

Graduate School *"BuildMoNa": Leipzig School of Natural Sciences – Building with Molecules and Nano-objects*
W. Janke (Principal Investigator)
Deutsche Forschungsgemeinschaft (DFG), Excellence Initiative Grant GSC185

Graduate School *Statistical Physics of Complex Systems*
W. Janke (with B. Berche, Nancy)
Deutsch-Französisches Doktorandenkollegium (DFDK) with "Co-tutelle de Thèse", jointly with Université de Lorraine, Nancy, France, and Coventry University, UK, and National Academy of Sciences of Ukraine, Lviv, Ukraine, as associated partner
Deutsch-Französische Hochschule (DFH-UFA), Grant No. CDFA-02-07

International Max Planck Research School (IMPRS) *Mathematics in the Sciences*
W. Janke (Scientific Member)
Max Planck Society and Klaus Tschira Foundation

Forschergruppe 877 *From Local Constraints to Macroscopic Transport*
W. Janke (Principal Investigator, project P9 in collaboration with K. Kroy)
Deutsche Forschungsgemeinschaft (DFG), Grant No. JA 483/29-1

Sonderforschungsbereich/Transregio SFB/TRR 102 *Polymers under Multiple Constraints: Restricted and Controlled Molecular Order and Mobility*
W. Janke (Principal Investigator, project B04)
Deutsche Forschungsgemeinschaft (DFG)

Nachwuchsforschergruppe *Funktion durch Selbstorganisation: Emergente Eigenschaften von Atom- und Molekülaggregaten*
P. Schierz, W. Janke
Europäischer Sozialfonds (ESF)

Nachwuchsforschergruppe *Werkzeuge und Technologien für die rationale Wirkstoffentwicklung*
J. Bock, W. Janke
Europäischer Sozialfonds (ESF)

Institute Partnership with the Institute for Condensed Matter Physics of the National Academy of Sciences of Ukraine, Lviv, Ukraine, *Polymers in Porous Environments and on Disordered Substrates*
W. Janke (with V. Blavatska, Lviv)
Alexander von Humboldt Foundation (AvH)

Molecular Conformation Mechanics of Proteins and Polymers
W. Janke
Deutsche Forschungsgemeinschaft (DFG), Grant No. JA 483/24-3

Mass Transport Models on Networks
W. Janke (twin project with H. Meyer-Ortmanns, Jacobs University Bremen)
Deutsche Forschungsgemeinschaft (DFG), Grant No. JA 483/27-1

Aggregation and Collapse of Polymers in Confinement
W. Janke, M. Marenz, J. Zierenberg
NIC Jülich (computer time grant for "JUROPA"), Grant No. HLZ21

11.23 Organizational Duties

Wolfhard Janke

- Director, Institute for Theoretical Physics (ITP), Universität Leipzig
- Director, Naturwissenschaftlich-Theoretisches Zentrum (NTZ), Universität Leipzig
- Member of Department Council ("Fakultätsrat"), Faculty for Physics and Earth Sciences, Universität Leipzig
- Member of the Steering Committee ("Direktorium") of the Graduate Centre *Mathematics/Computer Science and Natural Sciences*, Research Academy Leipzig
- Principal Investigator of the Graduate School "BuildMoNa"
- Scientific Member of the International Max Planck Research School (IMPRS) *Mathematics in the Sciences*
- Principal Investigator of the DFG Sonderforschungsbereich/Transregio SFB/TRR 102 *Polymers under Multiple Constraints: Restricted and Controlled Molecular Order and Mobility*

- Principal Investigator of the DFG Forschergruppe FOR877 *From Local Constraints to Macroscopic Transport*
- Member of the Priority Research Area PbF1 *Molecules and Nano-objects*, Universität Leipzig
- Member ot the Priority Research Area PbF2 *Mathematical Sciences*, Universität Leipzig
- Chairperson of the Programme Committee "Scientific Computing" of Forschungszentrum Jülich
- Member of the Scientific-Technical-Council of the Supervisory Board ("Aufsichtsrat") of the Forschungszentrum Jülich GmbH
- Spokesperson of the German-French Graduate College *Statistical Physics of Complex Systems* with Nancy (France), Coventry (England, UK) and Lviv (Ukraine) of the Deutsch-Französische Hochschule (DFH-UFA)
- Spokesperson of the German-Ukrainian Institute Partnership Leipzig-Lviv of the Alexander von Humboldt Foundation (AvH)
- External Member of the Jagiellonian University Graduate School *International Ph.D. Studies in Physics of Complex Systems*, Krakow, Poland
- *International Visiting Professor* of Coventry University, England, UK
- Permanent Member of the International Advisory Board for the Annual *Conference of the Middle European Cooperation in Statistical Physics (MECO)*
- Co-organizer of the SFB/TRR 102 Advanced Training Module *Introduction to Monte Carlo and Molecular Dynamics Simulation of Polymers* (with W. Paul, Universität Halle), Universität Halle, 07. February 2013 & Universität Leipzig, 08. February 2013
- Co-organizer of the "BuildMoNa" Modul 2013-B3 *Basic Concepts in Physics* (with P. Esquinazi and J. Haase), Universität Leipzig, 12./14. February 2013
- Co-organizer of the "BuildMoNa" Module 2013-T2 *Multifunctional Scaffolds: Modeling and Simulating Macromolecules* (with F. Kremer), Universität Leipzig, 20.–21. June 2013
- Member of the International Advisory Board for the XXV IUPAP *Conference on Computational Physics* CCP2013, Moscow, Russia, 20.–24. August 2013
- Organizer of the Workshop *CompPhys13* – 14th International NTZ Workshop on *New Developments in Computational Physics*, ITP, Universität Leipzig, 28.–30. November 2013
- Organizer of the Workshop *DEC13 – Droplet Evaporation/Condensation*, ITP, Universität Leipzig, 12./13. December 2013
- Member of the International Scientific Committee for the *Humboldt Kolleg: German-Turkish Cooperation in Physics: New Challenges in Science*, Ankara University, Ankara, Turkey, 11.–13. June 2014
- Chair of the Program Committee *Classical Statistical Mechanics and Complex Systems* of the XXVI IUPAP *Conference on Computational Physics* CCP2014, Boston, USA, 11.–14. August 2014
- Organizer of the Workshop *CompPhys14* – 15th International NTZ Workshop on *New Developments in Computational Physics*, ITP, Universität Leipzig, 27.–29. November 2014
- Guest Editor for the Special Issue of Condens. Matter Phys.: *Self-Organization and Collective Behaviour in Complex Systems*
- Editor "Computational Physics", Central European Journal of Physics, Krakow, Po-

land
- Member of Editorial Board, Condens. Matter Phys., Lviv, Ukraine
- External Reviewer for Deutsche Forschungsgemeinschaft (DFG), Humboldt-Stiftung (AvH), Studienstiftung des deutschen Volkes, Fond zur Förderung der wissenschaftlichen Forschung (FWF), Österreich, The Royal Society, UK, The Engineering and Physical Sciences Research Council (EPSRC), UK, Israel Science Foundation, Israel, National Science Foundation (NSF), USA, Natural Sciences and Engineering Research Council of Canada (NSERC), Canada, The Jeffress Memorial Trust, Bank of America, Virginia, USA, Universität Mainz, Germany, The University of Warwick, England, UK, Coventry University, England, UK, CECAM, Lyon, France
- Referee for Physical Review Letters, Physical Review B, Physical Review E, Journal of Chemical Physics, Europhysics Letters, Physics Letters A, Physics Letters B, The European Physical Journal B, Physica A, Proceedings of the Royal Physical Society, Journal of Physics A, Computer Physics Communications, JSTAT, Condens. Matter Phys., PLOS ONE, New Journal of Physics, International Journal of Modern Physics C

11.24 External Cooperations

Academic

- Institute of Physics, Jagiellonian University, Kraków, Poland
  Prof. Dr. Piotr Białas, Dr. Leszek Bogacz, Prof. Dr. Zdzisław Burda
- CEA/Saclay, Service de Physique Théorique, France
  Dr. Alain Billoire
- Institut für Physik, Universität Mainz, Germany
  Prof. Dr. Kurt Binder, Dr. Hsiao-Ping Hsu, Andreas Nußbaumer, Prof. Dr. Friderike Schmid
- Institut für Theoretische Physik, Universität Heidelberg, Germany
  Dr. Elmar Bittner
- Laboratoire de Physique des Matériaux (UMR CNRS No 7556), Université de Lorraine, Nancy, France
  Prof. Dr. Bertrand Berche, Dr. Christophe Chatelain, Dr. Olivier Collet, Prof. Dr. Malte Henkel, Prof. Dr. Dragi Karevski
- Groupe de Physique des Matériaux (UMR CNRS No 6634), Université de Rouen, France
  Dr. Pierre-Emmanuel Berche
- SUPA, School of Physics and Astronomy, University of Edinburgh, Scotland, UK
  Dr. Richard A. Blythe, Prof. Dr. Martin R. Evans, Dr. Bartłomiej Wacław
- Istituto Nazionale di Fisica Nucleare, Sezione di Milano-Bicocca, Milano, Italy
  Prof. Dr. Pablo Butera
- Jülich Supercomputing Centre (JSC), Forschungszentrum Jülich, Germany
  Prof. Dr. Peter Grassberger, PD Dr. Thomas Neuhaus

- IAC-1, Universität Stuttgart
  Prof. Dr. Rudolf Hilfer, Anjan Prasad Gantapara
- Complex Systems Division, Department of Theoretical Physics, Lunds Universitet, Lund, Sweden
  Prof. Dr. Anders Irbäck, Simon Mitternacht
- Department of Mathematics and the Maxwell Institute for Mathematical Sciences, Heriot-Watt University, Edinburgh, Scotland, UK
  Prof. Dr. Desmond A. Johnston
- Applied Mathematics Research Centre, Coventry University, England, UK
  Dr. Ralph Kenna, PD Dr. Christian von Ferber, Dr. Martin Weigel
- Inst. für Theoretische Physik, FU Berlin, Germany
  Prof. Dr. Hagen Kleinert
- Atominstitut, TU Wien, Austria
  Prof. Dr. Harald Markum, Dr. Rainer Pullirsch
- Jacobs Universität Bremen, Germany
  Prof. Dr. Hildegard Meyer-Ortmanns, Darka Labavić
- Applied Mathematics, Universitat Pompeu Fabra, Barcelona, Spain
  Dr. Ramon Villanova
- CERN (PH-SFT), Geneva, Switzerland
  Dr. Sandro Wenzel
- Department of Engineering of Physics, Ankara University, Turkey
  Prof. Dr. Handan Arkın (Olgar), Mustafa Bilsel, Buket Taşdizen
- Dept. of Physics, Hacettepe University, Ankara, Turkey
  Prof. Dr. Tarik Çelik, Gökhan Gökoğlu
- Institute for Condensed Matter Physics, National Academy of Sciences, Lviv, Ukraine
  Dr. Viktoria Blavatska, Prof. Dr. Yurij Holovatch
- Yerevan Physics Institute, Yerevan, Armenia
  Prof. Dr. David B. Saakian
- Landau Institute for Theoretical Physics, Chernogolovka, Russia
  Prof. Dr. Lev N. Shchur
- Center for Simulational Physics, The University of Georgia, Athens, USA
  Prof. Dr. Michael Bachmann, Jonathan Gross, Prof. Dr. David P. Landau
- Dept. of Physics, Florida State University, Tallahassee, USA
  Prof. Dr. Bernd A. Berg
- Dept. of Chemistry and Biochemistry, University of Oklahoma, Norman, USA
  Prof. Dr. Ulrich H.E. Hansmann
- Los Alamos National Laboratory, Los Alamos, USA
  Dr. Christoph Junghans, Dr. Thomas Vogel
- Dept. of Physics, Virginia Tech, Blacksburg, USA
  Prof. Dr. Michel Pleimling, Prof. Dr. Royce K.P. Zia

- Physics Department, Carnegie Mellon University, Pittsburgh, USA
  Prof. Dr. Robert H. Swendsen
- Computational Chemistry Unit Cell (CCUC), Department of Chemistry, Chulalongkorn University, Bangkok, Thailand
  Prof. Dr. Supot Hannongbua, Dr. Oraphan Saengsawang
- Laboratory of Statistical and Computational Physics, Institute of Physics, Academia Sinica, Nankang, Taipei, Taiwan
  Prof. Dr. Chin-Kun Hu
- The University of Tokyo, Japan
  Prof. Dr. Nobuyasu Ito
- Banaras Hindu University, Varanasi, India
  Prof. Dr. Sanjay Kumar
- Nagoya University, Japan
  Dr. Tetsuro Nagai, Prof. Dr. Yuko Okamoto
- Zhejiang Institute of Modern Physics, Zhejiang University, Hangzhou, P.R. China
  Prof. Dr. He-Ping Ying, Prof. Dr. Bo Zheng

11.25 Publications

Journals

H. Arkın, W. Janke: *Polymer-Attractive Spherical Cage System*, Eur. Phys. J. – Special Topics **216**, 181–190 (2013)

H. Arkın, W. Janke: *Gyration Tensor Based Analysis of the Shapes of Polymer Chains in an Attractive Spherical Cage*, J. Chem. Phys. **138**, 054904-1–8 (2013)

N. Fricke, W. Janke: *Self-Avoiding Walks on Strongly Diluted Lattices: Chain-Growth Simulations vs Exact Enumeration*, Eur. Phys. J. – Special Topics **216**, 175–179 (2013) [Fig. 1 selected for the cover page of this volume]

N. Fricke, J. Bock, W. Janke: *Diffusion and Polymers in Fractal, Disordered Environments*, diffusion-fundamentals.org **20**, 111-1–10 (2013)

D. Labavić, H. Nagel, W. Janke, H. Meyer-Ortmanns: *Caveats in Modeling a Common Motif in Genetic Circuits*, Phys. Rev. E **87**, 062706-1–11 (2013)

T. Nagai, Y. Okamoto, W. Janke: *Application of Simulated Tempering and Magnetizing to a Two-Dimensional Potts Model*, J. Stat. Mech.: Theor. Exp., P02039-1–21 (2013)

T. Nagai, Y. Okamoto, W. Janke: *Crossover Scaling in the Two-Dimensional Three-State Potts Model*, Condens. Matter Phys. **16**, 23605-1–8 (2013)

D.T. Seaton, S. Schnabel, D.P. Landau, M. Bachmann: *From Flexible to Stiff: Systematic Analysis of Structural Phases for Single Semiflexible Polymers*, Phys. Rev. Lett. **110**, 028103-1–5 (2013)

J. Zierenberg, M. Marenz, W. Janke: *Scaling Properties of a Parallel Implementation of the Multicanonical Algorithm*, Comput. Phys. Commun. **184**, 1155–1160 (2013)

in press

V. Blavatska, W. Janke: *Conformational Transitions in Random Heteropolymer Models*, J. Chem. Phys. **140**, 034904-1–7 (2014)

T. Chokbunpiam, R. Chanajaree, T. Remsungnen, O. Saengsawang, S. Fritzsche, C. Chmelik, J. Caro, W. Janke, S. Hannongbua: *N_2 in ZIF-8: Sorbate Induced Structural Changes and Self-Diffusion*, Micropor. Mesopor. Mater. **187**, 1–6 (2014)

E. Ehrenpreis, H. Nagel, W. Janke: *Numerical Survey of the Tunable Condensate Shape and Scaling Laws in Pair-Factorized Steady States*, J. Phys. A: Math. Theor. **47**, 125001-1–16 (2014)

M. Möddel, W. Janke, M. Bachmann: *Adsorption and Pattern Recognition of Polymers at Complex Surfaces with Attractive Stripe-like Motifs*, Phys. Rev. Lett. **112**, 148303-1–5 (2014)

M. Mueller, W. Janke, D.A. Johnston: *Nonstandard Finite-Size Scaling at First-Order Phase Transitions*, Phys. Rev. Lett. **112**, 200601-1–5 (2014)

J. Zierenberg, M. Wiedenmann, W. Janke: *Application of the Parallel Multicanonical Method to Lattice Gas Condensation*, J. Phys.: Conf. Ser. **510**, 012017-1–8 (2014)

M. Marenz, W. Janke: *Effect of Bending Stiffness on a Homopolymer Inside a Spherical Cage*, to appear in: *Computer Simulation Studies in Condensed-Matter Physics XXVII*, eds. D.P. Landau, H.-B. Schüttler, S.P. Lewis, M. Bachmann, Physics Procedia (2014), in print

M. Mueller, W. Janke, D.A. Johnston: *Transmuted Finite-Size Scaling at First-Order Phase Transitions*, to appear in: *Computer Simulation Studies in Condensed-Matter Physics XXVII*, eds. D.P. Landau, H.-B. Schüttler, S.P. Lewis, M. Bachmann, Physics Procedia (2014), in print

H. Nagel, D. Labavić, H. Meyer-Ortmanns, W. Janke: *Open Boundary Conditions in Stochastic Transport Processes with Pair-Factorized Steady States*, to appear in: *Computer Simulation Studies in Condensed-Matter Physics XXVII*, eds. D.P. Landau, H.-B. Schüttler, S.P. Lewis, M. Bachmann, Physics Procedia (2014), in print

J. Zierenberg, M. Marenz, W. Janke: *Application of Parallel Multicanonical Simulations to Systems with First and Second Order Phase Transition*, e-print `arXiv:1312.2213` (physics.comp-ph), in appear in: *Computer Simulation Studies in Condensed-Matter Physics XXVI*, eds. D.P. Landau, H.-B. Schüttler, S.P. Lewis, M. Bachmann, Physics Procedia (2014), in print

Talks

N. Fricke: *Self-Avoiding Walks on Critical Percolation Clusters*, SFG Workshop, Chemnitz, Germany, 09. April 2013

N. Fricke: *Scale-Free Enumeration of Self-Avoiding Walks on Critical Percolation Clusters*, XXV IUPAP International Conference on Statistical Physics, Seoul, South Korea, 22.–26. July 2013

N. Fricke: *Scale-Free Enumeration of Self-Avoiding Walks on Critical Percolation Clusters*, 14th International NTZ-Workshop on *New Developments in Computational Physics – CompPhys13*, Universität Leipzig, Germany, 28.–30. November 2013

J. Gross: *Interaction Range Dependency of Flexible Polymer Structural Phases*, 26th Annual CSP Workshop *Recent Developments in Computer Simulation Studies in Condensed Matter Physics*, The University of Georgia, Athens, USA, 27. February 2013

J. Gross, T. Vogel, M. Bachmann: *Adsorption of a Coarse-Grained Flexible Polymer on Nanocylinders – A Monte Carlo Study*, 14th International NTZ-Workshop on *New Developments in Computational Physics – CompPhys13*, Universität Leipzig, Germany, 28.–30. November 2013

M. Ivanov, W. Janke: *Polymer Adsorption onto a Stripe-Patterned Surface*, Retreat of SFB/TRR 102: Polymers under Multiple Constraints, Bad Blankenburg, Germany, 06.–08. March 2013

M. Ivanov: *Computer Simulations of Polymers*, SFB/TRR 102: Doctoral Students Seminar, Universität Leipzig, Germany, 13. August 2013

W. Janke: *Monte Carlo Methods in Classical Statistical Physics*, BuildMoNa Module B3 *Basic Concepts in Physics*, Universität Leipzig, Germany, 12. February 2013

W. Janke: *Scaling Properties of a Parallel Implementation of the Multicanonical Algorithm*, 26th CSP Workshop on *Recent Developments in Computer Simulation Studies in Condensed Matter Physics*, The University of Georgia, Athens, USA, 25. February – 01. March 2013

W. Janke: *Polymer Statistics in an Attractive Sphere*, DPG Frühjahrstagung, Universität Regensburg, Germany, 10.–15. March 2013

W. Janke: *Polymer Statistics in an Attractive Sphere*, Conference *MECO 38*, ICTP Trieste, Trieste, Italy, 25.–27. March 2013

W. Janke: *Exploring Critical Loop Gases with Worms*, Physics Seminar, Applied Mathematics Research Center (AMRC), Coventry University, England, UK, 25. April 2013

W. Janke: *Simulated Tempering and Magnetizing Study of Crossover Scaling in the 2d 3-State Potts Model*, invited talk, Workshop *Statistical Physics and Low Dimensional Systems – SPLDS*, Pont-à-Mousson, France, 15.–17. May 2013

W. Janke: *Constrained Polymer Statistics Inside a Spherical Cavity*, StatPhys25 Conference, Seoul, South Korea, 22.–26. July 2013

W. Janke: *Generalized Ensemble Simulations of Polymer Adsorption in an Attractive Spherical Cage*, invited talk, XXV IUPAP *Conference on Computational Physics CCP2013*, Moscow, Russia, 20.–24. August 2013

W. Janke: *Simulated Tempering and Magnetizing: Application to Crossover Scaling in the 2d 3-State Potts Model*, Statistical Physics Seminar, Applied Mathematics Research Centre (AMRC), Coventry University, England, UK, 24. September 2013

M. Marenz, W. Janke: *Effect of Bending Stiffness on a Homopolymer Inside a Spherical Cage*, 14th International NTZ-Workshop on *New Developments in Computational Physics – CompPhys13*, Universität Leipzig, Germany, 28.–30. November 2013

M. Marenz, W. Janke: *Effect of Bending Stiffness on a Homopolymer Inside a Spherical Cage*, Seminar of the cdfa-dfdk, Coventry, England, UK, 03. December 2013

M. Müller: *Transmuted Finite-Size Scaling at First-Order Phase Transitions with Exponential Degeneracy of Ordered States*, Seminar of the cdfa-dfdk, Coventry, England, Uk, 03. December 2013

M. Müller, M. Ivanov: *Statistical Data Analysis*, SFB/TRR 102: iRTG Workshop, Wittenberg, Germany, 11. September 2013

P. Schierz: *A GPU Accelerated Metropolis-Hastings Algorithm for Particle Simulations*, 2nd International Symposium *Computer Simulations on GPU – SimGpu2013*, Freudenstadt, Germany, 28. May 2013

P. Schierz: *GPU Computing for Molecular Dynamics – and Monte Carlo Simulations*, Seminar of the cdfa-dfdk, Nancy, France, 12. September 2013

P. Schierz: *Computer Simulations Study of Polymer Aggregation*, ESF-Nachwuchsforschergruppe *Funktion durch Selbstorganisation: Emergente Eigenschaften von Atom- und Molekülaggregaten*, Leipzig, Germany, 02. December 2013

S. Schnabel, W. Janke: *Microcanonical Flat-Histogram Sampling*, 26th Annual CSP Workshop *Recent Developments in Computer Simulation Studies in Condensed Matter Physics*, Athens, Georgia, USA, 27. February 2013

S. Schnabel, D.P. Landau: *Fictitious Spin Waves in a Frustrated Classical Antiferromagnet*, Cambridge, England, UK, 06. March 2013

S. Schnabel, D.P. Landau: *Fictitious Excitations in the Classical Heisenberg Antiferromagnet on the Kagome Lattice*, DPG Frühjahrstagung, Regensburg, Germany, 14. March 2013

B. Schott: *Physical Annealing in the Microcanonical Ensemble*, Guest Student Programme on Scientific Computing, Jülich Supercomputing Centre (JSC), FZ Jülich, Germany, 29. September 2013

J. Zierenberg: *Simulations of Aggregation in Homopolymer Systems*, 6th Annual BuildMoNa Conference, Leipzig, Germany, 05. March 2013

J. Zierenberg: *Simulations of Aggregation in Homopolymer Systems*, DPG Frühjahrstagung, Regensburg, Germany, 11. March 2013

J. Zierenberg: *Condensation of Lattice Gas and Aggregation of Lattice Polymers*, Seminar of the cdfa-dfdk, Coventry, England, UK, 03. July 2013

J. Zierenberg: *Application of the Parallel Multicanonical Method to Lattice Gas Condensation*, XXV IUPAP *Conference on Computational Physics CCP2013*, Moscow, Russia, 21. August 2013

J. Zierenberg: *Polymer Aggregation vs. Particle Condensation*, Workshop on *Droplet Evaporation/Condensation – DEC13*, Leipzig, Germany, 12. December 2013

Posters

U. Arsawang, S. Fritzsche, W. Janke, J. Caro, T. Remsungnen, S. Hannongbua: *Structural and Transport Properties of Hydrogen in ZIF-22*, International Conference *Diffusion Fundamentals V – Basic Principles of Diffusion Theory, Experiment and Application*, Universität Leipzig, Germany, 26.–28. August 2013

J. Bock, N. Fricke, W. Janke: *Kinetic Growth Random Walks*, XXV IUPAP *Conference on Computational Physics CCP2013*, Moscow, Russia, 20.–24. August 2013

T. Chokbunpiam, R. Chanajaree, O. Saengsawang, S. Fritzsche, C. Chmelik, W. Janke, J. Caro, T. Remsungnen, S. Hannongbua: *Diffusion and Adsorption of N_2 and C_2H_6 in ZIF-8 MD and MC Simulations*, International Conference *Diffusion Fundamentals V – Basic Principles of Diffusion Theory, Experiment and Application*, Universität Leipzig, Germany, 26.–28. August 2013

T. Chokbunpiam, R. Chanajaree, O. Saengsawang, S. Fritzsche, C. Chmelik, W. Janke, J. Caro, T. Remsungnen, S. Hannongbua: *N_2 and C_2H_6 in ZIF-8: Guest Induced Structural Changes*, 2013 International Workshop on *Frontiers of Theoretical and Computational Physics and Chemistry*, Ampur Mueng, Cholburi, Thailand, 09.-12. December 2013

E. Ehrenpreis, H. Nagel, W. Janke: *Numerical Survey of the Tunable Condensate Shape and Scaling Laws in Pair-Factorized Steady States* DPG Frühjahrstagung, Universität Regensburg, Germany, 10.–15. March 2013

N. Fricke, J. Bock, W. Janke: *Diffusion and Polymers in Fractal, Disordered Environments*, International Conference *Diffusion Fundamentals V – Basic Principles of Diffusion Theory, Experiment and Application*, Universität Leipzig, Germany, 26.–28. August 2013

N. Fricke, W. Janke: *Self-Avoiding Walks on Critical Percolation Clusters in 2–7 Dimensions*, DPG Frühjahrstagung, Universität Regensburg, Germany, 10.–15. March 2013

N. Fricke, W. Janke: *Diffusion and Self-Avoiding Walks on Percolation Clusters*, International Conference *Diffusion Fundamentals V – Basic Principles of Diffusion Theory, Experiment and Application*, Universität Leipzig, Germany, 26.–28. August 2013

S. Fritzsche, P. Schierz, W. Janke, S. Hannongbua, O. Saengsawang, C. Chmelik: *Diffusion Investigation for Hydrogen Guest Molecules in an Adapted Force Field for ZIF-11*, International Conference *Diffusion Fundamentals V – Basic Principles of Diffusion Theory, Experiment and Application*, Universität Leipzig, Germany, 26.–28. August 2013

M. Ivanov, M. Möddel, W. Janke: *Polymer Adsorption onto a Stripe-Patterned Surface*, XXV IUPAP *Conference on Computational Physics CCP2013*, Moscow, Russia, 20.–24. August 2013

M. Ivanov, W. Janke: *Polymer Adsorption onto a Stripe-Patterned Surface*, SFB/TRR 102: Miniworkshop, Schkeuditz, Germany, 08. November 2013

M. Ivanov, M. Möddel, W. Janke: *Polymer Adsorption onto a Stripe-Patterned Surface*, 14th International NTZ-Workshop on *New Developments in Computational Physics – CompPhys13*, Universität Leipzig, Germany, 28.–30. November 2013

M. Marenz, J. Zierenberg, W. Janke: *Simple Polymer in a Spherical Cage*, DPG Frühjahrstagung, Universität Regensburg, Germany, 10.–15. March 2013

M. Müller, D.A. Johnston, W. Janke: *Multicanonical Analysis of the Gonihedric Ising Model*, 14th International NTZ-Workshop on *New Developments in Computational Physics – CompPhys13*, Universität Leipzig, Germany, 28.–30. November 2013

M. Müller, D.A. Johnston, W. Janke: *Multicanonical Analysis of the Gonihedric Ising Model*, DPG Frühjahrstagung, Universität Regensburg, Germany, 10.–15. March 2013

H. Nagel, J. Vollmer, W. Janke: *Application of a Steady States Transport Model to Condensation of Water Droplets on a Substrate*, International Conference *Diffusion Fundamentals V – Basic Principles of Diffusion Theory, Experiment and Application*, Universität Leipzig, Germany, 26.–28. August 2013

H. Nagel, J. Vollmer, W. Janke: *Application of a Steady States Transport Model to Condensation of Water Droplets on a Substrate*, 14th International NTZ-Workshop on *New Developments in Computational Physics – CompPhys13*, Universität Leipzig, Germany, 28.–30. November 2013

P. Pilvar, S. Fritzsche, J. Caro, W. Janke: *Molecular Dynamics Investigation of the Transport of Hydrogen in ZIF-7*, International Conference *Diffusion Fundamentals V – Basic Principles of Diffusion Theory, Experiment and Application*, Universität Leipzig, Germany, 26.–28. August 2013

P. Schierz, S. Fritzsche, W. Janke, S. Hannongbua, O. Saengsawang, C. Chmelik: *Adsorption and Diffusion of Hydrogen Guest Molecules in the Metal-Organic Framework ZIF-11*, International MOF Symposium 2013, Dresden, Germany, 16.–17. September 2013

P. Schierz, J. Zierenberg, W. Janke: *Microcanonical Molecular Dynamics meets (Multi) Canonical Monte Carlo*, 14th International NTZ-Workshop on *New Developments in Computational Physics – CompPhys13*, Universität Leipzig, Germany, 28.–30. November 2013

J. Zierenberg, M. Marenz, W. Janke: *Scaling Properties of a Parallel Implementation of the Multicanonical Algorithm*, DPG Frühjahrstagung, Universität Regensburg, Germany, 10.–15. March 2013

J. Zierenberg, M. Wiedenmann, W. Janke: *Condensation of a Lattice Gas in Three Dimensions*, International Conference *Diffusion Fundamentals V – Basic Principles of Diffusion Theory, Experiment and Application*, Universität Leipzig, Germany, 26.–28. August 2013

11.26 Graduations

Doctorate

- Rainer Bischof
  Gaussian Critical Line in Anisotropic Mixed Quantum Spin Chains
  06. February 2013
- Sebastian Schoebl
  Macromolecules in Disordered Environments: From Flexible to Semiflexible Polymers
  22. February 2013

Diploma

- Christoph Vogelsberg
  The 2-Dimensional Ising Model with Minus Boundary Condition
  29. January 2013

Master

- Johannes Bock
  Kinetisch wachsende Zufallsläufe
  16. January 2013

Bachelor

- Andreas Wagner
  Kondensatbildung eines Transportprozesses im Steady State – Exemplarische Überprüfung von Kondensatsformen
  15. March 2013

11.27 Guests

- PD Dr. Thomas Neuhaus
  Jülich Supercomputing Centre, Forschungszentrum Jülich, Germany
  15. January – 15. February 2013
- Prof. Dr. Sanjay Kumar
  Department of Physics, Banaras Hindu University, Varanasi, India
  (Bio)polymers under Mechanical Force I and II
  27. May – 07. July 2013
- Dr. Hsiao-Ping Hsu
  Universität Mainz, Germany
  Polymer Simulations with PERM I and II
  19. – 22. June 2013

- Dr. Stefan Förster
  Universität Halle, Germany
  Single Polymer Deposition
  20. – 21. June 2013
- Prof. Dr. Kurt Kremer
  MPI für Polymerforschung, Mainz, Germany
  Multiscale Modeling I and II
  21. – 22. June 2013
- Dr. Viktoria Blavatska
  Institute for Condensed Matter Physics, Lviv, Ukraine
  Alexander von Humboldt Foundation Institute Partnership Programme
  July – August 2013
- M.Sc. Marjana Krasnytska
  National Academy of Sciences of Ukraine, Lviv, Ukraine
  NTZ/DFH-UFA/RALeipzig Colloquium (07. November 2013)
  Critical Behavior for the Potts Model on Uncorrelated Scale-Free Networks: Phase Diagram, Critical Exponents, Scaling Functions and Amplitude Ratios
  20. October – 09. November 2013
- M.Sc. Nicolas Allegra
  Université de Lorraine, Nancy, France
  Boundary Crossover in Non-Equilibrium Interfaces Growth Processes
  17. – 30. November 2013
- Dr. Nikolay Izmailyan
  Yerevan Physics Institute, Yerevan, Armenia
  NTZ Colloquium (05. December 2013)
  Universal Amplitude Ratios in $c = 1/2$ and $c = -2$ Universality Classes
  27. November – 07. December 2013
- Dr. Christophe Chatelain
  Université de Lorraine, Nancy, France
  Griffiths Phase in a Potts Model with Correlated Disorder
  27. – 30. November 2013
- Dr. Stefan Falkner
  Emory University, Atlanta, USA
  Renormalization Group for Quantum Walks
  27. – 30. November 2013
- Dr. Hsiao-Ping Hsu
  Universität Mainz, Germany
  Confined Semiflexible Chains in a Good Solvent: A Monte Carlo Test of Scaling Concepts
  27. – 30. November 2013
- PD Dr. Thomas Neuhaus
  Jülich Supercomputing Centre, Forschungszentrum Jülich, Germany
  Simulated Quantum Annealing for General Ising Models
  27. – 30. November 2013

- Dr. Francesco Parisen Toldin
  Universität Würzburg, Germany
  Critical Casimir Forces Between Homogeneous and Chemically Striped Surfaces
  27. – 30. November 2013
- Dr. Sergio Perez-Gaviro
  BIFI, University Zaragoza, Spain
  The Janus Family: A Special Purpose Computer Generation Devoted to Spin Glasses
  27. – 30. November 2013
- Prof. Dr. Bengt Petersson
  Humboldt Universität zu Berlin, Germany
  Magnetic Catalysis in 2 Color QCD at Finite Temperature
  27. – 30. November 2013
- Prof. Dr. Mark Taylor
  Hiram College, USA
  Partition Function Zeros and Finite-Size Scaling for Polymer Adsorption
  27. – 30. November 2013
- Dr. Andreas Tröster
  TU Wien, Österreich
  Fourier MC Simulation of Criticality in Solid and Hexatic Membranes
  27. – 30. November 2013
- Dr. Martin Weigel
  Coventry University, England, UK
  Corner Contribution to Cluster Numbers in the Potts Model
  27. – 30. November 2013
- M.Sc. Pierre Wendenbaum
  Université de Lorraine, Nancy, France
  Disentanglement of Two Qubits Coupled to an Ising Chain: Sudden Quench Dynamics
  27. – 30. November 2013
- Dr. David Yllanes
  "La Sapienza" Rome, Italy
  Numerical Study of the Branching Tree of States in Spin Glasses
  27. – 30. November 2013
- Prof. Dr. Michael Allen
  University of Warwick, Coventry, England, UK
  NTZ-Colloquium
  Computer Simulation of Peptide Adsorption
  27. November – 01. December 2013
- Dr. Elmar Bittner
  Universität Heidelberg, Germany
  MuCa vs WL: A Tight Race
  27. November – 01. December 2013
- Prof. Dr. Malte Henkel
  Université de Lorraine, Nancy, France

Statistical Mechanics of the Coagulation-Diffusion Process with a Stochastic Reset
27. November – 01. December 2013

- Prof. Dr. Ferenc Iglói
  Institute of Theoretical Physics, Research Institute for Solid State Physics and Optics, Budapest, Hungary
  Random Quantum Magnets in $d > 2$ Dimensions: Critical Behavior and Entanglement Entropy
  27. November – 01. December 2013
- Prof. Dr. Desmond A. Johnston
  Heriot-Watt University, Edinburgh, Scotland, UK
  Potts Models with Invisible States
  27. November – 01. December 2013
- M.Sc. Kai Qi
  Center for Simulational Physics, The University of Georgia, Athens, USA
  Autocorrelation Study for a Coarse-Grained Polymer Model
  27. November – 01. December 2013
- Dr. Christian von Ferber
  Coventry University, England, UK
  Environmental Impact on DNA Denaturation
  28. – 29. November 2013
- Prof. Dr. Michael Bachmann
  Center for Simulational Physics, The University of Georgia, Athens, USA
  Transitions in Small Systems
  28. – 30. November 2013
- Dr. Elmar Bittner
  Universität Heidelberg, Germany
  Muca vs WL in Droplet Models
  11. – 14. December 2013
- Dipl.-Phys. Andreas Nußbaumer
  Universität Mainz, Germany
  Gibbs-Thomson Effect in the 2D Ising Model
  11. – 14. December 2013
- PD Dr. Thomas Neuhaus
  Jülich Supercomputing Centre, Forschungszentrum Jülich, Germany
  Theory of Droplet/Evaporation Transition
  11. – 15. December 2013

12

Quantum Field Theory and Gravity

12.1 Vacuum interaction between topological objects

M. Bordag,

Boundary conditions play an important role in quantum field theory. On the one hand side they are generalizations of interactions which are concentrated on a region of higher co-dimensions. On the other hand, boundary conditions appear naturally when considering topological objects, for example boundary conditions can be found in some treatments of quantum field in black hole backgrounds, in the quantum Hall effect, in the physics of graphene etc. An interesting question appears about the vacuum quantum interaction of topological objects. As a first example in a larger project on this topic the vacuum interaction energy of two kinks was calculated. The results were extended to the vacuum interaction of two cosmic strings. Here the problem appears, that the background changes the topology of the space-time, thus providing a long range interaction. As a consequence it is not clear a'priori whether the subtraction of the empty space contribution will be sufficient to remove the ultraviolet divergences. This question was investigated in detail by two methods, the heat kernel expansion and a mode sum calculation. Both confirm, after nontrivial compensation, the validity of the subtraction procedure.

12.2 Casimir repulsion in sphere-plate geometry

M. Bordag,

The electromagnetic vacuum energy is considered in the presence of a perfectly conducting plane and a ball with dielectric permittivity ε and magnetic permeability μ, $\mu \neq 1$. The attention is focused on the Casimir repulsion in this system caused by the magnetic permeability of the sphere. In the case of a perfectly permeable sphere, $\mu = \infty$, the vacuum energy is estimated numerically. The short- and long-distance asymptotes corresponding to the repulsive force and respective low-temperature corrections and high-temperature limits are found for a wide range of μ. The constraints on the Casimir repulsion in this system are discussed. This work was supported by the Heisenberg-Landau program. Within this project one publication resulted.

I.G. Pirozhenko, M. Bordag. Casimir repulsion in sphere-plate geometry. *Phys. Rev. D*, 87:085031, 2013.

12.3 Deformations of quantum field theories, mathematical structure of low-dimensional quantum field theories, integrable models, QFT on noncommutative spaces

G. Lechner, J. Schlemmer, Y. Tanimoto, S. Waldmann, R. Longo, H. Grosse, R. Verch, T. Ludwig, S. Alazzawi, A. Andersson, C. Schützenhofer, A. Huber

In the project "deformations of quantum field theories" we pursue the question how to obtain models of interacting quantum fields by deformation procedures, sidestepping the problems of quantization and renormalization. In collaboration with J. Schlemmer (Vienna) and Y. Tanimoto (Göttingen), we investigated the equivalence of certain deformation procedures arising in the context of chiral field theories and massless integrable models, respectively. These results provide further evidence to the effect that the symmetric inner functions appearing in the context of Longo-Witten endomorphisms are closely connected to elastic two-particle S-matrices.

Another aspect of this circle of ideas is being developed in collaboration with R. Longo (Rome). Here we start from a field theory and investigate the structure of its half-localized endomorphism subnets arising from subnets of modular localized real subspaces. As in the context of existence proofs for local observables by modular nuclearity, the crucial question is here under which conditions on the underlying inner function compactly localized subspaces are still cyclic.

An extension of the algebraic construction of integrable models on two-dimensional Minkowski space to the case of a general particle spectrum transforming under some global gauge group was given in collaboration with C. Schützenhofer (Vienna). My PhD student S. Alazzawi (Vienna) analyzes the inverse scattering problem in this context, i.e. which two-particle S-matrices arise from local relativistic quantum field theories.

Regarding quantum field theory on noncommutative space(-times), I pursued two different research projects. Together with R. Verch, T. Ludwig, and H. Grosse (Vienna) we established an operator-algebraic version of the Wick rotation for quantum fields on Moyal space(-time) with commuting time. Together with S. Waldmann (Erlangen), there is ongoing research on the formulation of quantum field theories on spacetime manifolds which behave noncommutative only locally. Also the PhD student A. Andersson will be involved in this project.

There is also a project on the structure of thermal equilibrium states of certain deformed quantum field theories. Diploma student A. Huber (Vienna) contributed to this in his thesis, and could show that such models possess a wealth of KMS-functionals. However, the positivity aspects of these functionals, as required for a probability interpretation of the theory, are not settled yet, and are still analyzed in collaboration with J. Schlemmer (Vienna).

12.4 Structure of the gauge orbit space and study of gauge theoretical models

G. Rudolph, Sz. Charzynski[*], E. Fuchs H. Grundling[†], J. Huebschmann[‡] P. Jarvis[§], J. Kijowski[*], M. Schmidt

[*]U Warsaw
[†]U Sydney
[‡]U Lille
[§]U Hobart

The investigation of gauge theories in the Hamiltonian approach on finite lattices with emphasis on the role of nongeneric strata was continued.

As a further step towards a generalization of the results of [1] on stratified Kähler quantization to larger lattices, the defining relations for lattice gauge models with gauge group SU(2) have been derived [2]. E. Fuchs worked on the formulation of stratified Kähler quantization in terms of coherent states.

Based on [3], in collaboration with H. Grundling, the investigation of the structure of the algebra of observables and its representations for specific models of quantum lattice gauge theory in terms of gauge invariant quantities was continued. In [4], the observable algebra for an infinite lattice was constructed.

[1] J. Huebschmann, G. Rudolph, M. Schmidt, Commun. Math. Phys. **286**, Nr. 2 (2009) 459–494
[2] F. Fürstenberg, G. Rudolph, M. Schmidt: Defining relations for the orbit type strata of SU(2)-lattice gauge models (in preparation).
[3] J. Kijowski, G. Rudolph, J. Math. Phys. **43** (2002) 1796–1808;
J. Kijowski, G. Rudolph, J. Math. Phys. **46** (2005) 032303; Rep. Math. Phys. **55** (2005) 199
P. Jarvis, J. Kijowski, G. Rudolph, J. Phys. A **38** (2005) 5359
[4] Commun. Math. Phys. 318 (2013) 717-766

12.5 Quantum field theory on non-commutative geometries, quantum field theory and cosmology, generally covariant quantum field theory

R. Verch, A. Andersson, z. Avetisyan, T. Ludwig, M. Gransee, B. Eltzner, J. Zschoche

In non-commutative quantum field theory, the relation between the Euclidean and Lorentzian approach is investigated with T. Ludwig, in collaboration with H. Grosse and G. Lechner, with a focus on the non-commutative Wick-rotation. With A. Rennie, A. Andersson and K. van den Dungen, new approaches towards quantum field theory on general non-commutative geometries are being studied.

Recently, some new classes of distinguished states have been proposed in quantum field theory in curved spacetimes. In collaboration with C.J. Fewster it was shown that

such classes of states have problematic properties and cannot be viewed as physically reasonable states in general. In the course of that investigation, it was found that the Hadamard condition for quantum field states on curved spacetime manifolds is necessary for setting up a consistent perturbation theory for interacting quantum fields.
A further line of investigation in quantum field theory in curved spacetime centers around foundational issues in cosmology. This relates to questions of local thermodynamic equilibrium in cosmological spacetimes (M. Gransee), quantization of fluctuations in the early universe (B. Eltzner), and quantum pressure behaviour and the Chaplygin gas (J. Zschoche), and aspects of group representation theory and harmonic analysis on homogeneous spacetime (Z. Avetisyan)

12.6 Funding

Vacuum interaction between topological objects
Priv.-Doz. Dr. M. Bordag
DFG-Einzelprojekt BO1112/18-1

Spectral Zeta Functions and Heat Kernel Technique in Quantum Field Theory with Nonstandard Boundary Condition
M. Bordag
Heisenberg-Landau programme

New Trends and Applications of the Casimir Effect (CASIMIR)
Research Networking Program der ESF (European Research Foundation)
M. Bordag, member of the Steering Committee

Deformations of quantum field theories
G. Lechner, external collaborators at Vienna University
FWF project P22929-N16

Quantum field theory and locally noncommutative structures
A. Andersson
IMPRS fellowship

Group theory and harmonic analysis in cosmological spacetimes Z. Avetisyan
IMPRS fellowship

Foundational aspects of cosmology
B. Eltzner, M. Gransee, J. Zschoche
IMPRS fellowship

Quantum Theory of Lattice Gauge models
E. Fuchs
IMPRS fellowship

Quantum field theory and Moyal space(-time) in Euclidean and Lorentzian signature
T. Ludwig
IMPRS fellowship

12.7 Organizational Duties

Priv.-Doz. Dr. Michael Bordag

- Referee: J. Phys. A, Phys. Rev. D, J. Math. Phys.
- Member of the Steering Committee of the ESF Research Networking Program *New Trends and Applications of the Casimir Effect (CASIMIR)*

Dr. Gandalf Lechner

- Referee for Foundations of Physics, Communications in Mathematical Physics, Letters in Mathematical Physics, Reviews in Mathematical Physics, Forum of Mathematics, the Templeton Foundation, and mathscinet

Dr. J. Muñoz-Castañeda

- Organizer of the conference "Mathematical Structures in Quantum Systems", Benasque Centre for Science (Spain), July 2012. Editor of the proceedings, published in Nuovo Cimento C

Prof. Dr. G. Rudolph

- Referee: Class. Quant. Grav., J. Math. Phys., J. Geom. Phys., J. Phys. A, Rep. Math. Phys., Commun. Math. Phys.
- Referee for the German Research Council (DFG) and the Alexander von Humboldt Foundation

Dr. Matthias Schmidt

- Referee: J. Phys. A, Int. J. Mod. Phys. A, Class. Quant. Grav.

Prof. Dr. Rainer Verch

- Speaker, Profilbildender Forschungsbereich 2
- Quality Assurance Officer, Faculty of Physics and Earth Sciences (until Oct. 2013)
- Chairman of Examining Board, Physics and Meteorology (until Oct. 2013)
- Berufungsbeauftragter des Rektorats
- Associate Editor, Journal of General Relativity and Gravitation
- Book Series Editor, Fundamental Theories of Physics (Springer)
- IMPRS Board Member
- Referee for DFG and for Studienstiftung des Deutschen Volkes
- Referee: Ann. H. Poincaré, Commun. Math. Phys., Found. Phys., J. Phys. A, Rev. Math. Phys., Found. of Physics, Class. Quantum Grav., Gen. Rel. Grav.

12.8 External Cooperations

Academic

- II. Inst. f. Theoretische Physik, Universität Hamburg
  Prof. Dr. K. Fredenhagen
- Universität Göttingen
  Prof. Dr. D. Bahns, Dr. Y. Tanimoto

- Mathematisches Institut, Universität Münster
  Prof. Dr. R. Wulkenhaar
- Institut für Mathematik, Universität Paderborn
  Dr. Ch. Fleischhack
- Universität Würzburg
  Prof. Dr. S. Waldmann
- Universität Wien
  Dipl.Phys. S. Alazzawi, Prof. Dr. Harald Grosse, Dr. J. Schlemmer
- Department of Mathematics, University of York, England
  Dr. C.J. Fewster
- Universitá di Roma "Tor Vergata"
  Prof. Dr. R. Longo
- Dipartimento di Matematica, Universitá di Genova, Italy
  Prof. Dr. N. Pinamonti
- Université des Sciences et Technologies de Lille
  Prof. Dr. J. Huebschmann
- Polish Academy of Sciences, Center for Theoretical Physics, Warsaw
  Prof. Dr. J. Kijowski
  Dr. Sz. Charzynski
- National University, Dnepropetrovsk
  Prof. V. Skalozub
- VIK Dubna
  Dr. V. Nesterenko, Dr. I. Pirozhenko
- University of Tokyo
  Dr. Yoh Tanimoto
- University of New South Wales, Sydney
  Prof. H. Grundling
- Dep. of Mathematics, University of Wollongong, Australien
  Prof. Dr. A. Rennie
- University of Tasmania, Hobart
  Prof. Dr. P. Jarvis

12.9 Publications

Journals

Z. Avetisyan, R. Verch
Explicit harmonic and spectral analysis in Bianchi I-VII-type cosmologies.
Class. Quantum Grav. **30** (2013) 155006

C.J. Fewster, R. Verch
The necessity of the Hadamard condition.
Class. Quantum Grav. **30** (2013) 235027

H. Grundling, G. Rudolph
QCD on an Infinite Lattice
Commun. Math. Phys. **318** (2013) 717-766

M. Hofmann, G. Rudolph, M. Schmidt
On the reflection type decomposition of the adjoint reduced phase space of a compact semisimple Lie group. J. Math. Phys. **54** (2013) 083505

H. Grosse, G. Lechner, T. Ludwig, R. Verch
Wick rotation for quantum field theories on degenerate Moyal space(-time).
J. Math. Phys. **54** (2013) 022307

I.G. Pirozhenko, M. Bordag
Casimir repulsion in sphere-plate geometry.
Phys. Rev. D **87** (2013) 085031

J. Zschoche
The Chaplygin gas equation of state for the quantized free scalar field on cosmological spacetimes
Ann. H. Poincaré, July 2013 (online first publication), DOI: 10.1007/s00023-013-0281-5

Books

G. Rudolph, M. Schmidt
Differential Geometry and Mathematical Physics. Part I. Manifolds, Lie Groups and Hamiltonian Systems.
Springer Series in Theoretical and Mathematical Physics, 2013, 759 pages.

In press

B. Eltzner
Quantization of perturbations in inflation.
arXiv: 1305.5358, in press with J. Math. Phys.

Z. Avetisyan
A unified mode decomposition method for physical fields in homogeneous cosmology.
arXiv: 1212.2408, in press with Rev. Math. Phys.

A. Andersson
Operator deformation in quantum measurement theory
arXiv: 1304.2806, in press with Lett. Math. Phys.

R. Verch
Zeitreisen: Gravitation trifft Quantenphysik (Time Travel: Gravity Meets Quantum Physics)
arXiv: 1306.6091, erscheint im Sammelband “Raum und Materie”, Ev. Studienwerk Villigst (Hrsg.: E. Müller)

Talks

A. Andersson
Operator deformations in quantum measurement theory (T)
33th Workshop "Foundations and Constructive Methods of QFT", Göttingen, November 15–16, 2013

Z. Avetisyan
Mode decomposition and Fourier analysis of physical fields in homogeneous cosmology (T)
DPG-Frühjahrstagung, Jena, Fachsitzung MP, February 27, 2013

M. Bordag
Vakuumenergie und Casimir-Effekt
Kolloquiumsvortrag, Braunschweig (PTB), April 18, 2013

M. Bordag
Surface plasmons on graphene from quantum field theory
Seminarvortrag, VIK Dubna, September 9, 2013

G. Lechner
KMS functionals and KMS states for algebras of deformed quantum fields
Deformation Quantization Seminar, Universität Würzburg, November 2013

G. Lechner
Hyperbolic PDEs with star product potentials
Conference GEOQUANT 2013, Ewin-Schrödinger-Institut für Mathematische Physik, Wien, August 2013

G. Lechner
Non-Local Perturbations of Hyperbolic PDEs and QFT on Noncommutative Spacetimes
Conference Mathematics and Quantum Physics, Accademia dei Lincei, Rom, July 2013

G. Rudolph
Singular reduction and quantization
Workshop on Quantization and Reduction, Uni Erlangen, March 18–21, 2013

M. Schmidt
Costratified Hilbert space structure for lattice gauge models (T)
DPG-Frühjahrstagung, Jena, February 28, 2013

K. van den Dungen
Noncommutative Lorentzian manifolds (T)
33th Workshop "Foundations and Constructive Methods of QFT", Göttingen, November 15–16, 2013

Doctorate

- Zhirayr Avetisyan
  Mode decomposition and Fourier analysis of physical fields in homogeneous cosmology.
  January 2013

- Thomas Ludwig
  Wick rotation for quantum field theories on degenerate Moyal spaces
  February 2013
- Benjamin Eltzner
  Local thermal equilibrium on curved spacetimes and linear cosmological perturbation theory
  March 2013
- Jan Zschoche
  Quantum pressure inequalities and the Chaplygin gas equation of state
  September 2013

Diploma

- Robert Rauch (Humboldt-Universität, FB Mathematik)
  Konstruktion kommutativer spektraler Tripel auf semi-riemannschen Spin-Mannigfaltigkeiten
  October 2013
- Kevin Knauer
  Relativistic quantum teleportation
  March 2013

M.Sc.

- Adam Reichold
  Skalenalgebra einer Quantenfeldtheorie über Einparameterfamilien global hyperbolischer Raumzeiten
  January 2013

Bachelor

- Philip Liebel
  Ein Überblick über Quantenungleichungen
  April 2013
- Simone Rademacher
  Quantum energy inequalities
  October 2013
- Maik Reddiger
  On the geometry of Hamiltonian systems
  July 2013

12.10 Guests

- Dipl.-Phys. Sabina Allazzawi (Uni Wien)
  December 2–6, 2013

- I.G. Pirozhenko (VIK Dubna)
  January 13–26, 2013
- K. van den Dungen
  Dep. of Mathematics, University of Wollongong, Australia
  September 2013 – January 2014
- D. Vassilevich (Brazil)
  July 5–7, 2013

13

Statistical Physics

The focus of research in the SPT group is on low-dimensional and mesoscopic interacting systems. These systems are fascinating because on the one hand they allow to study fundamental questions of quantum statistical mechanics, and on the other hand they have a great potential for technological applications. The interplay of a reduced dimensionality with enhanced interaction effects, non-equilibrium physics, and possibly disorder allows the observation of many interesting phenomena, which pose a stimulating challenge for theoretical analysis. The mathematical language used for the description of these systems is quantum field theory, including techniques like functional integrals, renormalization group, instanton calculus, the Keldysh technique for non-equilibrium situations, and the replica method for disordered systems. These analytical tools are supplemented by the use of computer algebra (Mathematica) and numerical calculations (Matlab, Perl, C++). We try to combine the analysis of theoretically interesting problems with relevance to experiments on nanostructures.

Fractional quantum Hall (QH) systems display perhaps the richest and most beautiful physics of all condensed matter systems. They are a prime example for the idea that the whole is more than the sum of its parts, as low lying excitations of a fractional QH fluid carry only a fraction of the electron charge and are thus qualitatively different from the system constituents. Recently, interest in fractional QH physics has been reinvigorated by the prospect that quasiparticles (QPs) of the fractional QH state at filling fraction 5/2 may be non-abelian anyons, i.e. their braiding may not only give rise to a multiplication of the wave function with a complex phase, but in addition corresponds to a unitary transformation of the highly degenerate ground state. Due to the topological nature of braiding, these unitary transformations are robust against local perturbations and guarantee a high degree of stability of the quantum weave of braids, lending it to the construction of topological quantum bits. Future research in this field will concentrate on both the analysis of qualitative properties of topologically ordered systems and the description of experimentally relevant consequences in nanostructured systems.

Similarly to the edge states of QH systems, in single channel nanowires interactions strongly modify the dynamics of electrons. In the presence of strong spin-orbit coupling and in proximity to a superconductor, nanowires can support a topologically ordered state suitable for the formation of topological quantum bits. In multimode nanowires, a quantum phase transition between superconductor and diffusive metal can occur, which is tuned by an external magnetic field and is experimentally realized in niobium

and molybdenum-germanium systems. Comparatively small changes in the external magnetic field can give rise to a large change in conductivity. Quantum mechanical fluctuations of the superconducting phase can restore part of the density of states, which is reduced due to scattering of electrons off the superconducting order parameter.

B. Rosenow

13.1 Surface states and local spin susceptibility in doped three-dimensional topological insulators with odd-parity superconducting pairing symmetry

B. Zocher, B. Rosenow

Topological insulators are time-reversal-invariant systems with gapped bulk and protected massless Dirac modes at the surface. Semiconductors like the bismuth chalcogenides with strong spin-orbit coupling and a Fermi surface centered at the time-reversal-invariant momentum are of particular interest because of their single helical Dirac cone at the surface. Copper-doped Bi_2Se_3 is an unconventional superconductor (SC) [1] with non-trivial surface states and a band structure similar to that of Bi_2Se_3 but with shifted chemical potential. By now, the surface states in $Cu_xBi_2Se_3$ have been probed by

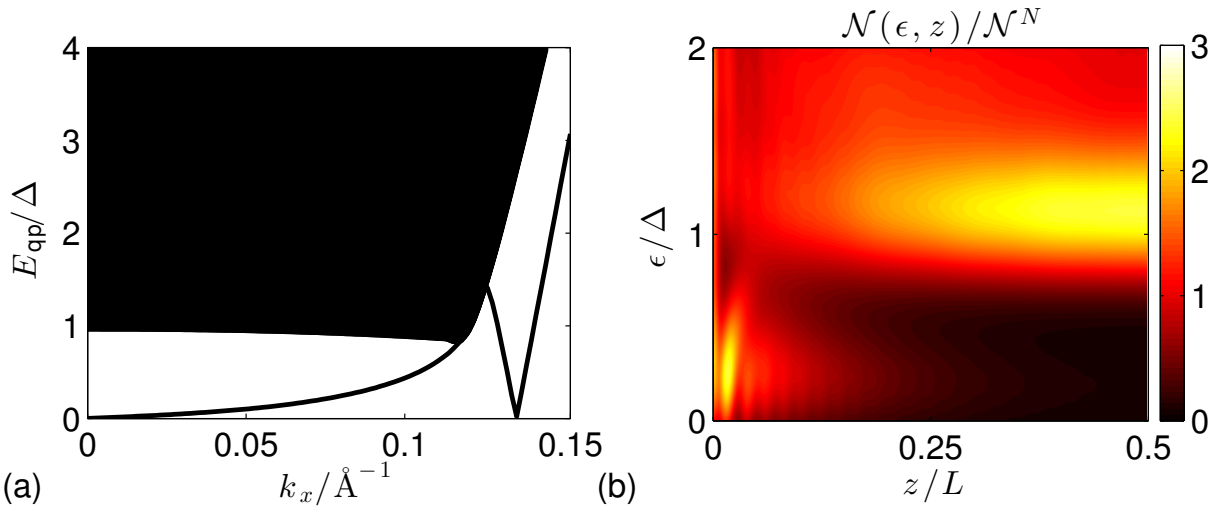

Figure 13.1: (a) Quasiparticle excitation spectrum and **(b)** local density of states of the three-dimensional topological superconductor. The surface is characterized by subgap Andreev states which decay exponentially into the bulk. The Andreev states for $k \approx 0$ originate from the odd-parity pairing while the states for $k \approx 0.14$ Å^{-1} originate from the band inversion of the topological insulator.

photoemission [1] and point contact spectroscopy [2]. However, the question about the pairing symmetry of $Cu_xBi_2Se_3$ cannot be clearly answered from point contact spectroscopy at the moment, and results obtained by complementary experimental techniques are desirable. Magnetic resonance methods are another class of powerful techniques to investigate the electronic properties locally. The Knight shift for example is determined

by the static spin susceptibility $K \sim \chi_s(\mathbf{q} = 0, \omega = 0)$, which is directly connected to the spin structure of the SC pairing. In conventional s-wave SCs with spin-singlet pairing, the Knight shift is significantly reduced and vanishes for $T = 0$ because spins pair up and longitudinal spin excitations cost the pair-breaking energy 2Δ. However, in SCs with strong spin-orbit coupling the spin susceptibility is suppressed as compared to the normal state but does not vanish for $T = 0$ due to coupling between up and down spins. We study characteristic features in the spin response of odd-parity pairing in doped topological insulators and predict clear signatures for magnetic resonance techniques.

Strong spin-orbit-coupled bands favor an odd-parity interorbital unequal-spin pairing. To gain insight into its topological non-trivial nature, we map this pairing symmetry onto the conduction band of the topological insulator, which yields an effective time-reversal invariant $p \pm ip$ pairing in three dimensions. Because of this topology, there is a pair of Majorana zero-energy modes located at each surface and protected by time-reversal symmetry. Additionally there are unconventional surface states [1] originating from the band inversion. The coexistence of the different modes gives rise to two characteristic length scales. The Dirac modes decay on the nm scale ξ_0 whereas the decay length ξ_1 for the Majorana modes is hundreds of nm. Hence, the local spin susceptibility shows different characteristic behavior in the bulk, at the surface, and within ξ_1 into the bulk.

[1] Y. S. Hor et al.: Phys. Rev. Lett. **104**, 057001 (2010)
[2] S. Sasaki et al.: Phys. Rev. Lett. **107**, 217001 (2011)
[3] B. Zocher and B. Rosenow: Phys. Rev. B **87**, 155138 (2013)

13.2 Many-flavor Phase Diagram of the (2+1)d Gross-Neveu Model at Finite Temperature

D.D. Scherer, J. Braun,* H. Gies†

*Institut für Kernphysik (Theoriezentrum), Technische Universität Darmstadt, Germany
†Theoretisch-Physikalisches Institut, Friedrich-Schiller-Universität Jena, Germany

The Gross-Neveu model [1] in (2 + 1)-dimensions exemplifies many of the intriguing properties of interacting Dirac fermions. From a theory perspective, it is an ideal laboratory to study the interplay of N flavors of massless fermions with dynamically generated collective excitations and the interaction driven mechanism of dynamical mass generation. From the viewpoint of applications, the study of effective low-energy quantum field theories of low-dimensional Dirac fermions has experienced a recent revival in the context of planar condensed-matter systems like graphene [2] (with $N = 2$) or the surface states of $3D$ topological insulators [3] ($N = 1$ or odd integer). The chiral Gross-Neveu model exhibits a quantum phase transition to a phase of broken discrete chiral symmetry as a function of the fermionic interaction strength. Despite being perturbatively non-renormalizable, it provides a paradigmatic example for an ultraviolet complete theory due to the existence of an interacting non-Gaußian renormalization group fixed point, intimately related to chiral symmetry breaking. Yet, many other low-dimensional fermionic systems develop interesting features or even phase transitions

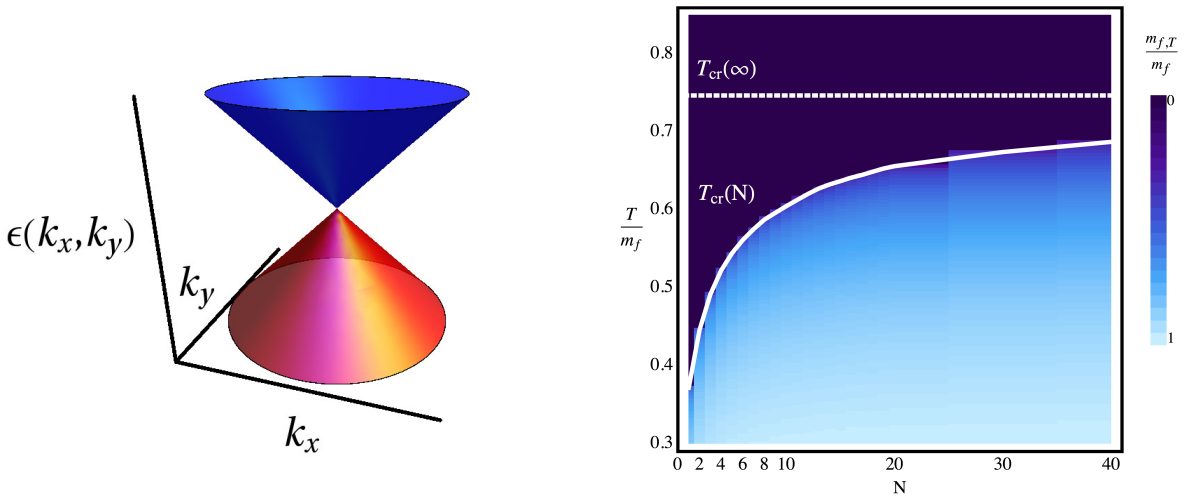

(a) **(b)**

Figure 13.2: (a): Schematic plot of the relativistic dispersion of 'massless' Dirac fermions moving in (2+1)-dimensional space-time as it occurs in the low-energy sector of condensed-matter systems, such as graphene. Massive Dirac modes are here generated dynamically from strong interactions. **(b)** Many-flavor phase diagram in the temperature (T)-flavor (N) plane as obtained from fRG calculations [4]. Dimensionful quantities are measured in units of the dynamically generated fermion mass m_f at zero temperature. The colorcode decribes the temperature and flavor dependence of the fermionic thermal mass $m_{f,T}$.

as a function of fermionic flavors N. For instance, convincing evidence has been collected for the fact that the $(2 + 1)$-dimensional Thirring model features chiral symmetry breaking only for flavor numbers below a critical value $N < N_{\rm cr}$. A similar behavior is observed in QED3. The occurrence of a critical flavor number in these models arises from a competition between symmetry stabilizing and destabilizing fluctuations. In this respect, the $(2+1)$-dimensional Gross- Neveu model behaves less dramatically as a function of N. Qualitatively, this can be understood from the fact that only one relevant bosonic degree of freedom corresponding to a "radial" $\mathbb{Z}_2$ mode cannot counterbalance the destabilizing fermion fluctuations at strong coupling. Still, the Gross-Neveu model is not completely structureless as a function of flavor number.

In Ref. [4], we study the finite-temperature phase diagram of the $(2 + 1)$-dimensional Gross-Neveu model within the framework of the functional renormalization group (fRG), see Fig. 13.2. In addition to the phase boundary, $T_{cr}(N)$, we particularly focused on the flavor-number dependence of the phase-diagram regions of (i) local order, (ii) the Ginzburg critical region and (iii) the classical region, all of which correspond to beyond-mean-field or finite-N phenomena. The non-analytic jump of the critical exponents from $2d$ Ising to mean field at $N \to \infty$ is realized by the size of the Ginzburg critical region vanishing with $1/N^x$. Our result $x \simeq 1$ is in accordance with other investigations in the literature [5].

[1] D. J. Gross and A. Neveu: Phys. Rev. D **10**, 3235 (1974)
[2] K. S. Novoselov et al.:, Nature **438**, 197 (2005)
[3] M. Z. Hasan and C. L. Kane: Rev. Mod. Phys. **82**, 3045 (2010)
[4] D. D. Scherer et al.: J. Phys. A: Math. Theor. **46**, 285002 (2013)

[5] J. B. Kogut et al.: Phys. Rev. D **58**, 096001 (1998) S. Caracciolo et al.: PoS LAT 2005, **187** (2006); Nucl. Phys. B **741**, 421 (2006); B. M. Mognetti: arXiv:hep-lat/0703020

13.3 Cancellation of quantum anomalies and bosonization of three-dimensional time-reversal symmetric topological insulators

H.-G. Zirnstein, B. Rosenow

Topological insulators [1, 2] are electronic materials that are insulating in the bulk, but feature conducting surface states which are protected against smooth perturbations, as long as these perturbations preserve certain symmetries. For instance, a time-reversal symmetric topological insulator will have conducting surface states even when the crystal structure is deformed or disorder is introduced, as these types of perturbations preserve time-reversal symmetry. However, applying a magnetic field breaks time-reversal symmetry and can introduce a band gap on the surface.

The robustness of surface states is explained by a topological classification of bulk materials. Two insulators are called topologically equivalent if one Hamiltonian can be smoothly deformed into the other without closing the band gap in the bulk. Moreover, the deformation is required to respect certain symmetries, like time-reversal symmetry. It has only recently been realized (see Ref. [1, 2]) that there are materials which are not topologically equivalent, i.e. which cannot be deformed into each other without going through a conducting phase. However, putting two such materials in close proximity is tantamount to interpolating from one material to the other across the interface, which means that the interface must host a conducting electron state. Moreover, smooth perturbations will not change the equivalence classes of the participating materials, and the gapless surface state is robust.

In Ref. [3], we consider the strong time-reversal symmetric topological insulator in three space dimensions, whose gapless surface states take the form of massless Dirac fermions. We study these surface states with the method of bosonization, and find that the resulting bosonic theory has a topological contribution due to a quantum anomaly of the surface Dirac fermions. In quantum field theory, the notion of a quantum anomaly refers to the phenomenon that symmetries, such as charge conservation or time-reversal symmetry, may be present in the classical Lagrangian, but are lost once the theory is quantized. We argue that the presence of a quantum anomaly is, in fact, the main reason for the existence of a surface state, by the principle that anomalies of surface and bulk must cancel. This is another way to look at the classification of topological insulators: the quantum theory of the bulk unexpectedly breaks the symmetries involved, and an additional surface state is required to make the theory well-defined. Inspecting other classes of topological insulators, we argue that this principle holds in general.

Moving beyond purely topological considerations, we also incorporate the dynamics of the surface electron states into the bosonic theory. Additionally, we discuss the thermodynamics of the bosonic theory and propose a representation of the surface Dirac fermions in terms of the bosonic fields.

[1] M. Z. Hasan and C. L. Kane: Rev. Mod. Phys. **82**, 3045 (2010)
[2] X.-L. Qi and S.-C. Zhang: Rev. Mod. Phys. **83**, 1057 (2011)
[3] H.-G. Zirnstein and B. Rosenow: Phys. Rev. B **88**, 085105 (2013)

13.4 Robustness of Topological Order in Semiconductor-Superconductor Nanowires in the Coulomb Blockade Regime

B. Zocher, M. Horsdal, B. Rosenow

Topological phases are quantum phases which cannot be described by a local order parameter. One characteristic property of topological phases is the dependence of the ground-state degeneracy on the topology of the manifold on which the system is defined [1]. Of particular interest are topological superconductors, which have been predicted to host Majorana bound states [2]. The p_x+ip_y superconductor (SC) for spinless fermions is a prototype system for topological SCs. Depending on the chemical potential, the ground state of the $p_x + ip_y$ SC is realized by the weak or the strong pairing phase, which can be distinguished topologically. In particular, the grand canonical ground state of the weak pairing phase on the torus depends on boundary conditions (BCs) for each of the two primitive directions. Here, the ground state with only periodic BCs is special and shows an odd parity, while the three ground states with at least one antiperiodic BC are characterized by an even parity. In contrast, the strong pairing phase and also the ordinary *s*-wave SC on the torus possess a fourfold degenerate even parity ground state. In Ref. [4], we have considered a quasi one-dimensional ring

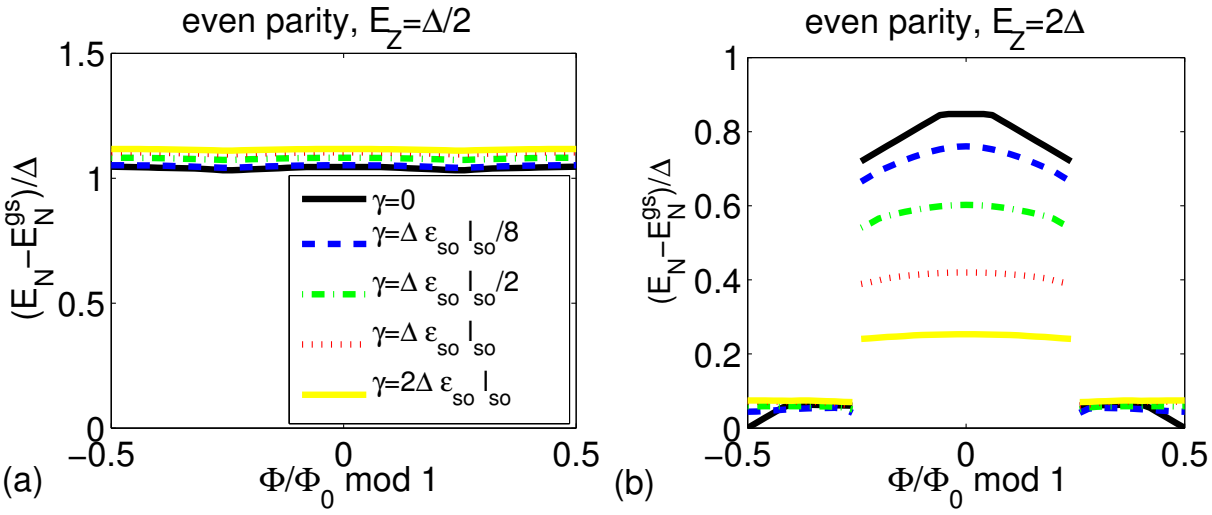

Figure 13.3: Lowest excitation energy for a ring-shaped nanowire as function of magnetic flux and for different variances of the electrostatic disorder potential. The curves represent the average over 50 random disorder configurations.

shaped SC nanowire and demonstrate that essential aspects of the above described topological degeneracy on the torus carry over to this simpler geometry. We focus on a

regime in which the quasiparticle gap Δ is larger than the single-particle level spacing d. In the Coulomb blockade regime, the total particle number and hence the parity of the SC nanowire are fixed by the charging energy $E_c > \Delta$ and the degeneracy of grand canonical ground states is reflected in the excitation energies, which can be observed in nonlinear Coulomb blockade transport. The lowest excited state above the ground state of a trivial SC with even parity involves two quasiparticles (QPs) and thus breaks a Cooper pair, incurring an excitation energy $\delta E \approx 2\Delta$, which is essentially independent of magnetic flux [3]. In contrast, the ground state for odd parity always has one QP, and hence the lowest excited state involves both annihilating and creating a QP which costs the excitation energy $d^2/\Delta \ll 2\Delta$. For nontrivial topological SCs the situation is very different. Here, ground states without unpaired particles at the Fermi energy have odd parity for periodic BC, and even parity for anti-periodic BC. Therefore, the excitation energy oscillates between d^2/Δ and 2Δ as function of magnetic flux with period h/e which is doubled as compared to the case of a trivial SC, see Fig. 13.3. This connection between the ground-state degeneracy on manifolds with nonzero genus and the h/e flux periodicity of ring structures demonstrates that these properties are a general consequence of topological order and that nonlinear Coulomb blockade transport is a suitable tool to investigate topological order.

[1] M. Oshikawa et al.: Ann. Phys. **322**, 1477 (2007)
[2] N. Read and D. Green: Phys. Rev. B **61**, 10267 (2000)
[3] B. Zocher et al.: Phys. Rev. Lett. **109**, 227001 (2012)
[4] B. Zocher et al.: New J. Phys. **15**, 085003 (2013)

13.5 Modulation of Majorana induced current cross-correlations by quantum dots

B. Zocher, B. Rosenow

Majorana bound states (MBSs) are zero-energy fermionic states which are their own anti-particles. Since quasiparticles in superconductors (SCs) are always superpositions of electron and hole components, the Majorana criterion can be realized in a peculiar way: a zero-energy quasiparticle in a SC has equal contributions from electrons and holes, and hence an exchange of electron and hole components leaves the quasiparticle invariant.

Recent experiments reported evidence of MBSs as end states in semiconductor-superconductor nanowires [1]. A possible probe for the nonlocal nature of MBSs is crossed Andreev reflection (CAR), the conversion of an incoming electron into an outgoing hole in a different lead, in contrast to local Andreev reflection, where electron and hole reside in the same lead. It has been shown theoretically that at sufficiently low voltages, CAR by the pair of MBS dominates transport [2]. However, for large voltages resonant tunneling of electrons and holes gives rise to negative cross-correlations, and the total crossed noise vanishes. In Ref. [4], we have focused on the physics of coupling a pair of MBSs to leads via quantum dots in the Coulomb blockade regime, see Fig. 13.4 **(a)**. Due to the finite wire length, the MBSs are tunnel coupled to each

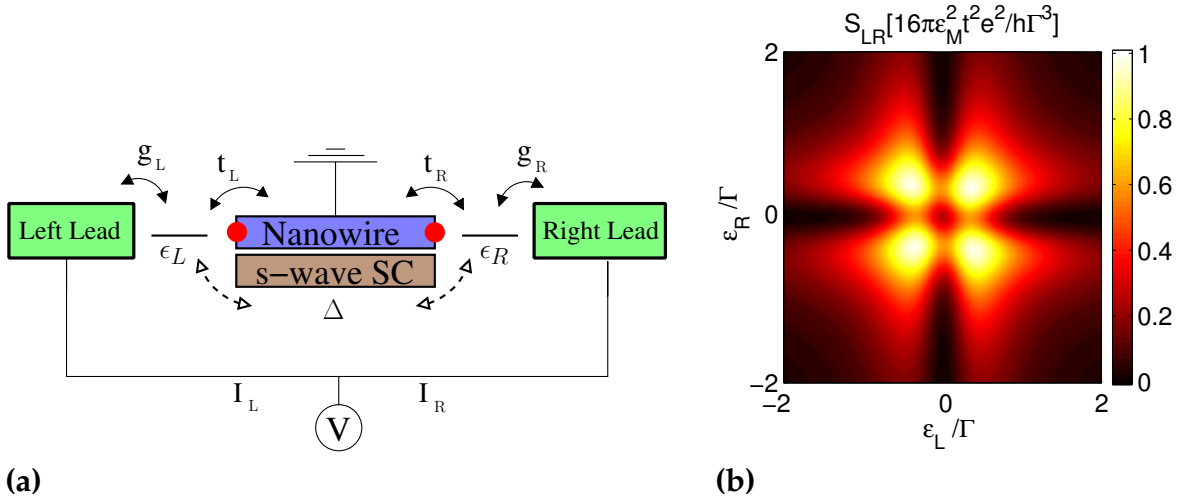

Figure 13.4: (a): Schematic setup for a system with a pair of Majorana bound states (red dots) coupled to quantum dots which themselves are coupled to biased lead electrodes. Crossed Andreev reflection can be detected by correlating the currents I_L and I_R that flow into the nanowire [3]. **(b)** Current cross-correlator S_{LR} for strong dot-lead coupling.

other and have an energy splitting $\epsilon_M \sim \Delta \exp(-L/\xi_{\mathrm{SM}})$, where ξ_{SM} is the coherence length in the semiconductor. Whenever one of the dots is aligned with the chemical potential of the superconductor, an MBS forms on that dot at exactly zero energy, even for ϵ_M finite. Hence, the MBSs at the ends of the wire are effectively uncoupled, and no CAR can be observed. When tuning the dots away from the chemical potential of the superconductor, the coupling between MBSs is restored. In addition, negative cross-correlations due to resonant tunneling are suppressed, and CAR becomes visible in positive current cross-correlations. Thus, the crossed current correlator provides a clear signature of non-local transport through a pair of MBSs in the form of a four-leaf clover feature as a function of ϵ_L and ϵ_R, see Fig. 13.4 **(b)**. These findings are in excellent agreement with results for a microscopic model of a spinless p-wave SC, persist in a more realistic model with several transverse channels, and are robust against addition of disorder.

[1] V. Mourik et al.: Science **336**, 1003 (2012)
[2] J. Nilsson et al.: Phys. Rev. Lett. **101**, 120403 (2008)
[3] A. Das et al.: Nature Commun. **3**, 1165 (2012)
[4] B. Zocher and B. Rosenow: Phys. Rev. Lett. **111**, 036802 (2013)

13.6 Shot Noise Signatures of Charges Fractionalization in the $\nu = 2$ Quantum Hall edge

M. Milletari, B. Rosenow

In contrast to three spatial dimensions, where excitations of an interacting many particle system often carry the same quantum numbers as in the non-interacting case, interactions in 1d systems completely change the character of the excitation spectrum. A

prototype model for this physics is the Luttinger model, where electrons are no longer well defined quasi-particles, and where electronic excitations decompose into spin and charge parts moving with different velocities [1]. An important example of 1d elec-

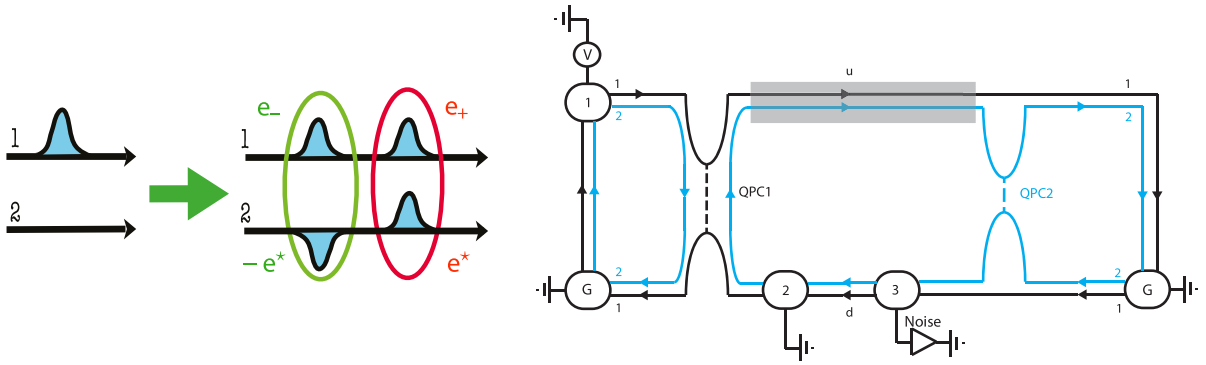

(a) **(b)**

Figure 13.5: (a) Charge Fractionalization in a $\nu = 2$ QH state. A charge pulse initially injected in edge mode 1 separates in a neutral (green) and charge (red) mode as a result of inter-channel interactions. The quasiparticles on edge mode 2 have charges $e^* = \sin 2\theta/2$ (where $\tan 2\theta = v_{12}/(v_1 - v_2)$ parametrizes the strength of interactions), while quasi particles on edge mode 1 have charges $e_\pm = e/2 \pm \sqrt{e^2/4 - (e^*)^2}$. **(b)** Sketch of a $\nu = 2$ Hall bar with a QPC1, where inner modes ("2", light blue) are fully reflected, while partial transmission of outer modes ("1", black) is possible. At QPC2, the opposite situation is realized. The shaded area is the interaction region, where partial energy relaxation takes place. The upper edge is biased with voltage V at contact 1, current noise is measured at contact 3.

tronic systems are the edge states of incompressible quantum Hall (QH) liquids, where the external magnetic field forces the excitations to be chiral (i.e. propagating only in one direction). In QH liquids at fractional filling fractions, due to strong interactions, elementary excitations carry a fractional charge that manifests itself in shot noise [2–4]. This fractional charge is universal and it is related to some topological invariants of the bulk state.

In our work [5] we have considered a QH state at integer filling fraction $\nu = 2$, whose edge dynamics is described in terms of two chiral edge modes co-propagating at different velocities v_1 and v_2. In the presence of a short range interaction v_{12} between them, a pulse of charge e injected into edge mode one at a first quantum point contact (QPC1) decomposes into a charge pulse and a neutral pulse, Fig. 13.5 **(a)**.

In the charge pulse, a charge e^* travels on mode two and e_+ on mode one. In the neutral pulse, there is a charge $-e^*$ on mode two and a charge e_- on mode one. In this way, by exciting edge channel one via a partially transmitting QPC1 (see Fig. 13.5 **(b)**, high frequency charge noise is generated on edge mode two [6]). At QPC2, allowing for partial transmission of channel two, both charges $\pm e^*$ traveling within the charge (neutral) pulse give rise to low frequency shot noise with a Fano factor $F = e^*/e$. The non triviality of this measurement consists in the fact that the shot-noise is measured in the charge neutral channel 2. As opposed to the QH state at fractional filling faction, the value of the fractional charge is not universal but instead depends on the specifics of the inter-mode interaction and the non-equilibrium nature of the state. Using the method of non-equilibrium bosonization [7, 8] within a quantum-quench model [9], we compute the shot noise at QPC2 in the asymptotic limit with particular emphasis on

its dependence on the strength of the interaction between the edge modes. Our results are in quantitative agreement with recent experimental results [10].

[1] T. Giamarchi: *Quantum Physics in One Dimension*, Oxford University Press (2003)
[2] X.G. Wen: *Quantum field Theory of Many-Body Systems*, Oxford University Press (2008)
[3] C.L. Kane, M.P.A. Fisher: Phys. Rev. Lett. **72**, 724 (1993)
[4] R. de-Picciotto et al.: Nature **389**, 162 (1997)
[5] M. Milletari, B. Rosenow: Phys. Rev. Lett. **111**, 136807 (2013)
[6] E. Berg et al.: Phys. Rev. Lett. **102**, 236402 (2009)
[7] I.P. Levkivskyi and E.V. Sukhorukov: Phys. Rev. Lett. **103**, 036801 (2009)
[8] D. B. Gutman et al.: Phys. Rev. B **81**, 085436 (2010)
[9] A.Iucci, M.A. Cazalilla: Phys. Rev. A **80**, 063619 (2009)
[10] H. Inoue et al.: arXiv:1310.0691

13.7 Superfluid Stiffness of a Driven Dissipative Condensate with Disorder

A. Janot, T. Hyart,[*] P.R. Eastham,[†] B. Rosenow

[*]Instituut-Lorentz, Universiteit Leiden, Netherlands
[†]School of Physics and CRANN, Trinity College, Dublin, Ireland

Perhaps the most spectacular manifestation of Bose-Einstein condensation, and its associated macroscopic quantum coherence, is superfluidity. Observations of macroscopic quantum coherence in driven systems, e.g. polariton condensates [1], have strongly stimulated experimental as well as theoretical efforts during the last decade. However, unlike the constituents of conventional condensates, such as cold atoms, polaritons have a finite lifetime. Thus, the polariton condensate is a non-equilibrium steady-state, in which the losses are compensated by particles flowing in from an external source. This leads to the interesting possibility of new universal behavior, different from that found in equilibrium [2]. Many similarities, nonetheless, appear to remain, at least in the absence of disorder: perturbatively, the forms of the correlation functions are the same as in equilibrium [3] (long-range order in three dimensions, and quasi-long-range order in two); superfluidity is predicted to survive [4] ($d \geq 2$); and the static behavior, in three dimensions, involves the standard O(2) critical exponents [2]. A new dynamical critical exponent has, however, been discovered [2]. We addressed the question of whether a driven quantum condensate is a superfluid, allowing for the effects of disorder and its non-equilibrium nature [5]. We predicted that for spatial dimensions $d < 4$ the superfluid stiffness vanishes once the condensate exceeds a critical size, and treated in detail the case $d = 2$. Thus a two-dimensional driven condensate is not formally a superfluid, except for zero disorder, although superfluid behavior would persist below a critical length scale. We identified this length scale labeled by $\mathcal{L}_s$, and the mechanism responsible for the destruction of superfluidity [5]. To this end we employed an effective Gross-Pitaevskii equation with disorder (disorder strength κ) as well as gain and loss term controlled by the parameter α. We found that the length scale

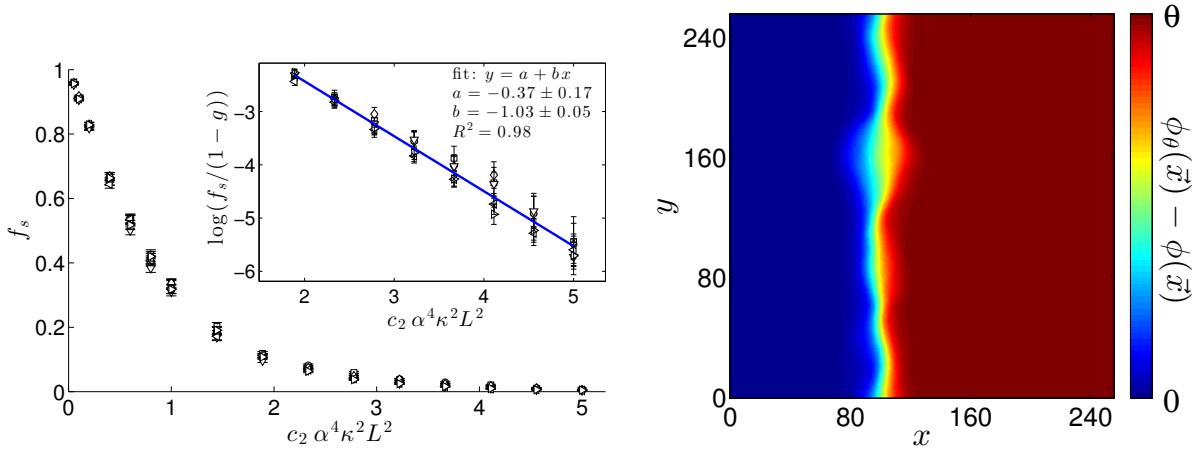

(a) **(b)**

Figure 13.6: (a) The numerically calculated stiffness f_s shows an exponential decay with increasing ratio $L^2/\mathcal{L}_s^2$ (inset: log plot of exponential tail). The superfluid depletion length is given by $\mathcal{L}_s \sim 1/\alpha^2\kappa$ where α encodes the non-equilibrium nature of the condensate and κ is an effective disorder strength. L is the system size. Points are shown for $L = 64$ and 96; $\alpha = 0.9, 1$ and 1.2. For each data point we simulated up to 1320 disorder realizations. **(b)** The condensate phase response due to a phase twist θ along x, in a typical disorder realization, exhibits a formation of a domain wall. Parameters used are $\alpha = 0.5$, $\kappa = 0.5$, $\theta = 1$.

at which superfluidity is lost decreases with increasing disorder and non-equilibrium nature, namely $\mathcal{L}_s \sim 1/\alpha^2\kappa$. In Fig. 13.6 **(a)** the behaviour of the superfluid stiffness as function of condensate size over $\mathcal{L}_s$ is shown. For a disordered driven condensate we have observed that the condensate-phase response to an external perturbation is localized in a domain wall, cf. Fig. 13.6 **(b)**. This reveals the responsible mechanism for the destruction of a rigid response.

As $\mathcal{L}_s$ decreases when moving away from equilibrium or the clean limit, our work shows that the universal properties of driven condensates are completely different from those of equilibrium ones, if there is any static disorder. These predictions could be tested by measuring the phase profiles and emission frequency of a polariton condensate in the presence of an imposed phase twist.

[1] J. Kasprzak et al.: Nature, **443**, 409 (2006)
[2] L. M. Sieberer et al.: Phys. Rev. Lett. **110**, 195301 (2013)
[3] A. Chiocchetta and I. Carusotto: EPL (Europhysics Letters) **102**, 67007 (2013); G. Roumpos et al.: PNAS **109**, 6467 (2012)
[4] J. Keeling: Phys. Rev. Lett. **107**, 080402 (2011)
[5] A. Janot et al.: Phys. Rev. Lett. **111**, 230403 (2013)

13.8 Coherent tunnelling across a quantum point contact in the quantum Hall regime

F. Martins,[*] S. Faniel,[†*] B. Rosenow, H. Sellier,[‡] S. Huant,[‡] M.G. Pala,[§] L. Desplanque,[¶] X. Wallart,[¶] V. Bayot,[*‡] B. Hackens[*]

*IMCN/NAPS, Université catholique de Louvain, Louvain-la-Neuve, Belgium
†ICTEAM/ELEN, Université catholique de Louvain, Louvain-la-Neuve, Belgium
‡Institut Néel, CNRS and Université Joseph Fourier, Grenoble, France
§IMEP-LAHC, Grenoble INP, Minatec, Grenoble, France
¶IEMN, Cité scientifique, Villeneuve d'Ascq, France

The unique properties of quantum Hall devices arise from the ideal one-dimensional edge states that form in a two-dimensional electron system at high magnetic field. Tunnelling between edge states across a quantum point contact (QPC) has already revealed rich physics, like fractionally charged excitations, or chiral Luttinger liquid. Thanks to scanning gate microscopy, we show that a single QPC can turn into an interferometer for specific potential landscapes. Spectroscopy, magnetic field and temperature dependences of electron transport reveal a quantitatively consistent interferometric behavior of the studied QPC. To explain this unexpected behavior, we put forward a new model which relies on the presence of a quantum Hall island at the centre of the constriction as well as on different tunnelling paths surrounding the island, thereby creating a new type of interferometer. This work sets the ground for new device concepts based on coherent tunnelling.

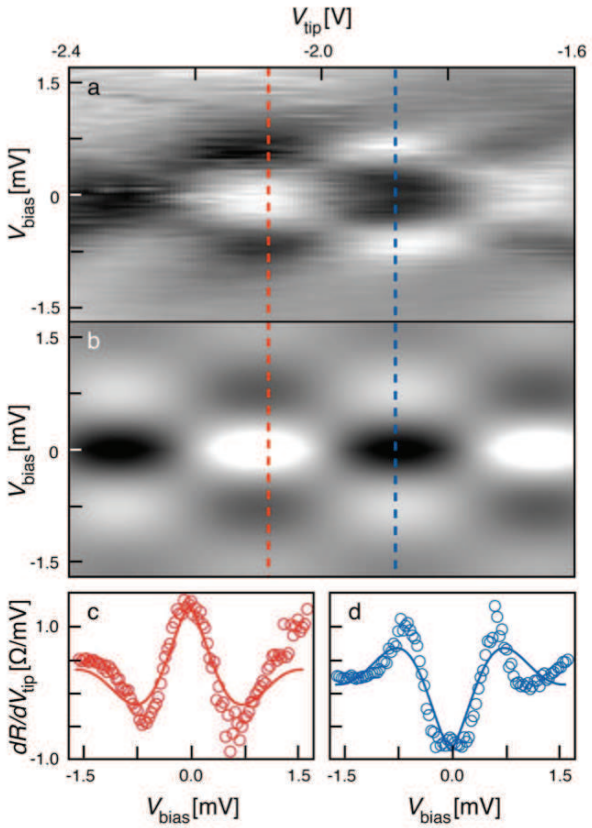

Figure 13.7: Evidence for coherent transport in spectroscopy. **(a)** dR/dV_{tip} as a function of the dc component of V_{tip} and V_{bias} at B = 9.5 T and T = 100 mK. Voltage modulation of V_{tip} was set to 50 mV. **(b)** 2D fit of dR/dV_{tip}. **(c-d)** Transresistance vs V_{bias} taken along the red **(c)** and blue **(d)** dashed lines in **(a-b)**. The circles correspond to the experimental data and the continuous lines to the fit.

We examine an unexplored regime of transport across a QPC where QH edge states are weakly coupled, but phase coherence is preserved [1]. The SGM tip is used as a nanogate to tune the potential landscape and hence edge states' pattern and coupling. At first sight, one expects that transport should be driven by tunnelling, and possibly by Coulomb blockade if a quantum Hall island were mediating transport between edge states. Indeed, SGM and magnetoresistance data corroborate with Coulomb blockade across a QHI located near the saddle point of the QPC. However, temperature dependence and scanning gate spectroscopy show clear signatures of quantum interferences. Instead of Coulomb diamonds, the spectroscopy displays a checkerboard pattern of maxima and minima, indicating that both V_{tip} and V_{bias} tune the interference of transiting electrons. Each bias independently adds a phase shift between interfering paths, so that the transresistance is modulated by a product of cosines and an exponential term accounting for a voltage-dependent dephasing induced by electrons injected at an energy eV_{bias}.

[1] F. Martins, S. Faniel, B. Rosenow, H. Sellier, S. Huant, M.G. Pala, L. Desplanque, X. Wallart, V. Bayot, and B. Hackens, Scientific Reports **3**, 1416 (2013).

13.9 Backscattering Between Helical Edge States via Dynamic Nuclear Polarization

A. Del Maestro,* T. Hyart, B. Rosenow

*Department of Physics, University of Vermont, Burlington, USA

We show that the non-equilibrium spin polarization of one dimensional helical edge states at the boundary of a two dimensional topological insulator can dynamically induce a polarization of nuclei via the hyperfine interaction. When combined with a spatially inhomogeneous Rashba coupling, the steady state polarization of the nuclei produces backscattering between the topologically protected edge states leading to a reduction in the conductance which persists to zero temperature. We study these effects in both short and long edges, uncovering deviations from Ohmic transport at finite temperature and a current noise spectrum which may hold the fingerprints for experimental verification of the backscattering mechanism [1].

We discuss the influence of dynamically polarized nuclear spins on the conductance of QSH edge channels depicted in Fig. 13.8. We argue that flip-flop scattering between electronic and nuclear spins creates a dynamic nuclear polarization, similar to behavior seen when helical edge states are coupled to a general spin bath. The nuclear polarization has the same effect as an external Zeeman field and gives rise to backscattering between helical edge states. The magnitude of the nuclear spin polarization is determined by the ratio of bias voltage and temperature. Thus, for a long edge of length $L \gg \ell$, the local temperature profile governed by a balance between Joule heating and electronic heat transport determines the conductance. We find a non-linear current-voltage characteristic at finite temperature and a peculiar relation between applied voltage and noise power, which together with hysteresis in the current-voltage characteristic are signatures of backscattering due to a dynamic nuclear polarization. Importantly, this

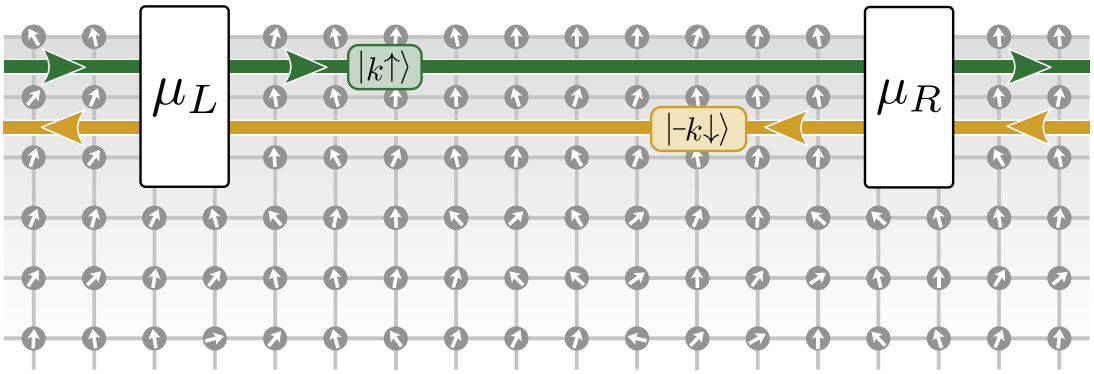

Figure 13.8: Quantum spin Hall edge states dynamically polarize nuclear spins via a hyperfine interaction. Although the edge states are drawn as sharp lines, their wavefunctions may overlap a large number of nuclei. Only one edge is shown, but there is an equivalent and independent transport channel at the opposite edge, where the spin polarizations are reversed.

mechanism stays effective in the low-temperature limit, similar to spin-flip scattering in $\nu = 2$ quantum Hall edges.

[1] Adrian Del Maestro, Timo Hyart, and Bernd Rosenow, Phys. Rev. B **87**, 165440 (2013).

13.10 Funding

Untersuchungen zum topologischen Quanten-Computing
B. Rosenow together with J. Smet (MPI FKF) and W. Dietsche (MPI FKF)
BMBF 01BM0900

Phasenrelaxation und Gegenstrom-Dissipation in Quanten-Hall Doppellagen
B. Rosenow
DFG-Projekt RO 2247/7-1

Robustheit geschützter Randzustände in topologischen Isolatoren
B. Rosenow (Teilprojektleiter)
ESF-Projekt 100124929

13.11 Organizational Duties

B. Rosenow

- Member of the Studienkommission of the Faculty of Physics and Earth Sciences
- Referee for Science, Phys. Rev. Lett., Phys. Rev. B, Europhys. Lett. Adv. Con. Matter, JSTAT, Physica A, NSF, Studienstiftung des Deutschen Volkes

13.12 External Cooperations

Academic

- University of Vermont, USA
  A. Del Maestro
- Technische Universität Darmstadt, Germany
  Prof. Dr. Jens Braun
- Friedrisch-Schiller-Universität Jena, Germany
  Prof. Dr. Holger Gies
- RWTH Aachen, Germany
  Prof. Dr. Carsten Honerkamp
- Universität Heidelberg, Germany
  Dr. Michael M. Scherer
- Universiteit Leiden, Netherlands
  Dr. Timo Hyart
- School of Physics and CRANN, Trinity College, Ireland
  Prof. Paul Eastham
- Weizmann Institute for Science, Israel
  Prof. Yuval Gefen, Prof. Ady Stern
- Harvard University, USA
  Prof. Bert Halperin

13.13 Publications

Journals

T. Hyart and B. Rosenow, *Influence of topological excitations on Shapiro steps and microwave dynamical conductance in bilayer exciton condensates*, Phys. Rev. Lett. **110**, 076806 (2013)

A. Del Maestro, T. Hyart, and B. Rosenow, *Backscattering Between Helical Edge States via Dynamic Nuclear Polarization*, Phys. Rev. B **87**, 165440 (2013)

B. Zocher, and B. Rosenow, *Surface states and local spin susceptibility in doped three-dimensional topological insulators with odd-parity superconducting pairing symmetry*, Phys. Rev. B **87**, 155138 (2013)

D. D. Scherer, J. Braun, H. Gies, *Many-flavor Phase Diagram of the (2+1)d Gross-Neveu Model at Finite Temperature*, J. Phys. A: Math. Theor. **46**, 285002 (2013)

H.-G. Zirnstein, and B. Rosenow, *Cancellation of Quantum Anomalies and Bosonization of the 3D Time-Reversal Symmetric Topological Insulator, Heinrich-Gregor Zirnstein, and Bernd Rosenow*, Phys. Rev. B **88**, 085105 (2013)

B. Zocher, M. Horsdal, and B. Rosenow, *Robustness of Topological Order in Semiconductor-Superconductor Nanowires in the Coulomb Blockade Regime*, NJP **15**, 085003 (2013)

B. Zocher and B. Rosenow, *Modulation of Majorana induced current cross-correlations by quantum dots*, Phys. Rev. Lett. **111**, 036802 (2013)

M. Milletari and B. Rosenow *Signatures of Charges Fractionalization in the $\nu = 2$ Quantum Hall edge*, Phys. Rev. Lett. **111**, 136807 (2013)

A. Janot, T. Hyart, P. R. Eastham, and B. Rosenow, *Superfluid Stiffness of a Driven Dissipative Condensate with Disorder*, Phys. Rev. Lett. **111**, 230403 (2013)

F. Martins, S. Faniel, B. Rosenow, M.G. Pala, H. Sellier, S. Huant, L. Desplanque, X. Wallart, V. Bayot, and B. Hackens, *Scanning gate spectroscopy of transport across a quantum Hall nano-island*, NJP **15**, 013049 (2013)

F. Martins, S. Faniel, B. Rosenow, H. Sellier, S. Huant, M.G. Pala, L. Desplanque, X. Wallart, V. Bayot, and B. Hackens, *Coherent tunnelling across a quantum point contact in the quantum Hall regime*, Scientific Reports **3**, 1416 (2013)

in press

Y. Dinaii, Y. Gefen, B. Rosenow, *Transmission phase lapses through a quantum dot in a strong magnetic field*, Physical Review Letters (2014)

Talks

B. Rosenow, Workshop Disorder, Dynamics, Frustration and Topology in Quantum Condensed Matter, Aspen Center for Physics, June 2013

B. Rosenow, Workshop Workshop on Interferometry and Interactions in Non-Equilibrium Meso- and NanoSystems, ICTP Trieste, April 2013

B. Rosenow, *Parity effects and crossed Andreev noise in transport through Majorana wires*, invited talk, DPG Frühjahrstagung, March 2013

B. Rosenow, *Exotic particles in two dimensions: interferometry with anyons*, Colloquium, University Trondheim, May 2013

B. Rosenow, *Non-equilibrium steady states and charge fractionalization in Luttinger liquids*, Theorie-Seminar, Universität Jena, June 2013

B. Rosenow, *Anyons in Fractional Quantum Hall States*, Seminar Nano- und Quantenphysik, Universität Basel, Mai 2013

B. Rosenow, *Non-equilibrium steady states and charge fractionalization in Luttinger liquids*, Seminar Festkörpertheorie, Harvard University, September 2013

B. Rosenow, *Parity effects and crossed Andreev noise in transport through Majorana wires*, FUB-WIS Minerva Group meeting, Weizmann Institute of Science, Oktober 2013

M. Milletari, *Non-equilibrium noise and charge fractionalization in a $\nu = 2$ Quantum Hall edge state*, Condensed Matter seminar, University of Maryland at College Park, USA, March 2013.

M. Milletari, *Non-equilibrium noise and charge fractionalization in a $\nu = 2$ Quantum Hall edge state*, APS March Meeting, Baltimore, USA, March 2013

B. Zocher, *Local spin susceptibility and surface states in doped three-dimensional topological insulators with odd-parity superconducting pairing symmetry*, DPG Frühjahrstagung, Regensburg, March 2013

Posters

A. Janot, *Depletion of Superfluidity in a disordered non-equilibrium Quantum Condensate*, Symposium Graduate School BuildMoNa, Leipzig, March 2013

M. Treffkorn, *Interference in single quantum point contacts*, Annual BuildMoNa Conference, Leipzig, March 2013

B. Zocher, *Modulation of Majorana induced current cross-correlations by quantum dots*, DPG Frühjahrstagung, Regensburg, March 2013

A. Janot, *Depletion of Superfluidity in a disordered non-equilibrium Quantum Condensate*, DPG Frühjahrstagung, Regensburg, March 2013

D. D. Scherer, *Interacting electrons on trilayer honeycomb lattices*,
DPG Frühjahrstagung, Regensburg, March 2013

M. Milletari, *Non-equilibrium noise and charge fractionalization in a $\nu = 2$ Quantum Hall edge state*, IPS Meeting, Singapore, February 2013

M. Horsdal, *Robustness of Topological Order in Semiconductor-Superconductor Nanowires in the Coulomb Blockade Regime*, Workshop Majorana Physics in Condensed Matter Physics, Erice, Italy, July 2013

A. Janot, *Superfluid Stiffness of a Driven Dissipative Condensate with Disorder*, Workshop on Non-Equilibrium Bosons: from Driven Condensates to Non-Linear Optics, Trieste, August 2013

B. Zocher, *Modulation of Majorana induced current cross-correlations by quantum dots*, Workshop, Topology and Nonequilibrium in Low-Dimensional Electronic Systems, Dresden, September, 2013

A. Janot, *Superfluid Stiffness of a Driven Dissipative Condensate with Disorder*, Mini Symposium: Quantum Coherent Structures: Quantum Structures for Energy Applications, Leipzig, October 2013

M. Treffkorn, *Scanning gate microscopy on quantum Hall point contacts*, Mini Symposium: Quantum Coherent Structures: Quantum Structures for Energy Application, Leipzig, October 2013

13.14 Graduations

Doctorate

- M. Milletari
  Non-equilibrium transport in quantum Hall edge states
  July 16
- B. Zocher
  Signatures of Majorana fermions and ground state degeneracies in topological superconductors
  December 16

Master

- C. Lehmann
  Effect of Interactions on Nuclear Polarization Induced Backscattering between Helical Edge States
  December 03

Bachelor

- E. Lohman
  Behavior of Majorana states in the 1d Kitaev model under manipulations of the chemical potential
  May 30

13.15 Guests

- Dr. Michael Wimmer
  Universiteit Leiden, Netherlands
  January 7
- Dr. Michael M. Scherer
  Universität Heidelberg, Germany
  January 23 - 24
- Dr. Timo Hyart,
  Universiteit Leiden, Netherlands
  January 27 - February 2
- Yehuda Dinaii
  Weizmann Institute for Science, Israel
  February 24 - March 3
- Prof. Yuval Gefen
  Weizmann Institute for Science, Israel
  April 22 - 24

14

Theory of Condensed Matter

14.1 Introduction

Major research topics of our groups include nonequilibrium phenomena and pattern formation in systems of various nature, e.g. in soft condensed matter and in biological systems. Modern analytic methods of statistical physics and computer simulations complement and stimulate each other. Cooperations with mathematicians, theoretical and experimental physicists, biologists and medical researchers in Germany, Europe and around the world are well established. Specifically we are interested in the following problems.

Stochastics and pattern formation (Behn). Noise induced phenomena like nonequilibrium phase transitions are studied with analytical and cumputational methods in stochastically driven nonlinear systems with many degrees of freedom. Methods of nonlinear dynamics and statistical physics are used to formulate and investigate mathematical models of the adaptive immune system. We describe the random evolution of idiotypic networks of the B-lymphocyte subsystem, and investigate the regulation of balance in the T-lymphocyte subsystem in allergy and during immunotherapy (cooperation with G. Metzner, Clinical Immunology).

Non-equilibrium dynamics in soft-condensed-matter systems (Kroy). Much of what we do can be summarized as Soft Mesoscopics, the study of of emerging properties in soft and biological matter. Studied phenomena range from desert dunes and ripples spontaneously developing as a generic consequence of aeolian sand transport, through non-equilibrium dynamics of hot nanoparticles, proteins and polymers, the viscoelastic and inelastic mechanics of the cytoskeleton, to the tension propagation in single DNA molecules under strong external fields. (Related experimental work is currently in progress at EXP1: MON, MOP, PWM.) A common theme is the presence of strong fluctuations and stochastic dynamics on the microscale. The emergence of the mesoscopic structure and transport is to be understood. The applied methods comprise a broad statistical mechanics toolbox including stochastic (integro-)differential equations, liquid-state theories, effective hydrodynamic equations, various systematic coarse-graining techniques, and massively parallel numerical simulations on GPUs.

Ulrich Behn, Klaus Kroy

14.2 Stochastic Phenomena in Systems with Many Degrees of Freedom

U. Behn, R. Kürsten, H. Stage*

*The University of Manchester, School of Physics and Astronomy, RISE intern

Arrays of coupled nonlinear dynamical systems driven by multiplicative or additive noise show close analogies to phase transitions in equilibrium [1]. Concepts such as ergodicity breaking, order parameter, critical behaviour, critical exponents etc. developed to describe equilibrium phase transitions can be transfered to noise induced nonequilibrium phase transitions.

For an infinite array of *globally* coupled overdamped anharmonic oscillators subject to additive Gaussian white noise [2], a mean-field like description is exact. In the stationary state, the mean field is determined by the stable fixed points of a self-consistency map [3].

We have proved the existence of a well-behaved critical manifold in the parameter space which separates a symmetric phase from a symmetry broken phase. Given two of the system parameters there is an unique critical value of the third. We show that the critical control parameter a_c is bounded by its limit values for weak and for strong noise. In these limits the mechanism of symmetry breaking differs. For weak noise the distribution is almost Gaussian and the symmetry is broken as the whole distribution is shifted in either the positive or the negative direction. For strong noise there is a symmetric double-peak distribution and the symmetry is broken as the weights of the peaks become different [5]. The qualitative behavior is the same for higher order saturation terms. Also in these cases, the critical point can be calculated for strong and for weak noise, and the limits are bounds for the critical point.

Introducing in the Langevin equation an additional, competing nonlinearity leads to richer behavior. Then the parameter space divides in three regions, a region with a symmetric phase, a region with a phase of broken symmetry, and a region where both phases coexist, cf. Fig. 14.1. The region of coexistence collapses into one of the others via a discontinuous phase transition whereas the transition between the symmetric phase and the phase of broken symmetry is continuous. We find optimal bounds also for the tricritical point where the three regions intersect which are assumed in the limits of weak and of strong noise.

During her internship, Helena Stage (a RISE intern mentored by Rüdiger Kürsten) elaborated on a simulation method for nonlinear stochastic differential equations, proposed in [4], to sample probability densities also in sparsely visited regions of the support.

[1] F. Sagués, J. García-Ojalvo, J.M. Sancho: Rev. Mod. Phys. **79**, 829 (2007)
[2] K. Kometani, H. Shimizu: J. Stat. Phys. **13**, 473 (1975)
[3] R. Desai, R. Zwanzig: J. Stat. Phys. **19**, 1 (1978)
[4] R. Kürsten: Masterarbeit, Universität Leipzig, 2012
[5] R. Kürsten, S. Gütter, U. Behn: Phys. Rev. E **88**, 022114 (2013)

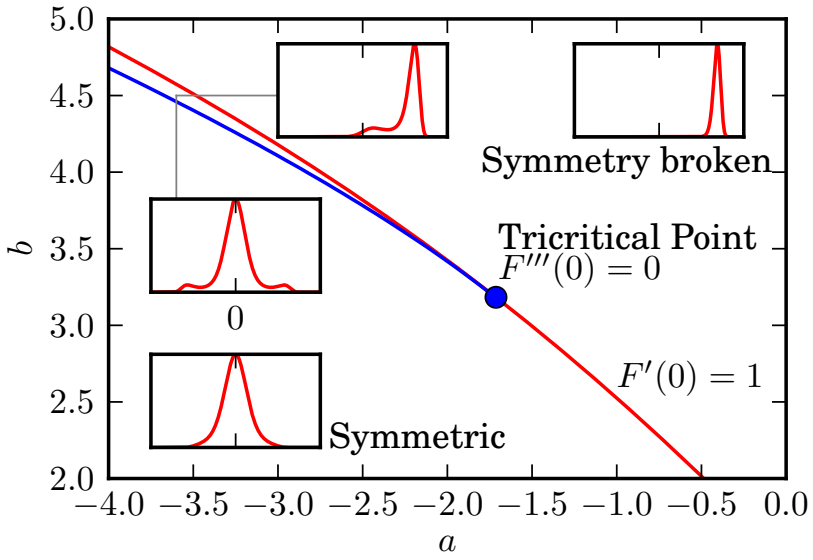

Figure 14.1: Phase diagram for a model with two competing nonlinearities, a cubic term and a quintic saturation term. The parameter plane is spanned by the main control parameter, the coefficient of the linear term a, and the coefficient of the cubic term b. The diagram shows a region of a symmetric phase, a region with a phase of broken symmetry, and a region where both phases coexist. The inserts show schematically the probability densities in the respective cases. The strength of the global coupling is $D = 1$, the strength of the noise is $\sigma = 1$. Figure by R. Kürsten.

14.3 Randomly Evolving Idiotypic Networks

U. Behn, N. Preuß, H. Schmidtchen, R. Schulz

The paradigm of idiotypic networks conceptualized a few decades ago by Niels Jerne [1] finds today a renewed interest mainly from the side of systems biology and from clinical research, cf. the recent reviews with focus on modeling [2], and on biological concepts and clinical applications [3].

We have considered the problem of self tolerance in the frame of a minimalistic model of the idiotypic network [4]. A node of this network represents a clone of B lymphocytes of the same idiotype which is encoded by a bit string. The links of the network connect nodes with (nearly) complementary strings. The population of a node survives if the number of occupied neighbours is not too small and not too large. There is an influx of lymphocytes with random idiotype from the bone marrow. Previous investigations have shown that this system evolves toward highly organized architectures, where the nodes can be classified into groups according to their statistical properties. The most interesting architecture, found in a certain regime of parameters, consists of a connected part (densely linked core groups and a hereto linked periphery), a hereof disconnected part (singletons), and groups of suppressed clones (stable holes). The building principles of these architectures can be analytically described [5] and the statistical results of simulations agree very well with results of a modular mean-field theory [6].

We performed simulations for the case that one or several nodes, playing the role of self, are permanently occupied. These self nodes influence their linked neighbours, the autoreactive clones, but are themselves not affected by idiotypic interactions. We observe that the group structure of the architecture is very similar to the case without self antigen, but organized such that the neighbours of the self are only weakly occupied, thus providing self tolerance, cf. Fig. 14.2. We also treated this situation in an adapted modular mean-field theory [7] which give results in good agreement with data from simulation. The model supports the view that autoreactive clones which naturally occur also in healthy organisms are controlled by anti-idiotypic interactions, and could be helpful to understand network aspects of autoimmune disorders [8].

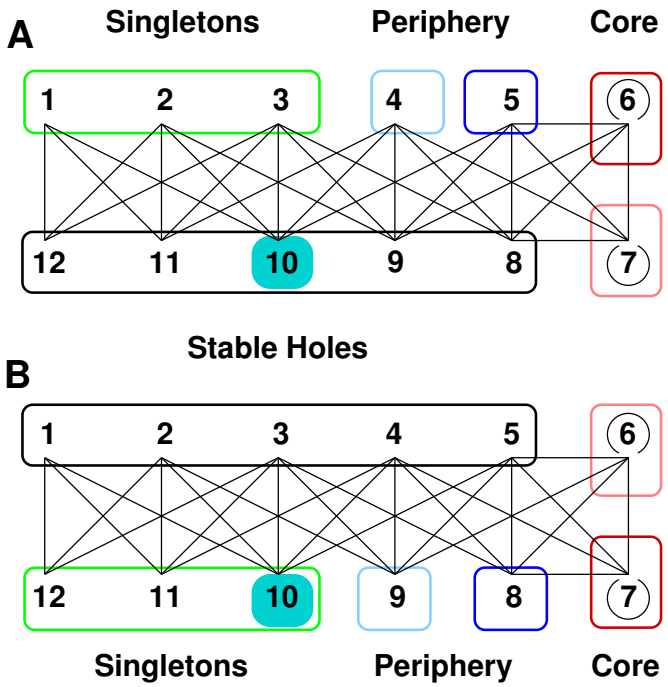

Figure 14.2: 12-group architecture with self. The lines indicate the existence of links between nodes of the connected groups. **(A)** We permanently occupy one of the hole groups, group 10 (cyan), thus mimicking the permanent presence of self. This state is not favourable since the self couples to singletons and periphery which have a high occupation. **(B)** Letting the thus prepared system evolve, it soon reaches a new steady state, still a 12-group architecture, but organized such that the self now belongs to the singletons and thus couples only to the almost empty stable holes. The self-recognizing idiotypes are controlled by the network, thus providing self tolerance. Figure from [8].

[1] N.K. Jerne: Ann. Inst. Pasteur Immunol. **125C**, 373 (1974)
[2] U. Behn: Immunol. Rev. **216** 142 (2007)
[3] U. Behn: *Idiotype Network*, in: Encyclopedia of Life Sciences, John Wiley & Sons, Ltd, Chichester, doi:10.1002/9780470015902.a0000954.pub2 (2011)
[4] M. Brede, U. Behn: Phys. Rev. E **67**, 031920 (2003)
[5] H. Schmidtchen, M. Thüne, U. Behn: Phys. Rev. E **86**, 011930 (2012)
[6] H. Schmidtchen, U. Behn: Phys. Rev. E **86**, 011931 (2012)
[7] R. Schulz: Diplomarbeit, Universität Leipzig, 2013
[8] R. Schulz, B. Werner, U. Behn: Frontiers in Immunology **5**, 00086 (2014)

14.4 T Cell Regulation and Immunotherapy

U. Behn, T. Lenich, G. Metzner*

*Institute of Clinical Immunology, University Leipzig

T helper cells play a significant role in immune responses to allergenic substances. There are several subtypes which differ in function according to their cytokine profiles. Immunologists distinguish four major lineages: Th1, Th2, Th17 and regulatory T cells (Treg). Among these, mainly specific Th2 cells are responsible for allergic reactions since they activate the production of IgE antibodies which provoke the well-known allergic symptoms. Allergen-specific immunotherapy consists of repeated injections of allergens aiming to induce a state of tolerance in the allergic individual. Specific immunotherapy has been carried out for more than one century based entirely on empirical grounds.

We previously have developed a mathematical model describing the nonlinear dynamics of Tregs, naive T helper cells, Th1 and Th2 subsets, and their major cytokines [1]. Administration of allergen according to empirical protocols is targeting the model from an allegic state with a prevalence of Th2 cells to a tolerant state, where a prevalent Treg population keeps both Th2 and Th1 cells low. The complexity of the model is reduced by investigating a stroboscobic map describing the maintenance phase of the therapy. One of the stable fixed points of this map describes the state after a successful therapy.

There is a number of other diseases where the T-cell balance is skewed which could be treated by inducing Tregs due to oral administration of antigen [2]. In this context it is of interest to develop in the frame of our model protocols which target the system into a favourable region of the state space. In his study Tobias Lenich found, applying an intelligent trial and error strategy, protocols which direct the system into the basin of attraction of the Th1-dominated fixed point of the stroboscobic map [3].

[1] F. Groß, G. Metzner, U. Behn: J. Theor. Biol. **269**, 70-78 (2011)
[2] H.L. Weiner, A.P. da Cunha, F. Quintana, H. Wu: Immunol. Rev. **241**, 241-259 (2011)
[3] T. Lenich: *Nichtlineare Dynamik des Th1-Th2-Treg Systems: Protokolle für spezifische Immuntherapien*, Bericht zum Theoretikum, Universität Leipzig, 2014

14.5 Melting of Pectin Gels

A. Kramer, R.R.R. Vincent*, B.W. Mansel†, K. Kroy, M.A.K. Williams†

*University of Barcelona, Institute for Bioengineering of Catalonia, Spain
†Massey University, Institute of Fundamental Sciences, New Zealand

Pectin is a polysaccharide of the plant cell wall that is thought to be a crucial player in the control of its mechanical functionality. We have analyzed the slow dynamics and linear and nonlinear viscoelasticity of pectin gels as a function of temperature, using various (micro-)rheological techniques and theory [1]. The nonlinear mechanical

response is found to be much more sensitive to temperature changes than the linear response, a property that is also observed in F-actin networks [2].

The temperature effects observed for pectin gels can be accounted for by the glassy wormlike chain (GWLC) model of self-assembled semiflexible filaments with some additional assumptions. Whereas the temperature effects observed in the linear response can be explained by assuming that the solvent viscosity decreases with temperature according to the Vogel-Fulcher equation, for nonlinear measurements structural properties of the network become more important.

Pronounced temperature effects were also observed for microtubules [3] and cells [4], the explanation of which is a focus of further investigations.

[1] R.R.R. Vincent et al.: New J. Phys. **15**, 1035002 (2013), doi:10.1088/1367-2630/15/3/035002
[2] C. Semmrich et al.: PNAS **51**, 20199 (2007), doi:10.1073/pnas.0705513104
[3] A. Kis et al.: Phys. Rev. Lett. **89**, 248101 (2002), doi:10.1103/PhysRevLett.89.248101
[4] T. Kießling et al.: New J. Phys. **15**, 045026 (2013), doi:10.1088/1367-2630/15/4/045026

14.6 DNA Tension Dynamics

K. Kroy, U. Keyser*, S. Sturm, O. Otto*, N. Laohakunakorn*

*Cavendish Laboratory, University of Cambridge, UK

The experimental investigation of biomolecules through single molecule manipulation techniques often relies on DNA or other semiflexible polymers as mechanically well-characterized, readily available linkers that easily bind both to other biological molecules and man-made structures. Whereas the strongly nonlinear stretching behaviour [1] of semiflexible polymers is routinely taken into account [2], the anomalously large friction that may be generated through internal polymer dynamics [3] has so far not been considered, although it may become a relevant factor for the analysis of high-speed force spectroscopy assays. In cooperation with experimentalists from the University of Cambridge, we provide measurements of, and a theoretical description for, the apparent relaxation timescale of a retracting "DNA handle" held on one end by an optical trap [4]. We obtain a semi-empirical formula for the effective relaxation timescale that should hold for all values of polymer length, polymer stiffness, solvent viscosity or trap strength and may be used as a convenient tool for the rational design of high-speed dynamic force spectroscopy setups.

[1] J. F. Marko, E. D. Siggia: Macromolecules **28**, 8759 (1995), doi:10.1021/ma00130a008
[2] C. Ray et al.: J. Phys. Chem. B **111**, 1963 (2007), doi:10.1021/jp065530h
[3] O. Hallatschek et al.: Phys. Rev. Lett. **94**, 077804 (2005), doi:10.1103/PhysRevLett.94.077804
[4] O. Otto et al. Nature communications **4**, 1780 (2013), doi:10.1038/ncomms2790

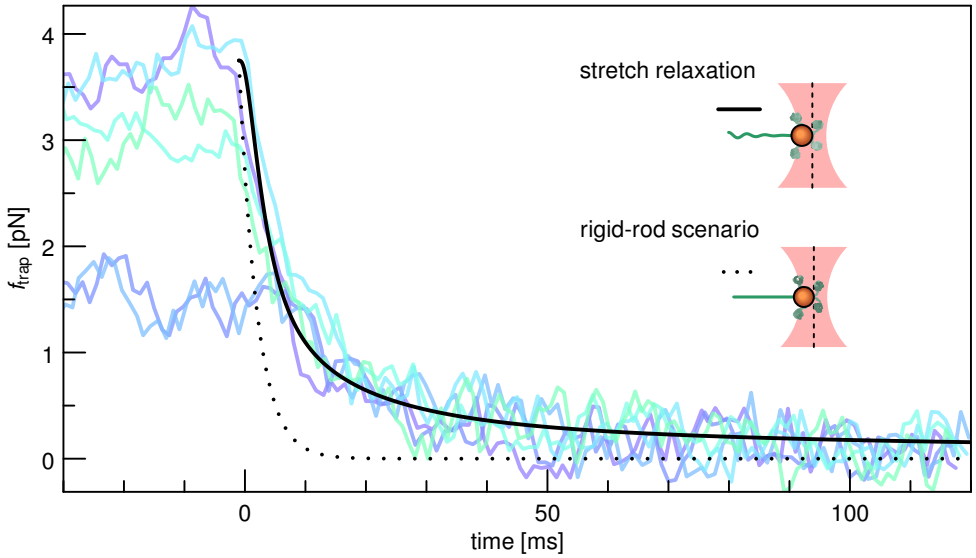

Figure 14.3: Force relaxation within optically trapped DNA. Although the overall friction coefficient of DNA scales linearly in its extension and is thus largest in a hypothetical scenario where bead and DNA relax towards the trap center as a single rigid object (dotted line), the experimentally observed force relaxation is severalfold slower, a discrepancy that can be explained theoretically by taking into account dynamic contraction effects (solid line).

14.7 Rapid Force Spectroscopy

K. Kroy, J.T. Bullerjahn, S. Sturm

Dynamic force spectroscopy is a well-established technique that allows the experimentalist to determine the free energy landscape of single molecules by probing their rupture behavior under external force. Conventional theories of dynamic force spectroscopy [1] rely on a quasistatic model of bond breaking that is well justified for current experimental setups, but fails to cover the high loading rates amenable to full-scale molecular dynamics simulations and, possibly, future high-speed force spectroscopy assays [2]. We extend these theories [3] to rapid force spectroscopy protocols by explicitly resolving the non-equilibrium internal bond dynamics. Our analytical predictions are exact for fast loading protocols and reduce to established quasistatic results in the limit of slow external loading. Their large range of applicability renders them an ideal companion to Bayesian methods of data analysis, yielding an accurate tool for analyzing and comparing force spectroscopy data from a wide range of experiments and simulations.

[1] O.K. Dudko et al.: Phys. Rev. Lett. **96**, 108101 (2006), doi:10.1103/PhysRevLett.96.108101
[2] M. Rief, H. Grubmüller: Chem. Phys. Chem. **3**, 255 (2002),
[3] J.T. Bullerjahn et al.: Theory of rapid force spectroscopy, under review.

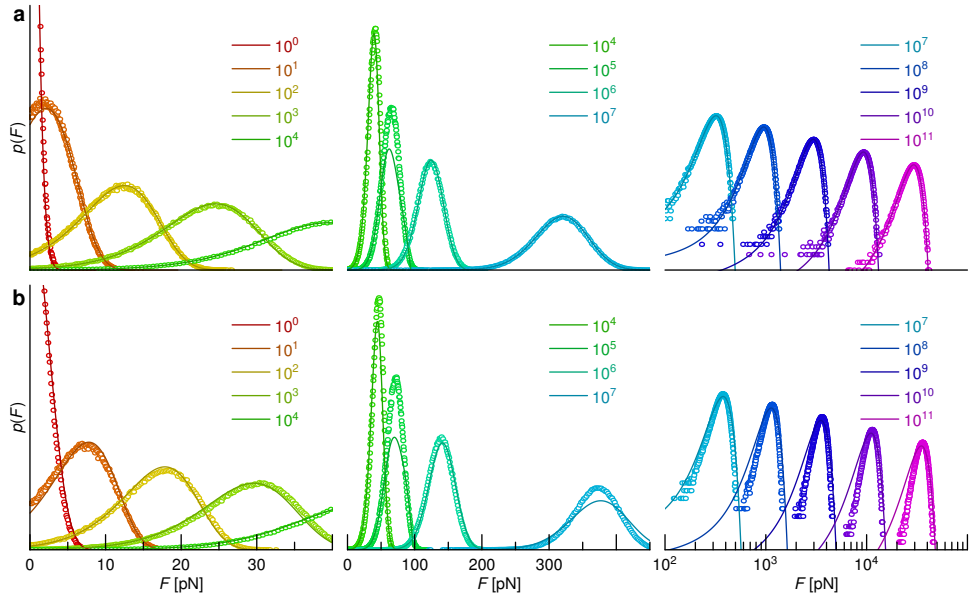

Figure 14.4: Analyzing numerically simulated force spectroscopy data. Using Brownian Dynamics simulations (data points), we have generated synthetic rupture force histograms for the two commonly used model binding potentials (**a** cusp-shaped, **b** linear-cubic) and over a wide range of external loading rates ($1 - 10^{11}$ pN/s). Whereas conventional quasi-static theories of force spectroscopy can only be applied up to a critical force level ($F \approx 80$ pN for our choice of parameters), our theory extends to arbitrarily high loading rates, using a single set of fit parameters for each of the two scenarios (solid lines).

14.8 Inelastic Mechanics of the Cytoskeleton and Cell Morphology

M. Kettner, K. Kroy, G. Zecua

The mechanical behavior of single animal cells is characterized by viscoelasticity. However, over long time scales, they can be described in analogy to a liquid drop, i.e., with an effective surface tension, mostly originated from the actin cortex underneath the plasma membrane. The surface tension minimizes the surface area.

There have been already attempts to explain the experimental finding with adherent cells on stiff substrates. Previous work predicts a constantly curved contour of the cell shape [1, 2]. These models describe the cell as a flat layer with a normal surface tension and a tangential line tension.

In contrast, we have developed a model which describes a sector of an adhered cell as a three-dimensional object, assuming that the cellular surface area becomes minimum while the pressure difference at the interface vanishes. In the spirit of the liquid analogy, one can show that the stable shape depends only on the geometry of the boundary conditions, given by cytoskeletal stress fibers, and not on the explicit value of the effective surface tension.

The minimal surface can be perturbed by small deviations of the pressure difference at the interface. In this way, it is possible to model observed active cellular expansion (or contraction) due to reinforcement processes of the actin network, or to changes in the osmotic pressure.

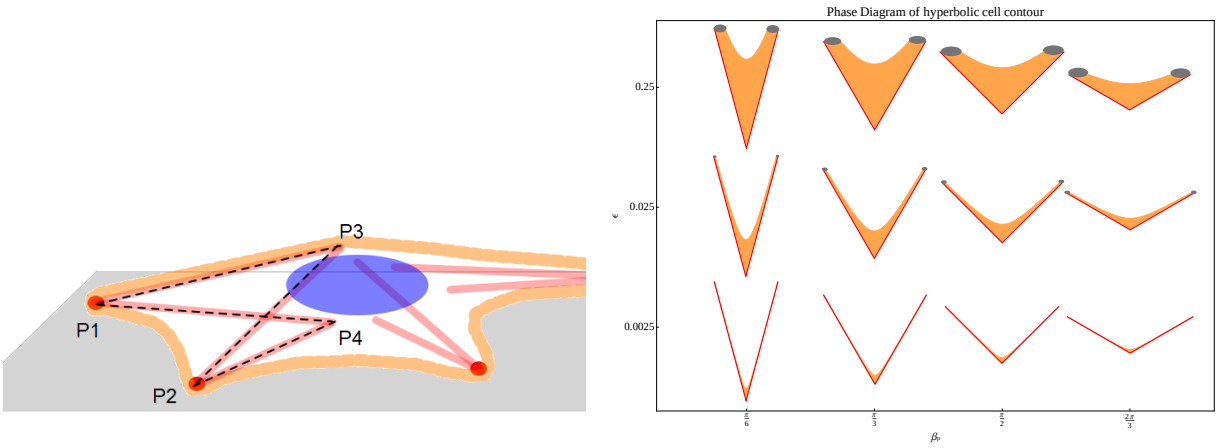

Figure 14.5: Left: Adhesion points and maximum cell height as fixed boundary conditions for the development of a minimal surface. The straight connections between the point of maximum cell height, P_3, and the adhesion points on the substrate, P_1 and P_2, can be interpreted as taut stress fibers that exhibit neglible bending. Right: Phase diagram of the cell contour with respect to tha opening angle β_p for different sizes of the cellular adhesion complex.

Biological tissue is expected to show similar mechanical properties as adherent cells because the mechanics of both are predominantly governed by prestressed fibrous actin networks. Therefore, the tissue interface is also assumed to minimize its area and take a shape of zero mean curvature. This allows us to apply our cellular model to the process of tissue growth an compare it to experimental observations [3].

[1] R. Bar-Ziv et al.: PNAS **961**, 10140 (1999), doi:10.1073/pnas.96.18.10140
[2] I.B. Bischofs et al.: Phys. Rev. Lett. **103**, 048101 (2009), doi:10.1103/PhysRevLett.103.048101
[3] C.M. Bidan et al.: PLoS ONE **7**, e36336 (20012), doi:10.1371/journal.pone.0036336

14.9 Self-propelled Swimmers

G. Falasco, K. Kroy, A. Würger*, G. Zecua

*Laboratoire Ondes et Matiere d'Aquitaine, Université de Bordeaux, France

We study the self-thermophoresis of artificial nano-swimmers, such as Janus particles. These are partly coated silica or polystyrene beads with a metal layer. They have an asymmetric temperature profile over their surface when heated through absorption of laser light.

Previous work has described the flow field around single spherical thermophoretic Janus particles [1]. However, there remain open questions concerning the motion of less symmetric swimmers, such as chiral dumbbells. A detailed study of the flow fields around asymmetric particles is the first step towards understanding collective motion and observed swarming behavior of an ensemble of swimmers.

We use the common approximation which reduces description of the interaction at the border between the particle and the solvent down to an effective slip velocity

around the swimmer. Then, we make a perturbative ansatz to obtain the solution of the Stokes equation for a two-component swimmer. More specifically, we study a Janus particle coupled by a rigid rod to an inactive cargo bead, see Fig. 14.6. Based on the reflection method, we further improve the superposition approximation for the bulk field around single Janus particles. From this point of view, it is possible to write down the hydrodynamic interaction between the swimmer's components as a contribution to the slip velocity of the whole vehicle.

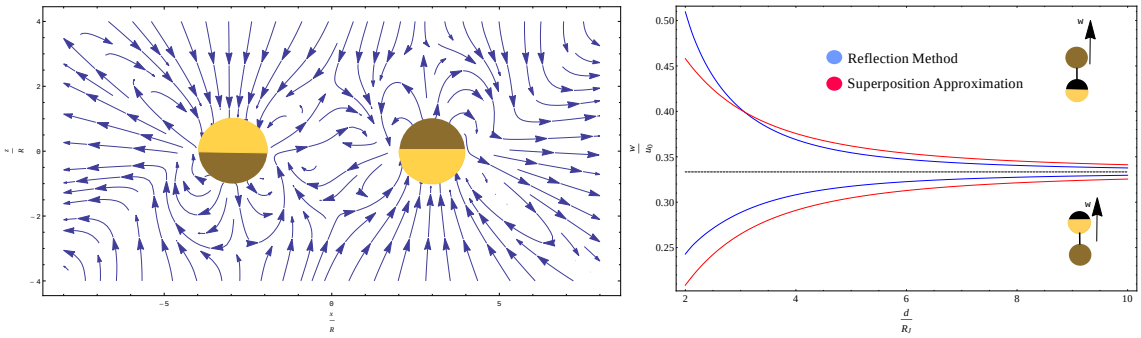

Figure 14.6: Left: Flow field around two active Janus particles, as a simple superposition. Right: For the case of a cargo particle coupled to a Janus swimmer, we compute the phoretic velocity. The picture shows the results obtained from the simple superposition and the from the reflection method.

On the side of the collective motion, we study the polarization of particles under external or self-generated temperature gradients. The non-uniform thermal field induces an asymmetric slip velocity, which in turn forces the Janus particle to align its symmetry axis along the thermal gradient. In the case of a large number of Janus particles, we can bring together the orienting viscous stress and rotational diffusion by means of the Smoluchowski equation for distribution function. This allows us to solve for an effective drift velocity and average orientation [2].

[1] T. Bickel et al.: Phys. Rev. E **88** 012301 (2013) doi:10.1103/PhysRevE.88.012301
[2] T.Bickel et al.: arXiv:1401.7833 [cond-mat.soft]

14.10 Nematic Microstructure in Biopolymer Solutions

M. Lämmel, K. Kroy, E. Jaschinski *, R. Merkel *

*Forschungszentrum Jülich, Germany

Domains of aligned filaments play an important role in solutions of semiflexible biopolymers. Such local order may, even in an intermediate density regime below the isotropic–nematic phase transition, appear as a precursor of bundle formation or as a consequence of shear induced ordering upon sample preparation and has therefore an important impact on the packing structure of a polymeric material. In the concentration range considered here, the physics of a meshwork of semiflexible or stiff polymers is dominated by its *tight entanglements* [1] and, since each filament in the meshwork

cannot cut though any other, it is effectively confined to a tube-like cage formed by surrounding filaments, within which it undergoes Brownian motion. This picture, as illustrated in Fig. 14.7, motivates for the following mean-field approach of the complicated many body problem. Starting from the worm-like chain model for a single filament one accounts for the network effects by introducing the tube that we represent in our model through a harmonic confinement potential. Its strength, which corresponds to the size of the tube, is self-consistently determined via a binary collision approximation (BCA) as proposed by Morse [2]. A local version [4] of this theory that predicts spatial tube radius fluctuations fared very well in comparison with extensive experiments on F-actin solutions [3].

In our present work we study the impact of (local) nematic order on the networks' microsructure, especially on the tube size. Therefore we extend our theoretical description and compare its predictions to extensive hybrid Monte Carlo/Brownian dynamics (MC/BD) simulations and new experiments with F-actin performed by our collaborators from the group of R. Merkel. Our general observation is in agreement with the expected relation that more ordered networks correspond to wider tubes, since each filament has more space to fluctuate. Within the above sketched BCA calculation we account for nematic order in a straight forward way by introducing a non-uniform distribution for the angle between two colliding filaments. Inserting, for example, Onsager's famous trail function [5] as orientational distribution, we calculate the mean tube size for any degree of nematic order, which results in the black curve shown in Fig. 14.7. The hybrid MC/BD simulations, kindly provided to us by D. Morse, are based on a Monte Carlo algorithm that samples the accessible phase space of the polymer solution by Brownian dynamics steps that account for the mutual impenetrability of colliding polymers. To impose order in these simulations, we aligned the filaments upon system initialization by a constant field (similar to a magnetic field for a ferromagnet), which is switched off before the MC run starts. In experiments it is much more subtle to control the degree of ordering. Here, our coworkers used two different setups: a relatively large micro-chamber, yielding more isotropic solutions, and a rather narrow micro-capillary, where shear alignment causes more pronounced nematic order. Since the ordering also depends on the actin concentration (whose direct influence on the tube size is scaled out in Fig. 14.7), these experiments allow for comparison between our theoretical prediction and the simulation results.

We also investigate the influence of the nematic order on the tube size distribution. Comparing its theoretical prediction with the experiments, we observe that accounting for polymer alignment results in better agreement. A systematic analysis will be part of the next steps of this project.

[1] D.C. Morse: Macromolecules **31**, 20 (1998)
[2] D.C. Morse: Phys. Rev. E **63**, 031502 (2001)
[3] J. Glaser et al.: Phys. Rev. Lett. **105**, 037801 (2010)
[4] J. Glaser and K. Kroy: Phys. Rev. E **84**, 051801 (2011)
[5] L. Onsager: Ann. N. Y. Acad. Sci. **51**, 627 (1949)

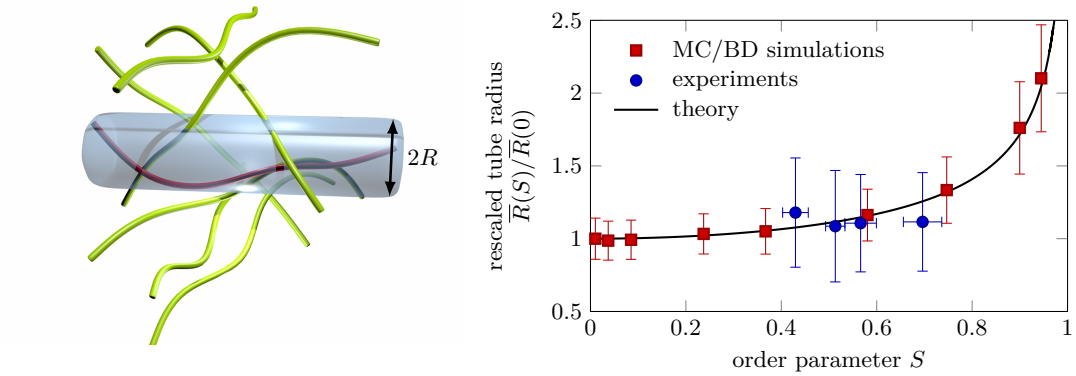

Figure 14.7: *Left:* Each polymer in the meshwork is effectively confined to a cage formed by its neighbor filaments. To first order, this cage can be represented as a homogeneous tube of size R. *Right:* The order dependence of the mean tube size $\overline{R}$ (rescaled by its isotropic value) as predicted by the self-consistently solved tube model compared to hybrid Monte Carlo/Brownian dynamics simulations (red squares) and experiments with F-actin solutions (blue dots). The order parameter $S = \frac{1}{2}\left\langle 3\cos^2(\theta) - 1\right\rangle$, where θ is the angle between two filaments (or filament segments), ranges from 0 for isotropic solutions to 1 for totally ordered systems.

14.11 Aeolian Sand Transport – Mesoscale Modeling

A. Meiwald, M. Lämmel, K. Kroy

Aeolian transport of sand is one of the most important geological processes on Earth and other rocky planets, creating a wide range of self-organized dynamic structures, like ripples or sand dunes. To understand the formation and evolution of those structures, it is thus necessary to investigate how granulates, like sand, are transported in turbulent flows. One knows, that the mass transport is most efficient, when the grains continuously jump downwind. The typical motion of those grains is called saltation. This highly erratic hopping process suggests a coarse-grained approach, where the (unknown) distribution of grain trajectories is represented by a single effective trajectory. This concept was successfully used in the past to explain the formation and dynamics of sand dunes [1]. However, such a drastic reduction lets slide all mesoscale properties of the transport mechanism, which are needed, for example, to describe sand ripples that have sizes comparable to the average hop length of the wind-blown grains. To improve the common picture in that sense, one can introduce a second transport mode, representing low-energetic reptating grains that are ejected by the saltating grains when impacting the sand bed [2]. As shown in our recent publication [3], an analytically treatable and numerically efficient description can be developed from this two-species approach, where the hopping grain population is represented by the given two types (e.g., see the video abstract accompanying our latest publication on http://youtu.beYFqmb_fSPYI).

In Ref. [3], we already showed that our two-species model reliably reproduces sand flux measurements from various wind tunnel experiments. Now, we investigate in detail how the mesoscale-structure of aeolian sand transport can be analyzed within our formalism and compare its predictions with the outcome of other models and various experimental data. In particular, we address the wind strength dependence

of the mean grain speed, the mean hop length, and the mean transport layer height. We also make contact to the transient regime of the sand transport by proposing a refined expression for the so-called saturation length, i.e. the length needed for the transport to reach its steady state. For all these mesoscale observables we find good agreement between the two-species predictions and a number of wind tunnel and field observations.

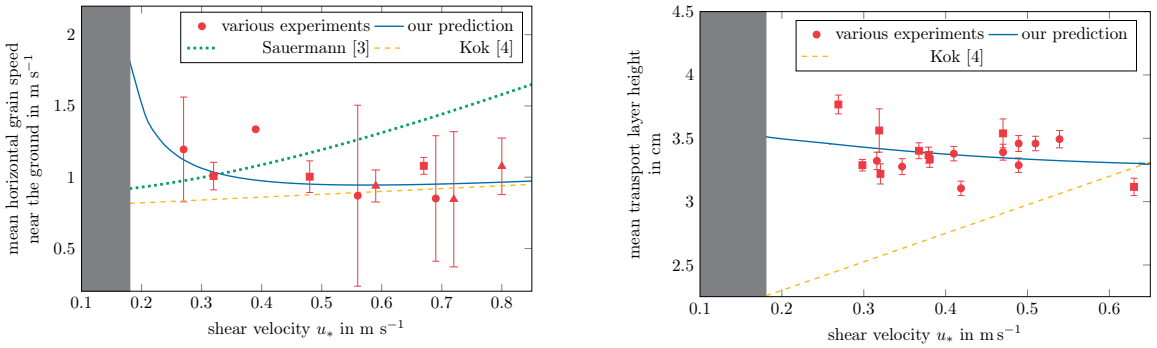

Figure 14.8: The mean grain speed (*left*) and transport layer height (*right*) as obtained from the two-species model compared to various wind tunnel experiments. We also show the prediction of the single trajectory approach [4] and the outcome of the numerical Comsalt model [5].

[1] K. Kroy et al.: Phys. Rev. Lett. **88**, 054301 (2002), doi:10.1103/PhysRevLett.88.054301
[2] B. Andreotti: J. Fluid Mech. **510**, 47 (2004), doi:10.1017/S0022112004009073
[3] M. Lämmel et al.: New J. Phys. **14**, 093037 (2012), doi:10.1088/1367-2630/14/9/093037
[4] G. Sauermann et al.: Phys. Rev. E. **64**, 031305 (2001), doi:10.1103/PhysRevE.64.031305
[5] J. Kok et al.: Rep. Prog. Phys. **75**, 106901 (2012), doi:10.1088/0034-4885/75/10/106901

14.12 Mutual Stabilization of Barchan Dunes

S. Auschra, M. Guthardt, M. Lämmel, K. Kroy

Crescent-shaped barchan dunes are among the most impressive structures observed in arid regions on Earth and Mars. Although they are isolated from nearby dunes by bedrock, models suggests that truly isolated barchans would be unstable with respect to their mass balance [1]. This indicates that some sort of interactions between the dunes in a dune field give rise to some size stabilization, resulting in the empirically observed uniform size distribution along the dune field [2, 3].

To uncover the underlying mechanism, we perform a mass stability analysis for a pair of consecutive dunes in a barchan field. Sand supplied from the horn of the windward dune to its downwind neighbor initiates a complex response of its shape and mass. Based on a dimensionally reduced description justified by a closeby shape attractor, a one-dimensional fixed-point equation for the mass balance of the downwind dune is derived and is going to be analyzed for stable solutions in the future.

[1] E. Fischer et al., Phys. Rev. E **77**, 031302 (2008)

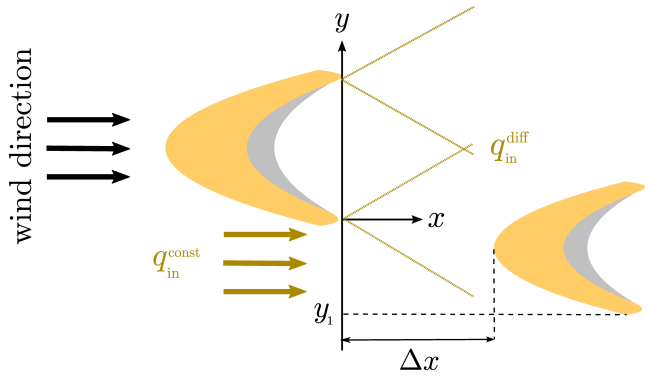

Figure 14.9: Sand exchange of two consecutive barchans. The downwind dune is fed by a homogeneous background sand flux $q_{\text{in}}^{\text{const}}$ and by sand escaping from the horns of its upwind neighbor $q_{\text{in}}^{\text{diff}}$.

[2] P. Hersen et al., Phys. Rev. E **69**, 011304 (2004)
[3] O. Duran et al., Nonlin. Processes Geophys. **69**, 455 (2011)

14.13 Inelastic Mechanics of Cells and Cell Aggregates

M. Gralka, K. Kroy

Semiflexible polymer networks, cells and tissues exist on vastly different length scales. Yet, they exhibit astonishing similarities in terms of their mechanics, prompting us to search for some underlying fundamental mechanical principles that can account for this remarkable unification. We apply the inelastic glassy wormlike chain model (iGWLC) for semiflexible polymer networks to cells and cell aggregates for the first time . The model can be understood as a combination of slow glassy viscoelastic dynamics (modeled on the basis of the standard model of the semiflexible polymers, the wormlike chain) with reversible crosslinker dynamics.

We show, analyzing the cell deformation response to strong force pulses, that the residual deformation persisting far beyond the pulse duration can be understood as a consequence of polymer slip in the cytoskeleton: while the viscoelastic deformation relaxes quickly, the inelastic part of the deformation decays very slowly such that the deformation may experimentally appear plastic, i.e. irreversible. Polymer slip is in the model associated with the breaking of transient crosslinks between polymers, described by a first-order rate equation with force-dependent rates.

This approach is validated by the realization that successive pulses are less and less effective at breaking bonds. Experiments on the time-dependence of the inelastic deformation unveiled quantitative limitations of this simplistic picture, which we could overcome by introducing a distribution of barrier heights in the bond description.

An important finding is that the Arrhenius parameters in the GWLC and in the description of the bonds should be treated as disparate quantities if the model is

applied to living cells at room temperature. Building on this insight, we were able to rationalize the power-law stress-relaxation in tissues as well as the stiffening of cells in response to an increasing oscillatory strain that was formerly believed to rely on active processes, entirely in terms of a passive inelastic mechanical model.

In summary, our findings demonstrate once more that the notion of semiflexible polymer networks, cells and tissues as viscoelastic materials is only valid under very special circumstances. For large deformations, the inelastic nature of biological materials becomes apparent. The iGWLC is well-equipped to describe a large body of experimental data, and, to our knowledge, is currently the only model that can account for power-law rheology, stiffening and softening in an semi-analytically tractable way[1] . Its generality makes the iGWLC a powerful tool to investigate and understand the unifying mechanical characteristics of biological matter.

[1] L. Wolff et al.: PLoS ONE **7(7)** e40063 (2012) doi:10.1371/journal.pone.0040063

14.14 Stochastic Dynamics of a Hot Brownian Particle

G. Falasco, M.V. Gnann, D. Rings *, K. Kroy

*Department of Physics and Astronomy, University of Leeds, Leeds, UK

Hot Brownian motion designates the diffusion of a colloidal particle kept at higher temperature than the solvent. Besides its relevance for applications involving laser heated nano-objects, such as photothermal spectroscopy and self-thermophoretic swimmers, it is also of significant theoretical interest. Indeed, since the solvent is characterized by an inhomogeneous temperature, the hot particle can be thought as a typical example of system in contact with a non-equilibrium bath.

Starting from the fluctuating hydrodynamic equations describing the coupled motion of solvent and particle, we derive generalized Langevin equations for the translation and rotation of the particle only [1]. Remarkably, a frequency dependent noise temperature which describes the energy spectrum of the thermal fluctuations replaces the constant temperature of an isothermal bath. Its appearance in the theory is due to the dynamical coupling between the temperature gradient in the fluid and the hydrodynamic modes exited by the particle itself.

From this central quantity all the statistical properties of the hot particle dynamics can be inferred. In particular, for the stationary state we retrieve the former results obtained by extensive molecular dynamics simulations [2, 3], consisting in Boltzmann distributions of the particle degrees of freedom, each of which appears to be thermalized at a different effective temperature [3]. Time dependent aspects, like the extension of linear response theory and fluctuation relations, are the subject of the ongoing research.

[1] G. Falasco et al., arXiv:1403.4040 [cond-mat.stat-mech]
[2] L. Joly et al., EPL **94(5)**, 50007 (2011)
[3] D. Chakraborty et al., EPL **96(6)**, 60009 (2011)

14.15 Funding

National Science Foundation, Kavli Institute of Theoretical Physics
M. Lämmel, S. Auschra, K. Kroy
NSF PHY11-25915

DAAD Scholarship for participation at "Fluid-Mediated Particle Transport in Geophysical Flows" at Kavli Institute of Theoretical Physics, Santa Barbara, USA
M. Lämmel

German-Israeli Foundation for Scientific Research and Development
K. Kroy (Principle Investigator), A. Meiwald
Grant No. 4411-1.02/8.44

Forschergruppe 877 From Local Constraints to Macroscopic Transport
K. Kroy (Principal Investigator), project P9 in collaboration with W. Janke
Deutsche Forschungsgemeinschaft (DFG), Grant No. KR 3381/3-1

Forschergruppe 877 From Local Constraints to Macroscopic Transport
K. Kroy (Principal Investigator), project P1 in collaboration with F. Cichos, M. Mertig
Deutsche Forschungsgemeinschaft (DFG), Grant No. KR 3381/2-2

Europäischen Sozialfonds (ESF) "How a polymer breaks a bond"
J.T. Bullerjahn

Europäischen Sozialfonds (ESF), Nachwuchsforschergruppe "Lösungen und Netzwerke steifer Polymere"
M. Lämmel

Europäischen Sozialfonds (ESF), Nachwuchsforschergruppe "Funktion durch Selbstorganisation: Emergente Eigenschaften von Atom- und Molekülaggregaten"
G. Falasco

Europäischen Sozialfonds (ESF), Nachwuchsforschergruppe "Werkzeuge und Technologien für die rationale Wirkstoffentwicklung"
G. Zecua

Nonlinear Stochastically Driven Systems with Many Degrees of Freedom
R. Kürsten, M.Sc.
IMPRS Fellowship

14.16 Organizational Duties

U. Behn

- Speaker of the Condensed Matter Theory Group
- Vertrauensdozent für die Nobelpreisträgertagungen in Lindau
- Bibliotheksbeauftragter of the Faculty
- Member of PbF2

- Scientific Member of the International Max Planck Research School "Mathematics in the Sciences"
- Referee: Bulletin of Mathematical Biology, Mathematical Biosciences and Engineering, Frontiers in Immunology
- Reviewer: Heinrich Böll Stiftung, Friedrich Ebert Stiftung

Klaus Kroy
- Member of the graduation committee
- Study counselor for physics
- Member of PbF1 and PbF2
- PI in DFG FOR 877 and Leipzig School of Natural Sciences Building with Molecules and Nano-objects (BuildMoNa)
- Scientific Member of the International Max Planck Research School Mathematics in the Sciences
- Nature Physics, Nature Nanotechnology, PNAS, PRL, JCP, Soft Matter, PRE, Physica A, EPJE, Aeolian Research, etc.
- Co-organizer of the Conference *Diffusion Fundamentals V*, 26–28 August 2013, Leipzig

Andrea Kramer
- Scientific Coordinator DFG Research Unit 877 *From Local Constraints to Macroscopic Transport*
- Scientific Manager Graduate School BuildMoNa
- Co-organizer of the Conference *Diffusion Fundamentals V*, 26–28 August 2013, Leipzig

14.17 External Cooperations

Academic

- Forschungszentrum Jülich GmbH, Germany
  Prof. Dr. R. Merkel, Dipl. E. Jaschinski
- University of Minnesota, USA
  Prof. Dr. David C. Morse
- Ben-Gurion University of the Negev, Israel
  Dr. H. Yizhaq, Dr. I. Katra, Prof. Dr. H. Tsoar
- Université de Rennes, France
  Dr. A. Valance
- Aarhus University, Denmark
  Prof. Dr. K.R. Rasmussen
- Cavendish Laboratory, University of Cambridge, UK
  Dr. U. Keyser, Dr. O. Otto, N. Laohakunakorn
- Max Planck Institute for Mathematics in the Sciences, Leipzig
  M. V. Gnann

- Department of Physics and Astronomy, University of Leeds, Leeds, UK
  D. Rings
- University of Barcelona, Spain
  Dr. R. Vincent
- Massey University, Palmerston North, New Zealand
  Prof. Dr. M. Williams, M. Sc. B. Minsel
- Université de Bordeaux, France
  Prof. Dr. A. Würger
- Joint Institute for Nuclear Research, Dubna, Russia
  Prof. Dr. N.M. Plakida
- Otto-von-Guericke-Universität Magdeburg
  Prof. Dr. J. Richter
- Institut für Klinische Immunologie
  Prof. Dr. G. Metzner
- Max Planck Institute for Evolutionary Biology, Plön
  Dr. B. Werner
- Technische Universität Dresden
  Prof. Dr. M. Mertig

14.18 Publications

Journals

M. Härtel, J. Richter, O. Götze, D. Ihle, S.-L. Drechsler: *Thermodynamics of the two-dimensional frustrated J_1 - J_2 Heisenberg ferromagnet in the collinear stripe regime: Susceptibility and correlation length*, Phys. Rev. B **87**, 054412 (2013)

R. Kürsten, S. Gütter, U. Behn: *Critical manifold of globally coupled overdamped anharmonic oscillators driven by additive Gaussian white noise*, Phys. Rev. E **88**, 022114 (2013), 10 pp.

N. Laohakunakorn, O. Otto, S. Sturm, K. Kroy, U.F. Keyser: *Dynamic single-molecule force spectroscopy using optical tweezers and nanopores*, Proc. SPIE **8810**, 88101F (2013), doi:10.1117/12.2027106

O. Otto, S. Sturm, N. Laohakunakorn, U.F. Keyser, K. Kroy: *Rapid internal contraction boosts DNA friction*. Nature communications **4**, 1780 (2013), doi:10.1038/ncomms2790

R.R.R. Vincent, B.W. Mansel, A. Kramer, K. Kroy, M.A.K. Williams: *Micro-rheological behaviour and nonlinear rheology of networks assembled from polysaccharides from the plant cell wall* New J. Phys. **15**, 1035002 (2013), doi:10.1088/1367-2630/15/3/035002

A.A. Vladimirov, D. Ihle, N.M. Plakida: *Spin excitations in an anisotropic J_1 - J_2 Heisenberg model*, Theor. Math. Phys. **177** (2), 1540 (2013)

In press

R. Schulz, B. Werner, U. Behn: *Self tolerance in a minimal model of the idiotypic network*, Frontiers in Immunology **5**, 00086 (2014), 12 pp.

Preprints

T.Bickel, G. Zecua, A. Würger: arXiv:1401.7833 [cond-mat.soft]

G. Falasco, M. V. Gnann, D. Rings, K.Kroy: arXiv:1403.4040 [cond-mat.stat-mech].

Under review

J. T. Bullerjahn, S. Sturm and K. Kroy: *Theory of rapid force spectroscopy*

Talks

U. Behn, F. Gross, D. Kröber, G. Metzner: *T-cell Regulation, Allergy, and Specific Immunotherapy: Mathematical Modeling*, 5th Annual World Congress of Vaccine 2013, Hangzhou, China, March 18-20, 2013, invited

U. Behn: *Evolution towards a complex architecture and self-tolerance in a minimal model of the idiotypic network*, European Conference on Complex Systems 2013, Barcelona, Spain, Satellite Meeting on Theoretical Immunology, September 19, 2013

M. Höll, U. Behn: *Globally Coupled Stratonovich Models: Self-consistent Theory of a Non-equilibrium Continuous Phase Transition*, DPG-Frühjahrstagung Regensburg, March 13, 2013

K. Kroy: *Hot Brownian motion*, International Summer School Fundamental Problems in Statistical Physics XIII, Leuven, Belgium, June 16-29, 2013

K. Kroy: *Interactions and Autonomous Transport of Hot Brownian Particles*, SPP 1726 Microswimmers - from single particle motion to collective behavior, Bonn, June 27, 2013

K. Kroy: *Theory of rapid single-molecule force spectroscopy*, Partnership: Vanderbilt-Leipzig - 4th Scientific Symposium, Leipzig, July 6-12, 2013

K. Kroy: *Where is the interesting physics in wind-blown sand?*, Fluid-Mediated Transport in Geophysical Flows, Santa Barbara, September 23 - December 20, 2013

K. Kroy: *Hot Brownian motion*, Workshop "Hot Nanostructures", Lorentz Center Leiden, October 21-25, 2013

K. Kroy: *How a polymer breaks a bond*, SFB TRR102, Schkeuditz, Nov 8, 2013

K. Kroy: *Science Cafe*, (public round table discussion), Leipzig, July 15, 2013

R. Kürsten, S. Gütter, U. Behn: *Globally Coupled Nonlinear Systems with Additive Noise*, DPG-Frühjahrstagung Regensburg, March 13, 2013

R. Kürsten: *Critical Manifold of Globally Coupled Overdamped Anharmonic Oscillators Driven by Additive Gaussian White Noise*, Workshop of the International Max Planck Reseach School Mathematics in the Sciences, Leipzig, July 5-6, 2013

Posters

A. Kramer, R.R.R. Vincent, B.W. Mansel, K. Kroy, M.A.K. Williams, *Melting of pectin gels*, Annual BuildMoNa Conference, Leipzig, March 4–5, 2013

A. Kramer, R.R.R. Vincent, B.W. Mansel, K. Kroy, M.A.K. Williams, *Melting of pectin gels*, DPG-Frühjahrstagung, Regensburg, March 10–15, 2013

J. T. Bullerjahn, S. Sturm, K. Kroy: *Improved modelling of forced Kramers rate*, DPG-Frühjahrstagung, Regensburg, March 10–15, 2013

J. T. Bullerjahn, S. Sturm, K. Kroy: *Improved modelling of forced Kramers rate*, International Summer School Fundamental Problems in Statistical Physics XIII, Leuven, Belgium, June 16-29, 2013

O. Otto, S. Sturm, N. Laohakunakorn, U. Keyser, K. Kroy: *Internal tension diffusion boosts DNA friction*, Diffusion Fundamentals, Leipzig, August 26-28th, 2013

M. Lämmel, A. Meiwald, K. Kroy: *Mesoscale modeling of aeolian sand transport*, Particle-Laden Flows in Nature, UC Santa Barbara, Kavli Institute for Theoretical Physics, December 16-19th, 2013

G. Falasco, M.V. Gnann, D. Rings, K. Kroy: *Frequency-dependent temperature of hot Brownian motion*, International Summer School Fundamental Problems in Statistical Physics XIII, Leuven, Belgium, June 16-29, 2013

G. Falasco, M.V. Gnann, D. Rings, D. Chakraborty, K. Kroy: *Frequency-dependent temperature of hot Brownian motion* Diffusion Fundamentals, Leipzig, August 26-28th, 2013

K. Kroy, F. Cichos *Propulsion and Interaction of Hot Brownian Swimmers*, SPP 1726 Microswimmers - from single particle motion to collective behavior, Bonn, December 2-3, 2013

14.19 Graduations

Diploma

- Robert Schulz
  Patterns for Large Idiotypic Networks and Self Tolerance: Extensions of the Mean Field Theory
  30 July 2013

Master

- Matti Gralka
  Inelastic mechanics of cells and cell aggregates
  March 2013
- Anne Meiwald
  Äolischer Sandtransport - Anwendbarkeit der Kontinuumsbeschreibung
  September 2013

Bachelor

- Mona Guthardt
  Coarse-grain Modelling of Barchan Dune Fields
  September 2013

14.20 Guests

- Dr. Gerhard Schmid
  Universität Augsburg
  January 22 - 23
- Prof. Lene Oddershede
  University of Copenhagen
  March 17-18
- Dr. Eric Bertin
  Laboratoire Interdisciplinaire de Physique (LIPhy), Grenoble, France
  March 28-30th
- Dr. Kirsten Martens
  Laboratoire Interdisciplinaire de Physique (LIPhy), Grenoble, France
  March 28-30th
- Dr. Samuel Sanchez Ordoñez
  Leibniz Institute for Solid State and Materials Research Dresden
  March 28-30th
- Prof. Dr. Giovanni Volpe
  Bilkent University, Ankara, Turkey
  March 28-30th
- Prof. Dr. A. Würger
  Université de Bordeaux
  Summer term appointed as Leibniz-Professor
- Prof. Dr. Thomas Voigtmann
  Univesität Konstanz
- Dr. Jaime Santos
  Centro de Fisica da Universidade do Minho, Braga, Portugal
  October 30

- M.Sc. Dmitrii Mishagli
  Odessa I.I. Mechnicov National University
  Since October 2013

15

Theory of Elementary Particles

15.1 Introduction

Our group is interested in the properties of matter at very high energies (small scales) or under other extreme conditions, covering a broad variety of research topics ranging from the study of elementary particles and their properties to the study of quantized matter fields in the presence of strong gravitational fields. The underlying theme of our research and teaching activity is the theory of such quantized fields in its various manifestiations, and applications, including:

1. Quantum fields on discrete spacetimes (lattices) and their numerical and theoretical study
2. Quantum fields on curved spacetimes
3. Applications of ideas from integrable systems to the study of quantum gauge theories

Quantum field theories on lattices are natural discretized counterparts of continuum models that describe elementary particles in quantum field theoretic models such as the standard model of particle physics. They were introduced in order to investigate certain non-perturbative features of these models in a controlled approximation that are inaccessible by other means, such as perturbation theory. A substantial fraction of the current work being done in this area are numerical simulations and the development of new theoretical methods leading to improved numerical schemes. Quantum gauge theories such as the standard model can also be treated as continuum field theories, and can thereby be studied using perturbative methods. The task of finding improved ways of handling perturbative calculations is an important aspect of quantum field theory and is actively pursued in our group. Quantum field theory in curved spacetime (QFTCS) is the theory of quantum fields propagating in a background, classical, curved spacetime. On account of its classical treatment of the metric, QFTCS cannot be a fundamental theory of nature. However, QFTCS is expected to provide an accurate description of quantum phenomena in a regime where the effects of curved spacetime may be significant, but effects of quantum gravity itself may be neglected. In particular, it is expected that QFTCS should be applicable to the description of quantum phenomena occurring in the early universe and near (and inside of) black holes, provided

that one does not attempt to describe phenomena occurring so near to singularities that curvatures reach Planckian scales and the quantum nature of the spacetime metric would have to be taken into account. Quantum field theory in curved spacetimes has provided important physical insights into the quantum nature of black holes, indicating that they should, if left alone, gradually evaporate due to the emission of quanta whose energies are distributed thermally at the famous Hawking temperature. More information may be found on the group's webpages, www.uni-leipzig.de/ tet

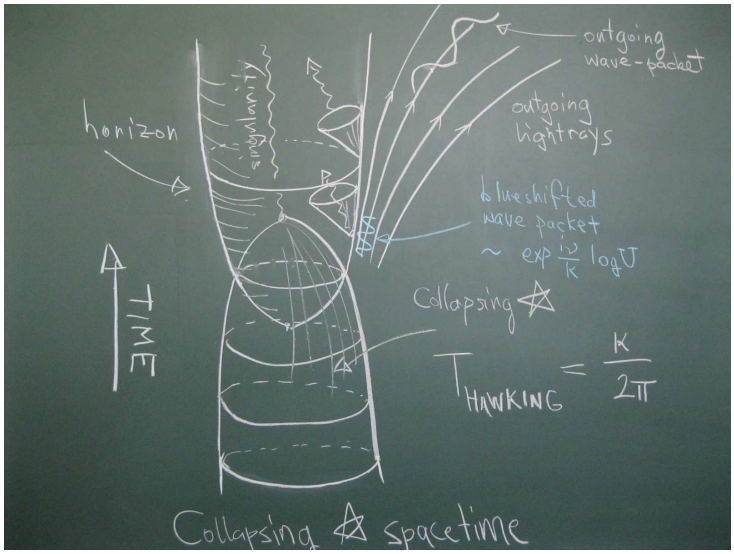

Figure 15.1: The Hawking Effect

Stefan Hollands

15.2 Computation of the invariants of the Gell-Mann–Low cocycle

M. Dütsch, S. Hollands

Under a simultaneous scaling of the coordinates $x \to \rho x$ ($\rho > 0$ arbitrary) and the masses $m \to m/\rho$ a *classical* field theory is invariant. But the corresponding *quantum* field theory (QFT) is changed. This change can equivalently be expressed by a finite renormalization Z_ρ of the interaction L: $L \to Z_\rho(L)$. In the framework of *causal perturbation theory* [3] (which we will use), this statement is due to the 'Main Theorem' of Stora and Popineau, which was refined in [1, 2, 4]. The map Z_ρ is the natural way to introduce the Gell-Mann–Low renormalization group and the concepts of running masses and running coupling constants in the mentioned framework. Actually the 1-parameter family $\{Z_\rho \,|\, \rho > 0\}$ is in general a cocycle, only for massless fields it is a group [1].

Using structural results, the computation of Z_ρ amounts to computing certain coefficients. Some of these numbers depend on the renormalization prescription used to construct the considered QFT-model. In most (possibly in all?) cases the conventions can be chosen such that these coefficients vanish. But there remain some coefficients

which are independent of any convention – we call them "invariants". In [5] it was observed that some of these invariants can be computed by a surface integral of the *unrenormalized* distributions, which are known by the Feynman rules. We want to generalize this result to all invariants. For this purpose, a main first step is to find a clear and simple identification of all invariants. To do this it seems to be helpful to take the renormalization group equation into account.

[1] R. Brunetti, M. Dütsch and K. Fredenhagen, *Perturbative algebraic quantum field theory and the renormalization groups* Adv. Theor. Math. Phys. **13** (2009), 1541–1599.
[2] M. Dütsch and K. Fredenhagen, *Causal perturbation theory in terms of retarded products, and a proof of the Action Ward Identity* Rev. Math. Phys. **16** (2004), 1291–1348.
[3] H. Epstein and V. Glaser, *The role of locality in perturbation theory* Ann. Inst. Henri Poincaré **19A** (1973), 211–295.
[4] S. Hollands and R. M. Wald, *On the renormalization group in curved spacetime* Commun. Math. Phys. **237** (2003), 123–160.
[5] S. Hollands, *Renormalized Quantum Yang-Mills Fields in Curved Spacetime* Rev. Math. Phys. **20** (2008), 1033–1172.

15.3 Operator product expansions in quantum field theory

S. Hollands, J. Holland

All quantum field theories with well-behaved ultra violet behavior are believed to have an operator product expansion (OPE). This means that the product of any two local fields located at nearby points x and y in spacetime can be expanded in the form $O_A(x)O_B(y) \sim \sum_C C^C_{AB}(x-y)\, O_C(y)$, where A, B, C are labels for the various local fields in the given theory (incorporating also their tensor character/spin), and where C^C_{AB} are certain numerical coefficient functions – or rather distributions – that depend on the theory under consideration, the coupling constants, etc. The sign "$\sim$" indicates that this can be understood as an asymptotic expansion: If the sum on the right side is carried out to a sufficiently large but finite order, then the remainder goes to zero fast as $x \to y$ in the sense of operator insertions into a quantum state, or into a correlation function. The operator product expansion is on the one hand an important tool for calculations in asymptotically free quatum field theories (such as Quantum Chromo Dynamics, QCD). However, it is also a very important theoretical structure. One would like to understand better the following questions:

1. In what precise sense, if any, is the expansion actually convergent (rather than only asymptotic)?

2. If one considers products of three or more operators, one can perform the expansion in different orders. Is there some sort of "associativity law," and if so, what is its precise nature?

3. The coefficients, C_{AB}^{C} are normally calculated by perturbative techniques relying on other auxiliary objects. Is there a *direct* way to calculate these recursively order-by-order in a small coupling expansion around those for a conformal fixed point (e.g. free field theory), and if so, what are the recursion formulas?

4. Does an expansion of this sort hold on curved spacetimes? Might the OPE be an appropropriate replacement for concepts such as S-matrices or path integrals in order to actually *define* quantum field theories in curved spacetime?

This is a longer term research project. The following papers report on progress concerning some of these important questions:

[1] S. Hollands and R. M. Wald, arXiv:1401.2026 [gr-qc].
[2] S. Hollands and C. Kopper, "The operator product expansion converges in perturbative field theory," Commun. Math. Phys. **313** (2012) 257 [arXiv:1105.3375 [hep-th]].
[3] J. Holland and S. Hollands, "Recursive construction of operator product expansion coefficients," arXiv:1401.3144 [math-ph].
[4] J. Holland and S. Hollands, "A small cosmological constant due to non-perturbative quantum effects," Class. Quant. Grav. **31** (2014) 125006 [arXiv:1305.5191 [gr-qc]].
[5] J. Holland and S. Hollands, "Operator product expansion algebra," J. Math. Phys. **54** (2013) 072302 [arXiv:1205.4904 [math-ph]].

15.4 Yangian Symmetry and scattering in gauge field theories

R. Kirschner, D. Chicherin, S. Derkachov

Integrable quantum systems are applied successfully to the study of the high-energy asymptotics and of the renormalization of composite operators in gauge theories.

These applications stimulated the development of the methods of integrable quantum systems. In the calculation of scattering amplitudes in maximally extended supersymmetric Yang Mills theory two superconformal symmetries have been discovered [1] which fit into the framework of Yangian symmetry [2].

We have proposed a convenient formulatation of this symmetry relying on the Quantum Inverse Scattering Method. The symmetry condition on the functions expressing the scattering amplitudes is formulated as an eigenvalue relation with the monodromy operator of a generalised Heisenberg spin chain.

A number of relations previously observed in the calculation of amplitudes can be derived directly from this symmetry condition. We have developed efficient methods for solving of the symmetry condition [3, 4].

[1] J. M. Drummond, J. Henn, G. P. Korchemsky and E. Sokatchev,
Dual superconformal symmetry of scattering amplitudes in N=4 super-Yang-Mills theory,
Nucl. Phys. B **828** (2010) 317, [arXiv:0807.1095 [hep-th]].
[2] J. M. Drummond, J. M. Henn and J. Plefka,
Yangian symmetry of scattering amplitudes in N=4 super Yang-Mills theory,
JHEP **0905** (2009) 046, [arXiv:0902.2987 [hep-th]].

[3] D. Chicherin and R. Kirschner, *Yangian symmetric correlators*, Nucl. Phys. B **877** (2013) 484 [arXiv:1306.0711 [math-ph]].
[4] D. Chicherin, S. Derkachov and R. Kirschner, *Yang-Baxter operators and scattering amplitudes in N=4 super-Yang-Mills theory*, Nucl. Phys. B **881** (2014) 467, [arXiv:1309.5748 [hep-th]].

15.5 Applications of numerical stochastic perturbation theory to lattice QCD

H. Perlt, A. Schiller

In collaboration with authors from different locations we have continued our research program using numerical stochastic perturbation theory (NSPT).

It is well known that lattice perturbation theory (LPT) is much more involved compared to its continuum QCD counterpart. The complexity of diagrammatic approaches increases rapidly beyond the one-loop approximation. By now only a limited number of results up to two-loop accuracy have been obtained.

Applying the standard Langevin dynamics [1, 2] to the problem of weak coupling expansions for lattice QCD, a powerful numerical approach for higher loop calculations – called numerical stochastic perturbation theory (NSPT) – has been proposed in [3].

With colleagues from the QCDSF collaboration we have calculated Wilson loops of various sizes up to 20 loops in SU(3) pure lattice gauge theory at different lattice sizes for Wilson gauge action using the technique of numerical stochastic perturbation theory [4]. This allowed us to investigate the perturbative series for various Wilson loops at high loop orders.

As a new application we have calculated [5] the SU(3) beta function from Wilson loops to 20th order numerical stochastic perturbation theory. An attempt has been made to include massless fermions, whose contribution is known analytically to 4th order. The question whether the theory admits an infrared stable fixed point is addressed.

The subtraction of hypercubic lattice corrections, calculated at one-loop order in LPT, is common practice, e.g., for determinations of renormalization constants in lattice hadron physics (see the next project). Together with colleagues from Regensburg and Dubna we started [6] a first check whether NSPT can by used to subtract hypercubic lattice corrections and provide (in a parametrization valid for arbitrary lattice couplings) the lattice corrections up to three-loop order for the SU(3) gluon and ghost propagators in Landau gauge. These propagators are ideal candidates for such a check, as they are available from lattice simulations to high precision and can be combined to a renormalization group invariant product (Minimal MOM coupling) for which a one-loop LPT correction was found to be insufficient to remove the bulk of the hypercubic lattice artifacts from the data.

[1] G. Parisi and Y. s. Wu, Sci. Sin. **24** (1981) 483.
[2] G. G. Batrouni, G. R. Katz, A. S. Kronfeld, G. P. Lepage, B. Svetitsky and K. G. Wilson, Phys. Rev. D **32** (1985) 2736.
[3] F. Di Renzo, E. Onofri, G. Marchesini and P. Marenzoni, Nucl. Phys. B **426** (1994) 675 [arXiv:hep-lat/9405019].

[4] R. Horsley, G. Hotzel, E.-M. Ilgenfritz, R. Millo, Y. Nakamura, H. Perlt, P. E. L. Rakow, G. Schierholz and A. Schiller, Phys. Rev. D **86** (2012) 054502 [arXiv:1205.1659 [hep-lat]].
[5] R. Horsley, H. Perlt, P. E. L. Rakow, G. Schierholz and A. Schiller, Phys. Lett. B **728** (2014) 1 [arXiv:1309.4311 [hep-lat]].
[6] J. Simeth, A. Sternbeck, E. -M. Ilgenfritz, H. Perlt and A. Schiller, PoS LATTICE **2013** (2013) 459 [arXiv:1311.1934 [hep-lat]].

15.6 Perturbatively improving regularization-invariant momentum scheme renormalization constants

H. Perlt, A. Schiller

Renormalization factors in lattice Quantum Chromodynamics (QCD) relate observables computed on finite lattices to their continuum counterparts in specific renormalization schemes. Therefore, their determination should be as precise as possible in order to allow for a reliable comparison with experimental results. One approach is based on lattice perturbation theory [1]. However, it suffers from its intrinsic complexity, slow convergence and the impossibility to handle mixing with lower-dimensional operators. Therefore, nonperturbative methods have been developed and applied. Among them the so-called regularization-invariant momentum (RI-MOM) scheme [2] is widely used because of its simple implementation.

Like (almost) all quantities evaluated in lattice QCD also renormalization factors suffer from discretization effects. One can attempt to cope with these lattice artifacts by extrapolating the nonperturbative scale dependence to the continuum (see Ref. [3]) or one can try to suppress them by a subtraction procedure based on perturbation theory. Here we were dealing with the latter approach.

In a recent paper of the QCDSF/UKQCD collaboration [4] a comprehensive discussion and comparison of perturbative and nonperturbative renormalization have been given. Particular emphasis was placed on the perturbative subtraction of the unavoidable lattice artifacts. For the simplest operators and lattice actions this can be done with reasonable effort in one-loop order completely by computing the corresponding diagrams for finite lattice spacing numerically. An alternative approach can be based on the subtraction of one-loop terms of order a^2 with a being the lattice spacing. The computation of those terms has been developed by the Cyprus group [6] and applied to various operators for different actions.

In collaboration with colleagues from QCDSF and Cyprus university we have used in this work [7] some of those results for the analysis of lattice Monte Carlo data of the QCDSF collaboration to determine as precisely as possible the renormalization constants in the so-called renormalization group invariant (RGI) scheme Z^{RGI}.

Ideally, Z^{RGI} depends only on the bare lattice coupling, but not on the momentum p. Computed on a lattice, however, it suffers from lattice artifacts, e.g., it contains contributions proportional to a^2p^2, $(a^2p^2)^2$ etc. For a precise determination it is essential to have these discretization errors under control.

Operator (multiplet)	Notation	Repre-sentation	Operator basis
$\bar{u}\,d$	O^S	$\tau_1^{(1)}$	O^S
$\bar{u}\,\gamma_\mu\,d$	O^V_μ	$\tau_1^{(4)}$	$O^V_1, O^V_2, O^V_3, O^V_4$
$\bar{u}\,\gamma_\mu\gamma_5\,d$	O^A_μ	$\tau_4^{(4)}$	$O^A_1, O^A_2, O^A_3, O^A_4$
$\bar{u}\,\sigma_{\mu\nu}\,d$	$O^T_{\mu\nu}$	$\tau_1^{(6)}$	$O^T_{12}, O^T_{13}, O^T_{14}, O^T_{23}, O^T_{24}, O^T_{34}$
$\bar{u}\,\gamma_\mu\overleftrightarrow{D}_\nu\,d$	$O_{\mu\nu} \to O^{v_{2,a}}$	$\tau_3^{(6)}$	$O_{\{12\}}, O_{\{13\}}, O_{\{14\}}, O_{\{23\}}, O_{\{24\}}, O_{\{34\}}$
$\bar{u}\,\gamma_\mu\overleftrightarrow{D}_\nu\,d$	$O_{\mu\nu} \to O^{v_{2,b}}$	$\tau_1^{(3)}$	$1/2(O_{11}+O_{22}-O_{33}-O_{44})$, $1/\sqrt{2}(O_{33}-O_{44}), 1/\sqrt{2}(O_{11}-O_{22})$

Table 15.1: Operators and their representations. The symbol {...} means total symmetrization. A detailed group theoretical discussion is given in [5].

We have studied the flavor-nonsinglet quark-antiquark operators given in Table 15.1. The corresponding renormalization factors $Z^{\text{RI-MOM}}$ have been measured (and chirally extrapolated) at $\beta = 5.20, 5.25, 5.29$ and 5.40 using $N_f = 2$ clover improved Wilson fermions with plaquette gauge action by the QCDSF/UKQCD collaboration [4].

The found final renormalization factors in the RGI scheme for the newly proposed subtraction technique of lattice artifacts are collected in Table 15.2 using the preferred

Op.	$Z^{\text{RGI}}\vert_{\beta=5.20}$	$Z^{\text{RGI}}\vert_{\beta=5.25}$	$Z^{\text{RGI}}\vert_{\beta=5.29}$	$Z^{\text{RGI}}\vert_{\beta=5.40}$
O^S	0.4530(34)	0.4475(33)	0.4451(32)	0.4414(30)
O^V	0.7163(26)	0.7253(26)	0.7308(25)	0.7451(24)
O^A	0.7460(41)	0.7543(40)	0.7590(39)	0.7731(37)
O^T	0.8906(43)	0.9036(42)	0.9108(41)	0.9319(39)
$O^{v_{2,a}}$	1.4914(55)	1.5131(55)	1.5266(54)	1.5660(53)
$O^{v_{2,b}}$	1.5061(37)	1.5218(37)	1.5329(36)	1.5534(35)

Table 15.2: Final Z^{RGI} values for $N_f = 2$ clover improved Wilson fermions at different lattice gauge couplings β.

QCDSF collaboration value $r_0\,\Lambda_{\overline{\text{MS}}} = 0.700$ on which the transformation from the measured $Z^{\text{RI-MOM}}$ to Z^{RGI} depends (with Sommer scale r_0), for details see the paper [7].

[1] S. Capitani, Phys. Rept. **382** (2003) 113 [arXiv:hep-lat/0211036]
[2] G. Martinelli, C. Pittori, C. T. Sachrajda, M. Testa and A. Vladikas, Nucl. Phys. B **445** (1995) 81 [arXiv:hep-lat/9411010]
[3] R. Arthur and P. A. Boyle (RBC and UKQCD Collaborations), Phys. Rev. D **83** (2011) 114511 [arXiv:1006.0422 [hep-lat]].
[4] M. Göckeler, R. Horsley, Y. Nakamura, H. Perlt, D. Pleiter, P. E. L. Rakow, A. Schäfer, G. Schierholz, A. Schiller, H. Stüben and J. M. Zanotti, (QCDSF/UKQCD Col-

laboration) Phys. Rev. D **82** (2010) 114511 [Erratum-ibid. D **86** (2012) 099903] [arXiv:1003.5756 [hep-lat]].
[5] M. Göckeler, R. Horsley, E.-M. Ilgenfritz, H. Perlt, P. E. L. Rakow, G. Schierholz and A. Schiller, Phys. Rev. D **54** (1996) 5705 [arXiv:hep-lat/9602029].
[6] M. Constantinou, V. Lubicz, H. Panagopoulos and F. Stylianou, JHEP **0910** (2009) 064 [arXiv:0907.0381 [hep-lat]].
[7] M. Constantinou, M. Costa, M. Göckeler, R. Horsley, H. Panagopoulos, H. Perlt, P. E. L. Rakow, G. Schierholz and A. Schiller, Phys. Rev. D **87** (2013) 9, 096019 [arXiv:1303.6776 [hep-lat]].

15.7 Funding

ERC Starting Grant
Prof. S. Hollands
QC & C 259562

DFG Grant
Dr. A Schiller
SCHI 422/9-1

15.8 Organizational Duties

Prof. S. Hollands
- Group leader
- Group speaker
- Erasmus coordinator
- Associate editor: General Relativity and Gravitation

Dr. A. Schiller
- Referee Phys. Rev. D
- Referee Europhysics Journal C

15.9 External Cooperations

Academic

- DESY Hamburg
  Prof. G. Schierholz (QCDSF collaboration)
- Edinburgh U.
  Dr. R. Horsley (QCDSF collaboration)
- Liverpool U.
  Dr. P.E.L. Rakow (QCDSF collaboration)
- Adalaide U.
  Dr. J. Zanotti (QCDSF collaboration)

- Cyprus U. Nikosia
  Prof. H. Panagopoulos and collaborators
- Regensburg U.
  Dr. A. Sternbeck
- Dubna, Russia
  Dr. E.-M. Ilgenfritz
- U. Chicago
  Prof. R. M. Wald

15.10 Publications

Journals

P. de Medeiros, S. Hollands: *Superconformal quantum field theory in curved spacetime*, Class. Quant. Grav. **30** (2013) 175015 [arXiv:1305.0499 [hep-th]]

P. de Medeiros, S. Hollands: *Conformal symmetry superalgebras*, Class. Quant. Grav. **30** (2013) 175016 [arXiv:1302.7269 [hep-th]]

K. Sanders, C. Dappiaggi, T.-P. Hack: *Electromagnetism, Local Covariance, the Aharonov-Bohm Effect and Gauss' Law*, doi:10.1007/s00220-014-1989-x, Commun. Math. Phys. **328** (2014) 625–667 [arXiv:1211.6420v2 [math-ph]]

M. Constantinou, M. Costa, M. Göckeler, R. Horsley, H. Panagopoulos, H. Perlt, P. E. L. Rakow, G. Schierholz, A. Schiller: *Perturbatively improving regularization-invariant momentum scheme renormalization constants*, Phys. Rev. D **87** (2013) 9, 096019 [arXiv:1303.6776 [hep-lat]]

R. Horsley, H. Perlt, P. E. L. Rakow, G. Schierholz, A. Schiller: *The SU(3) Beta Function from Numerical Stochastic Perturbation Theory*, Phys. Lett. B **728** (2014) 1 [arXiv:1309.4311 [hep-lat]]

M. Constantinou, M. Costa, M. Göckeler, R. Horsley, H. Panagopoulos, H. Perlt, P. E. L. Rakow, G. Schierholz, A. Schiller: *Perturbatively improving renormalization constants*, PoS LATTICE2013 (2013) 310 [arXiv:1310.6504 [hep-lat]]

R. Horsley, J. Najjar, Y. Nakamura, H. Perlt, D. Pleiter, P. E. L. Rakow, G. Schierholz, A. Schiller: *SU(3) flavour symmetry breaking and charmed states*, PoS LATTICE **2013** (2013) 249 [arXiv:1311.5010 [hep-lat]]

J. Simeth, A. Sternbeck, E.-M. Ilgenfritz, H. Perlt, A. Schiller: *Discretization Errors for the Gluon and Ghost Propagators in Landau Gauge using NSPT*, PoS LATTICE **2013** (2013) 459 [arXiv:1311.1934 [hep-lat]]

D. Chicherin, R. Kirschner: *Monodromy operators and symmetric correlators*, J. Phys. Conf. Ser. **474** (2013) 012014

D. Chicherin, S. Derkachov, R. Kirschner: *Yang-Baxter operators and scattering amplitudes in N=4 super-Yang-Mills theory*, Nucl. Phys. B **881** (2014) 467 [arXiv:1309.5748 [hep-th]]

D. Chicherin, R. Kirschner: *Yangian symmetric correlators*, Nucl. Phys. B **877** (2013) 484 [arXiv:1306.0711 [math-ph]]

R. Kirschner: *Integrable chains with Jordan-Schwinger representations*, J. Phys. Conf. Ser. **411** (2013) 012018

D. Chicherin, S. Derkachov, D. Karakhanyan, R. Kirschner: *Baxter operators with deformed symmetry*, Nucl. Phys. B **868** (2013) 652 [arXiv:1211.2965 [math-ph]]

Books

S. Hollands, R. M. Wald: *Quantum fields in curved spacetime*, arXiv:1401.2026 [gr-qc], invited contribution to "100 Years of General Relativity" monograph series.

in press

J. Holland, S. Hollands: *Recursive construction of operator product expansion coefficients*, arXiv:1401.3144 [math-ph] (preprint)

S. Hollands, A. Thorne: *Bondi mass cannot become negative in higher dimensions*, arXiv:1307.1603 [gr-qc], accepted for publication in Commun. Math. Phys.

J. Holland, S. Hollands: *A small cosmological constant due to non-perturbative quantum effects*, arXiv:1305.5191 [gr-qc], accepted for publication in Class. Quant. Grav.

K. Sanders: *On the construction of Hartle-Hawking-Israel states across a static bifurcate Killing horizon*, arXiv:1310.5537v1 [gr-qc] (preprint)

Talks

For the talks of Prof. S. Hollands, see http://www.uni-leipzig.de/~tet/?page_id=551

K. Sanders: *The construction of Hartle-Hawking-Israel states in static black holes spacetimes*, theoretical physics seminar, University of Leipzig, Germany, November 2013

15.11 Graduations

Master

- Bodnariuc, Ecaterina
  Numerical stochastic perturbation theory for SU(3) lattice gauge theory with twisted boundary conditions: application to Wilson loops
  August 2013

Bachelor

- Meischner, Jan
  Der Bethe-Ansatz fuer das eindimensionale Bose-Gas und die Heisenberg-Spinkette
  November 2013

15.12 Guests

- Prof. A. Ishisbashi
  Kinki U. Osaka
  19.-30. August 2013
- Prof. R. M. Wald
  U. Chicago
  11.-14. November 2013
- Prof. Müller-Preussker
  Humboldt-Universit"at
  19. November 2013
- Prof. V. G. Serbo
  U. Novosibirsk
  18.-19. Juli 2013
- Dr. Andre Sternbeck und Jakob Simeth
  U. Regensburg
  9.-10. Januar 2013
- Prof. B. Garbrecht
  TU München
  15.-16. April 2014
- Prof. J. Kunz
  U. Oldenburg
  13. Mai 2014

Author Index

D

E

F

G

H

J

K

L

M

N

O

P

R

S

T

U

V

W

Y

Z

Advances in Dielectrics
Series Editor: Friedrich Kremer

Friedrich Kremer *Editor*

Dynamics in Geometrical Confinement

Springer

ISSN 1862-6270
Phys. Status Solidi RRL
7 · No. 9 September
595–682 (2013)

physica status solidi RRL

www.pss-rapid.com

rapid research letters

9
2013

Review@RRL

One decade of fully transparent oxide thin-film transistors: fabrication, performance and stability

Heiko Frenzel, Alexander Lajn, and Marius Grundmann

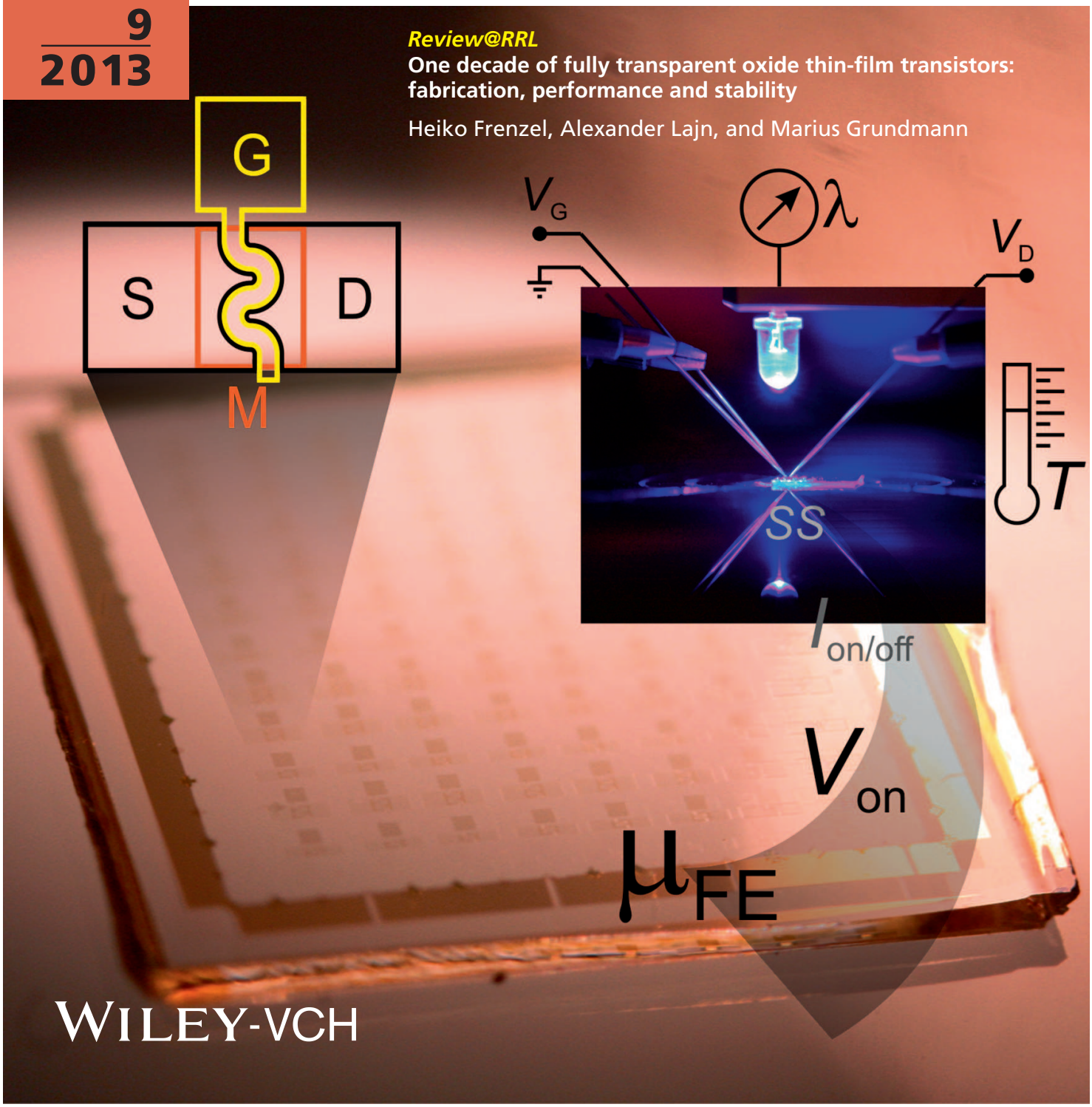

WILEY-VCH